JOINT INSTITUTE FOR NUCLEAR RESEARCH

PHYSICS OF ELEMENTARY PARTICLES AND ATOMIC NUCLEI

PARTICLES & NUCLEI

SCIENTIFIC REVIEW JOURNAL

Founded in December 1970

VOL.32

PART 3

Six issues per year

DUBNA 2001

ОБЪЕДИНЕННЫЙ ИНСТИТУТ ЯДЕРНЫХ ИССЛЕДОВАНИЙ

ФИЗИКА ЭЛЕМЕНТАРНЫХ ЧАСТИЦ И АТОМНОГО ЯДРА

ЭЧАЯ

НАУЧНЫЙ ОБЗОРНЫЙ ЖУРНАЛ

Основан в декабре 1970 года

ТОМ 32

ВЫПУСК 3

Выходит 6 раз в год

ДУБНА 2001

Зав. редакцией А.Н.Графова,
тел. (09621) 6-26-58;
E-mail address: pepan@jinr.ru
FAX +7(09621)6-73-19

ОИЯИ, «Физика элементарных частиц
и атомного ядра», 2001

«ФИЗИКА ЭЛЕМЕНТАРНЫХ ЧАСТИЦ И АТОМНОГО ЯДРА»
2001, ТОМ 32, ВЫП. 3

УДК 539.12.01

QED EFFECTS OF HIGHER ORDERS IN DIS

I. Akushevich[*]

North Carolina Cent. Univ., Durham, NC 27707 and TJNAF, Newport News, VA 23606, USA

E. Kuraev, B. Shaikhatdenov

Joint Institute for Nuclear Research, Dubna

The present status of theoretical description of deep inelastic scattering of leptons on protons with the account of radiative corrections (RC) in the leading and next-to-leading approximations is reviewed. For the process $ep \to ep\gamma$ along with RC coming from emission of virtual, soft and additional hard photons, there has been considered a e^+e^--pair production in the leading approximation. The Compton tensor with a heavy photon in the case of longitudinally polarized electron is presented. A cross section for a special experimental set-up with the tagging of additional hard photon is given to the nonleading order. A similar consideration is carried out for a cross channel, namely, electron–positron annihilation into hadrons with emission of a hard photon by initial leptons. Details of calculations are given in Appendices.

Дан обзор современного состояния теоретического описания процессов глубоконеупругого рассеяния лептонов на протонах с учетом радиационных поправок (РП) в лидирующем и следующем за лидирующим приближениях. Для процесса $ep \to ep\gamma$ наряду с РП от излучения виртуального, мягкого и жесткого дополнительного фотона в ведущем приближении также рассмотрено образование дополнительной e^+e^--пары. Приведен комптоновский тензор с тяжелым фотоном для случая продольно-поляризованного электрона. Для постановки опыта с детектированием дополнительного жесткого фотона представлено сечение с учетом нелидирующих поправок. Аналогичные результаты даны для кросс-канала — e^+e^--аннигиляции в адроны с излучением жесткого фотона начальными лептонами. В приложениях приводятся детали вычислений.

1. DEEP INELASTIC SCATTERING

Deep inelastic scattering (DIS) is one of the powerful tools in investigating a nucleon nature. It has played a key role to form our modern understanding of the substructure of hadrons. A number of experiments were performed at CERN, DESY, SLAC and elsewhere since the discovery of the proton structure in the late sixties. These experiments have provided very precise data in a wide kinematical region [1]. Renewed interest to the DIS was revived after measurement of the proton spin structure by EMC [2] (see also the review [3]). Till now the inclusive, semiinclusive and exclusive processes with both polarized

[*]On leave from the National Centre of Particle and High Energy Physics, 220040 Minsk, Belarus.

and unpolarized particles are widely investigated in many laboratories around the world.

Last years measurements of the observable quantities in DIS have the tendency to decrease both statistical and systematical errors comparing with the previous ones. Since radiative effects can give a substantial contribution to measured quantities the modern level of data analysis in experiments on DIS requires careful consideration of the QED radiative effects which can give substantial contribution to measured quantities. Usually a hard radiated photon cannot be registered in a detector. As is well understood the corrections due to soft photons and loop effects cannot be separated from observables in principle. Hence their contribution has to be calculated theoretically and subtracted from observed data. That's a reason why the calculation of radiative corrections is a very important field of theoretical particle physics.

Depending on the four-momentum transfer squared, Q^2, and the energy transfer, ν, there are three basic channels for lepton scattering on nuclei: elastic, quasielastic, and inelastic processes. In the case of elastic scattering ($\nu = Q^2/2M_A$, where M_A is a nuclear mass) leptons are scattered on a nucleus leaving the latter in its ground state. Quasielastic scattering ($\nu \sim Q^2/2M$, where M is a nucleon mass) corresponds roughly to direct collisions with the individual nucleons inside the nuclei. Inelastic scattering starts to appear when the pion threshold is reached ($\nu \geq Q^2/2M + m_\pi$, where m_π is a pion mass). At the Born level both Q^2 and ν are fixed completely by measuring the scattering angle and the energy (momentum) of scattered lepton. However at the level of radiative corrections, in the case of presence of real radiated photons, fixation is removed and the four-momentum of radiated photon has to be included in a kinematical variable calculation. Such elastic, quasielastic and inelastic processes with radiation of a real photon are known as radiative tails from the elastic ($\sigma_{\rm el}$) and the quasielastic ($\sigma_{\rm q}$) peaks and from the continuous spectrum ($\sigma_{\rm in}$) hereafter called shortly elastic, quasielastic and inelastic radiative tail.

The total radiative correction at the lowest order is obtained as a sum of these contributions together with loop corrections (σ_v) coming from effects of vacuum polarization and exchange by an additional virtual photon,

$$\sigma^{\rm rad.corr} = \sigma_{\rm in} + \sigma_{\rm q} + \sigma_{\rm el} + \sigma_v. \tag{1}$$

The lowest order radiative corrections in DIS on unpolarized proton target were first calculated by Mo and Tsai [4]. In this paper the integration region over the real photon phase space is divided into two parts by introducing an infinitesimal parameter. For values less than this parameter the integrals can be calculated analytically after some additional assumptions (arguments of structure functions are independent of photon momentum, only the leading power of photon energy is kept). The dependence on this unphysical infinitesimal parameter is a

shortcoming of this approach. A covariant formalism was developed in [5] in order to avoid the difficulties mentioned. The formulae of the lowest order RC are free of any approximation and rather compact, but are not visible as much as in the first approach. One of the shortcomings is the nonpositively defined expressions for inelastic radiative tail that make it unusable for Monte Carlo simulation of radiative processes. The excellent review of the model independent lowest order RC within this method can be found in [6]. Both approaches are widely used in practice. There are papers in which they were compared numerically [7, 8] and even analytically [9].

A complete set of the results for RC on unpolarized targets was obtained in [10]. The method was developed for the case of polarized proton and nuclear targets in [11,12]. QED correction to DIS cross section in the leading approximation was calculated in [13]. A lot of papers were devoted to electroweak radiative effects. We draw ones attention to the papers [14–17] in which the correction was calculated within a framework of electroweak theory basically for HERA kinematics. All cited papers were devoted to inclusive DIS. RC in the processes of semiinclusive and exclusive DIS electroproduction cannot be reduced to the inclusive case due to additional tensorial structures entering hadronic tensor and different phase space possible for hard radiated photon. Explicit results for these processes are given in papers [18–21]. Also we note papers [22–24] for RC to elastic and quasielastic ep scattering.

There is one more important task for theoreticians dealing with RC, namely a creation of computer tool which provides the procedure of accounting for RC to experimental data. One of the first codes applied in experiments on DIS at CERN were FERRAD [25] and TERAD [10] which were constructed on the basis of results of two discussed approaches, respectively. An exhaustive review of different codes can be found in [26]. We note recently developed codes gathering the best features and many years experience of data analysis. The Monte Carlo generator HERACLES [27] and semianalytical code HECTOR [28] are used in experiments at HERA. The code POLRAD 2.0 [29] and Monte Carlo generator RADGEN [9] are currently used in polarization experiments at CERN, DESY, SLAC and JLAB. For semiinclusive and exclusive cases the codes DIFFRAD [19] and HAPRAD [21] are intensively exploited. We note also the paper [30] where the approach to estimate a systematical error due to RC in polarized DIS is given.

Thus, we can conclude that the radiative correction of the lowest order is a well defined quantity. The open points here are basically related with a model dependent correction like a contribution of box diagrams or with generations to multiparticle measurements.

The next important step both from theoretical and experimental points of view is to take into account the second order radiative correction. So far, there are only approximate results even for model independent RC. Quite often results obtained by different authors are in disagreement and the quality of the approximations

made is not analyzed. The main approach here is the leading log approximation or put another way — the method of structure functions [31, 32]. Explicit results for inclusive higher order radiative correction within this approach were obtained in [13]. Correction to such a quite general quantity as the Compton tensor with heavy photon was discussed in [33]. If not to count a simple exponentiation formula, the higher order effects are not included in the procedure of RC accounting to experimental data. It is in the contradiction with currently performed experiments on Bhabha and $e\bar{e}$ annihilation where deeply analyzed second order correction is embedded into the standard scheme of data analysis.

The present review is just devoted to the consideration of different aspects of a theory of higher order effects in DIS. As such, it has something to do with the description of various sources of quantum corrections to the process. This way a very important second order contribution comes from elastic and quasielastic radiative tail. The kinematics is not trivial here and requires a careful consideration. These points and explicit results are discussed in Sec. 1.1. Very interesting measurements that allow one to obtain results for kinematical regions unreachable in normal DIS are experiments with photon tagging. RC come from higher order effects and are discussed in Sec. 1.2. Polarization effects for radiative processes can be considered in a quite general way by calculating the so-called Compton tensor for a heavy fermion. These results generalizing the ones obtained in [33] for unpolarized case are discussed in Sec. 1.3. And in Sec. 1.4, the hadronic cross section in $e\bar{e}$ annihilation with tagged photon is given.

1.1. QED Correction to Radiative Tail from Elastic Peak in DIS. Numerical analysis of the elastic radiative tail shows that its contribution is very important and can exceed the main measured process at the Born level. Therefore the next step is to calculate QED correction to the elastic radiative tail with the maximal possible accuracy. So far only the leading correction to elastic radiative tail due to double bremsstrahlung, which is part of the total second order correction, was treated numerically [16, 29] and the attempt to calculate the correction exactly was done in [34].

The structure of the cross section of elastic radiative tail is the following

$$\sigma^{\mathrm{ERT}} \sim \int\limits_{Q_h^2{}_{\min}} \mathrm{d}Q_h^2 \mathcal{K}(Q_h^2, Q^2, W^2)\mathcal{F}^2(Q_h^2), \tag{1.1.1}$$

where Q_h^2 is a momentum square transferred to hadronic system, and Q^2 and W^2 are leptonic kinematical variables measured. The quantity $\mathcal{K}$ is a kinematical factor known exactly and $\mathcal{F}$ is a nuclear form factor. Due to rapid fall of the form factor squared as a function of Q_h^2 the main integration region is close to the lower integration limit. In papers [16, 35] this fact was used to construct an approximation, where Q_h^2 is considered as a small parameter of order of the proton mass squared. In this paper we will also use this approximation to analyze

the correction to elastic radiative tail. The application of Sudakov technique will allow us to obtain compact explicit formulae for processes considered. The first effect which has to be considered is the one-loop correction and the emission of additional real photon. We will analyze both of them at leading and next-to-leading levels. Another effect contributing to the cross section is a lepton pair creation. We will calculate it in the leading log approximation.

Obtaining a second order correction to deep inelastic scattering is the main motivation of this part. However our results can be used in other cases. For instance, they can be considered as a radiative correction in measurements with hard photon detected in coincidence with scattered lepton (see [36], for example), that allows one to reach kinematical regions otherwise unreachable. That is why we do not concretize our notation usually used in DIS but instead try to keep it as general as possible. In the next section we introduce our notation and obtain results for the cross section of single bremsstrahlung using Sudakov technique. In Section 1.1.2. we give results for one-loop corrections. Double bremsstrahlung and contributions due to pair production are considered in Sections 1.1.3. and 1.1.4. and final remarks are given in Section 1.1.5. Some technical details are discussed in Appendices.

1.1.1. Single Bremsstrahlung. We study the process

$$\begin{aligned} &e(p_1)+p(p_2)\to e(p_1')+\gamma(k_1)+p(p_2'), \quad s=2p_1p_2,\\ &Q_h^2=-(p_2-p_2')^2, \quad Q^2=2p_1p_1', \quad k_1^2=0,\\ &p_1^2=p_1'^2=m^2, \quad p_2^2=p_2^{2'}=M^2, \quad q^2=-O_h^2\,, \end{aligned} \tag{1.1.2}$$

in the kinematical region

$$s\gg Q^2>Q_h^2\sim M^2, \qquad 2p_2p_1'\sim s. \tag{1.1.3}$$

The expression for differential cross section in Born approximation looks (details are given in Appendix A):

$$2\varepsilon_1'\frac{\mathrm{d}^3\sigma_0^\gamma}{\mathrm{d}^3p_1'}=\frac{4\alpha^3}{\pi^2}\int\frac{\mathrm{d}^2\mathbf{q}}{(\mathbf{q}^2+Q^2_{\min})^2}\frac{1}{1-b}\Phi^\gamma\Phi^{\mathrm{prot}}, \tag{1.1.4}$$

with $b=2p_2p_1'/s$ the energy fraction of the scattered electron. We imply the Sudakov parameterization of the 4-momenta in the problem (see Appendix A).

Note that due to the gauge invariance condition

$$q^\rho J_\rho^{(1)}\approx(\alpha_q p_2+q_\perp)^\rho J_\rho^{(1)}=0, \tag{1.1.5}$$

the quantity Φ^γ is constructed out of $(1/s)p_2J^{(1)}$ which may be rearranged as follows:

$$\begin{aligned} \frac{1}{s}p_2^\mu J_\mu^{(1)} &= -\frac{s}{s_1}|\mathbf{q}|e_q^\mu J_\mu^{(1)}, \quad e_q=\frac{\mathbf{q}}{|\mathbf{q}|},\\ s_1 &= s\alpha_q=(p_1'+k_1)^2+\mathbf{q}^2-m^2. \end{aligned} \tag{1.1.6}$$

Thus Φ^γ vanishes for small $\mathbf{q}^2$. The explicit expression for $\Phi^{\rm prot}$ is found to be

$$\Phi^{\rm prot} = 2(F_1^2 + \frac{\mathbf{q}^2}{M^2}F_2^2). \tag{1.1.7}$$

For Φ^γ we have (we refer for further details to Appendix A):

$$\Phi^\gamma = \frac{(1-b)^2 b(1+b^2)\mathbf{q}^2}{n_1 n}\,, \tag{1.1.8}$$

with

$$n = (\mathbf{p}_1' - b\mathbf{q})^2, \quad n_1 = (\mathbf{p}_1' - \mathbf{q})^2. \tag{1.1.9}$$

Another fact is that both $\Phi^\gamma/\mathbf{q}^2$ and $\Phi^{\rm prot}$ do not vanish in the limit of small momentum transfer $|\mathbf{q}|$, thus providing the logarithmic enhancement upon performing the $Q_h^2 \approx \mathbf{q}^2$ integration (Weizsäcker–Williams approximation). Indeed, the quantity $Q^2_{\rm min}$ entering the cross section is a small quantity,

$$Q^2_{\rm min} = M^2\left(\frac{Q^2}{(1-b)s}\right)^2 \ll M^2. \tag{1.1.10}$$

For completeness we put the phase volume of the scattered electron in terms of Sudakov variables:

$$\frac{{\rm d}^3 p_1'}{2\varepsilon_1'} = \frac{{\rm d}b}{2b}{\rm d}^2\mathbf{p}_1', \quad Q^2 = 2p_1 p_1' = \frac{\mathbf{p}_1^{'2}}{b}. \tag{1.1.11}$$

Note that the requirement $Q^2 > Q_h^2$ provides the absence of singularities while doing an integration over ${\rm d}^2\mathbf{q}$.

1.1.2. Virtual and Soft Photon Emission Contribution. The correction coming from the emission of virtual and soft photons (in the cms reference frame) can be drawn out of paper [33], in which the radiative corrections to the Compton tensor were calculated

$$2\varepsilon_1'\frac{{\rm d}^3\sigma_{B+V+S}}{{\rm d}^3 p_1'} = 2\varepsilon_1'\frac{{\rm d}^3\sigma_0^\gamma}{{\rm d}^3 p_1'}\left[1 + \frac{\alpha}{2\pi}\tilde{\rho} + \right.$$
$$\left. + \frac{\alpha}{4\pi}\frac{1}{1+b^2}\left(\tau_{11} + b(\tau_{12} + \tilde{\tau}_{12}) + b^2\tilde{\tau}_{11}\right)\right], \tag{1.1.12}$$

with

$$\begin{aligned}\tilde{\rho} &= 2(L-1)(2\ln\Delta-\ln b)+3L_h-\ln^2 b- \\ &- \frac{9}{2}-\frac{\pi^2}{3}+2\mathrm{Li}_2\left(\cos^2\frac{\theta}{2}\right), \qquad (1.1.13)\\ L &= \ln\frac{Q^2}{m^2}, \qquad L_h=\ln\frac{Q_h^2}{m^2},\\ \Delta &= \frac{\Delta E}{E}, \qquad \mathrm{Li}_2(x)=-\int\limits_0^x\frac{\ln(1-y)}{y}\mathrm{d}y.\end{aligned}$$

The Born cross section after substitution of Eq. (1.1.8) into Eq. (1.1.4) and neglect of subleading terms becomes

$$2\varepsilon_1'\frac{\mathrm{d}^3\sigma_0^\gamma}{\mathrm{d}^3p_1'}=\frac{4\alpha^3}{\pi^2}\int\frac{\mathrm{d}^2\mathbf{q}\mathbf{q}^2}{(\mathbf{q}^2+Q^2_{\min})^2}\frac{(1-b)(1+b^2)}{b(Q^2)^2}\Phi^{\mathrm{prot}},$$

where $\Delta E, E$ are the upper bound on the undetectable soft photon energy, and the energy of the initial electron, respectively; θ is the angle in the laboratory reference frame between the initial and the scattered electron momenta. Somewhat cumbersome functions τ_{ij} are explicitly given in Appendix D. It should be noted that they do not contain any large logarithms but include the quantity Q_h^2 which is small in our approximation. If one keeps only nonzero terms in the expansion over Q_h^2, then

$$\begin{aligned}\frac{1}{2}\Big(\tau_{11}+b(\tau_{12}+\tilde{\tau}_{12})+b^2\tilde{\tau}_{11}\Big) &= \left[3\log\frac{Q^2}{Q_h^2(1-b)}-1\right]\times\\ &\times(1+b^2)+4b\log(1-b)+[b^2+(1-b)^2]\times\\ &\times\left[\log^2\frac{(1-b)}{b}+\pi^2\right]+[1+(1-b)^2]\log^2(1-b)+\\ &+(3-2b)\log b. \qquad (1.1.14)\end{aligned}$$

The logarithms $\log Q_h^2$ cancel out exactly in the sum of (1.1.14) and $\tilde{\rho}$.

1.1.3. Two Hard Photons Emission Contribution. We will consider now the process of two hard photons emission:

$$e(p_1)+p(p_2)\to e(p_1')+\gamma(k_1)+\gamma(k_2)+p(p_2'). \qquad (1.1.15)$$

The relevant contribution to the cross section looks

$$\begin{aligned}2\varepsilon_1'\frac{\mathrm{d}^3\sigma}{\mathrm{d}^3p_1'} &= \frac{\alpha^4}{8\pi^4}\int\frac{\mathrm{d}^2\mathbf{q}}{(\mathbf{q}^2+Q^2_{\min})^2}\frac{\mathrm{d}x_1\mathrm{d}^2\mathbf{k}_1}{x_1x_2}\Phi^{\gamma\gamma}\Phi^{\mathrm{prot}},\\ Q^2_{\min} &= M^2\left(\frac{s_1}{s}\right)^2, \quad s_1=(p_1'+k_1+k_2)^2, \qquad (1.1.16)\end{aligned}$$

with the expression for $\Phi^{\rm prot}$ given earlier. The explicit form of $\Phi^{\gamma\gamma}$ can be found in Appendix B. The integration over $\mathrm{d}^2\mathbf{k}_1$ may be performed using the integrals given in Appendix C.

Concerning the region $Q_h^2 \ll Q^2$, the result is found to be *

$$\begin{aligned}\Phi^{\gamma\gamma} &= 16\mathbf{q}^2\left\{\frac{Q^2}{s_1^2}\left[\frac{s_1^2(1+b^2)}{d_1d_2d_1'd_2'}+\frac{d_1^2+d_1'^2}{bs_1^2d_2d_2'}+\frac{d_2^2+d_2'^2}{bs_1^2d_1d_1'}\right]-\right.\\ &- \frac{2}{Q^4}(1+\mathcal{P}_{12})\left[\frac{m^2}{d_1^2}\frac{x_2^2(b^2+(1-x_1)^2)}{b(1-x_1)^3}+\right.\\ &+ \left.\left.\frac{m^2}{d_1'^2}\frac{x_2^2b^2(1+(1-x_2)^2)}{(1-x_2)^3}\right]\right\}\end{aligned} \tag{1.1.17}$$

with the notations introduced

$$\begin{aligned}s_1 &= \frac{\mathbf{k}_1^2}{x_1}+\frac{\mathbf{k}_2^2}{x_2}+\frac{\mathbf{p}_1'^2}{b}, \qquad d_i = \frac{1}{x_i}(m^2x_i^2+\mathbf{k}_i^2),\\ d_i' &= \frac{1}{x_ib}[m^2x_i^2+(x_i\mathbf{p}_1'-b\mathbf{k}_i)^2],\end{aligned} \tag{1.1.18}$$

where $x_{1,2}$ are the energy fractions of hard photons, $x_1+x_2+b=1$. Besides we use the relations

$$\mathbf{k}_1+\mathbf{k}_2+\mathbf{p}_1'=0\,, \quad 2qp_1'=s_1b\,, \quad s_1=2qp_1=s\alpha_q.$$

An integration over $\mathrm{d}^2\mathbf{k}_1$ may be performed analytically and to a logarithmic accuracy it boils down to

$$\int\frac{\mathrm{d}^2\mathbf{k}_1}{\pi}\left[\frac{1}{d_1};\frac{1}{d_2};\frac{1}{d_1'};\frac{1}{d_2'}\right]=L\left[x_1;x_2;\frac{x_1}{b};\frac{x_2}{b}\right]. \tag{1.1.19}$$

The resulting contribution (again to a logarithmic accuracy) takes the following form

$$\begin{aligned}\int\mathrm{d}^2\mathbf{k}_1\Phi^{\gamma\gamma} &= \frac{16\pi\mathbf{q}^2L}{b(Q^2)^2}(1+\mathcal{P}_{12})x_2^2\times\\ &\times \left[\left(1+\frac{1}{(1-x_1)^2}+\frac{b^2}{(1-x_2)^2}\right)(1+b^2)+\right.\\ &+ \left.\frac{b^2}{(1-x_1)^4}+\frac{b^4}{(1-x_2)^4}\right],\\ \Delta &< x_i<1-b-\Delta.\end{aligned} \tag{1.1.20}$$

*Upon applying the crossing transformation to the amplitude of $e\bar{e}$ annihilation to $\gamma\gamma\gamma$ presented in paper [37].

Carrying out the integration of Eq. (1.1.17) over $\mathbf{k}_1$ and x_1 to a next-to-leading accuracy we obtain for the contribution to the differential cross section coming from emission of two hard photons

$$2\varepsilon_1'\frac{\mathrm{d}^3\sigma^{\gamma\gamma}}{\mathrm{d}^3p_1'} = \frac{2\alpha^4}{\pi^3}\int\frac{\mathrm{d}^2\mathbf{q}}{(\mathbf{q}^2+Q^2_{\min})^2}\frac{\mathbf{q}^2(T_{LL}+T_{NLO})}{b(Q^2)^2}\Phi^{\mathrm{prot}}, \tag{1.1.21}$$

where the leading and next-to-leading contributions read

$$\begin{aligned}
T_{LL} &= (L-1)[4(1-b)(1+b^2)\ln\frac{1-b}{\Delta}+\\
&+ (1-b)(1-b^2)\ln b-\frac{2}{3}(1-b)(7-2b+7b^2)],\\
T_{NLO} &= -\frac{1}{2}\frac{b^4+6b^2+1}{1+b}\log^2 b-\\
&- \frac{1}{3}(3-b^2)(3-b)\log b+\\
&+ \frac{8}{3}(1-b)(b^2+b+1)\log(1-b)-\\
&- (1-b)\left[\frac{1}{3}(15b^2-2b+15)+\right.\\
&+ \left.2\left(\mathrm{Li}_2(b)-\frac{\pi^2}{6}\right)\frac{b^4+6b^2+1}{1-b^2}\right].
\end{aligned} \tag{1.1.22}$$

There are two possible experimental set-ups we concern with: the first one in which a recoil proton is registered, and the second — pure inclusive set-up — with only a final lepton observed. Definitely, NLO contribution obtained can be counted valid only for the former experimental set-up, while in the latter case one can use the expression given above only to an LL accuracy.

The general answer for the cross section in Born approximation with the lowest order correction to the leading approximation is a sum of the contributions coming from virtual and real soft photons emission given above as well as from two hard photons emission and is free from dependence on the auxiliary parameter Δ.

The graphs given below illustrate behavior featured by the complete QED RC contribution to the cross section of DIS as well as the comparative contributions of the LL, NLO terms and of the correction due to pair production.

1.1.4. Contribution of Lepton Pair Production. Consider now the hard pair production process that takes place at the same order of perturbation theory as the two hard photons emission. In the same way we may conclude that the soft pair case as well as the case of double collinear kinematics does not contribute

to the radiative tail. Therefore we may consider only semicollinear kinematics of hard pair production of which there exist two different mechanisms [38]. One of these is the two-photon mechanism of pair creation. An electron from that pair having momentum p_1' is detected in experiment and the scattered electron moves close to the initial electron direction. This kinematics permits us to apply the Weizsäcker–Williams approximation,

$$\begin{aligned} 2\varepsilon_1' \frac{\mathrm{d}^3\sigma^{(1)}_{\mathrm{pair}}}{\mathrm{d}^3 p_1'} &= \frac{2\alpha^4}{\pi^3}\int \frac{\mathrm{d}^2\mathbf{q}}{(\mathbf{q}^2+Q^2_{\min})^2}\frac{\mathbf{q}^2 L}{b(Q^2)^2}\Phi^{\mathrm{prot}} \times \\ &\times \frac{\mathrm{d}\beta_-}{(1-\beta_-)^4}((1-\beta_- -b)^2+b^2)(1+\beta_-^2), \qquad (1.1.23) \\ s_1 &= Q^2\frac{1-\beta_-}{\beta_+}, \qquad b+\beta_-+\beta_+=1. \end{aligned}$$

The second mechanism is characterized by the bremsstrahlung mechanism of pair creation, with an electron from a pair to be detected. Leaving details to Appendix E let us present here the result

$$\begin{aligned} 2\varepsilon_1' \frac{\mathrm{d}^3\sigma^{(2)}_{\mathrm{pair}}}{\mathrm{d}^3 p_1'} &= \frac{2\alpha^4}{\pi^3}\int \frac{\mathrm{d}^2\mathbf{q}}{(\mathbf{q}^2+Q^2_{\min})^2}\frac{\mathbf{q}^2 L}{(Q^2)^2}\Phi^{\mathrm{prot}} \times \\ &\times \frac{b(1+\beta_-^2)\mathrm{d}\beta_-}{(1-\beta_-)^4}[(1-b-\beta_-)^2+b^2], \qquad (1.1.24) \\ s_1 &= Q^2\frac{1-\beta_-}{b\beta_-}. \end{aligned}$$

The integration over β_- can be performed analytically with additional assumption that $Q^2_{\min}$ has no β_- dependence. The result for the sum of these contributions is found to be

$$\begin{aligned} 2\varepsilon_1' \frac{\mathrm{d}^3\sigma_{\mathrm{pair}}}{\mathrm{d}^3 p_1'} &= \frac{2\alpha^4}{\pi^3}\int \frac{\mathrm{d}^2\mathbf{q}}{(\mathbf{q}^2+Q^2_{\min})^2}\frac{\mathbf{q}^2 L(1+b^2)}{b(Q^2)^2}\Phi^{\mathrm{prot}} \times \\ &\times \left(1-b+2(1+b)\log b+\frac{4}{3b}(1-b^3)\right). \qquad (1.1.25) \end{aligned}$$

1.1.5. Discussion. In this part the correction to radiative tail from elastic peak is studied in the kinematics when a final lepton is measured. Using Sudakov technique the contributions of loops (1.1.12), double photon bremsstrahlung (1.1.21) and a pair production (1.1.23,1.1.24) are calculated.

In this section we analyze obtained contributions numerically. Both the relative contributions of the processes considered and the total correction to the lowest order process are investigated within kinematical conditions of experiments on electron DIS at TJNAF and DESY (both for HERA and for HERMES). It is convenient to define the following quantities:

$$\delta = \frac{\sigma_L + \sigma_N + \sigma_p}{\sigma_0}, \quad \delta_{L,N,p} = \frac{\sigma_{L,N,p}}{\sigma_0}. \tag{1.1.26}$$

Here σ_0 stands for the cross section of radiative tail from elastic peak (1.1.4). Other σ's constitute the next order results. The quantity σ_p is a direct sum of two mechanisms of pair creations (1.1.23,1.1.24), whereas σ_L and σ_N are the leading (including mass singularities terms $\log(Q^2/m^2)$) and next-to-leading (independent of leptonic mass) terms. They are obtained upon summing up expressions given in Eqs. (1.1.12) and (1.1.21) after cancellation of infrared divergence.

The relative radiative correction to elastic radiative tail is important practically everywhere. The modern level of data analysis and very high experimental accuracies achieved in current experiments on DIS require that a generalization of standard radiative correction procedure be made in order to include a second order radiative correction. An extremely interesting region where the correction considered is important is actually high y domain. Remind, that this one (up to $y \sim 0.95$) is under investigation at TJNAF.

The main contribution to a second-order radiative correction comes from the effect of pair creation. Asymptotical behavior of σ_p for small $b = 1 - y$ is $1/b^2$ whereas the other cross sections feature only $1/b$ behavior. That is in fact a reason of the large correction in the region of high y. In the paper presented this particular contribution is calculated in the leading approximation only, therefore a study of the correction, induced by a pair production, at the next-to-leading level is highly desirable.

The relative contribution of the next-to-leading correction σ_N is not small with respect to the leading log contribution σ_L. In the region of large y the relative contribution σ_N/σ_L does not exceed 5%, whereas for small y it can reach as much as 20–30%. From the other hand the next-to-leading contribution completely fixes all uncertainties of leading log approximation thus leaving unknown only terms proportional to lepton mass squared and Q_h^2, which is effectively small due to behavior of form factors.

1.2. Tagged Photon with Next-to-Leading Accuracy. The radiative corrections to deep inelastic electron proton scattering due to hard real photon emission are very important in certain regions of the HERA kinematic domain. In fact, the initial-state collinear radiation leads to a reduction of the projectile electron energy and therefore to a shift of the effective Bjorken variables in the hard scattering process as compared to those determined from the actual measurement

of the scattered electron alone. Therefore, radiative events

$$e(p_1) + p(P) \to e(p_2) + \gamma(k) + X + (\gamma), \tag{1.2.1}$$

are to be carefully taken into account [4, 6, 39].

On the other hand, measuring the energy of the photons emitted very close to the incident electron beam direction [40–43] permits one to overlap the kinematical region of photoproduction ($Q^2 \approx 0$) and the DIS region with small transferred momenta (about a few GeV^2) within the high energy HERA experiments. Furthermore, these radiative events may be used to independently determine the proton structure functions F_2 and F_1 (and therefore F_L) in a single run without lowering the beam energies [36, 41]. Preliminary results of an F_2 analysis using such radiative events were recently presented by the H1 collaboration [44].

Our aim is to calculate the radiative corrections to neutral current deep inelastic events with simultaneous (exclusive) detection of a hard photon emitted very close to the direction of the incoming electron beam ($\theta_\gamma = \widehat{\mathbf{p_1 k}} \leq \theta_0 \approx \approx 5 \cdot 10^{-4}$ rad). In the case of the HERA collider, the experimental detection of photons emitted in this very forward direction is actually possible due to the presence of photon detectors (PD) that are part of the luminosity monitoring system of ZEUS and H1.

Let us briefly review the kinematics for the process under consideration. As the opening angle of the forward photon detector is very small, and since we will only consider cross sections where the tagged photon is integrated over the solid angle covered by this photon detector, we can parameterize these radiative events using the standard Bjorken variables x and y, that are determined from the measurement of the scattered electron,

$$x = \frac{Q^2}{2P \cdot (p_1 - p_2)}, \quad y = \frac{2P \cdot (p_1 - p_2)}{V}, \quad Q^2 = 2p_1 \cdot p_2 = xyV, \tag{1.2.2}$$

with $V = 2P \cdot p_1$, and the energy fraction z of the electron after initial state radiation of a collinear photon,

$$z = \frac{2P \cdot (p_1 - k)}{V} = \frac{\varepsilon - k^0}{\varepsilon}, \tag{1.2.3}$$

where ε is the initial electron energy, and k^0 is the energy seen in the forward photon detector.

An alternative set of kinematic variables that is especially adapted to the case of collinear radiation, is given by the *shifted* Bjorken variables [41],

$$\hat{Q}^2 = -(p_1 - p_2 - k)^2, \quad \hat{x} = \frac{\hat{Q}^2}{2P \cdot (p_1 - p_2 - k)}, \quad \hat{y} = \frac{P \cdot (p_1 - p_2 - k)}{P \cdot (p_1 - k)}. \tag{1.2.4}$$

The relations between the shifted and the standard Bjorken variables read [41]:

$$\hat{Q}^2 = zQ^2, \qquad \hat{x} = \frac{xyz}{z+y-1}, \qquad \hat{y} = \frac{z+y-1}{z}\,. \tag{1.2.5}$$

The cross section under consideration in the Born approximation, integrated over the solid angle of the photon detector ($0 \le \theta_\gamma \le \theta_0,\ \theta_0 \ll 1$), then takes the following form:

$$\frac{z}{y}\frac{\mathrm{d}^3\sigma_{\mathrm{Born}}}{\mathrm{d}x\,\mathrm{d}y\,\mathrm{d}z} = \frac{1}{\hat{y}}\frac{\mathrm{d}^3\sigma_{\mathrm{Born}}}{\mathrm{d}\hat{x}\,\mathrm{d}\hat{y}\,\mathrm{d}z} = \frac{\alpha}{2\pi}P(z,L_0)\tilde{\Sigma}, \tag{1.2.6}$$

where

$$\begin{aligned}\tilde{\Sigma} = \Sigma(\hat{x},\hat{y},\hat{Q}^2) \quad &= \quad \frac{2\pi\alpha^2(-\hat{Q}^2)}{\hat{Q}^2\hat{x}\hat{y}^2}F_2(\hat{x},\hat{Q}^2)\Big[2(1-\hat{y}) - 2\hat{x}^2\hat{y}^2\frac{M^2}{\hat{Q}^2} + \\ &+ \quad \left(1+4\hat{x}^2\frac{M^2}{\hat{Q}^2}\right)\frac{\hat{y}^2}{1+R}\Big],\end{aligned}$$

$$P(z,L_0) = \frac{1+z^2}{1-z}L_0 - \frac{2z}{1-z},\ R = R(\hat{x},\hat{Q}^2) = \left(1+4\hat{x}^2\frac{M^2}{\hat{Q}^2}\right)\frac{F_2(\hat{x},\hat{Q}^2)}{2\hat{x}F_1(\hat{x},\hat{Q}^2)} - 1,$$

$$\alpha(-\hat{Q}^2) = \frac{\alpha}{1-\Pi(-\hat{Q}^2)}\,,\ L_0 = \ln\left(\frac{\varepsilon^2\theta_0^2}{m^2}\right),\ \hat{Q}^2 = 2zp_1\cdot p_2 = 2z\varepsilon^2 Y(1-c),$$

$$Y = \frac{\varepsilon_2}{\varepsilon} = 1 - y + xy\frac{E_p(1+\beta_p)}{2\varepsilon}\,, \quad c = \cos(\widehat{\boldsymbol{p}_1\boldsymbol{p}_2}),$$

$$\hat{x} = \frac{\hat{Q}^2}{2P\cdot(zp_1-p_2)} = \frac{z\varepsilon Y(1-c)}{zE_p(1+\beta_p) - YE_p(1+\beta_p c)}\,, \quad \beta_p = \sqrt{1-M^2/E_p^2}\,,$$

$$\hat{y} = \frac{2P\cdot(zp_1-p_2)}{zV} = \frac{z(1+\beta_p) - Y(1+\beta_p c)}{z(1+\beta_p)}. \tag{1.2.7}$$

The quantities F_2 and F_1 are the proton structure functions, M and m are the proton and electron masses, respectively. In the cross section (1.2.6) we take into account terms proportional to $M^2/\hat{Q}^2$, which may be important at low Q^2. Note that the neglect of Z-boson exchange and γ–Z interference is a good approximation, because we are interested mostly in events with small momentum transfer $\hat{Q}^2$.* The energies of the initial and final electron, of the tagged photon

*The corresponding Born cross section including contributions from the Z can be found in Ref.42.

and of the initial proton (ε, ε_2, k^0, and E_p) are defined in the laboratory reference frame (i.e., the rest frame of HERA detectors). The cross section (1.2.6) agrees with [41, 42]. Also note that we explicitly included the correction from the vacuum polarization operator $\Pi(-\hat{Q}^2)$ in the virtual photon propagator. The aim of our work is to calculate the higher order QED radiative corrections for this process in the leading and next-to-leading logarithmic approximation.

Here we will restrict ourselves to the model independent QED radiative corrections related to the lepton line, which form a complete, gauge invariant subset for the neutral current scattering process. The remaining source of QED radiative corrections at the same order, such as virtual corrections with double photon exchange and bremsstrahlung off the partons are more involved and model dependent, they will be considered elsewhere. Our approach to the calculation of the QED corrections is based on the utilization of all essential Feynman diagrams that describe the observed cross section in the framework of the used approximation. The same approach was used recently for the calculation of the QED corrections for the small angle Bhabha scattering cross section at LEP1 [45].

This part is organized as follows. Section 1.2.1 is devoted to the corrections related with emission of virtual and soft real photons in the hard collinear photon emission DIS process. In Sec. 1.2.2 we consider the radiative corrections due to emission of two hard photons in the collinear kinematics (where we distinguish between the cases when both photons are emitted close to the initial electron direction and the case when one of the photons is emitted along the initial and the other one along the scattered electron direction) and the semicollinear kinematics, where the additional hard photon is emitted at a large angle. Section 1.2.3 collects the results obtained and discusses two experimental cases: an exclusive set-up, that assumes that a bare electron can be measured, and a calorimetric one. The Appendices are devoted to details of the calculation.

1.2.1. Virtual and Soft Photon Emission Corrections. In order to calculate the contributions from the virtual and soft photon emission corrections, we start from the expression for the Compton scattering tensor with a heavy photon [33, 46],

$$K_{\mu\nu} = (8\pi\alpha)^{-1} \sum_{\text{spins}} M_{\mu}^{e\gamma^* \to e'\gamma} (M_{\nu}^{e\gamma^* \to e'\gamma})^*, \tag{1.2.8}$$

where M_μ is the matrix element of the process of Compton scattering

$$\gamma^*(-q) + e(p_1) \to \gamma(k) + e(p_2), \tag{1.2.9}$$

and the index μ describes the polarization state of the virtual photon. This tensor is conveniently decomposed as follows:

$$\begin{aligned} K_{\mu\nu} &= \frac{1}{2}(P_{\mu\nu} + P^*_{\nu\mu}), \\ P_{\mu\nu} &= \tilde{g}_{\mu\nu}(B_g + \frac{\alpha}{2\pi}T_g) + \tilde{p}_{1\mu}\tilde{p}_{1\nu}(B_{11} + \frac{\alpha}{2\pi}T_{11}) + \\ &+ \tilde{p}_{2\mu}\tilde{p}_{2\nu}(B_{22} + \frac{\alpha}{2\pi}T_{22}) + \frac{\alpha}{2\pi}(\tilde{p}_{1\mu}\tilde{p}_{2\nu}T_{12} + \tilde{p}_{2\mu}\tilde{p}_{1\nu}T_{21}), \\ \tilde{g}_{\mu\nu} &= g_{\mu\nu} - \frac{q_\mu q_\nu}{q^2}\,, \qquad \tilde{p}_{1\mu} = p_{1\mu} - q_\mu\frac{p_1\cdot q}{q^2}\,, \\ \tilde{p}_{2\mu} &= p_{2\mu} - q_\mu\frac{p_2\cdot q}{q^2}\,, \qquad p_1 = q + p_2 + k. \end{aligned} \tag{1.2.10}$$

The expressions for the quantities B_{ij} corresponding to the Born approximation are *:

$$\begin{aligned} &B_g = \frac{1}{st}\left[(s+u)^2 + (t+u)^2\right] - 2m^2q^2\left(\frac{1}{s^2} + \frac{1}{t^2}\right), \quad B_{11} = \frac{4q^2}{st} - \frac{8m^2}{s^2}, \\ &B_{22} = \frac{4q^2}{st} - \frac{8m^2}{t^2}, \quad s = 2p_2\cdot k, \quad t = -2p_1\cdot k, \quad u = (p_2 - p_1)^2, \\ &q^2 = s + t + u, \quad p_1^2 = p_2^2 = m^2, \quad k^2 = 0. \end{aligned} \tag{1.2.11}$$

The one-loop QED corrections are contained in the quantities T_{ij}, whose explicit expressions are given in [33, 46]. Here we have to integrate them over the solid angle of the emitted photon corresponding to the shape of the photon detector. We need to keep only the terms singular in the limit $\theta_\gamma \to 0$, since after integration the constant terms contribute only proportional to $\theta_0^2 \sim 10^{-6}$ and can be safely neglected. Another simplification comes from the fact that we need only the symmetric (and real) part of the tensor K. This way, by using typical integrals

$$\int \frac{\mathrm{d}\Omega_k}{2\pi}\frac{1}{t} = -\frac{L_0}{2\varepsilon^2(1-z)}, \qquad \int \frac{\mathrm{d}\Omega_k}{2\pi}\frac{m^2}{t^2} = \frac{1}{2\varepsilon^2(1-z)^2}\,, \tag{1.2.12}$$

and using the expressions given in Appendix F we obtain the following expression for the Compton tensor integrated over the angular part of the photon phase space:

$$\int \frac{\mathrm{d}\Omega_k}{2\pi}K_{\mu\nu} = \left(-Q_l^2 g_{\mu\nu} + 4z p_{1\mu}p_{1\nu}\right)\frac{1}{2\varepsilon^2(1-z)}\left[\left(1 + \frac{\alpha}{2\pi}\rho\right)P(z, L_0) - \frac{\alpha}{2\pi}T\right],$$

*We have already dropped those terms that vanish in the high-energy limit when one integrates over any finite region of photon phase space.

$$\rho = 4\ln\frac{\lambda}{m}(L_Q - 1) - L_Q^2 + 3L_Q + 3\ln z + \frac{\pi^2}{3} - \frac{9}{2}\,, \tag{1.2.13}$$

$$T = \frac{1+z^2}{1-z}(A\ln z + B) - \frac{4z}{1-z}L_Q \ln z - \frac{2-(1-z)^2}{2(1-z)}L_0 + O(1),$$

$$A = -L_0^2 + 2L_0 L_Q - 2L_0\ln(1-z), \qquad B = \left(\ln^2 z - 2\mathrm{Li}_2(1-z)\right)L_0,$$

$$L_Q = \ln\frac{Q^2}{m^2}, \qquad \mathrm{Li}_2(x) = -\int\limits_0^x \frac{\mathrm{d}y}{y}\ln(1-y)\,.$$

The quantity λ, which enters into the expression for ρ, is a fictitious photon mass.

In the construction of the total expression for the tensor $K_{\mu\nu}$ we replaced $q_\mu = q_\nu = 0$, $p_{2\mu,\nu} = zp_{1\mu,\nu}$, bearing in mind the gauge invariance of hadronic tensor [47],

$$\begin{aligned} H_{\mu\nu} &= \frac{4\pi}{M}\left(W_2(x_h, Q_h^2)\tilde{P}_\mu\tilde{P}_\nu - M^2 W_1(x_h, Q_h^2)\tilde{g}_{\mu\nu}\right), \qquad (1.2.14)\\ x_h &= \frac{Q_h^2}{2P\cdot q_h}, \qquad \tilde{P}_\nu = P_\nu - q_{h\nu}\frac{P\cdot q_h}{q_h^2}. \end{aligned}$$

Here we imply $q_h = q$, $Q_h^2 = -q^2$.

Consider now the process with emission of a soft photon in addition to the emission of the hard one, which hits the PD. We imply the condition that the energy of the soft photon should be less than some small quantity $\delta\varepsilon$ (in the centre-of-mass system). In straightforward calculations, starting from Feynman diagrams, some care is to be paid in the evaluation of integrals over the phase volume of the soft photon, as some contributions are crucially dependent on the correlation between our two small parameters $\Delta = \delta\varepsilon/\varepsilon$ and θ_0. In our particular case $\theta_0 \ll \Delta \ll 1$, the result coincides with the one obtained using the approximation of classical currents for soft photons. The total effect for the sum of contributions of virtual and soft photon emission consists in the replacement of the quantity ρ by $\tilde{\rho}$ in Eq. (1.2.13) (see Eq. (45) in [33,46]):

$$\begin{aligned} \rho \to \tilde{\rho} &= 2(L_Q - 1)\ln\frac{\Delta^2}{Y} + 3L_Q + 3\ln z - \ln^2 Y - \frac{\pi^2}{3} - \qquad (1.2.15)\\ &- \frac{9}{2} + 2\mathrm{Li}_2\left(\frac{1+c}{2}\right). \end{aligned}$$

The final expression for the virtual and soft photon emission corrected tagged photon cross section has the form

$$\frac{z}{y}\frac{\mathrm{d}^3\sigma_{VS}}{\mathrm{d}x\,\mathrm{d}y\,\mathrm{d}z} = \left(\frac{\alpha}{2\pi}\right)^2 [P(z, L_0)\tilde{\rho} - T]\,\tilde{\Sigma}\,. \tag{1.2.16}$$

1.2.2. Double Hard Bremsstrahlung. Consider now the emission of an extra photon with the energy more than $\delta\varepsilon$. For the calculation of the contributions from real hard bremsstrahlung, which in our case correspond to double photon emission with at least one photon seen in the forward detector, we specify three specific kinematical domains: *i)* both hard photons strike the forward photon detector, i.e., both are emitted within a narrow cone around the electron beam ($\theta \leq \theta_0$); *ii)* one hard photon is tagged by the PD, while the other is collinear to the outgoing electron ($\theta_2 = \widehat{\mathbf{k}_2\mathbf{p}_2} \leq \theta_0'$); and finally *iii)* the second photon is emitted at large angles (i.e., outside the defined narrow cones) with respect to both incoming and outgoing electron momenta. We denominate the third kinematical domain as a semicollinear one. The contributions of the regions *i)* and *ii)* contain leading terms (quadratic in the large logarithms L_0, L_Q), whereas region *iii)* contains formally nonleading terms of order $L_0 \ln(1/\theta_0^2)$, which, however, give a contribution numerically larger than the leading ones since $\varepsilon\theta_0/m \ll 1/\theta_0$.

The calculation beyond the leading logarithmic approximation may be performed using the results of a paper of one of us [48]. The contribution from the kinematical region *i)* (with both hard photons being tagged), has the form (see Eq. (II 6) from [48]):

$$\frac{z}{y}\frac{\mathrm{d}^3\sigma_i^{\gamma\gamma}}{\mathrm{d}x\,\mathrm{d}y\,\mathrm{d}z} = \frac{\alpha^2}{8\pi^2}L_0\left[L_0\left(P_\Theta^{(2)}(z) + 2\frac{1+z^2}{1-z}\Big(\ln z - \frac{3}{2} - 2\ln\Delta\Big)\right) + \right.$$
$$\left. + \ 6(1-z) + \left(\frac{4}{1-z} - 1 - z\right)\ln^2 z - 4\frac{(1+z)^2}{1-z}\ln\frac{1-z}{\Delta}\right]\tilde{\Sigma} + O(1). \quad (1.2.17)$$

Here we use the notation $P_\Theta^{(2)}(z)$ for the Θ part of the second order term of the expansion of the electron nonsinglet structure function,

$$\begin{aligned}
D(z,L) &= \delta(1-z) + \frac{\alpha}{2\pi}P^{(1)}(z)L + \frac{1}{2}\left(\frac{\alpha}{2\pi}\right)^2 P^{(2)}(z)L^2 + \ldots \quad (1.2.18)\\
P^{(i)}(z) &= P_\Theta^{(i)}(z)\Theta(1-z-\Delta) + P_\delta^{(i)}\delta(1-z), \quad \Delta \to 0\ ,\\
P_\Theta^{(1)}(z) &= \frac{1+z^2}{1-z}\ , \quad P_\delta^{(1)} = \frac{3}{2} + 2\ln\,\Delta,\\
P_\Theta^{(2)}(z) &= 2\left[\frac{1+z^2}{1-z}\left(2\ln(1-z) - \ln z + \frac{3}{2}\right) + \frac{1}{2}(1+z)\ln z - 1 + z\right].
\end{aligned}$$

The parameter Δ serves as the infrared regularization parameter.

The contribution of the kinematical region *ii)* to the observed cross section depends on the event selection; in other words, on the method of measurement of the scattered particles.

In the case of exclusive event selection, when only the scattered electron is detected, while the photon that is emitted almost collinearly (i.e., within a small cone with opening angle $2\theta_0'$ around the momentum of the outgoing electron) goes unnoticed or is not taken into account in the determination of the kinematical variables, we have (see $\Pi 8$ from [48])

$$\begin{aligned}\frac{z}{y}\frac{\mathrm{d}^3\sigma_{ii}^{\gamma\gamma}}{\mathrm{d}x\,\mathrm{d}y\,\mathrm{d}z} &= \frac{\alpha^2}{4\pi^2}P(z,L_0)\int\limits_{\Delta/Y}^{y_2^{\max}}\frac{\mathrm{d}y_2}{1+y_2}\left[\frac{1+(1+y_2)^2}{y_2}(\widetilde{L}-1)+y_2\right]\Sigma_s,\\ \Sigma_s &= \Sigma(x_b,y_b,Q_b^2),\end{aligned} \tag{1.2.19}$$

where

$$\begin{aligned}\widetilde{L} &= \ln\left(\frac{\varepsilon\theta_0'}{m}\right)^2+2\ln Y,\quad y_2=\frac{x_2}{Y},\quad Y=\frac{\varepsilon_2}{\varepsilon},\quad y_2^{\max}=\frac{2z-Y(1+c)}{Y(1+c)},\\ x_b &= \frac{xyz(1+y_2)}{z-(1-y)(1+y_2)}\ ,\ y_b=\frac{z-(1-y)(1+y_2)}{z}\ ,\ Q_b^2=Q^2z(1+y_2)\ .\end{aligned} \tag{1.2.20}$$

More realistic (from the experimental point of view) is the calorimetric event selection, when only the sum of the energies of the outgoing electron and photon can be measured if the photon momentum lies inside the small cone with opening angle $2\theta_0'$ along the direction of the final electron. In this case we find

$$\begin{aligned}\frac{z}{y}\frac{\mathrm{d}^3\sigma_{ii,\mathrm{cal}}^{\gamma\gamma}}{\mathrm{d}x\,\mathrm{d}y\,\mathrm{d}z} &= \frac{\alpha^2}{4\pi^2}P(z,L_0)\int\limits_{\Delta/Y}^{\infty}\frac{\mathrm{d}y_2}{(1+y_2)^3}\left[\frac{1+(1+y_2)^2}{y_2}(\widetilde{L}-1)+y_2\right]\tilde{\Sigma}=\\ &= \frac{\alpha^2}{4\pi^2}P(z,L_0)\left[(\widetilde{L}-1)\left(2\ln\frac{Y}{\Delta}-\frac{3}{2}\right)+\frac{1}{2}\right]\tilde{\Sigma}.\end{aligned} \tag{1.2.21}$$

In the last equation we used the relation

$$\Sigma_s=\frac{1}{(1+y_2)^2}\tilde{\Sigma}, \tag{1.2.22}$$

which is valid for the calorimetric set-up.

Consider at last the semicollinear region *iii)*. The relevant contribution may be calculated using the quasireal electron method [49]:

$$\frac{z}{y}\frac{\mathrm{d}^3\sigma_{iii}^{\gamma\gamma}}{\mathrm{d}x\,\mathrm{d}y\,\mathrm{d}z}=\frac{\alpha}{2\pi}P(z,L_0)\frac{2\alpha}{\pi}\int\frac{\mathrm{d}^3k_2}{\omega_2}\frac{\alpha^2(Q_{sc}^2)}{Q_{sc}^4}I^\gamma,\quad I^\gamma=B_{\rho\sigma}(zp_1,p_2,k_1)\frac{H^{\rho\sigma}}{8\pi}. \tag{1.2.23}$$

The quantity $B_{\rho\sigma}(zp_1, p_2, k_1)$ is obtained from equation (1.2.11), where it is necessary to set $m = 0$. After some algebraic transformations we obtain

$$I^\gamma = \frac{1}{st}\left[F_2(x_{sc}, Q^2_{sc})\left(\frac{M^2}{Q^2_{sc}}x_{sc}G - V\Big[x_{sc}(z^2+(1-y)^2)V + (1-y)(zQ^2-s) - \right.\right.$$

$$\left.\left. - z(zQ^2-t)\Big]\right) - GF_1(x_{sc}, Q^2_{sc})\right], \qquad G = z^2Q^4 - 2st + Q^4_{sc}\ , \qquad (1.2.24)$$

$$x_{sc} = \frac{Q^2_{sc}}{V(z+y-1) - 2P\cdot k_2}, \quad s = 2p_2\cdot k_2, \quad t = -2zp_1\cdot k_2,$$

$$Q^2_{sc} = zQ^2 - s - t.$$

The angular integration in Eq. (1.2.23) is to be performed over the whole phase space, excepting the small cones along directions of motion of the initial and scattered electrons that correspond to the kinematic regions *i)* or *ii)*. The result (for details see Appendix G) has the form:

$$\begin{aligned}
\frac{z}{y}\frac{\mathrm{d}^3\sigma^{\gamma\gamma}_{iii}}{\mathrm{d}x\,\mathrm{d}y\,\mathrm{d}z} &= \left(\frac{\alpha}{2\pi}\right)^2 P(z, L_0)\left[\int\limits_\Delta^{x_2^t}\frac{\mathrm{d}x_2}{x_2}\frac{z^2+(z-x_2)^2}{z(z-x_2)}\ln\frac{2(1-c)}{\theta_0^2}\Sigma_t + \right.\\
&+ \left.\int\limits_\Delta^{x_2^s}\frac{\mathrm{d}x_2}{x_2}\frac{1+(1+y_2)^2}{1+y_2}\ln\frac{2(1-c)}{\theta_0'^2}\Sigma_s + Z\right]\ , \qquad (1.2.25)\\
\Sigma_t &= \Sigma(x_t, y_t, Q^2_t),
\end{aligned}$$

The logarithmic dependences on the infrared regulator Δ and on the angles θ_0, θ_0' are fully contained in the first two terms on the r.h.s., whereas the quantity Z represents an integral over the whole photon phase space of a well-behaved function, and it is free from collinear and infrared singularities. Its explicit expression is given in Appendix G.

The upper limits of the x_2 integration in (1.2.25) read

$$x_2^t = z - \frac{Y(1+c)}{2}\,, \qquad x_2^s = \frac{2z - Y(1+c)}{1+c}\,, \qquad (1.2.26)$$

and the arguments of Σ_t are

$$x_t = \frac{xy(z-x_2)}{z-x_2+y-1}\ , \quad y_t = \frac{z-x_2+y-1}{z-x_2}, \quad Q_t = Q^2(z-x_2). \quad (1.2.27)$$

An explicit expression for x_m, which is relevant for the calculation of Z, is given in Appendix G.

The formulae given above (see Eqs. (1.2.7), (1.2.16), (1.2.17), (1.2.19) or (1.2.21), and (1.2.25)) provide the complete answer for the leading and subleading contributions up to the second order of perturbation theory. The total sum of virtual, soft, and hard additional photons emission corrections to the radiative DIS cross section does not depend on the auxiliary parameter $\Delta = \delta\varepsilon/\varepsilon$, as it should be.

1.2.3. Results for Different Experimental Set-Ups. The sum of the contributions of the leading and next-to-leading corrections at order α^2, which are given explicitly in the expressions (1.2.16), (1.2.17), (1.2.19) or (1.2.21), and (1.2.25), may be written in the form

$$\frac{z}{y}\frac{\mathrm{d}^3\sigma}{\mathrm{d}x\,\mathrm{d}y\,\mathrm{d}z} = \left(\frac{\alpha}{2\pi}\right)^2 (\Sigma_i + \Sigma_f)\,. \tag{1.2.28}$$

The first term Σ_i is independent of the experimental selection of the scattered electron and has the form:

$$\begin{aligned}
\Sigma_i &= \left\{\frac{1}{2}L_0^2 P_\Theta^{(2)}(z) + P(z,L_0)\left[\frac{1-16z-z^2}{2(1+z^2)} + \left(3-2\ln Y + \frac{4z}{1+z^2}\right)\ln z + \right.\right. \\
&+ \ln^2 Y - 2\mathrm{Li}_2(z) + 2\mathrm{Li}_2\left(\frac{1+c}{2}\right) - \frac{2(1+z)^2}{1+z^2}\ln(1-z) + \\
&+ \left.\left.\frac{1-z^2}{2(1+z^2)}\ln^2 z\right]\right\}\tilde{\Sigma} + P(z,L_0)\,\tilde{\Sigma}\,\ln\frac{2(1-c)}{\theta_0^2}\left[\int\limits_0^{u_0}\frac{\mathrm{d}u}{u}(1+(1-u)^2)\times\right. \\
&\times \left.\left(\frac{\Sigma_t}{(1-u)\tilde{\Sigma}} - 1\right) - \int\limits_{u_0}^{1}\frac{\mathrm{d}u}{u}(1+(1-u)^2)\right] + P(z,L_0)\,Z, \qquad (1.2.29) \\
u &= \frac{x_2}{z}\,, \qquad u_0 = \frac{x_2^t}{z}\,,
\end{aligned}$$

where Z is given in Appendix G and the remaining notations are as above (see (1.2.17), (1.2.24), and (1.2.26)).

The second term in (1.2.28), denoted Σ_f, however, does explicitly depend on the event selection. It corresponds to the emission of a hard photon by the scattered electron. In the exclusive set-up, when only the scattered bare electron is measured, while the photon that is emitted close to the final electron's direction

is ignored, this contribution reads

$$\Sigma_f = \Sigma_f^{\rm excl} = P(z, L_0) \int\limits_0^{x_2^s/Y} {\rm d}y_2 \left[\left(\frac{1+(1+y_2)^2}{y_2} (L_Q + \ln Y - 1) + y_2 \right) \frac{1}{1+y_2} \times \right.$$

$$\left. \times \Theta \left(y_2 - \frac{\Delta}{Y} \right) + (L_Q + \ln Y - 1) \delta(y_2) \left(2 \ln \frac{\Delta}{Y} + \frac{3}{2} \right) \right] \Sigma_s. \qquad (1.2.30)$$

In this case the parameter θ_0', that separated the kinematic regions *ii)* and *iii)*, only plays the role of an auxiliary one; it has already cancelled in the above expression for the cross section.

As we will see below, this situation is quite different for the experimentally more realistic, calorimetric set-up, when the detector cannot distinguish between events with a bare electron and events when the electron is accompanied by a hard photon emitted within a small cone with opening angle $2\theta_0^{'}$ around the direction of the scattered electron. For this case we obtain

$$\begin{aligned} \Sigma_f = \Sigma_f^{\rm cal} &= P(z, L_0) \left[\frac{1}{2} \tilde{\Sigma} + \ln \frac{2(1-c)}{\theta_0^{'2}} \int\limits_0^{\infty} \frac{{\rm d}y_2}{y_2} \frac{1+(1+y_2)^2}{1+y_2} \times \right. \\ &\times \left. \left(\Sigma_s \Theta(y_2^{\max} - y_2) - \frac{\tilde{\Sigma}}{(1+y_2)^2} \right) \right]. \qquad (1.2.31) \end{aligned}$$

For the calorimetric event selection the parameter $\theta_0^{'}$ is a physical one and the final result therefore does depend on it. However, the mass singularity that is connected with the emission of the photon off the scattered electron is cancelled in accordance with the Kinoshita–Lee–Nauenberg theorem [50].

Note that the case of a coarse detector for the scattered electron, i.e., $\theta_0^{'} \sim$ $\sim O(1)$, agrees at the level of leading logarithms with the result of paper [51], that was obtained in the approximation of absence of emission along the scattered electron. Our result disagrees with the result of Bardin et al. [42] on the radiative corrections, as they neglected the interference of the emission of two photons; see [51] for a detailed discussion.

We note in conclusion that the set of Feynman diagrams considered here is gauge invariant and model independent but not complete. We have neglected the contributions with two virtual photons exchanged between electron and the target that appear at the same order of perturbation theory, as well as the interference with the contributions when the second photon is emitted by the hadronic side. However, the description of this part is definitely model dependent. The details and the numerical estimates may be found in [52].

1.3. Compton Tensor with Heavy Photon in the Case of Longitudinally Polarized Fermion. Here we shall restrict our consideration to the part of the Compton tensor, which contains the degree of polarization of the initial electron [53]. Our aim is to calculate soft and virtual QED radiative corrections to the tensor. The corrections are important for modern precise experiments in DIS. Possible applications of our results will be considered in Conclusions.

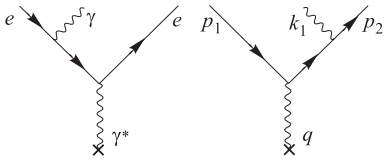

Fig. 1. The Born-level Feynman diagrams

Let us consider the process (see Fig. 1)

$$\gamma^*(q) \ + \ e(p_1) \ \longrightarrow \ \gamma(k_1) \ + \ e(p_2), \tag{1.3.1}$$

$$q^2 < 0, \qquad k_1^2 = 0, \qquad p_1^2 = p_2^2 = m^2, \qquad p_1 + q = p_2 + k_1,$$

where m is the electron mass.

The Compton tensor is defined as

$$K_{\rho\sigma} = (8\pi\alpha)^{-2}\Sigma M_\rho^{e\gamma^*\to e\gamma}(M_\sigma^{e\gamma^*\to e\gamma})^*. \tag{1.3.2}$$

Here the matrix element M describes the Compton scattering process (1.3.1),

$$M_\rho = M_{0\rho} + M_{1\rho} = \bar{u}(p_2)O_{\rho\mu}u(p_1)e^\mu(k_1),$$

$$O_{\rho\mu} = O_{\rho\mu}^{(0)} + \frac{\alpha}{4\pi}O_{\rho\mu}^{(1)}, \quad O_{\rho\mu}^{(0)} = \gamma_\rho\frac{\hat{p}_2 - \hat{q} + m}{t}\gamma_\mu + \gamma_\mu\frac{\hat{p}_1 + \hat{q} + m}{s}\gamma_\rho,$$

$$s = 2p_2k_1, \qquad t = -2p_1k_1. \tag{1.3.3}$$

Quantities $O_{\rho\mu}^{(0)}$ and $O_{\rho\mu}^{(1)}$ take into account the lowest and the first orders of perturbation theory, respectively. Here and in what follows, we use the following notation for scalar products of 4-vectors:

$$\hat{a} = \gamma_\mu a^\mu, \qquad ab = a_\mu b^\mu = a^0b^0 - \mathbf{ab},$$

and the polarization vector of the real photon is $e^\mu(k_1)$.

1.3.1. Radiative Corrections. Calculating the first order correction, we assume that all kinematical invariants of the process are large in comparison with the electron mass square:

$$s \sim -t \sim -u \sim -q^2 \gg m^2, \qquad u = -2p_1p_2, \qquad q^2 = s + t + u. \tag{1.3.4}$$

So, we will neglect the electron mass in all places, where it is possible. Note that for the unpolarized case in [33] the mass was taken into account.

The Compton tensor, defined in (1.3.2), is hermitian:

$$K_{\rho\sigma} = K^*_{\sigma\rho}. \tag{1.3.5}$$

We shall separate the contributions, associated with the electron polarization:

$$\begin{aligned} K_{\rho\sigma} &= K^0_{\rho\sigma} + \frac{\alpha}{4\pi}\left(K^1_{\rho\sigma} + K^{1*}_{\sigma\rho}\right), \qquad (1.3.6)\\ K^0_{\rho\sigma} &= B_{\rho\sigma} + \xi P^0_{\rho\sigma}, \qquad K^1_{\rho\sigma} = T_{\rho\sigma} + \xi P^1_{\rho\sigma}, \end{aligned}$$

where ξ is the degree of the initial electron polarization. Quantities $B_{\rho\sigma}$ and $T_{\rho\sigma}$ correspond to the case of unpolarized electron,

$$\begin{aligned} B_{\rho\sigma} &= B_g\tilde{g}_{\rho\sigma} + B_{11}\tilde{p}_{1\rho}\tilde{p}_{1\sigma} + B_{22}\tilde{p}_{2\rho}\tilde{p}_{2\sigma}, \qquad (1.3.7)\\ B_g &= \frac{1}{st}[(s+u)^2 + (t+u)^2] - 2m^2q^2\left(\frac{1}{s^2} + \frac{1}{t^2}\right),\\ B_{11} &= \frac{4q^2}{st} - \frac{8m^2}{s^2}, \qquad B_{22} = \frac{4q^2}{st} - \frac{8m^2}{t^2}\,. \end{aligned}$$

The new variables

$$\tilde{g}_{\rho\sigma} = g_{\rho\sigma} - \frac{q_\rho q_\sigma}{q^2}, \qquad \tilde{p}_{1\rho} = p^\rho_{1,2} - \frac{p_{1,2}q}{q^2}q^\rho \tag{1.3.8}$$

provide the explicit fulfillment of gauge conditions: $q_\rho K^{\rho\sigma} = 0$, $q_\sigma K^{\rho\sigma} = 0$. Quantity $T_{\rho\sigma}$ has a rather cumbersome form, it is given in [33].

For the case of the most general form of the electron polarization vector

$$u(p)\bar{u}(p) = (\hat{p}_1 + m)(1 - \xi\gamma_5\hat{a}) \tag{1.3.9}$$

one obtains (see also [11, 12])

$$\begin{aligned} P^0_{\rho\sigma} &= 4m\Bigg\{(p_1q\rho\sigma)\frac{qa - 2p_2a}{st} + (p_2q\rho\sigma)\left[\frac{qa}{t^2} + \frac{p_2a}{t}\left(\frac{1}{s} - \frac{1}{t}\right)\right] +\\ &+ (qa\rho\sigma)\left[\frac{q^2}{st} - \frac{1}{s} - \frac{1}{t} - m^2\left(\frac{1}{s^2} + \frac{1}{t^2}\right)\right]\Bigg\}, \qquad (1.3.10) \end{aligned}$$

where we used the notation

$$(abcd) \equiv \mathrm{i}\varepsilon_{\alpha\beta\gamma\delta}a^\alpha b^\beta c^\gamma d^\delta. \tag{1.3.11}$$

The above object obeys the Shouten identity:

$$(abcd)ef = (fbcd)ae + (afcd)be + (abfd)ce + (abcf)de. \tag{1.3.12}$$

In this part we shall consider only the case of longitudinally polarized fermion:

$$u(p_1)\bar{u}(p_1) = \hat{p}_1(1 - \xi\gamma_5). \tag{1.3.13}$$

This is the most interesting case for physical applications. In the Born approximation we obtain

$$\begin{aligned} P_{\rho\sigma} &= \xi\left[P^0_{\rho\sigma} + \frac{\alpha}{4\pi}P^1_{\rho\sigma}\right], \\ P^0_{\rho\sigma} &= P^{0t}_{\rho\sigma} + P^{0s}_{\rho\sigma} = \frac{2}{st}\Big[(u+t)(p_1q\rho\sigma) + (u+s)(p_2q\rho\sigma)\Big]. \end{aligned} \tag{1.3.14}$$

Here and below the upper indices t and s denote the contributions of Feynman diagrams with real photon emission from the initial and final electron lines, respectively. Using the explicit expressions for $P^{0t,s}_{\rho\sigma}$, it is easy to check the following relations:

$$q_\rho P^0_{\rho\sigma} = q_\sigma P^0_{\rho\sigma} = 0,\ (P^{0s,t}_{\sigma\rho})^* = P^{0s,t}_{\rho\sigma},\ P^{0s,t}_{\rho\sigma}q_\rho = 0,\ P^{0s,t}_{\rho\sigma}q_\sigma \neq 0, \tag{1.3.15}$$

$$\begin{aligned} P^{0t}_{\rho\sigma} &= \frac{1}{st}\Big[4(p_1p_2q\sigma)(p_{1\rho} + p_{2\rho}) + \\ &\qquad + 2(t-s)(p_1p_2\rho\sigma) + 2(s+u)(p_2q\rho\sigma)\Big], \\ P^{0s}_{\rho\sigma} &= \frac{1}{st}\Big[-4(p_1p_2q\sigma)(p_{1\rho} + p_{2\rho}) + \\ &\qquad + 2(s-t)(p_1p_2\rho\sigma) + 2(s+t)(p_1q\rho\sigma)\Big]. \end{aligned} \tag{1.3.16}$$

Note now, that we may consider only a half of the full set of eight one-loop Feynman diagrams. Namely, we take the t-type diagrams with real photon emission from the *initial* electron line (Fig. 2). To get the first order correction, we multiply the amplitudes of the one-loop graphs by the Born ones. The whole contribution (including the impact of the rest four one-loop diagrams) can be obtained, using the rearrangement ($\hat{H}$) and hermitization ($\hat{H}$) operators:

$$P^1_{\rho\sigma} = (1 + \hat{H})(1 - \hat{P})(P^{a,b} + P^{1c} + P^{1d})_{\rho\sigma} + P^{\rm soft}_{\rho\sigma}, \tag{1.3.17}$$

where the operators are defined as follows:

$$\hat{P}F(\rho,\sigma,p_1,p_2,q,s,t) = F(\rho,\sigma,p_2,p_1,-q,t,s), \qquad \hat{H}a_{\rho\sigma} = a^*_{\sigma\rho}\,. \tag{1.3.18}$$

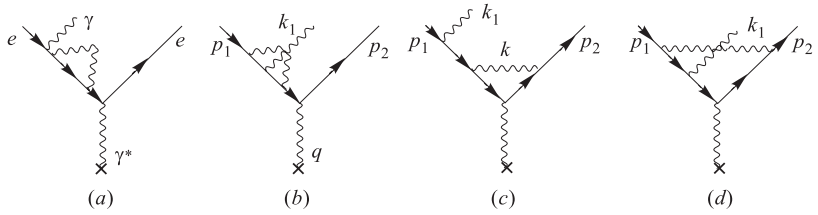

Fig. 2. One-loop virtual Feynman diagrams with photon emission by the *initial* electron

Note, that $\hat{P}P^{0s,t}_{\rho\sigma} = -P^{0t,s}_{\rho\sigma}$. The last term in Eq.(1.3.17) describes the contribution, coming from emission of an additional soft photon [33]:

$$P^{\rm soft}_{\rho\sigma} = P^0_{\rho\sigma}\delta^{\rm soft}, \tag{1.3.19}$$

$$\delta^{\rm soft} = -\frac{4\pi\alpha}{16\pi^3}\int\frac{{\rm d}^3k}{\omega}\left(\frac{p_1}{p_1k}-\frac{p_2}{p_2k}\right)^2 =$$

$$= \frac{\alpha}{\pi}\left[(L_u-1)\ln\frac{m^2(\Delta\varepsilon)^2}{\lambda^2\varepsilon_1\varepsilon_2}+\frac{1}{2}L_u^2-\frac{1}{2}\ln^2\frac{\varepsilon_1}{\varepsilon_2}-\frac{\pi^2}{3}+{\rm Li}_2\left(1+\frac{u}{4\varepsilon_1\varepsilon_2}\right)\right],$$

$$L_u = \ln\frac{-u}{m^2}, \qquad {\rm Li}_2(z) = -\int\limits_0^1\frac{{\rm d}x}{x}\ln(1-zx).$$

Here $\Delta\varepsilon$ is the maximal energy of soft photon; quantities $\varepsilon_{1,2} = p^0_{1,2}$ are the energies of the initial and the final electrons in the laboratory reference frame (in the rest reference frame of the target).

Considering the matrix elements of the Feynman graphs Fig. 2,*a,b*, we get

$$(M^a_\sigma + M^b_\sigma)(-i(4\alpha\pi)^2)^{-1} = \frac{\alpha}{2\pi}\bar{u}(p_2)\gamma_\sigma\left[mN_1\left(\hat{e}-\hat{k}_1\frac{p_1e}{p_1k_1}\right)+N_2\hat{k}_1\hat{e}\right]u(p_1),$$

$$N_1 = \frac{1}{2(t+m^2)}\left[1-\frac{t}{t+m^2}L_t\right], \tag{1.3.20}$$

$$N_2 = \frac{1}{2(t+m^2)}-\frac{2t^2+3m^2t+2m^4}{2t(t+m^2)^2}L_t+\frac{m^2}{t^2}\left[-{\rm Li}_2\left(1+\frac{t}{m^2}\right)+\frac{\pi^2}{6}\right].$$

One can see that only the structure in front of coefficient N_2 survives in the limit $m \to 0$. Really, the trace of the product of Dirac matrices, associated with N_1, has an odd number of matrices and gives an extra power of the mass. We would like to note that in the case of photon emission at small angles (which is not

under consideration now) the situation with the limit $m \to 0$ is more subtle and requires a special investigation (see [54], for instance).

After a simple algebraic transformation we get

$$P^{a,b}_{\rho\sigma} = 2\frac{2L_t - 1}{st}[2(p_1p_2q\sigma)p_{2\rho} + (u+s)((p_2q\rho\sigma) - (p_1p_2\rho\sigma))]. \quad (1.3.21)$$

The remaining contributions (see Fig. 2,*c,d*) are

$$P^{1c}_{\rho\sigma} = \frac{1}{t}\int \frac{\mathrm{d}^4k}{\mathrm{i}\pi^2}\ \frac{1}{a_0a_2a_q}\ \frac{1}{4}\mathrm{Tr}\left\{\hat{p}_2\gamma_\lambda(\hat{p}_2-\hat{k})\gamma_\sigma(\hat{p}_2-\hat{q}-\hat{k})\gamma_\lambda(\hat{p}_2-\hat{q})\gamma_\mu\hat{p}_1\gamma_5\tilde{O}^0_{\rho\mu}\right\} \quad (1.3.22)$$

and

$$P^{1d}_{\rho\sigma} = \int \frac{\mathrm{d}^4k}{\mathrm{i}\pi^2}\frac{1}{a_0a_1a_2a_q}\frac{1}{4}\mathrm{Tr}\left\{\hat{p}_2\gamma_\lambda(\hat{p}_2-\hat{k})\gamma_\sigma(\hat{p}_2-\hat{q}-\hat{k})\gamma_\mu(\hat{p}_1-\hat{k})\gamma_\lambda\hat{p}_1\gamma_5\tilde{O}^0_{\rho\mu}\right\}, \quad (1.3.23)$$

where

$$\begin{aligned} a_0 &= k^2-\lambda^2, \qquad a_1 = k^2 - 2p_1k, \\ a_2 &= k^2 - 2p_2k, \qquad a_q = (p_2-q-k)^2 - m^2. \end{aligned} \quad (1.3.24)$$

The matrix $\tilde{O}^0_{\rho\mu}$ differs from $O^0_{\rho\mu}$ (see Eq. (1.3.3)) by the reversal order of gamma matrices. Using the Table of integrals given in [53], one can perform the integration over the loop momentum in the right-hand sides of the expressions for P^{1c}, P^{1d}, and obtain the total expression for the Compton tensor. Its explicit form is given below.

Now we concentrate on the terms, which contain infrared singularities. There are three sources of them. The first one is the renormalization constant

$$Z_1 = 1 - \frac{\alpha}{2\pi}\left(\frac{1}{2}L_\Lambda + 2\ln\frac{\lambda}{m} + \frac{9}{4}\right), \quad L_\Lambda = \ln\frac{\Lambda^2}{m^2}, \quad (1.3.25)$$

which is required to remove the ultraviolet divergence of the vertex function, appearing in P^{1c}. The next source is a part of the box contribution P^{1d}, which comes from scalar loop integrals. Really, for the Feynman diagram Fig. 2,*d* the infrared terms are associated with the integral

$$\begin{aligned} I &= \int \frac{\mathrm{d}^4k}{\mathrm{i}\pi^2}\ \frac{1}{a_0a_1a_2a_q} = \\ &= \frac{1}{tu}\left[2L_u\ln\frac{m}{\lambda} - L_q^2 + 2L_tL_u - \frac{\pi^2}{6} - 2\mathrm{Li}_2(1-\frac{q^2}{u})\right], \quad (1.3.26) \\ L_q &= \ln\frac{-q^2}{m^2}, \qquad L_t = \ln\frac{-t}{m^2}. \end{aligned}$$

The third source is the emission of additional soft photons, which was considered above. The infrared singularities are cancelled out in the total sum.

Let us consider the contribution from one-loop corrections

$$P^t_{\rho\sigma} = (P^{a,b} + P^{1c} + P^{1d})_{\rho\sigma}. \tag{1.3.27}$$

Extracting the leading logarithmic terms and infrared singularities, we can present it as follows:

$$P^t_{\rho\sigma} = P^{0t}_{\rho\sigma}\left[-L_u^2 - 4(L_u - 1)\ln\frac{m}{\lambda} + 3L_u\right] + R^t_{\rho\sigma}. \tag{1.3.28}$$

After the hermitization and rearrangement operations, and adding the soft photon contribution, we come to the result

$$P_{\rho\sigma} = P^0_{\rho\sigma}\left\{1 + \frac{\alpha}{\pi}\left[(L_u - 1)\ln\frac{(\Delta\varepsilon)^2}{\varepsilon_1\varepsilon_2} + \frac{3}{2}L_u - \frac{1}{2}\ln^2\frac{\varepsilon_2}{\varepsilon_1} - \right.\right.$$
$$\left.\left. - \frac{\pi^2}{3} + \mathrm{Li}_2(\cos^2\frac{\theta}{2})\right]\right\} + \frac{\alpha}{4\pi}R_{\rho\sigma}. \tag{1.3.29}$$

Quantities $R^t_{\rho\sigma}$ and $R_{\rho\sigma}$ collect nonleading terms. They are free from infrared singularities.

Tensor $R^t_{\rho\sigma}$ can be presented in the form

$$R^t_{\rho\sigma} = A(2q\sigma\rho) + B(1q\sigma\rho) + C(12q\sigma)p_{1\rho} + D(12q\sigma)p_{2\rho} +$$
$$+ E(12q\sigma)q_\rho + F(12\sigma\rho). \tag{1.3.30}$$

The coefficients $A - F$ have a rather cumbersome form, we do not present them here. Note only that they obey the condition

$$Cp_1q + Dp_2q + Eq^2 - F = 0, \tag{1.3.31}$$

because of gauge invariance in respect to index ρ.

The rearrangement operation gives

$$\begin{aligned}(1-\hat{P})R^t_{\rho\sigma} &= (A+\tilde{B})(2q\sigma\rho) + (B+\tilde{A})(1q\sigma\rho) + (C-\tilde{D})(12q\sigma)p_{1\rho} + \\ &+ (D-\tilde{C})(12q\sigma)p_{2\rho} + (E+\tilde{E})(12q\sigma)q_\rho + (F+\tilde{F})(12\sigma\rho) \equiv \\ &\equiv A_1(1q\sigma\rho) + A_2(2q\sigma\rho) + B_1(12q\sigma)p_{1\rho} + B_2(12q\sigma)p_{2\rho} + \\ &+ C_1(12q\sigma)q_\rho + F_1(12\sigma\rho). \end{aligned} \tag{1.3.32}$$

Tests of the gauge invariance is an important check of our calculations:

$$q^\rho(1-\hat{P})R_{\rho\sigma} = B_1(12q\sigma)p_1q + B_2(12q\sigma)p_2q + C_1(12q\sigma)q^2 + F_1(12\sigma q) = 0,$$
$$q^\sigma(1-\hat{P})R_{\rho\sigma} = F_1(12q\rho) = 0. \tag{1.3.33}$$

These conditions yield

$$F_1 = 0, \qquad C_1 = -B_1\frac{p_1 q}{q^2} - B_2\frac{p_2 q}{q^2}\,,$$
$$B_1 p_{1\rho} + B_2 p_{2\rho} + C_1 q_\rho = B_1\tilde{p}_{1\rho} + B_2\tilde{p}_{2\rho}\,, \tag{1.3.34}$$
$$\tilde{p}_{1\rho} = p_{1\rho} - \frac{p_1 q}{q^2}q_\rho\,, \quad \tilde{p}_{2\rho} = p_{2\rho} - \frac{p_2 q}{q^2}q_\rho\,.$$

We checked these relations by straightforward calculations.

The last step is the hermitization, which gives

$$\begin{aligned} R_{\rho\sigma} &= (1+\hat{H})(1-\hat{P})R^t_{\rho\sigma} = \\ &= (A_1 + A_1^*)(1q\sigma\rho) + (A_2 + A_2^*)(2q\sigma\rho) + \\ &+ (12q\sigma)[B_1\tilde{p}_{1\rho} + B_2\tilde{p}_{2\rho}] - (12q\rho)[B_1^*\tilde{p}_{1\sigma} + B_2^*\tilde{p}_{2\sigma}], \end{aligned} \tag{1.3.35}$$

where

$$\begin{aligned} A_1 &= \frac{2}{st}\left[\frac{2u(2s-u)}{a}L_{qu} + \frac{4us}{a}\left(\frac{u}{a}L_{qu} - 1\right) + \frac{ub}{c} + \frac{2u^2+us-s^2}{c}L_{sq} + \right. \\ &+ \left.\frac{usb}{c^2}L_{sq} - 2c\zeta(2) - 2cL_{tu} + (2s-c)L_{qu} - \frac{uc}{s}G + \left(\frac{ub}{t} + c\right)\tilde{G} + 5c - 2s\right], \\ B_1 &= \frac{2}{st}\left[\frac{8u}{a}\left(1 - \left(\frac{u}{a}+1\right)L_{qu}\right) + \frac{6t}{b}L_{qt} + \frac{2(u^2-2s^2-su)}{cu}L_{sq} + \right. \\ &+ \frac{2b}{c}\left(1 + \frac{s}{c}L_{sq}\right) + \frac{2}{s}(2c-s)L_{tu} + \left(-2 - \frac{4c^2}{st} - \frac{12b}{t} - \frac{4s^2}{ut}\right)L_{qu} + \\ &+ \left.\frac{4b^2}{tu}L_{su} + \left(-2 + \frac{2uc}{s^2} - \frac{2t}{s}\right)G + \left(\frac{2b}{t} + \frac{2b^2}{t^2}\right)\tilde{G} + 6\right], \\ G &= (L_q - L_u)(L_q + L_u - 2L_t) - \frac{\pi^2}{3} - 2\mathrm{Li}_2\left(1 - \frac{q^2}{u}\right) + 2\mathrm{Li}_2\left(1 - \frac{t}{q^2}\right), \\ A_2 &= (s \leftrightarrow t)A_1, \qquad B_2 = -(s \leftrightarrow t)B_1, \qquad \tilde{G} = (s \leftrightarrow t)G. \end{aligned} \tag{1.3.36}$$

Note, that the above expressions are free from kinematical singularities. Really, in the limits $a \to 0$, $b \to 0$, and $c \to 0$ the quantities are finite. The symmetry between A_1, B_1 and A_2, B_2 takes place due to the initial symmetry between p_1 and p_2 in the traces.

1.3.2. Conclusions. Thus we calculated the part of the leptonic tensor, proportional to the degree of the initial longitudinal polarization. This tensor describes Compton scattering with one off-shell photon, which is related to a certain target. The main results of the paper are presented by Eqs.(1.3.29),(1.3.35).

The calculation allows one to obtain corrections, coming from one-loop effects, to quantities observable in different polarization experiments. Let us consider for definiteness the task of calculation of α^2 order radiative correction in polarized deep inelastic scattering. The results for the lowest order QED correction for nucleon and nuclear targets can be found in Refs. 11, 12. Both the Born cross section ($\sigma_{\rm Born}$) and the cross section at the level of radiative corrections ($\sigma_{\rm RC}$) can be split into unpolarized and polarized parts:

$$\sigma_{\rm Born,RC} = \sigma^{\rm unp}_{\rm Born,RC} + \xi_b \xi_t \sigma^{\rm pol}_{\rm Born,RC}\,, \tag{1.3.37}$$

where ξ_b and ξ_t are polarization degrees of the beam and target. The correction to asymmetry ($A = \sigma^{\rm pol}/\sigma^{\rm unp}$)

$$\Delta A = \frac{\sigma^{\rm pol}_{\rm RC}\sigma^{\rm unp}_{\rm Born} - \sigma^{\rm unp}_{\rm RC}\sigma^{\rm pol}_{\rm Born}}{\sigma^{\rm unp}_{\rm Born}(\sigma^{\rm unp}_{\rm Born} + \sigma^{\rm unp}_{\rm RC})} \tag{1.3.38}$$

is usually not large because of mutual cancellation of large factorizing terms. It is clear, that when a relatively small correction is obtained as a difference of two large terms, the radiatively corrected cross section has to be calculated with the most possible accuracy, and a special attention has to be paid to nonfactorizing terms like (1.3.36). The kinematical regions with very high y ($y \sim 0.9$) can be reachable in the current polarization experiments in DIS [55, 56]. In this region radiative corrections to the cross section are comparable with the Born cross section. Basically, it comes from the contributions of radiative tails from elastic and quasielastic peaks. This calculation firstly allows one to obtain the contribution of these tails with taking into account loop effects in the next-to-leading approximation.

Strictly speaking, the total QED correction $\sim \alpha^2$ to spin asymmetry Eq.(1.3.38) includes also contributions of double bremsstrahlung, lepton pair production and two-loop virtual corrections. The latter does not change kinematics of the general process, it can be easily derived using the results of Ref. 57. The leading contribution of two-loop corrections is factorized in front of the Born cross section, and it is exactly cancelled in the numerator of (1.3.38). Contrary, the radiative process has a different kinematics; and it is of particular interest in experiments. So, the elastic and quasielastic radiative tails, which have relatively large cross section, provide an important correction to polarized and unpolarized DIS. The contributions of double bremsstrahlung and lepton pair production can be calculated using analytical or Monte Carlo approach. We note that there are no infrared divergences in the case of correction to elastic and quasielastic radiative tails, so the integral over two photon phase space can be calculated straightforwardly (using Monte Carlo methods, for example). The corresponding corrections will be considered elsewhere.

Now new methods of experimental data processing, when experimental information about spin observables is extracted directly from polarized parts of cross sections (difference of observed cross sections with opposite spin configurations) [58], are actively developing. It makes new requirements for an accuracy of radiative correction calculations. We note that there is no any cancellation of leading contributions in this case, and factorizing terms in (1.3.28) give the basic contribution.

From the other hand, our result can be used as a contribution to the first order radiative correction to radiative polarized DIS, when radiated photon is tagged in calorimeter. Radiative events cover a much wider region of kinematical variables, so the detection of hard photons, for example, in deep inelastic scattering can provide additional physical information [41, 59] about structure functions in the region unreachable in current experiments. Note that radiative events are used also for luminosity measurements in experiments at HERA.

There is one particular phenomenon. Note, that $P^{(1)}_{\rho\sigma}$ contains not only the imaginary part, but also a certain real part, which comes from the imaginary parts of A_1 and B_1. The multiplication of this real part of $P^{(1)}_{\rho\sigma}$ with the ordinary symmetrical part of the hadronic tensor will give rise to a one-spin azimuthal asymmetry for the final electron [60]. The asymmetry is proportional to the degree of polarization of the initial electron. It is small (few percent) because of the extra power of $\alpha_{\rm QED}$ and the absence of large logarithms.

Here we considered the typical kinematical case when the photon can be resolved. The kinematical situation when photon is emitted close to initial or the scattered electron directions was considered in paper [61].

1.4. Hadronic Cross Sections in Electron-Positron Annihilation with Tagged Photon. Let us consider now the cross channel to DIS with hard photon tagging process — the initial state radiation of hard photon in the single virtual photon high-energy e^+e^--pair annihilation into hadrons [62].

1.4.1. Introduction. Experiments with tagged photons, radiated from the initial state in electron–proton and electron–positron collisions, can become particularly attractive. The reason is that these radiative processes will permit one to extract information about the final states at continuously varying values of the collision energy. To investigate deep inelastic scattering the authors of Ref. 41 suggested to use radiative events instead of running colliders at reduced beam energies. The method takes advantage of a photon detector (PD) placed in the very forward direction, as seen from the incoming electron beam. The effective beam energy, for each radiative event, is determined by the energy of the hard photon observed in PD. In fact, radiative events were already used to measure the structure function F_2 down to $Q^2 \geq 1.5$ GeV^2 [36, 63]. The specific theoretical work concerns the evaluation of QED radiative corrections (see Secs. 1,2) to the radiative Born cross section. With an accurate determination of the cross sections

and of the possible sources of background we believe that the use of radiative events may become particularly useful to carry investigations at various present and future machines.

The important role of the initial state radiation in the process of electron–positron annihilation was underlined in a series of papers by V.N. Baier and V.A. Khoze [64], where the radiative process was studied in detail in the Born approximation. In these papers the mechanism of returning to a resonant region was discovered. This mechanism consists in the preferable emission of photons from the initial particles, which provides a resonant kinematics of a subprocess. A utilization of radiative events can become a common type of investigations at various machines.

In this part we derive explicit formulae for the spectrum of tagged photons. The calculations are performed having an accuracy of the per-mille order as an aim. Formulae can be used at electron–positron colliders to investigate, for instance, hadronic final states at intermediate energies. A measurement of the total hadronic cross section at low energies is essential for high precision test of the Standard Model particularly for a precise determination of the fine structure constant $\alpha_{\rm QED}(M_Z)$ and of the muon anomalous magnetic moment $(g-2)_\mu$. The largest contribution to the errors for these quantities comes from the large indetermination still present on the measurement of the total hadronic cross section in electron–positron annihilation at the centre-of-mass energies of a few GeV. We will consider here the radiatively corrected cross section for the electron–positron annihilation process

$$e^-(p_1) \ + \ e^+(p_2) \ \longrightarrow \ \gamma(k) \ + \ H(q), \qquad k=(1-z)p_1\,, \tag{1.4.1}$$

where H is a generic hadronic state. The hard photon hitting the photon detector has a momentum k and an energy fraction $1-z$ with respect to the beam energy. In the following we assume that the photon detector is placed along the electron beam direction, and has an opening angle $2\theta_0 \ll 1$, such that $\varepsilon^2\theta_0^2 \gg m^2$, with m the electron mass, and ε the beam energy. To evaluate the process with an accuracy of the per mille requires a careful investigation of the radiative corrections. This part is organized as follows. In Section 1.4.2 we consider the cross section of the process (1.4.1) in the Born approximation. We give formulae suitable to study as differential distributions in hadronic channels, as well as the total (in terms of quantity R) and inclusive (in terms of hadron fragmentation functions) hadronic cross sections. In Sec. 1.4.3 we calculate separate contributions into radiatively corrected cross section of process (1.4.1) within the next–to–leading accuracy. In Sec. 1.4.3.1 the contribution due to virtual and soft photon emission is investigated. In Sec. 1.4.3.2 the case, when additional hard photon hits a photon detector is considered. In Sec. 1.4.3.3 the contribution due to hard photon emission, which does not hit a photon detector, is derived. In Sec. 1.4.4 we sum

up all the contributions and give the final result. In Conclusion we summarize the results and give some numerical illustrations.

1.4.2. The Born Approximation. In order to obtain the Born approximation for the cross section of the process (1.4.1), when the PD is placed in front of electron (positron) beam, we can use the quasireal electron method [49]. It gives

$$\mathrm{d}\sigma(k,p_1,p_2) = \mathrm{d}W_{p_1}(k)\sigma_0(p_1-k,p_2), \tag{1.4.2}$$

where $\mathrm{d}W_{p_1}(k)$ is the probability to radiate photon with energy fraction $1-z$ inside a narrow cone with the polar angle not exceeding $\theta_0 \ll 1$ around the incoming electron, and $\mathrm{d}\sigma_0$ is the differential cross section for the radiationless process of electron–positron annihilation into hadrons at the reduced electron beam energy. The form of both, $\mathrm{d}W_{p_1}(k)$ and $\sigma_0(p_1-k,p_2)$ is well known:

$$\mathrm{d}W_{p_1}(k) = \frac{\alpha}{2\pi}P_1(z,L_0)\mathrm{d}z\,, \quad P_1(z,L_0) = \frac{1+z^2}{1-z}L_0 - \frac{2z}{1-z}\,,$$
$$L_0 = \ln\frac{\varepsilon^2\theta_0^2}{m^2}\,. \tag{1.4.3}$$

We need further the general form of the lowest order cross section σ_0 for the process $e^+(z_1p_2)+e^-(zp_1)\to$ hadrons boosted along the beam axis ($\boldsymbol{p}_1$):

$$\sigma_0(z,z_1) = \frac{8\pi^2\alpha^2}{q^2|1-\Pi(q^2)|^2}\int T(q)\mathrm{d}\Gamma(q), \qquad T(q) = \frac{L_{\rho\sigma}H_{\rho\sigma}}{(q^2)^2}, \tag{1.4.4}$$

$$L_{\rho\sigma} = \frac{q^2}{2}\widetilde{g}_{\rho\sigma} + 2z^2\widetilde{p}_{1\rho}\widetilde{p}_{1\sigma},\ \mathrm{d}\Gamma(q) = (2\pi)^4\delta(q-\sum q_j)\prod\frac{\mathrm{d}^3q_j}{2\varepsilon_j(2\pi)^3}\,,$$
$$q = zp_1 + z_1p_2\,, \qquad q^2 = sz_1z,$$
$$\widetilde{g}_{\rho\sigma} = g_{\rho\sigma} - \frac{q_\rho q_\sigma}{q^2}\,, \qquad \widetilde{p}_{1\rho} = p_{1\rho} - \frac{p_1q}{q^2}q_\rho\,, \tag{1.4.5}$$

where q is the full 4-momentum of final hadrons, q_j is 4-momentum of an individual hadron, $s = 2p_1p_2 = 4\varepsilon^2$ is the full centre-of-mass energy squared, and $H_{\rho\sigma}$ is the hadronic tensor. The vacuum polarization operator $\Pi(q^2)$ of the virtual photon with momentum q is a known function [65] and will not be specified here.

The tensors $H_{\rho\sigma}$ and $L_{\rho\sigma}$ obey the current conservation conditions once saturated with the 4-vector q. The differential cross section with respect to the tagged photon energy fraction z can be obtained by performing the integration on the hadrons phase space. It takes the form

$$\frac{\mathrm{d}\sigma}{\mathrm{d}z} = \frac{\alpha}{2\pi}P_1(z,L_0)\ \sigma_0(z,1). \tag{1.4.6}$$

Each hadronic state is described by its own hadronic tensor. The cross section in Eqs. (1.4.2) and (1.4.4) is suitable for different uses and, as mentioned above, it can be used to check different theoretical predictions.

The sum of the contributions of all hadronic channels by means of the relation

$$\sum_h \int H_{\rho\sigma} \mathrm{d}\Gamma = f_h(q^2) \widetilde{g}_{\rho\sigma} \,, \tag{1.4.7}$$

can be expressed in terms of the ratio of the total cross section for annihilation into hadrons and muons $R = \sigma_h/\sigma_\mu$. For the $\mu^+\mu^-$ final state we get

$$f_\mu = \frac{q^2}{6\pi} K(q^2), \qquad K(q^2) = \left(1 + \frac{2m_\mu^2}{q^2}\right)\sqrt{1 - \frac{4m_\mu^2}{q^2}},$$

and so,

$$f_h(q^2) = \frac{q^2 R(q^2)}{6\pi} K(q^2). \tag{1.4.8}$$

Substituting this expression into the right-hand side of Eqs. (1.4.2) and (1.4.4) results in the replacement $\sigma_0(z, z_1) = R(q^2) 4\pi\alpha^2 K(q^2)/(3q^2)$.

In experiments of semiinclusive type one fixes an hadron with 3-momentum $\boldsymbol{q}_1$, energy ε_1 and mass M in every event and sum over all the rest. In this case instead of Eq. (1.4.7) we will have (similarly to the Deep Inelastic Scattering (DIS) case [51, 52, 66]):

$$\begin{aligned} &\sum_{h'} \int H_{\rho\sigma} \mathrm{d}\Gamma = H^{(1)}_{\rho\sigma} \frac{\mathrm{d}^3 q_1}{2\varepsilon_1 (2\pi)^3} \,, \\ &H^{(1)}_{\rho\sigma} = F_1(\eta, q^2) \widetilde{g}_{\rho\sigma} - \frac{4}{q^2} F_2(\eta, q^2) \widetilde{q}_{1\rho} \widetilde{q}_{1\rho}, \quad \eta = \frac{q^2}{2qq_1} > 1 \,, \end{aligned} \tag{1.4.9}$$

where we have introduced two dimentionless functions $F_1(\eta, q^2)$ and $F_2(\eta, q^2)$ in a way similar to the DIS case.

By introducing the dimentionless variable $\lambda = 2qq_1/(2zp_1q_1)$, we can write the corresponding cross section for radiative events in e^+e^- annihilation in the same form as in the case of deep inelastic scattering with a tagged photon [51, 52, 66]:

$$\begin{aligned} \frac{\mathrm{d}\sigma}{\mathrm{d}z} &= \frac{\alpha^2(q^2)}{2\pi} \frac{\alpha}{2\pi} P_1(z, L_0) \Sigma(\eta, \lambda, q^2) \frac{1}{(q^2)^2} \frac{\mathrm{d}^3 q_1}{\varepsilon_1} \,, \\ \Sigma(\eta, \lambda, q^2) &= F_1(\eta, q^2) + \frac{2F_2(\eta, q^2)}{\eta^2 \lambda^2} \left(\lambda - 1 - \frac{M^2}{q^2} \eta^2 \lambda^2\right). \end{aligned} \tag{1.4.10}$$

1.4.3. Radiative Corrections. For the radiative corrections (RC) to the cross section (1.4.6) we will restrict ourselves only to terms containing second and first powers of large logarithms L, and omit terms which don't contain them, i.e., we will keep leading and next-to-leading logarithmic contributions. We will consider in Section 3.1 the contribution from one-loop virtual photon as well as from the emission of soft real ones. In 3.2 we will discuss the double hard photon emission process.

1.4.3.1. Corrections Due to Virtual and Real Soft Photons. The interference of Born and one–loop contributions to the amplitude of the initial state radiation in annihilation of e^+e^- into hadrons can be obtained from the analogous quantity of hard photon emission in electron–proton scattering [51, 52, 66]. We do that by using the crossing transformation. For the contribution coming from the emission of real soft photons a straightforward calculation gives:

$$\frac{\mathrm{d}\sigma^S}{\mathrm{d}\sigma_0} = \frac{\alpha}{\pi}\left[2(L_s-1)\ln\frac{m\Delta\varepsilon}{\lambda\varepsilon} + \frac{1}{2}L_s^2 - \frac{\pi^2}{3}\right],$$

$$L_s = \ln\frac{s}{m^2} = L_0 + L_\theta, \qquad L_\theta = \ln\frac{4}{\theta^2}, \tag{1.4.11}$$

where λ is the *photon mass*, $\Delta\varepsilon$ is the energy carried by the soft photon. The sum of the two contributions is free from infrared singularities. It reads

$$\mathrm{d}\sigma^{V+S} = \frac{8\pi^2\alpha^2}{s|1-\Pi(q^2)|^2}\frac{\alpha}{2\pi}[\rho B_{\rho\sigma}(q) + A_{\rho\sigma}(q)]\frac{H_{\rho\sigma}(q)\mathrm{d}\Gamma(q)}{(q^2)^2}\frac{\alpha}{4\pi^2}\frac{\mathrm{d}^3k}{\omega}, \tag{1.4.12}$$

where

$$\rho = 4(L_s-1)\ln\Delta + 3L_q - \frac{\pi^2}{3} - \frac{9}{2}, \quad L_q = L_s + \ln z, \quad \Delta = \frac{\Delta\varepsilon}{\varepsilon} \ll 1, \tag{1.4.13}$$

where k and ω are the 3-momentum and the energy of the hard photon respectively. The tensors $A_{\rho\sigma}$ and $B_{\rho\sigma}$ have a rather involved form. The first can be obtained from the corresponding expressions of Refs. 13, 33. The tensor $B_{\rho\sigma}$ coincides with the one of the Born approximation. In the kinematical region where the hard photon is emitted close to the initial electron direction of motion one has

$$B_{\rho\sigma} = \frac{2}{z}\left(\frac{1+z^2}{y_1(1-z)} - \frac{2m^2z}{y_1^2}\right)L_{\rho\sigma}(q), \quad A_{\rho\sigma} = \frac{2}{q^2}A_g L_{\rho\sigma}(q), \quad q = zp_1 + p_2, \tag{1.4.14}$$

where tensor $L_{\rho\sigma}$ is given in Eq. (1.4.4), $y_1 = 2kp_1$, and quantity A_g reads

$$A_g = \frac{4zsm^2}{y_1^2} L_s \ln z + \frac{s}{y_1}\left[\frac{1+z^2}{1-z}(-2L_s \ln z - \ln^2 z + 2\mathrm{Li}_2(1-z) + \right.$$

$$\left. +2\ln\frac{y_1}{m^2}\ln z) + \frac{1+2z-z^2}{2(1-z)}\right], \qquad \mathrm{Li}_2(x) = -\int_0^1 \mathrm{d}t \frac{\ln(1-tx)}{t}. \quad (1.4.15)$$

Further integration over the hard photon phase space can be performed within the logarithmic accuracy by using the integrals

$$\int \frac{\mathrm{d}^3k}{2\pi k_0}\left[\frac{1}{y_1}, \frac{m^2}{y_1^2}, \frac{\ln(y_1/m^2)}{y_1}\right] = \left[\frac{1}{2}L_0, \frac{1}{2(1-z)}, \frac{1}{4}L_0^2 + \frac{1}{2}L_0\ln(1-z)\right]\mathrm{d}z.$$

The final expression for the Born cross section corrected for the emission of soft and virtual photons has the form

$$\frac{\mathrm{d}\sigma^{B+V+S}}{\mathrm{d}z} = \sigma_0(z,1)\left[\frac{\alpha}{2\pi}P_1(z,L_0) + \left(\frac{\alpha}{2\pi}\right)^2(\rho P_1(z,L_0) + N)\right],$$

$$N = -\frac{1+z^2}{1-z}\left[(L_0 + \ln z)\ln z - \frac{\pi^2}{3} + 2\mathrm{Li}_2(z)\right]L_0 - 2P_1(z,L_0)\ln\frac{\theta_0^2}{4} +$$

$$+\frac{1+2z-z^2}{2(1-z)}L_0 + \frac{4z}{1-z}L_0\ln z. \quad (1.4.16)$$

1.4.3.2. Two Hard Photons Tagged by the Detector. If an additional hard photon emitted by the initial-state electron hits the PD, we cannot use the quasireal electron method and have to calculate the corresponding contribution starting from Feynman diagrams.

We can use double hard photon spectra as given in Ref. 67 for annihilation diagrams only and write the cross section under consideration as follows

$$\frac{\mathrm{d}\sigma_{c1}^H}{\mathrm{d}z} = \sigma_0(z,1)\left(\frac{\alpha}{2\pi}\right)^2 L_0 \int_\Delta^{1-z-\Delta}\frac{\mathrm{d}x}{\xi}\left[\frac{\gamma\tau}{2}L_0 + (z^2+(1-x)^4)\times\right.$$

$$\left.\times\ln\frac{(1-x)^2(1-z-x)}{zx} + zx(1-z-x) - x^2(1-x-z)^2 - 2\tau(1-x)\right],$$

$$\xi = x(1-x)^2(1-z-x), \quad \gamma = 1+(1-x)^2, \quad \tau = z^2+(1-x)^2. \quad (1.4.17)$$

Here the variable x under the integral sign is the energy fraction of one hard photon. The quantity $1-z-x$ is the energy fraction of the second hard photon provided that their total energy fraction equals $1-z$. We write the index $c1$ in the left-hand side of Eq. (1.4.3) to emphasize that this contribution arises from the collinear kinematics, when the additional hard photon is emitted along the initial electron with 4-momentum p_1.

The integration in the right-hand side of Eq. (1.4.3) leads to the result

$$\begin{aligned}\frac{\mathrm{d}\sigma^H_{c1}}{\mathrm{d}z} &= \sigma_0(z,1)\left(\frac{\alpha}{2\pi}\right)^2\frac{L_0}{2}\left\{\left[P^{(2)}_{\Theta}(z)+2\frac{1+z^2}{1-z}\left(\ln z-\frac{3}{2}-2\ln\Delta\right)\right]L_0+\right.\\ &+ \left. 6(1-z)+\frac{3+z^2}{1-z}\ln^2 z-\frac{4(1+z)^2}{1-z}\ln\frac{1-z}{\Delta}\right\}, \qquad (1.4.18)\end{aligned}$$

where the quantity $P^{(2)}_{\Theta}(z)$ represents the so-called Θ term of the second-order electron structure function:

$$P^{(2)}_{\Theta}(z)=2\frac{1+z^2}{1-z}\left(\ln\frac{(1-z)^2}{z}+\frac{3}{2}\right)+(1+z)\ln z-2(1-z). \qquad (1.4.19)$$

1.4.3.3. Additional Hard Photon Emitted Outside PD. If an additional hard photon, emitted from the initial state, does not hit the PD situated in the direction of motion of the initial electron we distinguish the case when it is emitted in the direction close, within a small cone with angle $\theta' \ll 1$, to the direction of the initial positron. In this case we obtain:

$$\frac{\mathrm{d}\sigma^H_{c2}}{\mathrm{d}z}=\frac{\alpha}{2\pi}P_1(z,L_0)\int_{\Delta}^{1-\delta/z}\frac{\alpha}{2\pi}P_1(1-x,L')\sigma_0(z,1-x)\mathrm{d}x, \qquad (1.4.20)$$

where $L'=L_s+\ln(\theta'^2/4)$, $\delta=M^2/s$, and M^2 is the minimal hadron mass squared. We suppose that $z\sim 1$.

We have introduced the additional auxiliary parameter $\theta' \ll 1$ which, together with θ_0, separates collinear and semicollinear kinematics of the second hard photon. Contrary to θ_0, which is supposed to determine the PD acceptance, θ' will disappear in the sum of the collinear and semicollinear contributions of the

second photon. This last kinematical region gives

$$\begin{aligned}
\frac{\mathrm{d}\sigma_{sc}^{H}}{\mathrm{d}z} &= \left(\frac{\alpha}{2\pi}\right)^2 P_1(z,L_0)\int\frac{\mathrm{d}^3k_1}{2\pi\omega_1^3}\frac{16\pi^2\alpha^2}{(1-c^2)z^2}T(c,z,x),\\
T(c,z,x) &= \int\frac{H_{\rho\sigma}(q_2)\mathrm{d}\Gamma(q_2)}{s(q_2^2)^2|1-\Pi(q_2^2)|^2}\left[\frac{s}{2}((z-x_2)^2+z^2(1-x_1)^2)g_{\rho\sigma}+\right.\\
&+ \left. 2(z(1-x_1)-x_2)(z^2p_{1\rho}p_{1\sigma}+p_{2\rho}p_{2\sigma})\right],\\
x_1 &= \frac{x}{2}(1-c), \qquad x_2=\frac{x}{2}(1+c),\\
q_2 &= zp_1+p_2-k_1, \qquad c=\cos\widehat{\boldsymbol{k}_1\boldsymbol{p}_1}. \qquad (1.4.21)
\end{aligned}$$

The phase volume of the second photon is parametrized as:

$$\int\frac{\mathrm{d}^3k_1}{2\pi\omega^3}=\int\limits_{\Delta}^{\hat{x}}\frac{\mathrm{d}x}{x}\int\limits_0^{2\pi}\frac{\mathrm{d}\phi}{2\pi}\int\limits_{-1+\theta'^2/2}^{1-\theta_0^2/2}\mathrm{d}c, \qquad \hat{x}=\frac{2(z-\delta)}{1+z+c(1-z)}. \qquad (1.4.22)$$

Explicitly extracting the angular singularities we represent this expression as

$$\begin{aligned}
\frac{\mathrm{d}\sigma_{sc}^{H}}{\mathrm{d}z} &= \left(\frac{\alpha}{2\pi}\right)^2 P_1(z,L_0)\left[\Sigma_{sc}(z)+\ln\frac{4}{\theta_0^2}\int\limits_{\Delta}^{z-\delta}\frac{\mathrm{d}x}{x}\frac{z^2+(z-x)^2}{z^2}\times\right.\\
&\left.\times\sigma_0(z-x,1)+\ln\frac{4}{\theta'^2}\int\limits_{\Delta}^{1-\delta/z}\frac{\mathrm{d}x}{x}(1+(1-x)^2)\sigma_0(z,1-x)\right], \qquad (1.4.23)
\end{aligned}$$

$$\Sigma_{sc}=\frac{8\pi^2\alpha^2}{z^2}\int\limits_{-1}^{1}\mathrm{d}c\int\limits_{\Delta}^{\hat{x}}\frac{\mathrm{d}x}{x}\left[\frac{T(c,z,x)-T(1,z,x)}{1-c}+\frac{T(c,z,x)-T(-1,z,x)}{1+c}\right].$$

1.4.4.4. Complete QED Correction and Leading Logarithmic Approximation. The final result in the order $\mathcal{O}(\alpha)$ for radiative corrections

to radiative events can be written as follows:

$$\frac{\mathrm{d}\sigma}{\mathrm{d}z} = \frac{\alpha}{2\pi}P_1(z,L_0)\sigma_0(z,1)(1+r) = \frac{\alpha}{2\pi}P_1(z,L_0)\sigma_0(z,1) + \left(\frac{\alpha}{2\pi}\right)^2 \times$$
$$\times\Bigg\{L_0\left(\frac{1}{2}L_0P^{(2)}(z)+G\right)\sigma_0(z,1) + P_1(z,L_0)\Bigg[\int\limits_0^{1-\delta/z} C_1(x)\sigma_0(z,1-x)\mathrm{d}x +$$
$$+L_\theta\int\limits_0^{z-\delta} C_2(z,x)\sigma_0(z-x,1)\mathrm{d}x + \Sigma_{sc}\Bigg]\Bigg\}, \qquad (1.4.24)$$

where the last term is defined by Eq. (1.4.3) and

$$\begin{aligned}
C_1(x) &= P_1(1-x,L_s)\Theta(x-\Delta) + (L_s-1)(2\ln\Delta+\frac{3}{2})\delta(x),\\
C_2(z,x) &= \frac{z^2+(z-x)^2}{z^2x}\Theta(x-\Delta) + (2\ln\Delta+\frac{3}{2}-2\ln z)\delta(x),\\
G(z) &= \frac{1+z^2}{1-z}(3\ln z - 2\mathrm{Li}_2(z)) + \frac{1}{2}(1+z)\ln^2 z -\\
&- \frac{2(1+z)^2}{1-z}\ln(1-z) + \frac{1-16z-z^2}{2(1-z)} + \frac{4z\ln z}{1-z}. \qquad (1.4.25)
\end{aligned}$$

In order to include the higher order leading corrections to the tagged photon differential cross section and to show the agreement of our calculation with the well-known Drell–Yan representation for the total hadronic cross section at electron–positron annihilation [31]

$$\sigma(s) = \int\limits_\delta^1 \mathrm{d}x_1 \int\limits_{\delta/x_1}^1 \mathrm{d}x_2\; D(x_1,\alpha_{\mathrm{eff}})D(x_2,\alpha_{\mathrm{eff}})\sigma(x_1x_2s), \qquad (1.4.26)$$

where the electron structure functions include both nonsinglet and singlet parts

$$D(x_1,\alpha_{\mathrm{eff}}) = D^{NS}(x,\alpha_{\mathrm{eff}}) + D^S(x_1,\alpha_{\mathrm{eff}}), \qquad (1.4.27)$$

it is convenient to introduce the quantity

$$\Sigma = D(z,\bar{\alpha}_{\mathrm{eff}})\int\limits_{\delta/z}^1 \mathrm{d}x_1 \int\limits_{\delta/zx_1}^1 \mathrm{d}x_2\; D(x_1,\widetilde{\alpha}_{\mathrm{eff}})D(x_2,\hat{\alpha}_{\mathrm{eff}})\sigma_0(zx_1,x_2). \qquad (1.4.28)$$

Note that the shifted cross section in Eq. (1.4.26) has just the same meaning as in Eq. (1.4.4): $\sigma(x_1x_2s) = \sigma_0(x_1, x_2)$.

The structure functions [68, 69] entering RHS of Eq. (1.4.27) are

$$D^{NS}(x, \alpha_{\rm eff}) = \delta(1-x) + \sum_{n=1}^{\infty} \frac{1}{n!}\left(\frac{\alpha_{\rm eff}}{2\pi}\right)^n P_1^{\otimes n}(x), \tag{1.4.29}$$

$$D^{S}(x, \alpha_{\rm eff}) = \frac{1}{2!}\left(\frac{\alpha_{\rm eff}}{2\pi}\right)^2 R(x) + \frac{1}{3!}\left(\frac{\alpha_{\rm eff}}{2\pi}\right)^3 \left[2P_1 \otimes R(x) - \frac{2}{3}R(x)\right], \tag{1.4.30}$$

where

$$\begin{aligned} P_1(x) &= \lim_{\Delta\to 0}\left\{\frac{1+x^2}{1-x}\Theta(1-\Delta-x) + \left(\frac{3}{2} + 2\ln\Delta\right)\delta(1-x)\right\}, \\ R(x) &= 2(1+x)\ln x + \frac{1-x}{3x}(4+7x+4x^2), \\ P_1^{\otimes n} &= \underbrace{P_1(x)\otimes\cdots\otimes P_1(x)}_{n}, \qquad P_1(x)\otimes P_1(x) = \int\limits_x^1 P_1(t)P_1\left(\frac{x}{t}\right)\frac{{\rm d}t}{t}, \end{aligned}$$

and the effective electromagnetic couplings in the RHS of Eq. (1.4.28) are

$$\begin{aligned} \bar{\alpha}_{\rm eff} &= -3\pi\ln\left(1 - \frac{\alpha}{3\pi}L_0\right), \\ \widetilde{\alpha}_{\rm eff} &= -3\pi\ln\left(\frac{1-\frac{\alpha}{3\pi}L_s}{1-\frac{\alpha}{3\pi}L_0}\right), \\ \hat{\alpha}_{\rm eff} &= -3\pi\ln\left(1 - \frac{\alpha}{3\pi}L_s\right). \end{aligned} \tag{1.4.31}$$

At fixed values of z $(z < 1)$ the quantity Σ defines the leading logarithmic contributions into differential cross section for the events with tagged particles. That corresponds to only Θ terms in the expansion of the structure function $D(z, \bar{\alpha}_{\rm eff})$ before the integral sign in Eq. (1.4.28). If we consider photonic corrections (as do in the previous sections), it is needed to restrict ourselves to the nonsinglet part of the electron structure functions and with the first order terms in the expansion of all effective couplings, namely:

$$\bar{\alpha}_{\rm eff} \to \alpha L_0, \quad \widetilde{\alpha}_{\rm eff} \to \alpha L_\theta, \quad \hat{\alpha}_{\rm eff} \to \alpha L_s. \tag{1.4.32}$$

It is easy to see that in this case the leading contribution into differential cross section (1.4.3) can be obtained as an expansion of the quantity $\Sigma(z<1)$ by the powers of α, keeping the terms of the order α^2 in the production of D functions.

If we want to include the contribution due to e^+e^--pair (real and virtual) production it is required [70] to use both nonsinglet and singlet structure functions and effective couplings defined by Eq. (1.4.31). Note that the insertion into consideration of higher order corrections rises additional questions about concrete experimental conditions concerning registration of events with e^+e^- pairs.

The total hadronic cross section in e^+e^- annihilation can be obtained by integration of quantity Σ over z

$$\sigma(s)=\int\limits_{\delta}^{1}\mathrm{d}z\;D(z,\bar{\alpha}_{\mathrm{eff}})\int\limits_{\delta/z}^{1}\mathrm{d}x_1\int\limits_{\delta/zx_1}^{1}\mathrm{d}x_2\;D(x_1,\widetilde{\alpha}_{\mathrm{eff}})D(x_2,\hat{\alpha}_{\mathrm{eff}})\sigma(zx_1x_2s). \tag{1.4.33}$$

We can integrate the expression in the right side of Eq. (1.4.33) over the variable z provided the quantity $zx_1=y$ is fixed

$$\int\limits_{\delta}^{1}\mathrm{d}z\;D(z,\bar{\alpha}_{\mathrm{eff}})\int\limits_{\delta/z}^{1}\mathrm{d}x_1\;D(x_1,\widetilde{\alpha}_{\mathrm{eff}})=\int\limits_{\delta}^{1}\mathrm{d}z\int\limits_{y}^{1}\mathrm{d}y\;D(z,\bar{\alpha}_{\mathrm{eff}})\times$$

$$\times D\left(\frac{y}{z},\widetilde{\alpha}_{\mathrm{eff}}\right)=\int\limits_{\delta}^{1}\mathrm{d}y\;D(y,\bar{\alpha}_{\mathrm{eff}}+\widetilde{\alpha}_{\mathrm{eff}}),\quad \bar{\alpha}_{\mathrm{eff}}+\widetilde{\alpha}_{\mathrm{eff}}=\hat{\alpha}_{\mathrm{eff}}. \tag{1.4.34}$$

Using this result and definition of $\hat{\alpha}_{\mathrm{eff}}$ we indicate the equivalence of the Drell–Yan form of the total cross section as given by Eq. (1.4.26) and the representation of the cross section by Eq. (1.4.33).

Let us show now that D functions in expression for the quantity Σ have effective couplings as given by Eq. (1.4.31). By definition the nonsinglet electron structure function satisfies the equation [71]

$$D(x,s,s_0)=\delta(1-x)+\frac{1}{2\pi}\int\limits_{s_0}^{s}\frac{ds_1}{s_1}\alpha(s_1)\int\limits_{x}^{1}\frac{dz}{z}D(z)D\left(\frac{x}{z},\frac{s_1}{s_0}\right), \tag{1.4.35}$$

where $\alpha(s_1)$ is the electromagnetic running coupling

$$\alpha(s_1)=\alpha\left(1-\frac{\alpha}{3\pi}\ln\frac{s_1}{m^2}\right)^{-1},$$

and $s_0(s)$ is the minimal (maximal) virtuality of the particle, which radiates photons and e^+e^- pairs.

The structure function $D(z, \bar{\alpha}_{\rm eff})$ describes the photon emission and pair production inside narrow cone along the electron beam direction. In this kinematics $s_0 = m^2$, $s = \varepsilon^2\theta_0^2$. The corresponding iterative solution of Eq. (1.4.35) has the form (1.4.29) with $\alpha_{\rm eff} = \bar{\alpha}_{\rm eff}$. The structure function $D(x_1, \widetilde{\alpha}_{\rm eff})$ describes the events, when emitted (by the electron) particles escape this narrow cone. In this case $s_0 = \varepsilon^2\theta_0^2$, $s = 4\varepsilon^2$. The corresponding solution of Eq. (1.4.35) gives the structure function with $\alpha_{\rm eff} = \widetilde{\alpha}_{\rm eff}$. At last, the structure function $D(x_2, \hat{\alpha}_{\rm eff})$ is responsible for the radiation off the positron into the whole phase space. In this case $s_0 = m^2$, $s = 4\varepsilon^2$. Therefore we obtain D function with $\alpha_{\rm eff} = \hat{\alpha}_{\rm eff}$. The analogous consideration can be performed for the singlet part of structure functions.

When writing the representation (1.4.33) for the total cross section we, in fact, divide the phase space of the particles emitted by the electron on the regions inside and outside the narrow cone along electron beam direction. Therefore we can use this representation to investigate the events with tagged particles in both these regions. As we saw before the differential cross section for events with tagged particles inside the narrow cone is defined by the quantity $\Sigma(z < 1)$. In order to obtain the corresponding differential cross section for events with tagged particles outside this narrow cone we have to change the places of $\bar{\alpha}_{\rm eff}$ and $\widetilde{\alpha}_{\rm eff}$ in expression for $\Sigma(z, 1)$. This follows from the symmetry of representation (1.4.33) relative such change.

1.4.4. Conclusion. In sum, the formulae (1.4.34),(1.4.28) are the main results of this part.

Thus we calculated the cross section of e^+e^- annihilation with detection of a hard photon at small angles with respect to the electron beam. The general structure of a measured cross section, from which one should extract the annihilation cross section σ_0, looks

$$\sigma = \sigma_0\left[a_1\frac{\alpha}{\pi}L + b_1\frac{\alpha}{\pi} + a_2\left(\frac{\alpha}{\pi}\right)^2 L^2 + b_2\left(\frac{\alpha}{\pi}\right)^2 L + c_2\left(\frac{\alpha}{\pi}\right)^2\right] + \mathcal{O}(\alpha^3), \tag{1.4.36}$$

where L denotes some large logarithm. We calculated the terms a_1, b_1, a_2, b_2 and some contributions to c_2. The generalized formula (1.4.28) allows one to involve the leading terms of the order $\mathcal{O}(\alpha^3 L^3)$. In this way our formulae provide high theoretical precision.

Similar formulae can be obtained for an experimental set-up by tagging a definite hadron. By using e^+e^- machines such as BEPS, DAΦNE [72], VEPP, CLEO, SLAC–B/factory and others with luminosities of order $10^{33}\,\mathrm{cm}^2\cdot\mathrm{s}^{-1}$, one is in principle able to scan, by measuring the initial state radiation spectrum,

the whole energy region of hadron production with an effective luminosity of the order of $10^{31}\,\mathrm{cm}^2\cdot\mathrm{s}^{-1}$. Let's hope that further study would be pursuing on these issues from experimental as well as from theoretical point of view.

2. OUTLOOK

Results given in Sections 1.1 and 1.3 could be applied to elastic and quasi-elastic scattering off nuclei. Among possible there are channels with nuclei got excited or even broken apart.

At the moment a tagged photon set-up in DIS as well as annihilation channels (Sections 1.2, 1.4) are of some perspective to high-energy physics in testing QED (SM) predictions for effects induced by virtual corrections. The formulae given here guarantee the theoretical error to fall down to 0.1%.

We did not touch the problem of evaluation of Z, W bosons contribution, which was considered elsewhere, as well as that of double-photon exchange between a lepton and nucleon and a real photon emission by a nucleon (nuclei). The latter has not been investigated in detail up to now. An almost thorough numerical analysis of the RC to DIS was given in the papers cited in the introduction. Nevertheless, the results presented in the review could be used to create more advanced MC generators with accounting for RC at 0.1% level of accuracy. To the moment this programme has been carried out only partially.

APPENDIX A. DETAILS OF MATRIX ELEMENT CALCULUS: THE CASE OF SINGLE PHOTON BREMSSTRAHLUNG

Using the Sudakov decomposition of the 4-vectors in the problem

$$\begin{aligned}
&p_1' = \alpha_1'\tilde{p}_2 + b\tilde{p}_1 + p_{1\perp}', \quad k_1 = \alpha_1\tilde{p}_2 + x_1\tilde{p}_1 + k_{1\perp},\\
&q = p_2 - p_2' = \alpha_q\tilde{p}_2 + \beta_q\tilde{p}_1 + q_\perp,\\
&p_2' = \alpha_2'\tilde{p}_2 + \beta_2'\tilde{p}_1 + p_{2\perp}', \quad v_\perp p_1 = v_\perp p_2 = 0,\\
&\tilde{p}_1 = p_1 - p_2\frac{m^2}{s}, \quad \tilde{p}_2 = p_2 - p_1\frac{M^2}{s},
\end{aligned} \tag{A.1}$$

we have excluded parameters $\alpha_1, \alpha_1', \beta_q$ using the on-shell conditions

$$\begin{aligned}
&p_2^{'2} - M^2 = -s\beta_q(1-\alpha_q) - \mathbf{q}^2 - \alpha_q M^2 = 0,\\
&p_1^{'2} = sb\alpha_1' - \mathbf{p}_1^{'2} = 0, \quad k_1^2 = sx_1\alpha_1 - \mathbf{k}_1^2 = 0,
\end{aligned} \tag{A.2}$$

besides

$$\begin{aligned}\Phi^{\rm prot} &= \frac{1}{s^2}\,{\rm Sp}\,\{(\hat{p}_2'+M)\Gamma_\rho(\hat{p}_2+M)\tilde{\Gamma}_\sigma p_1^\rho p_1^\sigma\},\\ \Gamma_\rho &= F_1(q^2)\gamma_\rho+\frac{\sigma_{\mu\rho}q^\mu}{2M}F_2(q^2).\end{aligned}\tag{A.3}$$

Here $F_{1,2}(q^2)$ are the Dirac and Pauli form factors of a proton. For Φ^γ we have:

$$\begin{aligned}\Phi^\gamma &= -\frac{1}{s^2}\,{\rm Sp}\,\{\hat{p}_1' O_\mu \hat{p}_1 \tilde{O}^\mu\},\\ O_\mu &= \hat{p}_2\frac{\hat{p}_1-\hat{k}_1}{-2p_1k_1}\gamma_\mu+\gamma_\mu\frac{\hat{p}_1'+\hat{k}_1}{2p_1'k_1}\hat{p}_2,\end{aligned}\tag{A.4}$$

and then

$$q^2=-Q_h^2=-\frac{1}{1-\alpha_q}[\mathbf{q}^2+M^2\alpha_q^2]\approx-[\mathbf{q}^2+Q^2_{\rm min}],\tag{A.5}$$

with $Q^2_{\rm min}$ given in the text. The matrix element

$$M=\frac{1}{q^2}J_\sigma^{(1)}\bar{u}(p_2')\Gamma_\rho u(p_2)g^{\rho\sigma},\tag{A.6}$$

using the Gribov representation for the metric tensor

$$g^{\rho\sigma}=g_\perp^{\rho\sigma}+\left(\frac{2}{s}\right)(\tilde{p}_2^\rho\tilde{p}_1^\sigma+\tilde{p}_2^\sigma\tilde{p}_1^\rho)\approx\left(\frac{2}{s}\right)\tilde{p}_2^\sigma\tilde{p}_1^\rho,\tag{A.7}$$

may be put in a form

$$M=\frac{2s}{q^2}\left(\frac{1}{s}p_2^\sigma J_\sigma^{(1)}\right)\left(\frac{1}{s}\bar{u}(p_2')\Gamma_\rho u(p_2)p_1^\rho\right).\tag{A.8}$$

Note that each expressions in the parentheses on the r.h.s. of Eq. (A.8) do not depend on s in the limit $s\to\infty$. The expression for Φ^γ may be transformed using the following reduced expression

$$\begin{aligned}O_\mu = x_1\Big[sb\gamma_\mu\left(\frac{1}{n}-\frac{1}{n_1}\right) &+ \frac{1}{n_1}b\gamma_\mu\hat{q}\hat{p}_2-\frac{1}{n}\gamma_\mu\hat{p}_2\hat{q}\Big],\\ x_1 &= 1-b.\end{aligned}\tag{A.9}$$

to take the form given in Eq. (1.1.8).

APPENDIX B. DETAILS OF MATRIX ELEMENT CALCULUS: THE CASE OF DOUBLE PHOTON BREMSSTRAHLUNG

Let's first demonstrate that the matrix element of the process

$$\gamma^*(q) + e(p_1) \to e(p_1') + \gamma(k_1) + \gamma(k_2) \tag{B.1}$$

is explicitly proportional to $\mathbf{q}$ for small values of the latter, which is in fact the requirement of gauge invariance with respect to the virtual photon. The matrix element is described by six diagrams. With regard to the gauge invariance this set can be separated out to the two subsets in each of which the gauge condition is satisfied independently. Introducing the photon-permutating operator $\mathcal{P}_{12}$ we bring the matrix element to the form:

$$\mathcal{M} = (1 + \mathcal{P}_{12})Q\,, \qquad Q = \mathcal{M}_1 + \mathcal{M}_2 + \mathcal{M}_3\,, \tag{B.2}$$

where

$$\begin{aligned}
\mathcal{M}_1 &= \frac{1}{dd_1}\bar{u}(p_1')\hat{p}_2(\hat{p}_1 - \hat{k}_1 - \hat{k}_2 + m) \times \\
&\times \quad \hat{e}_2^*(\hat{p}_1 - \hat{k}_1 + m)\hat{e}_1^* u(p_1)\,, \qquad \text{(B.3)} \\
\mathcal{M}_2 &= \frac{1}{d_1 d_2'}\bar{u}(p_1')\hat{e}_2^*(\hat{p}_1 - \hat{k}_1 + \hat{q} + m)\hat{p}_2 \times \\
&\times \quad (\hat{p}_1 - \hat{k}_1 + m)\hat{e}_1^* u(p_1)\,, \qquad \text{(B.4)} \\
\mathcal{M}_3 &= \frac{1}{d' d_2'}\bar{u}(p_1')\hat{e}_2^*(\hat{p}_1 - \hat{k}_1 + \hat{q} + m) \times \\
&\times \quad \hat{e}_1^*(\hat{p}_1 + \hat{q} + m)\hat{p}_2 u(p_1)\,, \qquad \text{(B.5)}
\end{aligned}$$

and

$$\begin{aligned}
d &= d_1 + d_2 - \frac{1}{x_1 x_2}(x_1\vec{k}_2 - x_2\vec{k}_1)^2, \\
d' &= d_1' + d_2' + \frac{1}{x_1 x_2}(x_1\vec{k}_2 - x_2\vec{k}_1)^2.
\end{aligned}$$

The permutation operator $\mathcal{P}_{12}$ for the photons acts the following way

$$\mathcal{P}_{12} f(k_1, e_1; k_2, e_2) = f(k_2, e_2; k_1, e_1)\,, \qquad \mathcal{P}_{12}^2 = 1.$$

The quantity Q is gauge invariant regarding the virtual photon k since all permutations of this photon have been taken into account. Therefore Q is proportional to $q_\perp$ in the limit of $q_\perp \to 0$. Indeed, making use of the relations

$$Q = p_{2\mu}Q^\mu\,, \quad q_\mu Q^\mu = (\alpha_q\tilde{p}_2 + q_\perp)_\mu Q^\mu = 0\,, \tag{B.6}$$

we immediately obtain (neglecting the small contribution $\beta_q p_\mu Q^\mu \sim 1/s$)

$$Q = -\frac{q_{\perp\mu}}{\alpha_q} Q^\mu \,. \tag{B.7}$$

Then transform the quantities $\mathcal{M}_j$ to such a form that the noticed low $q_\perp$ behavior is present in their sum Q explicitly. The reason is that in this case all individual large (compared to $q_\perp$) contributions are mutually cancelled. The first step is to use the Dirac equations $\hat{p}_1 u(p_1) = m u_1$, $\bar{u}(p_1')\hat{p}_1' = m\bar{u}(p_1')$ and to rearrange the amplitudes $\mathcal{M}_j$ of Eq. (B.3),

$$\begin{aligned}
\mathcal{M}_1 &= \bar{u}(p_1')\Bigg\{ \frac{s\beta_1'}{d_1}\hat{e}_2^*(\hat{p}_1 - \hat{k}_1 + m)\hat{e}_1^* - \\
&- \frac{1}{d_1}\hat{p}_2\hat{q}\hat{e}_2^*(\hat{p}_1 - \hat{k}_1 + m)\hat{e}_1^* \Bigg\} u(p_1)\,, \\
\mathcal{M}_2 &= \bar{u}(p_1')\Bigg\{ +\frac{s(1-x_1)}{d_1 d_2'}\hat{e}_2^*(\hat{p}_1 - \hat{k}_1 + m)\hat{e}_1^* - \frac{1}{d_2'}\hat{e}_2^*\hat{p}_2\hat{e}_1^* + \\
&+ \frac{1}{d_1 d_2'}\hat{e}_2^*\hat{q}\hat{p}_2(\hat{p}_1 - \hat{k}_1 + m)\hat{e}_1^* \Bigg\} u(p_1)\,, \\
\mathcal{M}_3 &= \bar{u}(p_1')\Bigg\{ \frac{s}{d' d_2'}\hat{e}_2^*(\hat{p}_1 - \hat{k}_1 + m)\hat{e}_1^* + \frac{s}{d' d_2'}\hat{e}_2^*\hat{q}\hat{e}_1^* + \\
&+ \frac{1}{d' d_2'}\hat{e}_2^*(\hat{p}_1' + \hat{k}_2 + m)\hat{e}_1^*\hat{q}\hat{p}_2 \Bigg\} u(p_1)\,.
\end{aligned} \tag{B.8}$$

From these formulae it can be noted that the last terms in $\mathcal{M}_1, \mathcal{M}_2, \mathcal{M}_3$, up to terms of the order of

$$\frac{m^2}{E^2}\,, \quad \theta^2\,, \quad \frac{m}{E}\,\theta\,,$$

are proportional to $q_\perp$,

$$\hat{\tilde{p}}_2\hat{q} = \hat{\tilde{p}}_2(\alpha_q\hat{\tilde{p}}_2 + \beta_q\hat{p} + \hat{q}_\perp) = \hat{\tilde{p}}_2\hat{q}_\perp = -\hat{q}\hat{\tilde{p}}_2\,. \tag{B.9}$$

Next, one can see that the sum of the first three terms in Eqs. (B.8) is also proportional to $q_\perp$ since (for more details see [73])

$$A \equiv \frac{b}{d_1} + \frac{1-x_1}{d_1 d_2'} + \frac{1}{d' d_2'}\,, \qquad A|_{q_\perp \to 0} = 0\,. \tag{B.10}$$

Finally we consider the sum of the second terms of the quantities $\mathcal{M}_2, \mathcal{M}_3$ given in Eqs. (B.8). Using the relations ([73], Eq.(21)) and

$$(p_1' + k_1 + k_2)^2 = (p_1 - k)^2 = m^2 - \mathbf{k}^2 - s\alpha_k \,,$$

one immediately gets

$$-\frac{\hat{\tilde{p}}_2}{d_2'} + \frac{s(\alpha_q \hat{\tilde{p}}_2 + \hat{q}_\perp)}{d' d_2'} = \frac{s\hat{q}_\perp}{d' d_2'} + \frac{\hat{\tilde{p}}_2 \mathbf{q}^2}{d' d_2'} \,. \tag{B.11}$$

Therefore, from Eqs. (B.9), (B.10), (B.11) it is clearly seen that the property illustrated by Eq. (B.7)

$$(\mathcal{M}_1 + \mathcal{M}_2 + \mathcal{M}_3)\,|_{q_\perp \to 0} = 0$$

is evidently satisfied and consequently the quantity $Q = \sum_{j=1}^{3} \mathcal{M}_j$ became a sum of terms explicitly proportional to $q_\perp$,

$$\begin{aligned} Q &= \bar{u}(p_1')\Big\{ As\, \hat{e}_2^*(\hat{p}_1 - \hat{k}_1 + m)\hat{e}_1^* - \\ &- \frac{1}{d_1}\hat{\tilde{p}}_2 \hat{q}_\perp \hat{e}_2^*(\hat{p}_1 - \hat{k}_1 + m)\hat{e}_1^* - \\ &- \frac{\mathbf{q}^2}{d' d_2'}\hat{e}_2^*\hat{e}_1^*\hat{\tilde{p}}_2 + \frac{s}{d' d_2'}\hat{e}_2^*\hat{q}_\perp\hat{e}_1^* + \\ &+ \frac{1}{d_1 d_2'}\hat{e}_2^*\hat{q}_\perp\hat{\tilde{p}}_2(\hat{p}_1 - \hat{k}_1 + m)\hat{e}_1^* + \\ &+ \frac{1}{d' d_2'}\hat{e}_2^*(\hat{p}_1' + \hat{k}_2 + m)\hat{e}_1^*\hat{q}_\perp\hat{\tilde{p}}_2\Big\}u(p_1)\,. \end{aligned} \tag{B.12}$$

Calculating the contribution of the trace $\mathrm{Sp}\{p_1' Q p_1 \tilde{Q}\}$ we neglect masses whose contribution to the quantity $\Phi^{\gamma\gamma}$ may be restored using the general prescription [37]. The corresponding correction has the form:

$$\begin{aligned} \Delta_m \Phi^{\gamma\gamma} &= (1 + \mathcal{P}_{12})\Big\{ -\frac{4m^2}{d_1'^2}\frac{x_2^2 y_1(1 + y_1^2)}{(1 - x_2)^2} \times \\ &\times \frac{\mathbf{q}^2}{(\mathbf{q} - y_1\mathbf{p}_1')^2(\mathbf{q} - \mathbf{p}_1'/b)^2} - \\ &- \frac{4m^2}{d_1^2}\frac{\beta_2^2 z_1(1 + z_1^2)\mathbf{q}^2}{(\mathbf{q} - \mathbf{p}_1')^2(\mathbf{p}_1' - (1 - \beta_2)\mathbf{q})^2}\Big\}, \end{aligned} \tag{B.13}$$

where

$$y_1 = \frac{1 - x_2}{b}, \quad \beta_2 = \frac{x_2}{1 - x_1}, \quad z_1 = \frac{b}{1 - x_1}.$$

APPENDIX C. EVALUATION OF 2-DIMENSIONAL INTEGRALS

The azimuthal integration may be performed making use of the following equality:

$$\begin{aligned} J_{12\ldots n} &= \frac{1}{2\pi}\int_0^{2\pi} d\phi \prod_i [a_i + b_i \cos(\phi - \phi_i)]^{-1} = \\ &= \sum_{k=1}^{n} \frac{1}{r_k} \prod_{j\neq k}^{n} \frac{b_k}{b_{kj} + \mathrm{i} r_k \sin(\phi_k - \phi_j)}, \end{aligned} \tag{C.1}$$

with

$$\begin{aligned} r_i &= \sqrt{a_i^2 - b_i^2}, \qquad |a_i| > |b_i|, \\ b_{ij} &= b_i a_j - b_j a_i \cos(\phi_i - \phi_j). \end{aligned}$$

It is curious to note that the absence of the imaginary part provides an interesting algebraic identity. For $n = 2, n = 3$ it looks

$$\begin{aligned} J_{12} &= \frac{1}{d_{12}}\left(\frac{b_1}{r_1} b_{12} + \frac{b_2}{r_2} b_{21}\right), \quad d_{12} = a_{12}^2 - r_1^2 r_2^2, \\ a_{12} &= a_1 a_2 - b_1 b_2 \cos(\phi_1 - \phi_2), \\ J_{123} &= \frac{b_1^2}{r_1}\frac{a_{12}a_{13} - r_1^2 a_{23}}{d_{12}d_{13}} + \frac{b_2^2}{r_2}\frac{a_{21}a_{23} - r_2^2 a_{13}}{d_{12}d_{23}} + \\ &+ \frac{b_3^2}{r_3}\frac{a_{31}a_{32} - r_3^2 a_{12}}{d_{31}d_{32}}. \end{aligned} \tag{C.2}$$

This form is convenient for a subsequent integration over $\mathrm{d}\mathbf{k}_1^2$.

APPENDIX D. NLO CONTRIBUTIONS FROM VIRTUAL AND SOFT PHOTON EMISSION

To avoid the misprints we use here the notations of the paper [33]

$$\begin{aligned} s &= d_1', \quad t = -d_1, \quad u = -Q^2, \\ s + t + u &= q^2, \quad \tilde{f}(s,t) = f(t,s), \quad a = s + t, \\ b &= s + u, \qquad c = u + t. \end{aligned} \tag{D.1}$$

The quantities τ_{ij} encountered in the text (see Eq. (1.1.12)) may be written as

$$\begin{aligned}
\tau_{11} &= -G\left(1+\frac{u^2}{s^2}\right)-\tilde{G}\left(2+\frac{b^2}{t^2}\right)+2\left[\frac{b^2}{st}+\frac{2u}{a}+\right.\\
&+ \left.\frac{2}{a^2}(u^2-bt)\right]l_{qu}+\frac{b^2}{tc^2}(2c+t)l_{qs}+\frac{2u-s}{s}l_{qt}+\\
&+ \frac{1}{q^2}\left[\frac{4}{a}(bt-u^2)-4u-2q^2+t-\frac{b^2}{c}\right],\\
\tau_{12} &= \frac{c}{s^2}(u-s)G+\frac{1}{t^2}(uq^2-st)\tilde{G}-2\left[\frac{uq^2}{st}+\frac{2u-s+t}{a}+\right.\\
&+ \left.\frac{2}{a^2}(u^2-cs)\right]l_{qu}+\frac{2c+t}{c^2}\left(s-\frac{u}{t}q^2\right)l_{qs}-\\
&- \frac{c}{bs}(2u-s)l_{qt}+\frac{1}{q^2}\left[\frac{4}{a}(u^2-cs)+8u+3t-s+\frac{2}{c}us\right], \qquad \text{(D.2)}
\end{aligned}$$

and the additional notations look

$$\begin{aligned}
l_{qu} &= \ln\frac{q^2}{u}, \quad l_{qs}=\ln\frac{-q^2}{s}, \quad l_{qt}=\ln\frac{q^2}{t}, \quad l_{ut}=\ln\frac{u}{t},\\
G &= l_{qu}(l_{qt}+l_{ut})+2\mathrm{Li}_2\left(1-\frac{t}{q^2}\right)-\\
&\quad -2\mathrm{Li}_2\left(1-\frac{q^2}{u}\right)-2\mathrm{Li}_2(1). \qquad \text{(D.3)}
\end{aligned}$$

APPENDIX E. SEMICOLLINEAR KINEMATICS OF PAIR CREATION

The matrix element in the kinematics (1.1.2) may be put in a form (we extract the coupling constant):

$$M^{(1)}=\frac{1}{q_1^2}J_\nu I_\mu g^{\mu\nu}, \quad J_\nu=\bar{u}(p_-)\gamma_\nu u(p_1), \qquad \text{(E.1)}$$

where the current I describes a pair production by the photon with momentum q_1 off a proton. Using the Sudakov form of the 4-vectors p_- and q with basic 4-vectors p_1 and p_2,

$$p_-=\alpha_-\tilde{p}_2+\beta_-\tilde{p}_1+p_{-\perp}, \quad q=\alpha_q\tilde{p}_2+\beta_q\tilde{p}_1+q_\perp,$$

the representation of the metric tensor

$$g_{\nu\mu}=g_{\nu\mu\perp}+\frac{2}{s}p_{2\nu}p_{1\mu}$$

and the gauge condition

$$Iq = I(\beta_q p_1 + q_\perp) = 0, \quad \beta_q + \beta_- = 1,$$

we obtain for the matrix element squared and summed over spin states of electron:

$$\sum |M^{(1)}|^2 = \frac{1}{(q_1^2)^2}\left[-2q_1^2\mathbf{I}^2 + \frac{8}{\beta_q^2}\left(\mathbf{p}_-\mathbf{I}\right)^2\right]. \tag{E.2}$$

To calculate the quantity $\mathbf{I}^2$, we again present it in the form

$$\begin{aligned} I &= e_{q_1}\mathbf{I} = e_{q_1}^\mu e_q^\nu \frac{2s|\vec{q}|}{q^2 s_1} p_{2\rho} Y_\rho \bar{u}(p_1')O_{\mu\nu}v(p_+), \\ s_1 &= (p_2+q_1)^2, \qquad Y_\rho = \bar{u}(p_2)\Gamma_\rho u(p_2'). \end{aligned} \tag{E.3}$$

The phase volume is transformed the way to take the following form

$$\mathrm{d}\Gamma_4 = (2\pi)^{-8}\frac{1}{8s\beta_-\beta_+ b}\mathrm{d}^2q\mathrm{d}^2p_-\mathrm{d}\beta_-. \tag{E.4}$$

Using

$$\sum |\bar{u}(p_1')O_{\mu\nu}v(p_+)e_{q_1}^\mu e_q^\nu|^2 = 8\left[\frac{b}{\beta_+} + \frac{\beta_+}{b}\right],$$

we obtain the result for the cross section given in the text.

For the kinematics of bremsstrahlung mechanism the matrix element has the form

$$M^{(2)} = \frac{1}{k_1^2} I_\mu J_\nu g^{\mu\nu}, \quad k_1 = p_+ + p_1'. \tag{E.5}$$

Here it is convenient to use alternative basis vectors of Sudakov parameterization

$$\begin{aligned} p_+ &= \alpha_+ q + b_+\tilde{p}_1' + p_{+\perp},\ k_1 = a_1 q + b_1\tilde{p}_1' + k_{1\perp}, \\ g_{\mu\nu} &= g_{\mu\nu\perp} + \frac{2}{\tilde{s}}q^\nu p_1^{'\mu}, \quad k_1^2 = \frac{\mathbf{p}_+^2 + m^2 b_1^2}{b_1 - 1} > 0. \end{aligned} \tag{E.6}$$

Quite the same manipulations give

$$\sum |M^{(2)}|^2 = 2k_1^2\mathbf{I}^2 - \frac{8}{b_1^2}\left(\mathbf{k}_1\mathbf{I}\right)^2.$$

Performing the integration over $\mathrm{d}^2(p_+)_\perp$ to a logarithmic accuracy and expressing the parameter b_1 in terms of the standard Sudakov decomposition with basic 4-vectors p_1, p_2

$$b_1 = \frac{1-\beta_-}{b},$$

we immediately obtain the result given in the text.

APPENDIX F

In this section we collect the results of the angular integration of the definite structures of the Compton tensor in [33,46]. Using integrals similarly to (1.2.12) and retaining only terms that contain at least one large logarithm L_0 or L_Q, we obtain

$$\begin{aligned}
\frac{2\varepsilon^2}{Q_l^2}\int\frac{\mathrm{d}\Omega_k}{2\pi}T_g &= -\rho\left[\frac{1+z^2}{(1-z)^2}(L_0-1)+1\right]+\frac{1+z^2}{(1-z)^2}[A\ln z+B]-\\
&- \frac{4z}{(1-z)^2}L_Q\ln z-\frac{2-(1-z)^2}{2(1-z)^2}L_0,\\
2\varepsilon^2\int\frac{\mathrm{d}\Omega_k}{2\pi}T_{11} &= \frac{4z}{(1-z)^2}\rho L_0-\frac{2z(1+(1-z)^2)}{(1-z)^4}(A\ln z+B)-\\
&- A\frac{z(3-z)}{(1-z)^3}+\frac{2L_0}{(1-z)^3}\left(\frac{z(8z-3)}{1-z}\ln z+2z+z^2\right),\\
2\varepsilon^2\int\frac{\mathrm{d}\Omega_k}{2\pi}T_{22} &= \rho\left(\frac{4z}{(1-z)^2}L_0-\frac{8}{(1-z)^2}\right)+\frac{16}{(1-z)^2}\ln zL_Q-\\
&- \frac{2z(1+2(1-z)^2)}{(1-z)^4}(A\ln z+B)-A\frac{3z-1}{z(1-z)^3}+ \qquad \text{(F.1)}\\
&+ \frac{2L_0}{z(1-z)^3}\left(\frac{1+4z(z^2+z-1)}{1-z}\ln z+z^3-z^2+4z-1\right),\\
2\varepsilon^2\int\frac{\mathrm{d}\Omega_k}{2\pi}T_{21} &= \frac{2z^2}{(1-z)^4}(A\ln z+B)+\frac{3z-1}{(1-z)^3}A+\\
&+ \frac{2L_0}{(1-z)^3}\left(\frac{-1+4z-4z^2-4z^3}{1-z}\ln z-2z^2-2z+1\right),\\
2\varepsilon^2\int\frac{\mathrm{d}\Omega_k}{2\pi}T_{12} &= \frac{2z(2-z)}{(1-z)^4}(A\ln z+B)+\frac{3-z}{(1-z)^3}A+\\
&+ \frac{2L_0}{(1-z)^3}\left(\frac{3-8z}{1-z}\ln z-1-2z\right),
\end{aligned}$$

where ρ, A, and B are given by Eq. (1.2.13). It is remarkable to see that the relation

$$\int\frac{\mathrm{d}\Omega_k}{2\pi}\left[4zT_g+Q_l^2(T_{11}+z^2T_{22}+zT_{12}+zT_{21})\right]=0 \qquad \text{(F.2)}$$

is fulfilled, leading to the factorization of the virtual corrections in Eq. (1.2.13).

APPENDIX G

To perform the angular integration in (1.2.23) we first represent the integrand in the form

$$\frac{\varepsilon^2\alpha^2(Q^2_{sc})I^\gamma}{Q^4_{sc}} = \frac{F(t_1,t_2)}{t_1t_2}, \tag{G.1}$$

where $t_{1,2} = (1-c_{1,2})/2$, $c_{1,2} = \cos\theta_{1,2}$, and $\theta_{1,2}$ are the angles between nontagged photon momentum k_2 and the momenta of the initial and the scattered electrons. Note that $F(t_1,t_2)$ behaves regularly for $t_1 \to 0$ or $t_2 \to 0$. This can be easily seen by considering the limiting cases for the quantity I^γ.

For the case $t \to 0$, which corresponds to the second photon being emitted close to the direction of the incoming electron, one obtains from Eq. (1.2.24)

$$I^\gamma|_{t\to 0} = \frac{Q^2}{x_2 t}(z^2+(z-x_2)^2)\Bigg[x_t F_2(x_t,Q^2_t)\times$$

$$\times\left(\frac{M^2}{Q^2_t} - \frac{1-y}{x^2y^2(z-x_2)}\right) - F_1(x_t,Q^2_t)\Bigg], \tag{G.2}$$

while for the case $s \to 0$, corresponding to the second photon being almost collinear to the final electron,

$$I^\gamma|_{s\to 0} = -\frac{Q^2 z}{y_2 s}(1+(1+y_2)^2)\Bigg[x_b F_2(x_b,Q^2_b)\times$$

$$\times\left(\frac{M^2}{Q^2_b} - \frac{1-y}{x^2y^2z(1+y_2)}\right) - F_1(x_b,Q^2_b)\Bigg], \tag{G.3}$$

see Eqs.(1.2.20) and (1.2.27) for the notation. The r.h.s. of Eq. (G.1) is easily seen to be

$$\left.\frac{\varepsilon^2\alpha^2(Q^2_{sc})I^\gamma}{Q^4_{sc}}\right|_{t\to 0} = \frac{1}{t_1t_2}\frac{a}{16\pi x_2^2}\frac{z^2+(z-x_2)^2}{z(z-x_2)}\,\Sigma(x_t,y_t,Q^2_t), \tag{G.4}$$

$$\left.\frac{\varepsilon^2\alpha^2(Q^2_{sc})I^\gamma}{Q^4_{sc}}\right|_{s\to 0} = \frac{1}{t_1t_2}\frac{a}{16\pi x_2^2}\frac{1+(1+y_2)^2}{1+y_2}\,\Sigma(x_b,y_b,Q^2_b), \tag{G.5}$$

where $a = (1-\cos\theta)/2$.

For the phase space of the photon we use the following representation:

$$\int \frac{\mathrm{d}^3 k_2}{\omega_2} = \varepsilon^2 \int x_2 \, \mathrm{d}x_2 \, \mathrm{d}\Omega_2 = 4\varepsilon^2 \int x_2 \, \mathrm{d}x_2 \int \frac{\mathrm{d}t_1 \, \mathrm{d}t_2}{\sqrt{D}} \Theta(D),$$

$$D = (t_2 - y_-)(y_+ - t_2), \quad y_\pm = t_1(1-2a) + a \pm 2\sqrt{a(1-a)t_1(1-t_1)}. \tag{G.6}$$

The region of integration is determined by the conditions

$$\sigma_1 < t_1 < 1, \quad \sigma_2 < t_2 < 1, \quad D > 0, \quad \sigma_1 = \frac{\theta_0^2}{4}, \quad \sigma_2 = \frac{\theta_0'^2}{4}. \tag{G.7}$$

Using the substitution

$$t_2 \to t_2(t_1, u) = \frac{(a - t_1)^2 (1 + u^2)}{y_+ + u^2 y_-}, \tag{G.8}$$

and the identity

$$\int\limits_{\sigma_1}^{1} \mathrm{d}t_1 \int\limits_{\sigma_2}^{1} \mathrm{d}t_2 \frac{F(t_1, t_2)}{t_1 t_2 \sqrt{D}} \Theta(D) = \frac{\pi}{a} \left[F(a,0) \ln \frac{a}{\sigma_2} + F(0,a) \ln \frac{a}{\sigma_1} \right] +$$

$$+ 2 \int\limits_0^\infty \frac{\mathrm{d}u}{1+u^2} \lim_{\eta \to 0} \left[\int\limits_\eta^1 \frac{\mathrm{d}t_1}{t_1 |t_1 - a|} \left(F(t_1, t_2) - F(a,0) \right) + \right.$$

$$\left. + \int\limits_\eta^a \frac{\mathrm{d}t_1}{t_1 a} \left(F(a,0) - F(0,a) \right) \right], \tag{G.9}$$

which is valid for $\sigma_1, \sigma_2 \ll a$, we obtain for Z from Eq. (1.2.25) the following expression:

$$Z = -\frac{4(1-c)}{zQ^2} \int\limits_0^\infty \frac{\mathrm{d}u}{1+u^2} \lim_{\eta \to 0} \left[\int\limits_\eta^1 \frac{\mathrm{d}t_1}{t_1 |t_1 - a|} \times \right.$$

$$\left. \times \int\limits_0^{x_m} \frac{\mathrm{d}x_2}{x_2} (\Phi(t_1, t_2(t_1,u)) - \Phi(a,0)) + \int\limits_\eta^a \frac{\mathrm{d}t_1}{t_1 a} \int\limits_0^{x_m} \frac{\mathrm{d}x_2}{x_2} (\Phi(a,0) - \Phi(0,a)) \right], \tag{G.10}$$

where

$$\Phi(t_1,t_2) \;=\; \left.\frac{\alpha^2(Q^2_{sc})stI^\gamma}{Q^4_{sc}}\right|_{c_1=1-2t_1,\ c_2=1-2t_2(t_1,u),\ c=1-2a}. \qquad \text{(G.11)}$$

The upper limit of the x_2-integration, x_m, may be deduced from [42]. It has the form

$$x_m \;=\; \frac{z(e+p)-\Delta_m-Y(e+z)-(p-z)Yc}{z+e-Y+(p-z)c_1+Yc_2}, \qquad e=\frac{E_p}{\varepsilon},$$

$$p \;=\; \frac{P_p}{\varepsilon}, \qquad \Delta_m=\frac{(M+m_\pi)^2-M^2}{2\varepsilon^2}. \qquad \text{(G.12)}$$

This finally leads to Eq. (1.2.25).

It is important to note that while calculating Z one encounters neither collinear nor infrared singularities.

Acknowledgements. It's a pleasure to thank A. Arbuzov, N. Merenkov and H. Anlauf for fruitful collaboration. The work of I.A. was supported by the U.S. Department of Energy under contract DE–AC05–84ER40150. The work of E.K. and B.S. was supported by RFBR grant No.99-02-17730 and HLP grant No.2000-02.

REFERENCES

1. **Sloan T., Voss R., Smadja G.** — Phys. Rep., 1988, v.162, p.45.
2. **Ashman J. for EMC Coll.** — Nucl. Phys., 1989, v.B328, p.1.
3. **Anselmino M., Efremov A., Leader E.** — Phys. Rep., 1995, v.261, p.1.
4. **Mo L., Tsai Y.** — Rev. Mod. Phys., 1969, v.41, p.205.
5. **Bardin D.Y., Shumeiko N.M.** — Nucl. Phys., 1977, v.B127, p.242.
6. **Akhundov A., Bardin D., Kalinovskaya L. et al.** — Fortsch. Phys., 1996, v.44, p.373.
7. **Kuzhir P.P., Shumeiko N.M.** — Sov. J. Nucl. Phys., 1992, v.55, p.1086.
8. **Badelek B., Bardin D., Kurek K. et al.** — Z. Phys., 1995, v.C66, p.591.
9. **Akushevich I., Bottcher H., Ryckbosch D.** — In: Proc. of Hamburg Int. Conf. on Monte Carlo Generators for HERA Physics, 1998/99, p.554–565; hep-ph/9906408.
10. **Akhundov A.A., Bardin D.Y., Shumeiko N.M.** — Sov. J. Nucl. Phys., 1977, v.26, p.660.
11. **Kukhto T.V., Shumeiko N.M.** — Nucl. Phys., 1983, v.B219, p.412.
12. **Akushevich I.V., Shumeiko N.M.** — J. Phys., 1994, v.G20, p.513.
13. **Kuraev E.A., Merenkov N.P., Fadin V.S.** — YaF, 1988, v.47, p.1593.
14. **Bohm M., Spiesberger H.** — Nucl. Phys., 1987, v.B294, p.1081.
15. **Bardin D.Y., Burdik C., Khristova P.C. et al.** — Z. Phys., 1989, v.C42, p.679.

16. **Akushevich I.V., Ilichev A.N., Shumeiko N.M.** — Phys. Atom. Nucl., 1998, v.61, p.2154.
17. **Akushevich I.V., Ilichev A.N., Shumeiko N.M.** — J. Phys., 1998, v.G24, p.1995.
18. **Soroko A.V., Shumeiko N.M.** — Sov. J. Nucl. Phys., 1989, v.49, p.838.
19. **Akushevich I.** — Eur. Phys. J., 1999, v.C8, p.457.
20. **Akushevich I., Kuzhir P.** — Phys. Lett., 2000, v.B474, p.411.
21. **Akushevich I., Shumeiko N., Soroko A.** — Eur. Phys. J., 1999, v.C10, p.681.
22. **Maximon L.C., Parke W.C.** — Phys. Rev., 2000, v.C61, p.045502.
23. **Maximon L.C., Tjon J.A.** — nucl-th/0002058.
24. **Templon J.A., Vellidis C.E., Florizone R.E. et al.** — Phys. Rev., 2000, v.C61, p.014607.
25. FERRAD 3.5. This code was firstly created by J.Dress for EMC and further developed by M.Dueren.
26. **Magnussen N. et al.** — In: Proc. of Hamburg Workshop on Physics at HERA, Buchmüller W., Ingelman G. (eds.), 1991, v.3.
27. **Kwiatkowski A., Spiesberger H., Mohring H.J.** — Comp. Phys. Commun., 1992, v.69, p.155.
28. **Arbuzov A., Bardin D., Bluemlein J. et al.** — Comp. Phys. Commun., 1996, v.94, p.128.
29. **Akushevich I., Ilichev A., Shumeiko N. et al.** — Comp. Phys. Commun., 1997, v.104, p.201.
30. **Akushevich I., Nagaitsev A.** — J. Phys., 1998, v.G24, p.2235.
31. **Kuraev E.A., Fadin V.S.** — Sov. J. Nucl. Phys., 1985, v.41, p.466.
32. **Skrzypek M.** — Acta Phys. Polonica, 1992, v.B23, p.135.
33. **Kuraev E.A., Merenkov N.P., Fadin V.S.** — YaF, 1987, v.45, p.782.
34. **Akhundov A.A., Bardin D.Y., Shumeiko N.M.** — Sov. J. Nucl. Phys., 1986, v.44, p.988.
35. **Akushevich I.V., Kukhto T.V., Pacheco F.** — J. Phys., 1992, v.G18, p.1737.
36. **Favart L., Gruwe M., Marage P. et al.** — Z. Phys., 1996, v.C72, p.425.
37. **Berends F.A. et al.** — Phys. Lett., 1981, v.B103, p.124;
Berends F.A. et al. — Nucl. Phys., 1982, v.B206, p.61.
38. **Arbuzov A.B., Kuraev E.A., Merenkov N.P. et al.** — Nucl. Phys., 1996, v.B474, p.271.
39. **Spiesberger H. et al.** — In: Proc. of Hamburg Workshop on Physics at HERA, Buchmüller W., Ingelman G., (eds.), 1991, v.3.
40. **Jadach S., Jezabek M., Placzek W.** — Phys. Lett., 1990, v.B248, p.417.
41. **Krasny M.W., Placzek W., Spiesberger H.** — Z. Phys., 1992, v.C53, p.687.
42. **Bardin D., Kalinovskaya L., Riemann T.** — Z. Phys., 1997, v.C76, p.487.
43. **Ahmed T. et al.** — Z. Phys., 1995, v.C66, p.529.
44. **Klein M. for H1 Coll.** — In: Proc. of ICHEP'98 Conference, Vancouver, 1998, contributed paper no. 535.
45. **Arbuzov A.B. et al.** — Nucl. Phys., 1997, v.B485, p.457;
Merenkov N.P. et al. — Acta Phys. Polonica, 1997, v.B28, p.491.
46. **Kuraev E.A., Merenkov N.P., Fadin V.S.** — Sov. J. Nucl. Phys., 1987, v.45, p.486.
47. **Feynman R.P.** — Photon-Hadron Interactions. W.A. Benjamin, Inc., Reading, Massachusetts, 1972.
48. **Merenkov N.P.** — Sov. J. Nucl. Phys., 1988, v.48, p.1073.

49. **Baier V.N., Fadin V.S., Khoze V.A.** — Nucl. Phys., 1973, v.B65, p.381.
50. **Kinoshita T.** — J. Math. Phys. (N.Y.), 1962, v.3, p.650;
Lee T.D., Nauenberg M. — Phys. Rev., 1964, v.133, p.1549.
51. **Anlauf H., Arbuzov A.B., Kuraev E.A. et al.** — JETP Lett., 1997, v.66, p.391; Erratum ibid., 1998, v.67, p.305.
52. **Anlauf H., Arbuzov A., Kuraev E. et al.** — JHEP, 1998, v.9810, p.013.
53. **Akushevich I., Arbuzov A., Kuraev E.** — Phys. Lett., 1998, v.B432, p.222.
54. **Kleiss R.** — Z. Phys., 1987, v.C33, p.433.
55. **Adams D. et al.** — Phys. Rev., 1997, v.D56, p.5330.
56. **Ackerstaff K. et al.** — Phys. Lett., 1997, v.B404, p.383.
57. **Barbieri R., Mignaco J.A., Remiddi E.** — IL Nuovo Cim., 1972, v.A11, p.824.
58. **Gagunashvili N.D.** — Nucl. Instr. and Meth., 1994, v.A343, p.606;
Gagunashvili N.D. et al. — JINR Preprint E1–96–483, Dubna, 1996.
59. **Bluemlein J., Levman G., Spiesberger H.** — J. Phys., 1993, v.G19, p.1695.
60. **Arbuzov A.B., Kuraev E.A., Merenkov N.P. et al.** — YaF, 1996, v.59, p.878.
61. **Konchatnij M.I., Merenkov N.P.** — Pisma v ZhETF, 1999, v.69, p.645.
62. **Arbuzov A., Kuraev E., Merenkov N. et al.** — JHEP, 1998, v.9812, p.009.
63. **Aid S. et al.** — Nucl. Phys., 1996, v.B470, p.3.
64. **Baier V.N., Khoze V.A.** — ZhETF, 1965, v.48, p.946; YaF, 1965, v.2, p.287.
65. **Brown D.H., Worstell W.A.** — Phys. Rev., 1996, v.D54, p.3237;
Eidelman S. et al. — Z. Phys., 1995, v.C67, p.585;
Jegerlehner F. — In: Proc. of Karlsrue Workshop on Hadron Production Cross Sections at DAΦNE, Hagel U.V. et al. (eds.), 1996, v.1, p.81.
66. **Anlauf H., Arbuzov A., Kuraev E.A. et al.** — Phys. Rev., 1999, v.D59, p.014003.
67. **Arbuzov A.B. et al.** — Nucl. Phys., 1997, v.B483, p.83.
68. **Jadach S., Skrzypek M., Ward B.F.L.** — Phys. Rev., 1993, v.D47, p.3733.
69. **Nicrosini O., Trentadue L.** — Phys. Lett., 1987, v.B196, p.551.
70. **Catani S., Trentadue L.** — JETP Lett., 1990, v.51, p.83.
71. **Lipatov L.N.** — YaF, 1974, v.20, p.181;
Altarelli G., Parisi G. — Nucl. Phys., 1977, v.B126, p.298.
72. **Spagnolo S.** — KLOE memo No.139, 1998.
73. **Kuraev E.A., Schiller A., Serbo V.G. et al.** — Nucl. Phys., 2000, v.B570, p.359.

«ФИЗИКА ЭЛЕМЕНТАРНЫХ ЧАСТИЦ И АТОМНОГО ЯДРА»
2001, ТОМ 32, ВЫП. 3

УДК 530.12; 531.18; 531.12; 531.51; 539.12.01

TIME-REPARAMETRIZATION-INVARIANT DYNAMICS OF RELATIVISTIC SYSTEMS

B.M.Barbashov, V.N.Pervushin

Joint Institute for Nuclear Research, Dubna

M.Pawlowski

Soltan Institute for Nuclear Studies, Warsaw, Poland

The review is devoted to the description of the reparametrization-invariant dynamics of relativistic systems (special relativity, string, and general relativity) obtained by resolving constraints and constructing equivalent unconstrained systems. The constraint-shell actions allow us to give clear mathematical definitions of measurable quantities in both classical and quantum theories of the type of the geometric time interval, or the dynamic evolution parameter in the world space of dynamic variables, the energy density and the holomorphic (particle-like) variables in general relativity.

Обзор посвящен репараметризационно-инвариантному описанию динамики релятивистских систем (релятивистская частица, струна, вселенная в общей теории относительности). Такое описание достигается переходом на поверхность связей в фазовом пространстве.

Вычисление функции действия на поверхности связей (путем их решения) ведет к эквивалентным системам без связей, совместимым с простейшими вариационными принципами и с физически ясными, математически строгими определениями инвариантных измеряемых величин как в классической, так и в квантовой теориях, в частности, динамического эволюционного параметра в мировом пространстве переменных, плотности измеряемой энергии и частицеподобных (голоморфных) переменных в общей теории относительности.

1. INTRODUCTION

The modern physics grew from two different roots: the Newton mechanics and the Faraday–Maxwell electrodynamics. The first gave variational principles; the second, relativistic and gauge symmetries (see Fig. 1). Relativistic particles, strings, n branes, and general relativity are systems with constraints and are not compatible with the simplest variational principles of the Newton mechanics. One of the main difficulties is the invariance of relativistic system with respect to reparametrization of the coordinate time.

The problem of the self-consistent Hamiltonian description of relativistic systems (particles, strings, n branes, general relativity) has a long history [1–7]. There are two opposite approaches to solution of this problem in the generalized Hamiltonian formulation [1, 8–12].

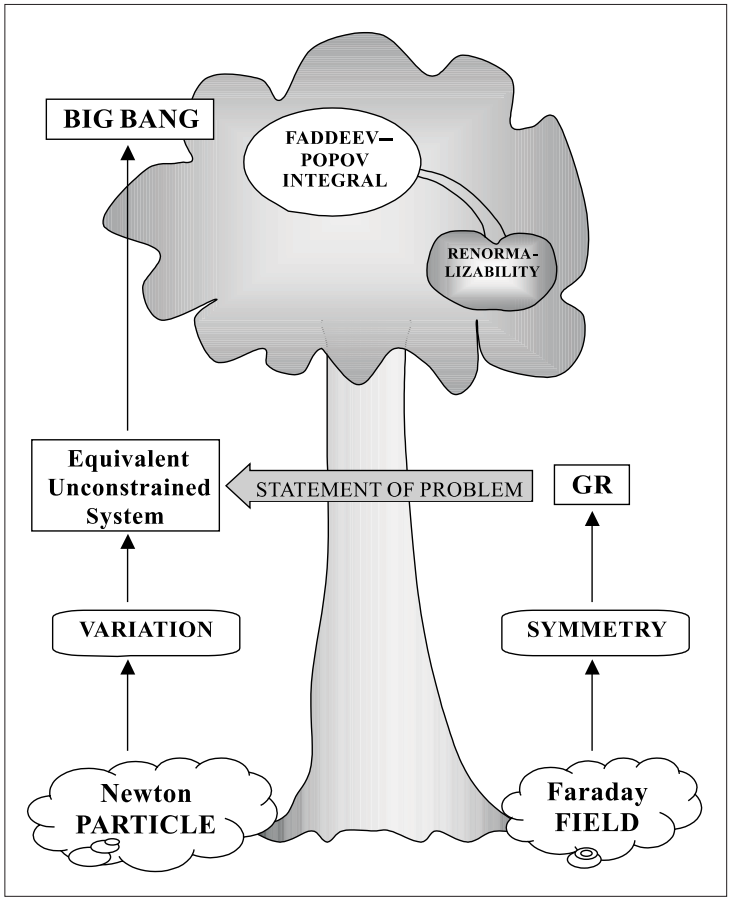

Fig. 1. The tree of modern theoretical physics grew from two different roots («particle» and «field») which gave the VARIATIONAL method and SYMMETRY principles for formulating modern physical theories as constrained systems. To obtain unambiguous physical results, one should construct Equivalent Unconstrained Systems compatible with the simplest variational method. It is just the problem discussed in the present paper

The first approach is the reduction of the extended phase space by fixing the gauge that breaks reparametrization invariance from the very beginning [2,6]. The defect of this approach is unclear correspondence between the reparametrization-noninvariant mathematical quantities and the invariant physical observables of the type of measurable time and energy; the quantum version of the first approach looks as attractable mathematical games with unnormalizable wave functions that are free from clear physical predictions.

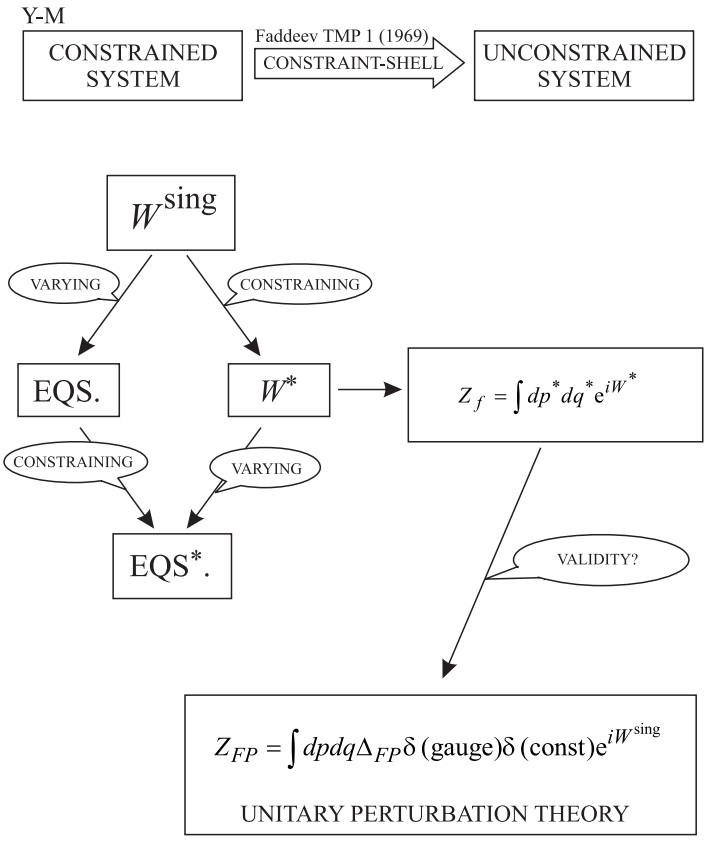

Fig. 2. An equivalent unconstrained system $W^*(p^*, q^*)$ can be obtained in the case when the operations of varying and constraining commute with each other to obtain equations (EQS.) of motion in terms of independent variables p^*, q^*. The next problem is to establish the range of validity of the standard Faddeev–Popov (FP) integral

The second approach is the reparametrization-invariant reduction of an action by the explicit resolving of the first class constraints to get an equivalent unconstrained system (see Fig. 2), so that one of the variables of the extended phase space (with a negative contribution to the energy constraint) converts into the *dynamic evolution parameter*, and its conjugate momentum becomes the nonzero Hamiltonian of evolution [3, 4, 7, 13–16].

An example of the application of such an invariant reduction of the action is the Dirac formulation of QED [17] directly in terms of the gauge-invariant (dressed) fields as the proof of the adequateness of the Coulomb gauge with the invariant content of classical equations. As was shown by Faddeev [18], the invariant reduction of the action is the way to obtain the unconstrained Feynman

integral for the foundation of the intuitive Faddeev–Popov functional integral in the non-Abelian gauge theories [19–21] (see Fig. 2).

In reparametrization-invariant relativistic theories, the constraining of actions does not kill superfluous variables. They are kept in the constrained action as the evolution parameter and the corresponding Hamiltonian. This fact is the main difference of reparametrization-invariant systems from the gauge-invariant ones where the operation of constraining removes all longitudinal components from the action. This difference explains why the gauge fixing is not compatible with reparametrization invariance.

To emphasize the importance of the superfluous variables in relativistic systems, we introduce the notion of the sector of «measurable quantities» including in it (together with the sector of the Dirac observables) the superfluous variables which cannot be removed by the gauge fixing, and which play important physical roles of the dynamic evolution parameter and the corresponding evolution Hamiltonian.

In special relativity (SR), the sector of «measurable quantities» coincides with the world space. The causal structure of this world space (given in the form of the light cones of future and past) determines the causal Green functions and the arrow of the *geometric time*. The latter is defined as the reparametrization-invariant geometric interval that is always greater than zero in accordance with equations of motion.

The application of the invariant reduction of extended actions in cosmology and general relativity [4, 7] allows one to formulate the dynamics of relativistic systems directly in terms of the invariant geometric time with the nonzero Hamiltonian of evolution, instead of the non-invariant coordinate time with the generalized zero Hamiltonian of evolution in the gauge-fixing method. The formulation in terms of the geometric time is based on the Levi-Civita canonical transformation [22–24] that converts the energy constraint into a new momentum, so that the new dynamic evolution parameter coincides with the geometric time, as one of the consequences of new equations of motion.

In the present paper, we apply the method of the invariant Hamiltonian reduction (with resolving the first class constraints and the Levi-Civita canonical transformations) to express reparametrization-invariant dynamics of relativistic systems in terms of the geometric time and to construct the causal Green functions in the form of the path integrals in the world space of dynamic variables.

The content of the paper is the following. In Section 2, we consider the extended version of classical mechanics. A relativistic particle is considered in Section 3. Section 4 is devoted to the generalized Hamiltonian formulation of a relativistic string and its invariant reduction. Section 5 is devoted to the reparametrization-invariant Hamiltonian reduction of general relativity. In Section 6, we discuss the reparametrization-invariant dynamics of the Early Universe. Section 7 is devoted to conformal relativity.

2. INVARIANT HAMILTONIAN REDUCTION: MECHANICS

To illustrate the time-reparametrization-invariant Hamiltonian reduction [4] and its difference from the gauge-fixing method, let us consider an extended form of a classical-mechanical system

$$W = \int\limits_{\tau^1}^{\tau_2} d\tau \left(p\dot{q} - \Pi_0 \dot{Q}_0 - \lambda[-\Pi_0 + H(p,q)] \right), \tag{1}$$

that is invariant under reparametrizations of the coordinate evolution parameter τ and «lapse» function λ

$$\tau \to \tau' = \tau'(\tau), \qquad \lambda \ \to \ \lambda' = \lambda \frac{d\tau}{d\tau'}. \tag{2}$$

The problem of the classical description is to obtain the evolution of the physical variables of the *world space* q, Q_0 in terms of the *geometric time* T defined as

$$dT := \lambda d\tau, \qquad T = \int\limits_0^{\tau} d\tau' \lambda(\tau'), \tag{3}$$

that is also invariant under reparametrizations (2).

The second problem (connected with quantization) is to present the effective action of the equivalent unconstrained theory directly in terms of T, the equations of which reproduce this evolution. The solution of the second problem will be called the *invariant Hamiltonian reduction*.

The resolving of the first problem for the considered system is trivial, as the equations of motion of this system

$$\dot{q} = \lambda \partial_p H, \qquad \dot{p} = -\lambda \partial_q H, \qquad \dot{Q}_0 = \lambda, \qquad \dot{\Pi}_0 = 0 \tag{4}$$

in terms of the geomeric time (3)

$$\frac{dq}{dT} = \partial_p H, \qquad \frac{dp}{dT} = -\partial_q H, \qquad \frac{dQ_0}{dT} = 1, \qquad \frac{d\Pi_0}{dT} = 0 \tag{5}$$

are completely equivalent to the equations of the conventional unconstrained mechanics in the *reduced phase space* (p, q)

$$W^M = \int\limits_{T(\tau_1)=T_1}^{T(\tau_2)=T_2} dT \left(p \frac{dq}{dT} - H(p,q) \right). \tag{6}$$

The problem is how to derive this system from the extended one (1) to apply the symplest Hamiltonian quantization with a clear physical interpretation of the invariant quantities.

The solution of the problem of the *invariant Hamiltonian reduction* considered in the present review is the explicit resolving of three equations of the extended system (1):
i) for the variable λ (treated as constraint)

$$\frac{\delta W}{\delta \lambda} = -\Pi_0 + H(p,q) = 0, \tag{7}$$

ii) for the momentum Π_0 with a negative contribution to the constraint (7)

$$\frac{\delta W}{\delta \Pi_0} = 0 \;\Rightarrow\; \frac{dQ_0}{d\tau} = \lambda, \tag{8}$$

iii) for its conjugate variable Q_0

$$\frac{\delta W}{\delta Q_0} = \frac{d\Pi_0}{d\tau} = 0. \tag{9}$$

(We call these three equations (7)–(9) the *geometric sector*.)

The resolving of the constraint (7) expresses the «ignorable» momentum Π_0 through $H(p,q)$ with a positive value $\Pi_0 = H(p,q) > 0$. The second equation (8) identifies the *dynamic evolution parameter* Q_0 with the proper time (3) $Q_0 = T$. It is not the gauge but the invariant solution of the equation of motion (8). The third equation (9) is the conservation law.

As a result of the invariant Hamiltonian reduction (i.e., a result of the substitution of $\Pi_0 = H$ and $Q_0 = T$ into the initial action (1)) this action is reduced to the one of the conventional mechanics (6) in terms of the proper time T, where the role of the nonzero Hamiltonian of evolution in the proper time T is played by the constraint-shell value of the «ignorable» momentum $\Pi_0 = H(p,q)$. In other words, this constraint-shell action $W(\text{constraint}) = W^M$ determines the nonzero Hamiltonian $H(p,q)$ in the proper time T, instead of the zero generalized Hamiltonian in the coordinate time τ in (1) $\lambda(-\Pi_0 + H)$.

Thus, the equivalent unconstrained system was constructed without any additional constraint of the type:

$$\lambda = 1, \qquad\qquad \tau = T \tag{10}$$

which confuse quantities of the measurable sector with noninvariant ones. This confusion is contradictable. The «gauge-fixing» identification of the coordinate evolution parameter τ and the geometric time $T = \lambda\tau$ in the form of the gauges (10) contradicts the difference of their Hamiltonians $\lambda(-\Pi_0 + H) \neq H(p,q)$.

The second difference of the «gauge-fixing» from the invariant Hamiltonian reduction is more essential, namely, the formulation of the theory in terms of the invariant geometric time (3) is achieved by the explicit resolving of the constraint (7) and equation of motion (8), as a result of which «ignorable» variables Π_0, Q_0 are excluded from the phase space.

In the present paper, we apply the invariant Hamiltonian reduction to relativistic particle, string, and general relativity.

3. SPECIAL RELATIVITY

3.1. Statement of the Problem. To answer the question: Why is the reparametrization-invariant reduction needed?, let us consider relativistic mechanics in the Hamiltonian form

$$W[P, X|N|\tau_1, \tau_2] = \int\limits_{\tau_1}^{\tau_2} d\tau[-P_\mu \dot{X}^\mu - \frac{N}{2m}(-P_\mu^2 + m^2)], \tag{11}$$

which is classically equivalent to the conventional square root form

$$W[X|\tau_1, \tau_2] = -m \int\limits_{\tau_1}^{\tau_2} d\tau \sqrt{\dot{X}^\mu \dot{X}_\mu}. \tag{12}$$

Both these actions are invariant with respect to reparametrizations of the *coordinate evolution parameter*

$$\tau \to \tau' = \tau'(\tau), \qquad N' d\tau' = N d\tau \tag{13}$$

given in the one-dimensional space with the invariant interval

$$dT := N d\tau, \qquad T = \int\limits_0^\tau d\bar{\tau} N(\bar{\tau}). \tag{14}$$

We called this invariant interval the *geometric time* [4] whereas the dynamic variable X_0 (with a negative contribution in the constraint) we called *dynamic evolution parameter*.

In terms of the geometric time (14) the classical equations of the generalized Hamiltonian system (11) take the form

$$\frac{dX_\mu}{dT} = \frac{P_\mu}{m}, \qquad \frac{dP_\mu}{dT} = 0, \qquad P_\mu^2 - m^2 = 0. \tag{15}$$

The classical problem is to find the evolution of the world space variables with respect to the geometric time T.

The quantum problem is to obtain the equivalent unconstrained theories directly in terms of the invariant times X_0 or T with the invariant Hamiltonians of evolution. The solution of the second problem is called the dynamic (for X_0), or geometric (for T) *reparametrization-invariant Hamiltonian reductions*.

3.2. Dynamic Unconstrained System. The dynamic reduction of the action (11) means the substitution of the explicit resolving of the energy constraint $(-P_\mu^2 + m^2) = 0$ with respect to the momentum P_0 into this action

$$\frac{\delta W}{\delta N} = 0 \quad \Rightarrow \quad P_0 = \pm\sqrt{m^2 + P_i^2}. \tag{16}$$

In accordance with two signs of the solution (16), after the substitution of (16) into (11), we have two branches of the dynamic unconstrained system

$$W(\text{constraint}) = W_\pm^D = \int\limits_{X_0(\tau_1)=X_0(1)}^{X_0(\tau_2)=X_0(2)} dX_0 \left[P_i \frac{dX_i}{dX_0} \mp \sqrt{m^2 + P_i^2}\right]. \tag{17}$$

The role of the time of evolution, in this action, is played by the variable X_0 that abandons the Dirac sector of «observables» P_i, X_i, but not the sector of «measurable» quantities. At the same time, its conjugate momentum P_0 converts into the corresponding Hamiltonian of evolution, values of which are energies of a particle.

This invariant reduction of the action gives an «equivalent» unconstrained system together with definition of the dynamic evolution parameter (X_0) corresponding to a nonzero Hamiltonian P_0.

Thus, we need the reparametrization-invariant Hamiltonian reduction to determine the dynamic evolution parameter and its invariant Hamiltonian for a reparametrization-invariant system and to apply the symplest canonical quantization to it.

In quantum relativistic theory, we get two Schrödinger equations

$$i\frac{d}{dX_0}\Psi_{(\pm)}(X|P) = \pm\sqrt{m^2 + P_i^2}\Psi_{(\pm)}(X|P), \tag{18}$$

with positive and negative values of P_0 and normalized wave functions

$$\Psi_\pm(X|P) = \frac{A_P^\pm \theta(\pm P_0)}{(2\pi)^{3/2}\sqrt{2P_0}} \exp\left(-iP_\mu X^\mu\right) \qquad \left([A_P^-, A_{P'}^+] = \delta^3(P_i - P_i')\right). \tag{19}$$

The coefficient A_P^+, in the secondary quantization, is treated as the operator of creation of a particle with positive energy; and the coefficient A_P^-, as the operator

of annihilation of a particle also with positive energy. The physical states are formed by action of these operators on the vacuum $\langle 0|, |0\rangle$ in the form of out-state ($|P\rangle = A_P^+|0\rangle$) with positive frequencies and in-state ($\langle P| = \langle 0|A_P^-$) with negative frequencies. This treatment means that positive frequencies propagate forward ($X_{02} > X_{01}$); and negative frequencies, backward ($X_{01} > X_{02}$), so that the negative values of energy are excluded from the spectrum to provide the stability of the quantum system in QFT [25]. For this causal convention the geometric time (14) is always positive in accordance with the equations of motion (15)

$$\left(\frac{dT}{dX_0}\right)_{\pm} = \pm\frac{m}{\sqrt{P_i^2+m^2}} \;\;\Rightarrow\;\; T(X_{02},X_{01}) = \pm\frac{m}{\sqrt{P_i^2+m^2}}(X_{02}-X_{01}) \geqslant 0. \tag{20}$$

In other words, instead of changing the sign of energy, we change that of the dynamic evolution parameter, which leads to the arrow of the geometric time (20) and to the causal Green function

$$\begin{aligned} G^c(X) &= G_+(X)\theta(X_0) + G_-(X)\theta(-X_0) = \\ &= i\int \frac{d^4P}{(2\pi)^4}\exp(-iPX)\frac{1}{P^2-m^2-i\epsilon}, \end{aligned} \tag{21}$$

where $G_+(X) = G_-(-X)$ is the «commutative» Green function [25]

$$G_+(X) = \int \frac{d^4P}{(2\pi)^3}\exp(-iPX)\delta(P^2-m^2)\theta(P_0) = \tag{22}$$

$$= \frac{1}{2\pi}\int d^3P d^3P' \langle 0|\Psi_-(X|P)\Psi_+(0|P')|0\rangle.$$

3.3. Path Integral for the Causal Green Functions. The question appears: How to construct the path integral without gauges?

To obtain the reparametrization-invariant form of the functional integral adequate to the considered gaugeless reduction (17) and the causal Green function (21), we use the version of composition law for the commutative Green function with the integration over the whole measurable sector $X_{1\mu}$

$$G_+(X-X_0) = \int G_+(X-X_1)\bar{G}_+(X_1-X_0)dX_1 \qquad \left(\bar{G}_+ = \frac{G_+}{2\pi\delta(0)}\right), \tag{23}$$

where $\delta(0) = \int dN$ is the infinite volume of the group of reparametrizations of

the coordinate τ. Using the composition law n times, we got the multiple integral

$$G_+(X-X_0)=\int G_+(X-X_1)\prod_{k=1}^{n}\bar{G}_+(X_k-X_{k+1})dX_k,\qquad (\ X_{n+1}=X_0\ ). \tag{24}$$

The continual limit of the multiple integral with the integral representation for δ function

$$\delta(P^2-m^2)=\frac{1}{2\pi}\int dN\exp\left[iN(P^2-m^2)\right]$$

can be defined as the path integral in the form of the average over the group of reparametrizations

$$G_+(X)=\int\limits_{X(\tau_1)=0}^{X(\tau_2)=X}\frac{dN(\tau_2)d^4P(\tau_2)}{(2\pi)^3}\prod_{\tau_1\leqslant\tau<\tau_2}\left\{d\bar{N}(\tau)\prod_{\mu}\left(\frac{dP_\mu(\tau)dX_\mu(\tau)}{2\pi}\right)\right\}\times$$

$$\times\exp\left(iW[P,X|N|\tau_1,\tau_2]\right), \tag{25}$$

where $\bar{N}=N/2\pi\delta(0)$, and W is the initial extended action (11).

3.4. Geometric Unconstrained System. The Hamiltonian of the unconstrained system in terms of the geometric time T can be obtained by the canonical Levi-Civita-type transformation [12, 22, 23]

$$(P_\mu,X_\mu)\Rightarrow\ (\Pi_\mu,Q_\mu) \tag{26}$$

to the variables (Π_μ,Q_μ) for which one of equations identifies Q_0 with the geometric time T. This transformation [22] converts the constraint into a new momentum

$$\Pi_0=\frac{1}{2m}[P_0^2-P_i^2],\qquad \Pi_i=P_i,\quad Q_0=X_0\frac{m}{P_0},\qquad Q_i=X_i-X_0\frac{P_i}{P_0} \tag{27}$$

and has the inverted form

$$P_0=\pm\sqrt{2m\Pi_0+\Pi_i^2},\ P_i=\Pi_i,\ X_0=\pm Q_0\frac{\sqrt{2m\Pi_0+\Pi_i^2}}{m},\ \ X_i=Q_i+Q_0\frac{\Pi_i}{m}. \tag{28}$$

After transformation (27) the action (11) takes the form

$$W=\int\limits_{\tau_1}^{\tau_2}d\tau\left[-\Pi_\mu\dot{Q}^\mu-N(-\Pi_0+\frac{m}{2})-\frac{d}{d\tau}S^{lc}\right],\qquad S^{lc}=(Q_0\Pi_0). \tag{29}$$

The invariant reduction is the resolving of the constraint $\Pi_0 = m/2$ which determines a new Hamiltonian of evolution with respect to the new dynamic evolution parameter Q_0, whereas the equation of motion for this momentum Π_0 identifies the dynamic evolution parameter Q_0 with the geometric time T ($dQ_0 = dT$). The substitution of these solutions into the action (29) leads to the reduced action of a geometric unconstrained system

$$W(\text{constraint}) = W^G = \int\limits_{T_1}^{T_2} dT \left(\Pi_i \frac{dQ_i}{dT} - \frac{m}{2} - \frac{d}{dT}(S^{lc}) \right) \qquad (S^{lc} = Q_0 \frac{m}{2}), \tag{30}$$

where variables Π_i, Q_i are cyclic ones and have the meaning of initial conditions in the comoving frame

$$\frac{\delta W}{\delta \Pi_i} = \frac{dQ_i}{d\tau} = 0 \Rightarrow Q_i = Q_i^{(0)}, \qquad \frac{\delta W}{\delta Q_i} = \frac{d\Pi_i}{d\tau} = 0 \Rightarrow \Pi_i = \Pi_i^{(0)}. \tag{31}$$

The substitution of all geometric solutions

$$Q_0 = T, \quad \Pi_0 = \frac{m}{2}, \quad \Pi_i = \Pi_i^{(0)} = P_i, \quad Q_i = Q_i^{(0)} \tag{32}$$

into the inverted Levi-Civita transformation (28) leads to the conventional relativistic solution for the dynamical system

$$P_0 = \pm\sqrt{m^2 + P_i^2}, \qquad P_i = \Pi_i^{(0)}, \qquad X_0(T) = T\frac{P_0}{m}, \qquad X_i(T) = X_i^{(0)} + T\frac{P_i}{m}. \tag{33}$$

The Schrödinger equation for the wave function

$$\frac{d}{idT}\Psi^{lc}(T, Q_i|\Pi_i) = \frac{m}{2}\Psi^{lc}(T, Q_i|\Pi_i), \tag{34}$$

$$\Psi^{lc}(T, Q_i|\Pi_i) = \exp\left(-iT\frac{m}{2}\right)\exp\left(i\Pi_i^{(0)}Q_i\right)$$

contains only one eigenvalue $m/2$ degenerated with respect to the cyclic momentum Π_i. We see that there are differences between the dynamic and geometric descriptions. The dynamic evolution parameter is given in the whole region $-\infty < X_0 < +\infty$, whereas the geometric one is only positive $0 < T < +\infty$, as it follows from the properties of the causal Green function (21) after the Levi-Civita transformation (27)

$$G^c(Q_\mu) = \int\limits_{-\infty}^{+\infty} d^4\Pi_\mu \frac{\exp\left(iQ^\mu\Pi_\mu\right)}{2m(\Pi_0 - m/2 - i\epsilon/2m)} = \frac{\delta^3(Q)}{2m}\theta(T), \qquad T = Q_0.$$

Two solutions of the constraint (a particle and antiparticle) in the dynamic system correspond to a single solution in the geometric system.

Thus, the reparametrization-invariant content of the equations of motion of a relativistic particle in terms of the geometric time is covered by two «equivalent» unconstrained systems: the dynamic and geometric. In both the systems, the invariant times are not *the coordinate evolution parameter*, but variables with the negative contribution into the energy constraint. The Hamiltonian description of a relativistic particle in terms of the geometric time can be achieved by the Levi-Civita-type canonical transformation, so that the energy constraint converts into a new momentum. Whereas, the dynamic unconstrained system suits for the secondary quantization and the derivation of the causal Green function that determine the arrow of the geometric time.

4. RELATIVISTIC STRING

4.1. The Generalized Hamiltonian Formulation. We begin with the action for a relativistic string in the geometrical form [26–28]

$$W = -\frac{\gamma}{2}\int d^2u\sqrt{-g}g^{\alpha\beta}\partial_\alpha x^\mu \partial_\beta x_\mu, \qquad u_\alpha = (u_0, u_1), \tag{35}$$

where the variables x_μ are string coordinates given in a space-time with a dimension D and the metric $(x_\mu x^\mu := x_0^2 - x_i^2)$; $g_{\alpha\beta}$ is a second-rank metric tensor given in the two-dimensional Riemannian space $u_\alpha = (u_0, u_1)$.

To formulate the Hamiltonian approach, one needs to separate the two-dimensional Riemannian space $u_\alpha = (u_0, u_1)$ on the set of space-like lines $\tau = \text{constant}$ in the form of the Dirac–Arnovitt–Deser–Misner parametrization of the two-dimensional metric

$$g_{\alpha,\beta} = \Omega^2 \begin{pmatrix} \lambda_1^2 - \lambda_2^2 & \lambda_2 \\ \lambda_2 & -1 \end{pmatrix}, \qquad \sqrt{-g} = \Omega^2\lambda_1 \tag{36}$$

with the invariant interval [2]

$$ds^2 = g_{\alpha\beta}du^\alpha du^\beta = \Omega^2[\lambda_1^2 d\tau^2 - (d\sigma + \lambda_2 d\tau)^2], \qquad u_\alpha = (u_0 = \tau, u_1 = \sigma), \tag{37}$$

where λ_1 and λ_2 are known in general relativity (GR) as the lapse function and shift «vector», respectively [29, 30]. The action (35) after the substitution (37) does not depend on the conformal factor Ω and takes the form

$$W = -\frac{\gamma}{2}\int\limits_{\tau_1}^{\tau_2} d\tau \int\limits_{\sigma_1(\tau)}^{\sigma_2(\tau)} d\sigma \left[\frac{(D_\tau x)^2}{\lambda_1} - \lambda_1 x'^2\right], \tag{38}$$

where

$$D_\tau x_\mu = \dot{x}_\mu - \lambda_2 x'_\mu \qquad (\dot{x} = \partial_\tau x,\ x' = \partial_\sigma x) \tag{39}$$

is the covariant derivative with respect to the two-dimensional metric (37). The metric (37), the action (38), and the covariant derivative (39) are invariant under the transformations

$$\tau \Rightarrow \widetilde{\tau} = f_1(\tau), \qquad \sigma \Rightarrow \widetilde{\sigma} = f_2(\tau, \sigma). \tag{40}$$

A similar group of transformations in GR is well-known as the «kinemetric» group of diffeomorphisms of the Hamiltonian description [31].

The variation of action (38) with respect to λ_1 and λ_2 leads to the equations

$$\frac{\delta W}{\delta \lambda_2} = \frac{x' D_\tau x}{\lambda_1} = 0 \ \Rightarrow\ \lambda_2 = \frac{\dot{x}x'}{x'^2}, \tag{41}$$

$$\frac{\delta W}{\delta \lambda_1} = \frac{(D_\tau x)^2}{\lambda_1^2} + x'^2 = 0 \ \Rightarrow\ \ \lambda_1^2 = \frac{(\dot{x}x')^2 - \dot{x}^2 x'^2}{(x'^2)^2}.$$

The solutions of these equations convert the action (38) into the standard Nambu–Gotto action of a relativistic string [28, 32]

$$W = -\gamma \int\limits_{\tau_1}^{\tau_2} d\tau \int\limits_{\sigma_1(\tau)}^{\sigma_2(\tau)} d\sigma \sqrt{(\dot{x}x')^2 - \dot{x}^2 x'^2}.$$

The generalized Hamiltonian form [8] is obtained by the Legendre transformation [10] of the action (38)

$$W = \int\limits_{\tau_1}^{\tau_2} d\tau \int\limits_{\sigma_1(\tau)}^{\sigma_2(\tau)} d\sigma \left(-p_\mu D_\tau x^\mu + \lambda_1 \phi_1\right) = \int\limits_{\tau_1}^{\tau_2} d\tau \int\limits_{\sigma_1(\tau)}^{\sigma_2(\tau)} d\sigma \left(-p_\mu \dot{x}^\mu + \lambda_1 \phi_1 + \lambda_2 \phi_2\right), \tag{42}$$

where

$$\phi_1 = \frac{1}{2\gamma}[p_\mu^2 + (\gamma x'_\mu)^2], \qquad \phi_2 = x'^\mu p_\mu, \tag{43}$$

and the generalized Hamiltonian

$$\mathcal{H} = \lambda_1 \phi_1 + \lambda_2 \phi_2 \tag{44}$$

is treated as the generator of evolution with respect to the coordinate time τ, and λ_1, λ_2 play the role of variables with the zero momenta

$$P_{\lambda_1} = 0, \qquad P_{\lambda_2} = 0 \tag{45}$$

considered as the first class primary constraints [8, 10]. The equations for λ_1, λ_2

$$\frac{\delta W}{\delta \lambda_1} = \phi_1 = 0, \qquad \frac{\delta W}{\delta \lambda_2} = \phi_2 = 0 \tag{46}$$

are known as the first class secondary constraints [8, 10]. The Hamiltonian equations of motion take the form

$$\frac{\delta W}{\delta x^\mu} = \dot{p}_\mu - \partial_\sigma[\gamma\lambda_1 x'_\mu + \lambda_2 p_\mu] = 0, \qquad \frac{\delta W}{\delta p^\mu} = p_\mu - \gamma\frac{D_\tau x_\mu}{\lambda_1} = 0. \tag{47}$$

The problem is to find solutions of the Hamiltonian equations of motion (47) and constraints (46) which are invariant with respect to the kinemetric transformations (40).

There is the problem of the solution of the linearized «gauge-fixing» equation in terms of the evolution parameter τ (as the object reparametrizations in the initial theory) being adequate to the initial kinemetric invariant and relativistic invariant system. In particular, the constraints mix the global motion of the «centre-of-mass» coordinates with local excitations of a string ξ_μ, which contradicts the relativistic invariance of internal degrees of freedom of a string. In this context, it is worth to clear up a set of questions: Is it possible to introduce the reparametrization-invariant evolution parameter for the string dynamics, instead of the noninvariant coordinate time (τ) used as the evolution parameter in the gauge-fixing method? Is it possible to construct the observable nonzero Hamiltonian of evolution of the «centre-of-mass» coordinates? What is relation of the «centre-of-mass» evolution to the unitary representations of the Poincare group?

4.2. The Separation of the «Centre-of-Mass» Coordinates. To apply the reparametrization-invariant Hamiltonian reduction discussed before to a relativistic string, one should define the *proper (geometric) time* in the form of the reparametrization-invariant functional of the lapse function (of type (14)), and to point out, among the variables, a *dynamic evolution parameter*, the equation of which identifies it with the proper time of type (8). We identify this *dynamic evolution parameter* with the time-like variable of the centre of mass of a string defined as the total coordinate

$$X_\mu(\tau) = \frac{1}{l(\tau)} \int\limits_{\sigma_1(\tau)}^{\sigma_2(\tau)} d\sigma x_\mu(\tau, \sigma), \qquad l(\tau) = \sigma_2(\tau) - \sigma_1(\tau). \tag{48}$$

Therefore, the invariant reduction requires to separate the «centre-of-mass» variables before variation of the action. We consider this separation on the level of the action (38) which after the substitution

$$x_\mu(\tau,\ \sigma) = X_\mu(\tau) + \xi_\mu(\tau,\ \sigma), \qquad x'_\mu(\tau,\ \sigma) = \xi'_\mu(\tau,\ \sigma) \tag{49}$$

takes the form

$$W = -\frac{\gamma}{2}\int\limits_{\tau_1}^{\tau_2} d\tau \left\{ \frac{\dot{X}^2 l(\tau)}{N_0(\tau)} + 2\dot{X}_\mu \int\limits_{\sigma_1(\tau)}^{\sigma_2(\tau)} d\sigma \frac{D_\tau \xi^\mu}{\lambda_1} + \int\limits_{\sigma_1(\tau)}^{\sigma_2(\tau)} d\sigma \left(\frac{(D_\tau \xi)^2}{\lambda_1} - \lambda_1 \xi'^2 \right) \right\}, \tag{50}$$

where the global lapse function $N_0(\tau)$ is defined as the functional of $\lambda_1(\tau, \sigma)$

$$\frac{1}{N_0[\lambda_1]} = \frac{1}{l(\tau)} \int\limits_{\sigma_1(\tau)}^{\sigma_2(\tau)} d\sigma \frac{1}{\lambda_1(\tau, \sigma)}. \tag{51}$$

To exclude the superfluous coordinates and momenta, the local variables ξ_μ are given (according to (48) and (49)) in the class of functions (with the nonzero Fourier harmonics) which satisfy the conditions

$$\int\limits_{\sigma_1(\tau)}^{\sigma_2(\tau)} d\sigma \xi_\mu = 0. \tag{52}$$

A definition of the conjugate momenta is consistent with (48) and the equation for the momentum p_μ (47) of the local momentum is given in the same class (52)

$$\int\limits_{\sigma_1(\tau)}^{\sigma_2(\tau)} d\sigma \frac{D_\tau \xi^\mu}{\lambda_1} = 0 \ . \tag{53}$$

Then we get

$$P_\mu = \int\limits_{\sigma_1(\tau)}^{\sigma_2(\tau)} d\sigma p_\mu(\tau, \sigma) = \frac{\delta W}{\delta \dot{X}^\mu} = -\gamma \frac{\dot{X}_\mu l}{N_0}, \quad \pi_\mu = \frac{\delta W}{\delta \dot{\xi}^\mu} = \gamma \frac{D_\tau \xi^\mu}{\lambda_1}. \tag{54}$$

This separation conserves the group of diffeomorphisms of the Hamiltonian [4] and leads to the Bergmann–Dirac generalized action

$$W = \int\limits_{\tau_1}^{\tau_2} d\tau \left[\left(\int\limits_{\sigma_1(\tau)}^{\sigma_2(\tau)} d\sigma [-\pi_\mu D_\tau \xi^\mu - \lambda_1 \mathcal{H}] \right) - P_\mu \dot{X}^\mu + N_0 \frac{P_\mu^2}{2\bar{\gamma}} \right] \quad (\bar{\gamma} = \gamma l(\tau)), \tag{55}$$

where $\mathcal{H}$ is the Hamiltonian of local excitations

$$\mathcal{H} = -\frac{1}{2\gamma}[\pi_\mu^2 + (\gamma \xi'_\mu)^2] \ . \tag{56}$$

The variation of the action (55) with respect to λ_1 results in the equation

$$\frac{\delta W}{\delta \lambda_1} = \mathcal{H} - \left(\frac{1}{l\bar{\lambda}_1^2}\right)\frac{P^2}{2\bar{\gamma}} = 0, \tag{57}$$

where

$$\bar{\lambda}_1(\tau,\sigma) = \frac{\lambda_1(\tau,\sigma)}{N_0(\tau)} \tag{58}$$

is the reparametrization-invariant component of the local lapse function. Here we have used the variation of the functional $N_0[\lambda_1]$ (51)

$$\frac{\delta N_0[\lambda_1]}{\delta \lambda_1} = \frac{1}{l(\tau)\bar{\lambda}_1^2}.$$

In accordance with our separation of dynamic variables onto the global and local sectors, the first class constraint (57) has two projections onto the global sector (zero Fourier harmonic) and the local one. The global part of the constraint (57) can be obtained by variation of the action (55) with respect to N_0 (after the substitution of (58) into (55))

$$\frac{\delta W}{\delta N_0} = \frac{P^2}{2\bar{\gamma}} - H = 0, \qquad H = \int\limits_{\sigma_1}^{\sigma_2} d\sigma \bar{\lambda}_1 \mathcal{H}, \tag{59}$$

or, in another way, by the integration of (57) multiplied by λ_1. Then, the local part of the constraint (57) can be obtained by the substitution of (59) into (57)

$$\bar{\lambda}_1\mathcal{H} - \frac{1}{l\bar{\lambda}_1}\int\limits_{\sigma_1}^{\sigma_2} d\sigma \bar{\lambda}_1 \mathcal{H} = 0. \tag{60}$$

The integration of the local part over σ is equal to zero if we take into account the normalization of the local lapse function

$$\frac{1}{l(\tau)}\int\limits_{\sigma_1(\tau)}^{\sigma_2(\tau)} d\sigma \frac{1}{\bar{\lambda}_1} = 1. \tag{61}$$

This follows from the definition of the global lapse function (51). We see that the local part (60) takes the form of an integral operator, orthogonal to the operator of integration over σ.

Finally, we can represent the action (55) in the equivalent form

$$W = \int\limits_{\tau_1}^{\tau_2} d\tau \left[\left(\int\limits_{\sigma_1(\tau)}^{\sigma_2(\tau)} d\sigma[-\pi_\mu D_\tau \xi^\mu]\right) - P_\mu \dot{X}^\mu - N_0\left(-\frac{P_\mu^2}{2\bar{\gamma}} + \mathcal{N}H\right)\right], \tag{62}$$

where the global lapse function N_0 and the local one $\bar{\lambda}_1$ are treated as independent variables, with taking the normalization (61) into account after the variation.

The invariant proper time T measured by the watch of an observer in the «centre-of-mass» frame of a string is given by the expression (according to (40) and (51))

$$\sqrt{\gamma}dT := N_0 d\tau = d\bar{\tau}, \quad \bar{\tau} = \int\limits_0^{\tau} d\tau' \left[\frac{1}{l(\tau')} \int\limits_{\sigma_1(\tau)}^{\sigma_2(\tau)} d\sigma \frac{1}{\lambda_1(\tau', \sigma)} \right]^{-1}. \qquad (63)$$

We include the constant $\sqrt{\gamma}$ to provide the dimension of the time measured by the watch of an observer.

Now we can see from (62) that the dynamics of the local degrees of freedom π, ξ, in the class of functions of nonzero harmonics (52), is described by the same kinemetric invariant and relativistic covariant equations (47) where x, p are changed by ξ, π, with the set of the first class (primary and secondary) constraints

$$P_{\lambda_1} = 0, \qquad P_{\lambda_2} = 0, \qquad \pi_\mu \xi'^\mu = 0, \qquad \bar{\lambda}_1 \mathcal{H} - \frac{1}{l\bar{\lambda}_1} \int\limits_{\sigma_1}^{\sigma_2} d\sigma \bar{\lambda}_1 \mathcal{H} = 0. \qquad (64)$$

We see that the separation of the «centre-of-mass» (CM) variables on the level of the action removes the interference terms which mix the CM variables with the local degrees of freedom; as a result, the new local constraints (64) do not depend on the total momentum P_μ, in contrast to the standard ones (92). In other words, there is the problem: when can one separate the CM coordinates of a relativistic string — before the variation of the action or after the variation of the action? The relativistic invariance dictates the first one, because an observer in the CM frame (which is the preferred frame for a string) cannot measure the total momentum of the string.

The first class local constraints (64) can be supplemented by the second class constraints

$$\bar{\lambda}_1 - 1 = 0, \qquad \lambda_2 = 0, \qquad n^\mu \xi_\mu = 0, \qquad n^\mu \pi_\mu = 0 \qquad (\ n_\mu = (1, 0, 0, 0)\ ) \quad (65)$$

so that the equations of the local constraint-shell action

$$W(\text{loc.constrs.}) = \int\limits_{\tau_1}^{\tau_2} d\tau \left[\left(\int\limits_{\sigma_1(\tau)}^{\sigma_2(\tau)} d\sigma \pi_i \dot{\xi}_i \right) - P_\mu \dot{X}^\mu - N_0 \left(-\frac{P_\mu^2}{2\bar{\gamma}} + H \right) \right] \quad (66)$$

coincide with the complete set of equations and the same constraints (64), (65) of the extended action, i.e., the operations of constraining and variation commute.

The substitution of the global constraint (59) with $\bar{\lambda}_1 = 1$ into the action (66) leads to the constraint-shell action

$$W_{\pm}^{D} = \int\limits_{X_0(\tau_1)}^{X_0(\tau_2)} dX_0 \left[\left(\int\limits_{\sigma_1(X_0)}^{\sigma_2(X_0)} d\sigma \pi_i \frac{d\xi_i}{dX_0} \right) + P_i \frac{dX_i}{dX_0} \mp \sqrt{P_i^2 + 2\bar{\gamma} H} \right]. \quad (67)$$

This action describes the dynamics of a relativistic string with respect to the time measured by an observer in the rest frame with the physical nonzero Hamiltonian of evolution. However, in this system, equations become nonlinear. To overcome this difficulty, we pass to the «centre-of-mass» frame.

4.3. Levi-Civita Geometrical Reduction. To express the dynamics of a relativistic string in terms of the proper time (63) measured by an observer in the comoving (i.e., «centre-of-mass») frame, we use the Levi-Civita–type canonical transformations [22, 24]

$$(P_\mu, X_\mu) \Rightarrow (\Pi_\mu, Q_\mu);$$

they convert the global part of the constraint (59) into a new momentum Π_0

$$\Pi_0 = \frac{1}{2\bar{\gamma}}[P_0^2 - P_i^2], \qquad \Pi_i = P_i, \qquad Q_0 = X_0 \frac{\bar{\gamma}}{P_0}, \qquad Q_i = X_i - X_0 \frac{P_i}{P_0}. \quad (68)$$

The inverted form of these transformations is

$$P_0 = \pm\sqrt{2\bar{\gamma}\Pi_0 + \Pi_i^2}, \;\; P_i = \Pi_i, \;\; X_0 = \pm Q_0 \frac{\sqrt{2\bar{\gamma}\Pi_0 + \Pi_i^2}}{\bar{\gamma}}, \;\; X_i = Q_i + Q_0 \frac{\Pi_i}{\bar{\gamma}}. \quad (69)$$

As a result of transformations (68), the extended action (62) in terms of the Levi-Civita geometrical variables takes the form (compare with (1))

$$W = \int\limits_{\tau_1}^{\tau_2} d\tau \left[\left(\int\limits_{\sigma_1(\tau)}^{\sigma_2(\tau)} d\sigma [-\pi_\mu D_\tau \xi^\mu] \right) - \Pi_\mu \dot{Q}^\mu - N_0(-\Pi_0 + H) - \frac{d}{d\tau}(Q_0 \Pi_0) \right]. \quad (70)$$

The Hamiltonian reduction means to resolve constraint (59) with respect to the momentum Π_0

$$\frac{\delta W}{\delta N_0} = 0 \Rightarrow \Pi_0 = H. \quad (71)$$

The equation of motion for the momentum Π_0

$$\frac{\delta W}{\delta \Pi_0} = 0 \Rightarrow \frac{dQ_0}{d\tau} = N_0 \quad (\text{i.e.,} \quad dQ_0 = N_0 d\tau) \quad (72)$$

identifies (according to our definition (63)) the new variable Q_0 with the proper time $\bar{\tau} = \sqrt{\gamma}T$, whereas the equation for Q_0

$$\frac{\delta W}{\delta Q_0} = 0 \Rightarrow \frac{d\Pi_0}{d\tau} = 0, \qquad \text{i.e.,} \ \frac{dH}{dT} = 0, \tag{73}$$

in view of (71), gives us the conservation law.

Thus, resolving the global energy constraint $\Pi_0 = H^R$, we obtain, from (70), the reduced action for a relativistic string in terms of the proper time $Q_0 = \bar{\tau}$

$$W^G = \int\limits_{T_1}^{T_2} dT \left[\left(\int\limits_{\sigma_1}^{\sigma_2} d\sigma[-\pi_\mu D_{\bar{\tau}} \xi^\mu] \right) + \Pi_i \frac{dQ_i}{dT} - H - \frac{d}{dT}(TH) \right], \tag{74}$$

where in analogy with (58) we introduced the factorized «shift-vector» $\lambda_2 = N_0 \bar{\lambda}_2$; in this case, the covariant derivative (39) takes the form

$$D_T \xi_\mu = \partial_T \xi_\mu - \bar{\lambda}_2 \xi'_\mu = \frac{D_\tau \xi_\mu}{N_0} \sqrt{\gamma}. \tag{75}$$

The reduced system (74) has trivial solutions for the global variables Π_i, Q_i

$$\frac{\delta W^G}{\delta \Pi_i} = 0 \Rightarrow \frac{dQ_i}{dT} = 0; \ Q_i = \text{const}, \tag{76}$$

$$\frac{\delta W^G}{\delta Q_i} = 0 \Rightarrow \frac{d\Pi_i}{dT} = 0, \ \Pi_i = \text{const}$$

which have the meaning of initial data.

If the solutions of equations (71), (72), and (76) for the system (74)

$$\Pi_0 = H := \frac{M^2}{2\bar{\gamma}}, \quad \Pi_i = P_i, \qquad Q_0 = T\sqrt{\gamma}, \quad Q_i = X_i(0), \tag{77}$$

are substituted into the inverted Levi-Civita canonical transformations (69)

$$P_0 = \pm\sqrt{M^2 + P_i^2}, \qquad X_0(\bar{\tau}) = T\frac{P_0}{\sqrt{\gamma} l} \ , \qquad X_i(\bar{\tau}) = Q_i + T\frac{P_i}{\sqrt{\gamma} l} \ , \tag{78}$$

the initial extended action (62) can be described in the rest frame of an observer who measures the energy P_0 and the time X_0 and sees the rest frame evolution of the «centre-of-mass» coordinates

$$X_i(X_0) = Q_i + X_0 \frac{P_i}{P_0} \ . \tag{79}$$

The Lorentz scheme of describing a relativistic system in terms of the time and energy (X_0, P_0) in the phase space $P_i, X_i, \pi_\mu, \xi_\mu$ is equivalent to the above-considered Levi-Civita scheme in terms of the proper time and the evolution Hamiltonian $(\bar{\tau}, H^R)$ in the phase space $\Pi_i, Q_i, \pi_\mu, \xi_\mu$, where the variables Π_i, Q_i are cyclic.

We identify the Levi-Civita scheme with the comoving frame with the energy

$$E_0 = -\frac{dW^G}{dT} = \frac{M^2}{2\sqrt{\gamma l}} + \frac{dS^{lc}}{dT} = \frac{M^2}{\sqrt{\gamma l}} \qquad (S^{lc} = T\frac{M^2}{2\sqrt{\gamma l}}). \tag{80}$$

This energy includes the time-surface S^{lc} term in the action (74). Then, the inverted Levi-Civita canonical transformations (69) (obtained on the level of the extended theory) play the role of the Lorentz transformation from the comoving frame to the rest frame

$$T\frac{M^2}{\sqrt{\gamma l}} - X_i^{(0)}P_i^{(0)} = \pm X_0|P_0| - X_iP_i. \tag{81}$$

4.4. Dynamics of the Local Variables. We restrict ourselves to an open string with the boundary conditions

$$\sigma_1(T) = 0, \qquad \sigma_2(T) = \pi, \qquad l(T) = \pi. \tag{82}$$

In the gauge-fixing method, by using the kinemetric transformation, we can put

$$\bar{\lambda}_1 = 1, \qquad \bar{\lambda}_2 = 0. \tag{83}$$

This requirement does not contradict the normalization of $\bar{\lambda}_1$ (61).

In view of (64), it means that the reduced Hamiltonian H (59) coincides with its density (56)

$$\bar{\phi}_1 = \mathcal{H} - \frac{1}{\pi}\int_0^\pi d\sigma\mathcal{H} = 0, \qquad \bar{\phi}_2 = \pi_\mu\xi'^\mu = 0. \tag{84}$$

In this case, the reparametrization-invariant equations for the local variables obtained by varying the action (74)

$$\frac{\delta W_s^G}{\delta\xi^\mu} = 0 \Rightarrow \partial_T\pi_\mu - \partial_\sigma(\bar{\lambda}_2\pi_\mu) = \gamma\partial_\sigma(\bar{\lambda}_1\xi'_\mu), \qquad \frac{\delta W_s^G}{\delta\pi^\mu} = 0 \Rightarrow \gamma D_T\xi_\mu = \bar{\lambda}_1\pi_\mu \tag{85}$$

lead to the D'Alambert equations

$$\partial_T^2\xi_\mu - \partial_\sigma^2\xi_\mu = 0. \tag{86}$$

The general solution of these equations of motion in the class of functions (52) with the boundary conditions (82) is given by the Fourier series

$$\xi_\mu(\bar\tau,\sigma)=\frac{1}{2\sqrt{\pi\gamma}}[\psi_\mu(z_+)+\psi_\mu(z_-)],\ \psi_\mu(z)=i\sum_{n\neq0}\mathrm{e}^{-inz}\frac{\alpha_{n\mu}}{n},\ z_\pm=\sqrt{\gamma}T\pm\sigma, \tag{87}$$

$$\xi'_\mu(\bar\tau,\sigma)=\frac{1}{2\sqrt{\pi\gamma}}[\psi'_\mu(z_+)-\psi'_\mu(z_-)],\qquad \pi_\mu(\bar\tau,\sigma)=\frac{1}{2}\sqrt{\frac{\gamma}{\pi}}[\psi'_\mu(z_+)+\psi'_\mu(z_-)].$$

The total coordinates $Q^{(0)}_\mu$ and momenta P_μ are determined by the reduced dynamics of the «centre-of-mass» (76), (77), (78), and the string mass M obtained from (59)

$$P^2_\mu=M^2=2\pi\gamma H=2\pi\gamma\int\limits_0^\pi d\sigma\mathcal{H}. \tag{88}$$

The substitution of ξ_μ and π_μ from (87) into (56) leads to the density

$$\mathcal{H}=-\frac{1}{4\pi}\left[\psi'^2_\mu(z_+)+\psi'^2_\mu(z_-)\right],$$

and from (88) we obtain, for the mass, the expression

$$M^2=-2\pi\gamma\bar L_0\ =-\frac{\gamma}{2}\int\limits_0^\pi d\sigma\left[(\psi'_\mu(z_+))^2+(\psi'_\mu(z_-))^2\right]. \tag{89}$$

The second constraint (84) in terms of the vector ψ'_μ in (87) takes the form

$$\xi'_\mu\pi^\mu=\frac{1}{4\pi}\left[\psi'^2_\mu(z_+)-\psi'^2_\mu(z_-)\right]=0\ \Rightarrow\quad \psi'^2_\mu(z_+)=\psi'^2_\mu(z_-)=\text{const.}, \tag{90}$$

and the first constraint (84) $\bar\phi_1=0$ is satisfied identically. After the substitution of the constant value (90) into (89) we obtain that const. $=-M^2/\pi\gamma$; thus, finally the reparamerization-invariant constraint takes the form

$$P^2_\mu+\pi\gamma\psi'^2_\mu(z_\pm)=0\qquad(\ P^2_\mu=M^2\ ). \tag{91}$$

Unlike this constraint, the gauge-fixing reparametrization-noninvariant constraint [27, 28]

$$\left(P_\mu+\sqrt{\pi\gamma}\psi'_\mu\right)^2=0 \tag{92}$$

contains the interference of the local and global degrees of freedom $\psi'_\mu P^\mu$. The latter violates the relativistic invariance of the local excitations which form the mass and spin of a string.

Equation (91) means that ψ'_μ is the modulo-constant space-like vector. The constraint (91) in terms of the Fourier components (87) takes the form

$$\psi'^2_\mu(z_\pm) = 2\sum_{n=-\infty}^{\infty} \bar{L}_n e^{-inz_\pm} = -\frac{M^2}{\pi\gamma}, \tag{93}$$

where $\bar{L}_n$ are the contributions of the nonzero harmonics

$$\bar{L}_0 = -\frac{1}{2}\sum_{k\neq 0} \alpha_{k\mu}\alpha^\mu_{-k}, \quad \bar{L}_{n\neq 0} = -\frac{1}{2}\sum_{k\neq 0,n} \alpha_{k\mu}\alpha^\mu_{n-k}. \tag{94}$$

From (93) we can see that the zero harmonic of this constraint determines the mass of a string

$$M^2 = -2\pi\gamma\bar{L}_0 = -\pi\gamma\sum_{k\neq 0}\alpha_{k\mu}\alpha_{-k\mu} \tag{95}$$

and coincides with the gauge-fixing value. However, the nonzero harmonics of constraint (93)

$$\bar{L}_{n\neq 0} = -\frac{1}{2}\sum_{k\neq 0,n}\alpha_{k\mu}\alpha_{n-k\mu} = 0, \qquad \bar{L}_{-n} = \bar{L}^*_n \tag{96}$$

(as we dicussed above) strongly differ from the nonzero harmonics of the gauge-fixing constraints (92) The latter (in the contrast to (91)) contains the mixing of the global motion of the centre of mass P_μ with the local excitations ψ_μ. It is clear that this mixing of the global and local motions violates the Poincare invariance of the local degrees of freedom.

The algebra of the local constraints (96) of the reparametrization-invariant dynamics of a relativistic string is not closed, as it does not contain the zero Fourier harmonic of the energy constraint (which has been resolved to express the dynamic equations in terms of the proper time).

The ideology of the invariant reduction (with the explicit resolving of constraints to exclude the superfluous variables of the type of the time-like component of the CM coordinates) can be extended onto the local constraints (84). These constraints in the form (91) can be also used to exclude the time component of the local excitations ξ_0, π_0 (with the negative contribution into energy) from the phase space, to proceed the stability of the system and the positive norm of quantum states

$$\xi'_0 = \frac{1}{2\sqrt{\pi\gamma}}[\psi'_0(z_+) - \psi'_0(z_-)], \qquad \pi_0 = \frac{1}{2}\sqrt{\frac{\gamma}{\pi}}[\psi'_0(z_+) + \psi'_0(z_-)], \tag{97}$$

where

$$\psi'_0(z_\pm) = \pm\left[(\psi'_i(z_\pm))^2 - \frac{M^2}{\pi\gamma}\right]^{1/2}. \tag{98}$$

The constraining (97) means that only the spatial components ξ_i, π_i are independent variables.

The choice of gauge (65) leads to $\xi_0 = \pi_0 = 0$ and fixes a contribution of the time-like component into the string mass. In this case, as was mentioned above, the equations for the reduced action coincide with the set of equations and the same constraints of the initial extended action. Finally, the explicit resolving of the local constraints takes the form

$$(\psi_i'(z_\pm))^2 = \frac{M^2}{\pi\gamma}. \tag{99}$$

The reparametrization-invariant dynamics of a relativistic string in the form of the first and second class constraints (64), (65) coincides with the Röhrlich approach to the string theory [33]. This approach is based on two points: i) the choice of the gauge condition

$$P_\mu \xi^\mu = 0, \;\; P_\mu \pi^\mu = 0 \Rightarrow G_n = P_\mu \alpha_n^\mu = 0, \;\; n \neq 0$$

and ii) the use of that condition for eliminating the states with negative norm, the physical state vectors being constructed in the «centre-of-mass» (CM) frame (in our scheme, the CM frame appears as a result of the geometric Levi–Civita reduction). This reference frame is the only preferred frame for quantizing such a composite relativistic object as the string, as only in this frame one can quantize the initial data. This is a strong version of the principle of correspondence with classical theory: the classical initial data become the quantum numbers of quantum theory. All previous attempts for quantization of the string fully ignored this meaning of the CM frame.

4.5. Quantum Theory. The Röhrlich approach distinguishes two cases: $M^2 = 0$ and $M^2 \neq 0$.

The first case, in our scheme, the equality $M^2 = 0$ together with the local constraints (96) forms the Virasoro algebra. The reparametrization-invariant version of the Virasoro algebra (with all its difficulties, including the $D = 26$ problem and the negative norm states) appears only in the case of the massless string $-2\pi\gamma\bar{L}_0 = M^2 = 0$.

The second case $M^2 \neq 0$ allows us to exclude the time Fourier components α_{n0}, and it is just these components that after quantization $[\alpha_{n,\mu}, \alpha^+_{m,\nu}] = -n\eta_{\mu\nu}\delta_{nm}$ $(n, m \neq 0)$ lead to the states with negative norm because of the system being unstable. This means that the state vectors in the CM frame are constructed only by the action on vacuum of the spatial components of the operators $a^+_{ni} = \alpha_{-ni}/\sqrt{n}, n > 0$

$$|\mathbf{\Phi}_\nu\rangle_{\mathrm{CM}} = \prod_{n=1}^{\infty} \frac{(a^+_{nx})^{\nu_{nx}}}{\sqrt{\nu_{nx}!}} \frac{(a^+_{ny})^{\nu_{ny}}}{\sqrt{\nu_{ny}!}} \frac{(a^+_{nz})^{\nu_{nz}}}{\sqrt{\nu_{nz}!}} |0\rangle, \tag{100}$$

where the three-dimensional vectors $\nu_n = (\nu_{nx}, \nu_{ny}, \nu_{nz})$ have only nonnegative integers as components. These state vectors automatically satisfy the constraint

$$\alpha_{n0}|\mathbf{\Phi}_\nu\rangle_{\mathrm{CM}} = 0, \qquad n > 0. \tag{101}$$

The physical states (100) are subjected to further constraints (96) with $n \geqslant 0$

$$\bar{L}_n|\mathbf{\Phi}_\nu\rangle_{\mathrm{CM}} = 0, \qquad n > 0, \qquad P^2 = M_\nu^2 = \pi\gamma\langle\mathbf{\Phi}_\nu \sum_{m\neq 0} \alpha_{-m,i}\alpha_{m,i}|\mathbf{\Phi}_\nu\rangle, \tag{102}$$

where $\bar{L}_n$ can be represented in the normal ordering form

$$\bar{L}_{n>0} = \sum_{k=1}^{\infty} \alpha_{k,i}^{+}\alpha_{n+k,i} + \frac{1}{2}\sum_{k>1}^{n-1} \alpha_{k,i}\alpha_{n-k,i}. \tag{103}$$

Constraints $G_n = \alpha_{n0} = 0, n > 0$ (101) and $\bar{L}_m, m \geqslant 0$ (102), taken together, represent the first class constraints, in accordance with the Dirac classification [8] as they form a closed algebra for $(n, m > 0)$

$$[G_n, G_m] = 0, \quad [\bar{L}_n, \bar{L}_m] = (n-m)\bar{L}_{n+m}, \quad [G_n, \bar{L}_m] = nG_{m+n}. \tag{104}$$

Therefore the conditions (101) eliminating the ghosts and the conditions (102) defining the physical vector states are consistent. Note that the commutator $[\bar{L}_n, \bar{L}_m]$ does not contain a c-number since $n \geqslant 0$ and $m \geqslant 0$.

On the operator level, equations determining the resolution of the constraints are fulfilled in a weak sense, as only the «annihilation» part of the constraints is imposed on the state vectors.

4.6. The Causal Green Functions. Now we can construct the causal Green function for a relativistic string as the analogy of the causal Green function for a relativistic particle (23)–(25) discussed in Section 3.3.

The Veneziano-type causal Green function is the spectral series with the Hermite polynomials $\langle\xi|\nu\rangle$ over the physical state vectors $|\mathbf{\Phi}_\nu\rangle = |\nu\rangle$

$$G_c(X|\xi_1, \xi_2) = G_+(X|\xi_1, \xi_2)\theta(X_0) + G_-(X|\xi_1, \xi_2)\theta(-X_0) = \tag{105}$$

$$= i\int \frac{d^4P}{(2\pi)^4} \exp(-iPX) \sum_\nu \frac{\langle\xi_1|\nu\rangle\langle\nu|\xi_2\rangle}{P^2 - M_\nu^2 - i\epsilon}.$$

The commutative Green function for a relativistic string $G_+(X|\xi_1, \xi_2)$ can be represented in the form of the Faddeev–Popov functional integral [19, 21] in the local gauge (65)

$$G_+(X|\xi_2,\xi_1) =$$

$$= \int\limits_{X(\tau_1)=0}^{X(\tau_2)=X} \frac{dN_0(\tau_2)d^4P(\tau_2)}{(2\pi)^3} \prod_{\tau_1\leqslant\tau<\tau_2} \left\{ d\bar{N}_0(\tau) \prod_\mu \left(\frac{dP_\mu(\tau)dX_\mu(\tau)}{2\pi} \right) \right\}, \quad (106)$$

$$F_+(\xi_2,\xi_1),$$

where we use the representation of the spectral series in the form of the functional integral

$$F_+(\xi_2,\xi_1) = \sum_\nu \langle\xi_2|\nu\rangle \exp\left\{iW[P,X,N_0,M_\nu]\right\} \langle\nu|\xi_1\rangle =$$

$$= \int\limits_{\xi_1}^{\xi_2} D(\xi,\pi)\Delta_{fp} \exp\left\{iW_{fp}\right\}, \quad (107)$$

$W[P,X,N_0,M_\nu]$ is the action (11) with the mass M_ν,

$$W_{fp} = \int\limits_0^{\tau(X_0)} d\tau \left[-\left(\int\limits_0^\pi d\sigma\pi_\mu\dot{\xi}^\mu \right) - P_\mu\dot{X}^\mu - N_0\left(-\frac{P^2}{2\pi\gamma} + H \right) \right] \quad (108)$$

is the constraint-shell action (66), and

$$D(\xi,\pi) = \prod_{\tau,\sigma}\prod_\mu \frac{d\xi_\mu d\pi_\mu}{2\pi}, \quad (109)$$

$$\Delta_{fp} = \prod_{\tau,\sigma} \delta(\phi_1))\delta(\pi_0)\delta(\phi_2))\delta(\xi_0)\det B^{-1},\ \det B = \det\left\{\phi_1,\phi_2,\pi_0,\xi_0\right\} \quad (110)$$

is the FP determinant given in the monograph [9].

5. HAMILTONIAN DYNAMICS OF GENERAL RELATIVITY

5.1. Action and Geometry. General relativity (GR) is given by the singular Einstein–Hilbert action with the matter fields

$$W(g|\mu) = \int d^4x\sqrt{-g}\left[-\frac{\mu^2}{6}R(g) + \mathcal{L}_{\rm matter} \right] \qquad \left(\mu^2 = M^2_{\rm Planck}\frac{3}{8\pi} \right) \quad (111)$$

and by a measurable interval in the Riemannian geometry

$$(ds)^2 = g_{\alpha\beta}dx^\alpha dx^\beta. \quad (112)$$

They are invariant with respect to general coordinate transformations

$$x_\mu \to x'_\mu = x'_\mu(x_0,x_1,x_2,x_3). \quad (113)$$

5.2. Variables and Hamiltonian. The generalized Hamiltonian approach to GR was formulated by Dirac and Arnovit, Deser and Misner [2] as a theory of a system with constraints in $3+1$ foliated space-time

$$(ds)^2 = g_{\mu\nu}dx^\mu dx^\nu = N^2dt^2 - {}^{(3)}g_{ij}\breve{d}x^i\breve{d}x^j \qquad (\breve{d}x^i = dx^i + N^i dt) \quad (114)$$

with the lapse function $N(t,\vec{x})$, three shift vectors $N^i(t,\vec{x})$, and six space components ${}^{(3)}g_{ij}(t,\vec{x})$ depending on the coordinate time t and the space coordinates $\vec{x}$. The Dirac-ADM parametrization of metric (114) characterizes a family of hypersurfaces $t = \mathrm{const}$. with the unit normal vector $\nu^\alpha = (1/N, -N^k/N)$ to a hypersurface and with the second (external) form

$$\frac{1}{N}({}^{(3)}\dot{g}_{ij}) - \Delta_i N_j - \Delta_j N_i \tag{115}$$

that shows how this hypersurface is embedded into the four-dimensional space-time.

Coordinate transformations conserving the family of hypersurfaces $t = \mathrm{const}$

$$t \to \tilde{t} = \tilde{t}(t), \qquad x_i \to \tilde{x}_i = \tilde{x}_i(t, x_1, x_2, x_3), \tag{116}$$

$$\tilde{N} = N\frac{dt}{d\tilde{t}}, \qquad \tilde{N}^k = N^i\frac{\partial\tilde{x}^k}{\partial x_i}\frac{dt}{d\tilde{t}} - \frac{\partial\tilde{x}^k}{\partial x_i}\frac{\partial x^i}{\partial\tilde{t}} \tag{117}$$

are called a kinemetric subgroup of the group of general coordinate transformations (113) [4, 5, 7, 31]. The group of kinemetric transformations is the group of diffeomorphisms of the generalized Hamiltonian dynamics. It includes reparametrizations of the nonobservable time coordinate $\tilde{t}(t)$) (116) that play the principal role in the procedure of the reparametrization-invariant reduction discussed in the previous Sections. The main assertion of the invariant reduction is the following: the dynamic evolution parameter is not the coordinate but the variable with a negative contribution to the energy constraint. (Recall that this reduction is based on the explicit resolving of the global energy constraint with respect to the conjugate momentum of the dynamic evolution parameter to convert this momentum into the Hamiltonian of evolution of the reduced system.)

A negative contribution to the energy constraint is given by the space-metric-determinant logarithm. Therefore, following papers [3, 4, 13, 14, 29, 34] we introduce an invariant evolution parameter $\varphi_0(t)$ as the zero Fourier harmonic component of this logarithm (treated, in cosmology, as the cosmic scale factor). This variable is distinguished in general relativity by the Lichnerowicz conformal-type transformation of field variables f with the conformal weight (n) [35]

$${}^{(n)}\bar{f} = {}^{(n)}f\left(\frac{\varphi_0(t)}{\mu}\right)^{-n}, \tag{118}$$

where $n = 2,\ 0,\ -3/2,\ -1$ for the tensor, vector, spinor, and scalar fields, respectively, $\bar{f}$ is the so-called conformal-invariant variable used in GR for the analysis of initial data [29,35]. In particular, for metric we get

$$g_{\mu\nu}(t,\vec{x}) = \left(\frac{\varphi_0(t)}{\mu}\right)^2 \bar{g}_{\mu\nu}(t,\vec{x}) \ \Rightarrow\ (ds)^2 = \left(\frac{\varphi_0(t)}{\mu}\right)^2 [\bar{N}^2 dt^2 - {}^{(3)}\bar{g}_{ij}\breve{dx}^i\breve{dx}^j]. \tag{119}$$

As the zero Fourier harmonic is extracted from the space metric determinant logarithm, the space metric $\bar{g}_{ij}(t,\vec{x})$ should be defined in a class of nonzero harmonics

$$\int d^3x \log ||\bar{g}_{ij}(t,\vec{x})|| = 0. \tag{120}$$

The transformational properties of the curvature $R(g)$ with respect to the transformations (119) lead to the action (111) in the form [4]

$$W(g|\mu) = W(\bar{g}|\varphi_0) - \int\limits_{t_1}^{t_2} dt \int\limits_{V_0} d^3x \varphi_0 \frac{d}{dt}\left(\frac{\dot{\varphi}_0\sqrt{\bar{g}}}{\bar{N}}\right). \tag{121}$$

This form defines the global lapse function N_0 as the average of the lapse function $\bar{N}$ in the metric $\bar{g}$ over the kinemetric invariant space volume

$$N_0(t) = \frac{V_0}{\int\limits_{V_0} d^3x \frac{\sqrt{\bar{g}(t,\vec{x}}}{\bar{N}(t,\vec{x})}}, \qquad \bar{g} = \det({}^{(3)}\bar{g}), \qquad V_0 = \int\limits_{V_0} d^3x, \tag{122}$$

where V_0 is a free parameter which in the perturbation theory has the meaning of a finite volume of the free coordinate space. The lapse function $\bar{N}(t,\vec{x})$ can be factorized into the global component $N_0(t)$ and the local one $\mathcal{N}(t,\vec{x})$

$$\bar{N}(t,\vec{x})\bar{g}^{-1/2} := N_0(t)\mathcal{N}(t,\vec{x}) := N_q, \tag{123}$$

where $\mathcal{N}$ fulfills normalization condition:

$$I[\mathcal{N}] := \frac{1}{V_0}\int \frac{d^3x}{\mathcal{N}} = 1 \tag{124}$$

that is imposed after the procedure of variation of action, to reproduce equations of motion of the initial theory. In the Dirac harmonical variables [1] chosen as

$$q^{ik} = \bar{g}\bar{g}^{ik}, \tag{125}$$

the metric (114) takes the form

$$(ds)^2 = \frac{\varphi_0(t)^2}{\mu^2} q^{1/2}\left(\ N_q^2 dt^2 - q_{ij}\breve{dx}^i\breve{dx}^j\right) \qquad (q = \det(q^{ij})). \tag{126}$$

The Dirac–Bergmann version of action (121) in terms of the introduced above variables reads [4, 5]

$$W = \int\limits_{t_1}^{t_2} dt \left\{ L + \frac{1}{2}\partial_t (P_0 \varphi_0) \right\}, \tag{127}$$

$$L = \left[\int\limits_{V_0} d^3x \left(\sum_F P_F \dot{F} - N^i \mathcal{P}_i \right) \right] - P_0 \dot{\varphi}_0 - N_0 \left[-\frac{P_0^2}{4V_0} + I^{-1} H(\varphi_0) \right], \tag{128}$$

where

$$\sum_F P_F \dot{F} = \sum_f p_f \dot{f} - \pi_{ij} \dot{q}^{ij}, \tag{129}$$

$$H(\varphi_0) = \int d^3x \mathcal{N} \mathcal{H}(\varphi_0) \tag{130}$$

is the total Hamiltonian of the local degrees of freedom,

$$\mathcal{H}(\varphi_0) = \frac{6}{\varphi_0^2} q^{ij} q^{kl} [\pi_{ik}\pi_{jl} - \pi_{ij}\pi_{kl}] + \frac{\varphi_0^2 q^{1/2}}{6} {}^{(3)}R(\bar{g}) + \mathcal{H}_f, \tag{131}$$

and

$$\mathcal{P}_i = 2[\nabla_k (q^{kl}\pi_{il}) - \nabla_i (q^{kl}\pi_{kl})] + \mathcal{P}_{if} \tag{132}$$

are the densities of energy and momentum and $\mathcal{H}_f, \mathcal{P}_f$ are contributions of the matter fields. In the following, we call the set of the field variables F (129) with the dynamic evolution parameter φ_0 the field world space. The local part of the momentum of the space metric determinant

$$\pi(t, x) := q^{ij}\pi_{ij} \tag{133}$$

is given in the class of functions with the nonzero Fourier harmonics, so that

$$\int d^3x \pi(t, x) = 0, \tag{134}$$

(compare with equations (53), (54), in the previous Section).

The geometric foundation of introducting the global variable (119) in GR was given in [34] as the assertion about the nonzero value of the second form in the whole space. This assertion (which contradicts the Dirac gauge $\pi = 0$) follows from the global energy constraint, as, in the lowest order of the Dirac perturbation theory, positive contributions of particle-like excitations to the zero Fourier harmonic of the energy constraint can be compensated only by the nonzero value of the second form.

The aim of this Section is to obtain the dynamic «equivalent» unconstrained system in the field world space (F, φ_0) by explicit resolving the global energy constraint and to find the geometric unconstrained system by the Levi–Civita-type canonical transformation considered for a particle and a string in the previous Sections.

5.3. Local Constraints and Equations of Motion. Following Dirac [1] we formulate generalized Hamiltonian dynamics for the considered system (127). It means the inclusion of momenta for $\mathcal{N}$ and N_i and appropriate terms with Lagrange multipliers

$$W^D = \int\limits_{t_1}^{t_2} dt \left\{ L^D + \frac{1}{2}\partial_t(P_0\varphi_0) \right\},$$

$$L^D = L + \int d^3x (P_{\mathcal{N}}\dot{\mathcal{N}} + P_{N^i}\dot{N}^i - \lambda^0 P_{\mathcal{N}} - \lambda^i P_{N^i}). \tag{135}$$

We can define extended Dirac Hamiltonian as

$$H^D = N_0 \left[-\frac{P_0^2}{4V_0} + I^{-1}H(\varphi_0) \right] + \int d^3x (\lambda^0 P_{\mathcal{N}} + \lambda^i P_{N^i}). \tag{136}$$

The equations obtained from variation of W^D with respect to Lagrange multipliers are called first class primary constraints

$$P_{\mathcal{N}} = 0, \qquad P_{N^i} = 0. \tag{137}$$

The condition of conservation of these constraints in time leads to the first class secondary constraints

$$\left\{H^D, P_{\mathcal{N}}\right\} = \mathcal{H} - \frac{\int d^3x \mathcal{N}\mathcal{H}}{V_0\mathcal{N}^2} = 0, \qquad \left\{H^D, P_{N^i}\right\} = \mathcal{P}_i = 0 \tag{138}$$

(compare with equations (59) and (64) in Section 4). For completeness of the system we have to include a set of secondary constraints. According Dirac we choose them in the form

$$\mathcal{N}(t, \vec{x}) = 1, \qquad N^i(t, \vec{x}) = 0, \tag{139}$$

$$\pi(t, \vec{x}) = 0, \qquad \chi^j := \partial_i(q^{-1/3}q^{ij}) = 0. \tag{140}$$

The equations of motion obtained for the considered system are

$$\frac{dF}{dT} = \frac{\partial H(\varphi_0)}{\partial P_F}, \quad -\frac{dP_F}{dT} = \frac{\partial H(\varphi_0)}{\partial F}, \tag{141}$$

where $H(\varphi_0)$ is given by the equation (130), and we introduced the invariant geometric time T

$$N_0 dt := dT. \tag{142}$$

5.4. Global Constraints and Equations of Motion. The physical meaning of the geometric time T, the dynamic variable φ_0 and its momentum is given by the explicit resolving of the zero-Fourier harmonic of the energy constraint

$$\frac{\delta W^E}{\delta N_0(t)} = -\frac{P_0^2}{4V_0} + H(\varphi_0) = 0. \tag{143}$$

This constraint has two solutions for the global momentum P_0:

$$(P_0)_\pm = \pm 2\sqrt{V_0 H(\varphi_0)} \equiv H_\pm^*. \tag{144}$$

The equation of motion for this global momentum P_0 in gauge (139) takes the form

$$\frac{\delta W^E}{\delta P_0} = 0 \Rightarrow \left(\frac{d\varphi}{dT}\right)_\pm = \frac{(P_0)_\pm}{2V} = \pm\sqrt{\rho(\varphi_0)}, \quad \rho(\varphi_0) = \frac{\int d^3x\mathcal{H}}{V_0} = \frac{H(\varphi_0)}{V_0}. \tag{145}$$

The integral form of the last equation is

$$T_\pm(\varphi_1, \varphi_0) = \pm \int_{\varphi_1}^{\varphi_0} d\varphi \rho^{-1/2}(\varphi), \tag{146}$$

where $\varphi_1 = \varphi_0(t_1)$ is the initial data. Equation obtained by varying the action with respect to φ_0 follows independently from the set of all other constraints and equations of motion.

In quantum theory of GR (like in quantum theories of a particle and string considered in Sections 3, 4), we get two Schrödinger equations

$$i\frac{d}{d\varphi_0}\Psi^\pm(F|\varphi_0, \varphi_1) = H_\pm^*(\varphi_0)\Psi^\pm(F|\varphi_0, \varphi_1) \tag{147}$$

with positive and negative eigenvalues of P_0 and normalizable wave functions with the spectral series over quantum numbers Q

$$\Psi^+(F|\varphi_0, \varphi_1) = \sum_Q A_Q^+ \langle F|Q\langle\rangle Q|\varphi_0, \varphi_1\rangle \theta(\varphi_0 - \varphi_1), \tag{148}$$

$$\Psi^-(F|\varphi_0, \varphi_1) = \sum_Q A_Q^- \langle F|Q\rangle^* \langle Q|\varphi_0, \varphi_1\rangle^* \theta(\varphi_1 - \varphi_0), \tag{149}$$

where $\langle F|Q\rangle$ is the eigenfunction of the reduced energy (144)

$$H_\pm^*(\varphi_0)\langle F|Q\rangle = \pm E(Q, \varphi_0)\langle F|Q\rangle, \tag{150}$$

$$\langle Q|\varphi_0,\varphi_1\rangle = \exp\,[-i\int\limits_{\varphi_1}^{\varphi_0} d\varphi E(Q,\varphi)],\ \langle Q|\varphi_0,\varphi_1\rangle^* = \exp\,[i\int\limits_{\varphi_1}^{\varphi_0} d\varphi E(Q,\varphi)]. \tag{151}$$

The coefficient A_Q^+, in «secondary» quantization, can be treated as the operator of creation of a universe with positive energy; and the coefficient A_Q^-, as the operator of annihilation of a universe also with positive energy. The «secondary» quantization means $[A_Q^-, A_{Q'}^+] = \delta_{Q,Q'}$. The physical states of a quantum universe are formed by the action of these operators on the vacuum $\langle 0|$, $|0\rangle$ in the form of out-state ($|Q\rangle = A_Q^+|0\rangle$) with positive «frequencies» and in-state ($\langle Q| = \langle 0|A_Q^-$) with negative «frequencies». This treatment means that positive frequencies propagate forward ($\varphi_0 > \varphi_1$); and negative frequencies, backward ($\varphi_1 > \varphi_0$), so that the negative values of energy are excluded from the spectrum to provide the stability of the quantum system in quantum theory of GR (similar in QFT in Section 3). In other words, instead of changing the sign of energy, we change that of the dynamic evolution parameter, which leads to the causal Green function

$$\begin{aligned} G_c(F_1,\varphi_1|F_2,\varphi_2) &= G_+(F_1,\varphi_1|F_2,\varphi_2)\theta(\varphi_2-\varphi_1) + \\ &+ G_-(F_1,\varphi_1|F_2,\varphi_2)\theta(\varphi_1-\varphi_2), \end{aligned} \tag{152}$$

where $G_+(F_1,\varphi_1|F_2,\varphi_2) = G_-(F_2,\varphi_2|F_1,\varphi_1)$ is the «commutative» Green function

$$G_+(F_2,\varphi_2|F_1,\varphi_1) = \langle 0|\Psi^-(F_2|\varphi_2,\varphi_1)\Psi^+(F_1|\varphi_1,\varphi_1)|0\rangle. \tag{153}$$

For this causal convention, the geometric time (146) is always positive in accordance with the equations of motion (145)

$$\left(\frac{dT}{d\varphi_0}\right)_{\pm} = \pm\sqrt{\rho} \quad \Rightarrow \quad T_{\pm}(\varphi_1,\varphi_0) = \pm\int\limits_{\varphi_1}^{\varphi_0} d\varphi\rho^{-1/2}(\varphi) \geqslant 0. \tag{154}$$

Thus, the causal structure of the field world space immediatly leads to the arrow of the geometric time (154) and the beginning of evolution of a universe with respect to the geometric time $T = 0$.

As we have seen in Sections 3 and 4, the way to obtain conserved integrals of motion in classical theory and quantum numbers Q in quantum theory is the Levi-Civita-type canonical transformation of the field world space (F,φ_0) to a geometric set of variables (V,Q_0) with the condition that the geometric evolution parameter Q_0 coincides with the geometric time $dT = dQ_0$ (see Fig. 3).

Equations (145), (146) in the homogeneous approximation of GR are the basis of observational cosmology where the geometric time is the conformal time

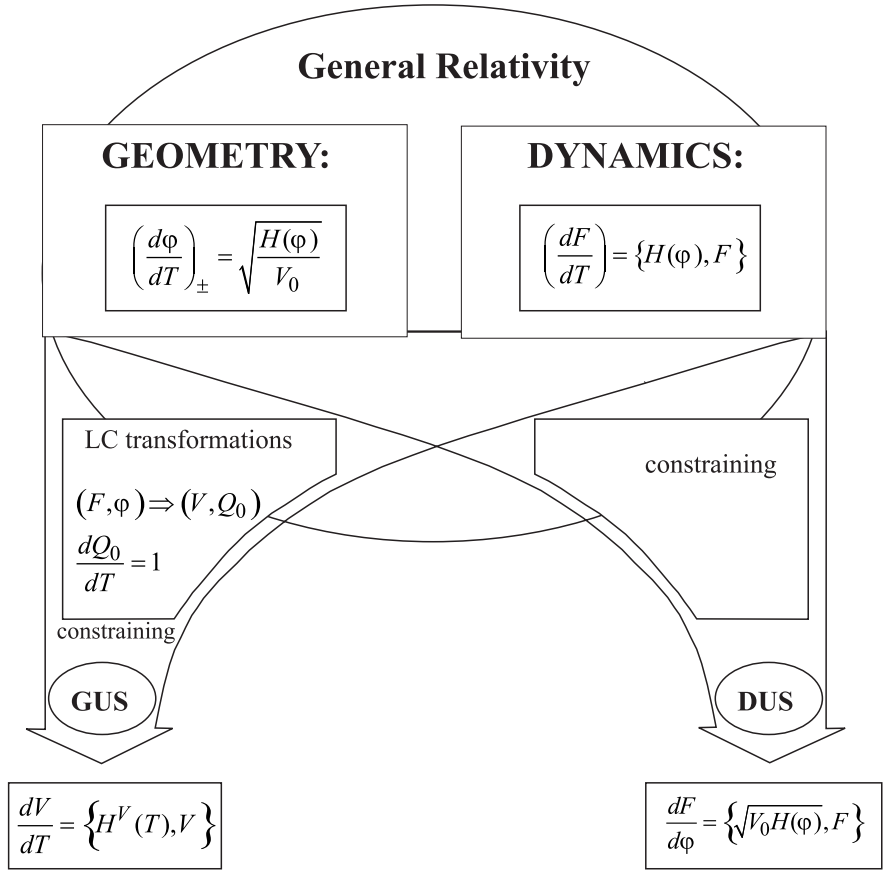

Fig. 3. Reparametrization-invariant dynamics of General Relativity is covered by the Dynamic Unconstrained Systems (DUS) and the Geometric Unconstrained Systems (GUS) connected by the Levi-Civita (LC) transformations of fields of MATTER into the vacuum fields of initial data with respect to geometric TIME

connected with the world time T_f of the Friedmann cosmology by the relation

$$dT_f = \frac{\varphi_0(T)}{\mu} dT, \tag{155}$$

and the dependence of scale factor (dynamic evolution parameter φ_0) on the geometric time T is treated as the evolution of the universe. In particular, equation (145) gives the relation between the present-day value of the dynamic evolution parameter $\varphi_0(T_0)$ and cosmological observations, i.e., the density of

matter ρ and the Hubble parameter

$$\mathcal{H}^{\rm e}_{\rm hub}=\frac{\mu\varphi_0'}{\varphi_0^2}=\frac{\mu\sqrt{\rho}}{\varphi_0^2}\qquad\Rightarrow\qquad\varphi_0(T_0)=\left(\frac{\mu\sqrt{\rho}}{\mathcal{H}_{\rm hub}}\right)^{1/2}:=\mu\Omega_0^{1/4},\qquad(156)$$

where $(0.6<(\Omega_0^{1/4})_{\rm exp}<1.2)$. The dynamic evolution parameter as the cosmic scale factor and a value of its conjugate momentum (i.e., a value of the dynamic Hamiltonian) as the density of matter (see equations (145), (146)) are objects of measurement in observational astrophysics and cosmology and numerous discussions about the Hubble parameter, dark matter, and hidden mass.

The general theory of reparametrization-invariant reduction described in the previous Sections can be applied also to GR. In accordance with this theory, the reparametrization-invariant dynamics of GR is covered by two unconsrained systems (dynamic and geometric) connected by the Levi-Civita canonical transformation which solves the problems of the initial data, conserved quantum numbers, and direct corrrespondence of standard classical cosmology with quantum gravity on the level of the generating functional of the unitary and causal perturbation theory [7, 15].

5.5. Equivalent Unconstrained Systems. Assume that we can solve the constraint equations and pass to the reduced space of independent variables (F^*,P_F^*). The explicit solution of the local and global constraints has two analytic branches with positive and negative values for scale factor momentum P_0 (144). Therefore, inserting solutions of all constraints into the action we get two branches of the equivalent Dynamic Unconstrained System (DUS)

$$W^{\rm DUS}_{\pm}[F|\varphi_0]=\int\limits_{\varphi_1}^{\varphi_2}d\varphi_0\left\{\left[\int d^3x\sum_{F^*}P_F^*\frac{\partial F^*}{\partial\varphi_0}\right]-H^*_{\pm}+\frac{1}{2}\partial_{\varphi_0}(\varphi_0H^*_{\pm})\right\},\qquad(157)$$

where φ_0 plays the role of evolution parameter and $H^*_{\pm}$ defined by equation (144) plays the role of the evolution Hamiltonian, in the reduced phase space of independent physical variables (F^*,P_F^*) with equations of motion

$$\frac{dF^*}{d\varphi_0}=\frac{\partial H^*_{\pm}}{\partial P_F^*},\qquad\qquad-\frac{dP_F^*}{d\varphi_0}=\frac{\partial H^*_{\pm}}{\partial F^*}.\qquad(158)$$

The evolution of the field world space variables (F^*,φ_0) with respect to the geometric time T is not contained in DUS (157). This geometric time evolution is described by supplementary equation (145) for nonphysical momentum P_0 (144) that follows from the initial extended system.

To get an equivalent unconstrained system in terms of the geometric time (we call it the Geometric Unconstrained System (GUS)), we need the Levi-Civita

canonical transformation (LC) [12, 22, 23] of the field world phase space

$$(F^*, P_F^*|\varphi_0, P_0) \Rightarrow (F_G^*, P_G^*|Q_0, \Pi_0) \tag{159}$$

which converts the energy constraint (143) into the new momentum Π_0 (see the similar transformations for a relativistic particle and a string in Sections 3, 4).

In terms of geometrical variables the action takes the form

$$W^G = \int_{t_1}^{t_2} dt \left\{ \left[\int d^3x \sum_{F_G^*} P_G^* \dot{F}_G^* \right] - \Pi_0 \dot{Q}_0 + N_0 \Pi_0 + \frac{d}{dt} S^{\mathrm{LC}} \right\}, \tag{160}$$

where $S^{-\mathrm{LC}}$ is generating function of LC transformations. Then the energy constraint and the supplementary equation for the new momentum take trivial form

$$\Pi_0 = 0\ ; \qquad \frac{\delta W}{\delta \Pi_0} = 0 \qquad \Rightarrow \qquad \frac{dQ_0}{dt} = N_0 \qquad \Rightarrow \qquad dQ_0 = dT. \tag{161}$$

Equations of motion are also trivial

$$\frac{dP_G^*}{dT} = 0, \qquad \frac{dF_G^*}{dT} = 0, \tag{162}$$

and their solutions are given by the initial data

$$P_G^* = P_G^{*\,0}, \qquad F_G^* = F_G^{*\,0}. \tag{163}$$

Substituting solutions of (161) and (162) into the inverted Levi-Civita transformations

$$F^* = F^*(Q_0, \Pi_0|F_G^*, P_G^*), \qquad \varphi_0 = \varphi_0(Q_0, \Pi_0|F_G^*, P_G^*) \tag{164}$$

and similar for momenta, we get formal solutions of (158) and (146)

$$F^* = F^*(T, 0|F_G^{*\,0}, P_G^{*\,0}),\ P_F^* = P_F^*(T, 0|F_G^{*\,0}, P_G^{*\,0}),\ \varphi_0 = \varphi_0(T, 0|F_G^{*\,0}, P_G^{*\,0}). \tag{165}$$

We see that evolution of the dynamic variables with respect to the geometric time (i.e., the evolution of a universe) is absent in DUS. The evolution of the dynamic variables with respect to the geometric time can be described in the form of the LC (inverted) canonical transformation of GUS into DUS (164), (165) (see Fig. 4).

There is also the weak form of Levi-Civita-type transformations to GUS $(F^*, P_F^*) \Rightarrow (\tilde{F}, \tilde{P})$ without action-angle variables and with a constraint

$$\tilde{\Pi}_0 - \tilde{H}(\tilde{Q}_0, \tilde{F}, \tilde{P}) = 0. \tag{166}$$

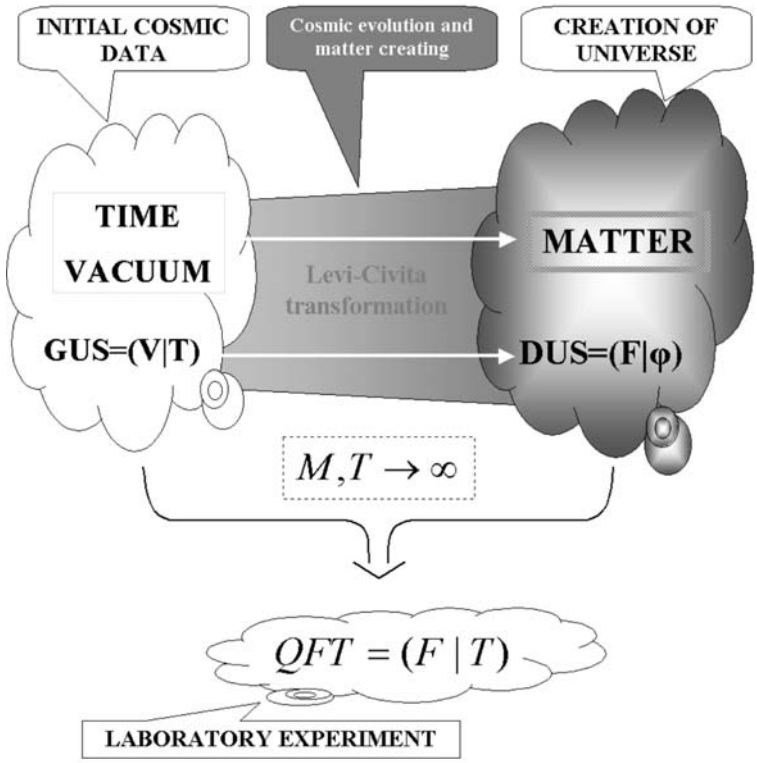

Fig. 4. Reparametrization-invariant dynamics of «Big Bang» of a quantum universe: the Dynamic Unconstrained System (DUS) describes creation of a universe in the field world space where we have only MATTER $F|\varphi$; the Geometric Unconstrained System (GUS) describes initial cosmic data (i.e., the Bogoliubov squeezed VACUUM) with respect to the geometric TIME measured by an observer; the inverse Levi-Civita canonical transformation describes the cosmic (Hubble) evolution and creation of matter from the VACUUM. The standard quantum field theory (QFT) in the form of the Faddeev–Popov generating functional for the unitary S matrix appears in the limits of tremendous mass, volume, and geometric lifetime of a universe

We get the constraint-shell action

$$\tilde{W}^{\mathrm{GUS}} = \int dT \left\{ \left[\int d^3x \sum_{\tilde{F}} \tilde{P} \frac{d\tilde{F}}{dT} \right] - \tilde{H}(T, \tilde{F}, \tilde{P}) \right\}, \qquad (167)$$

that allows us to choose the initial cosmological data with respect to the geometric time.

Recall that the considered reduction of the action reveals the difference of reparametrization-invariant theory from the gauge-invariant theory: in gauge-invariant theory the superfluous (longitudinal) variables are completely excluded from the reduced system; whereas, in reparametrization-invariant theory the superfluous (longitudinal) variables leave the sector of the Dirac observables (i.e., the phase space (F^*, P_F^*)) but not the sector of measurable quantities: superfluous (longitudinal) variables become the dynamic evolution parameter and dynamic Hamiltonian of the reduced theory.

5.6. Reparametrization-Invariant Path Integral. Following Faddeev–Popov procedure we can write down the path integral for local fields of our theory using constraints and gauge conditions (137)–(140):

$$Z_{\mathrm{local}}(F_1, F_2|P_0, \varphi_0, N_0) = \int\limits_{F_1}^{F_2} D(F, P_f)\Delta_s\bar{\Delta}_t \exp\left\{i\bar{W}\right\}, \tag{168}$$

where

$$D(F, P_f) = \prod_{t,x}\left(\prod_{i<k}\frac{dq^{ik}d\pi_{ik}}{2\pi}\prod_f\frac{df\,dp_f}{2\pi}\right) \tag{169}$$

are functional differentials for the metric fields (π, q) and the matter fields (p_f, f),

$$\Delta_s = \prod_{t,x,i}\delta(\mathcal{P}_i))\delta(\chi^j)\mathrm{det}\left\{\mathcal{P}_i, \chi^j\right\}, \tag{170}$$

$$\bar{\Delta}_t = \prod_{t,x}\delta(\mathcal{H}(\mu))\delta(\pi)\mathrm{det}\left\{\mathcal{H}(\varphi_0) - \rho, \pi\right\} \qquad \left(\rho = \frac{\int d^3x H(\varphi_0)}{V_0}\right) \tag{171}$$

are the F-P determinants, and

$$\bar{W} = \int\limits_{t_1}^{t_2} dt\left\{\int\limits_{V_0} d^3x\left(\sum_F P_F\dot{F}\right) - P_0\dot{\varphi}_0 - N_0\left[-\frac{P_0^2}{4V_0} + H(\varphi_0)\right] + \frac{1}{2}\partial_t(P_0\varphi_0)\right\} \tag{172}$$

is extended action of considered theory.

By analogy with a particle and a string considered in Sections 3 and 4 we define a commutative Green function as an integral over global fields (P_0, φ_0) and the average over reparametrization group parameter N_0

$$G_+(F_1, \varphi_1|F_2, \varphi_2) = \int\limits_{\varphi_1}^{\varphi_2}\prod_t\left(\frac{d\varphi_0 dP_0 d\tilde{N}_0}{2\pi}\right) Z_{\mathrm{local}}(F_1, F_2|P_0, \varphi_0, N_0), \tag{173}$$

where

$$\tilde{N} = N/2\pi\delta(0), \qquad \delta(0) = \int dN_0. \tag{174}$$

The causal Green function in the world field space (F, φ_0) is defined as the sum

$$\begin{aligned} G_c(F_1, \varphi_1 | F_2, \varphi_2) &= G_+(F_1, \varphi_1 | F_2, \varphi_2)\theta(\varphi_1 - \varphi_2) + \\ &+ G_+(F_2, \varphi_1 | F_2, \varphi_1)\theta(\varphi_2 - \varphi_1). \end{aligned} \tag{175}$$

This function will be considered as generating functional for the unitary S-matrix elements [25]

$$S[1,2] = \langle \text{out } (\varphi_2) | T_\varphi \exp \left\{ -i \int\limits_{\varphi_1}^{\varphi_2} d\varphi (H_I^*) \right\} | (\varphi_1) \text{ in} \rangle, \tag{176}$$

where T_φ is a symbol of ordering with respect to parameter φ_0, and $\langle \text{out } (\varphi_2)|$, $|(\varphi) \text{ in}\rangle$ are states of quantum univers in the lowest order of the Dirac perturbation theory ($\mathcal{N} = 1; \quad N^k = 0; \; q^{ij} = \delta_{ij} + h_{ij}$), H_I^* is the interaction Hamiltonian

$$H_I^* = H^* - H_0^*, \quad H^* = 2\sqrt{V_0 H(\varphi)}, \qquad H_0^* = 2\sqrt{V_0 H_0(\varphi)}, \tag{177}$$

H_0 is a sum of the Hamiltonians of «free» fields (gravitons, photons, massive vectors, and spinors) where all masses (including the Planck mass) are replaced by the dynamic evolution parameter φ_0 [7]. For example for gravitons the «free» Hamiltonian takes the form:

$$H_0(\varphi_0) = \int d^3x \left(\frac{6(\pi_{(h)})^2}{\varphi_0^2} + \frac{\varphi_0^2}{24} (\partial_i h)^2 \right) \quad (h_{ii} = 0; \quad \partial_j h_{ji} = 0). \tag{178}$$

In order to reproduce Faddeev–Popov integral for general relativity in infinite space-time [19], one should fix the dynamic evolution parameter at its present-day value $\varphi_0 = \mu$ (156), remove all the zero-mode dynamics $P_0 = \dot{\varphi}_0 = 0, N_0 = 1$, and neglect the surface Newton term in the Hamiltonian. We get

$$Z^{\text{FP}}(F_1, F_2) = Z_{\text{local}}(F_1, F_2 | P_0 = 0, \varphi_{0_{\text{exp}}} = \mu, N_0 = 1), \tag{179}$$

or

$$Z^{\text{FP}}(F_1, F_2) = \int\limits_{F_1}^{F_2} D(F, P_f) \Delta_s \Delta_t \exp \{ i W_{fp} \}, \tag{180}$$

where

$$W_{fp} = \int\limits_{-\infty}^{+\infty} dt \int d^3x \left(\sum_F P_F \dot{F} - \mathcal{H}_{fp}(\mu) \right), \qquad \mathcal{H}_{fp}(\mu) = \mathcal{H}(\mu) - \frac{\mu^2}{6} \partial_i \partial_j q^{ij}, \tag{181}$$

and

$$\Delta_t = \prod_{t,x} \delta(\mathcal{H}(\mu))\delta(\pi)\det\{\mathcal{H}(\mu), \pi\}. \tag{182}$$

The FP integral (180) is considered as the generating functional for unitary perturbation theory in terms of S-matrix elements

$$S[-\infty|+\infty] = \langle \text{out}|T\exp\left\{-i\int\limits_{-\infty}^{+\infty} dt H_I(\mu)\right\}|\text{in}\rangle. \tag{183}$$

Strictly speaking, the approximation (179) is not a correct procedure, as it breaks the reparametrization-invariance. The range of validity of FP integral (180) is discussed in next sections.

6. REPARAMETRIZATION-INVARIANT DYNAMICS OF EARLY UNIVERSE

6.1. Dynamic Unconstrained System. Possible states of a free quantum universe in S matrix (176) (see Fig. 5) are determined by the lowest order of the Dirac perturbation theory given by the well-known system of «free» conformal fields (118), (178) in a finite space-time volume [7, 36]

$$\begin{aligned} W_0^E &= \int\limits_{t_1}^{t_2} dt \left(\left[\int d^3x \sum_F P_F \dot{F} \right] - P_0\dot{\varphi}_0 - \right. \\ &- \left. N_0 \left[-\frac{P_0^2}{4V} + H_0(\varphi_0) \right] + \frac{1}{2}\partial_0(P_0\varphi_0) \right), \end{aligned} \tag{184}$$

where H_0 is a sum of the Hamiltonians of «free» fields (gravitons (178), photons, massive vectors, and spinors) where all masses (including the Planck mass) are replaced by the dynamic evolution parameter φ_0 [7].

The classical equations for the action (184)

$$\frac{dF}{dT} = \frac{\partial H_0}{\partial P_F}, \qquad -\frac{dP_F}{dT} = \frac{\partial H_0}{\partial F}, \qquad P_0 = \pm 2\sqrt{V_0 H_0} := H_0^* \tag{185}$$

contain two invariant times: the geometric T and the dynamic $\varphi_0^{\pm}$ connected by the geometro-dynamic (back-reaction) equation

$$\frac{d\varphi_0^{\pm}}{dT} = \pm\sqrt{\rho_0(\varphi_0^{\pm})}, \qquad \left(\rho_0 = \frac{H_0}{V_0}\right). \tag{186}$$

$$W^E(g,\Psi)=\int d^4x\left\{-\frac{\mu^2\sqrt{-g}}{6}R(g)+L_{\text{matter}}(g,\Psi)\right\},\ \mu=m_{\text{Planc}}\sqrt{\frac{3}{8\pi}}$$

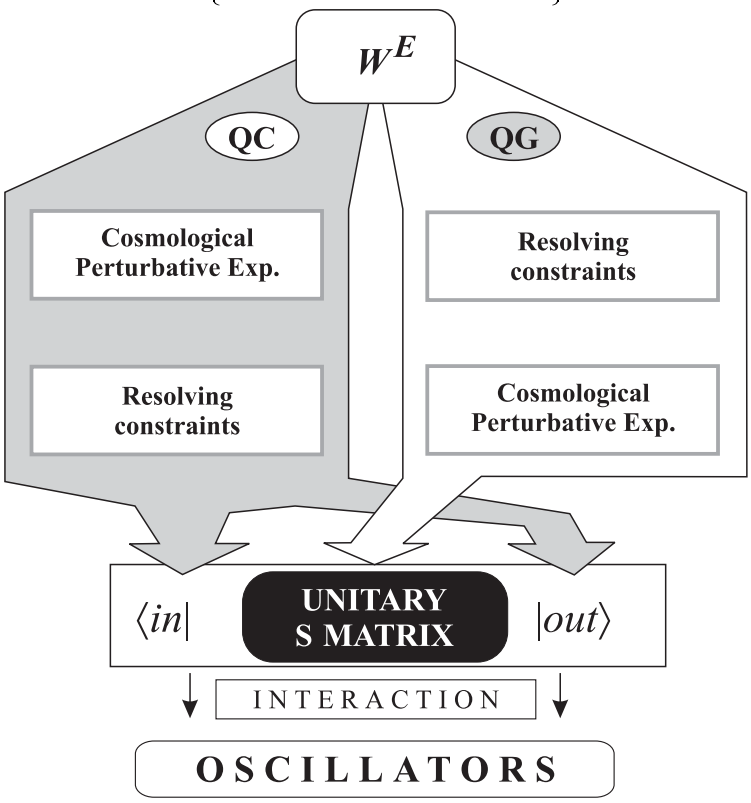

Fig. 5. To obtain the unitary S matrix in terms of invariants, one can use two ways: quantum cosmology (QC) and quantum gravity (QG). The first way (QC) is to formulate the cosmological perturbation theory and resolve constraints; this way is suitable for constructing «in» and «out» states as systems of «free oscillators». The second way (QG) is to resolve constraints and to formulate perturbation theory; this way is more suitable for constructing the unitary S matrix elements between the states of the Quantum Universe. Both the ways should be consistent

Solving the energy constraint we get the action for dynamic system

$$W_0^E(\text{constraint})=W_0^D=\int\limits_{\varphi(t_1)}^{\varphi(t_2)}d\varphi\left(\left[\int d^3x\sum_F P_F\partial_\varphi F\right]-H^*_{0\pm}+\frac{1}{2}\partial_\varphi(\varphi H^*_{0\pm})\right),\tag{187}$$

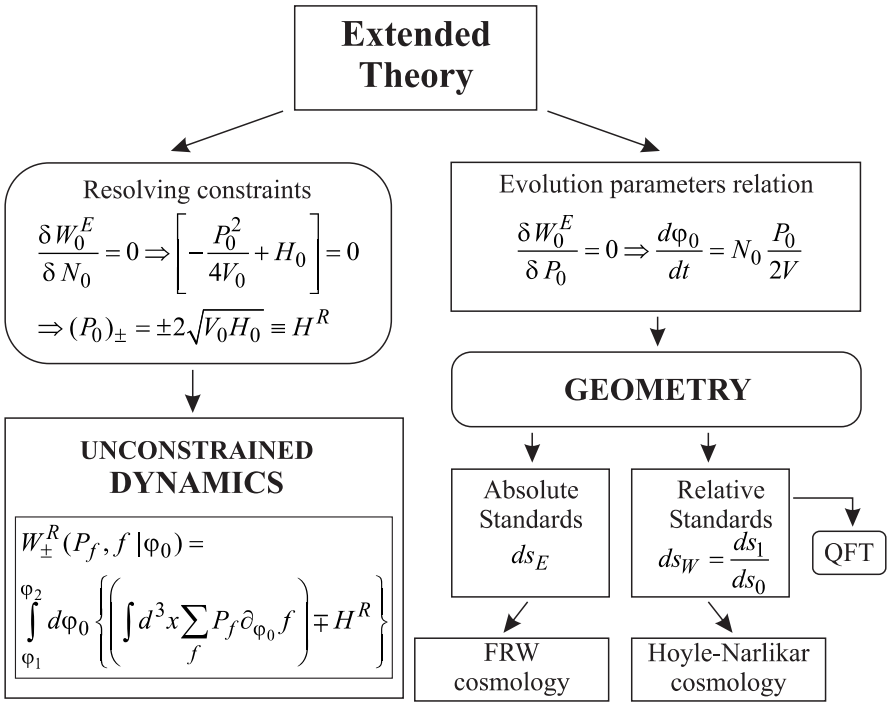

Freedman evolution goes from geometry

$$\frac{\delta W_0^E}{\delta P_0} = 0 \Rightarrow \frac{d\varphi_0}{N_0 dt} = \frac{P_0}{2V} = \pm\sqrt{\frac{H_0}{V}} \equiv \pm\sqrt{\rho_0(\varphi_0)} \xrightarrow{N_0 dt = dT} \frac{d\varphi_0}{dT} = \pm\sqrt{\rho_0(\varphi_0)}$$

Choosing "plus" sign we get

GEOMETRY (DYNAMICS) $\Rightarrow T(\varphi_0) = \int^{\varphi_0} \frac{d\varphi}{\sqrt{\rho_0(\varphi)}}$ Evolution of the universe

Fig. 6. The reduction means explicit resolving the energy constraint with respect to the momentum of the cosmic scale factor which gives a negative contribution to the constraint. As a result, we get an unconstrained version of «free» theory, where the cosmic scale factor φ_0 represents the dynamic evolution parameter, and its momentum converts into the reduced Hamiltonian ($H_O^R = 2\sqrt{V_0 H_0}$). However, the unconstrained dynamics is not sufficient to determine the geometrical interval of the proper time. The latter coincides with the Friedmann time for the absolute standard of measurement, in the FRW cosmology; or with the conformal time for the relative standard, in the Hoyle–Narlikar cosmology

that has two branches for a universe with a positive energy ($P_0 > 0$), and a universe with a negative energy ($P_0 < 0$). We interpret the branch with negative energy as an «antiuniverse» which propagates backward ($\varphi < 0$) with positive energy to provide the stability of a quantum system (see Fig. 6).

The content of matter in a universe is described by the number of particles $N_{F,k}$ and their energy $\omega_F(\varphi_0, k)$ (which depends on the dynamic evolution parameter φ_0 and quantum numbers k, momenta, spins, etc.). Detected particles are defined as the field variables $F = f$

$$f(x) = \sum_k \frac{C_f(\varphi_0)\exp(ik_i x_i)}{V_0^{3/2}\sqrt{2\omega_f(\varphi_0,k)}}\left(a_f^+(-k) + a_f^-(k)\right) \tag{188}$$

which diagonalize the operator of the density of matter

$$\begin{aligned} \rho_0 &= \sum_{f,k} \frac{\omega_f(\varphi_0,k)}{V_0}\hat{N}_{f,k}, \\ \hat{N}_f(a) &= \frac{1}{2}(a_f^+ a_f^- + a_f^- a_f^+) \end{aligned} \tag{189}$$

(see Fig. 7).

We restrict ourselves to gravitons ($f = h$) $C_h(\varphi_0) = \varphi_0\sqrt{12}$, $\omega_h(\varphi_0, k) = \sqrt{k^2}$ and massive vector particles ($f = v$) $C_v(\varphi_0) = 1$, $\omega_v(\varphi_0, k) = \sqrt{k^2 + y^2\varphi_0^2}$, where y is the mass in terms of the Planck constant.

6.2. Geometric Unconstrained System. The equations of motion (185) in terms of a^+, a^- [7] are not diagonal

$$i\frac{d}{dT}\chi := i\chi'_{a_f} = -\hat{H}_{a_f}\chi_{a_f}, \quad \chi_{a_f} = \begin{pmatrix} a_f^+ \\ a_f \end{pmatrix}, \quad \hat{H}_{a_f} = \begin{vmatrix} \omega_{a_f}, & -i\Delta_f \\ -i\Delta_f, & -\omega_{a_f} \end{vmatrix}, \tag{190}$$

where nondiagonal terms $\Delta_{f=h,v}$ are proportional to the Hubble parameter (156)

$$\Delta_{f=h} = \frac{\varphi'_0}{\varphi_0}, \qquad \Delta_{f=v} = -\frac{\omega'_v}{2\omega_v}, \qquad \varphi'_0 = \sqrt{\rho_0}. \tag{191}$$

The «geometric system» (b^+, b) is determined by the transformation to the set of variables which diagonalize equations of motion (185) and determine a set of integrals of motion of equations (185) (as conserved numbers $\{Q\}$).

To obtain integrals of motion and to choose initial conditions for a universe evolution we use the Bogoliubov transformations [37] and define «quasi-particles»

$$b^+ = \cosh(r)\,\mathrm{e}^{-i\theta}a^+ - i\sinh(r)\,\mathrm{e}^{i\theta}a, \quad b = \cosh(r)\,\mathrm{e}^{i\theta}a + i\sinh(r)\,\mathrm{e}^{-i\theta}a^+, \tag{192}$$

"The most important aspect of any phenomenon from mathematical point of view is that of a MEASURABLE QUANTITY. I shall therefore consider electrical phenomena chiefly with a view to their measurement, describing the methods of measurement, and defining the STANDARDS on which they depend."

Maxwell J.C. 1873. *A Treatise on Electricity and Magnetism* (Oxford)

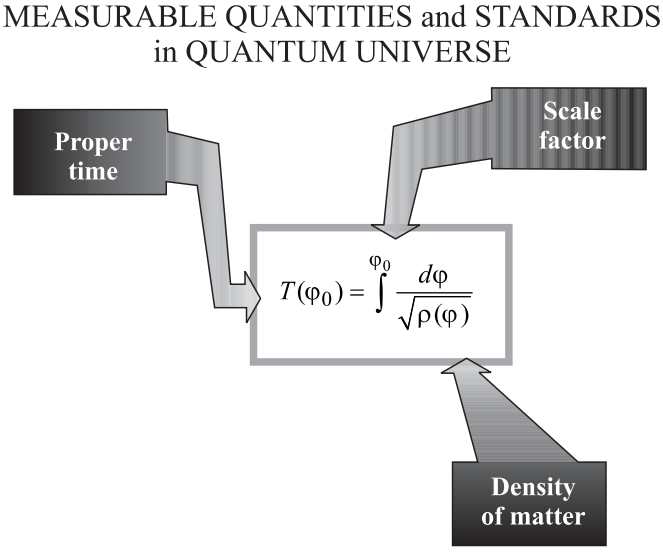

Fig. 7. The equation for dynamic evolution of the measurable time contains the energy density ρ which is treated as the measurable quantity in astrophysics and observational cosmology as the object of numerous discussions about the dark matter and hidden mass. Following the observational cosmology, we shall also treat this quantity ρ as the observable energy density and define «particles» as field variables in the holomorphic representation, which diagonalize this observable energy density

or

$$\chi_b = \begin{pmatrix} b^+ \\ b \end{pmatrix} = \hat{O}\chi_a,$$

which diagonalize the classical equations expressed in terms of particles (a^+, a), so that the number of quasiparticles is conserved

$$\frac{d(b^+b)}{dt} = 0, \qquad b = \exp\left(-i\int_0^T d\bar{T}\bar{\omega}_b(\bar{T})\right)b_0 \tag{193}$$

BOGOLIUBOV EQUATION
(state equations)

$$\underline{N}_0(r) = \cosh(2r) = {}_b\langle 0 \,|\, \hat{N}_a 0 \rangle_b \qquad \mathrm{H}_{\mathrm{Hubble}} = \frac{1}{\varphi}\frac{d\varphi}{dT} = \frac{\sqrt{\rho}}{\varphi}$$

$$\underline{\omega}_b^h = \omega_h \underline{N}_0 - \mathrm{H}_{\mathrm{Hubble}}\left[\sqrt{\underline{N}_0^2 - 1}\cos 2\theta + \underline{N}_0 \frac{\varphi d\theta}{d\varphi}\right]$$

$\underline{\omega}_b$ — quasiparticle energy

$$0 = \omega_h\sqrt{\underline{N}_0^2 - 1} - \mathrm{H}_{\mathrm{Hubble}}\left[\underline{N}_0 - \cos 2\theta + \sqrt{\underline{N}_0^2 - 1}\frac{\varphi d\theta}{d\varphi}\right]$$

$$\sqrt{\underline{N}_0^2 - 1}\sin 2\theta = -\frac{\varphi d\underline{N}_0}{2d\varphi}$$

$$\rho(\varphi) = \frac{{}_b\left\langle 0 \left| \sum_f \omega_f(\varphi) N_a^f \right| 0 \right\rangle_b}{V_0} = ?$$

Fig. 8. The Bogoliubov quasiparticles are defined as field variables which diagonalize the equations of motion and mark states of the universe by integrals of motion (i.e., quantum numbers in the corresponding quantum theory with a vacuum state $|0>_b$). The Bogoliubov transformation means the construction of a geometric unconstrained system (GUS), for which a new internal evolution parameter coincides with the conformal time. The Bogoliubov vacuum expectation value of the number of «particles» measured in the comoving frame, and the Hubble parameter (H_{Hubble})

(see Fig. 8). Functions r and θ in (192), and the quasiparticle energy $\bar{\omega}_b$ in (193) are determined by the equation of diagonalization

$$i\frac{d}{dT}\chi_b = [-i\hat{O}^{-1}\frac{d}{dT}\hat{O} - \hat{O}^{-1}\hat{H}_a\hat{O}]\chi_b \equiv -\begin{pmatrix} \bar{\omega}_b, & 0 \\ 0, & -\bar{\omega}_b \end{pmatrix}\chi_b \qquad (194)$$

in the form obtained in [7]

$$\bar{\omega}_{fb} = (\omega_f - \theta_f')\cosh(2r_f) - (\Delta_f \cos 2\theta_f)\sinh(2r_f), \qquad (195)$$

$$0 = (\omega_f - \theta'_f)\sinh(2r_f) - (\Delta_f \cos 2\theta_f)\cosh(2r_f), \qquad r'_f = -\Delta_f \sin\, 2\theta_f.$$

Equations (191)–(195) are closed by the definition of «observable particles» in terms of quasiparticles

$$\rho(\varphi) = \frac{H_0}{V} = \frac{\sum\limits_f \omega_f(\varphi)\{a_f^+ a_f\}}{V_0}, \ \{a^+ a\} = \{b_0^+ b_0\}\cosh 2r - \frac{i}{2}(b^{+2} - b^2)\sinh 2r \tag{196}$$

with

$$\bar\omega_{fb} = \sqrt{(\omega_f - \theta'_f)^2 + (r'_f)^2 - \Delta_f^2}, \qquad \theta'_f = -\frac{1}{2}\left(\frac{r'_f}{\Delta_f}\right)' \left[1 - \frac{(r'_f)^2}{\Delta_f^2}\right]^{-1/2}, \tag{197}$$

$$\cosh(2r_f) = \frac{\omega_f - \theta'_f}{\bar\omega_{fb}}.$$

The constrained system in terms of geometric variables is described by the action

$$\tilde W^G = \int dt \left\{ \sum_f \frac{i}{2}\left(b\partial_t b^+ - b^+\partial_t b\right)_f - \tilde\Pi_0 \dot Q_0 - N_0\left[-\tilde\Pi_0 + \sum_f \omega_b^f(Q_0) N_f(b)\right]\right\}, \tag{198}$$

where the new dynamic evolution parameter Q_0 coincides with geometric time T on the equations of motion

$$\frac{\delta \tilde W^E}{\delta \tilde\Pi_0} = 0 \qquad \Rightarrow \qquad dQ_0 = dT. \tag{199}$$

Reduction of this system leads to the weak version of Geometric Unconstrained System (167)

$$\tilde W^{\mathrm{GUS}} = \int dT \left\{ \sum_f \frac{i}{2}\left(b\partial_T b^+ - b^+\partial_T b\right)_f - \sum_f \omega_b^f(T) N_f(b)\right\}. \tag{200}$$

We choose the initial data appropriate for the dynamics described by GUS (200).

6.3. Quantization. The initial data b_0, b_0^+ of quasiparticle variables (193) form the set of quantum numbers in quantum theory.

Let us suppose that we manage to solve equations (193)–(197) with respect to the geometric time T in terms of conserved numbers b_0^+, b_0. This means that the wave function of a quantum universe can be represented in the form of a series over the conserved quantum numbers $Q = n_{f,k} = \langle Q|b_f^+ b_f|Q\rangle$ of the Bogoliubov

states (compare with the similar series for a relativistic string in Section 4)

$$\Phi_Q(T) = \prod_{f,n_f} \exp\left\{-i\int\limits_0^T dT n_f \bar{\omega}_b(T)\right\} \frac{(b_f^+)^{n_f}}{\sqrt{n_f!}}|0\rangle_b. \tag{201}$$

In this geometric system, we have an arrow of the geometric time T for a universe

$$T_+(\varphi_2,\varphi_1) = \int\limits_{\varphi_1}^{\varphi_2} d\varphi\rho(\varphi)^{-1/2} > 0, \qquad \varphi_2 > \varphi_1, \tag{202}$$

and for an antiuniverse

$$T_-(\varphi_2,\varphi_1) = -\int\limits_{\varphi_1}^{\varphi_2} d\varphi\rho(\varphi)^{-1/2} = \int\limits_{\varphi_2}^{\varphi_1} d\varphi\rho(\varphi)^{-1/2} > 0, \qquad \varphi_1 > \varphi_2. \tag{203}$$

The dynamic system (187) of particle variables a^+, a is connected with the geometric one by the Bogoliubov transformations. Using these transformations we can find wave functions of a universe, for $\varphi_2 > \varphi_1$ and an antiuniverse, for $\varphi_1 > \varphi_2$

$$\Psi_Q(T) = A_Q^+\Phi_Q(T_+(\varphi_2,\varphi_1))\theta(\varphi_2-\varphi_1) + A_Q^-\Phi_Q^*(T_-(\varphi_2,\varphi_1))\theta(\varphi_1-\varphi_2), \tag{204}$$

where the first term and the second one are positive ($P_0 > 0$) and negative ($P_0 < 0$) frequency parts of the solutions with the spectrum of quasiparticles $\bar{\omega}_b$, A_Q^+ is the operator of creation of a universe with a positive «frequency» (which propagates in the positive direction of the dynamic evolution parameter) and A_Q^- is the operator of annihilation of a universe (or creation of an antiuniverse) with a negative «frequency» (which propagates in the negative direction of the dynamic evolution parameter).

We can see that the creation of a universe in the field world space and the creation of dynamic particles by the geometric vacuum ($b^+|0\rangle = 0$) are two different effects.

The second effect disappears if we neglect gravitons and massive fields. In this case, $d\rho/d\varphi = 0$, and one can represent a wave function of a universe in the form of the spectral series over eigenvalues ρ_Q of the density ρ

$$\Psi(f|\varphi_2,\varphi_1) = \sum_Q \frac{A_Q^+}{\sqrt{2\rho_Q}} \exp\left\{-i(\varphi_2-\varphi_1)\sum \frac{\bar{\omega}_f n_f}{\sqrt{\rho_Q}}\right\}\langle f|Q\rangle + \tag{205}$$

$$+\sum_Q \frac{A_Q^-}{\sqrt{2\rho_Q}} \exp\left\{i(\varphi_2-\varphi_1)\sum \frac{\bar{\omega}_f n_f}{\sqrt{\rho_Q}}\right\}\langle f|Q\rangle^*,$$

where $\langle f|Q\rangle$ is a product of normalizable Hermite polynomials.

6.4. Evolution of Quantum Universe. The equations of diagonalization (194) for the Bogoliubov coefficients (192) and the quasiparticle energy $\bar{\omega}_b$ (195) play the role of the equations of state of the field matter in a universe. We can show that the choice of initial conditions for the «Big Bang» in the form of the Bogoliubov (squeezed) vacuum $b|0\rangle_b = 0$ reproduces all stages of the evolution of the Friedmann–Robertson–Walker universe in their conformal versions: anisotropic, inflation, radiation, and dust (see Fig. 9).

The squeezed vacuum (i.e., the vacuum of quasiparticles) is the state of «nothing». For small φ and a large Hubble parameter, at the beginning of a universe, the state of vacuum of quasiparticles leads to the density of matter [7]

$$ {}_b\langle 0|\rho(a^+,\ a)|0\rangle_b = \rho_0 \frac{1}{2}\left(\frac{\varphi^2(0)}{\varphi^2(T)} + \frac{\varphi^2(T)}{\varphi^2(0)}\right), \qquad \theta = \frac{\pi}{4}, \tag{206} $$

where $\varphi(0)$ is the initial value, and ρ_0 is the density of the Casimir energy of vacuum of «quasiparticles». The first term corresponds to the conformal version of the rigid state equation (in accordance with the classification of the standard cosmology) which describes the Kasner anisotropic stage $T_{\pm}(\varphi) \sim \pm\varphi^2$ (considered on the quantum level by Misner [38]). The second term of the squeezed vacuum density (206) (for an admissible positive branch) leads to the stage with inflation of the dynamic evolution parameter φ with respect to the geometric time T

$$ \varphi(T)_{(+)} \simeq \varphi(0)\exp\left[T\sqrt{2\rho_0}/\varphi(0)\right]. $$

It is the stage of intensive creation of «measurable particles». After the inflation, the Hubble parameter goes to zero, and gravitons convert into photon-like oscillator excitations with the conserved number of particles.

At the present-day stage, the Bogoliubov quasiparticles coincide with particles, so that the measurable density of energy of matter in a universe is a sum of relativistic energies of all particles

$$ \rho_0(\varphi) = \frac{E}{V_0} = \sum_{n_f} \frac{n_f}{V_0}\sqrt{k_{fi}^2 + y_f^2\varphi^2(T)}, \tag{207} $$

where y_f is the mass of a particle in units of the Planck mass. The case of massless particles ($y = 0, \rho_0(\varphi) = \text{constant}$) corresponds to the conformal version of radiation stage of the standard FRW-cosmology. And the massive particles at rest ($k = 0, \rho_0(\varphi) = \rho_{\text{baryons}}\varphi/\mu$) correspond to the conformal version of the dust universe of the standard cosmology with the Hubble law

$$ \varphi' = \pm\sqrt{\rho_0} \ \Rightarrow \ \ \varphi_{\pm}(T) = \left(\frac{\rho_{\text{baryons}}}{4\mu}\right)T^2, \qquad q = \frac{\varphi''\varphi}{\varphi'^2} = \frac{1}{2}. \tag{208} $$

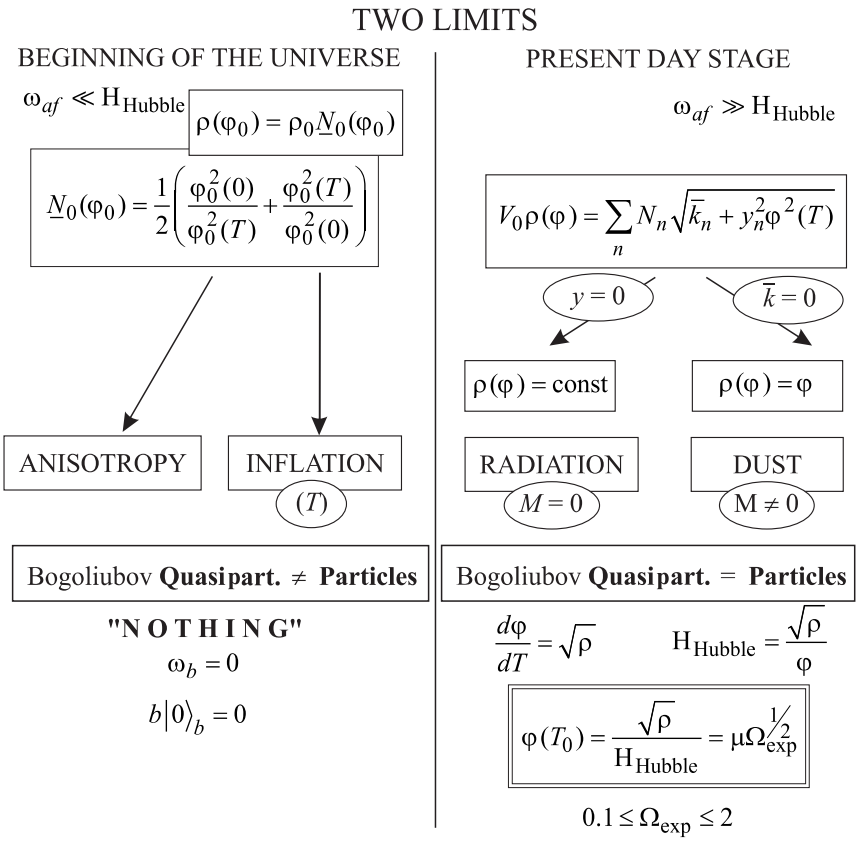

Fig. 9. These equations can be explicitly solved in two limits: at the beginning of the universe, and at the present-day stage. At the beginning of the universe in the state of the Bogoliubov vacuum, we get the density of measurable gravitons which corresponds to the well-known anisotropic stage. The anisotropic stage is changed by the stage of inflation-like increase of the cosmic scale factor with respect to the geometric (i.e., conformal) time. At the present-day stage, the Bogoliubov quasiparticles coincide with the measurable particles, so that the measurable energy of matter in the universe is a sum of relativistic energies of all particles in it. Neglecting masses, we get the conformal version of the radiation stage. Neglecting momenta, we get the conformal version of the dust stage, where an observer with the relative standard observes the Hubble law of the «accelerating» universe. According to the global equation for the cosmic scale factor φ_0 discussed before, it can be expressed in terms of astrophysical data of the observational cosmology, the density of matter, and the Hubble parameter in agreement with the value of the Newton coupling constant of gravity with $\Omega_{\rm theor} = 1$

The dynamic evolution parameter is expressed through the geometric time of a quantum asymptotic state of a universe $|\mathrm{out}\rangle$ and conserved quantum numbers of this state: energy E_{out} and density $\rho_0 = E_{\mathrm{out}}/V_0$.

It is well known that E_{out} is a tremendous energy (10^{79} GeV) in comparison with possible real and virtual deviations of the free Hamiltonian in the laboratory processes:

$$\bar{H}_0 = E_{\mathrm{out}} + \delta H_0, \quad \langle \mathrm{out}|\delta H_0|\mathrm{in}\rangle \ll E_{\mathrm{out}}. \tag{209}$$

We have seen that the dependence of the scale factor φ_0 on the geometric time T (or the «relation» of two classical unconstrained systems: dynamic and geometric) describes the «Big Bang» and evolution of a universe.

Therefore, from the point of view of unconstrained system «Big Bang» is the effect of evolution of the geometric interval with respect to the dynamic evolution parameter which goes beyond the scope of Hamiltonian description of a single classical unconstrained system.

Reparametrization-invariant dynamics of GR is covered by Geometric and Dynamic Unconstrained Systems connected by the Levi-Civita transformation of the matter fields into the vacuum fields of initial data with respect to geometric time (see Fig. 3).

6.5. QFT Limit of Quantum Gravity. The simplest way to determine the QFT limit of Quantum Gravity and to find the region of validity of the FP integral (180) is to use the quantum field version of the reparametrization-invariant integral (173) in the form of S-matrix elements [25] (see (176), (177)). We consider the infinite volume limit of the S-matrix element (177) in terms of the geometric time T for the present-day stage $T = T_0, \varphi(T_0) = \mu$, and $T(\varphi_1) = T_0 - \Delta T, T(\varphi_2) = T_0 + \Delta T = T_{\mathrm{out}}$. One can express this matrix element in terms of the time measured by an observer of an out-state with a tremendous number of particles in a universe using equation (208) $d\varphi = dT_{\mathrm{out}}\sqrt{\rho_{\mathrm{out}}}$ and approximation (209) to neglect «back-reaction». In the infinite volume limit, we get from (177)

$$d\varphi_0[H_I^*] = 2d\varphi_0\left(\sqrt{V_0(H_0+H_I)} - \sqrt{V_0 H_0}\right) = dT_{\mathrm{out}}[\hat{F}\bar{H}_I + O(1/E_{\mathrm{out}})], \tag{210}$$

where H_I is the interaction Hamiltonian in GR, and

$$\hat{F} = \sqrt{\frac{E_{\mathrm{out}}}{H_0}} = \sqrt{\frac{E_{\mathrm{out}}}{E_{\mathrm{out}} + \delta H_0}} \tag{211}$$

is a multiplier which plays the role of a form factor for physical processes observed in the «laboratory» conditions when the cosmic energy E_{out} is much greater than the deviation of the free energy

$$\delta H_0 = H_0 - E_{\mathrm{out}}; \tag{212}$$

due to creation and annihilation of real and virtual particles in the laboratory experiments.

The measurable time of the laboratory experiments $T_2 - T_1$ is much smaller than the age of the universe T_0, but it is much greater than the reverse «laboratory» energy δ, so that the limit

$$\int\limits_{T(\varphi_1)}^{T(\varphi_2)} dT_{\rm out} \Rightarrow \int\limits_{-\infty}^{+\infty} dT_{\rm out}$$

is valid. If we neglect the form factor (211) that removes a set of ultraviolet divergences, we get the matrix element (183) that corresponds to the standard FP functional integral (180) and S-matrix element (183) with the geometric (conformal) time T (instead of the coordinate time t) and with conformal-invariant fields $t \to T_{\rm out}$:

$$S[-\infty|+\infty] = \langle {\rm out}|T\exp\left\{-i\int\limits_{-\infty}^{+\infty} dT_{\rm out}\hat{F}H_I(\mu)\right\}|{\rm in}\rangle \qquad (\hat{F}=1). \quad (213)$$

Thus, the standard FP integral and the unitary S matrix for conventional quantum field theory (QFT) appears as the nonrelativistic approximation of tremendous mass of a universe and its very large lifetime (see Fig. 4). Now, it is evident that QFT are not valid for the description of the early universe given in the finite spatial volume and the finite positive interval of geometrical time $(0 \leqslant T \leqslant T_0)$ where T_0 is the «present-day value» for the early universe that only begins to create matter.

On the other hand, we revealed that standard QFT (that appears as the limit of quantum theory of the Einstein general relativity) speaks on the language of the conformal fields and coordinates. If we shall consider the standard QFT as the limit case of quantum gravity, we should recognize that, in QFT, we measure the conformal quantities, as QFT is expressed in terms of the conformal-invariant Lichnerowicz variables and coordinates including the conformal time ($T_{\rm out}$) as the time of evolution of these variables.

The conformal invariance of the variables can testify to the conformal invariance of the initial theory of gravity. What is this theory?

7. CONFORMAL RELATIVITY

7.1. Action and Geometry. There are observations [5,39,42] that the classical equations of Einsten's GR (111) are dynamically equivalent to the conformal-invariant theory described by the Penrose–Chernikov–Tagirov [43] action with a

negative sign

$$W(g|\Phi) = \int d^4x[-\sqrt{-g}\frac{\Phi^2}{6}R(g) + \Phi\partial_\nu(\sqrt{-g}g^{\mu\nu}\partial_\nu\Phi) + \mathcal{L}^c_{\rm matter}] \qquad (214)$$

and with the additional «dilaton» field Φ referred to as a conformal compensator and with the corresponding Lagrangian of fields of matter $\mathcal{L}^c_{\rm matter}$ [42].

The conformal-invariant version of Einstein's dynamics (214) is not compatible with the absolute standard of measurement of lengths and times given by the Einstein interval in the Riemannian geometry (112) as the latter is not conformal-invariant. As it was shown by Weyl in 1918 [44], a conformal-invariant theory corresponds to the relative standard of measurement of a conformal-invariant ratio of two intervals

$$(ds)_w = \frac{(ds_1)}{(ds_2)} \qquad (215)$$

given in the geometry of similarity as a manifold of Riemannian geometries connected by conformal transformations. The geometry of similarity is characterized by a measure of change of the length of a vector in its parallel transport. In the case (214), it is the gradient of the dilaton Φ [5, 39]. In the following, we call the theory (214) with intervals (215) the conformal relativity (CR), to differ it from the original Weyl [44] theory where the measure of change of the length of a vector in its parallel transport is a vector field.

Thus, the choice between two dynamically equivalent theories — general relativity (GR) and conformal relativity — (CR) (214) is the choice between the Riemannian geometry (112) and Weyl's geometry of similarity (215). The evident fact of the correspondence of the conformal-invariant theory (214) to the geometry of similarity (215) is ignored in the current literature (see, for example, paper [42]).

7.2. Variables and Hamiltonian. The dynamic equivalence of GR and CR becomes evident in the generalized Hamiltonian approach to solution of the problems of dynamics and initial data, as in both the theories, these problems are considered in terms of the Lichnerowicz conformal-invariant variables [29, 35].

In terms of the Lichnerowicz conformal-invariant variables formed by the determinant of the spatial metric $|^{(3)}g_{ij}| = \mathbf{g}$

$$f^{(n)}_c = f^{(n)}\mathbf{g}^{-n/6} \qquad (216)$$

GR (111) locally coincides with CR. The conformal-invariant dilaton in CR φ_c corresponds to the determinant of the space metric multiplied by the Planck constant in GR: μ ($\mathbf{g}^{1/6}\mu = \varphi_c$) [5] (see the Table).

In CR (214), we obtain the same Hamiltonian equations, the same reduction, and the same Levi-Civita transformation with the only one difference: the conformal variables, coordinates, and geometric time T are considered not as a mathematical tool, but as measurable quantities in the conformal relativity (214) [5].

Table. In terms of the Lichnerowicz conformal invariant variables (g_c), the Einstein general relativity (GR) (with the scale factor $\phi_g = \mu \parallel^3 g \parallel^{1/6}$) can be treated as the scalar version of the Weyl conformal invariant theory (with the scalar conformal field ϕ_c instead of the scale factor). In the Conformal Unified Theory (CUT), the Weyl scalar field forms both the Planck mass (in agreement with the present-day astrophysical data) and masses of elementary particles (in agreement with the principle of equivalence)

TWO VERSIONS	
GR	**CUT**
$\sqrt{-g}\left[-\frac{\mu^2 R}{6} + \mathcal{L}_{\rm mat}(g,\Psi)\right]$ (Lichnerowicz)	$\sqrt{-g}\left[-\frac{\Phi^2 R}{6} + \frac{\Phi}{\sqrt{-g}}\partial(\sqrt{-g}\partial\Phi) + \mathcal{L}_{\rm c}^{\rm SM}\right]$ $\Phi \propto$ modulus of Higgs field in SM
$N_c = N \parallel^{(3)} g \parallel^{-1/6}$	$N_c = N \parallel^{(3)} g \parallel^{-1/6}$
$g_{ij}^c =^{(3)} g_{ij} \parallel^{(3)} g \parallel^{-1/3}$	$g_{ij}^c =^{(3)} g_{ij} \parallel^{(3)} g \parallel^{-1/3}$
$\Phi_g = \mu \parallel^{(3)} g \parallel^{-1/6}$	$\Phi_c = \Phi \parallel^{(3)} g \parallel^{-1/6}$
$-N_c\frac{\phi_g^2}{6}R_c + \phi_g\partial(N_c\partial\phi_g) + N_c\mathcal{L}_{\rm mat}$	$-N_c\frac{\phi_c^2}{6}R_c + \phi_c\partial(N_c\partial\phi_c) + N_c\mathcal{L}_{\rm c}^{\rm SM}$
ABSOLUTE STANDARDS	RELATIVE STANDARDS
$(ds)^2 = g_{\mu\nu}dx^\mu dx^\nu$	$(ds)^2 = g_{\mu\nu}^c dx^\mu dx^\nu$
DIFFERENCES	
♦ mixing of internal evolution parameter and metric ♦ evolution of 3d-volume in FRW approximation ♦ singularity of 3d-volume	♦ separation of internal evolution parameter from metric ♦ evolution of particle masses ♦ 3d-volume conformal singularity moved to dynamics

7.3. Physical Consequences. In a space with the geometry of similarity, an observer can measure only the conformal-invariant ratio of lengths of two vectors (215). In particular, in the homogeneous approximation,

$$\varphi_c(t,x) = \varphi_0(t)a(t,x), \qquad a(t,x) = 1$$

a Weyl observer measures the conformal time by his watch and obtains the conformal version of the Friedmann cosmology, i.e., the Hoyle–Narlikar-type cosmology [40] with the conformal Hubble parameter $\mathcal{H}_{\rm hub}^c = \varphi'/\varphi$.

The action of conformal relativity (214) does not contain any dimensional parameter, except for a finite time interval and finite volume, as the universe has

the beginning $T = 0$ and the end $T = T_0$, i.e., the present-day stage, where the value of the scalar field

$$\varphi(T = T_0) = \frac{\sqrt{\rho_{\text{baryons}}}}{\mathcal{H}^c_{\text{hub}}} = \mu \tag{217}$$

coincides with the coupling constant of the Newton interaction, in agreement with equations of motion and astrophysical observational data (156) [5]. Equation (217) is not the gauge $\Phi(x) = \mu$ [39,42] but the experimental fit [5,7].

In the conformal cosmology, the Hubble law is explained by the evolution of the masses of elementary particles [5], so that the photon on a star remembers the «size» of a star atom at the moment of emission, and this «size» increases during the time of traveling; as a result, we get the red shift of a star photon in comparison with a photon emitted by a standard atom on the Earth at the moment of observation. The conformal version at the dust stage (208) corresponds to the «accelerating universe» with

$$q_c = \frac{\varphi''\varphi}{\varphi'^2} = \frac{1}{2}, \tag{218}$$

instead of $q_F = -1/2$ for the Friedmann version (with the measurable time $dT_F = (\varphi/\mu)dT$).

7.4. Quantum Conformal Relativity: Cosmological Scenario. The universe was created with a zero reduced energy from the state of «nothing» in the world space of the conformal-invariant variable F_c, φ_0 at the moment of the geometric time $T = 0$. The stability of quantum theory explains the arrow and beginning of the geometric time.

The classical and quantum evolutions of the universe coincide and are described by the Levi-Civita-type transformation (see Fig. 4) to the set of new variables $(F_c, \varphi_0) \Rightarrow (V, Q_0)$ where the new dynamic evolution parameter is the geometric time T ($dQ_0 = dT$). This transformation is the Bogoliubov one from «particle-like» variables (which diagonalize the measurable Hamiltonian) to «quasiparticle-like» variables (which diagonalize equations of motion). In particular, the Levi-Civita transformation defines the state of «nothing», i.e., initial data, as the vacuum of the Bogoliubov «quasipaticles», or squeezing vacuum.

The Levi-Civita evolution from «nothing» has four stages: «anisotropic», the squeezing vacuum «inflation» of the dilaton with respect to the geometric time, «radiation», and «dust» with accelerating evolution (218) (considered in Section 6). In the first two stages, the intensive creation of the matter fields (including gravitons) takes place, as «quasipaticles» differ from «particles».

In the last two stages, «quasipaticles» coincide with «particles», and these stages are the conformal version of the standard FRW cosmology.

7.5. Conformal Unified Theory. In the conformal theory (214), the Higgs mechanism of the formation of particle masses becomes superfluous and, moreover, it contradicts the equivalence principle, as, in the case of the standard Higgs mechanism, the Planck mass and masses of particles are formed by different scalar fields (see Fig. 10).

To save the equivalence principle we identify the modulus of the Higgs field with the Weyl dilaton [5, 39]. As a result, the Conformal Unified Theory (CUT) is described by the action [5, 39]

$$W_{\rm CUT} = -W_{\rm PCT} + W^c_{\rm SM}, \tag{219}$$

where $-W_{\rm PCT}(\varphi, g)$ is the Penrose–Chernikov–Tagirov action (214), and

$$W^c_{\rm SM}[\varphi, V, \psi, g] = \int d^4x \left(\mathcal{L}^{\rm SM}_{(\varphi=0)} + \sqrt{-g}[-\varphi F + \varphi^2 B]\right) \tag{220}$$

is the conformally invariant part of the SM action (i.e., the conventional SM action without the «free» part for the modulus of the Higgs $SU(2)$ doublet φ and without the Higgs mass term), B and F are the mass terms of the vector V and fermion ψ fields, respectively,

$$B = V_i \hat{Y}_{ij} V_j\,; \;\; F = \bar{\psi}_\alpha \hat{X}_{\alpha\beta}\psi_\beta, \tag{221}$$

$\hat{Y}$, $\hat{X}$ are the ordinary matrices of vector meson and fermion mass couplings in the WS theory multiplied by a rescaling parameter [5, 39].

The dilaton field φ forms both the Planck mass (in agreement with the present-day astrophysical data) and masses of elementary particles [5] (in agreement with the principle of equivalence). In other words, instead of the Higgs effect, we have the cosmic formation of all masses including the Planck one.

The effective Higgs potential could not be restored by the Coleman–Weinberg perturbation theory, as the vertices with scalar field interactions are eliminated from perturbation theory by the Bogoliubov transformations. Instead of the effective Higgs potential, in the exact theory, these interactions form cosmological evolution of the universe as the pure relativistic and quantum phenomenon which reproduces the conformal version of the standard Friedmann model (developed by Hoyle and Narlikar [40]).

The Weyl geometrization of the modulus of the Higgs field removes the Higgs potential with its problems of tremendous vacuum energy, monopole creation, the domain walls [41], and the violation of causality as the monotonous dependence ($\varphi(T)$). The conformal scalar field plays the role of the dynamic time and forms the Newton potential. As a consequence, the conformal version of the Higgs field loses its particle-like excitations [39] like the time component of the electromagnetic field. In CUT (219), we obtain the σ version of the Standard Model [4, 5, 39] without Higgs particles and with the prescription (211) which removes ultraviolet divergences from the SM sector.

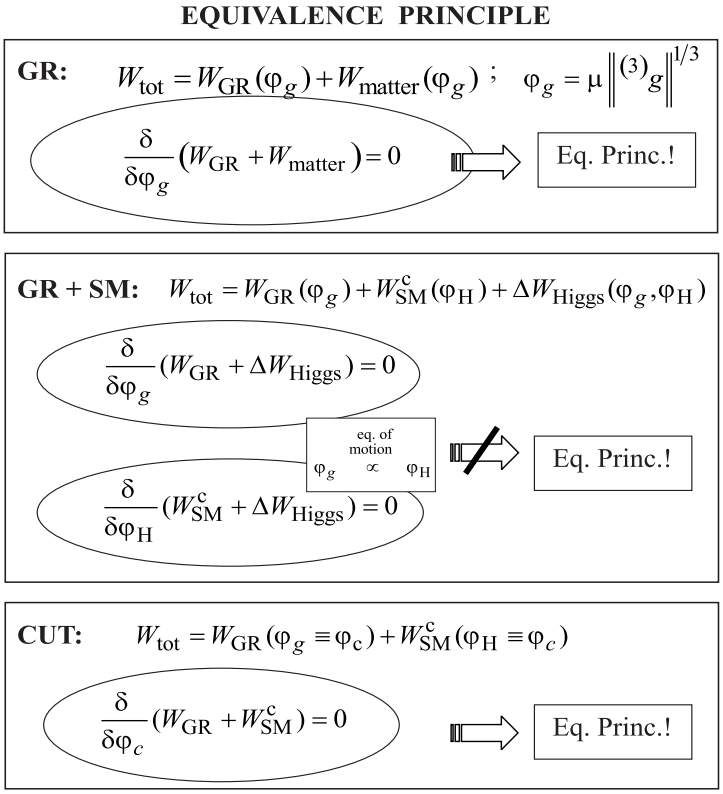

Fig. 10. In the Conformal Unified Theory (CUT), the Higgs mechanism of the formation of particle masses becomes superfluous, and, moreover, it contradicts the equivalence principle, as, in the case of a naive unification of general relativity (GR) and the Standard Model (SM), the Planck mass and masses of particles are of a different nature and are formed by different fields. The Weyl geometrization of the modulus of the Higgs field removes the Higgs potential with its problems of tremendous vacuum energy, monopole creation, and the domain walls

8. CONCLUSIONS

All relativistic systems (a particle, a string, a universe in general relativity) considered in the present review are given in their world spaces of dynamic variables by their singular actions (as integrals over the coordinate space) and by the geometric interval.

The peculiarity of relativistic systems is the invariance of their actions and the geometric intervals with respect to reparametrizations of the coordinate space, i.e., the general coordinate transformations, in general relativity. These

reparametrization-invariant relativistic theories are not compatible with the symplest variational principles of the Hamiltonian dynamics.

The main mystery of relativistic systems (which we tried to reveal in the review) is the following: the reparametrization symmetry means that the measurable geometric time is a time-like variable in the geometric world space (obtained by the Levi-Civita transformation to the action-angle-type variables) rather than the coordinate.

This mystery of the dynamic origin of the «time» was reliably covered by the gauge condition that the lapse-function is equal to unity.

This noninvariant gauge-fixing method of describing the Hamiltonian dynamics of relativistic systems was a real obstacle for understanding this dynamics. This noninvariant method confuses reparametrization-invariant (or measurable) quantities and noninvariant (nonobservable) ones and hides the necessity of constraining by the Levi-Civita transformation that converts ambiguous and attractive «mathematical games» with noninvariant quantities into a harmonious theory of invariant dynamics in the world space which includes an unambigouos description of quantum gravity with its relation to the standard cosmology of a classical universe.

To obtain the invariant dynamics, one should choose the dynamic evolution parameter and the homogeneous component of the lapse-function (separating the global motion of a relativistic system as a whole from the local one) to define the geometric time. This geometric time is converted into a new dynamic evolution parameter by the Levi-Civita canonical transformation.

The constraining of the initial dynamic system (to get a Dynamic Unconstrained System) loses the geometric time but determines the causal structure of a world space that follows from the stability of the quantum relativistic theory. Whereas, the constraining of the geometric system (after the Levi-Civita transformation in the strong version of the action-angle variables) loses any dynamics, as a Geometric Unconstrained System is only initial data with respect to the geometric time.

The evolution of the initial world space with respect to the geometric time (i.e., the evolution of a particle, a string, a universe) is described by the inverse Levi-Civita transformation.

The generating functionals for causal Green functions of the unitary perturbation theory in the form of path integrals are constructed by averaging over a space of the reparametrization group, instead of the gauge-fixing.

The operations of separation of the «centre-of-mass» coordinates and variation of the action do not commute. As a result, the invariant local constraints differ from the standard ones for a relativistic string. The invariant local constraints satisfy the Virasoro algebra only for the case of a string with a single value of the mass in the spectrum (in classical theory, this value is equal to zero) that corresponds to the light-like branch of the representation of the Poincare group.

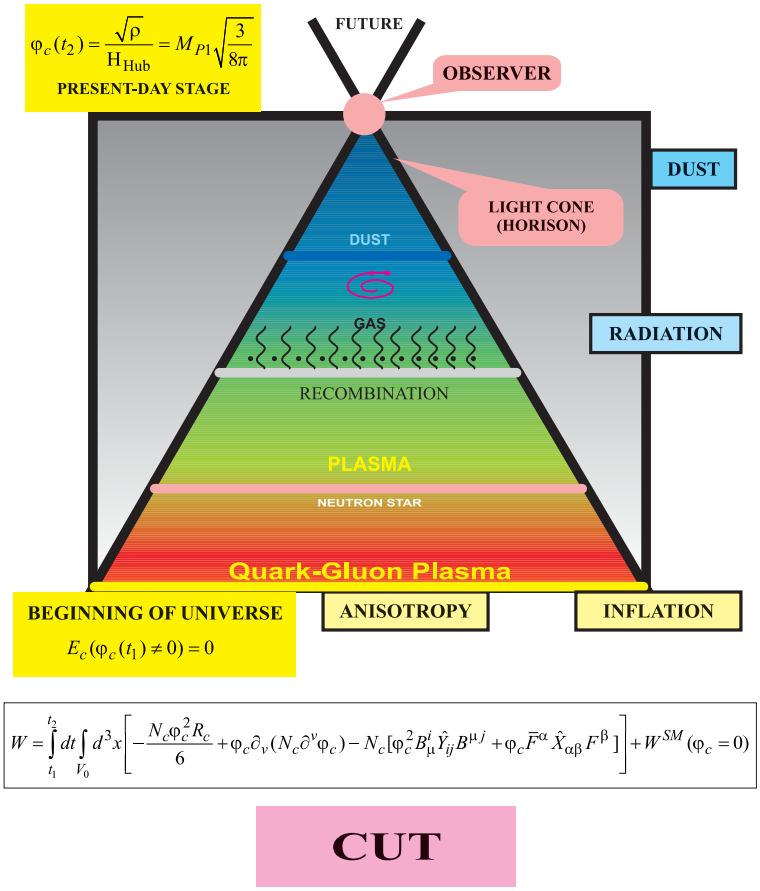

Fig. 11. Interactions of matter fields with a scalar field, in CUT, lead to the cosmic evolution of Quantum Universe with the set of predictions, including the Hoyle–Narlikar cosmology with the squeezed vacuum inflation, the accelerating evolution at the present-day dust stage. In CUT, we got the σ version of the Standard Model without Higgs particles, and with the «back-reaction» form factor to be free from the ultra-violet divergences for the precision calculations

In other words, for a string with a nontrivial spectrum of masses, the Virasoro algebra (with all its difficulties, including the $D = 26$ problem and the negative norm states) is an artefact of the reparametrization-noninvariant description.

To separate the global motion of a universe in general relativity, we used the wonderful effectivity of the Lichnerowicz conformal-invariant variables in solving the problems of the initial data and in formulating quantum field theory in the

Riemannian space. This effectivity was a signal of hidden conformal symmetry of the initial Einstein theory of gravitation. Really, the dynamics of Einstein's theory coincides with the dynamics of a conformal scalar field (dilaton) with the Penrose–Chernikov–Tagirov action with negative sign. However, the conformal-invariant theory is compatible with the Weyl geometry of similarity but not with the Riemannian one. The geometry of similarity converts the conformal-invariant Lichnerowicz variables from an effective mathematical tool to physical observables, consistent with large time and spatial volume limits of the obtained quantum gravity, where the standard Hamiltonian description of the evolution of matter fields with respect to the geometric time is possible.

The discovered conformal symmetry allows us to unify the conformal version of the Einstein theory with the Standard Model of electroweak and strong interactions on the basis of the equivalence principle that identifies the dilaton with the modulus of the Higgs field [5].

This unification of general relativity and Standard Model leads to a set of predictions, including the Hoyle–Narlikar cosmology with the «accelerating» evolution of the universe at the dust stage, the squeezed vacuum inflation from «nothing» at the beginning of the universe, and the negative result of the CERN experiment on the search of the Higgs particle [39], as the Weyl scalar field (like the determinant of the space metric in GR) has no particle-like excitations (see Fig. 11).

We would like to emphasize that we obtained the unification of a universe and an observer who appeared at the end of the evolution of the universe with respect to the geometric time; he measures the rhythm of the evolution by the rhythm of his heart and knows that any of his motions contributes to the global motion of the universe that forms its geometric time. «*Any motion*, if it makes sense, possesses also a *freedom*, and its task is to realize a good moral life, the final aim of which will be the *meaning of an everlasting existence*» (St. Maximus [45]).

Acknowledgements. We are happy to acknowledge interesting and critical discussions with A.M.Chervyakov, V.G.Kadyshevsky, H.Kleinert, E.A.Kuraev, V.V.Nesterenko, V.I.Smirichinski.

REFERENCES

1. **Dirac P.A.M.** — Proc. Roy. Soc., 1958, v.A246, p.333;
   Dirac P.A.M. — Phys. Rev., 1959, v.114, p.924.
2. **Arnovitt R., Deser S., Misner C.W.** — Phys. Rev., 1959, v.116, p.1322;
   Arnovitt R., Deser S., Misner C.W. — Phys. Rev., 1960, v.117, p.1595;
   Arnovitt R., Deser S., Misner C.W. — Phys. Rev., 1961, v.122, p.997.
3. **Isham C., Kuchar K.** — Ann. Phys. (NY), 1985, v.164, p.288;
   Hartle J.B., Kuchar K. — Phys. Rev., 1986, v.D34, p.2323;
   Hajicek P. — Nucl. Phys. Proc. Suppl., 1997, v.57, p.115.

4. **Gyngazov L.N., Pawlowski M., Pervushin V.N., Smirichinski V.I.** — Gen. Rel. and Grav., 1998, v.30, p.1749.
5. **Pawlowski M., Papoyan V.V., Pervushin V.N., Smirichinski V.I.** — Phys. Lett., 1998, v.444B, p.293.
6. **Fulop G., Gitman D.M., Tyutin I.V.** — Int. J. Theor. Phys., 1999, v.38, p.1941.
7. **Pervushin V.N., Smirichinski V.I.** — J. Phys. A: Math. Gen., 1999, v.32, p.6191.
8. **Dirac P.A.M.** — Lectures on Quantum Mechanics. Belfer Graduate School of Science, Yeshive University Press, New York, 1964.
9. **Hanson A.J., Regge T., Teitelboim C.** — Constrained Hamiltonian Systems. Accademia Nazionale dei Lincei, Rome, 1976.
10. **Gitman D.M., Tyutin I.V.** — Quantization of Fields with Constraints. Springer-Verlag, Berlin, 1990.
11. **Konopleva N.P., Popov V.N.** — Gauge Fields. M.: Atomizdat, 1972 (in Russian).
12. **Gogilidze S.A., Khvedelidze A.M., Pervushin V.N.** — Phys. Particles and Nuclei, 1999, v.30, p.66.
13. **Torre C.G.** — Class. Quantum Grav., 1991, v.8, p.1895.
14. **Khvedelidze A., Palii Yu., Papoyan V., Pervushin V.** — Phys. Lett., 1997, v.B402, p.263.
15. **Pawlowski M., Pervushin V.N.** — Reparametrization-Invariant Path Integral in GR and «Big Bang» of Quantum Universe. JINR Preprint E2-2000-67, Dubna, 2000; hep-th/0006116.
16. **Barbashov B.M., Pervushin V.N.** — Reparametrization-Invariant Dynamics of a Relativistic String. JINR Preprint E2-2000-100, Dubna, 2000, submitted to Th. Math. Phys.
17. **Dirac P.A.M.** — Can. J. Phys., 1955, v.33, p.650.
18. **Faddeev L.** — Teor. Mat. Fiz., 1969, v.1, p.3 (in Russian).
19. **Faddeev L.D., Popov V.N.** — Usp. Fiz. Nauk, 1973, v.111, p.427.
20. **DeWitt B.S.** — Phys. Rev., 1967, v.160, p.1113.
21. **Faddeev L., Popov V.** — Phys. Lett., 1967, v.B25, p.29.
22. **Levi-Civita T.** — Prace Mat.-Fiz., 1906, v.17, p.1.
23. **Shanmugadhasan S.** — J. Math. Phys., 1973, v.14, p.677.
24. **Gogilidze S.A., Khvedelidze A.M., Pervushin V.N.** — J. Math. Phys., 1996, v.37, p.1760;
Gogilidze S.A., Khvedelidze A.M., Pervushin V.N.— Phys. Rev., 1996, v.D53, p.2160.
25. **Schweber S.** — An Introduction to Relativistic Quantum Field Theory. Row, Peterson and Co. Evanston, Ill., Elmsford, N.Y., 1961.
26. **Brink L., Di Vecchia P., Howe P.** — Phys. Lett., 1976, v.B65, p.471.
27. **Green M.B., Schwarz J.H., Witten E.** — Superstring Theory. Cambridge University Press, Cambridge, New York, New Rochele, Melbourne, Sydney, 1986.
28. **Barbashov B.M., Nesterenko V.V.** — Introduction to the Relativistic String Theory. World Scientific, Singapore, New Jersey, London, Hong Kong, 1990.
29. **York J.W. (Jr.)** — Phys. Rev. Lett., 1971, v.26, p.1658;
Kuchar K. — J. Math. Phys., 1972, v.13, p.768.
30. **Brink L., Henneaux M.** — Lectures on String Theory. Paris, 1980.
31. **Zel'manov A.L.** — Doklady AN SSSR, 1976, v.227, p.78 (in Russian);
Vladimirov Yu.S. — Frame of References in Theory of Gravitation. M.: Energoizdat, 1982 (in Russian).

32. **Rebbi C.** — Phys. Rep., 1974, v.12, p.1.

33. **Röhrlich F.** — Phys. Rev. Lett., 1975, v.34, p.842;
Röhrlich F. — Nuovo Cim., 1977, v.A37, p.242.

34. **Pervushin V.N., Smirichinski V.I.** — Physics of Atomic Nuclei, 1998, v.61, p.142.

35. **Lichnerowicz A.** — Journ. Math. Pures and Appl., 1944, v.B37, p.23.

36. **Grib A.A., Mamaev S.G., Mostepanenko V.M.** — Quantum Effects in Intensive External Fields. M.: Atomizdat, 1980 (in Russian).

37. **Bogolubov N.N.** — J. Phys., 1947, v.11, p.23.

38. **Misner C.** — Phys. Rev., 1969, v.186, p.1319.

39. **Pawlowski M., Raczka R.** — Found. of Phys., 1994, v.24, p.1305.

40. **Narlikar J.V.** — Space Sci. Rev., 1989, v.50, p.523.

41. **Weinberg S.** — Rev. Mod. Phys., 1989, v.61, p.1;
Linde A.D. — Particle Physics and Inflationary Cosmology. M.: Nauka, 1990 (in Russian).

42. **Kallosh R., Kofman L., Linde A., Van Proeyen A.** — Superconformal Symmetry, Supergravity and Cosmology. CERN-TH/2000-118, 2000; hep-th/0006179.

43. **Penrose R.** — Relativity, Groups and Topology. Gordon and Breach, London, 1964;
Chernikov N., Tagirov E. — Ann. Ins. Henri Poincare, 1968, v.9, p.109.

44. **Weyl H.** — Sitzungsber. d. Berl. Akad. S., 1918, p.465.

45. **Meyndorf J.** — Byzantine Theology, Trends and Doctrinal Themes. Fordham University Press, New York, 1979.

«ФИЗИКА ЭЛЕМЕНТАРНЫХ ЧАСТИЦ И АТОМНОГО ЯДРА»
2001, ТОМ 32, ВЫП. 3

УДК 514.763.4

TOWARDS AN ALGEBRAIC CLASSIFICATION OF CALABI–YAU MANIFOLDS
Study of $K3$ Spaces

F. Anselmo

INFN–Bologna, Bologna, Italy

J. Ellis

Theory Division, CERN, CH-1211 Geneva, Switzerland

D.V. Nanopoulos

Dept. of Physics, Texas A & M University, College Station, TX 77843-4242, USA,
HARC, The Mitchell Campus, Woodlands, TX 77381, USA,
and Academy of Athens, 28 Panepistimiou Avenue, Athens 10679, Greece

G. Volkov

Theory Division, CERN, CH-1211 Geneva, Switzerland
and Theory Division, Institute for High-Energy Physics,
Protvino, Russia

We present an inductive algebraic approach to the systematic construction and classification of generalized Calabi–Yau (CY) manifolds in different numbers of complex dimensions, based on Batyrev's formulation of CY manifolds as toric varieties in weighted complex projective spaces associated with reflexive polyhedra. We show how the allowed weight vectors in lower dimensions may be extended to higher dimensions, emphasizing the roles of projection and intersection in their dual description, and the natural appearance of Cartan–Lie algebra structures. The 50 allowed extended four-dimensional vectors may be combined in pairs (triples) to form 22 (4) chains containing 90 (91) $K3$ spaces, of which 94 are distinct, and one further $K3$ space is found using duality. In the case of CY_3 spaces, pairs (triples) of the 10270 allowed extended vectors yield 4242 (259) chains with $K3$ (elliptic) fibers containing 730 additional $K3$ polyhedra. A more complete study of CY_3 spaces is left for later work.

На основе формулировки Батырева многообразий Калаби–Яо (КЯ) как торических множеств во взвешенных комплексных проективных пространствах, ассоциированных с рефлексивными полиэдрами, предложен индуктивный алгебраический подход к систематическому построению и классификации обобщенных многообразий КЯ для различных комплексных размерностей. Показано, как допустимые весовые векторы в низших размерностях могут быть расширены для высших размерностей. При этом отмечена роль проектирования и пересечения в их дуальном описании и естественное появление алгебраических структур Картана–Ли. Пятьдесят допустимых расширенных четырехмерных векторов могут быть скомбинированы в пары (тройки), формирующие 22 (4) цепочки, содержащие 90 (91) $K3$-пространств, из которых 94 являются особыми, а одно $K3$-пространство находится с использованием дуальности. В случае пространств CY_3

пары (тройки) из 10270 допустимых расширенных векторов дают 4242 (259) цепочек с $K3$ (эллиптическими)-расслоениями, содержащими 730 дополнительных $K3$-полиэдров. Более полное изучение CY_3-пространств будет приведено в следующей работе.

1. INTRODUCTION

One of the outstanding issues in both string theory and phenomenology is the choice of vacuum. Recent dramatic advances in the nonperturbative understanding of strings have demonstrated that all string theories, thought previously to be distinct, are in fact related by various dualities, and can be regarded as different phases of a single underlying theory, called variously M and/or F theory [1]. This deeper nonperturbative understanding does not alter the fact that many classical string vacua appear equally consistent at the perturbative level. However, the new nonperturbative methods may provide us with new tools to understand transitions between these classical vacua, and perhaps eventually provide a dynamical criterion for deciding which vacuum is preferred physically [2, 3].

Consistent string vacua are constrained by the principles of quantum mechanics applied to extended objects. At the classical level, these are expressed in the conformal symmetry of the supersymmetric world-sheet field theory. Consistent quantization of the string must confront a possible anomaly in conformal symmetry, as manifested in a net nonzero central charge of the Virasoro algebra. Early studies of the quantum mechanics of extended objects indicated that strings could not survive in the familiar dimension $D = 3 + 1$ of our space-time. The way initially used to cancel the conformal anomaly was to choose appropriately the dimension of the ambient space-time, for example, $D = 25 + 1$ for bosonic strings and $D = 9 + 1$ for the supersymmetric and heterotic strings.

This suggested that the surplus $n = 6$ real dimensions should be compactified. The simplest possibility is on a Calabi–Yau manifold [4], which is defined by the following conditions:

• It has a complex structure, with $N = 3$ complex dimensions required for the $D = 9 + 1 \to 3 + 1$ case of most direct interest, though all the cases $N = 1, 2, 3, 4, ...$ have some interest.

• It is compact.

• It has a Kähler structure.

• It has holonomy group $SU(n)$ or $Sp(n)$, e.g., $SU(3)$ in the $N = 3$ case.

It has subsequently been realized that one could compactify on an orbifold [5], rather than a manifold, and also that generalized heterotic strings could be formulated directly in $D = 3+1$ dimensions, with extra world-sheet degrees of freedom replacing the surplus space coordinates. More recently, the nonperturbative formulation of the theory in eleven or twelve dimensions, as M or F theory, has opened up new possibilities [6]. However, Calabi–Yau compactifications con-

tinue to play a key role in the search for realistic four-dimensional string models, motivating us to revisit their classification.

One of the most important tools in the investigation of such complex manifolds is the feature that their singularities are connected with the structure of Lie algebras. Kaluza was the first to attempt to understand this circumstance, and used this idea to embark on the unification of all the gauge interactions known at that time, namely electromagnetism and gravitation. These ideas were subsequently extended to non-Abelian gauge theories, and string theory can be regarded as the latest stage in the evolution of this programme.

The three-complex-dimensional CY manifolds can be situated in a sequence of complex spaces of increasing dimensions: two-real- (one-complex-)dimensional tori T_2, the two-complex-dimensional $K3$ spaces, the three-complex-dimensional CY_3 themselves, four-complex-dimensional CY_4, etc., whose topological structure and classification become progressively more complicated. Their topologies may be described by the Betti–Hodge numbers which count the numbers of distinct one-, two-, three-dimensional, ... cycles (holes,...). The topological data of the different CY manifolds determine their physical properties, such as the different numbers of generations N_g (which are related to the Euler characteristics of CY_3 spaces), etc. This emphasizes the desirability of approaching systematically the problem of their classification and the relations between, e.g., CY_3 manifolds with different values of the Euler characteristic and hence the number of generations N_g. Since some nonperturbative tools now exist for studying transitions between different CY manifolds, one could hope eventually to find some dynamical criterion for determining N_g.

The topologies and classification of the lower-dimensional spaces in this sequence are better known: although our ultimate objective is deeper understanding of CY_3 spaces, in this paper we study as a warm-up problem the simpler case of the two-complex-dimensional $K3$ hypersurfaces. These are of considerable interest in their own right, since, for example, they may appear as fibrations of higher-dimensional CY_n spaces. It is well known that any two $K3$ spaces are diffeomorphic to each other. This can be seen, for example, by using the polyhedron techniques of Batyrev [7] discussed in Sections 2 and 3, to calculate the Betti–Hodge invariants for all the $K3$ hypersurfaces corresponding to the $\mathbf{k}_4$ vectors we found. It is easy to check that Batyrev's results yield the same Euler number 24 for all $K3$ manifolds [8].

The quasi-homogeneous polynomial equations (hereafter called CY equations) whose zeroes define the CY spaces as hypersurfaces in complex projective space are defined (2.6), (2.7), (2.8), (2.9) by projective vectors $\mathbf{k}$, whose components specify the exponents of the polynomials. The number of CY manifolds is large but finite, as follows from the property of reflexivity introduced in Section 2. The central problem in the understanding of classification of these manifolds may be expressed as that of understanding the set of possible projective vectors

$\mathbf{k} = (k_1, \ldots, k_{n+1})$, the corresponding Lie algebras and their representations. More precisely, the classification of all CY manifolds contains the following problems:

• To study the structure of the $K3, CY_3, ...$ projective vectors $\mathbf{k}_n$, in particular, to find the links with the projective vectors of lower dimensions: $D = n-1, n-2, ...$

• To establish the web of connections between all the projective vectors $\mathbf{k}_n$ of the same dimension.

• To find an algebraic description of the geometrical structure for all projective vectors, and calculate the corresponding Betti–Hodge invariants.

• To establish the connections between the projective vectors $\mathbf{k}_n$, the singularities of the corresponding CY hypersurfaces, the gauge groups and their matter representations, such as the number of generations, N_g.

• To study the duality symmetries and hypermodular transformations of the projective vectors $\mathbf{k}_n$.

In addition to the topological properties and gauge symmetries already mentioned, it is now well known that string vacua may be related by duality symmetries. This feature is familiar even from simple compactifications on S_1 spaces of radius R, which revealed a symmetry: $R \to 1/R$ [9]. In the case of compactifications on tori, there are known to be S, T, and U dualities that interrelate five string theories and play key roles in the formulations of M and F theories [10]. Compactifications on different types of CY manifolds have also been used extensively in verifying these string dualities [10]. For example, in proving the duality between type-II A and type-II B string theories, essential use was made of the very important observation that all CY manifolds have mirror partners [7, 11–15]. Thus, duality in string theory found its origins in a duality of complex geometry.

Further information about string/M/F theory and its compactifications on CY manifolds can be obtained using the methods of *toric geometry*. The set of homogeneous polynomials of degree d in the complex projective space CP^n defined by the vector $\mathbf{k}_{n+1}$ with $d = k_1 + ...k_{n+1}$ defines a convex *reflexive* polyhedron *, whose intersection with the integer lattice corresponds to the polynomials of the CY equation. Therefore, instead of studying the complex hypersurfaces directly, one can study the geometry of polyhedrons. This method was first used to look for the solutions of the algebraic equations of degree five or more in terms of radicals [16]. Thus, the problem of classifying CY hypersurfaces is also connected with the problem of solving high-degree polynomial equations in terms of radicals. The solutions of quintic- and higher-degree algebraic equations in terms of radicals may be expressed using elliptic and hyperelliptic functions, respectively. Specifically, it is known that CY manifolds may be represented using double-periodic elliptic or multi-periodic hyperelliptic functions [17]. These functions

*The notion of a reflexive polyhedron is introduced and defined in Section 2.

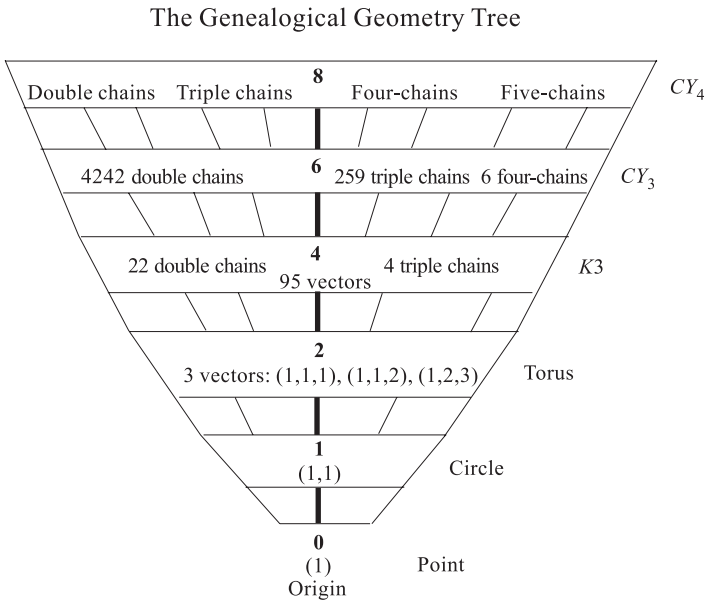

Fig. 1. The genealogical tree of reflexive projective vectors in different dimensions up to $d = 4$

have therefore been used to describe the behaviour of strings, and they should also be used to construct the ambient space-time in which strings move.

We embark here on a systematic classification of $K3$ manifolds, as a prelude to a subsequent classification of CY_3 manifolds, based on their construction in the framework of toric geometry. Within this approach, CY manifolds and their mirrors are toric varieties that can be associated with polyhedra in spaces of various dimensions. We propose here an inductive algebraic-geometric construction of the projective vectors $\mathbf{k}$ that define these polyhedra and the related $K3$ and CY spaces. This method has the potential to become exhaustive up to any desired complex dimensionality $d = 1, 2, 3, 4, 5, 6, ...$ (see Figure 1), limited essentially by the available computer power. As a first step in this programme, we present in this article a construction of $K3$ spaces, which is complete for those described by simple polynomial zeroes, and in principle for $K3$ spaces obtained as the complete intersections of pairs or triples of such polynomial zero loci. In the construction of projective vectors corresponding to hypersurfaces without an intersection with one internal point, the duality between a complex manifold and its mirror (which does contain an intersection) plays an important role. We discuss here also aspects of the CY_3 construction that are relevant for the classification of $K3$ spaces. We also indicate already how one may generate CY_3 manifolds

with elliptic fibrations or $K3$ fibers. More aspects of our CY_3 construction are left for later work.

To get the flavour of our construction, which is based on the formalism reviewed in Sections 2 and 3 [7] and is discussed in more detail in Sections 4 *et seq.*, consider first CP^1 space. Starting from the trivial unit «vector» $\mathbf{k}_1 \equiv (1)$, we introduce two *singly-extended* basic vectors

$$\mathbf{k}_1^{ex'} = (0,1),\ \mathbf{k}_1^{ex''} = (1,0), \tag{1.1}$$

obtained by combining $\mathbf{k}_1$ with zero in the two possible ways. The basic vectors (1.1) correspond to the sets of polynomials

$$\begin{aligned} x^n \cdot y \implies \{\, \boldsymbol{\mu}_1 \,\} = (n,\,1): \quad \boldsymbol{\mu}_1 \cdot \mathbf{k}_1^{ex'} = d = 1, \\ x \cdot y^m \implies \{\, \boldsymbol{\mu}_2 \,\} = (1,\,m): \quad \boldsymbol{\mu}_2 \cdot \mathbf{k}_1^{ex''} = d = 1, \end{aligned} \tag{1.2}$$

respectively. The only polynomial common to these two sequences is xy, which may be considered as corresponding to the trivial «vector» $\mathbf{k}_1 = (1)$. Consider now the composite vector $\mathbf{k}_2 = (1,1)$, which can be constructed out of the basic vectors (1.1), and is easily seen to correspond to the following three monomials of two complex arguments (x, y):

$$\begin{aligned} \{\, x^2, x \cdot y,\, y^2 \,\} \implies \boldsymbol{\mu}|_{i=1,2,3} &= \{\, (2,0), (1,1), (0,2) \,\} \implies \\ \boldsymbol{\mu}'|_{i=1,2,3} \equiv \boldsymbol{\mu}|_{i=1,2,3} - \mathbf{1} &= \{\, (1,-1), (0,0), (-1,+1) \,\}, \end{aligned} \tag{1.3}$$

where we have used the condition: $\boldsymbol{\mu} \cdot \mathbf{k}_2 = \mu_1 \cdot 1 + \mu_2 \cdot 1 = d = 2$, corresponding to $\boldsymbol{\mu}\,' \cdot \mathbf{k}_2 = 0$, and we denote by d the dimensionality of the projective vectors. It is convenient to parametrize (1.3) in terms of the new basis vector $\mathbf{e} = (-1, 1)$:

$$\boldsymbol{\mu}'|_{i=1,2,3} \implies (\mathbf{e})|_{i=1,2,3} = \{\, (-1), (0), (+1) \,\} \times \mathbf{e}. \tag{1.4}$$

The three points $(2,0), (1,1), (0,2)$ (or $-1, 0, +1$) corresponding to the composite vector $k_2 = (1,1)$ may be considered as composing a degenerate linear polyhedron with two integer vertices $\{(2,0), (0,2)\}$ (± 1) and one central interior point $(1,1)$ (0). As we see in more detail later, this polyhedron is self-dual, or reflexive as defined in Section 2.

To describe CY_1 spaces in CP^2 projective space, via the analogous projective vectors $\mathbf{k}_3 = (1,1,1), (1,1,2), (1,2,3)$, that are associated with the corresponding polynomial zero loci, one may introduce the two following types of extended vectors: the *doubly-extended basic* vectors

$$\mathbf{k}_1^{ex} = (0,0,1),\ (0,1,0),\ (1,0,0) \tag{1.5}$$

obtained by adding zero to the two-dimensional basic vectors (1.1) in all possible ways, and the three simple extensions of the composite vector $\mathbf{k}_2 = (1, 1)$:

$$\mathbf{k}_2^{ex} = (0, 1, 1),\ (1, 0, 1),\ (1, 1, 0). \tag{1.6}$$

Then, out of all the extended vectors (1.5) and (1.6) and the corresponding sets of monomials, one should consider only those pairs (triples) whose common monomials correspond to the composite vector $\mathbf{k}_2 = (1, 1)$ (to the unit vector) which produces the reflexive linear polyhedron with three integer points (a single point). The condition of reflexivity restricted to the extended vector pairs (triples), ... will also be very important for constructing the closed sets of higher-dimensional projective vectors (again reflexive).

For example, consider one such 'good' pair,

$$\mathbf{k}_2^{ex} = (0, 1, 1) \iff \mathbf{k}_1^{ex} = (1, 0, 0), \tag{1.7}$$

with the corresponding set of monomials,

$$\begin{aligned} \{x^m \cdot y^2\} &\implies \boldsymbol{\mu} = (m, 2, 0), \\ \{x^n \cdot y \cdot z\} &\implies \boldsymbol{\mu} = (n, 1, 1), \\ \{x^p \cdot z^2\} &\implies \boldsymbol{\mu} = (p, 0, 2), \\ \boldsymbol{\mu}_i \cdot \mathbf{k}_2^{ex} &= 2, \end{aligned} \tag{1.8}$$

and

$$\begin{aligned} \{x \cdot y^k \cdot z^l\} &\implies \boldsymbol{\mu} = (1, k, l), \\ \boldsymbol{\mu} \cdot \mathbf{k}_1^{ex} &= 1. \end{aligned} \tag{1.9}$$

The common action of these two extended vectors, (0,1,1) and (1,0,0), gives as results only the following three monomials:

$$\begin{aligned} \{x \cdot y^2,\ x \cdot y \cdot z,\ x \cdot z^2\} &\implies \\ \boldsymbol{\mu}|_{i=1,2,3} &= \{(1, 2, 0),\ (1, 1, 1),\ (1, 0, 2)\} \implies \\ \boldsymbol{\mu}|_{i=1,2,3} - \mathbf{1} &= \{(0, 1, -1),\ (0, 0, 0),\ (0, -1, 1)\} \implies \\ \mathbf{e}|_{i=1,2,3} &= \{(-1),\ (0),\ (1)\} \end{aligned} \tag{1.10}$$

which correspond to the CP^1 case. Such pairs or triples may be termed «reflexive» pairs or triples, because of the vertices $\mathbf{e}|_{i=1,2,3}$ above a generate (degenerate) reflexive polyhedron.

Such pairs, triples and higher-order sets of projective vectors $\mathbf{k}_1$ may be used to define *chains* of integer-linear combinations, as explained in more detail in Subsection 4.1:

$$m_1\mathbf{k}_1 + m_2\mathbf{k}_2 + \ldots \tag{1.11}$$

We use the term *eldest vector* for the leading entry in any such chain, with minimal values of $m_1, m_2, \ldots$ In the above case, there are just two distinct types of «reflexive» pairs: $\{(0,0,1),(1,1,0)\}$ and $\{(0,1,1),(1,0,1)\}$, which give rise to two such chains: $\{(1,1,1),(1,1,2)\}$ and $\{(1,1,2),\ (1,2,3)\}$. There is only one useful «reflexive» triple: $\{(0,0,1),(0,1,0),(1,0,0)\}$ defining a non-trivial three-vector chain. Together, these chains can be used to construct all three projective $\mathbf{k}_2$ vectors. The second possible «reflexive» triple $\{(0,1,1),(1,0,1),$ $(1,1,0)\}$ produces a chain that consists of only one projective $\mathbf{k}_3$ vector: $(1,1,1)$.

In addition to the zero loci of single polynomials, CY spaces may be found by higher-level contructions as the intersections of the zero loci of two or more polynomial loci. The higher-level CY_1 spaces found in this way are given in the last Section of this paper.

In the case of the $K3$ hypersurfaces in CP^3 projective space, our construction starts from the five possible types of extended vectors, with all their possible Galois groups of permutations. These types are the triply-extended basic vectors with the cyclic C_4 group of permutations,

$$\mathbf{k}_1^{ex} = (0,0,0,1):\ |C_4| = 4, \tag{1.12}$$

the doubly-extended composite vectors with the D_3 dihedral group of permutations,

$$\mathbf{k}_2^{ex} = (0,0,1,1):\ |D_3| = 6, \tag{1.13}$$

and the following singly-extended composite vectors with the cyclic C_4, alternating A_4 and symmetric S_4 groups of permutations, respectively:

$$\mathbf{k}_3^{ex} = (0,1,1,1):\ |C_4| = 4, \tag{1.14}$$

$$\mathbf{k}_3^{ex} = (0,1,1,2):\ |A_4| = 12, \tag{1.15}$$

$$\mathbf{k}_3^{ex} = (0,1,2,3):\ |S_4| = 24. \tag{1.16}$$

The A_4 and S_4 groups of permutations can be identified with the tetrahedral T and octahedral O rotation groups, respectively. Combining these 50 extended vectors in pairs, we find 22 pairs whose common actions correspond to reflexive polyhedra in the plane. These give rise to 22 chains (lattices parametrized by two positive integers), which together yield 90 $\mathbf{k}_4$ vectors based on such extended structures, that are discussed in more detail in Section 5. In addition, there exist just four triples constructed from the 10 extended vectors $(0,0,0,1)$ + permutations and $(0,0,1,1)$ + permutations whose common actions give a unique reflexive polyhedron on the line: $(-1),(0),(+1)$. The corresponding four triple chains (lattices parametrized by three positive integers) yield 91 $\mathbf{k}_4$ vectors, as discussed in Section 6. As also discussed there, it turns out that most of the $\mathbf{k}_4$ vectors obtained from the triple combinations are already included among those found

in the double chains, so that the combined number of distinct vectors is just 94. The total number of vectors is, however, 95 (see Table 1), because there exists, in addition to the above enumeration, a single vector $\mathbf{k}_4 = (7, 8, 9, 12)$ which has only a trivial intersection consisting just of the zero point. This can be found within our approach using the nontrivial projection structure of its dual, which is an example of the importance of duality in our classification, as discussed in Section 7.

To find all CY manifolds, and thereby to close their algebra with respect the duality between *intersection* and *projection* that is described in more detail in Sections 3 and 4, one must consider how to classify the projective structures of CY manifolds. Some of the 22 chains are dual with respect to the «intersection-projection» structure, but more analysis is required to close the CY algebra. As discussed in Section 7, it is useful for this purpose to look for the so-called *invariant* directions. To find all such *invariant* directions in the case of $K3$ spaces, one should consider all triples selected from the following five extended vectors: $(0,0,0,1), (0,0,1,1), (0,1,1,1), (0,1,1,2), (0,1,2,3)$, and their possible permutations, whose intersections give the following five types of *invariant* directions defined by two monomials:

$$\begin{aligned}
\boldsymbol{\pi}_1^\alpha &= \{(1,1,1,1) \to (0,1,1,3)\}, \ \alpha = 1, 2, \\
\boldsymbol{\pi}_2^\alpha &= \{(1,1,1,1) \to (0,0,0,3)\}, \ \alpha = 1, 2, 3, 4, \\
\boldsymbol{\pi}_3^\alpha &= \{(1,1,1,1) \to (0,0,1,3)\}, \ \alpha = 1, 2, 3, 4, \\
\boldsymbol{\pi}_4^\alpha &= \{(1,1,1,1) \to (0,0,0,4)\}, \ \alpha = 1, 2, 3, 4, \\
\boldsymbol{\pi}_5^\alpha &= \{(1,1,1,1) \to (0,0,1,4)\}, \ \alpha = 1, \qquad (1.17)
\end{aligned}$$

and the following three types of *invariant* directions defined by three monomials:

$$\begin{aligned}
\boldsymbol{\pi}_6^\alpha &= \{(0,2,1,1) \to (1,1,1,1) \to (2,0,1,1)\}, \ \alpha = 1, 2, \\
\boldsymbol{\pi}_7^\alpha &= \{(0,0,1,2) \to (1,1,1,1) \to (2,2,1,0)\}, \ \alpha = 1, 2, 3, 4, \\
\boldsymbol{\pi}_8^\alpha &= \{(0,0,0,2) \to (1,1,1,1) \to (2,2,2,0)\}, \ \alpha = 1, 2, 3, 4, \qquad (1.18)
\end{aligned}$$

respectively. Each double intersection of a pair of extended vectors from one of these triples gives the same «good» planar polyhedron whose intersection with the plane integer lattice Z_2 has just one interior point.

By this method, one can classify the projective vectors by projections, finding 78 projective vectors which can be characterized by their invariant directions. Taking into account the projective vectors with intersection-projection duality that have already been found by the double-intersection method, one can recover all 95 $K3$ projective vectors, including the exceptional vector $(7, 8, 9, 12)$ that was not found previously among the double and triple chains.

Table 1: **The algebraic structure of the 95 projective vectors characterizing $K3$ spaces. The numbers of points/vertices in the corresponding polyhedra (their duals) are denoted by N/V (N^*/V^*), and their Picard numbers are denoted by Pic (Pic*). In each case, we also list the double, triple chains and projective chains where the corresponding $K3$ vector may be found**

ℵ	$\mathbf{k}_4$	N	N^*	V	V^*	Pic	Pic*	Double chains	Triple chains	Projective chains
1	$(1,1,1,1)$	35	5	4	4	1	19	I, VII, X, XII	I	$\boldsymbol{\pi}_3,\ \boldsymbol{\pi}_4,\ \boldsymbol{\pi}_6$
2	$(1,1,1,2)$	34	6	6	5	2	18	I, IV, XI, XIV	I, II	$\boldsymbol{\pi}_1, \boldsymbol{\pi}_3, \boldsymbol{\pi}_5, \boldsymbol{\pi}_6, \boldsymbol{\pi}_7$
3	$(1,1,1,3)$	39	6	4	4	1	19	I, V, XX	I, III	$\boldsymbol{\pi}_8$
4	$(1,1,2,2)$	30	6	4	4	4	18	$II, IV, X,$ $XXI, XXII$	I, II, IV	$\boldsymbol{\pi}_2, \boldsymbol{\pi}_6, \boldsymbol{\pi}_7$
5	$(1,1,2,3)$	31	8	7	6	4	16	$IV, XI, XIII, XV$	$I, II,$	$\boldsymbol{\pi}_1, \boldsymbol{\pi}_3,\ \boldsymbol{\pi}_6,\ \boldsymbol{\pi}_7$
6	$(1,1,2,4)$	35	7	4	4	3	18	$IV,\ V,\ VI,\ XVI$	I, II, III	$\boldsymbol{\pi}_8$
7	$(1,1,3,4)$	33	9	5	5	4	16	$XI, XVII$	I, II	$\boldsymbol{\pi}_2, \boldsymbol{\pi}_6$
8	$(1,1,3,5)$	36	9	5	5	3	17	$V, XVIII$	I, III	$\boldsymbol{\pi}_8$
9	$(1,1,4,6)$	39	9	4	4	2	18	V, XIX	I, III	
10	$(1,2,2,3)$	24	8	6	5	7	16	$VII, VIII, XI,$ $XV, XXII$	I, II, IV	$\boldsymbol{\pi}_1,\ \boldsymbol{\pi}_3,\ \boldsymbol{\pi}_4,\ \boldsymbol{\pi}_7$
11	$(1,2,2,5)$	28	8	4	4	6	18	V, IX, XVI	I, III	$\boldsymbol{\pi}_8$
12	$(1,2,3,3)$	23	8	6	5	8	16	$II,\ III,\ XIV,\ XV$	I, II	$\boldsymbol{\pi}_1,\ \boldsymbol{\pi}_2,\ \boldsymbol{\pi}_7$
13	$(1,2,3,4)$	23	11	7	6	8	13	$XII, XIII,$ $XV, XXII$	II, IV	$\boldsymbol{\pi}_1,\ \boldsymbol{\pi}_3,\ \boldsymbol{\pi}_7$
14	$(1,2,3,5)$	24	13	8	7	8	12	$XIII, XIV, XV$	II	$\boldsymbol{\pi}_1, \boldsymbol{\pi}_3, \boldsymbol{\pi}_5, \boldsymbol{\pi}_7$
15	$(1,2,3,6)$	27	9	4	4	7	16	$VI,\ XV,\ XVI,\ XX$	II, III	$\boldsymbol{\pi}_8$
16	$(1,2,4,5)$	24	12	5	5	8	14	$XVII,\ XXI,\ XXII$	II, IV	$\boldsymbol{\pi}_1, \boldsymbol{\pi}_2$
17	$(1,2,4,7)$	27	12	5	5	7	15	$XVI, XVIII$	III	$\boldsymbol{\pi}_8$
18	$(1,2,5,7)$	26	17	6	6	8	12	$XVII$	II	$\boldsymbol{\pi}_1, \boldsymbol{\pi}_2$
19	$(1,2,5,8)$	28	14	5	5	7	14	$XVI, XVIII$	III	$\boldsymbol{\pi}_8$
20	$(1,2,6,9)$	30	12	4	4	6	16	XVI, XIX	III	
21	$(1,3,4,4)$	21	9	4	4	10	16	$II, VIII$	I, II	$\boldsymbol{\pi}_2, \boldsymbol{\pi}_7$
22	$(1,3,4,5)$	20	15	7	7	10	10	$XIII, XIV$	II	$\boldsymbol{\pi}_7$
23	$(1,3,4,7)$	22	17	6	6	10	10	$XIII$	II	$\boldsymbol{\pi}_3, \boldsymbol{\pi}_7$
24	$(1,3,4,8)$	24	12	5	5	9	14	VI, IX	II, III	$\boldsymbol{\pi}_8$
25	$(1,3,5,6)$	21	15	5	5	10	12	$III, XVII$	II	
26	$(1,3,5,9)$	24	15	5	5	9	13	$XVIII, XX$	III	$\boldsymbol{\pi}_8$
27	$(1,3,7,10)$	24	24	4	4	10	10	$XVII$	II	$\boldsymbol{\pi}_2$
28	$(1,3,7,11)$	25	20	5	5	9	11	$XVIII$	III	$\boldsymbol{\pi}_8$
29	$(1,3,8,12)$	27	15	4	4	8	14	XIX	III	
30	$(1,4,5,6)$	19	17	6	6	11	9	$VIII, XIII$	II	$\boldsymbol{\pi}_7$
31	$(1,4,5,10)$	23	13	4	4	10	14	VI	II, III	$\boldsymbol{\pi}_8$
32	$(1,4,6,7)$	19	20	6	6	11	9	$XVII$	II	
33	$(1,4,6,11)$	22	20	6	6	10	10	$IX, XVIII$	III	
34	$(1,4,9,14)$	24	24	4	4	10	10	$XVIII$	III	$\boldsymbol{\pi}_8$
35	$(1,4,10,15)$	25	20	5	5	9	11	XIX	III	
36	$(1,5,7,8)$	18	24	5	5	12	8	$XVII$	II	
37	$(1,5,7,13)$	21	24	5	5	11	9	$XVIII$	III	
38	$(1,5,12,18)$	24	24	4	4	10	10	XIX	III	
39	$(1,6,8,9)$	18	24	5	5	12	8	$XVII$	II	
40	$(1,6,8,15)$	21	24	5	5	11	9	$XVIII$	III	
41	$(1,6,14,21)$	24	24	4	4	10	10	XIX	III	
42	$(2,2,3,5)$	17	11	5	5	11	14	$VIII, XI$	I, II	$\boldsymbol{\pi}_4, \boldsymbol{\pi}_6, \boldsymbol{\pi}_7$
43	$(2,2,3,7)$	19	11	5	5	10	16	V, IX	I, III	$\boldsymbol{\pi}_8$
44	$(2,3,3,4)$	15	9	4	4	12	16	III, VII, XXI	I, IV	$\boldsymbol{\pi}_1,\ \boldsymbol{\pi}_2,\ \boldsymbol{\pi}_3,\ \boldsymbol{\pi}_4,\ \boldsymbol{\pi}_6$
45	$(2,3,4,5)$	13	16	7	7	13	9	$XII,\ XIV,\ XXII$	II, IV	$\boldsymbol{\pi}_1, \boldsymbol{\pi}_3, \boldsymbol{\pi}_5, \boldsymbol{\pi}_7$
46	$(2,3,4,7)$	14	18	6	6	13	10	$VIII, XIV$	II	$\boldsymbol{\pi}_1, \boldsymbol{\pi}_3, \boldsymbol{\pi}_4, \boldsymbol{\pi}_5, \boldsymbol{\pi}_7$
47	$(2,3,4,9)$	16	14	5	5	12	13	IX, XVI, XX	III	$\boldsymbol{\pi}_8$
48	$(2,3,5,5)$	14	11	6	5	14	14	II	I, II	$\boldsymbol{\pi}_2, \boldsymbol{\pi}_7$
49	$(2,3,5,7)$	13	20	8	8	14	6	$XIII$	II	$\boldsymbol{\pi}_3, \boldsymbol{\pi}_5, \boldsymbol{\pi}_7$
50	$(2,3,5,8)$	14	20	6	6	14	7	$XIII$	II	$\boldsymbol{\pi}_3, \boldsymbol{\pi}_7$
51	$(2,3,5,10)$	16	14	5	5	13	12	VI	II, III	$\boldsymbol{\pi}_8$
52	$(2,3,7,9)$	14	23	6	6	14	8	$XVII$	II	$\boldsymbol{\pi}_2$

Table 1: (cont.)

$\aleph$	$\mathbf{k}_4$	N	N^*	V	V^*	Pic	Pic*	Double chains	Triple chains	Projective chains
53	$(2,3,7,12)$	16	20	5	5	13	10	$XVIII$	III	$\boldsymbol{\pi}_8$
54	$(2,3,8,11)$	15	27	4	4	14	8	$XVII$	II	$\boldsymbol{\pi}_2$
55	$(2,3,8,13)$	16	23	5	5	13	9	$XVIII$	III	$\boldsymbol{\pi}_8$
56	$(2,3,10,15)$	18	18	4	4	12	12	XIX	III	
57	$(2,4,5,9)$	13	23	4	4	14	10	$VIII$	II	$\boldsymbol{\pi}_1,\boldsymbol{\pi}_4,\boldsymbol{\pi}_7$
58	$(2,4,5,11)$	14	19	5	5	13	11	IX,XVI	III	$\boldsymbol{\pi}_8$
59	$(2,5,6,7)$	11	23	5	5	15	7	$VIII$	II	$\boldsymbol{\pi}_3,\boldsymbol{\pi}_4,\boldsymbol{\pi}_7$
60	$(2,5,6,13)$	13	23	5	5	14	9	IX	III	$\boldsymbol{\pi}_8$
61	$(2,5,9,11)$	11	32	6	6	16	4	$XVII$	II	$\boldsymbol{\pi}_2$
62	$(2,5,9,16)$	13	29	5	5	15	6	$XVIII$	III	$\boldsymbol{\pi}_8$
63	$(2,5,14,21)$	15	27	4	4	14	8	XIX	III	
64	$(2,6,7,15)$	13	23	4	4	14	10	IX	III	$\boldsymbol{\pi}_8$
65	$(3,3,4,5)$	12	12	5	5	14	14	III	I	$\boldsymbol{\pi}_2,\boldsymbol{\pi}_3,\boldsymbol{\pi}_5,\boldsymbol{\pi}_6$
66	$(3,4,5,6)$	10	17	6	6	15	9	III,XII,XXI	IV	$\boldsymbol{\pi}_1,\boldsymbol{\pi}_2,\boldsymbol{\pi}_3$
67	$(3,4,5,7)$	9	24	7	8	16	4	XIV	II	$\boldsymbol{\pi}_3,\boldsymbol{\pi}_5,\boldsymbol{\pi}_7$
68	$(3,4,5,8)$	10	22	6	6	16	7	$VIII$	II	$\boldsymbol{\pi}_1,\boldsymbol{\pi}_3,\boldsymbol{\pi}_4,\boldsymbol{\pi}_7$
69	$(3,4,5,12)$	12	18	5	5	15	10	IX,XX	III	$\boldsymbol{\pi}_8$
70	$(3,4,7,10)$	10	26	5	6	17	3	$XIII$	II	$\boldsymbol{\pi}_3,\boldsymbol{\pi}_7$
71	$(3,4,7,14)$	12	18	5	5	16	10	VI	II,III	$\boldsymbol{\pi}_8$
72	$(3,4,10,13)$	10	35	5	5	17	3	$XVII$	II	$\boldsymbol{\pi}_2$
73	$(3,4,10,17)$	11	31	6	6	16	4	$XVIII$	III	$\boldsymbol{\pi}_8$
74	$(3,4,11,18)$	12	30	4	4	16	6	$XVIII$	III	$\boldsymbol{\pi}_8$
75	$(3,4,14,21)$	13	26	5	5	15	7	XIX	III	
76	$(3,5,6,7)$	9	21	5	5	16	8	III		$\boldsymbol{\pi}_1,\boldsymbol{\pi}_2$
77	$(3,5,11,14)$	9	39	4	4	18	2	$XVII$	II	$\boldsymbol{\pi}_2$
78	$(3,5,11,19)$	10	35	5	5	17	3	$XVIII$	III	$\boldsymbol{\pi}_8$
79	$(3,5,16,24)$	12	30	4	4	16	6	XIX	III	
80	$(3,6,7,8)$	9	21	4	4	16	10	III		$\boldsymbol{\pi}_1,\boldsymbol{\pi}_2,\boldsymbol{\pi}_3,\boldsymbol{\pi}_4$
81	$(4,5,6,9)$	8	26	5	6	17	4	XIV	II	$\boldsymbol{\pi}_3,\boldsymbol{\pi}_4,\boldsymbol{\pi}_5,\boldsymbol{\pi}_7$
82	$(4,5,6,15)$	10	20	5	5	16	9	XX	III	$\boldsymbol{\pi}_8$
83	$(4,5,7,9)$	7	32	5	6	18	2		II	$\boldsymbol{\pi}_3,\boldsymbol{\pi}_7$
84	$(4,5,7,16)$	9	27	5	5	17	6	IX	III	$\boldsymbol{\pi}_8$
85	$(4,5,13,22)$	9	39	4	4	18	2	$XVIII$	III	$\boldsymbol{\pi}_8$
86	$(4,5,18,27)$	10	35	5	5	17	3	XIX	III	
87	$(4,6,7,11)$	7	35	4	4	18	3	$VIII$	II	$\boldsymbol{\pi}_4,\boldsymbol{\pi}_5,\boldsymbol{\pi}_7$
88	$(4,6,7,17)$	8	31	5	5	17	4	IX	III	$\boldsymbol{\pi}_8$
89	$(5,6,7,9)$	6	30	5	6	18	2	III		$\boldsymbol{\pi}_2,\boldsymbol{\pi}_3,\boldsymbol{\pi}_5$
90	$(5,6,8,11)$	6	39	4	4	19	1		II	$\boldsymbol{\pi}_3,\boldsymbol{\pi}_7$
91	$(5,6,8,19)$	7	35	5	5	18	2	IX	III	$\boldsymbol{\pi}_8$
92	$(5,6,22,33)$	9	39	4	4	18	2	XIX	III	
93	$(5,7,8,20)$	8	28	4	4	18	6		III	$\boldsymbol{\pi}_8$
94	$(7,8,10,25)$	6	39	4	4	19	1		III	$\boldsymbol{\pi}_8$
95	$(7,8,9,12)$	5	35	4	4	19	1			$\boldsymbol{\pi}_2,\boldsymbol{\pi}_3,\boldsymbol{\pi}_4,\boldsymbol{\pi}_5$

Section 8 of this paper contains a systematic description how various gauge groups emerge associated with singularities in our construction of $K3$ spaces [18]. These are interesting because of their possible role in studies of F theory. Since this may be regarded as a decompactification of type-IIA string, understanding of duality between the heterotic string and type-IIA string in $D = 6$ dimensions can be used to help understand the duality between the heterotic string on T^2 and F theory on an elliptically-fibered $K3$ hypersurface [19]. The gauge group is directly defined by the ADE classification of the quotient singularities of hypersurfaces. The Cartan matrix of the Lie group in this case coincides up to a sign with

the intersection matrix of the blown-down divisors. There are two different mechanisms leading to enhanced gauge groups on the F-theory side and on the heterotic side. On the F-theory side, the singularities of the CY hypersurface give rise to the gauge groups, but on the heterotic side the singularities can give an enhancement of the gauge group if «small» instantons of the gauge bundle lie on these singularities [20]. This question has been studied in terms of the numbers of instantons placed on a singularity of type G, where G is a simply-laced group. Studies of groups associated with singularities of $K3$ spaces are also interesting because elliptic CY_n ($n = 3, 4$) manifolds with $K3$ fibers can be considered to study F-theory dual compactifications of the $E_8 \times E_8$ or $SO(32)$ string theory. To do this in toric geometry, it is possible to consider the $K3$ polyhedron fiber as a subpolyhedron of the CY_n polyhedron, and the Dynkin diagrams of the gauge groups of the type-IIA string (F-theory) compactifications on the corresponding threefold (fourfold) can then be seen precisely in the polyhedron of this $K3$ hypersurface. By extension, one could consider the case of an elliptic CY_4 with CY_3 fiber, where the last is a CY hypersurface with $K3$ fiber. We give in Section 8 several detailed examples of group structures associated with chains of $K3$ spaces, which our algebraic approach equips us to study systematically.

Finally, Section 9 provides a brief discussion of CY_3 manifolds and describes how additional CY spaces can be constructed at higher levels as the intersections of multiple polynomial loci. This discussion is illustrated by the examples of higher-level CY_1 and $K3$ spaces obtained via our construction of lower-level $K3$ and CY_3 spaces. We find, for example, 7 new polyhedra describing CY_1 spaces given by «level-one» intersections of pairs of polynomial loci, and three new «level-two» polyhedra given by triple intersections of polynomial loci. In looking for higher-level $K3$ spaces, we start from 100 types of extended vectors in five dimensions, corresponding to 10270 distinct vectors when permutations are taken into account. We find that these give rise to 4242 two-vector chains of CY_3 spaces, 259 triple-vector chains and 6 quadruple-vector chains. Analyzing their internal structures, we find 730 new $K3$ polyhedra at level one, of which 146 can be obtained as intersections of polynomials corresponding to simple polyhedra (points, line segments, triangles and tetrahedra). A complete characterization of higher-level $K3$ spaces given by multiple intersections of polynomial loci lies beyond our present computing scope, and we leave their further study to later work.

2. CALABI–YAU SPACES AS TORIC VARIETIES

We recall that an n-dimensional complex manifold is a $2 \cdot n$-dimensional Riemannian space with a Hermitean metric

$$ds^2 = g_{i\bar{j}} \cdot dz^i \cdot d\bar{z}^{\bar{j}} : \quad g_{ij} = g_{\bar{i}\bar{j}} = 0, \quad g_{i\bar{j}} = \bar{g}_{\bar{j}i} \tag{2.1}$$

on its n complex coordinates z_i. Such a complex manifold is Kähler if the $(1,1)$ differential two-form

$$\Omega \;=\; \frac{1}{2}\cdot i\cdot g_{i\bar{j}}\cdot dz^i\Lambda d\bar{z}^{\bar{j}}, \tag{2.2}$$

is closed, i.e., $d\Omega = 0$. In the case of a Kähler manifold, the metric (2.1) is defined by a Kähler potential:

$$g_{i\bar{j}} \;=\; \frac{\partial^2 K(z^i,\bar{z}^{\bar{j}})}{\partial z^i \partial \bar{z}^{\bar{j}}}. \tag{2.3}$$

The Kähler property yields the following constraints on components of the Cristoffel symbols:

$$\begin{aligned}\Gamma^i_{\bar{j}k} \;&=\; \Gamma^{\bar{i}}_{j\bar{k}} \;=\; \Gamma^i_{\bar{j}k} \;=\; 0,\\ \Gamma^{\bar{i}}_{\bar{j}\bar{k}} \;&=\; \Gamma^{\bar{i}}_{jk} \;=\; g^{\bar{i}s}\cdot\frac{\partial g_{\bar{k}s}}{\partial \bar{z}^{\bar{j}}},\end{aligned} \tag{2.4}$$

yielding in turn the following form

$$R_{\bar{i}j} \;=\; -\frac{\partial \Gamma^{\bar{k}}_{\bar{i}\bar{k}}}{\partial z^j} \tag{2.5}$$

for the Ricci tensor.

Since the only compact submanifold of C^n is a point [21], in order to find nontrivial compact submanifolds, one considers weighted complex projective spaces, $CP^n(k_1,k_2,...,k_{n+1})$, which are characterized by $(n+1)$ quasi-homogeneous coordinates $z_1,...,z_{n+1}$, with the identification:

$$(z_1,\ldots,z_{n+1}) \;\sim\; (\lambda^{k_1}\cdot z_1,\ldots,\lambda^{k_{n+1}}\cdot z_{n+1}). \tag{2.6}$$

The loci of zeroes of quasi-homogeneous polynomial equations in such weighted projective spaces yield compact submanifolds, as we explain in more detail in the rest of Section 2, where we introduce and review several of the geometric and algebraic techniques used in our subsequent classification. Other compact submanifolds may be obtained as the complete intersections of such polynomial zero constraints, as we discuss in more detail in Section 9.

2.1. The Topology of Calabi–Yau Manifolds in the Polyhedron Method. A CY variety X in a weighted projective space $CP^n(\mathbf{k}) = CP^n(k_1,...,k_{n+1})$ is given by the locus of zeroes of a transversal quasi-homogeneous polynomial $\wp$ of degree $\deg(\wp) = d$, with $d = \sum_{j=1}^{n+1} k_j$ [7, 13–15, 21–29]:

$$X \equiv X_d(k) \equiv \{[x_1,...,x_{n+1}] \in CP^n(k) | \wp(x_1,...,x_{n+1}) = 0\}. \tag{2.7}$$

The general polynomial of degree d is a linear combination

$$\wp = \sum_{\boldsymbol{\mu}} c_{\boldsymbol{\mu}} x^{\boldsymbol{\mu}} \tag{2.8}$$

of monomials $x^{\boldsymbol{\mu}} = x_1^{\mu_1} x_2^{\mu_2} ... x_{r+1}^{\mu_{r+1}}$ with the condition:

$$\boldsymbol{\mu} \cdot \mathbf{k} \, = \, d. \tag{2.9}$$

We recall that the existence of a *mirror symmetry*, according to which each Calabi–Yau manifold should have a dual partner, was first observed pragmatically in the literature [11–14, 27]. Subsequently, Batyrev [7] found a very elegant way of describing any Calabi–Yau hypersurface in terms of the corresponding *Newton polyhedron*, associated with degree-d monomials in the CY equation, which is the convex hull of all the vectors $\boldsymbol{\mu}$ of degree d. The Batyrev description provides a systematic approach to duality and mirror symmetry.

To each monomial associated with a vector $\boldsymbol{\mu}$ of degree d, i.e., $\boldsymbol{\mu} \cdot \mathbf{k} = d$, one can associate a vector $\boldsymbol{\mu}^{'} \equiv \boldsymbol{\mu} - \mathbf{e}_0 : \mathbf{e}_0 \equiv (1, 1, ..., 1)$, so that $\boldsymbol{\mu}^{'} \cdot \mathbf{k} = 0$. Using the new vector $\boldsymbol{\mu}^{'}$, hereafter denoted without the prime $(')$, it is useful to define the lattice Λ:

$$\Lambda = \{\boldsymbol{\mu} \in Z^{r+1} : \boldsymbol{\mu} \cdot \mathbf{k} = 0\} \tag{2.10}$$

with basis vectors e_i, and the dual lattice Λ^* with basis e_j^*, where $e_j^* \cdot e_i = \delta_{ij}$. Consider the polyhedron $\triangle$, defined to be the convex hull of $\{\boldsymbol{\mu} \in \Lambda : \mu_i \geqslant -1, \forall i\}$. Batyrev [7] showed that to describe a Calabi–Yau hypersurface*, such a polyhedron should satisfy the following conditions:

- The vertices of the polyhedron should correspond to the vectors $\boldsymbol{\mu}$ with integer components.
- There should be only one interior integer point, called the centre.
- The distance of any face of this polyhedron from the centre should be equal to unity.

Such an integral polyhedron $\triangle$ is called *reflexive*, and the only interior point of $\triangle(k_1 + ... + k_{r+1} = d)$ may be taken as the origin $(0, ..., 0)$. Batyrev [7] showed that the mirror polyhedron

$$\triangle^* \equiv \{\boldsymbol{\nu} \in \Lambda^* : \boldsymbol{\nu} \cdot \boldsymbol{\mu} \geqslant -1, \forall \boldsymbol{\mu} \in \triangle\} \tag{2.11}$$

of any reflexive integer polyhedron is also reflexive, i.e., is also integral and contains one interior point only. Thus Batyrev proved the existence of dual pairs of hypersurfaces M and M' with dual Newton polyhedra, $\triangle$ and $\triangle^*$.

*I.e., with trivial canonical bundle and at worst Gorenstein canonical singularities only.

Following Batyrev [7], to obtain all the topological invariants of the $K3, CY_3$, etc., manifolds, one should study the reflexive regular polyhedra in three, four, etc., dimensions. For this purpose, it is useful to recall the types of polyhedra and their duality properties. In three dimensions, the Descartes–Euler polyhedron formula relates the numbers of vertices, N_0, the number of edges, N_1 and numbers of faces, N_2:

$$1 \,-\, N_0 \,+\, N_1 \,-\, N_2 \,+1 \,=\, 0. \tag{2.12}$$

This formula yields:

$$\begin{aligned}
1 \,-\, 4 \,+\, 6 \,-\, 4 \,+1 \,=\, 0 \;&\Rightarrow\; \{3,3\} : \text{Tetrahedron} \\
1 \,-\, 8 \,+\, 12 \,-\, 6 \,+1 \,=\, 0 \;&\Rightarrow\; \{3,4\} : \text{Cube} \\
1 \,-\, 6 \,+\, 12 \,-\, 8 \,+1 \,=\, 0 \;&\Rightarrow\; \{4,3\} : \text{Octahedron} \\
1 \,-\, 20 \,+\, 30 \,-\, 12 \,+1 \,=\, 0 \;&\Rightarrow\; \{5,3\} : \text{Dodecahedron} \\
1 \,-\, 12 \,+\, 30 \,-\, 20 \,+1 \,=\, 0 \;&\Rightarrow\; \{3,5\} : \text{Icosahedron}
\end{aligned} \tag{2.13}$$

in the particular cases of the five Platonic solids, with the duality relations $T \leftrightarrow T$, $C \leftrightarrow O, D \leftrightarrow I$.

As we shall see later when we consider the $K3$ classification, it is interesting to recall the link between the classification of the five ADE simply-laced Cartan–Lie algebras and the finite rotation groups in three dimensions, namely, the cyclic and dihedral groups and the groups of the tetrahedron, octahedron (cube) and icosahedron (dodecahedron): $G_M \equiv C_n, D_n, T, O, I$, corresponding to the A_n, D_n series and the exceptional groups $E_{6,7,8}$, respectively [30]. Any cyclic group C_n of order n may be represented as the rotations in a plane around an axis $0x$ through angles $(2 \cdot m \cdot \pi)/n$ for $m = 0, 1, 2, ..., n-1$. This symmetry is realized by the group of symmetries of an oriented regular n-gon. The dihedral group D_n consists of the transformations in C_n and in addition n rotations through angles π around axes lying in planes orthogonal to $0x$, crossing $0x$ and making angles with one another that are multiples of $(2 \cdot \pi)/n$. This group has order $2 \cdot n$. In the case of three-dimensional space, there are three exceptional examples T, O, I of finite groups, related to the corresponding regular polyhedra. The order of the corresponding G_M is equal to the product of the number of the vertexes of the regular polyhedra with the number of edges leaving the vertex:

$$\begin{aligned}
|T| \;&=\; |A_4| \;=\; 12, \\
|O| \;&=\; |S_4| \;=\; 24, \\
|I| \;&=\; |A_5| \;=\; 60.
\end{aligned} \tag{2.14}$$

The dual polyhedron, whose vertices are the midpoints of the faces of the corresponding polyhedron, has the same group of symmetry, G_M. The finite groups

of orthogonal transformations in three-dimensional space do not consist only of rotations. It is remarkable to note that every finite group of rotations of three-space that preserves the sphere centred at the origin can be interpreted as a fractional-linear transformation of the Riemann sphere of a complex variable.

Finally, we recall that all $K3$ hypersurfaces have the following common values of the topological invariants: the Hodge number $h_{1,1}$ is 20, the Betti number $b_2 = 22$, and we have

$$Pic = h_{1,1} - (l(\Delta) - 4 - \sum_{\theta \in \Delta} l'(\theta)) \leqslant 20 \tag{2.15}$$

for the Picard number, where $l(\Delta)$ is the number of integer points in the polyhedron and $l'(\theta)$ is the number of integer interior points on the facets.

In the case of the CY_3 classification, a corresponding important role will be played by the structure and the duality properties of the four regular polyhedra known in four-dimensional Euclidean space [31]. The Descartes–Euler formulae for these cases become:

$$\begin{aligned}
1 - 5 + 10 - 10 + 5 - 1 = 0 &\quad \Rightarrow \quad \{3,3,3\} : \text{Pentahedroid} \\
1 - 16 + 32 - 24 + 8 - 1 = 0 &\quad \Rightarrow \quad \{3,3,4\} : \text{Hypercube} \\
1 - 8 + 24 - 32 + 16 - 1 = 0 &\quad \Rightarrow \quad \{4,3,3\} : \text{16-hedroid} \\
1 - 24 + 96 - 96 + 24 - 1 = 0 &\quad \Rightarrow \quad \{3,4,3\} : \text{24-hedroid} \\
1 - 600 + 1200 - 720 + 120 - 1 = 0 &\quad \Rightarrow \quad \{3,3,5\} : \text{120-hedroid} \\
1 - 120 + 720 - 1200 + 600 - 1 = 0 &\quad \Rightarrow \quad \{5,3,3\} : \text{600-hedroid}
\end{aligned} \tag{2.16}$$

with the duality relations $P \leftrightarrow P$, $H \leftrightarrow$16-hedroid, 24-hedroid$\leftrightarrow$24-hedroid, 120-hedroid$\leftrightarrow$600-hedroid.

We do not discuss these relations further in this paper, but do recall that each mirror pair of CY spaces, M_{CY} and M^*_{CY} has Hodge numbers that satisfying the mirror symmetry relation [7, 15]:

$$\begin{aligned}
h_{1,1}(M) &= h_{d-1,1}(M^*), \\
h_{d-1,1}(M) &= h_{1,1}(M^*).
\end{aligned} \tag{2.17}$$

This means that the Hodge diamond of M^*_{CY} is a mirror reflection through a diagonal axis of the Hodge diamond of M_{CY}. The existence of mirror symmetry is a consequence of the dual properties of CY manifolds. A pair of reflexive polyhedra $(\triangle, \triangle^*)$ gives a pair of mirror CY manifolds and the following identities

for the Hodge numbers for $n \geqslant 4$:

$$\begin{aligned} h_{1,1}(\triangle) &= h_{d-1,1}(\triangle^*) = \\ &= l(\triangle^*) - (d+2) - \sum_{\mathrm{codim}\Theta^*=1} l^{'}(\Theta^*) + \\ &+ \sum_{\mathrm{codim}\Theta^*=2} l'(\Theta^*) l^{'}\Theta, \end{aligned} \tag{2.18}$$

$$\begin{aligned} h_{1,1}(\triangle^*) &= h_{d-1,1}(\triangle) = \\ &= l(\triangle) - (d+2) - \sum_{\mathrm{codim}\Theta=1} l'(\Theta) + \\ &+ \sum_{\mathrm{codim}\Theta=2} l'(\Theta) l'(\Theta^*), \end{aligned} \tag{2.19}$$

$$h_{p,1} = \sum_{\mathrm{codim}\Theta^*=p+1} l^{'}(\Theta) \cdot l^{'}(\Theta^*), \;\; 1 < p < d-1. \tag{2.20}$$

Here, the quantities $l(\Theta)$ and $l'(\Theta)$ are the numbers of integer points on a face Θ of $\triangle$ and in its interior, and similarly for Θ^* and $\triangle^*$. An l-dimensional face Θ can be defined by its vertices $(v_{i_1} = ... = v_{i_k})$, and the dual face defined by $\Theta^* = \{m \in \triangle^* : (m, v_{i_1}) =, ..., = (m, v_{i_k}) = -1\}$ is an $(n-l-1)$-dimensional face of $\triangle^*$. Thus, we have a duality between the l-dimensional faces of $\triangle$ and the $(n-l-1)$-dimensional faces of $\triangle^*$. The last terms in (2.18), (2.19) correspond to the «twisted» contributions, and the last term corresponds to $d = 4$. In this case, if the manifold has $SU(4)$ group holonomy, then $h_{2,0} = h_{1,0} = 0$, and the remaining nontrivial Hodge number $h_{2,2}$ is determined by:

$$h_{2,2} = 2[22 + 2h_{1,1} + h_{3,1} - h_{2,1}]. \tag{2.21}$$

Some further comments about CY_3 spaces are made in Section 9.

2.2. The Web of CY Manifolds in the Holomorphic-Quotient Approach to Toric Geometry. It is well known that weighted projective spaces are examples of *toric varieties* [32]. The complex weighted projective space CP^n can be defined as

$$CP^n \equiv \frac{C^{n+1} - \mathbf{0}}{C^*}, \tag{2.22}$$

with the action C^*:

$$(x_1, ..., x_{n+1}) \Rightarrow (\lambda^{k_1} \cdot x_1, ..., \lambda^{k_{n+1}} \cdot x_{n+1}), \quad \lambda \in C \backslash 0. \tag{2.23}$$

The generalization of the projective space CP^n to a toric variety can be expressed in the following form:

$$\mho \equiv \frac{C^n - Z_\Sigma}{(C^*)^p}, \tag{2.24}$$

where, instead of removing the origin, as in the case of a simple projective space, here one removes a point set Z_Σ, and one takes the quotient by a suitable set of C^* actions. Thus, to understand the structure of certain geometrical spaces in the framework of toric geometry, one must specify the combinatorical properties of the Z_Σ and the actions C^*.

In the toric-geometry approach, algebraic varieties are described by a dual pair of lattices M and N, each isomorphic to Z^n, and a fan Σ^* [32] defined on N_R, the real extension of the lattice N. In the toric-variety description, the equivalence relations of projective vectors can be considered as diagrams in the lattice N, in which some vectors $\mathbf{v}_i$ satisfy linear relations (see later some examples in $P^2(1,1,1)$, $P^2(1,1,2)$, $P^2(1,2,3)$ projective spaces). The complex dimension of the variety coincides with the dimension of the lattice N. To determine the structure of a toric variety in higher dimensions $d > 2$, it is useful to introduce the notion of a fan [32, 33]. A fan Σ^* is defined as a collection of r-dimensional ($0 \leqslant r \leqslant d$) convex polyhedral cones with apex in 0, with the properties that with every cone it contains also a face, and that the intersection of any two cones is a face of each one.

In the holomorphic-quotient approach of Batyrev [7] and Cox [29], a single homogeneous coordinate is assigned to the system $\mho_\Sigma$ of varieties, in a way similar to the usual construction of P^n. This holomorphic-quotient construction gives immediately the usual description in terms of projective spaces, and turns out to be more natural in the descriptions of the elliptic, $K3$ and other fibrations of higher-dimensional CY spaces.

One can assign a coordinate $z_k : k = 1, ..., N$ to each one-dimensional cone in Σ. The integer points of $\Delta^* \cap N$ define these one-dimensional cones

$$(v_1, ..., v_N) = {\Sigma_1}^* \tag{2.25}$$

of the fan Σ^*. The one-dimensional cones span the vector space N_R and satisfy $(N - n)$ linear relations with nonnegative integer coefficients:

$$\sum_l k_j^l v_l = 0, \;\; k_j^l \geqslant 0. \tag{2.26}$$

These linear relations can be used to determine equivalence relations on the space $C^N \backslash Z_{\Sigma^*}$. A variety $\mho_{\Sigma^*}$ is the space $C^N \backslash Z_{\Sigma^*}$ modulo the action of a group which is the product of a finite Abelian group and the torus $(C^*)^{(N-n)}$:

$$(z_1, ..., z_N) \sim (\lambda^{k_j^1} z_1, ..., \lambda^{k_j^N} z_N), \;\; j = 1, ..., N - n. \tag{2.27}$$

The set Z_{Σ^*} is defined by the fan in the following way:

$$Z_{\Sigma^*} \equiv \bigcup_I ((z_1, ..., z_N) | z_i = 0, \forall i \in I), \tag{2.28}$$

where the union is taken over all index sets $I = (i_1, ..., i_k)$ such that $(v_{i_1}, ..., v_{i_k})$ do not belong to the same maximal cone in Σ^*, or several z_i can vanish simultaneously only if the corresponding one-dimensional cones v_i are from the same cone. It is clear from the above definitions that toric varieties can have often singularities, which will be very important for understanding the link between the topological properties of Calabi–Yau hypersurfaces and Cartan–Lie algebras: see the more systematic discussion in Section 8. The method of blowing up (blowing down) these singularities was developed in algebraic geometry: it consists of replacing the singular point or curve by a higher-dimensional (lower-dimensional) variety. The structure of the fan Σ^* determines what kind of singularities will appear in Calabi–Yau hypersurfaces. For example, if the fan Σ^* is simplicial, one can get only orbifold singularities in the corresponding variety [33].

The elements of Σ_1^* are in one-to-one correspondence with divisors

$$D_{v_i} = \mho_{\Sigma^*_{1i}}, \tag{2.29}$$

which are subvarieties given simply by $z_i = 0$. This circumstance was used [34] to give a simple graphic explanation of Cartan–Lie algebra (CLA) diagrams, whose Coxeter number could be identified with the intersections of the divisors D_{v_i}.

Two divisors, D_{v_i} and D_{v_j}, can intersect only when the corresponding one-dimensional cones v_i and v_j lie in a single higher-dimensional cone of the fan Σ^*. The divisors D_{v_i} form a free Abelian group $\mathrm{Div}\,(\mho_{\Sigma^*})$. In general, a divisor $D \in \mathrm{Div}\,(\mho_{\Sigma^*})$ is a linear combination of some irreducible hypersurfaces with integer coefficients:

$$qD = \sum a_i \cdot D_{v_i}. \tag{2.30}$$

If $a_i \geqslant 0$ for every i, one can say that $D > 0$. For a meromorphic function f on a toric variety, one can define a principal divisor

$$(f) \equiv \sum_i \mathrm{ord}_{D_i}(f) \cdot D_i, \tag{2.31}$$

where $\mathrm{ord}_{D_i}(f)$ is the order of the meromorphic function f at D_i. One can further define the zero divisor $(f)_0$ and the polar divisor $(f)_{\inf}$ of the meromorphic function f, such that

$$(f) = (f)_0 - (f)_{\inf}. \tag{2.32}$$

Any two divisors D_1, D_2 are linearly equivalent: $D_1 \sim D_2$, if their difference is a principal divisor, $D_1 - D_2 = (f)$ for some appropriate f. The quotient of all divisors $\mathrm{Div}\,(\mho_{\Sigma^*})$ by the principal divisors forms the Picard group.

The points of $\Delta \cap M$ are in one-to-one correspondence with the monomials in the homogeneous coordinates z_i. A general polynomial is given by

$$\wp = \sum_{m \in \Delta \cap M} c_m \prod_{l=1}^{N} z_l^{\langle v_l, m\rangle + 1}. \tag{2.33}$$

The equation $\wp = 0$ is well defined and $\wp$ is holomorphic if the condition

$$\langle v_l, m\rangle \geqslant -1 \ \forall\, l \tag{2.34}$$

is satisfied. The c_m parametrize a family M_Δ of CY surfaces defined by the zero locus of $\wp$.

2.3. Three Examples of CY_1 Spaces. As discussed in Section 1, three CY_1 spaces may be obtained as simple loci of polynomial zeroes associated with reflexive polyhedra. For a better understanding of the preceding formalism, we consider as warm-up examples the three elliptic reflexive polyhedron pairs Δ_i and Δ_i^*, which define the CY_1 surfaces $P^2(1,1,1)[3]$, $P^2(1,1,2)[4]$, and $P^2(1,2,3)[6]^*$. The first polyhedron $\Delta_I \equiv \Delta(P^2(1,1,1)[3])$ consists of the following ten integer points:

$$\begin{aligned}
z^3 &\Longrightarrow \mu_1^{(I)} = (-1,2),\\
xz^2 &\Longrightarrow \mu_2^{(I)} = (-1,1),\\
x^2z &\Longrightarrow \mu_3^{(I)} = (-1,0),\\
x^3 &\Longrightarrow \mu_4^{(I)} = (-1,-1),\\
yz^2 &\Longrightarrow \mu_5^{(I)} = (0,1),\\
xyz &\Longrightarrow \mu_6^{(I)} = (0,0),\\
x^2y &\Longrightarrow \mu_7^{(I)} = (0,-1),\\
y^2z &\Longrightarrow \mu_8^{(I)} = (1,0),\\
xy^2 &\Longrightarrow \mu_9^{(I)} = (1,-1),\\
y^3 &\Longrightarrow \mu_{10}^{(I)} = (2,-1)
\end{aligned} \tag{2.35}$$

*Here and subsequently, we use the conventional notation for such surfaces in n-dimensional projective space: $P^n(k_1,k_2,\ldots)[k_1+k_2+\ldots]$.

and the mirror polyhedron $\Delta_I^* \equiv \equiv \Delta^*(P^2(1,1,1)[3])$ consists of one interior point and three one-dimensional cones:

$$\begin{aligned} v_1^{(I)} &= (0,1), \\ v_2^{(I)} &= (1,0), \\ v_3^{(I)} &= (-1,-1). \end{aligned} \tag{2.36}$$

We use as a basis the exponents of the following monomials:

$$\begin{aligned} y^2z &\implies \mathbf{e}_1 = (-1,1,0), \\ yz^2 &\implies \mathbf{e}_2 = (-1,0,1), \end{aligned} \tag{2.37}$$

where the determinant of this lattice coincides with the dimension of the projective vector $\mathbf{k} = (1,1,1)$ (see Figure 2):

$$\det\{\mathbf{e}_1, \mathbf{e}_2, \mathbf{e}_0\} = \dim(\mathbf{k}) = 3, \tag{2.38}$$

where $\mathbf{e}_0$ is the unit vector (1,1,1).

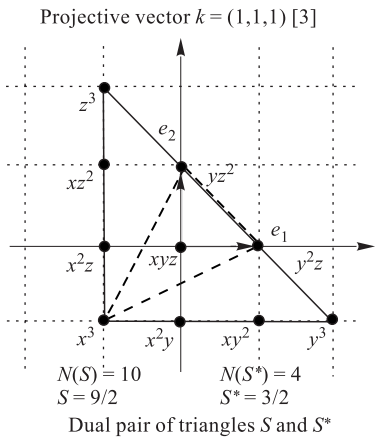

Fig. 2. The dual pair of reflexive plane polyhedra defined by the projective vector $(1,1,1)$ with $N(S) = 10$ and $N(S^*) = 4$ integer points, respectively. $SL(2,Z)$ transformations produce an infinite number of dual-pair triangles, conserving the areas $S = 9/2$ and $S^* = 3/2$, respectively

For this projective vector there exist 27 possibilities of choosing two monomials for constructing the basis. Of course, all these bases are equivalent, i.e., they are connected by the $SL(2,Z)$ modular transformations:

$$L_{i,j} = \begin{pmatrix} a & b \\ c & d \end{pmatrix},$$

where $a, b, c, d \in Z$ and $ad - bc = 1$. For the mirror polyhedron obtained from this vector, the basis should correspond to a lattice with determinant three times greater than (2.38), namely nine, for example:

$$\begin{aligned} \mathbf{e}_1 &= (-1,2,-1), \\ \mathbf{e}_2 &= (-1,-1,2), \end{aligned} \tag{2.39}$$

with

$$\det\{\mathbf{e}_1, \mathbf{e}_2, \mathbf{e}_0\} = \dim(\mathbf{k}) = 9, \tag{2.40}$$

where $\mathbf{e}_0$ is again the unit vector (1,1,1).

To describe this toric curve, one should embed it in the toric variety

$$P^2 = (C^3 \backslash 0)/(C \backslash 0), \tag{2.41}$$

where the equivalence relation

$$(x_1, x_2, x_3) \sim (\lambda x_1, \lambda x_2, \lambda x_3) \text{ for } \lambda \in C\backslash 0 \tag{2.42}$$

is a consequence of the equation:

$$q_1 \cdot v_1^{(I)} + q_2 \cdot v_2^{(I)} + q_3 \cdot v_3^{(I)} = 0, \tag{2.43}$$

where the $q_i = 1$, $i = 1, 2, 3$ are the exponents of λ. The corresponding general polynomial describing a CY surface is (setting $z_l \equiv x_l$):

$$\begin{aligned} \wp_I \; &= x_1^3 + x_2^3 + x_3^3 + x_1 x_2 x_3 + x_1^2 x_2 + \\ &+ x_1^2 x_3 + x_2^2 x_1 + x_2^2 x_3 + x_3^2 x_1 + \; x_3^2 x_2, \end{aligned} \tag{2.44}$$

and the Weierstrass equation can be written in the following form:

$$y^2 \cdot z \; = \; x^3 \; + \; a \cdot x \cdot y^3 \; + \; b \cdot z^3, \tag{2.45}$$

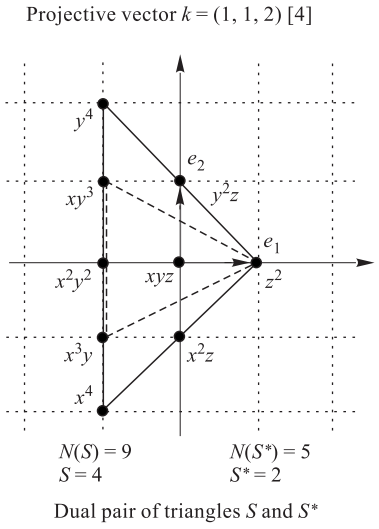

Fig. 3. The dual pair of reflexive plane polyhedra defined by the projective vector $(1, 1, 2)$ with $N(S) = 9$ and $N(S^*) = 5$ integer points, respectively. $SL(2, Z)$ transformations produce an infinite number of dual-pair triangles, conserving the areas $S = 4$ and $S^* = 2$, respectively

where we have set $x_1 = x, x_2 = y, x_3 = z$.

The second dual pair of triangle polyhedra $\Delta_{II} \equiv \Delta(P^2(1, 1, 2)[4])$ and its mirror $\Delta_{II}^* \equiv \Delta^*(P^2(1, 1, 2)[4])$ have nine points

$$\begin{aligned} y^4 &\implies \mu_1^{(II)} = (-1, 2), \\ xy^3 &\implies \mu_2^{(II)} = (-1, 1), \\ x^2y^2 &\implies \mu_3^{(II)} = (-1, 0), \\ x^3y &\implies \mu_4^{(II)} = (-1, -1), \\ x^4 &\implies \mu_5^{(II)} = (-1, -2), \\ y^2z &\implies \mu_6^{(II)} = (0, 1), \\ xyz &\implies \mu_7^{(II)} = (0, 0), \\ x^2z &\implies \mu_8^{(II)} = (0, -1), \\ z^2 &\implies \mu_9^{(II)} = (1, 0), \end{aligned} \tag{2.46}$$

and five points, respectively (see Figure 3).

We use as a basis the exponents of the following monomials:

$$\begin{aligned} z^2 &\implies \mathbf{e}_1 = (-1, -1, 1), \\ y^2z &\implies \mathbf{e}_2 = (-1, 1, 0), \end{aligned} \tag{2.47}$$

where the determinant of this lattice coincides with the dimension of the projective vector $\mathbf{k} = (1, 1, 2)$:

$$\det\{\mathbf{e}_1, \mathbf{e}_2, \mathbf{e}_0\} \;=\; \dim(\mathbf{k}) \;=\; 4, \tag{2.48}$$

where $\mathbf{e}_0$ is again the unit vector (1,1,1).

To get the mirror polyhedron with five integer points, four on the edges and one interior point, one should find a basis with lattice determinant twice (2.48), namely eight, for example:

$$\begin{aligned} \mathbf{e}_1 \;&=\; (-1, -1, 1), \\ \mathbf{e}_2 \;&=\; (-2, 2, 0). \end{aligned} \tag{2.49}$$

The following four points define four one-dimensional cones in $\Sigma_1(\Delta^*_{II})$:

$$\begin{aligned} v_1^{(3)} \;&=\; (1, 0), \\ v_2^{(3)} \;&=\; (-1, 0), \\ v_3^{(3)} \;&=\; (-1, -1), \\ v_4^{(3)} \;&=\; (-1, 1). \end{aligned} \tag{2.50}$$

Using the linear relations between the four one-dimensional cones, the corresponding $(C^*)^2$ is seen to be given by ($z_l \equiv \chi_l$):

$$(\chi_1, \chi_2, \chi_3, \chi_4) \Longrightarrow (\lambda\mu^2\chi_1, \lambda\chi_2, \mu\chi_3, \mu\chi_4), \tag{2.51}$$

and the general polynomial has the following nine terms:

$$\begin{aligned} \wp_{II} \;&=\; \chi_2^2\chi_3^4 + \chi_2^2\chi_3^3\chi_4 + \chi_2^2\chi_3^2\chi_4^2 + \chi_2^2\chi_3\chi_4^3 + \chi_2^2\chi_4^4 + \\ &+\; \chi_1\chi_2\chi_3^2 + \chi_1\chi_2\chi_3\chi_4 + \chi_1\chi_2\chi_4^2 + \chi_1^2 \end{aligned} \tag{2.52}$$

in this case.

The vectors $\mathbf{k} = (1, 1, 1)$ and $\mathbf{k} = (1, 1, 2)$ have three common monomials and a related reflexive segment-polyhedron, corresponding to the projective vector $\mathbf{k}_2 = (1, 1)$ of CP^1. This circumstance can be used further in the construction of the projective algebra in which these two vectors appear in the same chain.

The last CY_1 example involves the plane of the projective vector $\mathbf{k} = (1, 2, 3)$, whose polyhedron $\Delta_{III} \equiv \Delta(P^2(1, 2, 3)[6])$ and its mirror partner $\Delta^*_{III} \equiv$ $\equiv \Delta^*(P^2(1, 2, 3)[6])$ both have seven self-dual points, and one can check the

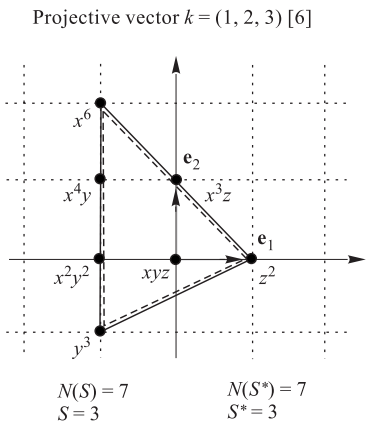

Fig. 4. The self-dual pair of reflexive plane polyhedra defined by the projective vector (1,2,3) with $N(S) = = 7$ and $N(S^*) = 7$ integer points. $SL(2, Z)$ transformations produce an infinite number of the dual-pair triangles, conserving the areas $S = 3$ and $S^* = 3$, respectively

existence of the following six one-dimensional cones (see Figure 4):

$$\begin{aligned} z^2 &\Longrightarrow v_1^{(III)} = (1,0), \\ x^2y^2 &\Longrightarrow v_2^{(III)} = (-1,0), \\ x^3z &\Longrightarrow v_3^{(III)} = (0,1), \\ y^3 &\Longrightarrow v_4^{(III)} = (-1,-1), \\ x^4y &\Longrightarrow v_5^{(III)} = (-1,1), \\ x^6 &\Longrightarrow v_6^{(III)} = (-1,2). \end{aligned} \quad (2.53)$$

We use as a basis the exponents of the following monomials:

$$\begin{aligned} z^2 &\Longrightarrow \mathbf{e}_1 = (-1,-1,1), \\ x^3z &\Longrightarrow \mathbf{e}_2 = (2,-1,0), \end{aligned} \quad (2.54)$$

where the determinant of this lattice coincides with the dimension of the projective vector $\mathbf{k} = (1, 2, 3)$:

$$\det\{\mathbf{e}_1, \mathbf{e}_2, \mathbf{e}_0\} = \dim(\mathbf{k}) = 6. \quad (2.55)$$

As in the case of the two projective vectors $\mathbf{k} = (1, 1, 1)$ and $\mathbf{k} = (1, 1, 2)$, the vectors $\mathbf{k} = (1, 1, 2)$ and $\mathbf{k} = (1, 2, 3)$ also have three common monomials, corresponding to the reflexive segment polyhedron described by the vector $\mathbf{k}_2 = (1, 1)$ in CP^1 projective space. Hence these vectors will appear in the second chain of the plane projective algebra.

Thus one can see that, with these three plane projective vectors, $\mathbf{k} = (1, 1, 1)$, $\mathbf{k} = (1, 1, 2)$, $\mathbf{k} = (1, 2, 3)$, one finds only triangle reflexive polyhedra intersecting the integer planar lattice in $10+4^*$, $9+5^*$, $7+7^*$ points. Of course, on the plane one can find other reflexive polyhedra, whose intersection with the integer plane lattice will give new CP^1 surfaces corresponding to different polygons with more than three vertices, such as a reflexive pair of square and rhombus. These new figures can be obtained using the techniques of extended vectors.

In the following, we will go on to study reflexive polyhedron pairs in three-dimensional space. The corresponding general polynomial can be expressed in terms of six variables, and contains seven monomials:

$$\begin{aligned} \wp_{III} &= z_1^2 z_3 + z_2^2 z_3 z_4^2 z_5^2 z_6^2 + z_1 z_2 z_3^2 z_5^2 z_6^3 + z_2^2 z_4^3 z_5 + \\ &+ z_2^2 z_3^2 z_4 z_5^3 z_6^4 + z_2^2 z_3^3 z_5^4 z_6^6 + z_1 z_2 z_3 z_4 z_5 z_6. \end{aligned} \quad (2.56)$$

The C^{*4} action is determined by the following linear relations:

$$\begin{aligned} v_1^{(III)} \; + \; v_2^{(III)} &= 0, \\ 2v_1^{(III)} \; + \; v_4^{(III)} \; + \; v_5^{(III)} \; &= \; 0, \\ v_1^{(III)} \; + \; v_3^{(III)} \; + \; v_4^{(III)} &= 0, \\ 3v_1^{(III)} \; + \; 2v_4^{(III)} \; + \; v_6^{(III)} &= 0 \end{aligned} \tag{2.57}$$

between the elements of $\Sigma_1(\Delta^*_{III})$, and is given by

$$(z_1, z_2, z_3, z_4, z_5, z_6) \longrightarrow (\lambda\mu^2\nu\rho^3 z_1, \lambda z_2, \nu z_3, \mu\nu\rho^2 z_4, \mu z_5, \rho z_6). \tag{2.58}$$

One can introduce the following birational map between $P^2(1,2,3)[6]$ and $\mho_{\Sigma^*}$:

$$z_1^2 z_3 \; = \; y_3^2, \tag{2.59}$$

$$z_2^2 z_4^3 z_5 \; = \; y_2^3, \tag{2.60}$$

$$z_2^2 z_3^3 z_5^4 z_6^6 \; = \; y_1^6. \tag{2.61}$$

Then, a dimensionally-reduced example of a CY manifold embedded in a toric variety is described by the weight vector $k = (1,2,3)$ and the zero locus of the Weierstrass polynomial

$$\wp_{III} = y_1^6 \; + \; y_2^3 \; + \; y_3^2 \; + \; y_1 y_2 y_3 + \; y_1^4 y_2 \; + \; y_1^2 y_2^2 \; + \; y_1^3 y_3. \tag{2.62}$$

The elliptic Weierstrass equation can be written in the weighted projective space $P^2(1,2,3)[6]$ as

$$y^2 = x^3 \; + \; a \cdot x \cdot z^4 \; + \; b \cdot z^6 \tag{2.63}$$

with the following equivalence relation

$$(x, y, z) \; \sim \; (\lambda^2 x, \lambda^3 y, \lambda z), \quad \lambda \in C\backslash 0 \tag{2.64}$$

in this case.

These examples illustrate how toric varieties can be defined by the quotient of $C^k\backslash Z_\Sigma$, and not only by a group $(C\backslash 0)^{k-n}$. One should divide $C^k\backslash Z_\Sigma$ also by a finite Abelian group $G(v_1, ..., v_k)$, which is determined by the relations between the D_{v_i} divisors. In this case, the toric varieties can often have orbifold singularities, $C^k\backslash G$. For example, the toric variety defined by (2.63) looks near the points $y = z = 0$ and $x = z = 0$ locally like $C^2\backslash Z_2$ (related to the $SU(2)$ algebra) and $C^2\backslash Z_3$ (related to the $SU(3)$ algebra), respectively, as seen in Figure 5.

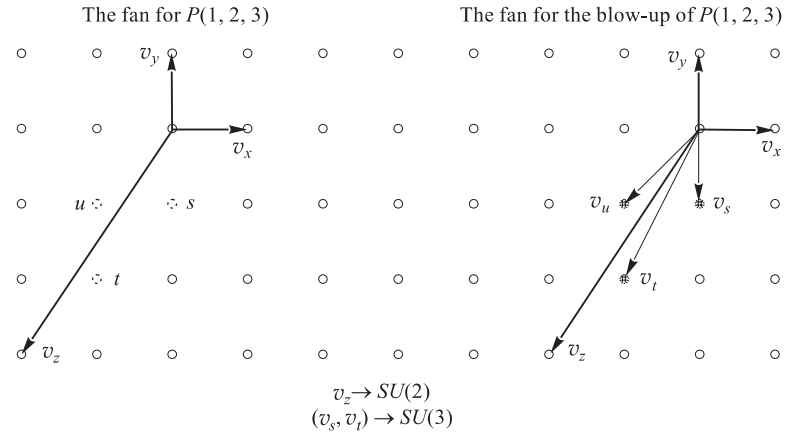

Fig. 5. The toric variety $P(1,2,3)$ with two orbifold singularities at the points $y = z = 0$ and $x = z = 0$ can be blown up by extra divisors $D(v_u)$ and $D(v_s)$, $D(v_t)$, respectively

3. GAUGE GROUP IDENTIFICATIONS FROM TORIC GEOMETRY

3.1. Calabi–Yau Spaces as Toric Fibrations. As discussed in Section 2, any Calabi–Yau manifold can be considered as a hypersurface in a toric variety, with a corresponding reflexive polyhedron Δ with a positive-integer lattice Λ, associated with a dual polyhedron Δ^* in the dual lattice Λ^*. The toric variety is determined by a fan Σ^*, consisting of the cones which are given by a triangulation of Δ^*. A large subset of reflexive polyhedra and their corresponding Calabi–Yau manifolds can be classified in terms of their fibration structures. In this way, it is possible, as we discuss later, to connect the structures of all the projective vectors of the one dimensionality with the projective vectors of other dimensionalities, and thereby construct a new algebra in the set of all «reflexive» projective vectors that gives the full set of CY_d hypersurfaces in all dimensions: $d = 1, 2, 3, ...$

In order to embark on this programme, it is useful first to review two key operations, *intersection* and *projection*, which can give possible fibration structures for reflexive polyhedra [34]:

• There may exist a projection operation $\pi : \Lambda \to \Lambda_{n-k}$, where Λ_{n-k} is an $(n-k)$-dimensional sublattice, and $\pi(\Delta)$ is also a reflexive polyhedron, and

• there may exist an intersection projection J through the origin of a reflexive polyhedron, such that $J(\Delta)$ is again an $(n-l)$-dimensional reflexive polyhedron, and

• these operations may exhibit the following duality properties:

$$\begin{aligned} \Pi(\Delta) &\Leftrightarrow J(\Delta^*) \\ J(\Delta) &\Leftrightarrow \Pi(\Delta^*). \end{aligned} \tag{3.1}$$

For a reflexive polyhedron Δ with fan Σ over a triangulation of the facets of Δ^*, the CY hypersurface in variety $\mathcal{O}_\Sigma$ is given by the zero locus of the polynomial:

$$\wp = \sum_{\mu \in \Delta \cap M} c_{\boldsymbol{\mu}} \cdot \prod_{i=1}^{N} z_i^{\langle \mathbf{v}_i \cdot \boldsymbol{\mu} \rangle + 1}. \tag{3.2}$$

One can consider the variety $\mathcal{O}_\Sigma$ as a fibration over the base $\mathcal{O}_{\Sigma_{\rm base}}$ with generic fiber $\mathcal{O}_{\Sigma_{\rm fiber}}$. This fibration structure can be written in terms of homogeneous coordinates. The fiber as an algebraic subvariety is determined by the polyhedron $\Delta^*_{\rm fiber} \subset \Delta^*_{\rm CY}$, whereas the base can be seen as a projection of the fibration along the fiber. The set of one-dimensional cones in $\Sigma_{\rm base}$ (the primitive generator of a cone is zero or $\tilde{v}_i$) is the set of images of one-dimensional cones in $\Sigma_{\rm CY}$ (with primitive generator v_j) that do not lie in $N_{\rm fiber}$. The image $\Sigma_{\rm base}$ of $\Sigma_{\rm CY}$ under $\Pi : N_{\rm CY} \to N_{\rm base}$ gives us the following relation:

$$\Pi v_i \; = \; r_i^j \cdot \tilde{v}_j, \tag{3.3}$$

if Πv_i is in the set of one-dimensional cones determined by $\tilde{v}_j$ $r_i^j \in N$, otherwise $r_i^j = 0$.

Similarly, the base space is the weighted projective space with the torus transformation:

$$(\tilde{x}_1, ..., \tilde{x}_{\tilde{N}}) \;\; \sim (\lambda^{\tilde{k}_j^1} \cdot \tilde{x}_1, ..., \lambda^{\tilde{k}_j^{\tilde{N}}} \cdot \tilde{x}_{\tilde{N}}), \;\; j = 1, ..., \tilde{N} - \tilde{n}, \tag{3.4}$$

where the $\tilde{k}_j^i$ are integers such that $\sum_j \tilde{k}_i^j \tilde{v}_j = 0$. The projection map from the variety $\mathcal{O}_\Sigma$ to the base can be written as

$$\tilde{x}_i = \prod_j x_j^{r_j^i}, \tag{3.5}$$

corresponding to the following redefinitions of the torus transformation for $\tilde{x}_i$:

$$\Pi : \tilde{x}_i \to \lambda^{k_l^j \cdot r_j^i} \cdot \tilde{x}_i, \;\; \sum k_l^j \cdot r_j^i \cdot \tilde{v}_i = 0. \tag{3.6}$$

In the toric description of $K3$ surfaces with elliptic fibers, denoted by $\Delta^*{}_{\rm fiber}$, one can consider the following divisors: $D_{\rm fiber}$, $D_{\rm section}$, D_{v_a} and D_{v_b}. The last pair of divisors correspond to lattice points of Δ^* that are «above» or «below» the fiber, respectively. Let us consider the case when all divisors D_{v_a} (or D_{v_b}) shrink to zero size. In this case, there appears a $K3$ hypersurface with two point singularities, which belong to the ADE classification. The process of blowing up these singularities gives the primordial $K3$ manifold, and its intersection structure is given by the structure of the edges. The Cartan–Lie algebra (CLA) diagrams

of the gauge groups that appear when the exceptional fibers are blown down to points are nothing but the edge diagrams of the upper and lower parts of Δ^* without vertices, respectively. A simple well-known example with elliptic fiber and with base P^1 is given by the following Weierstrass equation for the fiber:

$$y^2 = x^3 \, + \, f(z_1, z_2) \cdot x \cdot z^4 \, + \, g(z_1, z_2) \cdot z^6, \tag{3.7}$$

where the coefficients $f(z_1, z_2), g(z_1, z_2)$ are functions on the base.

In the following parts of this Section, we discuss some examples of $K3$ spaces from our general classification, and explain the identification of their corresponding gauge groups.

3.2. Examples of $K3$ Toric Fibrations with $J = \Pi$ Weierstrass Structure. As a first example, we consider the case of the elliptic $K3$ hypersurface with elliptic fiber $P^2(1, 2, 3)[6]$ defined by the integer positive lattice with basis (we explain this lattice basis later in terms of our algebraic description):

$$\begin{pmatrix} \mathbf{e}_1 \\ \mathbf{e}_2 \\ \mathbf{e}_3 \end{pmatrix} = \begin{pmatrix} -m & n & 0 & 0 \\ -2 & -2 & 1 & 0 \\ -1 & -1 & -1 & 1 \end{pmatrix},$$

where we consider the following 12 pairs of integer numbers (m, n) which are taken from the numbers: $1, 2, 3, 4, 5, 6$,

$$\{\,(1,1),\,(1,2),\,(1,3),\,(1,4),\,(1,5),\,(1,6),\,(2,3),\,(2,5)\,(3,4),\,(4,5),\,(5,6)\}.$$

With this choice of the pairs, the basis above determines a self-dual set of 12 projective $\mathbf{k}_4$ vectors:

$$\begin{aligned}
m = 1,\, n = 1 &\implies \mathbf{k}_4 = (1,1,4,\ 6\ )[12], \Longleftrightarrow (5,6,22,33) \\
m = 1,\, n = 2 &\implies \mathbf{k}_4 = (1,2,6,\ 9\ )[18], \Longleftrightarrow (3,5,16,24) \\
m = 1,\, n = 3 &\implies \mathbf{k}_4 = (1,3,8,\ 12)[24], \Longleftrightarrow (2,5,14,21) \\
m = 1,\, n = 4 &\implies \mathbf{k}_4 = (1,4,10,15)[30], \Longleftrightarrow DI^{'} \\
m = 1,\, n = 5 &\implies \mathbf{k}_4 = (1,5,12,16)[36], \Longleftrightarrow \text{self-dual} \\
m = 1,\, n = 6 &\implies \mathbf{k}_4 = (1,6,14,21)[42], \Longleftrightarrow \text{self-dual} \\
m = 2,\, n = 3 &\implies \mathbf{k}_4 = (2,3,10,15)[30], \Longleftrightarrow \text{self-dual} \\
m = 2,\, n = 5 &\implies \mathbf{k}_4 = (2,5,14,21)[42], \Longleftrightarrow (1,3,8,12) \\
m = 3,\, n = 4 &\implies \mathbf{k}_4 = (3,4,14,21)[42], \Longleftrightarrow DI^{''} \\
m = 3,\, n = 5 &\implies \mathbf{k}_4 = (3,5,16,24)[48], \Longleftrightarrow (1,2,6,9) \\
m = 4,\, n = 5 &\implies \mathbf{k}_4 = (4,5,18,27)[54], \Longleftrightarrow DI^{'''} \\
m = 5,\, n = 6 &\implies \mathbf{k}_4 = (5,6,22,33)[66], \Longleftrightarrow (1,1,4,6).
\end{aligned} \tag{3.8}$$

Later this set will emerge as the intersection-projection symmetric XIX chain ($J = \Pi$) of our algebraic classification. In this example, one can see that the projective vectors corresponding to the tetrahedra produce a self-dual set. We also show in (3.8) the duality relations between six other vectors and some of the vectors from Table 1.

However, three of the projective vectors in (3.8), $\mathbf{k}_4 = (1,4,10,15)[30]$, $(3,4,14,21)[42]$ and $(4,5,18,27)[54]$, correspond to polyhedra with five vertices, and their duals can be found among higher-level $K3$ spaces. They are found by double intersections (DI) among the five-dimensional extensions of the $K3$ vectors shown in Table 1:

$$\begin{aligned}
\mathbf{k}_4 = (1,4,10,15)[30] &\overset{DI'}{\Longleftrightarrow} \{\mathbf{k}_5^{ex} = (0,1,6,8,15)[30]\} \bigcap \\
&\bigcap \{\mathbf{k}_5^{ex} = (6,1,0,14,21)[42]\}, \\
\mathbf{k}_4 = (3,4,14,21)[42] &\overset{DI''}{\Longleftrightarrow} \{\mathbf{k}_5^{ex} = (2,1,0,6,9)[18]\} \bigcap \\
&\bigcap \{\mathbf{k}_5^{ex} = (0,1,2,4,7)[14]\}, \\
\mathbf{k}_4 = (4,5,18,27)[54] &\overset{DI'''}{\Longleftrightarrow} \{\mathbf{k}_5^{ex} = (1,0,1,4,6)[12]\} \bigcap \\
&\bigcap \{\mathbf{k}_5^{ex} = (0,1,1,3,5)[10]\}
\end{aligned} \tag{3.9}$$

as discussed in more detail in Section 6.

The ascending Picard numbers for polyhedra in this chain include:

$$\begin{aligned}
(\Delta(P^3(1,6,14,21)[42]) : \aleph &= 24(24^*),\ \mathrm{Pic} = 10(10^*) \\
\approx (\Delta(P^3(1,5,12,18)[36]) : \aleph &= 24(24^*),\ \mathrm{Pic} = 10(10^*) \\
\subset (\Delta(P^3(1,4,10,15)[30]) : \aleph &= 25(20^*),\ \mathrm{Pic} = 9(11^*) \\
\subset (\Delta(P^3(1,3,8,12)[24]) : \aleph &= 27(15^*),\ \mathrm{Pic} = 8(14^*) \\
\subset (\Delta(P^3(1,2,6,9)[18]) : \aleph &= 30(12^*),\ \mathrm{Pic} = 6(16^*) \\
\subset (\Delta(P^3(1,1,4,6)[12]) : \aleph &= 39(9),\ \mathrm{Pic} = 2(18^*) \subset \ldots\ldots
\end{aligned} \tag{3.10}$$

In the case of the mirror polyhedron chain, there is the inverse property: $\Delta^*(P^3(1,6,14,21)[42])$ corresponds to the maximal member of the set of mirror polyhedra. These Picard numbers are listed in Table 1, together with those of the other $K3$ spaces.

In the chain (3.8), the mirror polyhedra, Δ^*, have an intersection plane H^*_{fiber} through the interior point which defines an elliptic-fiber triangle with seven integer points, $P^2(1,2,3)[6]$ (see Figures 6,7):

$$\Delta^*_{\mathrm{fiber}} = \Delta^* \bigcap H^*_{\mathrm{fiber}}. \tag{3.11}$$

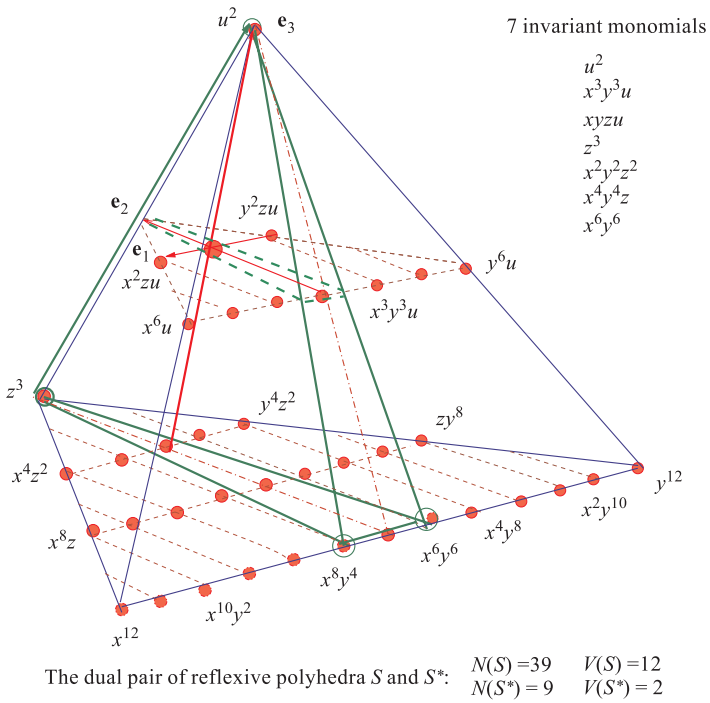

Fig. 6. The dual pair of reflexive planar polyhedra defined by the eldest projective vector (1,1,4,6) with $N(S) = 39$ and the youngest projective vector (5,6,22,33) with $N(S^*)$=9 integer points (marked by circles), respectively. $SL(3, Z)$ transformations produce an infinite number of dual pairs of tetrahedra, conserving the volumes $\mathrm{Vol}\,(S) = 12$, $\mathrm{Vol}\,(S^*) = 6$, respectively

By mirror symmetry in the polyhedron Δ, a projection operator π can be defined: $\pi : M \to M_{n-1}$, where M_{n-1} is an $(n-1)$-dimensional sublattice, such that $\pi(\Delta)$ is a reflexive polyhedron in M_{n-1}. This reflexive polyhedron also consists of seven points, so it is self-dual. Also, one can find a planar intersection H through Δ and through the interior point, which also produces the reflexive polyhedron with seven points, namely the fiber $P^2(1, 2, 3)[6]$ (see Figures 6,7):

$$\Delta_{\mathrm{fiber}} = \Delta \bigcap H_{\mathrm{fiber}}. \tag{3.12}$$

The dual pair of tetrahedra $\Delta(P^3(1, 1, 4, 6)[12])$ and $\Delta(P^3(5, 6, 22, 33)[66])$ consist of 39 and 9 points, respectively, as seen in Figure 6. They are the biggest and smallest polyhedra in the chain (3.8), and all other tetrahedra in this chain can

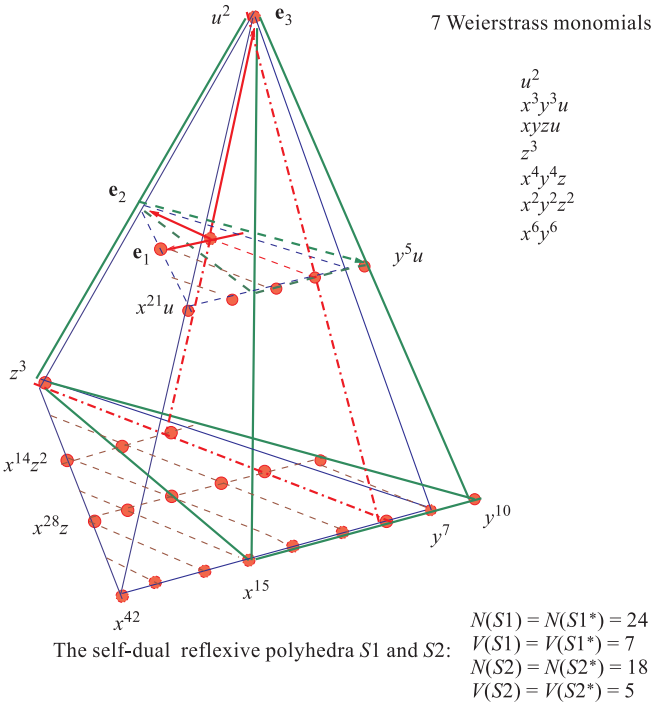

Fig. 7. The self-dual polyhedra in the chain XIX determined by projective vector (1,6,14,21) with $N(S1) = 24$ and vector (2,3,10,15) with $N(S2) = 18$ integer points, respectively. $SL(3, Z)$ transformations produce an infinite number of dual pairs of tetrahedra, conserving the volumes $\mathrm{Vol}\,(S1) = 7$ and $\mathrm{Vol}\,(S2) = 5$, respectively

be found in this Figure. This contains, in particular, the two self-dual polyhedra $\Delta(P^3(1, 6, 14, 21)[42])$ and $\Delta(P^3(2, 3, 10, 15)[30])$ consisting of $24 + 24^*$ and $18 + 18^*$ points, respectively, as seen in Figure 7:

$$\begin{aligned}&(0, 0, 1),\ (0, 1, -1),\ (-1, -2, -1),\ (6, -2, -1),\\ &(0, 0, 1),\ (0, 1, -1),\ (-2, -2, -1),\ (3, -2, -1).\end{aligned} \tag{3.13}$$

We now consider the intersection of the three-dimensional polyhedron $\Delta(P^3(1, 6, 14, 21)[42])$ with the two-dimensional plane H through the interior point. The intersection of this plane with the polyhedron, $H \bigcap \Delta$, forms a reflexive polyhedron fiber $P^2(1, 2, 3)$ with seven points. The equation of this plane in canonical coordinates μ_1, μ_2, μ_3 is: $m_1 = 0$. The fiber consists of the following

polyhedron points:

$$\begin{aligned} v_0 &= (0,\underline{0,0}),\\ v_1 &= (0,\underline{-1,0}),\\ v_2 &= (0,\underline{0,1}),\\ v_3 &= (0,\underline{1,-1}),\\ v_4 &= (0,\underline{0,-1}),\\ v_5 &= (0,\underline{-1,-1}),\\ v_6 &= (0,\underline{-2,-1}). \end{aligned} \tag{3.14}$$

Here and subsequently, the components of the vector corresponding to the fiber are underlined.

With respect to this fiber, the base is one-dimensional: P^1, and its fan F_2 consists of the divisors corresponding to the interior point and two divisors corresponding to two rays, $R_1 = +\mathbf{e}_1$ and $R_2 = -\mathbf{e}_1$, with directions from the point $(0,-2,-1)$ to the point $(6,-2,-1)$ and from the point $(0,-2,-1)$ to $(-1,-2,-1)$, respectively. The points of $\pi_B^{-1}(R_i)$ (i.e., the points projected onto R_i by π_B) for the rays R_i, $(i=1=+, i=2=-)$ are of the form $(\pm\ldots,b,c)$, where $(0,b,c)$ is the point of the fiber.

The 16 points of $\pi_B^{-1}(R_1)$ are listed in Table 2: they correspond to the divisors D_{v_i}, which produce the E_8 algebra [34]. Also, from this Table one can easily read the Coxeter numbers/weights. There is only one point in $\pi_B^{-1}(R_2)$, namely

$$\tilde{v}_1^1 = (-1,\underline{-2,-1}) \tag{3.15}$$

which therefore does not correspond to any nontrivial group.

Table 2. The points of $\pi_B^{-1}(R_1)$

Coxeter #	$v_6^{(i)}$	$v_5^{(i)}$	$v_1^{(i)}$	$v_4^{(i)}$	$v_0^{(i)}$
1	$(1,\underline{-2,-1})$	$(1,\underline{-1,-1})$	$(1,\underline{-1,0})$	$(1,\underline{0,-1})$	$(1,\underline{0,0})$
2	$(2,\underline{-2,-1})$	$(2,\underline{-1,-1})$	$(2,\underline{-1,0})$	$(2,\underline{0,-1})$	$---$
3	$(3,\underline{-2,-1})$	$(3,\underline{-1,-1})$	$(3,\underline{-1,0})$	$---$	$---$
4	$(4,\underline{-2,-1})$	$(4,\underline{-1,-1})$	$---$	$---$	$---$
5	$(5,\underline{-2,-1})$	$---$	$---$	$---$	$---$
6	$(6,\underline{-2,-1})$	$---$	$---$	$---$	$---$

3.3. Example of Gauge-Group Identification. Consider again the toric variety determined by the dual pair of polyhedra $\Delta(P^3(1,1,4,6)[12])$ and its dual Δ^* shown in Figure 6. The mirror polyhedron contains the intersection H^* through the interior point, the elliptic fiber $P^2(1,2,3)$. For all integer points of Δ^* (apart from the interior point), one can define in a convenient basis the corresponding complex variables:

$$\begin{aligned} v_1 &= (0,\underline{-2,-3}) \to z_1,\\ v_2 &= (0,\underline{-1,-2}) \to z_2,\\ v_3 &= (0,\underline{-1,-1}) \to z_3,\\ v_4 &= (0,\underline{0,-1}) \to z_4,\\ v_0 &= (0,\underline{0,0}),\\ v_6 &= (0,\underline{1,0}) \to z_6,\\ v_7 &= (0,\underline{0,1}) \to z_7, \end{aligned} \tag{3.16}$$

and

$$\begin{aligned} v_8 &= (-1,\underline{-4,-6}) \to z_8,\\ v_9 &= (1,\underline{0,0}) \to z_9. \end{aligned} \tag{3.17}$$

There are some linear relations between integer points inside the fiber:

$$\begin{aligned} v_1 + 2v_6 + 3v_7 &= 0,\\ v_2 + v_6 + 2\cdot v_7 &= 0,\\ v_3 + v_6 + v_7 &= 0,\\ v_4 + v_6 + v_7 &= 0 \end{aligned} \tag{3.18}$$

and also the following relation between points in Δ^*:

$$v_8 + v_9 + 4v_6 + 6v_7 = 0. \tag{3.19}$$

The polyhedron $\Delta(P^3(1,1,4,6))$ contains 39 points, which can be subdivided as follows. There are seven points in the fiber $P^2(1,2,3)$, determined by the intersection of the plane $m_1 + 2m_2 + 3m_3 = 0$ and the positive integer lattice. This plane separates the remaining 32 points in 16 «left» and 16 «right» points.

These «left» and «right» points define singularities of the E_{8_L} and E_{8_R} types, respectively, which may be illustrated as follows. The plane

$H(\Delta) = m_1 + 2m_2 + 3m_3$ contains the following seven points:

$$\begin{aligned}
t_1 &= (5, \underline{-1, -1}) \to (z_8^6 z_9^6) \cdot (\underline{z_1^6 z_2^4 z_3^3 z_4^2}),\\
t_2 &= (3, \underline{0, -1}) \to (z_8^4 z_9^4) \cdot (\underline{z_1^4 z_2^3 z_3^3 z_4^2 z_6}),\\
t_3 &= (2, \underline{-1, 0}) \to (z_8^3 z_9^3) \cdot (\underline{z_1^3 z_2^2 z_3^2 z_4 z_7}),\\
t_4 &= (1, \underline{1, -1}) \to (z_8^2 z_9^2) \cdot (\underline{z_1^2 z_2^2 z_3 z_4^2 z_6^2}),\\
t_5 &= (0, \underline{0, 0}) \to (z_8 z_9) \cdot (\underline{z_1^6 z_2^4 z_3^3 z_4^2}),\\
t_6 &= (-1, \underline{2, -1}) \to (\underline{z_2 z_4^2 z_6^3}),\\
t_7 &= (-1, \underline{-1, 1}) \to (\underline{z_3 z_7^2}).
\end{aligned} \tag{3.20}$$

The Weierstrass equation for the E_{8_L} group based on the polyhedron $\Delta(P^3(1,1,4,6))$ can be written in the form:

$$\begin{aligned}
&\underline{z}_6^3 + \underline{z}_6^2 \cdot (a_2^{(1)} z_8 z_9^3 + a_2^{(2)} z_9^4) +\\
&+\underline{z}_1^4 \cdot \underline{z}_6 \cdot (a_4^{(1)} z_8^3 z_9^5 + a_4^{(2)} z_8^2 z_9^6 + a_4^{(3)} z_8 z_9^7 + a_4^{(4)} z_9^8) +\\
&+\underline{z}_1^6 \cdot (a_6^{(1)} z_8^5 z_9^7 + a_6^{(2)} z_8^4 z_9^8 + a_6^{(3)} z_8^3 z_9^9 + a_6^{(4)} z_8^2 z_9^{(10)} + a_6^{(5)} z_8 z_9^{(11)} + a_6^{(6)} z_9^{(12)}) =\\
&= \underline{z}_7^2 + a_1 \cdot \underline{z}_6 \underline{z}_7 \cdot z_9^2 + \underline{z}_7 \cdot (a_3^{(1)} z_8^2 z_9^4 + a_3^{(2)} z_8 z_9^{(5)}).
\end{aligned} \tag{3.21}$$

The second Weierstrass equation for the E_{8_R} group can be obtained from this equation by interchanging the variables desrcibing the base: $z_8 \leftrightarrow z_9$*. The Weierstrass triangle equation can be presented in the following general form, where we denote $\underline{z}_6 = x$, $\underline{z}_7 = y$:

$$y^2 + a_1 \cdot x \cdot y + a_3 \cdot y = x^3 + a_2 \cdot x^2 + a_4 \cdot x + a_6, \tag{3.22}$$

where the a_i are polynomial functions on the base. The Weierstrass equation can be written in more simplified form as:

$$y^2 = x^3 + x \cdot f + g, \tag{3.23}$$

with discriminant

$$\Delta = 4f^3 + 27g^2. \tag{3.24}$$

In the zero locus of the discriminant, some divisors D_i define the degeneration of the torus fiber.

In addition to the method [34] described above, there is a somewhat different way to find the singularity type [35]. As we saw in the above example, the

*The coefficients a_i correspond to the notations of [35].

polynomials f and g can be homogeneous of orders 8 and 12, respectively, with a fibration that is degenerate over 24 points of the base. For this form of Weierstrass equation, there exists the ADE classification of degenerations of elliptic fibers. In this approach, the type of degeneration of the fiber is determined by the orders of vanishing of the functions f, g and δ. In the case of the general Weierstrass equation, a general algorithm for the ADE classification of elliptic singularities was considered by Tate [36]. For convenience, we repeat in Table 3 some results of Tate's algorithm, from which one can recover the $E_8 \times E_8$ type of Lie-algebra singularity for the (1,1,4,6) polyhedron.

Table 3. Lie algebras obtained from Tate's algorithm [36]: $a_{j;k} = a_j/\sigma^k$

Type	Group	$k(a_1)$	$k(a_2)$	$k(a_3)$	$k(a_4)$	$k(a_6)$	$k(\Delta)$
I_0	—	0	0	0	0	0	0
I_1	—	0	0	1	1	1	1
I_2	$SU(2)$	0	0	1	1	1	1
I_{2k}^{ns}	$Sp(2k)$	0	0	k	k	$2k$	$2k$
I_{2k}^{s}	$SU(2k)$	0	1	k	k	$2k$	$2k$
I_{2k+1}^{s}	$SU(2k+1)$	0	1	k	$k+1$	$2k+1$	$2k+1$
III	$SU(2)$	1	1	1	1	2	3
IV_s	$SU(3)$	1	1	1	2	3	4
I_0^{*ns}	G_2	1	1	2	2	3	6
I_1^{*s}	$SO(10)$	1	1	2	3	5	7
I_{2k-3}^{*ns}	$SO(4k+1)$	1	1	k	$k+1$	$2k$	$2k+3$
I_{2k-3}^{*s}	$SO(4k+2)$	1	1	k	$k+1$	$2k+1$	$2k+3$
I_{2k-2}^{*ns}	$SO(4k+3)$	1	1	$k+1$	$k+1$	$2k+1$	$2k+4$
I_{2k-2}^{*s}	$SO(4k+4)$	1	1	$k+1$	$k+1$	$2k+1$	$2k+4$
IV^{*ns}	F_4	1	2	2	3	4	8
IV^{*s}	E_6	1	2	2	3	5	8
III^*	E_7	1	2	3	3	5	9
II^*	E_8	1	2	3	4	5	10

4. THE COMPOSITE STRUCTURE OF PROJECTIVE VECTORS

We now embark in more detail on our construction of the projective vectors $\mathbf{k}$ which determine CY hypersurfaces, as previewed briefly in the Introduction and based on the polyhedron technique and the concept of duality [7] reviewed

in Section 2. We develop this construction inductively, studying the structure of these vectors initially in low dimensions and then proceeding to higher ones.

4.1. Initiation to the Dual Algebra of CY Projective Vectors. Our starting point is the trivial zero-dimensional «vector»,

$$\mathbf{k}_1 = (1), \tag{4.1}$$

which defines the trivial self-dual polyhedron comprising a single point, with the simplest possible associated monomial:

$$x \Rightarrow \mu_1 = 1 \Rightarrow \mu_1' = (0). \tag{4.2}$$

The next step is to consider the only polyhedron on the line R^1 which is also self-dual, and whose intersection with the integer lattice on the line contains three integer points:

$$\mu_1' = (-1),\ \mu_1' = (0),\ \mu_1' = (+1). \tag{4.3}$$

The projective vector corresponding to this linear polyhedron is

$$\mathbf{k}_2 = (1, 1), \tag{4.4}$$

which can be constructed from the $\mathbf{k}_1$ vector, by the following procedure.

We extend the vector $\mathbf{k}_1$ to a two-dimensional vector in CP_1, by inserting a zero component in all possible ways:

$$\begin{aligned} \mathbf{k}_1^{ex'} &= (0, 1) \\ \mathbf{k}_1^{ex''} &= (1, 0). \end{aligned} \tag{4.5}$$

The following monomials correspond to these «extended» vectors:

$$\begin{aligned} \mu^{'} &= (\nu, 1) \Rightarrow x^{\nu} \cdot y \\ \mu^{''} &= (1, \xi) \Rightarrow x \cdot y^{\xi} \end{aligned} \tag{4.6}$$

with the arbitrary integer numbers ν, ξ. From all the possible $\mathbf{k}$ pairs:

$$(\mathbf{k}^{ex'} \Leftrightarrow \mathbf{k}^{ex'}),\ (\mathbf{k}^{ex''} \Leftrightarrow \mathbf{k}^{ex''}),\ (\mathbf{k}^{ex'} \Leftrightarrow \mathbf{k}^{ex''}), \tag{4.7}$$

we select only those whose intersections give a reflexive polyhedron. In this simple two-dimensional case, only a single pair is so selected, namely $\mathbf{k}_1^{ex'}$ and $\mathbf{k}_1^{ex''}$:

$$\mathbf{k}_1^{ex'} \bigcap \mathbf{k}_1^{ex''} = 1, \tag{4.8}$$

and the reflexive polyhedron comprises just a single point. The corresponding monomial is $x \cdot y$, whose degree is unity for both variables: $\deg_x = 1$ and $\deg_y = 1$.

We now introduce a second operation on these «extended» vectors $\mathbf{k}^{'\cdots}$, which is «dual» to the intersection, namely the «sum» operation:

$$\mathbf{k}_1^{ex'} \bigcup \mathbf{k}_1^{ex''} = \mathbf{k}_2 = (0,1) + (1,0) = (1,1). \tag{4.9}$$

In this simple case, one has three quadratic monomials:

$$\begin{aligned} x^2 \Rightarrow \mu_1 &= (2,0) \Rightarrow \mu_1' = (-1); \\ x \cdot y \Rightarrow \mu_2 &= (1,1) \Rightarrow \mu_2' = (0); \\ y^2 \Rightarrow \mu_3 &= (0,2) \Rightarrow \mu_3' = (+1). \end{aligned} \tag{4.10}$$

If a projective vector is multiplied by a positive integer number $m \in Z^+$, it still determines the same hypersurface. Therefore, we should also consider sums of such vectors, characterized by two positive integer numbers, $m,\ n$:

$$m \cdot \mathbf{k}_1^{ex'} + n \cdot \mathbf{k}_1^{ex''}. \tag{4.11}$$

It turns out that, in order to get a reflexive polyhedron with only one interior point, the numbers m and n have to be lower than certain maximal values: $m_{\max}$ and $n_{\max}$, respectively. In our first trivial example, we find that

$$m_{\max} = 1,\ \ n_{\max} = 1. \tag{4.12}$$

In general, the set of all pairs (m,n) with $m \leqslant m_{\max}$ and $n \leqslant n_{\max}$ generate a «chain» of possible reflexive polyhedra, which happens to be trivial in this simple case.

Following the previous procedure, to construct all possible vectors on the plane we should start from two vectors, $\mathbf{k}_1$ and $\mathbf{k}_2$, «extended» to dimension three in CP_2 space:

$$\begin{aligned} &\mathbf{k}_1^{ex'} = (0,0,1),\ \mathbf{k}_1^{ex''} = (0,1,0),\ \mathbf{k}_1^{ex'''} = (1,0,0), \\ &\mathbf{k}_2^{ex'} = (0,1,1),\ \mathbf{k}_2^{ex''} = (1,1,0),\ \mathbf{k}_2^{ex'''} = (1,0,1). \end{aligned} \tag{4.13}$$

The next step consists in finding all possible pairs of these three-dimensional vectors whose intersection gives the only reflexive polyhedron of dimension two, which corresponds to the polyhedron projective vector $\mathbf{k}_2 = (1,1)$. Only two pairs (plus cyclic permutations) satisfy this constraint:

$$[\mathbf{k}_1^{ex'}(0,0,1)] \bigcap [\mathbf{k}_2^{ex''}(1,1,0)] = [\mathbf{k}_2(1,1)]_J \tag{4.14}$$

and

$$[\mathbf{k}_2^{ex'}(0,1,1)] \bigcap [\mathbf{k}_2^{ex''}(1,1,0)] \;=\; [\mathbf{k}_2(1,1)]_J. \tag{4.15}$$

In these two cases, the corresponding monomials are:

$$\begin{aligned} x^2 \cdot z \Rightarrow \mu_1 = (2,0,1) \;\Rightarrow\; (-1),\\ x \cdot y \cdot z \Rightarrow \mu_2 = (1,1,1) \;\Rightarrow\; (0),\\ y^2 \cdot z \Rightarrow \mu_3 = (0,2,1) \;\Rightarrow\; (+1), \end{aligned} \tag{4.16}$$

and

$$\begin{aligned} x^2 \cdot z^2 \Rightarrow \mu_1 = (2,0,2) \;\Rightarrow\; (-1),\\ x \cdot y \cdot z \Rightarrow \mu_2 = (1,1,1) \;\Rightarrow\; (0),\\ y^2 \Rightarrow \mu_3 = (0,2,0) \;\Rightarrow\; (+1), \end{aligned} \tag{4.17}$$

respectively. These lead to the two following chains:

$$\begin{aligned} I. \qquad \mathbf{k}_3(1) \;&=\; 1 \cdot \mathbf{k}_1^{ex'} + 1 \cdot \mathbf{k}_2^{ex''} \;=\; (1,1,1);\; m=1,\, n=1,\\ \mathbf{k}_3(2) \;&=\; 2 \cdot \mathbf{k}_1^{ex'} + 1 \cdot \mathbf{k}_2^{ex''} \;=\; (1,1,2);\; m=2,\, n=1,\\ m_{\max} \;&=\; \dim(\mathbf{k}_2^{ex''}) = 2, \quad n_{\max} = \dim(\mathbf{k}_1^{ex'}) = 1 \end{aligned} \tag{4.18}$$

and

$$\begin{aligned} II. \qquad \mathbf{k}_3(2) \;&=\; 1 \cdot \mathbf{k}_2^{ex'} + 1 \cdot \mathbf{k}_2^{ex'''} \;=\; (1,1,2);\; m=1,\, n=1,\\ \mathbf{k}_3(3) \;&=\; 2 \cdot \mathbf{k}_2^{ex'} + 1 \cdot \mathbf{k}_2^{ex'''} \;=\; (1,2,3);\; m=2,\, n=1,\\ m_{\max} \;&=\; \dim(\mathbf{k}_2^{ex''}) = 2, \quad n_{\max} = \dim(\mathbf{k}_2^{ex'}) = 2. \end{aligned} \tag{4.19}$$

Where the eldest vectors are given on the first lines of the two preceding equations, and we note that the vector $(1,1,2)$ is common to both chains.

It turns out that, also in higher dimensions, some $\mathbf{k}$ vectors are common to more than one chain. Thus it is possible to make a transition from one chain to another by passing through the common vectors. The algebra of projective vectors with the two operations $\bigcap$ and $\bigcup$ should be closed under duality symmetry:

$$J \;\Longleftrightarrow\; \Pi, \tag{4.20}$$

where the symbols J and Π denote two dual conjugate operations: *intersection* and *projection*, respectively. In this way, all vectors $\mathbf{k}_d$ can be found. This structure underpins the idea of a web of transitions between all Calabi–Yau manifolds.

4.2. General Formulation of Calabi–Yau Algebra. In the spirit of the simple constructions of the previous subsection, we can also construct the corresponding closed $\mathbf{k}_4$ algebra in the case of $K3$ hypersurfaces. However, before giving the results, we first briefly formulate a theorem underlying the construction of a $\mathbf{k}_{d+1}$ projective vector, determining an associated reflexive $d+1$-dimensional polyhedron and CY_d hypersurface, starting from $\mathbf{k}_d$ projective vectors, which determine a d-dimensional reflexive polyhedron with one interior point and a corresponding CY_{d-1} hypersurface. This theorem underlies our systematic inductive algebraic construction of CY manifolds.

The theorem is based on two general points:

• First: from the vector $\mathbf{k}_d$, we construct the «extended» vectors $\mathbf{k}_{d+1}^{ex}$ using the rule:

$$(*)\quad \mathbf{k}_d = (k_1, ..., k_2) \stackrel{\pi^{-1}}{\Longrightarrow} \mathbf{k}_{d+1}^{ex(i)} = (k_1, ..., 0^i, ..., k_d). \tag{4.21}$$

• Second: we consider only those pairs of all possible «extended» vectors, $\mathbf{k}_{d+1}^{ex(i)}$ and $\mathbf{k}_{d+1}^{ex(j)}$ with $0 \leqslant i, j \leqslant d$, whose intersection gives the reflexive polyhedron of dimension d with only one interior point. We denote this operation by:

$$(**)\qquad \mathbf{k}_{d+1}^{ex(i)} \bigcap \mathbf{k}_{d+1}^{ex(j)} = [\mathbf{k}_d]_J. \tag{4.22}$$

The statement of the theorem is:

• If by the rule (*) one can get, from the projective $\mathbf{k}_d$ vector, a set of «extended» vectors $\mathbf{k}_{d+1}^{ex(i)}$, $0 \leqslant i \leqslant d$, and for any pair of such «extended» $\mathbf{k}_{d+1}^{ex(i)}$-vectors the conditions (**) are fulfilled, then the sum of these two «extended» vectors will give an eldest projective vector $\mathbf{k}_{d+1}$, which determines a reflexive polyhedron with only one interior point.

• Two finite positive integer numbers, $n_{\max}, m_{\max} \in Z_+$, exist such that any linear combination of two vectors $\mathbf{k}_{d+1}^{i,j}(n,m)$, with integer coefficients $m \leqslant m_{\max}$; $n \leqslant n_{\max}$ produce a CY hypersurface. We call «chain» the set of vectors generated by any such pair of «extended» vectors:

$$\begin{gathered} p \cdot \mathbf{k}_{d+1}^{i,j}(n,m) = m \cdot \mathbf{k}_{d+1}^{ex(i)} + n \cdot \mathbf{k}_{d+1}^{ex(j)}, \\ \mathbf{k}_{d+1}^{i,j}(1,1) = \mathbf{k}_{d+1}^{i,j}(\text{eld}). \end{gathered} \tag{4.23}$$

• The intersection of the vector $\mathbf{k}_{d+1}^{i,j}(m,n)$ with the vector $\mathbf{k}_{d+1}^{ex(i)}$ is equal to the intersection of this vector with the vector $\mathbf{k}_{d+1}^{ex(j)}$:

$$[\mathbf{k}_{d+1}^{i,j}(m,n)] \bigcap [\mathbf{k}_{d+1}^{ex(j)}] = [\mathbf{k}_{d+1}^{i,j}(m,n)] \bigcap [\mathbf{k}_{d+1}^{ex(i)}]. \tag{4.24}$$

We can also formulate a converse theorem:

• If one can decompose a reflexive projective vector $\mathbf{k}_{d+1}$ as the sum of two reflexive projective vectors $\mathbf{k}^{'}_{d+1}$ and $\mathbf{k}^{''}_{d+1}$, then there exists the intersection of the vector $\mathbf{k}_{d+1}$ with either of these two vectors, which defines a projective vector $\mathbf{k}_d$ and a reflexive polyhedron with only one interior point.

The above theorem provides a description of all CY_{d+1} hypersurfaces with d-dimensional fibers in terms of two positive-integer parameters. Similarly, one can also consider the intersections of three (or more) «doubly-extended» vectors $\mathbf{k}^{ex(')}_{d+1}$, $\mathbf{k}^{ex('')}_{d+1}$, $\mathbf{k}^{ex(''')}_{d+1}$ (by «doubly-extended» we mean that they may be obtained by inserting two zero components in $\mathbf{k}_{d-1}$ vectors). One should check that this intersection gives a reflexive polyhedron in the $d-2$ space:

$$[\mathbf{k}^{ex(2^{'})}_{d-1}] \bigcap [\mathbf{k}^{ex(2^{''})}_{d-1}] \bigcap [\mathbf{k}^{ex(2^{'''})}_{d-1}] = [\mathbf{k}_{d-1}]_J. \tag{4.25}$$

In this way, one may obtain a $3, 4, ..., \leqslant d$ positive-integer parameter description of the $(d+1)$-dimensional polyhedra with $(d-1), (d-2), ...$-dimensional fiber sections:

$$p \cdot \mathbf{k}_{d+1} = m \cdot \mathbf{k}^{ex(2^{'})}_{d-1} + n \cdot \mathbf{k}^{ex(2^{''})}_{d-1} + l \cdot \mathbf{k}^{ex(2^{'''})}_{d-1}. \tag{4.26}$$

Finally, one can obtain additional lists of $\mathbf{k}_{d+1}$ vectors by using three «extended» vectors, $\mathbf{k}^{ex^r}_d$, $\mathbf{k}^{ex^i}_d$ $\mathbf{k}^{ex^j}_d$ (and similarly using four $\mathbf{k}^{ex}_{...}$, etc.), and a special algebra of summing these vectors only if the following three conditions are fulfilled:

$$\begin{aligned} &1.[\mathbf{k}^{ex^r}_d] \bigcap [\mathbf{k}^{ex^i}_d] = [\mathbf{k}_{d-1}]^{'}_J, \\ &2.[\mathbf{k}^{ex^i}_d] \bigcap [\mathbf{k}^{ex^j}_d] = [\mathbf{k}_{d-1}]^{''}_J, \\ &3.[\mathbf{k}^{ex^j}_d] \bigcap [\mathbf{k}^{ex^r}_d] = [\mathbf{k}_{d-1}]^{'''}_J. \end{aligned} \tag{4.27}$$

In this way, one may obtain a complete description of the positive-integer lattice which defines all reflexive $\mathbf{k}$ vectors.

5. TWO-VECTOR CHAINS OF $K3$ SPACES

We now embark on a parametrization of the $\mathbf{k}_4$ vectors defining $K3$ hypersurfaces with fiber sections. Our description of $K3$ hypersurfaces is based on the above understanding of the composite and dual structure of the projective $\mathbf{k}_4$ vectors. As already mentioned, we find a link between this structure and the finite subgroups of the group of rotations of three-space, namely the cyclic and dihedral

groups and the symmetry groups of the Platonic solids — the tetrahedron, the octahedron-cube and the icosahedron-dodecahedron:

- $C_n : n = 1, 2, 3, ...$ — the cyclic group of finite rotations in the plane around an axis «1» by the angles $\alpha = 2\pi/n$;
- $D_n : n = 2, 3, 4, ...$ — the dihedral group, comprising all these rotations together with all the reflections of a second axis «n» lying in this plane, which is orthogonal to the axis «l», and producing with respect to each other the angle $\alpha/2$;
- T — the finite group of the transformations leaving invariant the regular tetrahedron, with 12 parameters;
- O — the finite group of the transformations leaving invariant the regular cube and octahedron, with 24 parameters;
- I — the finite group of the transformations leaving invariant the regular icosahedron and dodecahedron, with 60 parameters.

We use the polyhedron technique introduced in the previous Section, taking into account all its duality, intersection and projection properties to study the projective-vector classification of $K3$ spaces.

5.1. Two-Dimensional Integer Chains of $K3$ Hypersurfaces. In the $K3$ case, as already foreshadowed in the Introduction, the classification can start from a basis of five types of «extended» vectors. We recall that the structure of the three «planar» projective vectors $\mathbf{k}_3 = (1, 1, 1), (1, 1, 2), (1, 2, 3)$ can easily be understood on the basis of the doubly-extended vector $\mathbf{k}_1^{ext} = (0, 0, 1)$ and the singly-extended vector $\mathbf{k}_2^{ext} = (0, 1, 1)$. The structure of the underlying composite vector $\mathbf{k}_2 = (1, 1)$ is also obvious. The full list of $K3$ projective vectors is obtainable from the algebra of the following five extended vectors: the maximally-extended vector of the form

$$\mathbf{k}_C^{\text{ext}} = (0, 0, 0, 1) \tag{5.1}$$

with its 4 cyclic permutations, the doubly-extended dihedral vector of the form

$$\mathbf{k}_D^{\text{ext}} = (0, 0, 1, 1) \tag{5.2}$$

with its 6 dihedral permutations, the singly-extended tetrahedral vector of the form

$$\mathbf{k}_T^{\text{ext}} = (0, 1, 1, 1) \tag{5.3}$$

with its 4 cyclic permutations, the extended octahedral vector of the form

$$\mathbf{k}_O^{\text{ext}} = (0, 1, 1, 2) \tag{5.4}$$

with its 12 permutations, and finally the extended icosahedral vector of the form

$$\mathbf{k}_I^{\text{ext}} = (0, 1, 2, 3) \tag{5.5}$$

with its 24 permutations, for a total of 50 extended vectors.

Using the algebra of combining pairs of these 50 extended $\mathbf{k}^i$ vectors, we obtain 90 distinct $\mathbf{k}_4$ vectors in 22 double chains with a regular planar k-gon intersection: $k > 3$ with only one interior point, as seen in Table 1. Combining three extended $\mathbf{k}^i$ vectors, we obtain four triple chains with self-dual line-segment intersection-projections and one interior point, which contain 91 distinct vectors, of which only four $\mathbf{k}_4$ vectors are different from the 90 vectors found previously, as also seen in Table 1. Of course, there are some vectors which have a regular planar k-gon in their intersection and no line-segment intersection. Further, as we see later in Section 7, there is just one vector, $\mathbf{k}_4 = (7, 8, 9, 12)$, which has only a single point intersection, i.e., the intersection consists of the zero point alone, and can be determined by the intersection-projection

$$J(\Delta) \leftrightarrow \Pi(\Delta^*), \qquad \Pi(\Delta) \leftrightarrow J(\Delta^*) \tag{5.6}$$

duality, where the polyhedra Δ and Δ^* determine a dual pair of $K3$ hypersurfaces. We recall that the sum of the integer points in intersection, $J(\Delta)$, and in projection, $\Pi(\Delta^*)$, is equal to $14 = 4 + 10, 5 + 9, 6 + 8, 7 + 7, 8 + 6, 9 + 5, 10 + 4$ for the plane intersection-projection and $6 = 3 + 3$ for the line-segment intersection-projection. This duality plays a very important role in our description. Eleven of the 22 two-vector chains found previously satisfy directly the following condition:

$$\begin{aligned} J(\Delta^n) &= \Pi(\Delta^n) = \Delta^{n-1}, \\ \Pi(\Delta^{n*}) &= J(\Delta^{n*}) = \Delta^{n-1^*}, \end{aligned} \tag{5.7}$$

which means that the number of integer points in the intersection of the polyhedron (mirror polyhedron) forming the reflexive polyhedron of lower dimension is equal to the number of projective lines crossing these integer points of the polyhedron (mirror). The projections of these lines on a plane in the polyhedron and a plane in its mirror polyhedron reproduce, of course, the reflexive polyhedra of lower dimension. Only for self-dual polyhedra one can have

$$J(\Delta^n) = \Pi(\Delta^n) = \Pi(\Delta^{n*}) = J(\Delta^{n*}) = \Delta^{n-1} = \Delta^{n-1^*}, \tag{5.8}$$

namely the most symmetrical form of these relations.

Following the recipe presented as our central Theorem in Section 4, we present Table 4, which lists all the $\mathbf{k}_4$ projective vectors derived from *pairs* of extended vectors of lower dimension, which fall into the 22 chains listed. In each case, we list the maximum integers m, n in the chains, which are determined by the dimensions of the extended $\mathbf{k}_i$ vectors. This Table includes all the 90 projective $\mathbf{k}_4$ vectors found using our construction. All of these $\mathbf{k}_4$ vectors define $K3$ hypersurfaces which could be obtained using the Z^n symmetry coset action*.

*They may also be used to construct higher-level CY_1 spaces as the intersections of polynomial loci, as discussed in Section 9.

Table 4. The 22 chains of $K3$ obtained using pairs of $\mathbf{k}_4$ projective vectors. The number of $K3$ spaces in each chain is denoted by N

Chain	$\mathbf{k}_i \bigcap \mathbf{k}_j$	$\Delta_{\rm Int}, \Delta^*_{\rm Int}$	$\mathbf{k}(K3) = m \cdot \mathbf{k}_i + n \cdot \mathbf{k}_j$	$\sum m + \sum n$	$\max(m,n)$	N
I	$(0001) \bigcap (1110)$	$(10,4)$	(n,n,n,m)	$1 \cdot m + 3 \cdot n$	$m=1, n=3$	3
IV	$(0001) \bigcap (1120)$	$(9,5)$	$(n,n,2n,m)$	$1 \cdot m + 4 \cdot n$	$m=1, n=4$	4
XV	$(0001) \bigcap (1230)$	$(7,7)$	$(n,2n,3n,m)$	$1 \cdot m + 6 \cdot n$	$m=1, n=6$	6
X	$(0011) \bigcap (1100)$	$(9,5)$	(n,n,m,m)	$2 \cdot m + 2 \cdot n$	$m=2, n=2$	4
XI	$(0011) \bigcap (1101)$	$(9,5)$	$(n,n,m,m+n)$	$2 \cdot m + 3 \cdot n$	$m=3, n=2$	6
V	$(0011) \bigcap (1102)$	$(9,5)$	$(n,n,m,m+2n)$	$2 \cdot m + 4 \cdot n$	$m=4, n=2$	6
$XXII$	$(0011) \bigcap (1210)$	$(7,7)$	$(n,2n,m+n,m)$	$2 \cdot m + 4 \cdot n$	$m=3, n=3$	6
XVI	$(0011) \bigcap (1203)$	$(7,7)$	$(n,2n,m,m+3n)$	$2 \cdot m + 6 \cdot n$	$m=6, n=2$	9
II	$(0111) \bigcap (1011)$	$(10,4)$	$(n,m,m+n,m+n)$	$3 \cdot m + 3 \cdot n$	$m=3, n=3$	4
$XIII$	$(0111) \bigcap (1012)$	$(8,6)$	$(n,m,m+n,m+2n)$	$3 \cdot m + 4 \cdot n$	$m=4, n=3$	9
III	$(0111) \bigcap (3012)$	$(4,10)$	$(3n,m,m+n,m+2n)$	$3 \cdot m + 6 \cdot n$	$m=6, n=2$	9
$XVII$	$(0111) \bigcap (1023)$	$(7,7)$	$(n,m,m+2n,m+3n)$	$3 \cdot m + 6 \cdot n$	$m=6, n=3$	12
VI	$(0112) \bigcap (1012)$	$(9,5)$	$(n,m,n+m,2m+2n)$	$4 \cdot m + 4 \cdot n$	$m=4, n=4$	6
$VIII$	$(0112) \bigcap (1120)$	$(5,9)$	$(n,m+n,m+2n,2m)$	$4 \cdot m + 4 \cdot n$	$m=3, n=4$	9
VII	$(0112) \bigcap (2110)$	$(9,5)$	$(2n,m+n,m+n,2m)$	$4 \cdot m + 4 \cdot n$	$m=3, n=1$	3
$XVIII$	$(0112) \bigcap (1023)$	$(7,7)$	$(n,m,m+2n,2m+3n)$	$4 \cdot m + 6 \cdot n$	$m=6, n=4$	16
XIV	$(0112) \bigcap (2130)$	$(6,8)$	$(2n,m+n,m+3n,2m)$	$4 \cdot m + 6 \cdot n$	$m=5, n=3$	8
IX	$(0112) \bigcap (2103)$	$(5,9)$	$(2n,m+n,m,2m+3n)$	$4 \cdot m + 6 \cdot n$	$m=6, n=3$	12
XIX	$(0123) \bigcap (1023)$	$(7,7)$	$(n,m,2m+2n,3m+3n)$	$6 \cdot m + 6 \cdot n$	$m=6, n=6$	12
XX	$(0123) \bigcap (2103)$	$(7,7)$	$(2n,m+n,2m,3m+3n)$	$6 \cdot m + 6 \cdot n$	$m=3, n=3$	12
XXI	$(0123) \bigcap (3120)$	$(7,7)$	$(3n,m+n,2m+2n,3n)$	$6 \cdot m + 6 \cdot n$	$m=2, n=2$	4
XII	$(0123) \bigcap (3210)$	$(5,9)$	$(3n,m+2n,2m+n,3m)$	$6 \cdot m + 6 \cdot n$	$m=2, n=2$	4

For illustration, we give in Table 5 the eldest vectors in each chain, i.e., the first members of all 22 chains, which have $m=1, n=1$. As one can see, some vectors are common to more than one chain. Using our understanding of the origins of the intersections, and duality, we can classify these 22 chains in five classes, as indicated by the groupings in Table 5, which correspond to the intersections, as indicated.

It should be noted, however, that the above doubly-extended vector structure does not exhaust the full list of possible $K3$ projective vectors. The projective vectors

$$\begin{aligned} (\mathbf{k}_4)_{91} &= (4,5,7,9), \\ (\mathbf{k}_4)_{92} &= (5,6,8,11), \\ (\mathbf{k}_4)_{93} &= (5,7,8,20), \\ (\mathbf{k}_4)_{94} &= (7,8,10,25), \\ (\mathbf{k}_4)_{95} &= (7,8,9,12) \end{aligned} \tag{5.9}$$

Table 5. The eldest vectors $\mathbf{k}_i$ in the 22 $K3$ chains which have $m = n = 1$

Chain	d	$\mathbf{k}_i$	$\mathbf{k}_i$	(Δ, Δ^*)	$(\Delta_{\rm Int}, \Delta^*_{\rm Int})$
I	$d = 1 \cdot m + 3 \cdot n$	(n, n, n, m)	$(1, 1, 1, 1)$	$(35, 5)$	$(10, 4)$
II	$d = 3 \cdot m + 3 \cdot n$	$(n, m, m + n, m + n)$	$(1, 1, 2, 2)$	$(30, 6)$	$(10, 4)$
III	$d = 3 \cdot m + 6 \cdot n$	$(3n, m, m + n, m + 2n)$	$(1, 2, 3, 3)$	$(23, 8)$	$(4, 10)$
IV	$d = 1 \cdot m + 4 \cdot n$	$(n, n, 2n, m)$	$(1, 1, 1, 2)$	$(34, 6)$	$(9, 5)$
V	$d = 2 \cdot m + 2 \cdot n$	(n, n, m, m)	$(1, 1, 1, 1)$	$(35, 5)$	$(9, 5)$
VI	$d = 2 \cdot m + 3 \cdot n$	$(n, n, m, m + n)$	$(1, 1, 1, 2)$	$(34, 6)$	$(9, 5)$
VII	$d = 2 \cdot m + 4 \cdot n$	$(n, n, m, m + 2n)$	$(1, 1, 1, 3)$	$(39, 6)$	$(9, 5)$
$VIII$	$d = 4 \cdot m + 4 \cdot n$	$(n, m, m + n, 2m + 2n)$	$(1, 1, 2, 4)$	$(35, 7)$	$(9, 5)$
IX	$d = 4 \cdot m + 4 \cdot n$	$(2n, m + n, m + n, 2m)$	$(1, 1, 1, 1)$	$(35, 5)$	$(9, 5)$
X	$d = 4 \cdot m + 4 \cdot n$	$(n, m + n, m + 2n, 2m)$	$(1, 2, 2, 3)$	$(24, 8)$	$(5, 9)$
XI	$d = 4 \cdot m + 6 \cdot n$	$(2n, m + n, m, 2m + 3n)$	$(1, 2, 2, 5)$	$(28, 8)$	$(5, 9)$
XII	$d = 6 \cdot m + 6 \cdot n$	$(3n, m + 2n, 2m + n, 3m)$	$(1, 1, 1, 1)$	$(35, 5)$	$(5, 9)$
$XIII$	$d = 3 \cdot m + 4 \cdot n$	$(n, m, m + n, m + 2n)$	$(1, 1, 2, 3)$	$(31, 8)$	$(8, 6)$
XIV	$d = 4 \cdot m + 6 \cdot n$	$(2n, m + n, m + 3n, 2m)$	$(1, 1, 1, 2)$	$(34, 6)$	$(6, 8)$
XV	$d = 1 \cdot m + 6 \cdot n$	$(n, 2n, 3n, m)$	$(1, 1, 2, 3)$	$(31, 8)$	$(7, 7)$
XVI	$d = 2 \cdot m + 6 \cdot n$	$(m, n, 2n, 3n + m)$	$(1, 1, 2, 4)$	$(35, 7)$	$(7, 7)$
$XVII$	$d = 3 \cdot m + 6 \cdot n$	$(n, m, m + 2n, , m + 3n)$	$(1, 1, 3, 4)$	$(33, 9)$	$(7, 7)$
$XVIII$	$d = 4 \cdot m + 6 \cdot n$	$(n, m, m + 2n, 2m + 3n)$	$(1, 1, 3, 5)$	$(36, 9)$	$(7, 7)$
XIX	$d = 6 \cdot m + 6 \cdot n$	$(n, m, 2m + 2n, 3m + 3n)$	$(1, 1, 4, 6)$	$(39, 9)$	$(7, 7)$
XX	$d = 6 \cdot m + 6 \cdot n$	$(2n, m + n, 2m, 3m + 3n)$	$(1, 1, 1, 3)$	$(39, 6)$	$(7, 7)$
XXI	$d = 6 \cdot m + 6 \cdot n$	$(3n, m + n, 2m + 2n, 3m)$	$(2, 3, 3, 4)$	$(15, 9)$	$(7, 7)$
$XXII$	$d = 2 \cdot m + 4 \cdot n$	$(n, 2n, m + n, m)$	$(1, 1, 2, 2)$	$(30, 6)$	$(7, 7)$

have no planar reflexive polyhedron intersections, and therefore were not included in this list. To obtain most of the additional $\mathbf{k}_4$ vectors (5.10), one must consider chains constructed from three extended vectors of the type $\mathbf{k}^{ex} = (0, 0, 1)$ and $\mathbf{k}^{ex} = (0, 1, 1)$, with all possible permutations, having in the intersection the line-segment polyhedron consisting of three integer points. All these chains will be $J_1 - \Pi_1$ self-dual: $J_1 = \Pi_1 = 3$. It is easy to see that only four different such triple chains can be built, as discussed in Section 6. These chains are much longer than the previous two-vector chains, although their total number, 91, is also less than the full number of all $K3$ vectors. The projective vectors

$$\begin{aligned} (\mathbf{k}_4)_{12} &= (3, 5, 6, 7), \\ (\mathbf{k}_4)_{13} &= (3, 6, 7, 8), \\ (\mathbf{k}_4)_{14} &= (5, 6, 7, 9), \\ (\mathbf{k}_4)_{95} &= (7, 8, 9, 12) \end{aligned} \tag{5.10}$$

are not involved in these chains. However, the union of the doubly-extended and triply-extended vector chains gives a total of 94 $\mathbf{k}_4$ projective vectors. Only the $\mathbf{k}_4 = (7, 8, 9, 12)$ vector has just a point-intersection structure, and is not found by either the double- or triple-vector constructions, as discussed in more detail in Section 7.

To preview how it arises, note that, by $J - \Pi$ duality, we know that to $\mathbf{k} = (1, 1, 1, 1)$, which has three intersection planes (1,1,1) with ten points, there must correspond a $\mathbf{k}$ which has three different π projections with four points. Since it should have a nontrivial projection structure, namely a four-point planar polyhedron with one interior point in three independent directions, its external points should satisfy the following condition:

$$\frac{1}{4}\{M_1 + M_2 + M_3 + M_4\} = M_0 = (1, 1, 1, 1). \tag{5.11}$$

In three-space, these points can only be taken as:

$$\begin{aligned} M_1 &= (4, 1, 0, 0),\ M_2 = (0, 3, 1, 0), \\ M_3 &= (0, 0, 4, 0),\ M_4 = (0, 0, 0, 3). \end{aligned} \tag{5.12}$$

One can easily check that this polyhedron has three projections: π_{x_1}, π_{x_2}, π_{x_3}, with four points giving the $(1, 1, 1)$ planar polyhedron. The four points M_i (5.12) give the exceptional vector $\mathbf{k} = (7, 8, 9, 12)$. By projection, one can see that the five integer points of this polyhedron produce the $(1, 1, 1)$ planar polyhedron with four points.

5.2. Invariant Monomials and the $J - \Pi$ Structure of Calabi–Yau Equations. The experience provided by working with $K3$ hypersurfaces can aid in the classification of Calabi–Yau manifolds. Also for this more complicated case, one should use the duality conditions: one must be prepared to study the intersection structures of polyhedra and their mirrors and/or to study the projection structures for polyhedra and mirror polyhedra.

This «intersection-projection» structure of the $\mathbf{k}_4$ vectors from doubly-, triply- and quadruply-extended vectors allows us to introduce the concept of *invariant* monomials in the CY equations. These invariant monomials are homogeneous under the action of the extended vectors, i.e., if

$$\mathbf{z}' = \lambda^{\mathbf{k}_j^{ex}} \cdot \mathbf{z},\ \ j = 1, 2, 3, ..., \tag{5.13}$$

then

$$\mathbf{z}'^{\boldsymbol{\mu}} = \lambda^{\mathbf{k}_j^{ex} \cdot \boldsymbol{\mu}} \cdot \mathbf{z}^{\boldsymbol{\mu}} = \lambda^{d_j} \cdot \mathbf{z}^{\boldsymbol{\mu}}, \tag{5.14}$$

where $d_j = \dim(\mathbf{k}_j^{ex})$ and $j = 1, 2, 3, ...$ is the number of extended $\mathbf{k}_j^{ex}$ vectors. The invariant monomials, $\wp_i$, correspond to the reflexive polyhedra produced by the invariant set Ψ_{inv} which is the same for all the chains.

These extended vectors can be formed from the following five familiar types of projective vectors of lower dimensions:

$$\begin{aligned} &\mathbf{k}_1 = (0,0,1), \\ &\mathbf{k}_2 = (0,1,1), \\ &\mathbf{k}_3 = (1,1,1),\ \mathbf{k}_3 = (1,1,2),\ \mathbf{k}_3 = (1,2,3). \end{aligned} \tag{5.15}$$

A chain of $\mathbf{k}_4$ projective vectors can be generated from the linear sums of extended vectors, for example, for $j = 1, 2$ one can get:

$$\begin{aligned} \mathbf{k}_4(m,n) &= m \cdot \mathbf{k}_1^{ex} + n \cdot \mathbf{k}_2^{ex} \\ \text{if } \mathbf{k}_1^{ex} &\bigcap \mathbf{k}_2^{ex} = \{\wp_i : \wp_i \in \Sigma_{\text{inv}}\}. \end{aligned} \tag{5.16}$$

The invariant monomials are universal for all the $\mathbf{k}_4$ vectors in this chain.

To construct the $\mathbf{k}_4$ vectors determining $K3$ hypersurfaces, i.e., determining the corresponding polyhedra with the property of reflexivity, one has to give a correct set of invariant monomials. We have constructed the 22 sets of invariant monomials corresponding to the doubly-extended vector structures among the $\mathbf{k}_4$ projective vectors. In this case, these sets of the invariant monomials give in the intersection reflexive polyhedra of lower dimensions. The number of invariant monomials for this doubly-extended vector structure is given by

$$31 = 1 + 4 \times 2 + 22, \tag{5.17}$$

where the last number corresponds to the Betti number for $K3$ hypersurfaces: $b_2 = 22$. The structure of the $\mathbf{k}_4$ projective vectors obtained from the triply-extended vectors, namely $\mathbf{k}^{ex} = (0,0,0,1)$ and $\mathbf{k}^{ex} = (0,0,1,1)$, is given by the following four types of invariant monomials:

$$\begin{aligned} \Psi_{I_3} &: (2,0,1,1),\ (0,2,1,1),\ (1,1,1,1,) \Rightarrow x^2 \cdot z \cdot u,\ y^2 \cdot z \cdot u,\ x \cdot y \cdot z \cdot u, \\ \Psi_{II_3} &: (2,2,1,0),\ (0,0,1,2),\ (1,1,1,1,) \Rightarrow x^2 \cdot y^2 \cdot z,\ z \cdot u^2,\ x \cdot y \cdot z \cdot u, \\ \Psi_{III_3} &: (2,2,2,0),\ (0,0,0,2),\ (1,1,1,1,) \Rightarrow x^2 \cdot y^2 \cdot z^2,\ u^2,\ x \cdot y \cdot z \cdot u, \\ \Psi_{IV_3} &: (2,0,0,2),\ (0,2,2,0),\ (1,1,1,1,) \Rightarrow x^2 \cdot u^2,\ y^2 \cdot z^2,\ x \cdot y \cdot z \cdot u. \end{aligned} \tag{5.18}$$

The four chains corresponding to these sets of invariant monomials are (see Tables 4,5,6, and 7):

$$\begin{aligned}
\mathbf{k}_4(\Psi_{I_3}) &= M\cdot(1,1,0,0)+N\cdot(0,0,1,0)+\\
&+L\cdot(0,0,0,1)=(M,M,N,L),\\
\mathbf{k}_4(\Psi_{II_3}) &= M\cdot(1,0,0,1)+N\cdot(0,1,0,1)+\\
&+L\cdot(0,0,1,0)=(M,N,L,M+N),\\
\mathbf{k}_4(\Psi_{III_3}) &= M\cdot(1,0,0,1)+N\cdot(0,1,0,1)+\\
&+L\cdot(0,0,1,1)=(M,N,L,M+N+L),\\
\mathbf{k}_4(\Psi_{IV_3}) &= M\cdot(1,0,1,0)+N\cdot(0,1,0,1)+\\
&+L\cdot(0,0,1,1)=(M,N,M+L,N+L).
\end{aligned}\tag{5.19}$$

In these chains*, the sets of projective vectors are subject to the following additional projective restrictions:

$$\begin{aligned}
\mathbf{k}_4(\Psi_{I_3})\cdot\mathbf{e}_I &= 0, \quad \mathbf{e}_I=(-1,1,0,0),\\
\mathbf{k}_4(\Psi_{II_3})\cdot\mathbf{e}_{II} &= 0, \quad \mathbf{e}_{II}=(-1,-1,0,1),\\
\mathbf{k}_4(\Psi_{III_3})\cdot\mathbf{e}_{III} &= 0, \quad \mathbf{e}_{III}=(-1,-1,-1,1),\\
\mathbf{k}_4(\Psi_{IV_3})\cdot\mathbf{e}_{IV} &= 0, \quad \mathbf{e}_{IV}=(1,-1,-1,1).
\end{aligned}\tag{5.20}$$

Corresponding to these chains, the following triple intersections

$$\mathbf{k}_M^{ex}\bigcap\mathbf{k}_N^{ex}\bigcap\mathbf{k}_L^{ex}=\Psi_{I_3},\,\Psi_{II_3},\,\Psi_{III_3},\,\Psi_{IV_3}.\tag{5.21}$$

have the above-mentioned invariant monomials.

The $K3$ algebra has the interesting consequence that all the $\{1+4+22\}$ invariant monomials that give «good» planar reflexive polyhedra in the 22 two-vector chains also can be found by triple constructions. Therefore it is interesting to list now the 22 types of invariant monomials whose origin is also connected with the triple intersections of all types of projective vectors, the triply-extended vectors $\mathbf{k}_1^{ex}=(0,0,0,1)$, the doubly-extended vectors $\mathbf{k}_2^{ex}=(0,0,1,1)$, and the singly-extended vectors, $\mathbf{k}_3^{ex}=(0,1,1,1),(0,1,1,2),(0,1,2,3)$.

These monomials, $\mathbf{z}^{\boldsymbol{\mu}}$, are invariant under action of the extended vectors

$$\begin{aligned}
\mathbf{k}_i^{ex}\cdot\boldsymbol{\mu} &= \dim(\mathbf{k}_i^{ex}),\\
\mathbf{k}_j^{ex}\cdot\boldsymbol{\mu} &= \dim(\mathbf{k}_j^{ex}),\\
\mathbf{k}_l^{ex}\cdot\boldsymbol{\mu} &= \dim(\mathbf{k}_l^{ex}).
\end{aligned}\tag{5.22}$$

*There is in fact another «good» triple intersection of the extended vectors $(1,1,0,0)$, $(0,0,1,1)$, $(0,0,0,1)$, but the chain $I_3'=(M,M,N,N+L)$ it produces has the same three invariant monomials, $(0,2,1,1)+(2,0,1,1)+(1,1,1,1)$ as the I_3 chain, which includes all its projective vectors.

The directions of the possible projections Π are determined* by the degenerate monomial $(x \cdot y \cdot z \cdot u) \Rightarrow \boldsymbol{\mu} = (1,1,1,1)$ and by the exponents of the following 22 invariant monomials, $\mu = (\mu_1, \mu_2, \mu_3, \mu_4)$:

$$\begin{aligned}
&\underline{(3,0,0,0),\ (3,1,0,0),\ (3,1,1,0),}\ (3,2,0,0),\\
&(3,2,1,0),\ (3,3,0,0),\ (3,3,1,0),\\
&\underline{(4,0,0,0),\ (4,1,0,0),}\ (4,1,1,0),\ (4,2,0,0),\\
&(4,2,1,0), (4,3,0,0),\ (4,3,1,0),\ (4,4,0,0),\ (4,4,1,0),\\
&(6,0,0,0),\ (6,1,0,0),\ (6,2,0,0),\ (6,3,0,0),\\
&(6,4,0,0),\ (6,6,0,0),
\end{aligned} \tag{5.23}$$

where the underlines pick out those triple intersections where the intersections of pairs of vectors also specify reflexive polyhedra, which will be important later. The four other types of possible projections were already defined above.

The algebraic-geometry sense of $(J,\Pi)(\Delta) \leftrightarrow (\Pi, J)(\Delta^*)$ duality for $K3$ hypersurfaces can be interpreted through the invariant monomials: the list of the invariant monomials for the two-extended-vector classification and the list of all of the three-extended-vector classification are the same, and the total number of them is equal to $31 = 1 + 4 \times 2 + 22$. The $J(\Delta, \Delta^*) \leftrightarrow \Pi(\Delta^*, \Delta)$ duality can be interpreted at a deeper level for $J = \Pi$ chains: the invariant monomials are identical for corresponding CY equation and for its mirror equation. The projection–projection structure gives additional information about the form of the corresponding CY equation. For example, this structure determines the subset of monomials corresponding to the invariant monomials. As a result, the homogeneous CY equation can be written in according in terms of the intersection–projection structure of the projective $\mathbf{k}$ vectors:

$$\wp(\mathbf{z}) = \sum_{i}^{J} \mathbf{z}^{\mathbf{m}_0^i} \{ \sum_{p}^{\Pi} a^p_{\mathbf{m}_0^i}\, \mathbf{z}^{n_p \cdot \mathbf{e}^{\Pi}} \} = 0. \tag{5.24}$$

Here the $\mathbf{z}^{\mathbf{m}_0^i}$ are the invariant monomials which are defined by intersection structure, the vector $\mathbf{e}^{\Pi}$ is the direction of the projection, and the n_p are integer numbers.

6. THREE-VECTOR CHAINS OF $K3$ SPACES

As already mentioned, one can find additional chains of $K3$ projective vectors $\mathbf{k}_4$ if one considers systems of three extended vectors of the type $\mathbf{k}_1^{ex} = (0,0,0,1)$

*Additional constraints on the invariant monomials are given in Section 7, reducing their number to 9 = 1 + 3 + 5.

Table 6. The 18 $K3$ hypersurfaces in the three-vector chain I_3: $\mathbf{k} = (M, M, N, L) = = M \cdot (1,1,0,0) + N \cdot (0,0,1,0) + L \cdot (0,0,0,1)$. Here and subsequently, the symbol $\aleph$ in the first column denotes the location of the corresponding vector in Table 1. The numbers in the last columns indicate their locations in the corresponding chains

$\aleph$	M	M	N	L	$[d]$	(Δ, Δ^*)	I	II	IV	V	VII	X	XI	III
$J(\Delta)$	–	–	–	–	–	–	10	10	9	9	9	9	9	–
$\pi(\Delta^*)$	–	–	–	–	–	–	4	4	5	5	5	5	5	–
$\pi(\Delta^)$	–	–	–	–	–	–	–	10	–	–	$9'$	–	–	–
$J(\Delta^*)$	–	–	–	–	–	–	–	4	–	–	$5'$	–	–	–
1	1	1	1	1	[4]	$(35, 5^*)$	1	–	–	–	1	1	–	–
2	1	1	1	2	[5]	$(34, 6^*)$	2	–	1	–	–	–	1	–
3	1	1	1	3	[6]	$(39, 6^*)$	3	–	–	1	–	–	–	–
4	1	1	2	2	[6]	$(30, 6^*)$	–	1	2	–	–	2	–	–
5	1	1	2	3	[7]	$(31, 8^*)$	–	–	3	–	–	–	2	–
6	1	1	2	4	[8]	$(35, 7^*)$	–	–	4	2	–	–	–	–
7	1	1	3	4	[9]	$(33, 9^*)$	–	–	–	–	–	–	4	–
8	1	1	3	5	[10]	$(36, 9^*)$	–	–	–	3	–	–	–	–
9	1	1	4	6	[12]	$(39, 9^*)$	–	–	–	5	–	–	–	–
10	2	2	1	3	[8]	$(24, 8^*)$	–	–	–	–	2	–	3	–
11	2	2	1	5	[10]	$(28, 8^*)$	–	–	–	4	–	–	–	–
42	2	2	3	5	[12]	$(17, 11^*)$	–	–	–	–	–	–	5	–
43	2	2	3	7	[14]	$(19, 11^*)$	–	–	–	6	–	–	–	–
12	3	3	1	2	[9]	$(23, 8^*)$	–	2	–	–	–	–	–	–
44	3	3	2	4	[12]	$(15, 9^*)$	–	–	–	–	3	–	–	–
65	3	3	4	5	[15]	$(12, 12^*)$	–	–	–	–	–	–	–	1
21	4	4	1	3	[12]	$(21, 9^*)$	–	3	–	–	–	–	–	–
48	5	5	2	3	[15]	$(14, 11^*)$	–	4	–	–	–	–	–	–

and $\mathbf{k}_2^{ex} = (0,0,1,1)$, which have in their intersections only three integer points or only three invariant monomials. As also already remarked, there are only four different chains, corresponding to the four kinds of invariant monomial triples. We have also commented that these new chains yield only four additional $K3$ vectors, whilst the remaining vector, $\mathbf{k}_4 = (7,8,9,12)$, can be constructed out of four extended vectors, as discussed in the following Section. The relationship between the two- and three-vector constructions, and their substantial overlap, is the subject of this Section.

6.1. The Three-Vector Chain I_3: $\mathbf{k}_4 = (M,\ M,\ N,\ L)$. In this chain, the dimension $(d = 2M + N + L)$ and the eldest vector is $\mathbf{k}_{\rm eld} = (1,1,1,1)$, whose invariant monomials are $(2,0,1,1) + (0,2,1,1)$. The relations between this three-vector chain and the previously-discussed two-vector chains can easily be found.

We consider the first three vectors in Table 6, which also form the two-vector chain I:

$$\begin{aligned} I: \quad & m \cdot (1,1,1,0) + n \cdot (0,0,0,1) = (m,m,m,n) \rightarrow \\ & M = N = m = [\dim]\{(0,0,0,1)\} = 1, \\ & L = n \leqslant [\dim]\{(1,1,1,0)\} = 3. \end{aligned} \tag{6.1}$$

Similarly, one can consider four vectors $(2,2,1,1)$, $(3,3,1,2)$, $(4,4,1,3)$, and $(5,5,2,3)$, which form the two-vector chain II:

$$\begin{aligned} II: \quad & m \cdot (1,1,1,0) + n \cdot (1,1,0,1) = (m+n,m+n,m,n) \rightarrow \\ & N = m \leqslant [\dim]\{(1,1,0,1)\} = 3, \\ & L = n \leqslant [\dim]\{(1,1,1,0)\} = 3, \\ & M = m + n < 6. \end{aligned} \tag{6.2}$$

The four vectors $(1,1,2,1)$, $(1,1,2,2)$, $(1,1,2,3)$, and $(1,1,2,4)$ from the two-vector chain IV have the following relations with this triple chain:

$$\begin{aligned} IV: \quad & m \cdot (1,1,2,0) + n \cdot (0,0,0,1) = (m,m,2m,n) \rightarrow \\ & M = m \leqslant [\dim]\{(0,0,0,1)\} = 1, \\ & N = 2m = 2, \\ & L = n \leqslant [\dim]\{(1,1,2,0)\} = 4. \end{aligned} \tag{6.3}$$

The six vectors $(1,1,1,3)$, $(1,1,2,4)$, $(1,1,3,5)$, $(1,1,4,6)$, $(2,2,1,5)$, and $(2,2,3,7)$ in Table 6 correspond to the two-vector chain V:

$$\begin{aligned} V: \quad & m \cdot (1,1,0,2) + n \cdot (0,0,1,1) = (m,m,n,2m+n) \rightarrow \\ & M = m \leqslant [\dim]\{(0,0,1,1)\} = 2, \\ & N = n \leqslant [\dim]\{(1,1,0,2)\} = 4, \\ & L = 2m + n <= 8. \end{aligned} \tag{6.4}$$

The next three vectors $(1,1,1,1)$, $(3,3,2,4)$, and $(2,2,1,3)$ from the two-vector chain VII have the following connection to this triple chain:

$$\begin{aligned} VII: \quad & m \cdot (1,1,2,0) + n \cdot (1,1,0,2) = (m+n,m+n,2m,2n) \rightarrow \\ & M = m + n < 4, \\ & N = 2m < 4, \\ & L = 2n < 4. \end{aligned} \tag{6.5}$$

Two vectors $(1,1,1,1)$ and $(1,1,2,2)$ correspond to the two-vector chain X:

$$\begin{aligned} X: \quad & m\cdot(1,1,0,0)+n\cdot(0,0,1,1)=(m,m,n,n)\rightarrow \\ & M=m\leqslant 2, \\ & N=n\leqslant 2, \\ & L=n\leqslant 2. \end{aligned} \tag{6.6}$$

Finally, the values of M,N,L of the five projective vectors $(1,1,1,2)$, $(1,1,2,3)$, $(1,1,3,4)$, $(2,2,1,3)$, and $(2,2,3,5)$ correspond to the fact that they are also from the two-vector chain XI:

$$\begin{aligned} XI: \quad & m\cdot(1,1,0,1)+n\cdot(0,0,1,1)=(m,m,n,m+n)\rightarrow \\ & M=m\leqslant 2, \\ & N=n\leqslant 3, \\ & L=m+n\leqslant 5. \end{aligned} \tag{6.7}$$

6.2. The Three-Vector Chain II_3: $\mathbf{k}_4=(M,N,L,M+N)$. In this chain, shown in Table 7, the dimension $d=2M+2N+L$, there is a symmetry: $M\leftrightarrow N$, the eldest vector $\mathbf{k}_{\text{eld}}=(1,1,1,2)$, and the invariant monomials are $(2,2,1,0)+(0,0,1,2)$. Comparing this chain with the previous two-vector chains, one can see clearly the possible values of M,N,L for the projective vectors $(M,N,L,M+N)$. For example, if one compares the four vectors $(1,1,2,2)$, $(1,2,3,3)$, $(1,3,4,4)$, and $(2,3,5,5)$ in this triple chain with their structure in the two-vector chain II, one finds the following relations:

$$\begin{aligned} II: \quad & m\cdot(1,0,1,1)+n\cdot(0,1,1,1)=(m,n,m+n,m+n)\rightarrow \\ & M=m\leqslant [\dim]\{(0,1,1,1)\}=3, \\ & N=n\leqslant [\dim]\{(1,0,1,1)\}=3, \\ & L=m+n<6. \end{aligned} \tag{6.8}$$

Similarly, we find the following relations between the values of M,N,L in the triple chain and the values of m,n for double chains:

$$\begin{aligned} IV: \quad & m\cdot(1,1,0,2)+n\cdot(0,0,1,0)=(m,m,n,2m)\rightarrow \\ & M=N=m\leqslant [\dim]\{(0,0,1,0)\}=1, \\ & L=n\leqslant [\dim]\{(1,1,0,2)\}=4. \end{aligned} \tag{6.9}$$

$$\begin{aligned} VI: \quad & m\cdot(1,0,2,1)+n\cdot(0,1,2,1)=(m,n,2m+2n,m+n)\rightarrow \\ & M=m\leqslant [\dim]\{(0,1,2,1)\}=4, \\ & N=n\leqslant [\dim]\{(1,0,2,1)\}=4, \\ & L=2m+2n<8. \end{aligned} \tag{6.10}$$

$$
\begin{aligned}
VIII: \quad & m\cdot(1,0,2,1)+n\cdot(1,1,0,2)=(m+n,n,2m,m+2n)\rightarrow\\
& M=m+n\leqslant 8,\\
& N=n\leqslant[\dim]\{(1,0,2,1)\}=4,\\
& L=2m\leqslant 2[\dim]\{(1,1,0,2)\}=8.
\end{aligned}
\tag{6.11}
$$

$$
\begin{aligned}
XI: \quad & m\cdot(1,0,1,1)+n\cdot(0,1,0,1)=(m,n,m,m+n)\rightarrow\\
& M=m\leqslant[\dim]\{(0,1,0,1)\}=2,\\
& N=n\leqslant[\dim]\{(1,0,1,1)\}=3,\\
& L=m.
\end{aligned}
\tag{6.12}
$$

$$
\begin{aligned}
XIII: \quad & m\cdot(1,0,2,1)+n\cdot(0,1,1,1)=(m,n,2m+n,m+n)\rightarrow\\
& M=m\leqslant[\dim]\{(0,1,1,1)\}=3,\\
& N=n\leqslant[\dim]\{(1,0,2,1)\}=4,\\
& L=2m+n.
\end{aligned}
\tag{6.13}
$$

$$
\begin{aligned}
XIV: \quad & m\cdot(1,0,2,1)+n\cdot(1,2,0,3)=(m+n,2n,2m,m+3n)\rightarrow\\
& M=m+n,\\
& N=2n\leqslant 2[\dim]\{(1,0,2,1)\}=8,\\
& L=2m\leqslant 2[\dim]\{(1,2,0,3)\}=12.
\end{aligned}
\tag{6.14}
$$

$$
\begin{aligned}
XV: \quad & m\cdot(1,2,0,3)+n\cdot(0,0,1,0)=(m,2m,n,3m)\rightarrow\\
& M=m\leqslant[\dim]\{(0,0,1,0)\}=1,\\
& N=2m\leqslant 2[\dim]\{(0,0,1,0)\}=2,\\
& L=n\leqslant[\dim]\{(1,2,0,3)\}=6.
\end{aligned}
\tag{6.15}
$$

$$
\begin{aligned}
XVII: \quad & m\cdot(1,2,0,3)+n\cdot(0,1,1,1)=(m,2m+n,n,3m+n)\rightarrow\\
& M=m\leqslant[\dim]\{(0,1,1,1)\}=3,\\
& N=2m+n,\\
& L=n\leqslant[\dim]\{(1,2,0,3)\}=6.
\end{aligned}
\tag{6.16}
$$

$$
\begin{aligned}
XXII: \quad & m\cdot(1,0,2,1)+n\cdot(0,1,0,1)=(m,n,2m,m+n)\rightarrow\\
& M=m\leqslant[\dim]\{(0,1,0,1)\}=2,\\
& N=n\leqslant[\dim]\{(1,0,2,1)\}=6,\\
& L=2m.
\end{aligned}
\tag{6.17}
$$

Table 7. The 45 $K3$ hypersurfaces in the II_3 chain: $\mathbf{k} = (M, N, L, Q = N + M) =$ $= M \cdot (1, 0, 0, 1) + N \cdot (0, 1, 0, 1) + L \cdot (0, 0, 1, 0)$

ℵ	M	N	L	Q	$[d]$	(Δ, Δ^*)	II	IV	VI	$VIII$	XI	$XIII$	XIV	XV	$XVII$	$XXII$
–	–	–	–	–	–	$J(\Delta)$	10	9	9	5	9	8	6	7	7	7
–	–	–	–	–	–	$\pi(\Delta^*)$	4	5	5	9	5	6	8	7	7	7
–	–	–	–	–	–	$\pi(\Delta)$	10	–	9	$5'$	–	–	–	–	7	–
–	–	–	–	–	–	$J(\Delta^*)$	4	–	5	$9'$	–	–	–	–	7	–
2	1	1	1	2	[5]	$(34, 6^*)$		1			1		1			
4	1	1	2	2	[6]	$(30, 6^*)$	1	2								1
5	1	1	3	2	[7]	$(31, 8^*)$		3			2	1		1		
6	1	1	4	2	[8]	$(35, 7^*)$		4	1							
10	1	2	2	3	[8]	$(24, 8^*)$				1	3			2		2
12	1	2	3	3	[9]	$(23, 8^*)$	2						2	3		
13	1	2	4	3	[10]	$(23, 11^*)$						2		4		3
14	1	2	5	3	[11]	$(24, 13^*)$						3	3	5		
15	1	2	6	3	[12]	$(27, 9^*)$			2					6		
7	1	3	1	4	[12]	$(33, 9^*)$					4				1	
21	1	3	4	4	[12]	$(21, 9^*)$	3			3						
24	1	3	8	4	[16]	$(24, 12^*)$			3							
16	1	4	2	5	[12]	$(24, 12^*)$									2	4
22	1	4	3	5	[13]	$(20, 15^*)$						4	5			
31	1	4	10	5	[20]	$(23, 13^*)$			4							
25	1	5	3	6	[15]	$(21, 15^*)$									3	
30	1	5	4	6	[16]	$(19, 17^*)$				4		5				
32	1	6	4	7	[18]	$(19, 20^*)$									4	
36	1	7	5	8	[21]	$(18, 24^*)$									5	
39	1	8	6	9	[24]	$(18, 24^*)$									6	
42	2	3	2	5	[12]	$(17, 11^*)$				2	5					
45	2	3	4	5	[14]	$(13, 16^*)$							4			5
48	2	3	5	5	[15]	$(14, 11^*)$	4									
51	2	3	10	5	[20]	$(16, 14^*)$			5							
18	2	5	1	7	[15]	$(26, 17^*)$									7	
49	2	5	3	7	[17]	$(13, 20^*)$						7				
59	2	5	6	7	[20]	$(11, 23^*)$				7						
52	2	7	3	9	[21]	$(14, 23^*)$									9	
61	2	9	5	11	[27]	$(11, 32^*)$									13	
23	3	4	1	7	[15]	$(22, 17^*)$						6				
46	3	4	2	7	[16]	$(14, 18^*)$				5			6			
67	3	4	5	7	[19]	$(9, 24^*)$							7			
71	3	4	14	7	[28]	$(12, 18^*)$			6							
50	3	5	2	8	[18]	$(14, 20^*)$						8				
68	3	5	4	8	[20]	$(10, 22^*)$				8						
27	3	7	1	10	[21]	$(24, 24^*)$									8	
70	3	7	4	10	[24]	$(10, 26^*)$						9				
54	3	8	2	11	[24]	$(15, 27^*)$									10	
72	3	10	4	13	[30]	$(10, 35^*)$									11	
77	3	11	5	14	[33]	$(9, 39^*)$									12	
57	4	5	2	9	[20]	$(13, 23^*)$				6						
81	4	5	6	9	[24]	$(8, 26^*)$							8			
83	4	5	7	9	[25]	$(7, 32^*)$										
87	4	7	6	11	[28]	$(7, 35^*)$				9						
90	5	6	8	11	[30]	$(6, 39^*)$										

6.3. The Three-Vector Chain III_3: $\mathbf{k}_4 = (M, N, L, M + N + L)$. In this chain, shown in Table 8, the dimension $d = 2M + 2N + 2L$, there is $M \leftrightarrow N \leftrightarrow L$

symmetry, the eldest vector $\mathbf{k}_{\rm eld} = (1,1,1,3)$, and the invariant monomials are $(2,2,2,0)+(0,2,2,2)$. We see in the Table the appearance of the following two-vector chains

$$\begin{aligned} V: \quad & m\cdot(1,1,0,2) + n\cdot(0,0,1,1) = (m,m,n,2m+n) \rightarrow \\ & M = N = m \leqslant [\dim]\{(0,0,1,1)\} = 2, \\ & L = n \leqslant [\dim]\{(1,1,0,2)\} = 4. \end{aligned} \tag{6.18}$$

$$\begin{aligned} VI: \quad & m\cdot(1,0,1,2) + n\cdot(0,1,1,2) = (m,n,m+n,2m+2n) \rightarrow \\ & M = m \leqslant [\dim]\{(0,1,1,2)\} = 4, \\ & N = n \leqslant [\dim]\{(1,0,1,2)\} = 4, \\ & L = m+n. \end{aligned} \tag{6.19}$$

$$\begin{aligned} IX: \quad & m\cdot(1,0,1,2) + n\cdot(0,2,1,3) = (m,2n,m+n,2m+3n) \rightarrow \\ & M = m \leqslant [\dim]\{(0,2,1,3)\} = 6, \\ & N = 2n \leqslant 2[\dim]\{(1,0,1,2)\} = 8, \\ & L = m+n. \end{aligned} \tag{6.20}$$

$$\begin{aligned} XVI: \quad & m\cdot(1,0,2,3) + n\cdot(0,1,0,1) = (m,n,2m,3m+n) \rightarrow \\ & M = m \leqslant [\dim]\{(0,1,0,1)\} = 2, \\ & N = n \leqslant [\dim]\{(1,0,2,3)\} = 6, \\ & L = 2m. \end{aligned} \tag{6.21}$$

$$\begin{aligned} XVIII: \quad & m\cdot(1,0,1,2) + n\cdot(0,1,2,3) = (m,n,m+2n,2m+3n) \rightarrow \\ & M = m \leqslant [\dim]\{(0,1,2,3)\} = 6, \\ & N = n \leqslant [\dim]\{(1,0,1,2)\} = 4, \\ & L = m+2n. \end{aligned} \tag{6.22}$$

$$\begin{aligned} XIX: \quad & m\cdot(1,0,2,3) + n\cdot(0,1,2,3) = (m,n,2m+2n,3m+3n) \rightarrow \\ & M = m \leqslant [\dim]\{(0,2,1,3)\} = 6, \\ & N = n \leqslant [\dim]\{(1,0,2,3)\} = 6, \\ & L = 2m+2n. \end{aligned} \tag{6.23}$$

$$\begin{aligned} XX: \quad & m\cdot(2,0,1,3) + n\cdot(0,2,1,3) = (2m,2n,m+n,3m+3n) \rightarrow \\ & M = 2m \leqslant 2[\dim]\{(0,2,1,3)\} = 12, \\ & N = 2n \leqslant 2[\dim]\{(2,0,1,3)\} = 12, \\ & L = m+n. \end{aligned} \tag{6.24}$$

Table 8. The 48 $K3$ hypersurfaces in the III_3 chain: $\mathbf{k} = (M, N, L, Q = N+M+L) =$ $= M \cdot (1,0,0,1) + N \cdot (0,1,0,1) + L \cdot (0,0,1,1)$

ℵ	M	N	L	Q	$[d]$	(Δ, Δ^*)	V	VI	IX	XVI	$XVIII$	XIX	XX
–	–	–	–	–	–	$J(\Delta)$	9	9	5	7	7	7	7
–	–	–	–	–	–	$\pi(\Delta^*)$	5	5	9	7	7	7	7
–	–	–	–	–	–	$\pi(\Delta)$	–	9	–	–	7	7	7
–	–	–	–	–	–	$J(\Delta^*)$	–	5	–	–	7	7	7
3	1	1	1	3	[6]	$(39, 6^*)$	1						1
6	1	1	2	4	[8]	$(35, 7^*)$	2	1		1			
8	1	1	3	5	[10]	$(36, 9^*)$	3				1		
9	1	1	4	6	[12]	$(39, 9^*)$	4					1	
11	1	2	2	5	[10]	$(28, 8^*)$	5		1	2			
15	1	2	3	6	[12]	$(27, 9^*)$		2		3			2
17	1	2	4	7	[14]	$(27, 12^*)$				4	2		
19	1	2	5	8	[16]	$(28, 14^*)$				5	3		
20	1	2	6	9	[18]	$(30, 12^*)$				6		2	
24	1	3	4	8	[16]	$(24, 12^*)$		3	3				
26	1	3	5	9	[18]	$(24, 15^*)$					4		
28	1	3	7	11	[22]	$(25, 20^*)$					8		
29	1	3	8	12	[24]	$(27, 15^*)$						3	
31	1	4	5	10	[20]	$(23, 13^*)$		4					
33	1	4	6	11	[22]	$(22, 20^*)$			5		5		
34	1	4	9	14	[28]	$(24, 24^*)$					9		
35	1	4	10	15	[30]	$(25, 20^*)$						4	
37	1	5	7	13	[26]	$(21, 24^*)$					6		
38	1	5	12	18	[36]	$(14, 18^*)$						5	
40	1	6	8	15	[30]	$(21, 24^*)$					7		
41	1	6	14	21	[42]	$(24, 24^*)$						6	
43	2	2	3	7	[14]	$(19, 11^*)$	6		2				
47	2	3	4	9	[18]	$(16, 14^*)$			4	7			3
51	2	3	5	10	[20]	$(16, 14^*)$		5					
53	2	3	7	12	[24]	$(16, 20^*)$					11		
55	2	3	8	13	[26]	$(16, 23^*)$					10		
56	2	3	10	15	[30]	$(18, 18^*)$						7	
58	2	4	5	11	[22]	$(14, 19^*)$			6				
60	2	5	6	13	[26]	$(13, 23^*)$			7				
62	2	5	9	16	[32]	$(13, 29^*)$					14		
63	2	5	14	21	[42]	$(15, 27^*)$						9	
64	2	6	7	15	[30]	$(13, 23^*)$			9				
69	3	4	5	12	[24]	$(12, 18^*)$			8				
71	3	4	7	14	[28]	$(12, 18^*)$		6					
73	3	4	10	17	[34]	$(11, 31^*)$					13		
74	3	4	11	18	[36]	$(12, 30^*)$					12		
75	3	4	14	21	[42]	$(13, 26^*)$						8	
78	3	5	11	19	[38]	$(10, 35^*)$					15		
79	3	5	16	24	[48]	$(12, 30^*)$						10	
82	4	5	6	15	[30]	$(10, 20^*)$							4
84	4	5	7	16	[32]	$(9, 27^*)$			10				
85	4	5	13	22	[44]	$(9, 39^*)$					16		
86	4	5	18	27	[54]	$(10, 35^*)$						11	
88	4	6	7	17	[34]	$(8, 31^*)$			11				
91	5	6	8	19	[38]	$(7, 35^*)$			12				
92	5	6	22	33	[66]	$(9, 39^*)$						12	
93	5	7	8	20	[40]	$(8, 28^*)$							
94	7	8	10	25	[50]	$(6, 39^*)$							

6.4. The Three-Vector Chain IV_3: $\mathbf{k}_4 = (M,\ N,\ M+L,\ N+L)$. In this case (see Table 9), we have the dimension $d = 2M + 2N + 2L$, the eldest vector $\mathbf{k}_{\text{eld}} = (1,1,1,1)$, and the invariant monomials are $(2,0,0,2) + (0,2,2,0)$. This three-vector chain includes the following vectors form the two-vector construction:

$$\begin{aligned} VII: \quad & m \cdot (2,1,1,0) + n \cdot (0,1,1,2) = (2m, m+n, m+n, 2n) \rightarrow \\ & M = 2m \leqslant 4, \\ & N = m+n \leqslant 4, \\ & L = n-m \geqslant 0. \end{aligned} \tag{6.25}$$

$$\begin{aligned} X: \quad & m \cdot (1,1,0,0) + n \cdot (0,0,1,1) = (m,m,n,n) \rightarrow \\ & M = m \leqslant 2, \\ & N = m \leqslant 2, \\ & L = n-m \geqslant 0. \end{aligned} \tag{6.26}$$

$$\begin{aligned} XII: \quad & m \cdot (3,2,1,0) + n \cdot (0,1,2,3) = (3m, 2m+n, m+2n, 3n) \rightarrow \\ & M = 3m, \\ & N = 2m+n, \\ & L = 2n-2m, \\ & (m,n) = (1,2),\ (2,1)\,;\ (1,1),\ (1,4),\ (4,1),\ (2,5),\ (5,2). \end{aligned} \tag{6.27}$$

$$\begin{aligned} XXI: \quad & m \cdot (1,2,3,0) + n \cdot (1,2,0,3) = (m+n, 2m+2n, 3m, 3n) \rightarrow \\ & M = m, \\ & N = 2m, \\ & L = m, \\ & (m,n) = (1,1), (1,2),\ (2,1);\ (1,5),\ (5,1),\ (4,5),\ (5,4). \end{aligned} \tag{6.28}$$

$$\begin{aligned} XXII: \quad & m \cdot (1,0,2,1) + n \cdot (0,1,0,1) = (m,n,2m,m+n) \rightarrow \\ & M = m \leqslant [\dim]\{(0,1,0,1)\} = 2, \\ & N = n \leqslant [\dim]\{(1,0,2,1)\} = 4, \\ & L = m. \end{aligned} \tag{6.29}$$

Table 9. The 8 $K3$ hypersurfaces in the IV_3 chain: $\mathbf{k} = (M, N, M+L, N+L) = M \cdot (1,0,1,0) + N \cdot (0,1,0,1) + L \cdot (0,0,1,1)$

$\aleph$	M	N	$M+L$	$N+L$	$[d]$	(Δ, Δ^*)	VII	X	XII	XXI	$XXII$
–	–	–	–	–	–	$J(\Delta)$	7	9	5	7	7
–	–	–	–	–	–	$\pi(\Delta^*)$	7	5	9	7	7
–	–	–	–	–	–	$\pi(\Delta)$	–	–	$5'$	$7'$	–
–	–	–	–	–	–	$J(\Delta^*)$	–	–	$9'$	$7'$	–
1	1	1	1	1	[4]	$(35, 5^*)$	1	1	1	–	–
4	1	1	2	2	[6]	$(30, 6^*)$	–	2	–	1	1
10	1	2	2	3	[8]	$(24, 8^*)$	2	–	–	–	–
13	1	2	3	4	[10]	$(23, 11^*)$	–	–	2	–	2
16	1	2	4	5	[12]	$(24, 12^*)$	–	–	–	2	3
44	2	3	3	4	[12]	$(15, 9^*)$	3	–	–	3	–
45	2	3	4	5	[14]	$(13, 16^*)$	–	–	3	–	4
66	3	4	5	6	[18]	$(10, 17^*)$	–	–	4	4	–

7. THE DUAL $K3$ ALGEBRA FROM FOUR-DIMENSIONAL EXTENDED VECTORS

As discussed in the Introduction, the enumeration of $K3$ reflexive polyhedra obtained at level zero from pairs of projective vectors (Section 5) and triples (Section 6) is not quite complete. The one remaining example, corresponding to $\mathbf{k}_4 = (7, 8, 9, 12)$, can be found using the intersection–projection and duality properties outlined in Section 3, as we now discuss. This method can be used to build projective-vector chains using the rich projective structure of $K3$ vectors. For example, one can construct a chain with, as youngest vector, $\mathbf{k}_4 = (7, 8, 10, 25)$, which is dual to the eldest vector $\mathbf{k}_4 = (1, 1, 1, 3)$ contained in the triple chain III_3. Similarly, one can consider other cases, e.g., building a chain with youngest vector $\mathbf{k}_4 = (5, 6, 8, 11)$, contained in the triple chain II_3.

7.1. The Dual π Projective-Vector Structure of $K3$ Hypersurfaces. We obtained in Section 6, as an interesting application of the $K3$ algebra, all the $1 + (4 \times 2) + 22$ invariant monomials of the 22 double-intersection $K3$ chains via the triple intersections of $K3$ extended vectors. These invariant monomials correspond to particular directions relative to the reflexive polyhedra, which can be used to find the projection structures of the vectors. In particular, they can be used to find all the projective vectors which have no planar-intersection structure at all. Because of duality, their polyhedra have sufficient invariant directions that the projections on the corresponding perpendicular planes give reflexive planar polyhedra. Examples include the youngest vectors which are dual to the eldest

vectors as well as other relations in the corresponding chain, e.g., as we shall see, the remaining $K3$ vector (7,8,9,12) is dual to (1,1,1,1), (7,8,10,25) is dual to (1,1,1,3), etc.

To understand this more deeply, we consider triple chains built using a special subalgebra of the four-dimensional extended vectors: $\mathbf{k}_3^{ex(i)} = (0,0,0,1)$, $(0,0,1,1)$, $(0,1,1,1)$, $(0,1,1,2)$, and $(0,1,2,3)$, with all possible permutations. We consider triples $\mathbf{k}_3^{ex(i,j,l)}$ of these vectors with the property that each pair $(i,j),(j,l),(l,i)$ gives a reflexive planar polyhedron:

$$[\mathbf{k}_3^{ex(i)}] \bigcap [\mathbf{k}_3^{ex(j)}] = [\mathbf{k}_3]. \tag{7.1}$$

We note that the triple intersections of these triples of extended vectors always define an invariant direction, $\boldsymbol{\pi}$. In some cases, the triple intersection contains just two monomial vectors, and $\boldsymbol{\pi}$ is simply defined by their difference:

$$[\mathbf{k}_3^{ex(i)}] \bigcap [\mathbf{k}_3^{ex(j)}] \bigcap [\mathbf{k}_3^{ex(r)}] \Rightarrow \boldsymbol{\pi}_N = \{\boldsymbol{\mu} - \boldsymbol{\mu}_0\}, \tag{7.2}$$

where $\boldsymbol{\mu}_0 = (1,1,1,1)$ is the basic monomial $z^{\boldsymbol{\mu}_0+\mathbf{1}} = x \cdot y \cdot z \cdot u$. These cases are listed in Table 10.

These pairs of invariant monomials correspond to directions $\boldsymbol{\pi}_i = \boldsymbol{\mu}_i - \boldsymbol{\mu}_0$ in the exponent/monomial hyperspace given by the following vectors $\boldsymbol{\mu}_N$,

Table 10. Triples of $\mathrm{k}_3{}^{ex}$ vectors giving invariant directions $\boldsymbol{\pi}_N = \boldsymbol{\mu}_N - \boldsymbol{\mu}_0$ defined by pairs of monomials. Also indicated are the sizes of the corresponding polyhedra Δ and the two-vector chains to which they belong

$\boldsymbol{\pi}_N^{(\alpha)}$	$\mathbf{k}_3^{ex(i)}$	$\mathbf{k}_3^{ex(j)}$	$\mathbf{k}_3^{ex(p)}$	$\Delta_{J_{ij}}$	$\Delta_{J_{jp}}$	$\Delta_{J_{pi}}$	inv. monom	$\boldsymbol{\mu}_N$
$\boldsymbol{\pi}_1^{(1)}$	$(0,0,1,1)$	$(1,2,0,1)$	$(1,2,1,0)$	7_{XXII}	9_{VI}	7_{XXII}	$x^3 \cdot z \cdot u$	$(3,0,1,1)$
$\boldsymbol{\pi}_1^{(2)}$	$(0,0,1,1)$	$(1,2,0,3)$	$(1,2,3,0)$	7_{XVI}	7_{XXI}	7_{XVI}	$x^3 \cdot z \cdot u$	$(3,0,1,1)$
$\boldsymbol{\pi}_2^{(1)}$	$(0,1,1,1)$	$(1,0,1,1)$	$(1,1,0,1)$	10_{II}	10_{II}	10_{II}	u^3	$(0,0,0,3)$
$\boldsymbol{\pi}_2^{(2)}$	$(0,1,1,1)$	$(1,0,1,1)$	$(1,3,0,2)$	10_{II}	4_{III}	7_{XVII}	u^3	$(0,0,0,3)$
$\boldsymbol{\pi}_2^{(3)}$	$(0,1,1,1)$	$(1,0,3,2)$	$(1,3,0,2)$	7_{XVII}	7_{XXI}	7_{XVII}	u^3	$(0,0,0,3)$
$\boldsymbol{\pi}_2^{(4)}$	$(0,1,1,1)$	$(3,0,1,2)$	$(3,1,0,2)$	4_{III}	7_{XIX}	4_{III}	u^3	$(0,0,0,3)$
$\boldsymbol{\pi}_3^{(1)}$	$(1,1,1,0)$	$(0,1,2,1)$	$(2,1,0,1)$	8_{XIII}	9_{VII}	8_{XIII}	$y^3 \cdot u$	$(0,3,0,1)$
$\boldsymbol{\pi}_3^{(2)}$	$(1,1,1,0)$	$(0,1,2,1)$	$(2,1,0,3)$	8_{XIII}	6_{XIV}	4_{III}	$y^3 \cdot u$	$(0,3,0,1)$
$\boldsymbol{\pi}_3^{(3)}$	$(1,1,1,0)$	$(0,1,2,3)$	$(2,1,0,3)$	4_{III}	7_{XX}	4_{III}	$y^3 \cdot u$	$(0,3,0,1)$
$\boldsymbol{\pi}_3^{(4)}$	$(0,1,2,1)$	$(1,2,3,0)$	$(2,1,0,3)$	7_{XVIII}	5_{XII}	6_{XIV}	$y^3 \cdot u$	$(0,3,0,1)$
$\boldsymbol{\pi}_4^{(1)}$	$(0,1,1,2)$	$(1,0,1,2)$	$(1,2,1,0)$	9_{VI}	9_{VII}	5_{VIII}	y^4	$(0,0,4,0)$
$\boldsymbol{\pi}_4^{(2)}$	$(0,1,1,2)$	$(1,2,1,0)$	$(2,0,1,1)$	5_{VIII}	5_{VIII}	5_{VIII}	y^4	$(0,0,4,0)$
$\boldsymbol{\pi}_5^{(1)}$	$(1,0,1,2,)$	$(1,2,0,3)$	$(1,2,3,0)$	5_{IX}	7_{XXI}	6_{XIV}	$x^4 \cdot y$	$(4,1,0,0)$

$N = 1, 2, 3, 4, 5$:

$$\begin{aligned} \boldsymbol{\mu}_1 &= (3,0,1,1), \\ \boldsymbol{\mu}_2 &= (0,0,0,3), \\ \boldsymbol{\mu}_3 &= (0,3,0,1), \\ \boldsymbol{\mu}_4 &= (0,0,4,0), \\ \boldsymbol{\mu}_5 &= (4,1,0,0), \end{aligned} \tag{7.3}$$

as can be seen in Table 10.

In other cases, the triple intersections contain three points which form a degenerate linear polyhedron, which also defines a unique direction $\boldsymbol{\pi}$ determined by three points, one of which $(\boldsymbol{\mu}_0)$ corresponds to the origin:

$$[\mathbf{k}_3^{ex(i)}] \bigcap [\mathbf{k}_3^{ex(j)}] \bigcap [\mathbf{k}_3^{ex(r)}] \Rightarrow \boldsymbol{\pi}_N = \{\boldsymbol{\mu}_+ - \boldsymbol{\mu}_0\} = \{\boldsymbol{\mu}_0 - \boldsymbol{\mu}_-\}, \tag{7.4}$$

as seen in Table 11.

It is easy to see that five of the invariant monomials from Table 10 produce a reflexive three-dimensional polyhedron. For example, from $\boldsymbol{\mu}_2$, $\boldsymbol{\mu}_3$, $\boldsymbol{\mu}_4$, and $\boldsymbol{\mu}_5$ one obtains the following exceptional vector whose associated polyhedron has no intersection substructure:

$$\begin{aligned} \boldsymbol{\mu}_\alpha \cdot \mathbf{k}_4 &= d = k_1 + k_2 + k_3 + k_4, \quad \alpha = 0, 2, 3, 4, 5, \\ \mathbf{k}_4 &= (7, 8, 9, 12)[d = 36], \end{aligned} \tag{7.5}$$

Table 11. Triples of $\mathbf{k}_3^{ex}$ vectors defining directions $\boldsymbol{\pi}_N$ determined by three invariant monomials

$\boldsymbol{\pi}_N^{(\alpha)}$	$\mathbf{k}_3^{ex(i)}$	$\mathbf{k}_3^{ex(j)}$	$\mathbf{k}_3^{ex(p)}$	$\Delta_{J_{ij}}$	$\Delta_{J_{jp}}$	$\Delta_{J_{pi}}$	$\boldsymbol{\mu}_+$	$\boldsymbol{\mu}_-$
$\boldsymbol{\pi}_6^{(1)}$	$(0,0,1,1)$	$(1,1,0,1)$	$(1,1,1,0)$	9_{XI}	10_{II}	9_{XI}	$(0,2,1,1)$	$(2,0,1,1)$
$\boldsymbol{\pi}_6^{(2)}$	$(0,0,1,1)$	$(1,1,0,2)$	$(1,1,2,0)$	9_{V}	9_{VII}	9_{V}	$(0,2,1,1)$	$(2,0,1,1)$
$\boldsymbol{\pi}_7^{(1)}$	$(0,1,1,1)$	$(1,0,1,1)$	$(1,1,0,2)$	10_{II}	8_{XIII}	8_{XIII}	$(0,0,1,2)$	$(2,2,1,0)$
$\boldsymbol{\pi}_7^{(2)}$	$(0,1,1,1)$	$(1,0,2,1)$	$(1,1,0,2)$	8_{XIII}	5_{VIII}	8_{XIII}	$(0,0,1,2)$	$(2,2,1,0)$
$\boldsymbol{\pi}_7^{(3)}$	$(0,1,1,1)$	$(1,0,2,1)$	$(1,2,0,3)$	8_{XIII}	6_{XIV}	7_{XVII}	$(0,0,1,2)$	$(2,2,1,0)$
$\boldsymbol{\pi}_7^{(4)}$	$(0,1,2,1)$	$(1,0,2,1)$	$(1,1,0,2)$	9_{VI}	5_{VIII}	5_{VIII}	$(0,0,1,2)$	$(2,2,1,0)$
$\boldsymbol{\pi}_8^{(1)}$	$(0,1,1,2)$	$(1,0,1,2)$	$(1,1,0,2)$	9_{VI}	9_{VI}	9_{VI}	$(0,0,0,2)$	$(2,2,2,0)$
$\boldsymbol{\pi}_8^{(2)}$	$(0,1,1,2)$	$(1,0,1,2)$	$(1,2,0,3)$	9_{VI}	5_{IX}	7_{XVIII}	$(0,0,0,2)$	$(2,2,2,0)$
$\boldsymbol{\pi}_8^{(3)}$	$(0,1,1,2)$	$(1,0,2,3)$	$(1,2,0,3)$	7_{XVIII}	7_{XX}	7_{XVIII}	$(0,0,0,2)$	$(2,2,2,0)$
$\boldsymbol{\pi}_8^{(4)}$	$(0,1,1,2)$	$(2,0,1,3)$	$(2,1,0,3)$	5_{IX}	7_{XIX}	5_{IX}	$(0,0,0,2)$	$(2,2,2,0)$

where we used the constraint

$$\boldsymbol{\mu}_0 = \frac{1}{4} \cdot (\boldsymbol{\mu}_2 + \boldsymbol{\mu}_3 + \boldsymbol{\mu}_4 + \boldsymbol{\mu}_5). \tag{7.6}$$

Thus duality enables us to identify the missing 95th $K3$ vector, which was not generated previously in our systematic study of the two- and three-vector chains. We recall that they contain totals of 90 and 91 vectors, respectively, of which only 94 were distinct.

Similarly, using these invariant monomials, one can find the rest of the exceptional $\mathbf{k}_4$ vectors, $(3,5,6,7)$, $(3,6,7,8)$, $(5,6,7,9)$ which were not included in the triple chains, together with $(3,4,5,6)$. They have intersection polyhedra that are not linear. These other exceptional $\mathbf{k}_4$ vectors are defined as follows

$$\begin{aligned} \boldsymbol{\mu}_\alpha \cdot \mathbf{k}_4 &= d, \quad \alpha = 0,1,2,3,3', \\ \mathbf{k}_4 &= (3,5,6,7)[d=21], \end{aligned} \tag{7.7}$$

where again the following constraint has been used

$$\begin{aligned} &\boldsymbol{\mu}_0 = \frac{1}{4} \cdot (\boldsymbol{\mu}_1 + \boldsymbol{\mu}_2 + \boldsymbol{\mu}_3 + \boldsymbol{\mu}_3') = \\ &= (3,1,0,1) + (0,0,0,3) + (1,0,3,0) + (0,3,1,0), \end{aligned}$$

and

$$\begin{aligned} \boldsymbol{\mu}_\alpha \cdot \mathbf{k}_4 &= d, \quad \alpha = 0,1,2,3,4, \\ \mathbf{k}_4 &= (3,6,7,8)[d=24], \end{aligned} \tag{7.8}$$

with the constraint:

$$\begin{aligned} &\boldsymbol{\mu}_0 = \frac{1}{4} \cdot (\boldsymbol{\mu}_1 + \boldsymbol{\mu}_2 + \boldsymbol{\mu}_3 + \boldsymbol{\mu}_4) = \\ &= (3,0,1,1) + (0,0,0,3) + (1,0,3,0) + (0,4,0,0). \end{aligned}$$

We also find

$$\begin{aligned} \boldsymbol{\mu}_\alpha \cdot \mathbf{k}_4 &= d, \quad \alpha = 2,3,3',5, \\ \mathbf{k}_4 &= (5,6,7,9)[d=27], \end{aligned} \tag{7.9}$$

where the following constraint also has been used

$$\begin{aligned} &\boldsymbol{\mu}_0 = \frac{1}{4} \cdot (\boldsymbol{\mu}_2 + \boldsymbol{\mu}_3 + \boldsymbol{\mu}_3' + \boldsymbol{\mu}_5) = \\ &= (0,0,0,3) + (0,3,0,1) + (0,1,3,0) + (4,0,1,0), \end{aligned}$$

and

$$\begin{aligned} \boldsymbol{\mu}_\alpha \cdot \mathbf{k}_4 &= d, \quad \alpha = 1, 2, 3, 3', \\ \mathbf{k}_4 &= (3, 4, 5, 6)[d = 18], \end{aligned} \tag{7.10}$$

where the following constraint also has been used

$$\begin{aligned} &\boldsymbol{\mu}_0 = \frac{1}{4} \cdot (\boldsymbol{\mu}_1 + \boldsymbol{\mu}_2 + \boldsymbol{\mu}_3 + \boldsymbol{\mu}_3') = \\ &= (3, 1, 1, 0) + (0, 0, 0, 3) + (1, 0, 3, 0) + (0, 3, 0, 1). \end{aligned}$$

7.2. Projective Chains of $K3$ Spaces Constructed from $\boldsymbol{\pi}_N$ Vectors. Using the invariant directions found in the previous Subsection, one can construct new triple chains:

$$p \cdot [\mathbf{k}_4]_{\boldsymbol{\pi}_N} = m \cdot \mathbf{k}^{ex(i)} + n \cdot \mathbf{k}^{ex(j)} + r \cdot \mathbf{k}^{ex(l)} \tag{7.11}$$

each corresponding to a direction $\boldsymbol{\pi}$ determined by an intersection of invariant monomial pairs. Each good projective vector in such a chain, determined by an invariant direction, contains the monomial/projective direction in its polyhedron. With respect to this direction, the polyhedron is projected onto a «good» planar reflexive polyhedron. If the projective vector appears in several different chains, its polyhedron will have «good» projections corresponding to each of these chains. This property can be used to make a classification by their projections of the projective vectors and their reflexive polyhedra. One finds that 78 projective $K3$ vectors out of 95 have such projective property. Taking into account the rest of the vectors which already were known from double-intersection $J = \Pi$-symmetric chains, one can recover all 95 projective $K3$ vectors.

The distribution of the 3-dimensional set of positive-integer numbers m, n, r depends on the dimension of the three extended vectors $d^{(i)} = \sum_\alpha \{\mathbf{k}_3^{ex(i)}\}_\alpha$, $i = 1, 2, 3$, participating in the construction of the chain, can have some «blank spots», corresponding to «false vectors» which do not correspond to any reflexive polyhedron. The origin of this phenomenon is connected with the structure of Calabi–Yau algebra, i.e., some of the projective vectors have different expansions (double-, triple-,...) in terms of the extended vectors. So, for example, if a vector is *forbidden* in two-vector expansions, it should also be forbidden in triple-, etc., expansions, which is what we call a false vector. The self-consistency of the algebra entails the absences of some combinations of integer numbers m, n, r, even though all of them are below their maximum values. We already have met and discussed this phenomenon in the classification of triple-vector chains.

Table 12. Extended vectors $\mathbf{k_4}$ in the chain $\boldsymbol{\pi}_2^{(1)}$ with $\Pi = 4$ with: $Q \cdot \mathbf{k} = (N+ +L, M+L, M+N, M+N+L) = M \cdot (0,1,1,1) + N \cdot (1,0,1,1) + L \cdot (1,1,0,1)$ **and** $d = 3M + 3N + 3L$**, whose youngest vector is** $\mathbf{k}_{\rm young} = (7,8,9,12)$

$\aleph$	$\mathbf{k}_4$	[det]	M	N	L	(Δ, Δ^*)	$\Pi - J^*$	Chain
95	$(7,8,9,12)$	[36]	5	4	3	$(5,35)$	$4-10$	$-$
89	$(5,6,7,9)$	[27]	4	3	2	$(6,30)$	$4-10$	III
80	$(3,6,7,8)$	[24]	5	2	1	$(9,21)$	$4-10$	III
76	$(3,5,6,7)$	[21]	4	2	1	$(9,21)$	$4-10$	III
66	$(3,4,5,6)$	[18]	3	2	1	$(10,17)$	$4-10$	III
65	$(3,3,4,5)$	[15]	2	2	1	$(12,12)$	$4-10$	III
44	$(2,3,3,4)$	[24]	2	1	1	$(7,26)$	$4-10$	III

As seen in Table 10, one can give examples of triple intersections giving just one good vector which has three different projections with $\Pi = 4$:

$$\begin{aligned}
[\mathbf{k}_4]_{\boldsymbol{\pi}_1^{(2)}} \bigcap [\mathbf{k}_4]_{\boldsymbol{\pi}_2^{(2)}} \bigcap [\mathbf{k}_4]_{\boldsymbol{\pi}_3^{(4)}} \quad &\Rightarrow \quad (3,5,6,7)[21], \\
[\mathbf{k}_4]_{\boldsymbol{\pi}_1^{(2)}} \bigcap [\mathbf{k}_4]_{\boldsymbol{\pi}_2^{(2)}} \bigcap [\mathbf{k}_4]_{\boldsymbol{\pi}_4^{(2)}} \quad &\Rightarrow \quad (3,6,7,8)[24], \\
[\mathbf{k}_4]_{\boldsymbol{\pi}_2^{(2)}} \bigcap [\mathbf{k}_4]_{\boldsymbol{\pi}_3^{(3)}} \bigcap [\mathbf{k}_4]_{\boldsymbol{\pi}_3^{(1)}} \quad &\Rightarrow \quad (5,6,7,9)[27]. \qquad (7.12)
\end{aligned}$$

Moreover, the exceptional vector, which has four different projections with $\Pi = 4$, is given by the intersection of four such chains, i.e.:

$$[\mathbf{k}_4]_{\boldsymbol{\pi}_2^{(1)}} \bigcap [\mathbf{k}_4]_{\boldsymbol{\pi}_3^{(2)}} \bigcap [\mathbf{k}_4]_{\boldsymbol{\pi}_4^{(2)}} \bigcap [\mathbf{k}_4]_{\boldsymbol{\pi}_5^{(1)}} \quad \Rightarrow \quad (7,8,9,12)[36]. \quad (7.13)$$

To understand this in more detail, we consider one chain with projection $\Pi = 4$, which is determined by the invariant direction $\boldsymbol{\pi}_2^{(1)}$. The vectors of this chain are represented as linear combinations with positive-integer coefficients, M, N, L, of the following three projective vectors, taken from the third line in Table 10:

$$\begin{aligned}
\mathbf{k}_4(\boldsymbol{\pi}_2^{(1)}) \quad &= \quad M \cdot (0,1,1,1) + N \cdot (1,0,1,1) + L \cdot (1,1,0,1) = \\
&= \quad (\,N + L,\, M + L,\, M + N,\, M + N + L\,). \qquad (7.14)
\end{aligned}$$

The basis is constructed out of the exceptional invariant monomials determining the $\boldsymbol{\pi}$ directions. Projecting on the perpendicular plane gives us planar reflexive polyhedra, so the third basis vector

$$\mathbf{e}_3 = (-1,-1,-1,2) \;\Rightarrow\; (0,0,0,3). \qquad (7.15)$$

is common to all the chains discussed in this Subsection.

Table 13. The $K3$ hypersurfaces in chain III with intersection $J = 4$: $\mathbf{k}(III) = (3n, m, m+n, m+2n) = m \cdot (0,1,1,1) + n \cdot (3,0,1,2)$, $d = 3m + 6n$ with level $l = m + n$, $m_{\max} = 6, n_{\max} = 2$

ℵ	$\mathbf{k}_i$[dim]	$\Delta(J=4)$	$\Delta^*(\Pi = 10)$	(Π, J^*)
12	$(3,1,2,3)[9]$	$23 = 4_L + 4_J + 15_R$	$8^* = 3^*_L + 4^*_J + 1^*_R$	$(10, 4^*)$
44	$(3,2,3,4)[12]$	$15 = 7_L + 4_J + 4_R$	$9^* = 4^*_L + 3^*_C + 2^*_R$	$(9, 5^*); (7, 7^*)$
25	$(6,1,3,5)[15]$	$21 = 16_L + 4_J + 1_R$	$15^* = 7^*_L + 7^*_J + 1^*_R$	$(7, 7^*)$
65	$(3,3,4,5)[15]$	$12 = 4_L + 4_J + 4_R$	$12^* = 1^*_L + 10^*_J + 1^*_R$	$(4, 10)$
66	$(3,4,5,6)[18]$	$10 = 2_L + 4_J + 4_R$	$17^* = 8^*_L + 3^*_C + 6^*_R$	$(7, 7)$
76	$(3,5,6,7)[21]$	$9 = 1_L + 4_J + 4_R$	$21^* = 11^*_L + 3^*_C + 7^*_R$	$(4, 10)$
80	$(3,6,7,8)[24]$	$9 = 1_L + 4_J + 4_R$	$21^* = 12^*_L + 3^*_C + 6^*_R$	$(4, 10)$
89	$(6,5,7,9)[27]$	$6 = 1_L + 4_J + 1_R$	$30^* = 17^*_L + 3^*_C + 10^*_R$	$(4, 10)$

Looking at the distribution of allowed integers, M, N, L, we see «blank spots» such as $M = N = L = 1$, corresponding to the «false vector» $(2,2,2,3)$, which is forbidden by the double-vector classification: it would require $m = 2$ in the chain $(2,2,2,3) = m \cdot (1,1,1,0) + n \cdot (0,0,0,1)$, but actually $m_{\max} = 1$ for this chain. Also, all the polyhedra corresponding to these projective vectors have the other invariant directions $\boldsymbol{\pi}^{(2)}_3 \to (1,0,3,0)$ with $\Pi = 4$ and should produce the following triple-vector expansion chain:

$$\begin{aligned} \mathbf{k}_4(\boldsymbol{\pi}^{(2)}_3) &= M \cdot (0,1,1,1) + N \cdot (1,0,1,2) + L \cdot (3,2,1,0) = \\ &= (\,N + 3L,\, M + 2\,L,\, M + N + L,\, M + 2\,N\,). \end{aligned} \tag{7.16}$$

Projecting on the perpendicular plane to the vector

$$\boldsymbol{e}_3 = (0,-1,2,-1) \;\Rightarrow\; (1,0,3,0) \tag{7.17}$$

gives us planar reflexive polyhedron with 4 points. This chain is a little longer and contains other projective vectors. Similarly, one can find using the other projective directions, $\boldsymbol{\pi}^{(\alpha)}_4$ and $\boldsymbol{\pi}^{(1)}_5$, two new triple expansion chains. Together these four invariant directions, $\boldsymbol{\pi}^{(\alpha)}_i$, $i = 2,3,4,5$, with the constructions of the corresponding triple projective chains contain 40 projective vectors (see Table 1).

One can compare the projection set, $\boldsymbol{\pi}^{(1)}_2$ and $\Pi = 4$, with the double-vector-intersection chain with $J = 4$. It is interesting to note that six vectors from the projective chain shown in Table 12 also appear in the III-intersection chain with $J = 4$ shown in Table 13. Conversely, the chain shown in this latter Table has just two vectors: $(3,1,2,3), (1,3,5,6)$ that are not contained in Table 12. The intersection structure of the III chain shown in Table 13 is obtained from the

following two vectors:

$$\begin{aligned}\mathbf{k}_4(III) &= m\cdot(0,1,1,1)+n\cdot(3,0,1,2)= \\ &= (\,3n,\, m,\; m+n,\, m+2n\,), \\ &\quad 1\leqslant m\leqslant 6,\quad 1\leqslant n\leqslant 2.\end{aligned} \tag{7.18}$$

The corresponding four invariant monomials are

$$\begin{aligned}\boldsymbol{\mu}_0^1 &= (0,0,0,3)\Rightarrow u^3, \\ \boldsymbol{\mu}_0^2 &= (1,0,3,0)\Rightarrow x\cdot z^3, \\ \boldsymbol{\mu}_0^3 &= (2,3,0,0)\Rightarrow x^2\cdot y^3, \\ \boldsymbol{\mu}_0^4 &= (1,1,1,1)\Rightarrow x\cdot y\cdot z\cdot u,\end{aligned} \tag{7.19}$$

and the corresponding basis can be chosen in the form

$$\begin{aligned}\mathbf{e}_1 &= (0,-m-n,m,0), \\ \mathbf{e}_2 &= (0,-1,2,-1), \\ \mathbf{e}_3 &= (-1,-1,-1,2).\end{aligned} \tag{7.20}$$

The canonical expression for the determinant of this lattice is

$$\det(\mathbf{e}_1,\mathbf{e}_2,\mathbf{e}_3,\mathbf{e}_0)=3\cdot m+6\cdot n=d, \tag{7.21}$$

where $\mathbf{e}_0\equiv(1,1,1,1)$.

7.3. Example of a $J,\Pi=10$ Double-Intersection Chain. To see another aspect of mirror symmetry and duality, consider the II chain with intersection $J(\Delta)=\Pi(\Delta)=10$ and $J(\Delta^*)=\Pi(\Delta^*)=4$ shown in Table 14. The decomposition of this chain is in terms of the following two vectors:

$$\begin{aligned}\mathbf{k_4} &= m\cdot(0,1,1,1)+n\cdot(1,0,1,1)= \\ &= (\,n,\, m,\; m+n,\, m+n\,), \\ &\quad 1\leqslant m\leqslant 3,\quad 1\leqslant n\leqslant 3.\end{aligned} \tag{7.22}$$

The basis of the lattice in which the polyhedral intersection with the set of positive-integer points corresponds to Table 14 is the following:

$$\begin{aligned}\mathbf{e}_1 &= (-m,n,0,0), \\ \mathbf{e}_2 &= (-1,-1,1,0), \\ \mathbf{e}_3 &= (-1,-1,0,1),\end{aligned} \tag{7.23}$$

and the corresponding determinant is

$$\det(\mathbf{e}_1,\mathbf{e}_2,\mathbf{e}_3,\mathbf{e}_0)=3\cdot m+3\cdot n=d, \tag{7.24}$$

Table 14. The $K3$ hypersurfaces in chain II with intersection $J = 10$: $\mathbf{k}(II) = = (n, m, m+n, m+n) = m \cdot (0,1,1,1) + n \cdot (1,0,1,1)$ with $d = 3m + 3n$, $q = 1$, $m_{\max} = 3, n_{\max} = 3$

ℵ	$\mathbf{k}_i$[dim]	$\Delta(J = 10)$	$\Delta^*(\Pi = 4)$	(Π, J^*)
4	$(1,1,2,2)[6]$	$30 = 10_L + 10_J + 10_R$	$6^* = 1^*_L + 4^*_J + 1^*_R$	$(10, 4^*)$
12	$(1,2,3,3)[9]$	$23 = 10_L + 10_J + 3_R$	$8^* = 3^*_L + 4^*_J + 1^*_R$	$(10, 4^*)$
21	$(1,3,4,4)[12]$	$21 = 10_L + 10_J + 1_R$	$9^* = 4^*_L + 4^*_J + 1^*_R$	$(10, 4^*)$
48	$(2,3,5,5)[15]$	$14 = 3_L + 10_J + 1_R$	$11^* = 4^*_L + 4^*_J + 3^*_R$	$(10, 4^*)$

where $\mathbf{e}_0 = (1,1,1,1)$ again. The ten corresponding invariant monomials are:

$$\begin{aligned}
\boldsymbol{\mu}_0^1 &= (3,3,0,0) \Rightarrow x^3 \cdot y^3,\\
\boldsymbol{\mu}_0^2 &= (2,2,1,0) \Rightarrow x^2 \cdot y^2 \cdot z,\\
\boldsymbol{\mu}_0^3 &= (1,1,2,0) \Rightarrow x \cdot y \cdot z^2,\\
\boldsymbol{\mu}_0^4 &= (0,0,3,0) \Rightarrow z^3,\\
\boldsymbol{\mu}_0^5 &= (2,2,0,1) \Rightarrow x^2 \cdot y^2 \cdot u,\\
\boldsymbol{\mu}_0^6 &= (1,1,1,1) \Rightarrow x \cdot y \cdot z \cdot u,\\
\boldsymbol{\mu}_0^7 &= (0,0,2,1) \Rightarrow z^2 \cdot u,\\
\boldsymbol{\mu}_0^8 &= (1,1,0,2) \Rightarrow x \cdot y \cdot u^2,\\
\boldsymbol{\mu}_0^9 &= (0,0,1,2) \Rightarrow z \cdot u^2,\\
\boldsymbol{\mu}_0^{10} &= (0,0,0,3) \Rightarrow u^3.
\end{aligned} \tag{7.25}$$

For the vector $\mathbf{k}_4 = (1,1,2,2)$, one can consider the basis

$$\begin{aligned}
\mathbf{e}_1 &= (-3,3,0,0),\\
\mathbf{e}_2 &= (-1,-1,1,0),\\
\mathbf{e}_3 &= (-1,-1,0,1)
\end{aligned} \tag{7.26}$$

with determinant 18, in which the dual pair of polyhedra:

$$\begin{aligned}
1_L \,+\, 10_J \,+\, 1_R &= 12,\\
4^*_L \,+\, 4^*_J \,+\, 4^*_R &= 12^*
\end{aligned} \tag{7.27}$$

both contain 12 points and 12 mirror points, respectively.

7.4. Example of a Chain with $\Pi = 5$ and Eldest Vector $\mathbf{k}_4 = (7,8,10,25)$. Now we present in Table 15 a projective chain with $\Pi = 5$, constructed from the invariant direction $\boldsymbol{\pi}_8^{(1)}$ with the invariant monomials $(0,0,0,2) + (2,2,2,0)$.

The 14 projective vectors of this chain are represented as linear combinations with positive-integer coefficients, M, N, L, Q, $Q = 2, 1$, of the following three vectors:

$$\begin{aligned} Q \cdot \mathbf{k}_4(\boldsymbol{\pi}_8^{(1)}) &= M \cdot (0,1,1,2) + N \cdot (1,0,1,2) + L \cdot (1,1,0,2) = \\ &= (N + L,\, M + L,\, M + N,\, 2 \cdot M + 2 \cdot N + 2 \cdot L). \end{aligned} \tag{7.28}$$

Projecting on the perpendicular plane gives us planar reflexive polyhedra, so the third basis vector

$$\mathbf{e}_3 = (-1,-1,-1,1) \;\Rightarrow\; (0,0,0,2) \tag{7.29}$$

is common to all the chain discussed in this Subsection.

There can be constructed additional three chains, $\boldsymbol{\pi}_8^{(2,3,4)}$, with the same invariant direction, (0,0,0,2), (2,2,2,0), and the same youngest vector, but with the different triple intersections and therefore with the different projective chains. Together one can find inside all of four projective chains, $\boldsymbol{\pi}_8^{(\alpha)}$, $\alpha = 1, 2, 3, 4$, a total of 33 projective vectors (see Table 1).

Table 15. The $K3$ hypersurfaces in the $\boldsymbol{\pi}_8^{(1)}$ chain with projection $\Pi = 5$ related to the IX with $J = 5$: $Q \cdot \mathbf{k} = (N + L,\ M + L,\ M + N,\ 2M + 2N + 2L) = M \cdot (0,1,1,2) + N \cdot (1,0,1,2) + L \cdot (1,1,0,2)$ with $d = 4M + 4N + 4L$, $\mathbf{k}_{\rm eld} = (1,1,1,3)$ $\mathbf{k}_{\rm young} = (7,8,10,25)$, $Q = 2$ or 1

ℵ	$\mathbf{k}_4$	[det]	M	N	L	Q	(Δ, Δ^*)	$\Pi - J^*$	chain
94	$(7,8,10,25)$	[50]	11	9	5	2	$(6, 39^*)$	$5-9$	–
93	$(8,7,5,20)$	[40]	2	3	5	1	$(8, 28^*)$	$5-9$	–
91	$(5,6,8,19)$	[38]	9	7	3	2	$(7, 35^*)$	$5-9$	IX
88	$(7,6,4,17)$	[34]	9	5	3	2	$(8, 31^*)$	$5-9$	IX
84	$(4,5,7,16)$	[32]	4	3	1	1	$(9, 27^*)$	$5-9$	IX
82	$(4,5,6,15)$	[30]	7	5	3	2	$(10, 20^*)$	$5-9$	IX
69	$(3,4,5,12)$	[48]	3	2	1	1	$(7, 35^*)$	$5-9$	IX
64	$(2,6,7,15)$	[30]	6	3	1	2	$(13, 23^*)$	$5-9$	IX
60	$(2,5,6,13)$	[26]	9	3	1	2	$(13, 23^*)$	$5-9$	IX
58	$(2,4,5,11)$	[22]	7	3	1	2	$(14, 19^*)$	$5-9$	IX
47	$(2,3,4,9)$	[36]	5	3	1	2	$(9, 27^*)$	$5-9$	IX
43	$(2,2,3,7)$	[14]	3	3	1	2	$(19, 11^*)$	$5-9$	IX
11	$(1,2,2,5)$	[20]	3	1	1	2	$(15, 15^*)$	$5-9$	IX
3	$(1,1,1,3)$	[12]	1	1	1	2	$(39, 6^*)$	$5-9$	IX

It is interesting to note that the chain $\boldsymbol{\pi}_8^{(1)}$ has 11 $\mathbf{k}_4$ vectors with $\Pi = 5$ in common with the IX_J chain where $J = 5$, whose structure is obtained from the following two vectors:

$$\begin{aligned} \mathbf{k}_4(IX) &= m \cdot (0,1,1,2) + n \cdot (2,1,0,3) = \\ &= (\,2n,\, m\,+\,n,\, m,\, 2m\,+\,3n\,), \\ &\quad 1 \leqslant m \leqslant 6, \quad 1 \leqslant n \leqslant 4. \end{aligned} \tag{7.30}$$

The chain IX of $\mathbf{k}_4$ projective vectors with the structure $5_{J=\triangle} \leftrightarrow 9_{\Pi=\triangle}$ is presented in Table 16. The lattice determinant and the basis are given by the following expressions:

$$\begin{aligned} \mathbf{e}_1 &= (0, -m, m+n, 0), \\ \mathbf{e}_2 &= (-1, 2, -2, 0), \\ \mathbf{e}_3 &= (-1, -1, -1, 1), \end{aligned} \tag{7.31}$$

and

$$\det(\mathbf{e}_1, \mathbf{e}_2, \mathbf{e}_3, \mathbf{e}_0) = 4 \cdot m \,+\, 6 \cdot n = d, \tag{7.32}$$

where $\mathbf{e}_0 = (1,1,1,1)$.

The possible values of m and n for this chain are also determined by the dimensions of the extended vectors, $d(\mathbf{k}^{ex(i)}) = 6$ and $d(\mathbf{k}^{ex(j)}) = 4$, with the

Table 16. The $K3$ **hypersurfaces in the chain** IX**:** $\mathbf{k}=(2n, m+n, m, 2m+3n)= = m \cdot (0,1,1,2) + n \cdot (2,1,0,3)$ **with** $d = 4m + 6n$**,** $m_{\max} = 6, n_{\max} = 3$ **and** $\mathbf{k}_{\text{eld}} = (1,2,2,5)[10]$

N	$\mathbf{k}$[dim]	$\Delta(J = \underline{5})$	$\Delta^*(\Pi = 9)$	$(\Delta_J, \Delta^*{}_\Pi)$
11	$(2,2,1,5)[10]$	$28 = 7_L + 5_J + 16_R$	$8^* = 3^*_L + 4^*_C + 1^*_R$	$(10')$
43	$(2,3,2,7)[14]$	$19 = 7_L + 5_J + 7_R$	$11^* = 1_L + 9_J + 1_R$	$(5_\Pi, 9_J)$
24	$(4,3,1,8)[16]$	$24 = 3_L + 5_J + 16_R$	$12^* = 1_L + 5_J + 6_R$	$(5_\Pi, 9_J)$
33	$(6,4,1,11)[22]$	$22 = 1_L + 5_J + 16_R$	$20^* = 1_L + 5_J + 14_R$	$(7_\Pi \in 9_\Pi)$
47	$(2,4,3,9)[18]$	$16 = 7_L + 5_J + 4_R$	$14^* = 6_L + 7_J + 1_R$	$(7_\Pi \in 9_\Pi)$
58	$(2,5,4,11)[22]$	$14 = 7_L + 5_J + 2_R$	$19^* = 9_L + 9_J + 11_R$	$(5_\Pi, 9_J)$
60	$(6,5,2,13)[26]$	$13 = 1_L + 5_J + 7_R$	$23^* = 1_L + 9_J + 13_R$	$(5_\Pi, 9_J)$
69	$(4,5,3,12)[24]$	$12 = 3_L + 5_J + 4_R$	$18^* = 6_L + 7_J + 5_R$	$(7_\Pi \in 9_\Pi)$
64	$(2,7,6,15)[30]$	$13 = 7_L + 5_J + 1_R$	$23^* = 13_L + 9_J + 1_R$	$(5_\Pi, 9_J)$
84	$(4,7,5,16)[32]$	$9 = 3_L + 5_J + 1_R$	$27^* = 13_L + 9_J + 5_R$	$(5_\Pi, 9_J)$
88	$(6,7,4,17)[34]$	$8 = 1_L + 5_J + 2_R$	$31^* = 9_L + 9_J + 13_R$	$(5_\Pi, 9_J)$
91	$(6,8,5,19)[38]$	$7 = 9_L + 5_J + 1_R$	$35^* = 16_L + 7_J + 12_R$	$(5_\Pi, 9_J)$

additional constraint $n_{\max} = 3 < \dim(0,1,1,2)$ (see Table 16):

$$\begin{aligned} p \cdot \mathbf{k}_4(IX) \;&=\; m \cdot (0,1,1,2) \,+\, n \cdot (2,0,1,3), \\ p = 1 \;&\rightarrow\; 1 \leqslant m \leqslant 6;\,,\; 1 \leqslant n \leqslant 3. \end{aligned} \tag{7.33}$$

The 5 invariant monomials for this chain are the following:

$$\begin{aligned} \boldsymbol{\mu}_0^1 &= (1,4,0,0) \;\Rightarrow\; x \cdot y^4, \\ \boldsymbol{\mu}_0^2 &= (2,2,2,0) \;\Rightarrow\; x^2 \cdot y^2 \cdot z^2, \\ \boldsymbol{\mu}_0^3 &= (3,0,4,0) \;\Rightarrow\; x^3 \cdot z^4, \\ \boldsymbol{\mu}_0^4 &= (1,1,1,1) \;\Rightarrow\; x \cdot y \cdot z \cdot u, \\ \boldsymbol{\mu}_0^5 &= (0,0,0,2) \;\Rightarrow\; u^2. \end{aligned} \tag{7.34}$$

7.5. Example of a $J = \Pi = 9$ Chain. To see another aspect of mirror symmetry and duality, we now consider the chain VI with intersection $J(\Delta) = \Pi(\Delta) = 9$ and $J(\Delta^*) = \Pi(\Delta^*) = 5$ shown in Table 15, which is constructed from the extended vectors $\mathbf{k}^i = (0,1,1,2)$ and $\mathbf{k}^j = (1,0,1,2)$. In this case, duality gives very simple connections between the numbers of integer points in the dual polyhedron pair, as seen in Table 17.

The canonical basis for chain VI is:

$$\begin{aligned} \mathbf{e}_1 \;&=\; (-m,n,0,0), \\ \mathbf{e}_2 \;&=\; (-1,-1,1,0), \\ \mathbf{e}_3 \;&=\; (-1,-1,-1,1) \end{aligned} \tag{7.35}$$

with the following restriction on the determinant

$$\det(\mathbf{e}_1,\mathbf{e}_2,\mathbf{e}_3,\mathbf{e}_0) = 4 \cdot m \,+\, 4 \cdot n = d, \tag{7.36}$$

where $\mathbf{e}_0 = (1,1,1,1)$.

Table 17. The $K3$ hypersurfaces in the chain VI: $\mathbf{k}(VI) = (n, m, m+n, 2m+2n) =$ $= m \cdot (0,1,1,2) + n \cdot (1,0,1,2)$

N	$\mathbf{k}_4$	$\Delta(J=9)$	$\Delta^*(\Pi=5)$	$\Delta_\Pi, \Delta^*{}_J$
6	$(1,1,2,4)[8]$	$35 = 13_L + 9_{J,\Pi} + 13_R$	$7^* = 1^*_L + 5^*_{\Pi,J} + 1^*_R$	$(9_{\Pi,J}, 5_{J,\Pi})$
15	$(2,1,3,6)[12]$	$27 = 5_L + 9_{J,\Pi} + 13_R$	$9^* = 1^*_L + 5^*_{\Pi,J} + 4^*_R$	$(9_{\Pi,J}, 5_{J,\Pi})$
24	$(3,1,4,8)[16]$	$24 = 2_L + 9_{J,\Pi} + 13_R$	$12^* = 1^*_L + 5^*_{\Pi,J} + 6_R$	$(9_{\Pi,J}, 5_{J,\Pi})$
31	$(4,1,5,10)[20]$	$23 = 1_L + 9_{J,\Pi} + 13_R$	$13^* = 1^*_L + 5^*_{\Pi,J} + 7_R$	$(9_{\Pi,J}, 5_{J,\Pi})$
24	$(3,2,5,10)[20]$	$16 = 2_L + 9_{J,\Pi} + 5_R$	$14^* = 3^*_L + 5^*_{\Pi,J} + 6^*_R$	$(9_{\Pi,J}, 5_{J,\Pi})$
71	$(3,4,7,14)[28]$	$12 = 2_L + 9_{J,\Pi} + 1_R$	$18^* = 7^*_L + 5^*_{\Pi,J} + 6^*_R$	$(9_{\Pi,J}, 5_{J,\Pi})$

The possible values of m and n for this chain are determined by the dimensions of the extended vectors, without any unexpected puzzles:

$$\begin{aligned} p \cdot \mathbf{k}_4(VI) \;&=\; m \cdot (0,1,1,2) \,+\, n \cdot (1,0,1,2), \\ p = 1 \;&\rightarrow\; 1 \leqslant m \leqslant 4; \;\; 1 \leqslant n \leqslant 4, \end{aligned} \tag{7.37}$$

and the following:

$$\begin{aligned} \boldsymbol{\mu}_0^1 = (4,4,0,0) \;&\Rightarrow\; x^4 \cdot y^4, \\ \boldsymbol{\mu}_0^2 = (3,3,1,0) \;&\Rightarrow\; x^3 \cdot y^3 \cdot z, \\ \boldsymbol{\mu}_0^3 = (2,2,2,0) \;&\Rightarrow\; x^2 \cdot y^2 \cdot z^2, \\ \boldsymbol{\mu}_0^4 = (1,1,3,0) \;&\Rightarrow\; x \cdot y \cdot z^3, \\ \boldsymbol{\mu}_0^5 = (0,0,4,0) \;&\Rightarrow\; z^4, \\ \boldsymbol{\mu}_0^6 = (2,2,0,1) \;&\Rightarrow\; x^2 \cdot y^2 \cdot u, \\ \boldsymbol{\mu}_0^7 = (1,1,1,1) \;&\Rightarrow\; x \cdot y \cdot z \cdot u, \\ \boldsymbol{\mu}_0^8 = (0,0,2,1) \;&\Rightarrow\; z^2 \cdot u, \\ \boldsymbol{\mu}_0^9 = (0,0,0,2) \;&\Rightarrow\; u^2. \end{aligned} \tag{7.38}$$

are the 9 invariant monomials Ψ_{inv} for this chain.

Analogously, one can consider the projective chain $\boldsymbol{\pi}_7^{(\alpha)}(\Pi = 5)$ with the youngest vector (5,6,8,11), and compare it with the double-intersection chain $VIII$, constructed from the extended vectors $\mathbf{k}(VIII) = m \cdot (0,1,1,2) + n \cdot (1,1,2,0)$; $(d = 4m + 4n.\ m_{\max} = 3, n_{\max} = 4)$, $\mathbf{k}_{\mathrm{eld}} = (1,2,3,2)[8]$. Among the 95 $K3$ projective vectors, 26 have such an invariant-direction structure, and therefore can be found in corresponding projective chains (see Table 1).

8. $K3$ HYPERSURFACES AND CARTAN–LIE ALGEBRA GRAPHS

We discuss in this Section more details of the emergence of Cartan–Lie algebra graphs in our construction of CY spaces.

8.1. Cartan–Lie Algebra Graphs and the Classification of Chains of Projective Vectors. As we commented already in the Introduction and in Section 2, the structure of the projective $\mathbf{k}_4$ vectors in 22 chains leads to interesting relations with the five classical regular dual polyhedron pairs in three-dimensional space: the one-dimensional point, two-dimensional line segment and three-dimensional tetrahedron, octahedron-cube and icosahedron-dodecahedron. There are also interesting correspondences with the Cartan–Lie algebra CLA graphs for the five types of groups in the $\mathrm{ADE}_{6,7,8}$ series: see Figure 8. The $\mathrm{CLA}_{J,\Pi}$ graphs, which can be seen in the polyhedra of the corresponding $\mathbf{k}_4$ projective vectors, follow

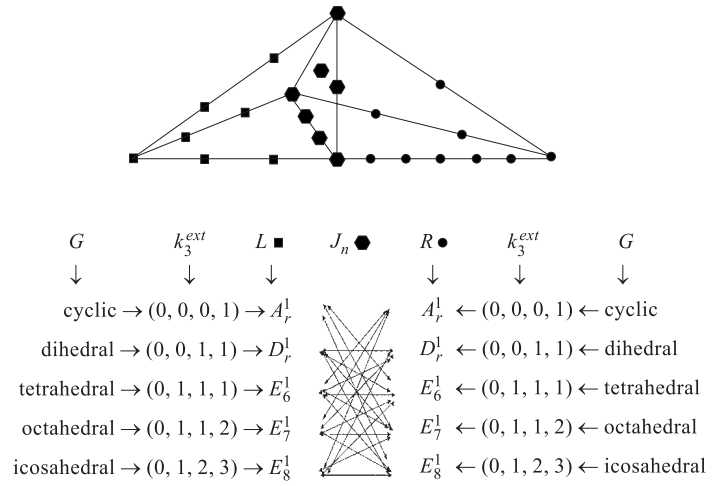

Fig. 8. Illustration of the Cartan–Lie algebra diagram classification of the $22(=[13+1]+8^*)$ chains of $K3$ polyhedra shown in Table 18. Here G denotes the cyclic, dihedral, tetrahedron, octahedron-cube, and icosahedron-dodecahedron subgroups of $SU(2)$, L/R denote left/right integer points and CLA_J diagrams, J_n — the type of intersection, and the $\mathbf{k}_3$ are all the possible planar vectors. We find $r_{\max L}=17$ or $r_{\max R}=17$ for the A_r^1 series, and $r_{\max L}=16$ or $r_{\max R}=16$ for the D_r^1 series. In the example shown here, one can see the polyhedron with the projective vector: $\mathbf{k}_4=(1,1,3,4)[9]$

completely the structure of the five possible extended vectors:

$$\begin{aligned}
\mathbf{k}_C^{ext}&=(0,0,0,1) \quad \leftrightarrow \quad A_r,\\
\mathbf{k}_D^{ext}&=(0,0,1,1) \quad \leftrightarrow \quad D_r,\\
\mathbf{k}_T^{ext}&=(0,1,1,1) \quad \leftrightarrow \quad E_6,\\
\mathbf{k}_O^{ext}&=(0,1,1,2) \quad \leftrightarrow \quad E_7,\\
\mathbf{k}_I^{ext}&=(0,1,2,3) \quad \leftrightarrow \quad E_8.
\end{aligned} \tag{8.1}$$

We give in Table 18 the ADE structures and the CD_J diagrams of all the eldest $K3$ projective vectors from the 22 double chains. An illustration is given in Figure 8, and the rest of this Section discusses the examples of chains XV to XIX, illustrating the power of our systematic approach.

8.2. The $K3$ Chain XV with Graphs in the $E_8^{(1)}-A_r^{(1)}$ Series. Here we give the list of $\mathbf{k}_4$ vectors which can be constructed from the Weierstrass vectors $\mathbf{k}_3\equiv(1,2,3)$ and $\mathbf{k}_1=(1)$, shown as chain XV in Table 19. The number of $\mathbf{k}_4$ vectors in this chain is determined by the positive-integer numbers: $m=1, n\leqslant 6$, according to the dimensions of the corresponding component $\mathbf{k}^i$.

Table 18. The eldest vectors $(m = n = 1)$ for all the 22 chains of $K3$ hypersurfaces, and the corresponding Cartan–Lie algebra diagrams CLA_J

N	$\mathbf{k}_i$(eldest)	Structure	max $\Delta(J)$	CLA_J	min $\Delta^*(\Pi)$
I	$(1,1,1,1)[4]$	$(0,1,1,1)_{e6}+(1,0,0,0)_a$	$35=10_{e6}+10_{J=\triangle}+15_a$	$E_6^{(1)}\leftrightarrow A_{12}^{(1)}$	$5^*=1^*_{e6}+3^*_C+1^*_a$
II	$(1,1,2,2)[6]$	$(0,1,1,1)_{e6}+(1,0,1,1)_{e6}$	$30=10_{e6}+10_{J=\Pi=\triangle}+10_{e6}$	$E_6^{(1)}\leftrightarrow E_6^{(1)}$	$6^*=1^*_{e6}+4^*_{\Pi=J=\triangle}+1^*_{e6}$
III	$(3,1,2,3)[9]$	$(0,1,1,1)_{e6}+(3,0,1,2)_{e8}$	$23=4_{e6}+4_{J=\triangle}+15_{e8}$	${G_2}^{(1)}\leftrightarrow E_8^{(1)}$	$8^*=3^*_{e6}+4^*_{J=\triangle}+1^*_{e8}$
IV	$(1,1,1,2)[5]$	$(0,1,1,2)_{e7}+(1,0,0,0)_a$	$34=13_{e7}+9_{J=\triangle}+12_a$	$E_7^{(1)}\leftrightarrow A_9^{(1)}$	$6^*=1^*_{e6}+4^*_C+1^*_a$
V	$(1,1,1,3)[6]$	$(0,1,1,2)_{e7}+(1,0,0,1)_d$	$39=13_{e7}+9_{J=\triangle}+17_d$	$E_7^{(1)}\leftrightarrow D_{10}^{(1)}$	$6^*=1^*_{e7}+4^*_C+1_d$
VI	$(1,1,2,4)[8]$	$(0,1,1,2)_{e7}+(1,0,1,2)_{e7}$	$35=13_{e7}+9_{J=\Pi=\triangle}+13_{e7}$	$E_7^{(1)}\leftrightarrow E_7^{(1)}$	$7^*=1^*_{e7}+5^*_{\Pi=\triangle}+1^*_{e7}$
VII	$(1,1,1,1)[4]$	$(0,1,1,2)_{e7}+(2,1,1,0)_{e7}$	$35=13_{e7}+9_{J=\triangle}+13_{e7}$	$E_7^{(1)}\leftrightarrow E_7^{(1)}$	$5^*=1^*_L+3^*_C+1^*_R$
$VIII$	$(1,2,3,2)[8]$	$(0,1,1,2)_{e7}+(1,1,2,0)_{e7}$	$24=12_{e7}+5_{J=\triangle}+7_{e7}$	$E_7^{(1)}\leftrightarrow F_4^{(1)}$	$8^*=3^*_{e7}+4^*_C+1^*_{e7}$
IX	$(2,2,1,5)[10]$	$(0,1,1,2)_{e7}+(2,1,0,3)_{e8}$	$28=7_{e7}+5_{J=\triangle}+16_{e8}$	$F_4^{(1)}\leftrightarrow E_8^{(1)}$	$8^*=3^*_{e7}+4^*_C+1^*_{e8}$
X	$(1,1,1,1)[4]$	$(0,0,1,1)_d+(1,1,0,0)_d$	$35=13_d+9_{J=\square}+13_d$	$D_8^{(1)}\leftrightarrow D_8^{(1)}$	$5^*_{\Pi=\diamond}=1^*_d+3^*_C+1^*_d$
XI	$(1,1,1,2)[5]$	$(0,0,1,1)_d+(1,1,0,1)_{e6}$	$34=15_d+9_{J=\square}+10_{e6}$	$D_8^{(1)}\leftrightarrow E_6^{(1)}$	$6^*=1^*_d+4^*_C+1^*_{e6}$
XII	$(1,1,1,1)[4]$	$(0,1,2,3)_{e8}+(3,2,1,0)_{e8}$	$13=4_{e8}+5_{J=\Pi=\square}+4_{e8}$	$G_2^{(1)}\leftrightarrow G_2^{(1)}$	$11^*=1^*_{e8}+9^*_{\Pi=J=\square}+1^*_{e8}$
$XIII$	$(1,1,2,3)[7]$	$(0,1,1,1)_{e6}+(1,0,1,2)_{e7}$	$31=10_{e6}+8_{J=\Pi=\square}+13_{e7}$	$E_6^{(1)}\leftrightarrow E_7^{(1)}$	$8^*=1^*_{e6}+6^*_{\Pi,J}+1^*_{e7}$
XIV	$(1,1,1,2)[5]$	$(0,1,1,2)_{e6}+(2,1,3,0)_{e8}$	$18=7_{e6}+6_{J=\Pi=\square}+5_{e8}$	$F_4^{(1)}\leftrightarrow G_2^{(1)}$	$10^*=1^*_{e6}+8^*_{\Pi=J=\square}+1^*_{e8}$
$XXII$	$(1,2,1,2)[6]$	$(0,1,1,2)_{e7}+(1,1,0,0)_d$	$30=13_{e7}+7_{J=\Pi=\square}+10_d$	$E_7^{(1)}\leftrightarrow D_7$	$6^*=1^*_{e7}+4^*_J+1^*_d$
XV	$(1,1,2,3)[7]$	$(0,1,2,3)_{e8}+(1,0,0,0)_a$	$31=16_{e8}+7_{J=\triangle}+8_a$	$E_8^{(1)}\leftrightarrow A_6^{(1)}$	$8^*=1^*_{e8}+6^*_C+1^*_a$
XVI	$(1,1,2,4)[8]$	$(0,1,2,3)_{e8}+(1,0,0,1)_d$	$35=16_{e8}+7_{J=\triangle}+12_d$	$E_8^{(1)}\leftrightarrow D_8$	$7^*=1^*_{e8}+5^*_C+1^*_{e8}$
$XVII$	$(1,1,3,4)[9]$	$(0,1,2,3)_{e8}+(1,0,1,1)_{e6}$	$33=16_{e8}+7_{J=\Pi=\triangle}+10_{e6}$	$E_8^{(1)}\leftrightarrow E_6^{(1)}$	$9^*=1^*_{e8}+7^*_{\Pi=J=\triangle}+1^*_{e6}$
$XVIII$	$(1,1,3,5)[10]$	$(0,1,2,3)_{e8}+(1,0,1,2)_{e7}$	$36=16_{e8}+7_{J=\Pi=\triangle}+13_{e7}$	$E_8^{(1)}\leftrightarrow E_7^{(1)}$	$9^*=1^*_{e8}+7^*_{\Pi=J=\triangle}+1^*_{e7}$
XIX	$(1,1,4,6)[12]$	$(0,1,2,3)_{e8}+(1,0,2,3)_{e8}$	$39=16_{e8}+7_{J=\Pi=\triangle}+16_{e8}$	$E_8^{(1)}\leftrightarrow E_8^{(1)}$	$9^*=1^*_{e8}+7^*_{\Pi=J=\triangle}+1^*_{e8}$
XX	$(1,1,1,3)[6]$	$(0,1,2,3)_{e8}+(2,1,0,3)_{e8}$	$21=7_{e8}+7_{J=\Pi=\triangle}+7_{e8}$	$F_4^{(1)}\leftrightarrow F_4^{(1)}$	$9^*=1^*_{e8}+7^*_{\Pi=J=\triangle}+1^*_{e8}$
XXI	$(3,2,4,3)[12]$	$(0,1,2,3)_{e8}+(3,1,2,0)_{e8}$	$15=4_{e8}+7_{J=\Pi=\triangle}+4_{e8}$	$G_2^{(1)}\leftrightarrow G_2^{(1)}$	$9^*=1^*_{e8}+7^*_{\Pi=J=\triangle}+1^*_{e8}$

Table 19. The $K3$ hypersurfaces in the chain XV: $\mathbf{k} = (m, 2\cdot m, 3\cdot m, n) = m\cdot(1,2,3,0) + n\cdot(0,0,0,1)$: $d = 6m+n$, $m_{\max} = 1, n_{\max} = 6$, $\mathbf{k}_{\text{eld}} = (1,2,3,1)[7]$

ℵ	m,n	$\mathbf{k}[d]$	$\Delta(J=7)$	Group	$\Delta^*(\Pi=7)$
5	1, 1	$(1,2,3,1)[7]$	$31 = 8_L + 7_J + 16_R$	${A_6^{(1)}}_L$	$8^* = 1_L^* + 6_C^* + 1_R^*$
10	1, 2	$(1,2,3,2)[8]$	$24 = 10_L + 7_J + 7_R$	${A_7^{(1)}}_L$	$8^* = 3_L^* + 4_C^* + 1_R^*$
12	1, 3	$(1,2,3,3)[9]$	$23 = 12_L + 7_J + 4_R$	${A_8^{(1)}}_L$	$8^* = 4_L^* + 3_C^* + 1_R^*$
13	1, 4	$(1,2,3,4)[10]$	$23 = 14_L + 7_J + 2_R$	${A_9^{(1)}}_L$	$11^* = 3_L^* + 3_C^* + 1_R^*$
14	1, 5	$(1,2,3,5)[11]$	$24 = 16_L + 7_J + 1_R$	${A_{10}^{(1)}}_L$	$13^* = 9_L^* + 3_C^* + 1_R^*$
15	1, 6	$(1,2,3,6)[12]$	$27 = 19_L + 7_J + 1_R$	${A_{11}^{(1)}}_L$	$9^* = 5_L^* + 3_C^* + 1_R^*$

The basis for this chain, see Figure 9, can be written in the the following form:

$$\begin{aligned} \mathbf{e}_1 &= (-n, 0, 0, m), \\ \mathbf{e}_2 &= (-2, 1, 0, 0), \\ \mathbf{e}_3 &= (-3, 0, 1, 0). \end{aligned} \tag{8.2}$$

The determinant of this canonical basis coincides, of course, with the dimensions of the $\mathbf{k}_4$ vectors:

$$\det(\mathbf{e}_1, \mathbf{e}_2, \mathbf{e}_3, \mathbf{e}_0) = 6\cdot m + 1\cdot n = d, \tag{8.3}$$

where $\mathbf{e}_0 = (1,1,1,1)$. The decomposition of this chain is again determined by the dimension of the extended vectors $d(\mathbf{k}^{ex(i)}) = k_1^{ex(i)} + k_2^{ex(i)} + k_3^{ex(i)} + k_4^{ex(i)}$, as seen in Table 19:

$$\begin{aligned} \mathbf{k}_4(XV) = m\cdot(1,2,3,0) \quad &+ \quad n\cdot(0,0,0,1), \\ m = 1, \qquad &1 \leqslant n \leqslant 6. \end{aligned} \tag{8.4}$$

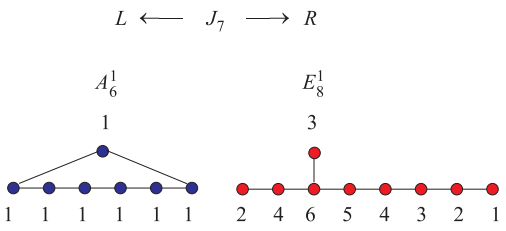

Fig. 9. The ${A_6^{(1)}}_L - {E_8^{(1)}}_R$ graph from the eldest $(1,2,3,1)[7]$ polyhedron in chain XV: $31 = 8_L + 7_J + 16_R$

The seven invariant monomials corresponding to this chain are:

$$\begin{aligned}
\boldsymbol{\mu}_0^1 = (6,0,0,1) &\Rightarrow x^6 \cdot u,\\
\boldsymbol{\mu}_0^2 = (4,1,0,1) &\Rightarrow x^4 \cdot y \cdot u,\\
\boldsymbol{\mu}_0^3 = (2,2,0,1) &\Rightarrow x^2 \cdot y^2 \cdot u,\\
\boldsymbol{\mu}_0^4 = (0,3,0,1) &\Rightarrow y^3 \cdot u,\\
\boldsymbol{\mu}_0^5 = (3,0,1,1) &\Rightarrow x^3 \cdot z \cdot u,\\
\boldsymbol{\mu}_0^6 = (1,1,1,1) &\Rightarrow x \cdot y \cdot z \cdot u,\\
\boldsymbol{\mu}_0^7 = (0,0,2,1) &\Rightarrow z^2 \cdot u.
\end{aligned} \tag{8.5}$$

Considering the dual pairs for these vectors, one can see that the singularities of the eldest vector $\mathbf{k}_4 = (1,2,3,1)$ correspond to some graphs of the ${A_6^{(1)}}_L - {E_8^{(1)}}_R$ series, as seen in Figure 9. For instance, if one looks at the integer points in the edges of the polyhedron on the left (right) side of the intersection by the hyperplane $\mathbf{k}^i = (0,1,2,3)$, one sees graphs with ${A_6^{(1)}}_L$ and ${E_8^{(1)}}_R$ Lie algebras. Going to the last minimal $\mathbf{k} = (1,2,3,6)$ of this chain, we find that the right graph degenerates and left points reproduce $A_{11}^{(1)}$ with the maximum possible rank in this chain. Thus, the six $\mathbf{k}$ vectors in this chain produce the following graphs in the A series: $A_6^{(1)}, A_7^{(1)}, A_8^{(1)}, A_9^{(1)}, A_{10}^{(1)}, A_{11}^{(1)}$.

8.3. The $K3$ Chain XVI with Graphs in the $E_8^{(1)} - D_r$ Series. The basis for the chain shown in Table 20 is

$$\begin{aligned}
\mathbf{e}_1 &= (-m,n,0,0),\\
\mathbf{e}_2 &= (0,-2,1,0),\\
\mathbf{e}_3 &= (-1,-1,-1,1),
\end{aligned} \tag{8.6}$$

with

$$\det(\mathbf{e}_1,\mathbf{e}_2,\mathbf{e}_3,\mathbf{e}_0) = 6\cdot m + 2\cdot n = d, \tag{8.7}$$

where $\mathbf{e}_0 = (1,1,1,1)$ again. The decomposition of this chain is completely determined by the dimensions of the vectors shown in Table 20:

$$\begin{aligned}
p\cdot\mathbf{k}_4(XVI) &= m\cdot(0,1,2,3) + n\cdot(1,0,0,1),\\
p = 1^* &\rightarrow 1 \leqslant m \leqslant 2;\ 1 \leqslant n \leqslant 6,\\
p = 2 &\rightarrow m = n = 2.
\end{aligned} \tag{8.8}$$

Table 20. The $K3$ hypersurfaces in the chain XVI: $\mathbf{k} = (n, m, 2m, 3m + n) = m\cdot(0, 1, 2, 3)+n\cdot(1, 0, 0, 1)$: $(d = 6m + 2n)$, $m_{\max} = 2, n_{\max} = 6$, $\mathbf{k}_{\text{eld}} = (1, 1, 2, 4)[8]$

ℵ	$\mathbf{k}[d]$	$\Delta(J = 7)$	Group	$\Delta^*(\Pi = 7)$	$(\Pi(\Delta), J(\Delta^*))$
6	$(1, 1, 2, 4)[8]$	$35 = 16_L + 7_J + 12_R$	D_{8R}	$7^* = 1^*_L + 5^*_C + 1^*_R$	$(9, 5^*)$
11	$(2, 1, 2, 5)[10]$	$28 = 7_L + 7_J + 14_R$	D_{9R}	$8^* = 1^*_L + 4^*_C + 3^*_R$	$(10, 4^*)$
15	$(3, 1, 2, 6)[12]$	$27 = 4_J + 7_J + 16_R$	D_{10R}	$9^* = 1^*_L + 4^*_C + 4^*_R$	$(9, 5^*)$
17	$(4, 1, 2, 7)[14]$	$27 = 2_L + 7_J + 18_R$	D_{11R}	$12^* = 1^*_L + 4^*_C + 7^*_R$	$(7, 7^*)$
19	$(5, 1, 2, 8)[16]$	$28 = 1_L + 7_J + 14_R$	D_{12R}	$14^* = 1^*_L + 4^*_C + 9^*_R$	$(7, 7^*)$
20	$(6, 1, 2, 9)[18]$	$30 = 1_L + 7_J + 22_R$	D_{13R}	$12^* = 1^*_L + 4^*_C + 7^*_R$	$(7, 7^*)$
47	$(3, 2, 4, 9)[18]$	$16 = 4_L + 7_J + 5_R$	—	$14^* = 3^*_L + 5^*_C + 6^*_R$	$(7, 7^*)$
58	$(5, 2, 4, 11)[22]$	$14 = 1_L + 7_J + 6_R$	—	$19^* = 3^*_L + 4^*_C + 12^*_R$	$(5, 9^*)$

The seven invariant monomials corresponding to this chain are the following:

$$\begin{aligned}
\boldsymbol{\mu}_0^1 &= (2, 6, 0, 0) \quad \Rightarrow \quad x^2 \cdot y^6, \\
\boldsymbol{\mu}_0^2 &= (2, 4, 1, 0) \quad \Rightarrow \quad x^2 \cdot y^4 \cdot z, \\
\boldsymbol{\mu}_0^3 &= (2, 2, 2, 0) \quad \Rightarrow \quad x^2 \cdot y^2 \cdot z^2, \\
\boldsymbol{\mu}_0^4 &= (2, 0, 3, 0) \quad \Rightarrow \quad x^2 \cdot z^3, \\
\boldsymbol{\mu}_0^5 &= (1, 3, 0, 1) \quad \Rightarrow \quad x \cdot y^3 \cdot u, \\
\boldsymbol{\mu}_0^6 &= (1, 1, 1, 1) \quad \Rightarrow \quad x \cdot y \cdot z \cdot u, \\
\boldsymbol{\mu}_0^7 &= (0, 0, 0, 2) \quad \Rightarrow \quad u^2.
\end{aligned} \tag{8.9}$$

The example of the ${E_8^{(1)}}_L - D_{8R}$ graph associated with the eldest $(1, 1, 2, 4))[8]$ polyhedron in Table 20 is shown in Figure 10.

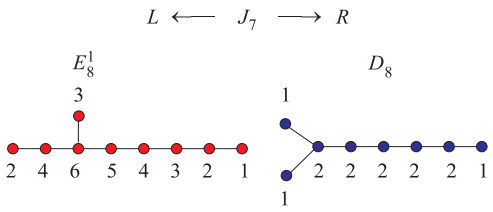

Fig. 10. The ${E_8^{(1)}}_L - D_{8R}$ graph from the eldest $(1, 1, 2, 4)[8]$ polyhedron in the chain XVI: $33 = 16_L + 7_J + 10_R$

8.4. The $J = \Pi$ Symmetric Chain $XVII$ with Exceptional Graph $E_6 \times E_8$. We show in Table 21 the projective vectors constructed from $\mathbf{k}_3^{ex} = (0,1,1,1)$ and $\mathbf{k}_3^{ex} = (1,0,2,3)$. In this case, the number of points in the maximal polyhedron with $m = n = 1$ can easily be calculated: $33 = (10)_L + (7)_{\text{int}} + (16)_R$. The «right» $15_R + 1_R$ points form the graph for the affine $E_8^{(1)}$ Lie algebra, as shown in Figure 11:

$$\begin{aligned} 6 = 1 + 1 + 1 + 1 + 1 + 1 \quad &\Rightarrow \quad \{(P_{x_0})_1 + (P_{x_1})_2 + (P_{x_2})_3 + \\ &+ \quad (P_{x_3})_4 + (P_{x_4})_5 + (P_{x_5})_6\}, \\ 3 = 3 \quad &\Rightarrow \quad \{(P_{x_6,x_6',x_6''})_3\}, \\ 6 = 4 + 2 \quad &\Rightarrow \quad \{(P_{x_7,x_7',x_7'',x_7'''})_4 + (P_{x_8,x_8'})_2\}. \end{aligned} \tag{8.10}$$

The «left» points in this polyhedron, $9_L + 1_L$, correspond to the $E_6^{(1)}$ affine series with the Coxeter numbers:

$$\begin{aligned} 3 = 1 + 1 + 1 \quad &\Rightarrow \quad \{(P_{x_1})_1 + (P_{x_2})_2 + (P_{x_3})_3\}, \\ 3 = 2 + 1 \quad &\Rightarrow \quad \{(P_{x_4,x_4'})_2 + (P_{x_0})_1\}, \\ 3 = 2 + 1 \quad &\Rightarrow \quad \{(P_{x_5,x_5'})_2 + (P_{x_6})_1\}. \end{aligned} \tag{8.11}$$

Table 21. The $K3$ hypersurfaces in the chain $XVII$: $\mathbf{k} = (n, m, m+2n, m+3n) =$ $= m \cdot (0,1,1,1) + n \cdot (1,0,2,3)$: $d = 3m + 6n$, $\max(m,n) = (6,3)$

ℵ	$\mathbf{k}[d]$	Δ	Δ^*
7	$(1,1,3,4)[9]$	$33 = 10_L + 7_{J=\Pi} + 16_R$	$9^* = 1_L^* + 7_{\Pi=J}^* + 1_R^*$
16	$(1,2,4,5)[12]$	$24 = 10_L + 7_{J=\Pi} + 7_R$	$12^* = 4_L^* + 7_{\Pi=J}^* + 1_R^*$
25	$(1,3,5,6)[15]$	$21 = 10_L + 7_{J=\Pi} + 4_R$	$15^* = 7_L^* + 7_{\Pi=J}^* + 1_R^*$
32	$(1,4,6,7)[18]$	$19 = 10_L + 7_{J=\Pi} + 2_R$	$20^* = 12_L^* + 7_{\Pi=J}^* + 1_R^*$
36	$(1,5,7,8)[21]$	$18 = 10_L + 7_{J=\Pi} + 1_R$	$24^* = 16_L^* + 7_{\Pi=J}^* + 1_R^*$
39	$(1,6,8,9)[24]$	$18 = 10_L + 7_{J=\Pi} + 1_R$	$24^* = 16_L^* + 7_{\Pi=J}^* + 1_R^*$
18	$(2,1,5,7)[15]$	$26 = 3_L + 7_{J=\Pi} + 16_R$	$17^* = 1_L^* + 7_{\Pi=J}^* + 9_R^*$
27	$(3,1,7,10)[21]$	$24 = 1_L + 7_{J=\Pi} + 16_R$	$24^* = 1_L^* + 7_{\Pi=J}^* + 16_R^*$
52	$(2,3,7,9)[21]$	$14 = 3_L + 7_{J=\Pi} + 4_R$	$23^* = 7_L^* + 7_{\Pi=J}^* + 9_R^*$
54	$(3,2,8,11)[24]$	$15 = 1_L + 7_{J=\Pi} + 7_R$	$27^* = 4_L^* + 7_{\Pi=J}^* + 16_R^*$
61	$(2,5,9,11)[27]$	$11 = 1_L + 7_{J=\Pi} + 3_R$	$32^* = 9_L^* + 7_{\Pi=J}^* + 16_R^*$
72	$(3,4,10,13)[30]$	$10 = 1_L + 7_{J=\Pi} + 2_R$	$35^* = 12_L^* + 7_{\Pi=J}^* + 16_R^*$
77	$(3,5,11,14)[33]$	$9 = 1_L + 7_{J=\Pi} + 1_R$	$39^* = 16_L^* + 7_{\Pi=J}^* + 16_R^*$

For $m_{\max} = d(\mathbf{k}(1,2,3)) = 6$ and $n_{\min} = 1$, the corresponding polyhedron contains 18 points: $18 = (10)_L + (7)_{\text{int}} + (1)_R$. Conversely, for $m_{\min} = 1$ and $n_{\max} = 3 = \dim(\mathbf{k}(1,1,1))$, the self-dual vector $\mathbf{k} = (3,1,7,10)$ has 24 integer points: $24 = (1)_L + (7)_{\text{int}} + (16)_R$. Finally, the polyhedron with $m = 5$ and $n = 3$ contains the minimal possible number of integer points, namely $9 = (1)_L + (7)_{\text{int}} + (1)_R$. This minimal vector $(3,5,11,14)[33]$ is the dual conjugate of the vector $\mathbf{k} = (1,1,4,6)[12]$.

The canonical basis of the chain shown in Table 21 is:

$$\begin{aligned} \mathbf{e}_1 &= (-m, n, 0, 0), \\ \mathbf{e}_2 &= (-2, -1, 1, 0), \\ \mathbf{e}_3 &= (-1, 0, -1, 1), \end{aligned} \tag{8.12}$$

with

$$\det(\mathbf{e}_1, \mathbf{e}_2, \mathbf{e}_3, \mathbf{e}_0) = 3 \cdot m + 6 \cdot n = d, \tag{8.13}$$

where $\mathbf{e}_0 = (1,1,1,1)$. The possible values of m and n for this chain are determined in the standard way from the dimensions of the extended vectors, $d(\mathbf{k}^{ex(j)}) = 6$ and $d(\mathbf{k}^{ex(i)}) = 3$, as seen in Table 21:

$$\begin{aligned} p \cdot \mathbf{k}_4(XVII) &= m \cdot (0,1,1,1) + n \cdot (1,0,2,3), \\ p = 1^* &\rightarrow 1 \leqslant m \leqslant 6,\ 1 \leqslant n \leqslant 3, \\ p = 2 &\rightarrow m = n = 2, \\ p = 3 &\rightarrow m = n = 3. \end{aligned} \tag{8.14}$$

The seven invariant monomials corresponding to this chain are the following:

$$\begin{aligned} \boldsymbol{\mu}_0^1 = (6,3,0,0,) &\Rightarrow x^6 \cdot y^3, \\ \boldsymbol{\mu}_0^2 = (4,2,1,0,) &\Rightarrow x^4 \cdot y^2 \cdot z, \\ \boldsymbol{\mu}_0^3 = (2,1,2,0,) &\Rightarrow x^2 \cdot y \cdot z, \\ \boldsymbol{\mu}_0^4 = (0,0,3,0,) &\Rightarrow z^3, \\ \boldsymbol{\mu}_0^5 = (3,2,0,1,) &\Rightarrow x^3 \cdot y^2 \cdot u, \\ \boldsymbol{\mu}_0^6 = (1,1,1,1,) &\Rightarrow x \cdot y \cdot z \cdot u, \\ \boldsymbol{\mu}_0^7 = (0,1,0,2,) &\Rightarrow y \cdot u^2 \end{aligned} \tag{8.15}$$

and the corresponding ${E_6^{(1)}}_L - {E_8^{(1)}}_R$ graph associated with the eldest $(1,1,3,4)$ [9] polyhedron in chain $XVII$ is shown in Table 22 and Figure 11.

Table 22. The group singularities of the dual pairs of elliptic polyhedra in chain $XVII$

$P^3(\mathbf{k})$	$H(\Delta)$	$H(\Delta^*)$	$G_L(\Delta)$	$G_R(\Delta)$	$G_L(\Delta^*)$	$G_R(\Delta^*)$
$(1,1,3,4)$	$m_1+m_2+m_3=0$	$m_1^*=0$	E_6	E_8	$SU(1)$	$SU(1)$
$(1,2,4,5)$	$m_1+m_2+m_3=0$	$m_1^*=0$	E_6	F_4	G_2	$SU(1)$
$(1,3,5,6)$	$m_1+m_2+m_3=0$	$m_1^*=0$	E_6	G_2	F_4	$SU(1)$
$(1,4,6,7)$	$m_1+m_2+m_3=0$	$m_1^*=0$	E_6	$SU(2)$	E_7	$SU(1)$
$(1,5,7,8)$	$m_1+m_2+m_3=0$	$m_1^*=0$	E_6	$SU(1)$	E_8	$SU(1)$
$(1,6,8,9)$	$m_1+m_2+m_3=0$	$m_1^*=0$	E_6	$SU(1)$	E_8	$SU(1)$

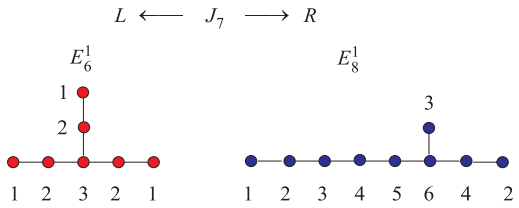

Fig. 11. The ${E_6^{(1)}}_L - {E_8^{(1)}}_R$ graph associated with the eldest $(1,1,3,4)[9]$ polyhedron in chain XVII: $33 = 10_L + 7_J + 16_R$

8.5. The $J=\Pi$ Symmetric Chain $XVIII$ with Exceptional Graph $E_7 \times E_8$. This chain can be built from the vectors $\mathbf{k}_4^{ex^i} = (0,1,1,2)$ and $\mathbf{k}_4^{ex^j} = (1,0,2,3)$, with positive integers $m \leqslant 6$ and $n \leqslant 4$. The maximal ($m=n=1$) polyhedron in this chain is again completely determined by the dimensions 4 and 6 of the projective vectors $\mathbf{k}_4^{ex^i}$ and $\mathbf{k}_4^{ex^j}$, respectively:

$$36 = (13)_L + (7)_{J=\Pi} + (16)_R. \tag{8.16}$$

The «right» $15_R + 1_R$ and «left» $12_L + 1_L$ points produce the graphs for the affine $E_8^{(1)}$ and $E_7^{(1)}$ Lie algebras, respectively, as seen in Figure 12. The vector $\mathbf{k} = (3,4,9,14)[28]$ is self-dual with $E_8^{(1)}$ graphs for the dual polyhedron pair. The «minimal» vector $\mathbf{k}$ gives the following set of integer lattice points in the polyhedron:

$$(1)_L + (7)_{\text{int}} + (1)_R = 9. \tag{8.17}$$

The canonical basis for the chain shown in Table 23 is:

$$\begin{aligned} \mathbf{e}_1 &= (-m,n,0,0), \\ \mathbf{e}_2 &= (-2,-1,1,0), \\ \mathbf{e}_3 &= (-1,-1,-1,1), \end{aligned} \tag{8.18}$$

Table 23. The $K3$ hypersurfaces in the chain $XVIII$: $\mathbf{k} = (n, m, m+2n, 2m+3n) = m \cdot (0,1,1,2) + n \cdot (1,0,2,3)$: $d = 4m + 6n$, $m_{\max} = 6, n_{\max} = 4$

$\aleph$	$\mathbf{k}[d]$	Δ	Δ^*
8	$(1,1,3,5)[10]$	$36 = 13_L + 7_{J=\Pi} + 16_R$	$9^* = 1^*_L + 7^*_{\Pi=J} + 1^*_R$
17	$(1,2,4,7)[14]$	$27 = 13_L + 7_{J=\Pi} + 7_R$	$12^* = 4^*_L + 7^*_{\Pi=J} + 1^*_R$
26	$(1,3,5,9)[18]$	$24 = 13_L + 7_{J=\Pi} + 4_R$	$15^* = 7^*_L + 7^*_{\Pi=J} + 1^*_R$
33	$(1,4,6,11)[22]$	$22 = 13_L + 7_{J=\Pi} + 2_R$	$20^* = 12^*_L + 7^*_{\Pi=J} + 1^*_R$
37	$(1,5,7,13)[26]$	$21 = 13_L + 7_{J=\Pi} + 1_R$	$24^* = 16^*_L + 7^*_{\Pi=J} + 1^*_R$
40	$(1,6,8,15)[30]$	$21 = 13_L + 7_{J=\Pi} + 1_R$	$24^* = 16^*_L + 7^*_{\Pi=J} + 1^*_R$
19	$(2,1,5,8)[16]$	$28 = 5_L + 7_{J=\Pi} + 16_R$	$14^* = 1^*_L + 7^*_{\Pi=J} + 6^*_R$
28	$(3,1,7,11)[22]$	$25 = 2_L + 7_{J=\Pi} + 16_R$	$20^* = 1^*_L + 7^*_{\Pi=J} + 12^*_R$
34	$(4,1,9,14)[28]$	$24 = 1_L + 7_{J=\Pi} + 16_R$	$24^* = 1^*_L + 7^*_{\Pi=J} + 16^*_R$
55	$(3,2,8,13)[26]$	$16 = 2_L + 7_{J=\Pi} + 7_R$	$23^* = 4^*_L + 7^*_{\Pi=J} + 12^*_R$
53	$(2,3,7,12)[24]$	$16 = 5_L + 7_{J=\Pi} + 4_R$	$20^* = 7^*_L + 7^*_{\Pi=J} + 6^*_R$
74	$(4,3,11,18)[36]$	$12 = 1_L + 7_{J=\Pi} + 4_R$	$30^* = 7^*_L + 7^*_{\Pi=J} + 16^*_R$
73	$(3,4,10,17)[34]$	$11 = 2_L + 7_{J=\Pi} + 2_R$	$31^* = 12^*_L + 7^*_{\Pi=J} + 12^*_R$
62	$(2,5,9,16)[32]$	$13 = 5_L + 7_{J=\Pi} + 1_R$	$29^* = 16^*_L + 7^*_{\Pi=J} + 6^*_R$
78	$(3,5,11,19)[38]$	$10 = 2_L + 7_{J=\Pi} + 1_R$	$35^* = 16^*_L + 7^*_{\Pi=J} + 12^*_R$
85	$(4,5,13,22)[44]$	$9 = 1_L + 7_{J=\Pi} + 1_R$	$39^* = 16^*_L + 7^*_{\Pi=J} + 16^*_R$

with

$$\det(\mathbf{e}_1, \mathbf{e}_2, \mathbf{e}_3, \mathbf{1}) = 4 \cdot m + 6 \cdot n = d. \tag{8.19}$$

The possible values of m and n for this chain fill up the dimensions of the extended vectors $d(\mathbf{k}^{ex(j)}) = 6$ and $d(\mathbf{k}^{ex(i)}) = 4$, as seen in Table 23:

$$\begin{aligned} p \cdot \mathbf{k}_4(XVIII) &= m \cdot (0,1,1,2) + n \cdot (1,0,2,3), \\ p = 1^* &\rightarrow 1 \leqslant m \leqslant 6,\ 1 \leqslant n \leqslant 4, \\ p = 2 &\rightarrow m = n = 2, \\ p = 3 &\rightarrow m = n = 3, \\ p = 4 &\rightarrow m = n = 4. \end{aligned} \tag{8.20}$$

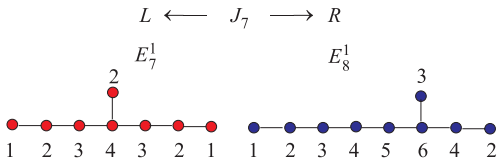

Fig. 12. The ${E_7^{(1)}}_L - {E_8^{(1)}}_R$ graphs associated with the $(1,1,3,5)[10]$ polyhedron in chain $XVIII$: $36 = 13_L + 7_J + 16_R$

Table 24. The group singularities of the dual pairs of elliptic polyhedra in chain $XVIII$

$P^3(\mathbf{k})$	$H(\Delta)$	$H(\Delta^*)$	$G_L(\Delta)$	$G_R(\Delta)$	$G_L(\Delta^*)$	$G_R(\Delta^*)$
$(1,1,3,5)$	$m_1+m_2+2m_3=0$	$m_1^*=0$	E_7	E_8	$SU(1)$	$SU(1)$
$(1,2,4,7)$	$m_1+m_2+2m_3=0$	$m_1^*=0$	E_7	F_4	G_2	$SU(1)$
$(1,3,5,9)$	$m_1+m_2+2m_3=0$	$m_1^*=0$	E_7	G_2	F_4	$SU(1)$
$(1,4,6,11)$	$m_1+m_2+2m_3=0$	$m_1^*=0$	E_7	$SU(2)$	E_7	$SU(1)$
$(1,5,7,13)$	$m_1+m_2+2m_3=0$	$m_1^*=0$	E_7	$SU(1)$	E_8	$SU(1)$
$(1,6,8,15)$	$m_1+m_2+2m_3=0$	$m_1^*=0$	E_7	$SU(1)$	E_8	$SU(1)$

The seven invariant monomials corresponding to this chain are the following:

$$\begin{aligned}
\boldsymbol{\mu}_0^1 &= (6,4,0,0,) \quad \Rightarrow \quad x^6\cdot y^4,\\
\boldsymbol{\mu}_0^2 &= (4,3,1,0,) \quad \Rightarrow \quad x^4\cdot y^3\cdot z,\\
\boldsymbol{\mu}_0^3 &= (2,2,2,0,) \quad \Rightarrow \quad x^2\cdot y^2\cdot z^2,\\
\boldsymbol{\mu}_0^4 &= (0,1,3,0,) \quad \Rightarrow \quad y\cdot z^3,\\
\boldsymbol{\mu}_0^5 &= (3,2,0,1,) \quad \Rightarrow \quad x^3\cdot y^2\cdot u,\\
\boldsymbol{\mu}_0^6 &= (1,1,1,1,) \quad \Rightarrow \quad x\cdot y\cdot z\cdot u,\\
\boldsymbol{\mu}_0^7 &= (0,1,0,2,) \quad \Rightarrow \quad y\cdot u^2.
\end{aligned} \tag{8.21}$$

The ${E_7^{(1)}}_L - {E_8^{(1)}}_R$ graph associated with the eldest $(1,1,3,5))[10]$ polyhedron in chain $XVIII$ can be seen in Table 24 and Figure 12.

8.6. Chain XIX with $(7_J, 7_\Pi)$ Weierstrass Triangle Fibrations. We now consider the chain XIX of $\mathbf{k}_4$ projective vectors with E_{8L} and E_{8R} graphs. This chain starts from the $m=n=1$ polyhedron, which is left-right symmetric with respect to the intersection $P^2(1,2,3)$. This polyhedron $P^3(1,1,4,6)$ contains $39 = 16_L + (7)_{J=\Pi} + 16_R$ integer points: see Table 25 and Figure 13. The minimal vector $\mathbf{k} = (5,6,22,33)[66]$ is the dual conjugate of the eldest vec-

Table 25. The $K3$ hypersurfaces in the $J = \Pi$ symmetric chain XIX with $\mathbf{k} = (n, m, 2m + 2n, 3m + 3n) = m \cdot (0, 1, 2, 3) + n \cdot (1, 0, 2, 3)$: $d = 6m + 6n$, $m_{\max} = 6, n_{\max} = 6$, $\mathbf{k}_{\text{eld}} = (1, 1, 4, 6)[12]$

ℵ	$\mathbf{k}_4$	$\Delta(J = \Pi = 7)$	$\Delta^*(\Pi = J = 7)$
9	$(1, 1, 4, 6)[12]$	$39 = 16_L + 7_{J=\Pi} + 16_R$	$9^* = 1^*_L + 7^*_{\Pi=J} + 1^*_R$
20	$(1, 2, 6, 9)[18]$	$30 = 16_L + 7_{J=\Pi} + 7_R$	$12^* = 4^*_L + 7^*_{\Pi=J} + 1^*_R$
29	$(1, 3, 8, 12)[24]$	$27 = 16_L + 7_{J=\Pi} + 4_R$	$15^* = 7^*_L + 7^*_{\Pi=J} + 1^*_R$
35	$(1, 4, 10, 15)[30]$	$25 = 16_L + 7_{J=\Pi} + 2_R$	$20^* = 12^*_L + 7^*_{\Pi=J} + 1^*_R$
38	$(1, 5, 12, 18)[36]$	$24 = 16_L + 7_{J=\Pi} + 1_R$	$24^* = 16^*_L + 7^*_{\Pi=J} + 1^*_R$
41	$(1, 6, 14, 21)[42]$	$24 = 16_L + 7_{J=\Pi} + 1_R$	$24^* = 16^*_L + 7^*_{\Pi=J} + 1^*_R$
56	$(2, 3, 10, 15)[30]$	$18 = 7_L + 7_{J=\Pi} + 4_R$	$18^* = 7^*_L + 7^*_{\Pi=J} + 4_R$
75	$(3, 4, 14, 21)[42]$	$13 = 4_L + 7_{J=\Pi} + 2_R$	$26^* = 12^*_L + 7^*_{\Pi=J} + 7_R$
63	$(2, 5, 14, 21)[42]$	$15 = 7_L + 7_{J=\Pi} + 1_R$	$27^* = 16^*_L + 7^*_{\Pi=J} + 4^*_R$
79	$(3, 5, 16, 24)[48]$	$12 = 4_L + 7_{J=\Pi} + 1_R$	$30^* = 16^*_L + 7^*_{\Pi=J} + 7^*_R$
86	$(4, 5, 18, 27)[54]$	$10 = 2_L + 7_{J=\Pi} + 1_R$	$35^* = 16^*_L + 7^*_{\Pi=J} + 12^*_R$
92	$(5, 6, 22, 33)[66]$	$9 = 1_L + 7_{J=\Pi} + 1_R$	$39^* = 16^*_L + 7^*_{\Pi=J} + 16^*_R$

tor $\mathbf{k} = (1, 1, 4, 6)[12]$, the vector $\mathbf{k} = (1, 6, 14, 21)[42]$ is self-dual, and its dual pair of $K3$ polyhedra yield the self-dual $E_8^{(1)}$ graph.

The basis of the chain shown in Table 25 is the following:

$$\begin{aligned} \mathbf{e}_1 &= (-m, n, 0, 0), \\ \mathbf{e}_2 &= (-2, -2, 1, 0), w \\ \mathbf{e}_3 &= (-1, -1, -1, 1), \end{aligned} \tag{8.22}$$

with

$$\det(\mathbf{e}_1, \mathbf{e}_2, \mathbf{e}_3, \mathbf{e}_0) = 6 \cdot m + 6 \cdot n = d, \tag{8.23}$$

where $\mathbf{e}_0 = (1, 1, 1, 1)$. The possible values of m and n for this chain are completely determined by the dimensions of the vectors $d(\mathbf{k}^{ex(j)}) = 6$ and $d(\mathbf{k}^{ex(i)}) = = 6$ (see Table 25):

$$\begin{aligned} p \cdot \mathbf{k}_4(XIX) &= m \cdot (0, 1, 2, 3) + n \cdot (1, 0, 2, 3), \\ p = 1^* &\rightarrow 1 \leqslant m \leqslant 6, \ 1 \leqslant n \leqslant 6, \\ p = 2 &\rightarrow m = n = 2, \\ p = 3 &\rightarrow m = n = 3, \\ p = 4 &\rightarrow m = n = 4, \\ p = 6 &\rightarrow m = n = 6. \end{aligned} \tag{8.24}$$

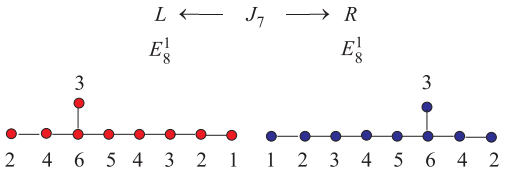

Fig. 13. The $E_8^{(1)}{}_L - E_8^{(1)}{}_R$ graph obtained from the eldest $(1,1,4,6)[12]$ polyhedron in chain XIX: $39 = 16_L + 7_J + 16_R$

Table 26. The group singularities of the dual pairs of elliptic polyhedra in chain XIX

$P^3(\mathbf{k})$	$H(\Delta)$	$H(\Delta^*)$	$G_L(\Delta)$	$G_R(\Delta)$	$G_L(\Delta^*)$	$G_R(\Delta^*)$
$(1,1,4,6)$	$m_1+2m_2+3m_3=0$	$m_1^*=0$	E_8	E_8	$SU(1)$	$SU(1)$
$(1,2,6,9)$	$m_1+2m_2+3m_3=0$	$m_1^*=0$	E_8	F_4	G_2	$SU(1)$
$(1,3,8,12)$	$m_1+2m_2+3m_3=0$	$m_1^*=0$	E_8	G_2	F_4	$SU(1)$
$(1,4,10,15)$	$m_1+2m_2+3m_3=0$	$m_1^*=0$	E_8	$SU(2)$	E_7	$SU(1)$
$(1,5,12,18)$	$m_1+2m_2+3m_3=0$	$m_1^*=0$	E_8	$SU(1)$	E_8	$SU(1)$
$(1,6,14,21)$	$m_1+2m_2+3m_3=0$	$m_1^*=0$	E_8	$SU(1)$	E_8	$SU(1)$

The seven invariant monomials corresponding to this chain are the following:

$$\begin{aligned}
\boldsymbol{\mu}_0^1 &= (6,6,0,0) \quad \Rightarrow \quad x^6\cdot y^6,\\
\boldsymbol{\mu}_0^2 &= (4,4,1,0) \quad \Rightarrow \quad x^4\cdot y^4\cdot z,\\
\boldsymbol{\mu}_0^3 &= (2,2,2,0) \quad \Rightarrow \quad x^2\cdot y^2\cdot z^2,\\
\boldsymbol{\mu}_0^4 &= (0,1,3,0) \quad \Rightarrow \quad y\cdot z^3,\\
\boldsymbol{\mu}_0^5 &= (3,3,0,1) \quad \Rightarrow \quad x^3\cdot y^3\cdot u,\\
\boldsymbol{\mu}_0^6 &= (1,1,1,1) \quad \Rightarrow \quad x\cdot y\cdot z\cdot u,\\
\boldsymbol{\mu}_0^7 &= (0,0,0,2) \quad \Rightarrow \quad u^2.
\end{aligned} \tag{8.25}$$

Using these invariant monomials and basis, the CY equations for all the $\mathbf{k}(l=m+n)$ projective vectors of this chain can be written in the following form:

$$F(\mathbf{z})_{m,n} = \sum_{j=1}^{j=7} \mathbf{z}^{\boldsymbol{\mu}_0^j}\{\sum_{p=1}^{p=\Pi_{jL}} a^{pL}_{\boldsymbol{\mu}_0^j}\cdot \mathbf{z}^{n_{pL}\cdot(-\mathbf{e}_1)} + \sum_{p=1}^{p=\Pi_{jR}} a^{pR}_{\boldsymbol{\mu}_0^j}\cdot \mathbf{z}^{-n_{pR}\cdot(-\mathbf{e}_1)}\}, \tag{8.26}$$

where the basis vector $\mathbf{e}_1 = (m,-n,0,0)$. The $E_8^{(1)}{}_L - E_8^{(1)}{}_R$ graph obtained from the eldest $(1,1,4,6)[12]$ polyhedron in chain XIX is shown in Table 26 and Figure 13.

9. PERSPECTIVES ON THE FURTHER CLASSIFICATION OF CY_3 AND $K3$ SPACES

Although a fuller study of CY_3 spaces lies outside the scope of this paper, a preliminary study is of interest here, for the following reason. In addition to the 95 $K3$ spaces (Table 1) related to the zeroes of single polynomials discussed in previous Sections, others can be found by «higher-level» constructions as the intersections of the loci of zeroes of quasi-homogeneous polynomials, which are obtainable from CY_3 spaces, as we now discuss.

When going on to consider the general construction of $\mathbf{k}_5$ projective vectors in CP^4 that describe CY_3 hypersurfaces, we start from the 95 simple extensions of these $K3$ vectors as well as 5 multiple extensions of lower-dimensional vectors, together with all their possible permutations. In accordance with the previous five forms of extended vectors, one finds the following sets and permutations: quadruply-extended basic vectors with the cyclic C_5 group of permutations:

$$\mathbf{k}_1^{ex} = (0,0,0,0,1), \quad |C_5| = 5, \tag{9.1}$$

triply-extended composite vectors with the dihedral D_5 group of permutations

$$\mathbf{k}_2^{ex} = (0,0,0,1,1), \quad |D_5| = 10, \tag{9.2}$$

the following doubly-extended composite vectors with the D_5', A_5', and A_5 groups of permutations

$$\mathbf{k}_3^{ex} = (0,0,1,1,1), \quad |D_5'| = 10, \tag{9.3}$$

$$\mathbf{k}_3^{ex} = (0,0,1,1,2), \quad |A_5'| = 30, \tag{9.4}$$

$$\mathbf{k}_3^{ex} = (0,0,1,2,3), \quad |A_5| = 60, \tag{9.5}$$

we recall that the alternating group of permutations A_5 can be identified with the icosahedral symmetry group I. All the other extended $\mathbf{k}_5$ vectors can be obtained similarly from 95 $K3$ vectors, utilising the symmetric group S_5 or some subgroups. The full set of extended $\mathbf{k}_5$ vectors is displayed in Table 27. As noted in its caption, the total number of extended vectors is 10 270.

As an illustration how our method may be used to classify CY_3 manifolds, we now describe briefly how to obtain the complete list of $\mathbf{k}_5$ vectors with $K3$ intersections, which we find to be distributed in 4242 chains. To build the chains for CY_3 which have a double-vector structure, each of which is parametrized by a pair of positive integers, one should find the «good» pairs of «extended» vectors (i.e., those whose intersection gives a reflexive $K3$ hypersurface), which involves checking all the $10\ 270 \times 10\ 271/2 = 52\ 731\ 315$ possible pairs of vectors from Table 27. It was just such a search by computer that led to the 4242 double

Table 27. The 100 distinct types of five-dimensional «extended» projective vectors used to construct CY_3 spaces, listed together with the orders of their permutation groups. Including these permutations, the total number of extended vectors is 10 270

ℵ	$\mathbf{k}_{5ex}^{(i)}$	$G(\mathrm{perm})$	ℵ	$\mathbf{k}_{5ex}{}^{(i)}$	$G(\mathrm{perm})$
i	(0, 0, 0, 0, 1)	5	46	(0, 2, 3, 4, 7)	120
ii	(0, 0, 0, 1, 1)	10	47	(0, 2, 3, 4, 9)	120
iii	(0, 0, 1, 1, 1)	10	48	(0, 2, 3, 5, 5)	60
iv	(0, 0, 1, 1, 2)	30	49	(0, 2, 3, 5, 7)	120
v	(0, 0, 1, 2, 3)	60	50	(0, 2, 3, 5, 8)	120
1	(0, 1, 1, 1, 1)	5	51	(0, 2, 3, 5, 10)	120
2	(0, 1, 1, 1, 2)	20	52	(0, 2, 3, 7, 9)	120
3	(0, 1, 1, 1, 3)	20	53	(0, 2, 3, 7, 12)	120
4	(0, 1, 1, 2, 2)	30	54	(0, 2, 3, 8, 11)	120
5	(0, 1, 1, 2, 3)	60	55	(0, 2, 3, 4, 7)	120
6	(0, 1, 1, 2, 4)	60	56	(0, 2, 3, 10, 15)	120
7	(0, 1, 1, 3, 4)	60	57	(0, 2, 4, 5, 9)	120
8	(0, 1, 1, 3, 5)	60	58	(0, 2, 4, 5, 11)	120
9	(0, 1, 1, 4, 6)	60	59	(0, 2, 5, 6, 7)	120
10	(0, 1, 2, 2, 3)	60	60	(0, 2, 5, 6, 13)	120
11	(0, 1, 2, 2, 5)	60	61	(0, 2, 5, 9, 11)	120
12	(0, 1, 2, 3, 3)	60	62	(0, 2, 5, 9, 16)	120
13	(0, 1, 2, 3, 4)	120	63	(0, 2, 5, 14, 21)	120
14	(0, 1, 2, 3, 5)	120	64	(0, 2, 6, 7, 15)	120
15	(0, 1, 2, 3, 6)	120	65	(0, 3, 3, 4, 5)	60
16	(0, 1, 2, 4, 5)	120	66	(0, 3, 4, 5, 6)	120
17	(0, 1, 2, 4, 7)	120	67	(0, 3, 4, 5, 7)	120
18	(0, 1, 2, 5, 7)	120	68	(0, 3, 4, 5, 8)	120
19	(0, 1, 2, 5, 8)	120	69	(0, 3, 4, 5, 12)	120
20	(0, 1, 2, 6, 9)	120	70	(0, 3, 4, 7, 10)	120
21	(0, 1, 3, 4, 4)	60	71	(0, 3, 4, 7, 14)	120
22	(0, 1, 3, 4, 5)	120	72	(0, 3, 4, 10, 13)	120
23	(0, 1, 3, 4, 7)	120	73	(0, 3, 4, 10, 17)	120
24	(0, 1, 3, 4, 8)	120	74	(0, 3, 4, 11, 18)	120
25	(0, 1, 3, 5, 6)	120	75	(0, 3, 4, 14, 21)	120
26	(0, 1, 3, 5, 9)	120	76	(0, 3, 5, 6, 7)	120
27	(0, 1, 3, 7, 10)	120	77	(0, 3, 5, 11, 14)	120
28	(0, 1, 3, 7, 11)	120	78	(0, 3, 5, 11, 19)	120
29	(0, 1, 3, 8, 12)	120	79	(0, 3, 5, 16, 24)	120
30	(0, 1, 4, 5, 6)	120	80	(0, 3, 6, 7, 8)	120
31	(0, 1, 4, 5, 10)	120	81	(0, 4, 5, 6, 9)	120
32	(0, 1, 4, 6, 7)	120	82	(0, 4, 5, 6, 15)	120
33	(0, 1, 4, 6, 11)	120	83	(0, 4, 5, 7, 9)	120
34	(0, 1, 4, 9, 14)	120	84	(0, 4, 5, 7, 16)	120
35	(0, 1, 4, 10, 15)	120	85	(0, 4, 5, 13, 22)	120
36	(0, 1, 5, 7, 8)	120	86	(0, 4, 5, 18, 27)	120
37	(0, 1, 5, 7, 13)	120	87	(0, 4, 6, 7, 11)	120
38	(0, 1, 5, 12, 18)	120	88	(0, 4, 6, 7, 17)	120
39	(0, 1, 6, 8, 9)	120	89	(0, 5, 6, 7, 9)	120
40	(0, 1, 6, 8, 15)	120	90	(0, 5, 6, 8, 11)	120
41	(0, 1, 6, 14, 21)	120	91	(0, 5, 6, 8, 19)	120
42	(0, 2, 2, 3, 5)	60	92	(0, 5, 6, 22, 33)	120
43	(0, 2, 2, 3, 7)	60	93	(0, 5, 7, 8, 20)	120
44	(0, 2, 3, 3, 4)	60	94	(0, 7, 8, 10, 25)	120
45	(0, 2, 3, 4, 5)	120	95	(0, 7, 8, 9, 12)	120

chains mentioned above, together with their eldest vectors. For more complete information about these chains, see [37].

These chains give many CY_3 projective vectors, but not all. The complete list also includes the «good» triples which have elliptic fibres. This requires looking for good triples among the following five types of five-dimensional extended vectors:

$$\begin{aligned} &1.\quad (0,0,0,0,1) \Rightarrow 5,\\ &2.\quad (0,0,0,1,1) \Rightarrow 10,\\ &3.\quad (0,0,1,1,1) \Rightarrow 10,\\ &4.\quad (0,0,1,1,2) \Rightarrow 30,\\ &5.\quad (0,0,1,2,3) \Rightarrow 60, \end{aligned} \tag{9.6}$$

where the number after the arrow on each line of (9.7) corresponds to the number of permutations in each case. We have found 259 such good triples, together with their eldest vectors, corresponding to 259 elliptic chains. The union of the $K3$ and elliptic projective vectors still does not yield the full dual set of $\mathbf{k_5}$ projective vectors. We must also construct another set of chains using quadruples from among the following multiply-extended vectors:

$$\begin{aligned} &1.\quad (0,0,0,0,1) \Rightarrow 5,\\ &2.\quad (0,0,0,1,1) \Rightarrow 10. \end{aligned} \tag{9.7}$$

The number of CY_3 chains found in this way is just six.

In addition to these 4242 double, 259 triple and 6 quadruple CY_3 chains (to be compared with the 22 double and 4 triple $K3$ chains found previously), one must find all the vectors whose intersection contains only one central interior point (to be compared with the exceptional $K3$ vector $(7,8,9,12)$). We have found just two such examples in the case of CY_3, namely $(41,48,51,52,64)$ and $(51,60,64,65,80)$, again using the intersection-projection duality technique. The eldest vectors for all the CY_3 projective vector chains we have found can be obtained from [37].

In the cases of dimension higher than three, the concept of intersection–projection duality is richer, and leads to one important and by now well-known consequence [7,33], namely the isomorphism between different homology groups for dual pairs of CY_d manifolds M, M^*, and specifically the following relation:

$$H^{p,q}(M) \sim H^{d-p,q}(M^*) \tag{9.8}$$

for $0 \leqslant p,q \leqslant d$. We leave a more complete discussion of duality of CY_3 spaces to future work, limiting our discussion here of their ramifications for the classification of $K3$.

Our construction based on the 10270 extended vectors obtained from the $100(= 95 + 5)$ types of projective vectors in lower dimensions $n = 1, 2, 3, 4$ shown in Table 27 yielded all the 4242 $(259, ...)$ eldest vectors representing CY_3 spaces with $K3$ (elliptic, ...) fibers. However, this method of construction simultaneously provides a new *higher-level* list of $K3$ spaces defined by planar polyhedra. To explain this, let us first assign to all $K3$ spaces defined by n-dimensional projective vectors *level zero*, and denote them by Π_0. Then, *level one* $K3$ spaces consist of all the «good» intersections* of two $(n+1)$-dimensional extended vectors, denoted by Π_1. This yields a list of reflexive polyhedra that is more complete than the previous list of polyhedra obtained from n-dimensional projective vectors, i.e., $\Pi_0 \subseteq \Pi_1$. Continuing, one may define the set of all «good» intersections of *level two*, Π_2, by considering the intersections of three $(n + 2)$-dimensional extended vectors, and similarly for the higher levels $3, 4, ...$:

$$\Pi_0 \subseteq \Pi_1 \subseteq \Pi_2 \subseteq ... \subseteq \Pi_{\rm last} \tag{9.9}$$

until this process gives us no new reflexive polyhedra. Since the number of distinct reflexive polyhedra in any dimension is finite, e.g., the maximal number of integer points for planar polyherdra is 10, for $K3$ polyhedra it is 39, etc., there exists a maximum last level, after which one cannot find any new types of polyhedra.

Following this approach in the simple case of CY_1 spaces, we recall that we found three planar polyhedra (triangles) at level zero, determined by the three projective vectors $(1, 1, 1)$, $(1, 1, 2)$ and $(1, 2, 3)$. At level one, constructing the 22 chains of $K3$ projective vectors via the 22 «good» intersections of the five types of four-dimensional extended vectors, we now find 7 new planar polyhedra in 9 of the 22 two-vector $K3$ chains, differing from the previous three triangles by the numbers of vertices (V, V^*) and/or by the numbers of integer points (N, N^*) and/or by the areas of these planar polyhedra, as shown in Table 28. To look for further new polyhedra at level 2, one should consider the five following types of vectors: $(1), (1, 1), (1, 1, 1), (1, 1, 2)$, and $(1, 2, 3)$, extended to five dimensions. Taking into account all the 50 possible permutations, and looking for the «good» triple intersections, we find among the 259 «good» planar reflexive polyhedra mentioned above just three distinct new polyhedra, which are exhibited in Table 29.

Extending this procedure, we found among the 4242 chains of CY_3 spaces with «good» intersections 730 new $K3$ polyhedra at level one, many with multiple realizations as in Tables 28 and 29. As an example how such new $K3$ spaces emerge, consider the following two-vector CY_3 chain: $m(0, 1, 1, 4, 6)+$

*In the sense that they give n-dimensional reflexive polyhedra.

Table 28. The 7 distinct new planar polyhedra, representing new CY_1 spaces, that are found as double intersections involving 9 of the 22 two-vector $K3$ chains. Two realizations each are given for 2 of the new polyhedra

ℵ	$\mathbf{k}_{4ex}^{(i)}$	$\mathbf{k}_{4ex}^{(i)}$	N, N^*	V, V^*
1	$(0,0,1,1)$	$(1,1,0,0)$	$9, 5^*$	$4, 4^*$
	$(0,0,1,1)$	$(1,1,0,1)$	$9, 5^*$	$4, 4^*$
2	$(0,0,1,1)$	$(1,2,0,1)$	$7, 7^*$	$4, 4^*$
3	$(0,1,1,1)$	$(1,0,1,2)$	$8, 6^*$	$4, 4^*$
4	$(0,1,1,1)$	$(3,0,1,2)$	$4, 10^*$	$3, 3^*$
5	$(0,1,1,2)$	$(1,1,2,0)$	$5, 9^*$	$3, 3^*$
	$(0,1,1,2)$	$(2,0,1,3)$	$5, 9^*$	$3, 3^*$
6	$(0,1,1,2)$	$(2,1,3,0)$	$6, 8^*$	$4, 4^*$
7	$(0,1,2,3)$	$(3,2,1,0)$	$5, 9^*$	$4, 4^*$

Table 29. The 3 distinct new planar polyhedra, representing new CY_1 spaces, that are obtainable as triple intersections of five-dimensional extended projective vectors, the sum of which gives the eldest CY_3 projective vector. Three realizations each are given for 2 of the new polyhedra

ℵ	$\mathbf{k}_{5ex}^{(i)}$	$\mathbf{k}_{5ex}^{(i)}$	$\mathbf{k}_{5ex}^{(i)}$	N, N^*	V, V^*
1	$(0,0,0,1,1)$	$(0,1,1,0,0)$	$(1,0,1,0,1)$	$8, 6^*$	$5, 5^*$
2	$(0,0,0,1,1)$	$(0,1,1,0,1)$	$(1,0,1,1,0)$	$7, 7^*$	$5, 5^*$
	$(0,0,0,1,1)$	$(0,1,1,0,1)$	$(1,1,2,0,0)$	$7, 7^*$	$5, 5^*$
	$(0,0,1,1,1)$	$(1,1,0,0,1)$	$(0,1,0,1,2)$	$7, 7^*$	$5, 5^*$
3	$(0,0,0,1,1)$	$(1,1,1,0,0)$	$(0,1,2,0,1)$	$6, 8^*$	$5, 5^*$
	$(0,0,0,1,1)$	$(0,1,2,0,1)$	$(2,1,0,1,0)$	$6, 8^*$	$5, 5^*$
	$(0,0,1,1,1)$	$(0,1,0,1,2)$	$(1,0,2,1,0)$	$6, 8^*$	$5, 5^*$

$+n(1,0,1,4,6)$. The maximum values of m and n are determined by the dimensions of these extended vectors, namely $d = 12$. This chain contains 46 different $\mathbf{k}_5$ projective vectors. The four-dimensional pentahedroid corresponding to the eldest vector in this chain is shown in Figure 14. As can be seen there, in addition to its 5 vertices, the pentahedroid has 10 one-dimensional edges, 10 two-dimensional triangular faces, and 5 three-dimensional tetrahedral facets.

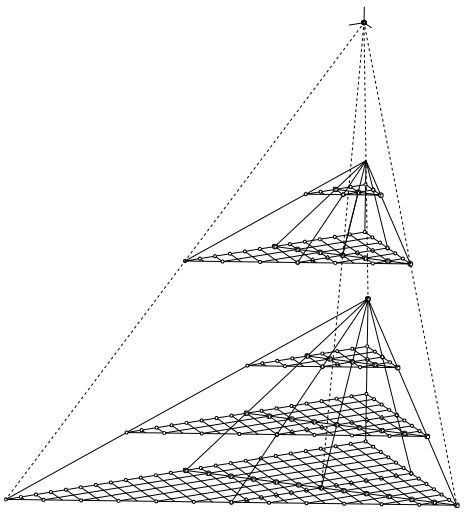

Fig. 14. The 4-dimensional pentahedroid corresponding to the CY_3 space specified by the eldest vector $\mathbf{k}_5 = (1,1,2,8,12)[24]$ in the two-vector chain $m(0,1,1,4,6)+$ $+n(1,0,1,4,6)$. The number of integer points in this pentahedroid is $N(S) = 335$, and the volume $S = 72$. $SL(4,Z)$ transformations produce an infinite number of polyhedroids, conserving the volume

This pentahedroid contains two realizations of the tetrahedron corresponding to $\mathbf{k}_4 = (1,1,4,6)$, whose intersection contains an elliptic fibre corresponding to $\mathbf{k}_3 = (1,2,3)$.

A snapshot of the complete $m(0,1,1,4,6)+n(1,0,1,4,6)$ chain is shown in Figure 15, where the number of points N in each member of the chain is plotted as a function of $d = k_1 + k_2 + k_3 + k_4 + k_5$ for each of the allowed values of m. We note a systematic tendency for N to *decrease* as d increases. (The structure of the chain is, of course, symmetric under the interchange: $n \leftrightarrow m$). The corresponding plot for the dual polyhedra is shown in Figure 16: here we see that the number of points N^* *increases* as d increases.

To get another impression of the rich new structures emerging at levels one and above, we consider a «tetrahedron subalgebra» of our $K3$ algebra, i.e., we consider only those projective vectors corresponding to point- and segment-polyhedra, triangles and tetrahedra. With this restriction, we start from only 32 $K3$ projective vectors, corresponding to four-vertex tetrahedra and five of our previous extended vectors. In this way, the number of reflexive polyhedra at level one is reduced to just 632, consisting of 460 tetrahedra and 172 reflexive polyhedra with numbers of vertices between 5 and 10. In this list of 632 polyhedra, there are actually only 146 distinct new types of polyhedra, as shown in

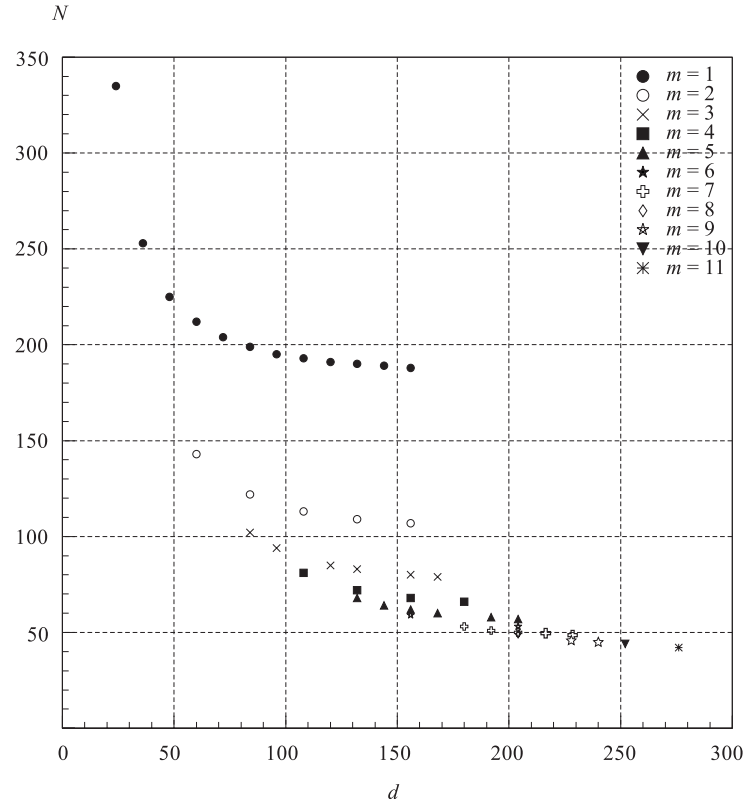

Fig. 15. The number of points N found in different members of the chain $m(0,1,1,4,6)+n(1,0,1,4,6)$, plotted as a function of $d = k_1 + k_2 + k_3 + k_4 + k_5$ for different values of m

Table 30. More information about them can be obtained from [37]: we leave their more detailed study to later work.

The method described here has a very simple geometrical interpretation. According to the chain structure, each CY_3 can have a complex internal structure, and correspondingly its vector can be extended as a sum of two $K3$, three elliptic, four two-component or five single-component extended vectors. Another nice feature of this chain structure is that it gives us complete information about the integer lattice which determines all the CY equations. Moreover, it also gives us the possibility of summarizing the singularity structure of CY_3 spaces. As we discussed in Section 8, the $K3$ polyhedron structure gives us a systematic way of classifying the corresponding Cartan–Lie algebra graphs. It will be interesting to make a full corresponding analysis for CY_3 hypersurfaces, taking duality into

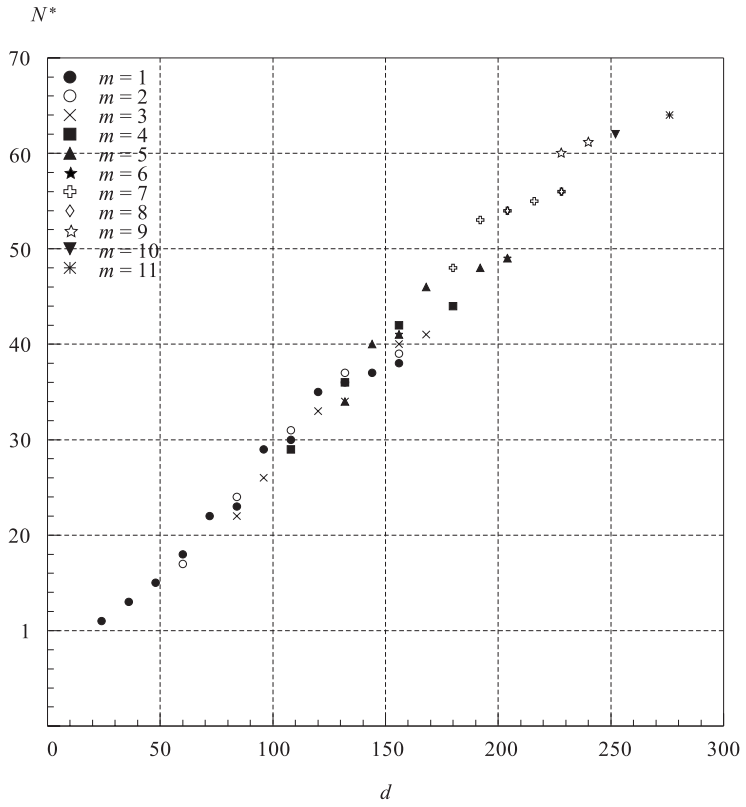

Fig. 16. The number of points N^* found in the polyhedra dual to the previous $m(0,1,1,4,6)+n(1,0,1,4,6)$ chain, plotted as a function of $d = k_1+k_2+k_3+k_4+k_5$ for different values of m

account. This method could also provide the full classification of Betti–Hodge topological numbers for CY_3 manifolds. Moreover, this algebraic method enables us to «walk» between different dimensions, e.g., to classify CY_4, ...$_5$,... manifolds (Figure 1). The greatest limitations may be our abilities to analyze this algebra and/or the available computer resources.

A fuller analysis of our structural classification of the $\mathbf{k}_5$ vectors for CY_3 manifolds will be given in later work. An important aspect of this procedure is that we can study the structures of the positive-integer lattices which correspond to the $\mathbf{k}$ vectors, introducing the corresponding modular (for two-dimensional sublattices) and hypermodular (for 3-, 4- or higher-dimensional lattices) transformations. These yield duality groups that are more general than the well-known S, T and U dualities, including them as subgroups. Moreover, the study of the

Table 30. The 146 distinct new polyhedra, representing new $K3$ spaces, that are obtainable as double intersections of projective vectors in the «tetrahedron subalgebra» containing only point- and segment-polyhedra, triangles and tetrahedra. Many of these have several different realizations as double intersections: more details can be found in [37]

א	N, N^*	V, V^*	Pic, Pic*	א	N, N^*	V, V^*	Pic, Pic*	א	N, N^*	V, V^*	Pic, Pic*
1	$31, 6^*$	$6, 5^*$	$2, 18^*$	51	$14, 19^*$	$7, 6^*$	$13, 8^*$	101	$22, 20^*$	$5, 5^*$	$10, 11^*$
2	$28, 9^*$	$7, 6^*$	$4, 16^*$	52	$26, 8^*$	$6, 5^*$	$4, 17^*$	102	$20, 16^*$	$5, 5^*$	$10, 13^*$
3	$29, 7^*$	$6, 5^*$	$4, 17^*$	53	$25, 14^*$	$6, 6^*$	$7, 13^*$	103	$24, 18^*$	$5, 5^*$	$9, 12^*$
4	$22, 8^*$	$6, 5^*$	$7, 16^*$	54	$15, 21^*$	$5, 5^*$	$12, 10^*$	104	$15, 21^*$	$4, 4^*$	$14, 10^*$
5	$31, 9^*$	$6, 5^*$	$3, 17^*$	55	$22, 16^*$	$6, 6^*$	$9, 11^*$	105	$21, 15^*$	$4, 4^*$	$10, 14^*$
6	$21, 12^*$	$7, 6^*$	$8, 13^*$	56	$12, 18^*$	$6, 7^*$	$13, 10^*$	106	$10, 26^*$	$5, 6^*$	$15, 7^*$
7	$17, 20^*$	$7, 7^*$	$11, 9^*$	57	$17, 13^*$	$6, 6^*$	$10, 13^*$	107	$10, 32^*$	$6, 6^*$	$16, 4^*$
8	$22, 14^*$	$6, 6^*$	$8, 13^*$	58	$24, 12^*$	$5, 5^*$	$7, 14^*$	108	$19, 14^*$	$5, 5^*$	$11, 13^*$
9	$24, 12^*$	$6, 5^*$	$7, 14^*$	59	$15, 15^*$	$4, 4^*$	$14, 12^*$	109	$16, 26^*$	$5, 5^*$	$13, 8^*$
10	$20, 12^*$	$6, 6^*$	$10, 13^*$	60	$20, 11^*$	$7, 6^*$	$9, 14^*$	110	$12, 27^*$	$5, 5^*$	$15, 7^*$
11	$20, 20^*$	$6, 6^*$	$10, 10^*$	61	$10, 20^*$	$5, 6^*$	$16, 9^*$	111	$15, 15^*$	$5, 5^*$	$12, 13^*$
12	$13, 14^*$	$6, 6^*$	$13, 11^*$	62	$11, 14^*$	$6, 6^*$	$14, 12^*$	112	$10, 23^*$	$6, 6^*$	$15, 7^*$
13	$26, 8^*$	$6, 5^*$	$5, 17^*$	63	$24, 18^*$	$5, 5^*$	$8, 12^*$	113	$6, 34^*$	$5, 6^*$	$18, 2^*$
14	$26, 7^*$	$6, 5^*$	$5, 17^*$	64	$16, 17^*$	$6, 6^*$	$11, 11^*$	114	$25, 11^*$	$5, 5^*$	$8, 15^*$
15	$18, 8^*$	$6, 5^*$	$9, 16^*$	65	$8, 26^*$	$5, 6^*$	$17, 5^*$	115	$15, 15^*$	$4, 4^*$	$13, 13^*$
16	$24, 10^*$	$6, 6^*$	$6, 15^*$	66	$14, 11^*$	$7, 6^*$	$12, 14^*$	116	$14, 16^*$	$5, 5^*$	$12, 13^*$
17	$11, 11^*$	$4, 4^*$	$15, 15^*$	67	$8, 26^*$	$6, 7^*$	$17, 3^*$	117	$9, 27^*$	$5, 5^*$	$16, 6^*$
18	$21, 17^*$	$7, 7^*$	$9, 11^*$	68	$21, 19^*$	$6, 6^*$	$10, 10^*$	118	$10, 26^*$	$6, 6^*$	$16, 6^*$
19	$14, 15^*$	$6, 6^*$	$12, 11^*$	69	$12, 12^*$	$4, 4^*$	$14, 14^*$	119	$22, 14^*$	$5, 5^*$	$9, 14^*$
20	$23, 11^*$	$5, 5^*$	$7, 15^*$	70	$10, 17^*$	$5, 6^*$	$15, 11^*$	120	$7, 31^*$	$5, 6^*$	$17, 3^*$
21	$10, 20^*$	$7, 7^*$	$15, 7^*$	71	$9, 15^*$	$4, 4^*$	$16, 12^*$	121	$15, 15^*$	$5, 5^*$	$13, 12^*$
22	$7, 23^*$	$5, 6^*$	$17, 5^*$	72	$8, 23^*$	$5, 6^*$	$16, 8^*$	122	$15, 15^*$	$4, 4^*$	$12, 14^*$
23	$10, 14^*$	$5, 6^*$	$15, 12^*$	73	$24, 12^*$	$6, 6^*$	$8, 14^*$	123	$19, 11^*$	$5, 5^*$	$10, 14^*$
24	$12, 12^*$	$6, 6^*$	$13, 13^*$	74	$19, 11^*$	$4, 4^*$	$11, 14^*$	124	$12, 18^*$	$6, 6^*$	$14, 10^*$
25	$6, 30^*$	$4, 4^*$	$18, 4^*$	75	$11, 19^*$	$4, 4^*$	$17, 10^*$	125	$11, 17^*$	$5, 5^*$	$14, 11^*$
26	$25, 11^*$	$6, 6^*$	$6, 14^*$	76	$19, 11^*$	$4, 4^*$	$10, 17^*$	126	$20, 14^*$	$6, 6^*$	$7, 14^*$
27	$12, 12^*$	$4, 4^*$	$16, 14^*$	77	$8, 24^*$	$5, 6^*$	$16, 7^*$	127	$14, 16^*$	$5, 5^*$	$13, 12^*$
28	$21, 9^*$	$4, 4^*$	$9, 17^*$	78	$31, 11^*$	$5, 5^*$	$5, 16^*$	128	$19, 17^*$	$5, 5^*$	$11, 12^*$
29	$15, 15^*$	$5, 6^*$	$11, 12^*$	79	$20, 22^*$	$5, 5^*$	$11, 10^*$	129	$12, 24^*$	$5, 5^*$	$15, 8^*$
30	$12, 12^*$	$4, 4^*$	$14, 16^*$	80	$26, 10^*$	$6, 5^*$	$3, 17^*$	130	$12, 20^*$	$6, 6^*$	$13, 10^*$
31	$31, 8^*$	$5, 5^*$	$4, 17^*$	81	$26, 10^*$	$5, 5^*$	$7, 16^*$	131	$12, 24^*$	$5, 5^*$	$14, 9^*$
32	$17, 11^*$	$6, 5^*$	$9, 16^*$	82	$19, 11^*$	$4, 4^*$	$10, 16^*$	132	$7, 26^*$	$5, 6^*$	$17, 5^*$
33	$20, 10^*$	$5, 5^*$	$9, 16^*$	83	$16, 14^*$	$5, 5^*$	$12, 14^*$	133	$11, 28^*$	$7, 7^*$	$15, 5^*$
34	$18, 12^*$	$5, 5^*$	$11, 14^*$	84	$14, 16^*$	$6, 6^*$	$12, 12^*$	134	$9, 33^*$	$5, 5^*$	$16, 4^*$
35	$15, 12^*$	$4, 4^*$	$13, 13^*$	85	$23, 13^*$	$5, 5^*$	$9, 14^*$	135	$14, 28^*$	$5, 5^*$	$14, 7^*$
36	$9, 21^*$	$4, 4^*$	$17, 9^*$	86	$23, 10^*$	$5, 5^*$	$8, 15^*$	136	$10, 29^*$	$6, 6^*$	$15, 5^*$
37	$25, 17^*$	$6, 6^*$	$8, 12^*$	87	$14, 16^*$	$6, 5^*$	$14, 11^*$	137	$11, 25^*$	$5, 5^*$	$15, 8^*$
38	$15, 21^*$	$5, 5^*$	$13, 10^*$	88	$12, 18^*$	$6, 6^*$	$15, 10^*$	138	$17, 26^*$	$6, 6^*$	$12, 8^*$
39	$17, 10^*$	$6, 5^*$	$11, 15^*$	89	$29, 13^*$	$5, 5^*$	$6, 15^*$	139	$15, 18^*$	$5, 5^*$	$13, 11^*$
40	$10, 23^*$	$6, 6^*$	$16, 7^*$	90	$17, 19^*$	$5, 5^*$	$12, 11^*$	140	$11, 19^*$	$5, 5^*$	$16, 10^*$
41	$13, 28^*$	$7, 7^*$	$14, 6^*$	91	$11, 19^*$	$4, 4^*$	$16, 10^*$	141	$20, 25^*$	$5, 5^*$	$11, 9^*$
42	$24, 21^*$	$5, 5^*$	$9, 11^*$	92	$14, 16^*$	$6, 6^*$	$13, 11^*$	142	$10, 26^*$	$5, 5^*$	$16, 7^*$
43	$9, 24^*$	$5, 5^*$	$17, 7^*$	93	$10, 24^*$	$6, 6^*$	$15, 6^*$	143	$11, 25^*$	$6, 6^*$	$15, 7^*$
44	$12, 30^*$	$6, 6^*$	$15, 5^*$	94	$8, 34^*$	$5, 6^*$	$17, 3^*$	144	$9, 33^*$	$5, 5^*$	$17, 4^*$
45	$21, 9^*$	$5, 5^*$	$8, 16^*$	95	$14, 16^*$	$5, 5^*$	$14, 12^*$	145	$11, 13^*$	$5, 5^*$	$14, 13^*$
46	$16, 11^*$	$6, 5^*$	$11, 13^*$	96	$16, 15^*$	$7, 6^*$	$12, 12^*$	146	$9, 36^*$	$5, 5^*$	$17, 3^*$
47	$11, 16^*$	$7, 7^*$	$13, 9^*$	97	$11, 31^*$	$5, 5^*$	$16, 5^*$				
48	$26, 10^*$	$6, 5^*$	$6, 15^*$	98	$9, 30^*$	$6, 7^*$	$16, 4^*$				
49	$18, 12^*$	$6, 5^*$	$11, 13^*$	99	$14, 10^*$	$6, 5^*$	$12, 15^*$				
50	$12, 22^*$	$6, 7^*$	$14, 8^*$	100	$9, 28^*$	$6, 7^*$	$16, 5^*$				

geometric properties of the one-dimensional complex torus, two-dimensional $K3$ hypersurfaces and Calabi–Yau manifolds with dimensions $d = 3, 4, ...$ gives insight into the possible rank and dimensions of the Lie algebras which may be important for the understanding of the nature of the symmetries used in high-energy physics.

Acknowledgements. G.V. thanks H.Dahmen, G.Harigel, L.Fellin, V.Petrov, A.Zichichi and the CERN Theory Division for support. We all thank F.Cindolo and A.Toukhtarov for technical help and support. The work of D.V.N. was supported in part by DOE grant No. DE-FG-0395ER40917.

REFERENCES

1. **Schwarz J.** — Nucl. Phys. Proc. Suppl., 1997, v.B55, p.1;
   Polchinski J. — String Duality: A Colloquium, Rev. Mod. Phys., 1996, v.68, p.1245; TASI Lectures on D-Branes, NSF-ITP-96-145; hep-th/9611050;
   Sen A. — Unification of String Dualities, Nucl. Phys. Proc. Suppl., 1997, v.58, p.5; An Introduction to Nonperturbative String Theory, MRI-PHY-P980235; hep-th/9802051;
   Duff M. — M-Theory (The theory formerly known as strings), Int. J. Mod. Phys., 1996, v.A11, p.5623;
   Townsend P. — Four Lectures on M-Theory, DAMTP-R-96-58; hep-th/9612121;
   Douglas M. — Superstring Dualities, Dirichlet Branes and the Small Scale Structure of Space, RU-96-91; hep-th/9610041;
   Förste S., Louis J. — Quaternions and M-Theory in Spaces with Boundaries, HEP-UK-0002; hep-th/9612198;
   Vafa C. — Lectures on Strings and Dualities, HUTP-97-A009; hep-th/9702201;
   Ibáñez L.E., Uranga A. — $D = 6, N = 1$ String Vacua and Duality, FTUAM-97-9; hep-th/9707075;
   Gómez C., Hernández R. — Fields, Strings and Branes, IFT-UAM-CSIC-97-4; hep-th/9711102.
2. **Polchinski J.** — Dirichlet-Branes and Ramond-Ramond Charges, Phys. Rev. Lett., 1995, v.75, p.4724;
   Townsend P. — D-Branes from M-Branes, Phys.Lett., 1995, v.B360, p.13;
   Bachas C. — Lectures on D-Branes, CPHT-CL-615-0698; hep-th/9806199;
   Bachas C. — Scales of String Theory, Class. Quant. Grav., 2000, v.17, p.1.
3. **Aldazabal G., Ibáñez L.E., Quevedo F.** — A D-Brane Alternative to the MSSM, FTUAM-2000-001; hep-ph/0001083;
   Berglund P., Ellis J., Faraggi A., Nanopoulos D.V., Qiu Z. — Elevating the Free-Fermion $Z_2 \times Z_2$ Orbifold Model to a Compactification of F-Theory, ACT-12-98; hep-th/9812141;
   Antoniadis I. — Mass Scales in String and M-Theory, CPHT-CL741; hep-th/9909212.
4. **Calabi E.** — On Kahler Manifolds with Vanishing Canonical Class, in: Algebraic Geometry and Topology, A Symposium in Honor of S. Lefshetz, 1955, Princeton University Press, Princeton, NJ, 1957;
   Yau S.-T. — Calabi's Conjecture and Some New Results in Algebraic Geometry, Proc. Nat. Acad. Sci., 1977, v.74, p.1798;
   Candelas P., Horowitz G., Strominger A., Witten E. — Nucl. Phys., 1985, v.B258, p.46;
   Hübsch T. — Calabi–Yau Manifolds — A Bestiary for Physicists. World Scientific Pub. Co., Singapore, 1992.
5. **Satake I.** — On a Generalization of the Notion of Manifold, Proc. Nat. Acad. Sci. USA, 1956, v.42, p.359;

Dixon L., Harvey J.A., Vafa C., Witten E. — Strings on Orbifolds, Nucl. Phys., 1985, v.B261, p.678, and 1986, v.B274, p.285.

6. **Schwarz J.H.** — Introduction to M-Theory and AdS/CFT Duality, CALT-68-2204; hep-th/9812037 and references therein;
Duff M. — TASI Lectures on Branes, Black Holes and Anti-de Sitter Space, UM-TH-99-07; hep-th/9912164;
Greene B. — D-Brane Topology Changing Transitions, Nucl. Phys., 1998, v.B525, p.284;
Greene B., Lazaroiu C., Raugas M. — D-Branes on Non-Abelian Threefold Quotient Singularities, Nucl. Phys., 1999, v.B553, p.711.
7. **Batyrev V.** — Dual Polyhedra and Mirror Symmetry for Calabi–Yau Hypersurfaces in Toric Varieties, J. Algebraic Geom., 1994, v.3, p.493;
Batyrev V. — Variations of the Mixed Hodge Structure of Affine Hypersurfaces in Algebraic Tori, Duke Math. J., 1993, v.69, p.349;
Batyrev V., Cox D. — On the Hodge Structure of Projective Hypersurfaces in Toric Varieties, Duke Math. J., 1994, v.75, p.293.
8. **Aspinwall P.** — K3 Surfaces and String Duality, RU-96-98; hep-th/9611137;
Kreuzer M., Skarke H. — Classification of Reflexive Polyhedra in Three Dimensions, Adv. Theor. Math. Phys., 1998, v.2, p.847;
Nikulin V.V. — Surfaces of Type K3 with Finite Automorphism Group and Picard Group of Rank Three, Proc. Steklov Math. Inst.,1985, v.3, p.95;
Kreuzer M., Skarke H. — Reflexive Polyhedra, Weights and Toric Calabi–Yau Fibrations, HUB-EP-00/03, TUW-00/01, math.AG/0001106.
9. **Font A., Ibáñez L., Lüst D., Quevedo F.** — Strong-Weak Coupling Duality and Nonperturbative Effects in String Theory, Phys. Lett., 1990, v.B249, p.35;
Sen A. — Strong-Weak Coupling Duality in Four-Dimensional Field Theory, Int. J. Mod. Phys., 1994, v.A9, p.3707;
Hull C., Townsend P. — Unity of Superstring Dualities, Nucl. Phys., 1995, v.B438, p.109;
Duff M. — Strong/Weak Coupling Duality from the Dual String, Nucl. Phys., 1995, v.B442, p.47;
Townsend P. — The Eleven-Dimensional Supermembrane Revisited, Phys. Lett., 1995, v.B350, p.184;
Witten E. — String Theory Dynamics in Various Dimensions, Nucl. Phys., 1995, v.B443, p.85;
Sen A. — String-String Duality Conjecture in Six Dimensions and Charged Solitonic Strings, Nucl. Phys., 1995, v.B450, p.103;
Schwarz J., Sen A. — Nucl. Phys., 1994, v.B411, p.35.
10. **Alvarez-Gaume L., Zamora F.** — Duality in Quantum Field Theory (and String Theory), CERN-TH/97-257; hep-th/9709180.
11. **Dixon L.** — Some World-Sheet Properties of Superstring Compactifications on Orbifolds and Otherwise, in: Superstrings, Unified Theories, and Cosmology, 1987. World Scientific Pub. Co., Singapore, New Jersey, Hong Kong, 1988, p.67.
12. **Lerche W., Vafa C., Warner N.** — Chiral Rings in N=2 Superconformal Theories, Nucl. Phys., 1989, v.B324, p.251.
13. **Candelas P., Lynker M., Schimmrigk R.** — Calabi–Yau Manifolds in Weighted P_4, Nucl. Phys., 1990, v.B341, p.383.
14. **Roan S.** — The Mirror of Calabi–Yau Orbifold, Internat. J. Math., 1991, v.2, p.439.
15. **Aspinwall P., Greene B., Morrison D.** — The Monomial-Divisor Mirror Map, alg-geom/9309007.
16. **King B.** — Beyond the Quartic Equation. Birkhäuser, Boston, 1996;
Ribenboim P. — Fermat's Last Theorem. Springer-Verlag, New York, 1999.

17. **Lang S.** — Elliptic Functions. Addison-Wesley Pub. Co., Reading, Massachusetts, 1973.

18. **Bershadsky M., Johansen A., Pantev T., Sadov V., Vafa C.** — F-Theory, Geometric Engineering and $N = 1$ Dualities, Nucl. Phys., 1997, v.B505, p.153;
Katz S., Vafa C. — Geometric Engineering of $N = 1$ Quantum Field Theories, Nucl. Phys., 1997, v.B497, p.196;
Katz S., Vafa C. — Matter from Geometry, Nucl. Phys., 1997, v.B497, p.146;
Douglas M., Katz S., Vafa C. — Small Instantons, del Pezzo Surfaces and Type-II Theory, Nucl. Phys., 1997, v.B497, p.155.

19. **Duff M., Minasian R., Witten E.** — Evidence for Heterotic/Heterotic Duality, Nucl. Phys., 1996, v.B465, p.413;
Witten E. — Small Instantons in String Theory, Nucl. Phys., 1996, v.B460, p.541;
Polchinski J., Witten E. — Evidence for Heterotic — Type I String Duality, Nucl. Phys., 1996, v.B460, p.525;
Sethi S., Vafa C., Witten E. — Constraints on Low-Dimensional String Compactifications, Nucl. Phys., 1996, v.B480, p.213;
Horava P., Witten E. — Eleven-Dimensional Supergravity on a Manifold with Boundary, Nucl. Phys., 1996, v.B475, p.94;
Candelas P., Perevalov E., Rajesh G. — F-Theory Duals of Nonperturbative Heterotic $E_8 \times E_8$ Vacua in Six Dimensions, Nucl. Phys., 1997, v.B502, p.613;
Morrison D., Vafa C. — Compactifications of F-Theory on Calabi–Yau Threefolds–I, Nucl. Phys., 1996, v.B473, p.74;
Aldazabal G., Font A., Ibáñez L.E., Uranga A.M. — New Branches of String Compactifications and Their F-Theory Duals, Nucl. Phys., 1997, v.B492, p.119;
Klemm A., Lian B., Roan S-S., Yau S. — Calabi–Yau Fourfolds for M- and F-Theory Compactifications, Nucl. Phys., 1998, v.B518, p.515;
Aspinwall P., Katz S., Morrison D. — Lie Groups, Calabi–Yau Threefolds, and F-Theory, DUKE-CGTP-00-02, OSU-Math-2000-3; hep-th/0002012.

20. **Douglas M.** — Enhanced Gauge Symmetry in M-Theory, JHEP, 1997, 9707, p.004;
Greene B., Morrison D., Strominger A. — Black Hole Condensation and the Unification of String Vacua, Nucl. Phys., 1995, v.B451, p.109;
Strominger A. — Massless Black Holes and Conifolds in String Theory, Nucl. Phys., 1995, v.B451, p.96;
Strominger A. — Statistical Hair on Black Holes, Phys. Rev. Lett., 1996, v.77, p.3498;
Strominger A. — Black Hole Condensation and Duality in String Theory, Nucl. Phys. Proc. Suppl., 1996, v.46, p.204.

21. **Schlichenmaier M.** — An Introduction to Riemann Surfaces, Algebraic Curves and Moduli Spaces. Springer-Verlag, Berlin, Heildeberg, 1989.

22. **Shafarevich I.** — Basic Algebraic Geometry 1,2. Springer-Verlag, Berlin, 1994.

23. **Kostrikin A., Shafarevich I.** — Algebra. Springer-Verlag, Berlin, 1990.

24. **Dimka A.** — Singularities and Topology of Hypersurfaces. Springer-Verlag, Berlin, 1992.

25. **Barth W., Peters C., Van de Ven A.** — Compact Complex Surfaces. Springer-Verlag, Berlin, 1984.

26. **Miranda R.** — Smooth Models for Elliptic Threefolds, in: The Birational Geometry of Degenerations, R. Friedman and D.R. Morrison (eds.), Birkhäuser, Boston, 1983.

27. **Greene B., Plesser M.** — Duality in Calabi–Yau Moduli Spaces, Nucl. Phys., 1990, v.B338, p.38.

28. **Lamotke K.** — Regular Solids and Isolated Singularities, Advanced Lectures in Mathematics. Braunschweig, Wiesbaden, Vieweg, 1986.

29. **Cox D.** — Recent Developments in Toric Geometry, in: Proc. Sympos. Pure Math., v.62, Part 2, Amer. Math. Soc., Providence, RI, 1997; alg-geom/9606016.

30. **Du Val P.** — Homographies, Quaternions and Rotations. Clarendon Press, Oxford, 1964;
Dimca A. — Singularities and Topology of Hypersurfaces. Springer-Verlag, New York, 1992;
Barth W., Peters C., Van de Ven A. — Compact Complex Surfaces. Springer-Verlag, Berlin, Heidelberg, 1984.

31. **Parker Manning H.** — Geometry of Four Dimensions. Dover Pub. Inc., New York, 1956.

32. **Fulton W.** — Introduction to Toric Varieties. Princeton Univ. Press, Princeton, NJ, 1993.

33. **Greene B.R.** — String Theory on Calabi–Yau Manifolds, CU-TP-812; hep-th/9702155.

34. **Candelas P., Font A.** — Duality Between the Webs of Heterotic and Type II Vacua, Nucl. Phys., 1998, v.B511, p.295;
Candelas P., Perevalov E., Rajesh G. — Toric Geometry and Enhanced Gauge Symmetry of F-Theory/Heterotic Vacua, Nucl. Phys., 1997, v.B507, p.445;
Candelas P., Perevalov E., Rajesh G. — Matter from Toric Geometry, Nucl. Phys., 1998, v.B519, p.225;
Candelas P., Skarke H. — F-Theory, SO(32) and Toric Geometry, Phys. Lett., 1997, v.B413, p.63;
Perevalov E., Skarke H. — Enhanced Gauge Symmetry in Type II and F-Theory Compactifications: Dynkin Diagrams from Polyhedra, Nucl. Phys., 1997, v.B505, p.679;
Perevalov E. — On the Hypermultiplet Moduli Space of Heterotic Compactifications with Small Instantons; hep-th/9812253;
Skarke H. — String Dualities and Toric Geometry: An Introduction, UTTG-09-97; hep-th/9806059.

35. **Bershadsky M., Intriligator K., Kachru S., Morrison D.R., Sadov V., Vafa C.** — Geometric Singularities and Enhanced Gauge Symmetries, Nucl. Phys., 1996, v.B481, p.215.

36. **Tate J.** — Algorithm for Determining the Type of a Singular Fiber in an Elliptic Pencil, in: Modular Functions of One Variable IV, Lecture Notes in Math., v.476. Springer-Verlag, Berlin, 1975.

37. Files containing these lists are available on request from `Francesco.Anselmo@cern.ch`.

«ФИЗИКА ЭЛЕМЕНТАРНЫХ ЧАСТИЦ И АТОМНОГО ЯДРА»
2001, ТОМ 32, ВЫП. 3

УДК 539.12

ЭКСПЕРИМЕНТАЛЬНЫЙ СТАТУС ЭЛЕКТРИЧЕСКОЙ И МАГНИТНОЙ ПОЛЯРИЗУЕМОСТЕЙ ПРОТОНА

П.С.Баранов, А.И.Львов, В.А.Петрунькин, Л.Н.Штарков

Физический институт им. П.Н.Лебедева РАН, Москва

Впервые выполнен совместный анализ всех (ранних и поздних) экспериментальных данных по дифференциальному сечению упругого γp-рассеяния при энергиях фотонов $\omega < 150$ МэВ с целью определения электрической (α_p) и магнитной (β_p) поляризуемостей протона. Фитирование данных теоретическим сечением с двумя свободными параметрами α_p и β_p, полученным на основе s-канальных дисперсионных соотношений при конечной энергии, дает мировые средние экспериментальные значения поляризуемостей протона: $\alpha_p^{\text{эксп}} = 11{,}7 \pm 0{,}8 \pm 0{,}7$ и $\beta_p^{\text{эксп}} = 2{,}3 \pm 0{,}9 \pm 0{,}7$ (в ед. 10^{-4} фм^3), где первая погрешность (комбинированная) учитывает статистические и систематические погрешности экспериментальных сечений, а вторая — теоретические неопределенности дисперсионного сечения. Отмечается, что более полные и точные данные при $\omega \lesssim 100$ МэВ позволят в будущем уменьшить теоретические и экспериментальные погрешности в извлекаемых значениях α_p и β_p.

For the first time a global analysis of all (early and recent) experimental data on the differential cross section of elastic γp scattering at photon energies $\omega < 150$ MeV is fulfilled in order to determine the electric (α_p) and (β_p) polarizabilities of the proton. Fit of the data with the two free parameters α_p and β_p embedded into a theoretical cross section obtained on the basis of finite-energy s-channel dispersion relations gives the world-average for the values of the proton electromagnetic polarizabilities: $\alpha_p^{\text{exp}} = 11.7 \pm 0.8 \pm 0.7$ and $\beta_p^{\text{exp}} = 2.3 \pm 0.9 \pm 0.7$ (in units of 10^{-4} fm^3), where the first error (combined) takes into account statistical and systematic errors of the experimental cross section and the second error does theoretical uncertainties in the dispersion cross section. It is emphasized that more complete and precise data at $\omega \lesssim 100$ MeV will enable one to reduce theoretical and experimental errors in the extracted values of α_p and β_p.

1. ВВЕДЕНИЕ

В последние годы заметно вырос интерес к изучению свойства поляризуемости нуклонов и пионов, то есть наведения у них дипольных моментов внешним электромагнитным полем, и его влияния на различные двухфотонные процессы с участием этих частиц. В этой связи на электронных ускорителях BNL, MAMI, SAL и других исследовательских центров выполнены новые измерения [1–8] дифференциального сечения упругого рассеяния фотона (УРФ) на протоне при низких энергиях падающего фотона в л.с. $\omega \leq 150$ МэВ и в окрестности Δ_{33}-резонанса, и по полученным данным

повторно определены значения электрической и магнитной поляризуемостей протона α_p и β_p соответственно. Из данных по другим процессам извлекались также поляризуемости нейтрона, заряженного и нейтрального пионов*. Найденные разными группами экспериментальные значения поляризуемостей нейтрона и пионов плохо согласуются между собой; здесь необходимы как более точные измерения соответствующих сечений, так и развитие методов извлечения поляризуемостей из данных. Положение с экспериментальными значениями поляризуемостей протона в целом лучше, и его анализу посвящена настоящая работа. В отличие от [4,8] мы обсуждаем как поздние, так и ранние данные по УРФ на протоне ниже порога фоторождения пионов, часть которых не использовалась прежде для определения поляризуемостей α_p и β_p.

Впервые значения α_p и β_p были экспериментально определены в Физическом институте им. П.Н.Лебедева (ФИАН) [23, 24]. С пучком тормозного излучения измерялось дифференциальное сечение УРФ протоном при углах рассеяния фотона в л.с. $\theta \geq 75^\circ$ в трех энергетических интервалах с шириной $20 \div 40$ МэВ и со средними энергиями падающего фотона $\langle\omega\rangle$, равными 55 [23], 83 и 109 МэВ [24]. По числу точек углового распределения (5 точек) работа [23] и до настоящего времени остается наиболее полной при низких энергиях. Систематические погрешности в полученных значениях сечения равны $6\,\%$ в [23] и $1-3,7\,\%$ в [24] (по поводу последней см. разд. 2). Статистическая погрешность была $4-6\,\%$. Оказалось, что экспериментальное дифференциальное сечение при фиксированном угле θ и разных ω лежит ниже дифференциального сечения Поуэлла [25], которое описывает рассеяние фотона на точечном протоне с аномальным магнитным моментом (а.м.м.). В [23, 24] наблюдаемое отклонение интерпретировалось как специфическое проявление структуры протона в двухфотонном процессе, то есть как влияние на УРФ свойства поляризуемости протона [26–28]. Чтобы определить поляризуемости протона, экспериментальные значения сечений фитировались безмодельным низкоэнергетическим, то есть разложенным по ω с точностью до ω^2- или ω^3-членов, дифференциальным сечением, зависящим от неизвестных параметров α_p и β_p [28, 29]. В результате были получены экспериментальные значения α_p и β_p, воспроизведенные в табл. 1.

*История попыток определить электрическую поляризуемость нейтрона α_n в экспериментах по рассеянию реакторных нейтронов тяжелыми ядрами насчитывает четыре десятилетия [9]. Этим методом были получены значения $\alpha_n^{\text{эксп}} = (12{,}0 \pm 1{,}5\ (\text{стат.}) \pm 2{,}0\ (\text{сист.})) \cdot 10^{-4}$ фм^3 [10] и $\alpha_n^{\text{эксп}} = (0 \pm 5) \cdot 10^{-4}$ фм^3 [11]. Впрочем, выполненный в [12] анализ показал, что систематическая ошибка в значении $\alpha_n^{\text{эксп}}$ из [10], по-видимому, сильно занижена. С приблизительно той же точностью поляризуемости нейтрона можно извлекать также из данных по неупругому [13,14] и упругому [15,16] γd-рассеянию. После первых экспериментов в 80-е годы [17,18] поляризуемости пионов извлекались в последнее время из данных о процессах $\gamma\gamma \to \pi^+\pi^-$ и $\gamma\gamma \to \pi^0\pi^0$ (см., например, [19–22]).

Таблица 1. Поляризуемости протона (в ед. 10^{-4} фм^3) по публикациям экспериментальных работ

Ссылка	α_p	β_p	$\alpha_p+\beta_p$	$\alpha_p-\beta_p$	Теор. прибл.	
					Теория	$\alpha_p+\beta_p$
Gol60 [23]	9 ± 2	2 ∓ 2	—	—	LEX	11
Bar74 [24]	$10{,}7\pm1{,}1$	$-0{,}7\pm1{,}6$	$10{,}0\pm2{,}3$	—	LEX	—
Fed91 [1]	—	—	$12{,}2\pm3{,}5\pm1{,}5$	$9{,}1\pm4{,}0\pm2{,}0$	LEX	—
			$11{,}9\pm3{,}9\pm1{,}7$	$8{,}0\pm4{,}4\pm2{,}2$	DR	—
	$10{,}9\pm2{,}2\pm1{,}3$	$3{,}3\mp2{,}2\mp1{,}3$	—	—	LEX	14,2
Fed95 [4]	—	—	$15{,}8\pm4{,}5\pm0{,}1$	$11{,}9\pm5{,}3\pm0{,}2$	DR	—
Zie92 [2]	—	—	—	$7{,}03^{+2,49+2,14}_{-2,27-2,05}$	DR	—
	$10{,}6^{+1,25+1,07}_{-1,19-1,03}$	$3{,}6^{-1,25-1,07}_{+1,19+1,03}$	—	—	DR	14,2
Hal93 [3]	$9{,}8\pm0{,}4\pm1{,}1$	$4{,}4\mp0{,}4\mp1{,}1$	—	$5{,}5\pm0{,}7\pm2{,}1$	DR	14,2
Mac95 [4]	—	—	$15{,}0\pm2{,}9\pm1{,}1$	$10{,}8\pm1{,}1\pm1{,}4$	DR	—
	$12{,}5\pm0{,}6\pm0{,}7$	$1{,}7\mp0{,}6\mp0{,}7$	—	—	DR	14,2
Ton98 [8]	—	—	$13{,}23\pm0{,}86^{+0,20}_{-0,49}$	$10{,}11\pm1{,}74^{+1,22}_{-0,86}$	DR	—

Примечание. Последние две колонки указывают тип применяемой теории — низкоэнергетическое разложение (LEX) или дисперсионные соотношения (DR), а также использовалось ли при фите теоретическое значение суммы $\alpha_p+\beta_p \simeq 14,2$ (или 11,0 в ранней работе [23]). Строка Fed95 означает результаты работы [1], исправленные ее авторами в [4]. Строка Ton98 представляет результат глобального фита работ [1–7, 24]. Смысл приведенных погрешностей различен в разных работах. В [23] указанная погрешность — только статистическая, а в [24] — полная. В [1–3] раздельно даны статистические и систематические погрешности. В [4,8] указаны полные экспериментальные погрешности и оценки модельной зависимости

Отметим, что в использованном в [23] фитирующем сечении параметр β_p заменялся на $11-\alpha_p$ (здесь и далее для поляризуемостей приняты единицы 10^{-4} фм^3) и варьировался только параметр α_p. Таким образом, сумма поляризуемостей приравнивалась к известному в то время теоретическому значению $(\alpha_p+\beta_p)^{\text{теор}}=11$ [27], тогда как ее современное значение равно

$(14{,}0 \pm 0{,}5)$ [24, 30–32]*. Систематическая погрешность $6\,\%$ в экспериментальных сечениях при фитировании данных [23] не принималась во внимание. В [24] оба параметра α_p и β_p определялись независимо, так как статистические и систематические погрешности в измеренных сечениях относительно малы. Отметим, что из сравнения безмодельного низкоэнергетического сечения УРФ на протоне (обозначаемого далее LEX) с предсказаниями дисперсионной теории [36–38], которая удовлетворительно согласуется с экспериментальными данными ниже Δ_{33}-резонанса, следует, что область применимости LEX лежит при $\omega \lesssim 80$ МэВ (зависит от угла θ), в то время как измерения в [24] были выполнены в интервале энергий фотона $80 \div 110$ МэВ. В рамках определенных модельных предположений дисперсионная теория указала также на возможность определить значения суммы $(\alpha_p + \beta_p)^{\text{эксп}}$ и разности $(\alpha_p - \beta_p)^{\text{эксп}}$ из данных при $\omega \leq 150$ МэВ, где неопределенности в предсказаниях минимальны, без использования разложения фитирующего дифференциального сечения УРФ на протоне по ω [36, 37, 39, 40] (см. также п. 3.2). Этот путь используется в настоящей работе.

После работ [23, 24] длительное время измерения поляризуемостей протона не проводились. Работы [1–4] были стимулированы, с одной стороны, прогрессом в технике эксперимента (см. разд. 2), с другой — расчетами поляризуемостей протона в различных теоретических подходах (см., например, [31, 41–44]). В частности, было показано, что в нерелятивистской кварковой модели (НКМ), не учитывающей мезонное облако, не удается одновременно воспроизвести экспериментальные значения электрической поляризуемости протона, квадрата его зарядового радиуса и энергии низколежащих возбуждений [31, 41, 42]. Расхождения вычисленных значений $\alpha_p^{\text{НКМ}}$ и $\langle r^2 \rangle_p^{\text{НКМ}}$ с экспериментальными составляют не $\sim 20\,\%$, как часто принято считать (см., например, гл. 1 и 5 в книге [45]), а около 3 раз. Все это привело к осознанию возможности и важности более точного измерения поляризуемостей протона. Определение значений $\alpha_p^{\text{эксп}}$ и $\beta_p^{\text{эксп}}$ с точностью $5{-}10\,\%$ и $20{-}30\,\%$ соответственно является проверкой предсказаний разных дисперси-

*Впервые значение $(\alpha_p + \beta_p)^{\text{теор}} = 14{,}1 \pm 0{,}3$ получено в [24] из дисперсионного правила сумм [27, 33] (см. формулу (11)) с привлечением данных по полному сечению адронного фотопоглощения на протоне. Ранее соответствующий дисперсионный интеграл вычислялся в работе [30], авторы которой не упоминают о его связи с суммой $\alpha_p + \beta_p$. Приведенное в [30] значение интеграла дает $(\alpha_p + \beta_p)^{\text{теор}} = 14{,}2 \pm 0{,}3$. Полученное недавно значение $(\alpha_p + \beta_p)^{\text{теор}} = 13{,}69 \pm 0{,}14$ [32] учитывает только статистическую погрешность использованных сечений. Полная неопределенность в значении $(\alpha_p + \beta_p)^{\text{теор}}$ в основном определяется систематической погрешностью, которая составляет $\sim 2-3\,\%$ или $\pm(0{,}3{-}0{,}4)$. На центральное значение результата [32] повлияло использование сечений, найденных с помощью мультипольного анализа фоторождения [34], занижающего сечение фотопоглощения в околопороговой области. При использовании другого анализа [35] центральное значение $(\alpha_p + \beta_p)^{\text{теор}}$ поднимается до 14,0.

онных правил сумм (ПС) [31], в частности, широко используемого ПС для $\alpha_p + \beta_p$ [27, 33], и разных моделей структуры адронов [41–44, 46, 47]. Но несмотря на значительные усилия точность измерений сечения УРФ на протоне в работах [1–4] оказалась все-таки недостаточно высокой (см. разд. 2), так что погрешности полученных в них значений $\alpha_p^{\text{эксп}}$, $(\alpha_p - \beta_p)^{\text{эксп}}$ и $(\alpha_p + \beta_p)^{\text{эксп}}$ лежат в пределах $10 - 50\,\%$, а значений $\beta_p^{\text{эксп}}$ — $50 - 100\,\%$ (см. табл. 1)*. Такая ситуация предполагает необходимость привлечения или получения дополнительных экспериментальных данных.

В настоящей работе с целью уменьшения полных (комбинированных) и теоретических (модельных) погрешностей в экспериментальных значениях поляризуемостей протона их определение проводится по всему массиву мировых данных по дифференциальному сечению УРФ на протоне при энергиях $\omega < 150$ МэВ. Этот массив состоит из 94 экспериментальных точек, а именно: 48 поздних из [1–4] и 46 ранних из [23, 24, 48–52]. Статистический анализ показывает совместимость друг с другом экспериментальных данных, полученных разными группами, и возможность их объединения в одном фите. Внимание уделяется и теоретическим ошибкам в значениях $\alpha_p^{\text{эксп}}$ и $\beta_p^{\text{эксп}}$, возникающим из-за различных модельных неопределенностей в фитирующем дисперсионном сечении, меньшим при низких и большим при средних энергиях фотона ω.

Далее в разд. 2 приводится краткий обзор ранних и поздних низкоэнергетических данных по УРФ на протоне, используемых в нашем анализе. В разд. 3 обсуждаются теоретические сечения, используемые при фитировании данных. В разд. 4 описана методика фитирования данных с учетом их статистических и систематических погрешностей. В разд. 5 приводятся результаты фитирования данных отдельных групп и глобального фитирования всего массива сечений. Раздел 6 содержит выводы и рекомендации для будущих экспериментов по определению поляризуемостей протона.

2. НИЗКОЭНЕРГЕТИЧЕСКИЕ ЭКСПЕРИМЕНТАЛЬНЫЕ ДАННЫЕ

Все экспериментальные данные по УРФ на протоне в интервале энергий $\omega = 30 \div 150$ МэВ, где вклад ω^2-членов, зависящих от α_p и β_p, в низкоэнергетическое дифференциальное сечение реально наблюдаем, можно условно разбить на две группы. В одну входят данные [23, 24, 48–52], полученные в 50–70-х годах (см. обзор [53]), в другую — данные последних лет [1–4].

*Потребность в более точном измерении поляризуемостей протона возникает и в связи с измерениями поляризуемостей нейтрона в опытах по упругому γd-рассеянию, в которых определяется сумма поляризуемостей протона и нейтрона (см., например, [16]).

Ранние работы были выполнены с пучками тормозного излучения, полученными на циклических электронных ускорителях первого поколения. В них процесс УРФ на протоне наблюдался, как правило, по рассеянному фотону, который регистрировался телескопом сцинтилляционных счетчиков с очень плохим энергетическим разрешением. Такой метод наблюдения не позволял надежно выделять УРФ на протоне на фоне других электромагнитных процессов, например $\gamma p \to e^+e^-\gamma' p$, при углах рассеяния фотона $\theta \lesssim 60^\circ$ и энергии $\omega \lesssim 80$ МэВ. Экспериментальные точки, относящиеся к этой кинематической области, не использовались авторами оригинальных работ в последующем анализе. Они не включены и в массив данных, которые мы далее фитируем.

Поздние работы [1–4] выполнены на электронных ускорителях следующего поколения, обладающих гораздо лучшим коэффициентом заполнения пучка («duty factor»): микротрон Иллинойского университета MUSL-2 (сейчас разобран), электронный ускоритель с растяжителем в Саскачеване (SAL), микротрон в Майнце MAMI-A (сейчас работает как первая ступень микротрона MAMI-B). Наиболее важной особенностью работ [1–4] была регистрация рассеянных фотонов спектрометрами полного поглощения с большими кристаллами NaI(Tl), которые позволяли измерять энергию конечного фотона ω' с точностью несколько процентов.

2.1. Работы 50—70-х годов. В работах [48–52], где измерялось дифференциальное сечение УРФ на протоне, поляризуемости протона α_p и β_p не определялись.

В ФИАНе [48] измерения были выполнены при $\omega \approx 100$ МэВ для трех значений угла θ. Статистические погрешности в полученных значениях сечения равняются в среднем $20\,\%$. Систематическую погрешность авторы не приводят. Поэтому экспериментальные точки [48] не пригодны для фитирования в рамках принятой нами процедуры, учитывающей зависимость χ^2 от систематической погрешности экспериментальных сечений (см. разд. 4). Они не включены нами в массив фитируемых данных.

Из трех работ [49], выполненных в Чикагском университете, в последней получены наиболее точные данные. Она включает также ранние результаты, в которые авторы внесли значительные поправки на многократные фоновые процессы в экспериментальные сечения для малых углов θ. В соответствии со сказанным в начале этого раздела только данные при угле $\theta > 60^\circ$ включены в табл. 2. Статистические погрешности в полученных сечениях равны $\sim 5\,\%$, систематическая — $8\,\%$.

В [50] энергетическая зависимость сечения для углов $\theta = 50^\circ$ и 90° показана в виде сплошных полос, ширина которых определяет статистическую точность данных ($\approx 15\,\%$). Число энергетических интервалов соответствует числу изломов в представленных таким образом сечениях. В работе отмечено, что данные при $\theta = 50^\circ$ и $\omega \leq 80$ МэВ сильно искажены фоном. По-

этому в дальнейшем мы используем сечения при $\theta = 50^\circ$ только для энергий $\omega > 80$ МэВ. Систематическая погрешность сечений из [50] равна $\sim 10\,\%$.

Таблица 2. Экспериментальные данные по УРФ на протоне в области энергий фотонов до 150 МэВ. Указаны число экспериментальных точек n, систематическая погрешность δ, а также энергии, углы и дифференциальные сечения в лаб. системе

Ссылка	n	δ, %	ω, МэВ	θ, град	$d\sigma/d\Omega$, нб/ср
Gov56 [48] *	3	–	97	45	$14,0 \pm 1,7$
				90	$13,5 \pm 1,3$
				135	$22,5 \pm 4,5$
Oxl58 [49]	4	8	60	70	$10,6 \pm 0,8$
				90	$10,8 \pm 0,4$
				120	$11,8 \pm 0,5$
				150	$14,7 \pm 0,6$
Hym59 [50]	12	10	88	50	$13,9 \pm 4,0$
			99	50	$13,2 \pm 3,8$
			109	50	$12,3 \pm 3,8$
			120	50	$12,8 \pm 8,3$
			60	90	$10,9 \pm 1,8$
			70	90	$10,9 \pm 1,9$
			78	90	$10,9 \pm 1,8$
			87	90	$10,8 \pm 1,5$
			95	90	$10,6 \pm 1,4$
			106	90	$10,5 \pm 1,3$
			118	90	$9,8 \pm 2,0$
			128	90	$9,4 \pm 4,0$
Gol60 [23]	5	6	55	75	$11,2 \pm 0,8$
				90	$11,0 \pm 0,5$
				120	$13,4 \pm 0,8$
				135	$15,6 \pm 0,8$
				150	$19,3 \pm 0,7$
Ber61 [51] **	2	10	120	134,5	$14,9 \pm 2,0$
			139	133,9	$18,9 \pm 1,9$
Fri67 [52]	16	7	80	50	$11,8 \pm 2,4$
			95	50	$9,4 \pm 2,4$
			105	50	$9,4 \pm 2,4$
			115	50	$8,2 \pm 2,4$
			125	50	$4,7 \pm 6,0$
			55	90	$10,6 \pm 1,4$
			75	90	$10,6 \pm 1,4$
			95	90	$10,6 \pm 1,4$
			115	90	$9,9 \pm 1,9$
			125	90	$9,7 \pm 2,8$
			135	90	$4,7 \pm 7,0$
			65	135	$15,3 \pm 4,7$
			75	135	$16,5 \pm 4,7$
			95	135	$18,9 \pm 4,7$
			115	135	$14,2 \pm 4,7$
			125	135	$18,9 \pm 9,4$
Bar74a [24]	3	1	80,9	90	$11,5 \pm 0,6$
			85,4	90	$10,9 \pm 0,4$
			109,9	90	$10,3 \pm 0,6$
Bar74b [24] (см. текст)	4	3,7	81,9	150	$14,4 \pm 1,2$
			86,3	150	$13,7 \pm 1,0$
			106,7	150	$16,0 \pm 0,8$
			111,1	150	$14,4 \pm 0,6$

(продолжение таблицы 2)

Ссылка	n	δ, %	ω, МэВ	θ, град	$d\sigma/d\Omega$, нб/ср
Fed91 [1] (см. текст)	16	3	33,5	60	$15,0 \pm 1,6$
			37,5	60	$16,1 \pm 1,4$
			44,2	60	$11,0 \pm 1,5$
			48,2	60	$12,0 \pm 1,4$
			55,0	60	$13,5 \pm 1,3$
			59,0	60	$11,7 \pm 1,2$
			65,8	60	$12,7 \pm 1,2$
			70,0	60	$12,2 \pm 1,0$
			33,5	135	$14,6 \pm 1,8$
			37,5	135	$15,0 \pm 1,5$
			44,2	135	$20,5 \pm 1,8$
			48,2	135	$14,8 \pm 1,6$
			55,0	135	$14,9 \pm 1,5$
			59,0	135	$15,7 \pm 1,4$
			65,8	135	$15,3 \pm 1,5$
			70,0	135	$13,5 \pm 1,3$
Zie92 [2] **	2	4,3	98	180	$18,4 \pm 3,4$
			132	180	$21,8 \pm 1,2$
Hal93 [3] **	12	4	135	45,6	$8,4 \pm 1,9$
			140	45,4	$8,1 \pm 1,5$
			146	45,2	$7,8 \pm 1,4$
			138	60,4	$8,3 \pm 4,5$
			144	60,1	$4,7 \pm 3,4$
			149	59,9	$9,2 \pm 3,2$
			132	82,9	$12,4 \pm 1,2$
			139	82,6	$13,0 \pm 1,1$
			145	82,3	$11,5 \pm 0,9$
			130	136,4	$18,3 \pm 1,4$
			138	136,1	$20,9 \pm 1,3$
			146	135,9	$19,7 \pm 1,3$
Mac95 [4] (tagged)	8	3,5	73,2	90	$10,4 \pm 1,7$
			81,8	90	$9,0 \pm 1,6$
			89,8	90	$10,7 \pm 1,5$
			96,8	90	$8,6 \pm 1,4$
			73,2	135	$14,3 \pm 1,8$
			81,8	135	$16,1 \pm 1,8$
			89,8	135	$16,7 \pm 1,7$
			96,8	135	$16,0 \pm 1,6$
Mac95 [4] (untagged)***	10	2,9	105	90	$9,5 \pm 1,4$
			115	90	$12,1 \pm 1,6$
			125	90	$11,2 \pm 1,0$
			135	90	$11,4 \pm 1,6$
			145	90	$13,1 \pm 2,4$
			105	135	$14,6 \pm 2,5$
			115	135	$15,9 \pm 2,0$
			125	135	$14,9 \pm 1,8$
			135	135	$18,8 \pm 1,4$
			145	135	$18,4 \pm 2,0$

*Данные этой работы не включены в фит из-за отсутствия информации о систематической погрешности.

**Большинство данных из работ [3,51] относятся к энергиям выше 150 МэВ и здесь опущены. Сечения, приведенные в [2, 3, 51] в с.ц.м., даны в таблице в лаб. системе.

***Указанные погрешности в сечениях при каждом угле рассеяния сильно коррелированы, что необходимо учитывать при построении функции χ^2 (см. [4] и раздел 4).

В работе [51], выполненной на бетатроне Иллинойского университета, УРФ на протоне наблюдалось по одновременной регистрации протона отдачи и рассеянного фотона. Только два из полученных значений экспериментального сечения относятся к области $\omega < 150$ МэВ. Их статистические и систематические погрешности одинаковы и равны $10\,\%$.

В MIT [52] определялась энергетическая зависимость сечения для трех углов θ. Получено 19 экспериментальных точек со статистическими погрешностями $\approx 25\%$ и систематической погрешностью $7\,\%$. Окончательные значения сечений объявлены через 10 лет после первых публикаций.

О работах [23, 24], где впервые достаточно надежно определена электрическая поляризуемость протона и было установлено, что $\alpha_p^{\text{эксп}} > \beta_p^{\text{эксп}}$, мы уже говорили в разд. 1. Здесь ограничимся одним важным замечанием, касающимся точности работы [24]. Абсолютная нормировка сечения рассеяния фотонов на протонах в [24] выполнялась по мониторному процессу — рассеянию фотонов на атомных электронах. При вычислении сечения рассеяния фотона на электроне учитывались радиационные поправки. Угол рассеяния фотонов θ_e в мониторном процессе выбирался так, чтобы рассеянные фотоны на протонах и электронах имели одинаковую энергию ω'; этот угол определяется отношением масс электрона и протона и углом рассеяния в основном процессе: $\sin(\theta_e/2) = \sin(\theta/2)\sqrt{m_e/M}$. Тогда при определении экспериментального отношения сечений основного и мониторного процессов систематическая погрешность, связанная с недостаточным знанием многих факторов, включая энергетическую зависимость эффективности регистрации фотона γ-телескопом, сокращается. В действительности нужный угол рассеяния в мониторном сеансе был выдержан только для $\theta = 90^\circ$. По техническим причинам изменить геометрию мониторного сеанса для полного совпадения энергетических интервалов (увеличить θ_e) при переходе к $\theta = 150^\circ$ было нельзя, и в этом случае γ-телескоп регистрировал фотоны с энергией на ~ 8 МэВ больше, чем в основном процессе. Поправка на изменение эффективности регистрации γ-телескопа с ростом энергий фотонов в [24] вводилась. Однако анализ, проведенный в рамках данной работы, показал, что связанная с этим максимальная погрешность может привести к увеличению систематической погрешности получаемых сечений УРФ до $3,7\%$.

Поэтому в рамках принятой нами процедуры фитирования и построения функции χ^2 (см. формулу (16) в разд. 4) мы рассматриваем данные работы [24] при углах 90° и 150° как два независимых набора данных с систематической погрешностью 1 и $3,7\,\%$ соответственно.

2.2. Работы 90-х годов. В работе [1] были выполнены первые измерения сечений УРФ на протоне с мечеными фотонами. На микротроне MUSL-2 сечения измерены в интервале энергий ω от 33 до 70 МэВ при $\theta = 60^\circ$ и 135°. Статистические погрешности полученных в этой работе сечений равны

$8-13\,\%$, систематическая — $3\,\%$ В дальнейшем авторы [1] обнаружили неточность калибровки γ-детекторов, связанную с учетом мертвого времени, и скорректировали (уменьшили) первоначальные сечения на $3-4\,\%$ (см., например, рис. 9 в [4]). В настоящей работе мы используем эти исправленные значения сечений [54].

В работе [2], выполненной на микротроне MAMI-A с мечеными фотонами, произведено уникальное измерение сечения УРФ при $\theta = 180^\circ$. Наблюдение процесса проводилось по регистрации протона отдачи, вылетающего под углом 0°, с помощью магнитного спектрометра. Измерения сделаны для энергий $\omega = 98$ и 132 МэВ с статистическими погрешностями $18,5$ и $5,5\,\%$ соответственно. Систематическая погрешность в полученных сечениях равна $4,3\%$.

В работе [3], выполненной на ускорителе SAL с тормозным пучком фотонов, дифференциальное сечение УРФ измерялось как выше, так и ниже порога фоторождения пионов на установке, регистрирующей только рассеянный фотон. Это стало возможным благодаря использованию большого NaI(Tl)-спектрометра фотонов с энергетическим разрешением $1,5\,\%$. Статистические и систематические погрешности в полученных сечениях равны $10-20$ и $4\,\%$ соответственно. В наших целях мы используем только малую часть этих данных, относящуюся к допороговым энергиям $\omega \leq 150$ МэВ.

Следует отметить, что полученные дифференциальные сечения представлены в [3] двумя способами: как функции энергии при фиксированных углах и как угловые распределения при фиксированных энергиях (149 МэВ в нашем случае). Мы проводили определение поляризуемостей, используя оба варианта представления сечений, и нашли, что их результаты немного отличаются. В первом значение $\alpha_p^{\text{эксп}}$ на $\sim 1,3\cdot 10^{-4}$ фм^3 больше, а значение $\beta_p^{\text{эксп}}$ на $\sim 0,6\cdot 10^{-4}$ фм^3 меньше, чем во втором, что, впрочем, находится в пределах статистических погрешностей. В работе [3] непосредственно измерялись энергетические распределения при фиксированных положениях γ-детектора, а угловые распределения при фиксированном ω выводились из них на основе дальнейших предположений о форме энергетической зависимости дифференциального сечения, которое имеет излом (касп) вблизи пионного порога. В нашей работе мы предпочли использовать первичные энергетические, а не вторичные угловые зависимости — всего 12 точек.

В работе [4], сделанной также на ускорителе SAL, измерения выполнялись с большими NaI(Tl)-детекторами в интервале энергий $\omega = 73 \div 148$ МэВ при углах $\theta = 90^\circ$ и 135°. Система мечения позволяла отдельно метить фотоны с энергиями $\omega \leq 100$ МэВ. В немеченых событиях спектр конечных фотонов при энергиях $\omega' \leq 80$ МэВ был загрязнен фотонами, не связанными с УРФ на протоне. Их источником служит, например, реакция $\gamma p \to e^+e^-\gamma' p$, а также распад π^0-мезонов, рождаемых фотонами тормозного спектра, максимальная энергия которого (148 МэВ) немного превышала порог фоторо-

ждения π^0-мезонов (144,7 МэВ). Поэтому сечения при $\omega < 100$ МэВ определялись только по событиям с мечеными фотонами, а при $\omega > 100$ МэВ — по немеченым событиям. Статистические погрешности в значениях сечений при $\omega < 100$ МэВ и $\omega > 100$ МэВ равны $10-17$ и $\sim 13\,\%$ соответственно. Систематическая погрешность измерений с мечеными фотонами в среднем равна $3,5\,\%$, а с тормозными фотонами — $2,9\,\%$.

Отметим, что энергия электронного пучка, использованного в работе [4], была фиксированной, так что энергетическая зависимость сечения УРФ с тормозными фотонами получалась в результате анализа спектра регистрируемых фотонов. Из-за конечного энергетического разрешения детектора получаемые сечения в выбранных пяти интервалах энергий от 100 до 150 МэВ имеют сильно коррелированные статистические погрешности, что следует учитывать при использовании метода χ^2. В табл. 2 приведены сечения только с диагональными элементами матрицы погрешностей [4]. Использовать буквально указанные погрешности для представления результатов эксперимента [4] нельзя. Правильная процедура обсуждается в [4] (см. также разд. 4).

В [8] сумма и разность поляризуемостей протона α_p и β_p извлекались из данных [1–4, 24] при $\omega \leq 150$ МэВ и полученных совсем недавно на ускорителях BNL и MAMI данных [5–7], относящихся к окрестности Δ_{33}-резонанса. Фитирование всех этих данных, выполненное в [8], показало, что получаемое значение разности $(\alpha_p - \beta_p)^{\text{эксп}}$ весьма чувствительно к деталям теоретического описания УРФ выше порога фоторождения пионов (см. разд. 3 и 5). Поэтому далее мы не используем данные по УРФ при $\omega > 150$ МэВ,

Все данные по дифференциальному сечению γp-рассеяния при $\omega \leq 150$ МэВ собраны в табл. 2, где для каждой работы приводится число экспериментальных точек (n), систематическая погрешность (δ) и сами сечения при энергии ω для угла θ со статистическими погрешностями. Из табл. 2 видно, что систематические погрешности измерений сечения УРФ на протоне в работах последних лет приблизительно в два раза меньше, чем в ранних работах, за исключением [24]. Однако статистическая точность измерений низкоэнергетического сечения, достигнутая в ранних работах, не только не уступает точности измерений последних лет, но в ряде работ ее превосходит. По числу полученных экспериментальных точек ранние и поздние работы практически совпадают. Несомненным достоинством работ 90-х годов являются измерения энергетической зависимости сечения УРФ. К недостаткам этих работ относится бедная информация по угловому распределению, асимметрия которого относительно угла $\theta = 90^\circ$ чувствительна к величине магнитной поляризуемости протона и модельным поправкам в теоретическом сечении. Поэтому при определении мировых средних значений поляризуемостей протона $\alpha_p^{\text{эксп}}$ и $\beta_p^{\text{эксп}}$ все еще желательно фитировать всю совокупность не очень многочисленных и не очень точных экспериментальных данных по УРФ на протоне.

3. ФИТИРУЮЩИЕ ДИФФЕРЕНЦИАЛЬНЫЕ СЕЧЕНИЯ

В этом разделе обсуждаются низкоэнергетическое и дисперсионное дифференциальные сечения УРФ на протоне, которые обычно используются при фитировании экспериментальных данных и определении экспериментальных значений поляризуемостей протона $\alpha_p^{\text{эксп}}$ и $\beta_p^{\text{эксп}}$. Специально обращается внимание на область применимости и точность теоретических дифференциальных сечений.

3.1. Низкоэнергетическое приближение. Разложение дифференциального сечения УРФ на протоне по степеням энергии падающего фотона в л.с. ω есть следствие низкоэнергетических теорем для амплитуды рассеяния T_{fi} ($f = \gamma' p'$ и $i = \gamma p$, конечное и начальное состояния), выведенных без использования теории возмущений по константе сильной связи из общих принципов квантовой теории поля: релятивистская, калибровочная, P-, T-инвариантности, полнота системы состояний и т.д. Так, по теореме Тирринга [55], справедливой также во всех порядках по константе тонкой структуры $e^2 = 1/137$ ($\hbar = c = 1$), амплитуда УРФ на любой заряженной частице (ион, ядро, адрон) в пределе нулевой энергии ω совпадает с классической томсоновской амплитудой $T_{fi}^{\text{T}} = -(e^2/M)\mathbf{e}\cdot\mathbf{e}'$, где e и M — заряд и масса частицы, а $\mathbf{e}$ и $\mathbf{e}'$ — векторы поляризации начального и конечного фотонов.

Теорема Гелл-Манна–Гольдбергера–Лоу [56,57] утверждает, что постоянные коэффициенты при линейных по ω спин-тензорных структурах разложения амплитуды УРФ на протоне выражаются через заряд e, массу M и а.м.м. λ. Однако все ω-члены в амплитуде зависят от спина протона и не вносят линейный по ω вклад в дифференциальное сечение для неполяризованных протонов.

Обобщение этих низкоэнергетических теорем на ω^2-члены амплитуды УРФ было получено в работах [26,28,58–61], где доказано, что соответствующие коэффициенты разложения выражаются через e, M, λ и две структурные константы α_p и β_p, получившие названия поляризуемостей протона.

В рамках того же квантово-полевого подхода выведены новые формулы и для самих поляризуемостей, которые кроме известных из нерелятивистской теории сумм по возбужденным состояниям протона имеют дополнительные релятивистские поправки, выражающиеся через e, M, λ и зарядовый радиус протона [28,58,60–62]. Схожесть полученных формул с нерелятивистскими послужила основанием для принятого названия констант α_p и β_p. Обобщенная низкоэнергетическая теорема открыла возможность вывести дифференциальное сечение УРФ на протоне с точностью до ω^2-членов и тем самым поставила задачу экспериментального определения поляризуемостей α_p и β_p на реальную основу. Такое низкоэнергетическое дифференциальное сечение, выведенное впервые в [28a], при явном учете кроссинг-симметрии амплитуды

T_{fi} принимает в лабораторной системе вид

$$\frac{d\sigma}{d\Omega} = \frac{1}{2}\Big(\frac{e^2}{M}\Big)^2\Big(\frac{\omega'}{\omega}\Big)^2\Bigg\{1+\cos^2\theta+\frac{\omega\omega'}{M^2}\Big[1+2\lambda+\frac{9}{2}\lambda^2+3\lambda^3+\frac{3}{4}\lambda^4-$$

$$-(2+4\lambda+5\lambda^2+2\lambda^3)\cos\theta+(1+2\lambda+\frac{1}{2}\lambda^2-\lambda^3-\frac{1}{4}\lambda^4)\cos^2\theta\Big]-$$

$$-\frac{2M\omega\omega'}{e^2}[\alpha_p(1+\cos^2\theta)+2\beta_p\cos\theta]+O(\omega^2\omega'^2)\Bigg\}, \qquad (1)$$

где $\omega' = \omega/[1+(\omega/M)(1-\cos\theta)]$ — энергия конечного фотона в л.с. Последний член в квадратных скобках в формуле (1) получается из-за интерференции томсоновского вклада в амплитуде с теми ω^2-вкладами, которые зависят от поляризуемостей α_p и β_p. Если его отбросить, то (1) переходит в сечение Поуэлла $d\sigma^{\Pi}/d\Omega$. Еще раз подчеркнем, что при выводе формулы (1) никаких предположений о структуре протона и механизмах его взаимодействия с фотоном не делалось*. Поэтому дифференциальное сечение (1) называют безмодельным, и оно может рассматриваться как операциональное определение поляризуемостей α_p и β_p через УРФ на протоне. Если в (1) исключить фактор фазового объема $(\omega'/\omega)^2$, то видно, что низкоэнергетическое разложение идет по единственному кроссинг-симметричному параметру $\omega\omega'$. Таким образом, формула (1) фактически справедлива до ω^3-членов включительно (см. [29]). Для краткости мы обозначаем низкоэнергетическое разложение дифференциального сечения (1) как LEX.

Использование LEX для фитирования экспериментальных данных и определения значений поляризуемостей $\alpha_p^{\text{эксп}}$ и $\beta_p^{\text{эксп}}$ оправданно, если «редуцированное экспериментальное сечение»

$$\frac{d\tilde{\sigma}^{\text{эксп}}}{d\Omega} = \Big(\frac{\omega}{\omega'}\Big)^2\,\frac{d\sigma^{\text{эксп}}}{d\Omega} \qquad (2)$$

при фиксированном угле рассеяния θ линейно зависит от $\omega\omega'$. Как имеющиеся данные удовлетворяют этому требованию, показано на рис. 1, где даны экспериментальные сечения при $\theta = 90^\circ$ и 135°. Там же показана теоретическая зависимость от $\omega\omega'$ других низкоэнергетических сечений, а также дисперсионного сечения. Видно, что отбрасываемые в LEX члены

*В [26,28,29,60,61] низкоэнергетические теоремы выведены в низшем по e^2 приближении. Радиационные поправки к формуле (1) вычислялись в [63,64]. При интересующих нас энергиях ω и углах θ эти поправки сводятся к сдвигу поляризуемостей протона на пренебрежимо малую величину порядка $e^4/M^3 = 0,005\cdot 10^{-4}$ фм^3.

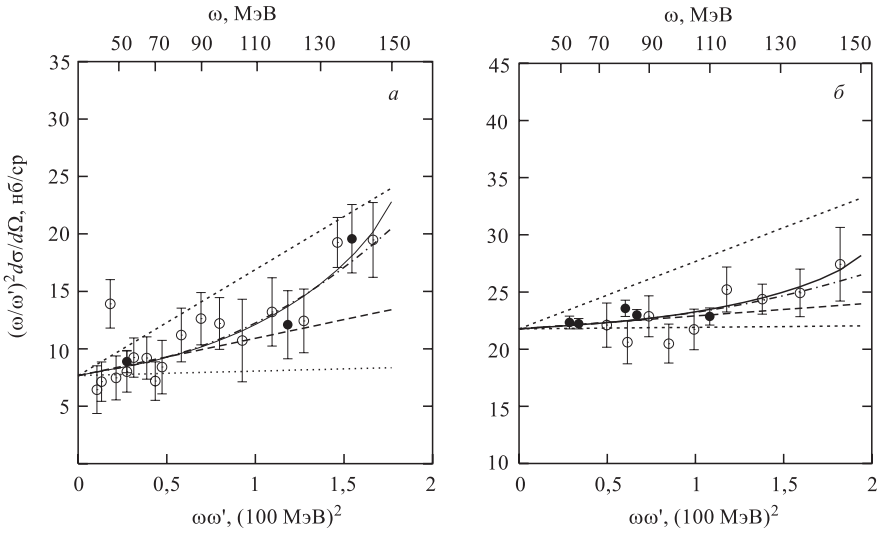

Рис. 1. Зависимость редуцированного дифференциального сечения γp-рассеяния (2) от $\omega\omega'$ при фиксированном угле $\theta = 90^\circ$ (*а*) или 135° (*б*). Точечные кривые — сечение Поуэлла (верхняя кривая) и Клейна–Нишины–Тамма (нижняя кривая); они отличаются учетом и, соответственно, неучетом аномального магнитного момента протона. Пунктирная кривая — сечение LEX (1) при $\alpha_p = 12,1$ и $\beta_p = 2,1$. Штрихпунктирная кривая (ELEX) включает поправки Δ_1 и Δ_2 (см. текст). Сплошная кривая — предсказания дисперсионных соотношений. Данные из работ [23, 24, 49, 51] (черные кружки) и [1, 4] (светлые кружки)

$O(\omega^2\omega'^2)$ при $\omega \geq 80$ МэВ не малы. Чтобы иметь возможность фитировать все данные при $\omega < 150$ МэВ простым алгебраическим выражением, добавим к формуле (1) $\omega^2\omega'^2$-поправку, ответственную за нелинейный рост «редуцированного сечения». Общая структура такой поправки имеет вид

$$\Delta_1 = \left(\frac{\omega'}{\omega}\right)^2 \omega^2\omega'^2 A(\theta), \tag{3}$$

где $A(\theta)$ — полином третьей степени от $\cos\theta$ [65], значение которого при фиксированном θ будем считать новым свободным параметром*. Другая по-

*При одновременном фитировании данных, относящихся к разным углам θ, нужно варьировать наряду с α_p и β_p еще четыре коэффициента полинома $A(\theta)$, что приводит к заметному увеличению ошибок в извлекаемых значениях $\alpha_p^{\text{эксп}}$ и $\beta_p^{\text{эксп}}$. Все или часть из этих коэффициентов можно вычислить в рамках дисперсионного подхода (см. п. 3.2), но это вносит в низкоэнергетическое сечение модельную зависимость. Такова плата за расширение области применимости формулы (1).

правка к формуле (1), влияющая на результаты фитирования, возникает от интерференции ω-членов в низкоэнергетической амплитуде с кубичной по ω амплитудой Лоу [51, 56], учитывающей вклад ближайшего к физической области значений кинематических переменных полюса в t-канале от обмена нейтральным пионом. Она имеет вид*

$$\Delta_2 = \left(\frac{\omega'}{\omega}\right)^2 \frac{e^2}{M}\frac{\omega^2\omega'^2}{M^2}\frac{g_{\pi NN}F_{\pi\gamma\gamma}}{8\pi(m_\pi^2 - t)}[1 + 3\lambda + \lambda^2 - (1+\lambda)\cos\theta](1-\cos\theta)^2. \tag{4}$$

В (4) $t = -2\omega\omega'(1-\cos\theta)$ — квадрат передаваемого протону 4-импульса, m_π — масса нейтрального пиона, а произведение констант πNN-взаимодействия и распада $\pi^0 \to \gamma\gamma$ отрицательно (в соответствии со структурой аномалии в алгебре токов и эффективных киральных лагранжианах; см., например, [67]) и дается выражением

$$g_{\pi NN}F_{\pi\gamma\gamma} = -16\pi\sqrt{\frac{g_{\pi NN}^2}{4\pi}\frac{\Gamma_{\pi^0\to\gamma\gamma}}{m_\pi^3}} = -(0,331 \pm 0,012)\ \text{ГэВ}^{-1}. \tag{5}$$

В (5) подставлены следующие численные значения констант: $g_{\pi NN}^2/4\pi = (13{,}75 \pm 0{,}55)$ [68], $\Gamma_{\pi^0\to\gamma\gamma} = (7{,}74 \pm 0{,}55)$ эВ [69]. Выделение интерференционного вклада (4) в отдельное слагаемое объясняется его резкой полюсной зависимостью от t. Пренебречь этой t-зависимостью нельзя. Действительно, при $\omega \geq 70$ МэВ и $\theta \geq 90^\circ$ значения $|t| \geq m_\pi^2$ и разложение Δ_2 в степенной ряд по t/m_π^2 невозможно. Следовательно, дифференциальное сечение (1) с поправками (3) и (4), которое будем обозначать как ELEX, не является последовательным низкоэнергетическим приближением, и его следует рассматривать как одно из простых аппроксимирующих выражений. Область применимости ELEX, как видно из рис. 1, простирается до энергий $\omega \approx 130{-}140$ МэВ. ELEX удобно использовать при фитировании экспериментальных сечений, измеренных при одном угле θ и разных энергиях ω. В этом случае имеются два неизвестных параметра: $\alpha_p(1+\cos^2\theta) + 2\beta_p\cos\theta$ и $A(\theta)$. Выполнив процедуру фитирования для двух углов, например $\theta_1 = 90^\circ$ и $\theta_2 = 135^\circ$, получаем два экспериментальных значения первого параметра и, решая систему из двух уравнений, находим сами поляризуемости $\alpha_p^{\text{эксп}}$ и $\beta_p^{\text{эксп}}$. Далее мы используем ELEX только для независимой проверки фитов с дисперсионным дифференциальным сечением из-за невозможности применить такой «модельно-независимый» анализ ко всем данным в табл. 2 из-за их скудости,

*Впервые влияние поправок Δ_1 и Δ_2 на значения $\alpha_p^{\text{эксп}}$ и $\beta_p^{\text{эксп}}$, извлекаемые из экспериментальных данных, обсуждалось в [65, 66]. Однако из-за неправильного определения знака поправки Δ_2 найденные там значения $(\alpha_p - \beta_p)^{\text{эксп}}$ заметно отличаются от современных.

недостаточной точности и больших погрешностей в получаемых значениях $\alpha_p^{\text{эксп}}$ и $\beta_p^{\text{эксп}}$.

3.2. Дисперсионный подход. Теперь кратко обсудим дисперсионный расчет дифференциального сечения УРФ на протоне, которое в разд. 5 используется для фитирования данных из табл. 2 и определения экспериментальных значений поляризуемостей протона. В отличие от низкоэнергетических сечений LEX и ELEX область практической применимости дисперсионного дифференциального сечения значительно шире. Так, в [38] в рамках дисперсионного подхода получено удовлетворительное описание всех данных по УРФ на протоне при энергии $\omega \lesssim 1,0$ ГэВ, включая поляризационные характеристики. Дальнейшее изложение следует работам [31,36,38], к которым мы отсылаем за отсутствующими ниже деталями.

Из [70,71] известно, что общая амплитуда УРФ на протоне T_{fi} для начальных и конечных частиц с произвольными поляризациями выражается через шесть скалярных амплитуд, зависящих от двух кинематических переменных, например, от энергии и угла рассеяния фотона. В релятивистском расчете удобно использовать свободные от кинематических особенностей и связей амплитуды $A_{k=1\ldots6}(\nu,t)$ [72] от инвариантных переменных $\nu=(s-u)/4M=\omega+t/4M$ и t, где s, u, t — мандельстамовские переменные. По определению четные по ν амплитуды $A_k(\nu,t)$ при фиксированном и по крайней мере малом $|t|\le 12m_\pi^2$ являются аналитическими функциями во всей комплексной плоскости ν (см. [73,74]), исключая полюсы и разрезы на вещественной оси, и удовлетворяют дисперсионному соотношению при конечной энергии [31,36,72]:

$$\operatorname{Re}A_k(\nu,t)=\frac{a_k(t)}{\nu^2-\dfrac{t^2}{16M^2}}+\frac{2}{\pi}P\int\limits_{\nu_{\text{пор}}(t)}^{\nu_{\text{макс}}(t)}\frac{\nu'\operatorname{Im}A_k(\nu',t)}{\nu'^2-\nu^2}d\nu'+$$
$$+\frac{1}{\pi}\operatorname{Re}\int_0^\pi\frac{\nu'^2A_k(\nu',t)}{\nu'^2-\nu^2}\,d\varphi\Big|_{\nu'=\nu_{\text{макс}}(t)\exp(i\varphi)}. \qquad (6)$$

Первый член в правой части (6) — однонуклонный полюсный вклад $A_k^{\text{пол}}(\nu,t)$, в числителе которого стоит линейная функция t с известными коэффициентами, зависящими от заряда e, массы M и а.м.м. λ протона. Взятый отдельно вклад $A_k^{\text{пол}}(\nu,t)$ приводит к дифференциальному сечению Поуэлла [25]. Второй член, интегральный вклад $A_k^{\text{инт}}(\nu,t)$, учитывает низшие адронные возбуждения протона в промежуточных состояниях УРФ на протоне. Нижний предел интегрирования $\nu_{\text{пор}}(t)$ равен порогу фоторождения одиночных пионов на протоне по переменной ν при фиксированном t: $\nu_{\text{пор}}(t)=m_\pi+m_\pi^2/2M+t/4M$. Выбор верхнего предела $\nu_{\text{макс}}(t)=\omega_{\text{макс}}+t/4M$ определяется реальной возможностью вычислить мнимую часть $A_k(\nu,t)$ в интервале от $\nu_{\text{пор}}(t)$ до $\nu_{\text{макс}}(t)$, используя условие унитарности для амплитуды

T_{fi} в e^2-приближении:

$$2\,\mathrm{Im}\,T_{fi} = \sum_n (2\pi)^4 \delta(P_n - P_i)\, T^*_{nf} T_{ni} \tag{7}$$

и результаты мультипольных анализов экспериментальных данных по фоторождению пионов на протоне. В (7) суммирование выполняется по всем разрешенным законами сохранения состояниям адронов $|n\rangle = |\pi N\rangle$, $|\pi\pi N\rangle, \ldots$ с полным 4-импульсом P_n. Фактически в численных расчетах используются формулы, являющиеся следствием (7) и связывающие мнимые части амплитуд $A_k(\nu, t)$ с квадратичными формами от мультипольных амплитуд пионного фоторождения. Если $\omega_{\text{макс}}$ положить равным 1,5 ГэВ, то в расчетах интегрального вклада $A_k^{\text{инт}}(\nu, t)$ можно ограничиться πN- и $\pi\pi N$-вкладами (см. ниже).

Третий член в (6), так называемый асимптотический вклад $A_k^{\text{ас}}(\nu, t)$, учитывает связь «высокоэнергетического» поведения амплитуды $A_k(\nu, t)$ с низкоэнергетическим. Предполагая применимость асимптотического степенного разложения по ν амплитуды $A_k(\nu, t)$, предсказываемого полюсной моделью Редже, на полуокружности с радиусом $\nu_{\text{макс}}(t)$, по которой проводится интегрирование, получаем следующее выражение для асимптотического вклада*:

$$A_k^{\text{ас}}(\nu, t) \approx \sum_R \frac{b_k^R(t)(2M\alpha'_R \nu_{\text{макс}}(t))^{\alpha_R(t)-n_k}}{\alpha_R(t) - n_k} \times$$

$$\times \left[1 + \frac{\alpha_R(t) - n_k}{\alpha_R(t) - n_k - 2} \left(\frac{\nu}{\nu_{\text{макс}}(t)}\right)^2 + \ldots\right]. \tag{8}$$

В (8) $\alpha_R(t) = \alpha_R(0) + \alpha'_R t$ — траектории полюсов Редже $R = P$ (померон), f_2, a_2, π, σ, $\ldots$, обмен которыми в t-канале УРФ на протоне приводит к слагаемым с разной зависимостью от ν в асимптотиках амплитуд $A_k(\nu, t)$. Интерсепты $\alpha_R(0)$ и наклоны α'_R траекторий $\alpha_R(t)$ известны из эксперимента: $\alpha_P(0) \approx 1,1$, $\alpha_{f_2,a_2}(0) \approx 0{,}5$, $\alpha_\pi(0) \approx 0$, $\alpha_\sigma(0) \approx -0,5$; $\alpha'_P \approx 0{,}2$ ГэВ$^{-2}$, $\alpha'_{f_2,a_2,\pi,\sigma} \approx 0{,}9$ ГэВ$^{-2}$. Целые числа $n_{1,2} = 0$, $n_{3,5,6} = 2$, $n_4 = 3$ определяют сигнатуру (четность спинов) полюсов Редже $\tau_R = (-1)^{n_k}$, вносящих вклад в асимптотику амплитуды $A_k(\nu, t)$; $b_k^R(t)$ — вещественные функции t, пропорциональные вычетам в полюсах R. Масштаб и t-зависимость функций $b_k^R(t)$, как правило, можно определить только грубо, привлекая экспериментальную информацию о процессах взаимодействия фотона с протоном

*При выводе (8) не учитывается теоретически возможный вклад фиксированного полюса или кронекеровского члена [75] в асимптотику амплитуды $A_k(\nu, t)$, так как убедительного экспериментального свидетельства его существования нет [30, 76].

при энергии $\omega \geq 1{,}5$ ГэВ и дополнительные модельные представления. С учетом P, C-симметрии и сигнатуры τ_R главные вклады в $A_k^{\text{ас}}(\nu, t)$ вносят траектории $\alpha_R(t)$ с интерсептом $\alpha_R(0) > -1$: P, $f_2(1270)$, $a_2(1320)$, σ (или $f_0(400{-}1200)$) при $k = 1, 3, 5, 6$; P, $f_2(1270)$, $a_2(1320)$, π при $k = 2$; $a_1(1260)$, $f_1(1285)$ при $k = 4$. Таким образом, из (8) следует, что асимптотические вклады $A_k^{\text{ас}}(\nu, t)$ зависят от нескольких ненадежно определяемых функций $b_k^R(t)$, которые могут быть уточнены на основе будущих более полных и более точных экспериментальных данных по УРФ на протоне при разных ν и t, в частности, по асимметрии рассеяния линейно поляризованных фотонов на протонах при $\omega \geq 1{,}5$ ГэВ. Отметим, что асимптотические вклады (8) из-за присутствия в знаменателе выражения $\alpha_R(t) - n_k$ имеют полюсы, характерные для обмена частицами в t-канале, в частности, π- и σ-мезонами.

В допороговой области, где $\nu \leq m_\pi + m_\pi^2/2M$, $|t| \leq 3{,}5 m_\pi^2$ и $\nu^2/\nu_{\text{макс}}^2(t) \ll 1$, задача определения вкладов $A_k^{\text{ас}}(\nu, t)$ несколько упрощается, так как они, во-первых, перестают практически зависеть от ν, то есть $A_k^{\text{ас}}(\nu, t) \approx A_k^{\text{ас}}(0, t)$. Во-вторых, при относительно малых t вместо (8) можно использовать одно- или двухполюсную аппроксимацию

$$A_k^{\text{ас}}(\nu, t) \approx a_k \frac{M_k^2}{M_k^2 - t}, \quad k = 1, 3, 4, 5, 6 \tag{9}$$

и

$$A_2^{\text{ас}}(\nu, t) \approx a_2 \frac{M_2^2}{M_2^2 - t} + \frac{g_{\pi NN} F_{\pi\gamma\gamma}}{t - m_\pi^2} \frac{\Lambda_\pi^2 - m_\pi^2}{\Lambda_\pi^2 - t}, \tag{10}$$

где a_k — не определенные пока константы, а M_k — массы эффективных промежуточных частиц в t-канале. Мы явно выделили в $A_2^{\text{ас}}(\nu, t)$ быстроменяющийся с изменением t вклад от π^0-обмена, в котором в отличие от (4) учтен комбинированный формфактор πNN- и $\pi^0\gamma\gamma$-вершин с $\Lambda_\pi = 0{,}7$ ГэВ. Другие вклады в (9) и (10) не так резко зависят от t, так как массы эффективных частиц M_k лежат в пределах от 0,5 до 1,0 ГэВ. Согласно (8) асимптотические вклады $A_{1,2}^{\text{ас}}(\nu, t)$ пропорциональны $\nu_{\text{макс}}(t)$, а $A_{3,4,5,6}^{\text{ас}}(\nu, t)$ убывают как $1/\nu_{\text{макс}}(t)$ или быстрее. Если $\nu_{\text{макс}}(t)$ достаточно большое, можно ожидать, что вклады $A_{3,4,5,6}^{\text{ас}}(\nu, t)$ малы по сравнению с интегральными вкладами $A_{3,4,5,6}^{\text{инт}}(\nu, t)$. Для величин $A_{3+6}^{\text{ас}}(0, 0) = A_3^{\text{ас}}(0, 0) + A_6^{\text{ас}}(0, 0)$ и $A_{3+6}^{\text{инт}}(0, 0) = A_3^{\text{инт}}(0, 0) + A_6^{\text{инт}}(0, 0)$ это прямо следует из дисперсионного ПС для $\alpha_p + \beta_p$,

записанного в виде [72]*:

$$\alpha_p+\beta_p=-\frac{1}{2\pi}\left(A^{\text{инт}}_{3+6}(0,0)+A^{\text{ас}}_{3+6}(0,0)\right)=$$
$$=\frac{1}{2\pi^2}\left(\int\limits_{\nu_{\text{пор}}(0)}^{\nu_{\text{макс}}(0)}\frac{\sigma_{\text{пол}}(\nu)}{\nu^2}d\nu+\int\limits_{\nu_{\text{макс}}(0)}^{\infty}\frac{\sigma_{\text{пол}}(\nu)}{\nu^2}d\nu\right). \qquad (11)$$

В (11) под знаками интегралов стоит умноженное на $1/\nu^2$ полное сечение адронного фотопоглощения на протоне. В интервале энергий ν от 1,3 до 20 ГэВ оно хорошо воспроизводится феноменологической формулой $\sigma_{\text{пол}}(\nu)=A_p+B_{f_2+a_2}/\sqrt{\nu}$, где $A_p\approx 100$ мкб и $B_{f_2+a_2}\approx 57$ мкб·ГэВ$^{1/2}$, учитывающей обмены P-, f_2- и a_2-траекториями Редже [79]. В сумме поляризуемостей

$$(\alpha_p+\beta_p)^{\text{теор}}=14,0\pm 0,5, \qquad (12)$$

вычисленной с помощью (11), при $\nu_{\text{макс}}(0)=1{,}5$ ГэВ вклад второго интеграла, который получен путем преобразования соответствующего интеграла по полуокружности в (6), составляет всего 6%. Далее предполагается, что неравенство $|A^{\text{инт}}_{3+6}(\nu,t)|\gg|A^{\text{ас}}_{3+6}(\nu,t)|$ выполняется не только при нулевых, но, по крайней мере, и малых ν и t. Асимптотические вклады $A^{\text{ас}}_{3,4,5}(\nu,t)$ имеют дополнительный фактор малости по сравнению с вкладом $A^{\text{ас}}_{6}(\nu,t)$. Он обусловлен тем, что амплитуды $A_{3,4,5}(\nu,t)$ при больших ν описывают УРФ на протоне с переворотом спинов частиц, которое, как известно из эксперимента, подавлено в несколько раз по сравнению с рассеянием без переворота спинов [80, 81]. Следовательно, вклады $A^{\text{ас}}_{3,4,5}(\nu,t)$ еще меньше, чем $A^{\text{ас}}_{3+6}(\nu,t)$, и коэффициенты $a_{3,4,5}$ в (9) будем считать равными нулю. В этом приближении естественными параметрами амплитуд $A_k(\nu,t)$ и дифференциального сечения являются остающиеся коэффициенты $a_{1,2,6}$ и массы $M_{1,2,6}$. Коэффициенты $a_{1,2,6}$ в (9) и (10) можно выразить через $\alpha_p-\beta_p$, $\alpha_p+\beta_p$ и γ_π, где последняя величина есть спиновая поляризуемость назад (см., например, [82]). Для этого нужно воспользоваться первым равенством в (11) и соотношениями $2\pi(\alpha_p-\beta_p)=-(A^{\text{инт}}_1(0,0)+A^{\text{ас}}_1(0,0))$ и

*ПС (11) все еще не имеет устоявшегося названия. Например, в [38] оно называется ПС Балдина–Лапидуса, а в [32] — ПС Балдина. Отметим, что ПС (11), строго говоря, справедливо с точностью до вещественной аддитивной константы C, которая появляется из-за принципиальной возможности добавить к аналитической функции $A_3(\nu,t)+A_6(\nu,t)$ постоянное слагаемое (вклад фиксированного полюса $J=2$), не изменяя ее особенностей [77]. Константу C можно попытаться определить экспериментально. В частности, поэтому в разд. 5 мы варьируем α_p и β_p как независимые параметры. Фиксированный полюс $J=2$ меняет асимптотическое поведение амплитуды УРФ вперед и, следовательно, влияет на энергетическую зависимость дифференциального сечения $d\sigma/dt$ при высоких энергиях. Используя данные FNAL по $d\sigma/dt$ при $\omega=50\div 130$ ГэВ [78], можно получить достаточно сильное ограничение $|C|\lesssim 0,02\cdot 10^{-4}$ фм^3.

$2\pi M\gamma_\pi = -(A^{\text{инт}}_{2+5}(0,0) + A^{\text{ас}}_{2+5}(0,0))$. В результате вместо трех дисперсионных соотношений (6) для амплитуд $A_{1,2,6}(\nu,t)$ получаем

$$\operatorname{Re} A_1(\nu,t) = A_1^{\text{пол}}(\nu,t) + A_1^{\text{инт}}(\nu,t) - \left[A_1^{\text{инт}}(0,0) + 2\pi(\alpha_p - \beta_p)\right]\frac{M_1^2}{M_1^2 - t}, \quad (13)$$

$$\operatorname{Re} A_{2+5}(\nu,t) = A_{2+5}^{\text{пол}}(\nu,t) + A_{2+5}^{\text{инт}}(\nu,t) -$$

$$-\left[A_{2+5}^{\text{инт}}(0,0) + 2\pi M\gamma_\pi - \frac{g_{\pi NN}F_{\pi\gamma\gamma}}{m_\pi^2}\right]\frac{M_2^2}{M_2^2 - t} + \frac{g_{\pi NN}F_{\pi^0\gamma\gamma}}{t - m_\pi^2}\frac{\Lambda_\pi^2 - m_\pi^2}{\Lambda_\pi^2 - t}, \quad (14)$$

$$\operatorname{Re} A_{3+6}(\nu,t) = A_{3+6}^{\text{пол}}(\nu,t) + A_{3+6}^{\text{инт}}(\nu,t) - \left[A_{3+6}^{\text{инт}}(0,0) + 2\pi(\alpha_p + \beta_p)\right]\frac{M_6^2}{M_6^2 - t}. \quad (15)$$

Для величин $\alpha_p - \beta_p$ и γ_π, как и для $\alpha_p + \beta_p$, из дисперсионных соотношений (6) можно вывести правила сумм при конечной энергии. В [31, 72, 83] такие правила сумм использовались для более или менее точных расчетов значений $\alpha_p - \beta_p$ и γ_π. Однако при фитировании низкоэнергетических экспериментальных данных дисперсионным сечением некоторые из его параметров варьируют: $\alpha_p - \beta_p$ в [2], $\alpha_p - \beta_p$ и $\alpha_p + \beta_p$ в [1, 4], $\alpha_p - \beta_p$, $\alpha_p + \beta_p$ и γ_π в [8]. При одном и том же массиве фитируемых точек с ростом числа варьируемых параметров точность получаемых экспериментальных значений этих параметров, конечно, уменьшается. Далее мы обсудим основные источники неопределенностей, возникающие при расчете дисперсионного сечения, в частности, из-за разброса используемых значений параметров, которые не варьируются.

3.3. Источники теоретических неопределенностей. Численный расчет интегральных вкладов $A_k^{\text{инт}}(\nu,t)$ вносит сравнительно малые неопределенности в дисперсионное дифференциальное сечение и, соответственно, в значения параметров, определяемых при фитировании данных в допороговой области. Основной вклад в $A_k^{\text{инт}}(\nu,t)$ вносит интегрирование по области $\nu' \leq 0{,}5$ ГэВ. Используя два набора довольно точных при $\nu' \leq 0{,}5$ ГэВ «экспериментальных» мультипольных амплитуд фоторождения одиночных пионов на протоне, как основной — SAID из [34] и как альтернативный — HDD из [35], можно оценить погрешность, возникающую при определении значений $\alpha_p^{\text{эксп}}$ и $\beta_p^{\text{эксп}}$. Численные значения всех теоретических (модельных) погрешностей приводятся в разд. 5. Главное различие между наборами [34] и [35] заключается в пороговом поведении s-волновой амплитуды E_{0+}. Мы изменяем также резонансную амплитуду M_{1+} на $\pm 2\,\%$ так, как это описано в [84]. Учет парного фоторождения пионов, которое начинает вносить заметный вклад в полное сечение $\sigma_{\text{полн}}(\gamma p \to \text{адроны})$, при $\omega \gtrsim 0{,}4$ ГэВ мало изменяет доминирующие интегральные вклады $A_1^{\text{инт}}(\nu,t)$ и $A_{3+6}^{\text{инт}}(\nu,t)$. В дисперсионных соотношениях (13)–(15) сильное подавление интегральных вкладов от больших ν' происходит из-за вычитаний, например, из-за присутствия

члена $A^{\text{инт}}_{3+6}(\nu,t) - A^{\text{инт}}_{3+6}(0,0)M_6^2/(M_6^2-t)$ в (15). Это легко проверить при $t=0$ и убедиться, что вычитание приводит к появлению дополнительного обрезающего фактора ν^2/ν'^2 под знаком интеграла. Для получения верхней оценки погрешности, связанной с учетом парного фоторождения пионов, мы рассматриваем в разд. 5 случай, когда оно вообще опускается.

Как показывают расчеты, основная неопределенность возникает при учете асимптотических вкладов в дисперсионных соотношениях (13)–(15). При разных k роль $A^{\text{ас}}_k(\nu,t)$, как мы уже отметили ранее, не одинакова. Вклад $A^{\text{ас}}_1(\nu,t)$ почти целиком определяет экспериментальное значение разности поляризуемостей $\alpha_p^{\text{эксп}} - \beta_p^{\text{эксп}} \approx 10$, и от значения массы M_1 заметно зависят результаты фитирования. В настоящей работе выбрано $M_1 = 0{,}5$ ГэВ, хотя в [38] для удовлетворительного описания данных выше Δ_{33}-резонанса приходилось брать $M_1 = 0,6$ ГэВ, которое там называлось «массой σ-мезона». В асимптотическом вкладе $A^{\text{ас}}_{2+5}(\nu,t)$ (14) первый член относительно мал и множитель $M_2^2/(M_2^2-t)$ не так существен. Вклад самого π^0-обмена заметен, и неопределенности в значениях Λ_π и (5) следует учитывать. Однако при малых t изменение Λ_π не имеет самостоятельного значения и сводится к сдвигу коэффициента a_{2+5} и, соответственно, γ_π. В дальнейшем мы берем $\Lambda_\pi = 0{,}7$ ГэВ, а спиновую поляризуемость без вклада π^0-обмена меняем в пределах точности теоретического расчета [85]: $\gamma_\pi^{(\text{non}-\pi^0)} = \gamma_\pi - g_{\pi NN}F_{\pi\gamma\gamma}/2\pi M m_\pi^2 = (5{,}5 \pm 1{,}8)\cdot 10^{-4}$ фм^4. Так как вклад $A^{\text{ас}}_{3+6}(\nu,t)$ сам по себе мал, то результаты фитирования практически не зависят от значения M_6.

4. ФИТИРОВАНИЕ С УЧЕТОМ СИСТЕМАТИЧЕСКИХ ПОГРЕШНОСТЕЙ

При определении физических параметров (поляризуемостей протона) из нескольких ($N_{\text{эксп}}$) независимых экспериментов по измерению дифференциальных сечений γp-рассеяния возникает необходимость совместного учета как статистических, так и систематических погрешностей. Для каждого отдельно взятого эксперимента $j = 1,\dots N_{\text{эксп}}$, рассматриваемого в данном анализе, относительные систематические погрешности измеряемых сечений $\sigma_{ij}^{\text{эксп}} \equiv \sigma^{\text{эксп},\,j}(\omega_{ij},\theta_{ij})$, $i = 1,\dots n_j$ слабо зависят от энергий или углов рассеяния фотонов и в основном сводятся к неопределенности в общей нормировке k_j этих сечений. Коэффициенты k_j можно рассматривать как неизвестные параметры обобщенного теоретического описания экспериментов, при котором теоретические сечения $\sigma_{ij}^{\text{теор}} \equiv \sigma(\omega_{ij},\theta_{ij};\alpha_p,\beta_p)$, зависящие от поляризуемостей протона, должны согласовываться с перемасштабированными экспериментальными сечениями $k_j\sigma_{ij}^{\text{эксп}}$. Тот факт, что величины k_j равны единице в пределах неопределенностей δ_j абсолютизации сечений отдельных экспе-

риментов, можно рассматривать как независимое «измерение» этих величин. Соответственно функция χ^2 записывается как [86]

$$\chi^2(k;\ \alpha_p, \beta_p) = \sum_{j=1}^{N_{\text{эксп}}} \left\{ \sum_{i=1}^{n_j} \left(\frac{k_j \sigma_{ij}^{\text{эксп}} - \sigma_{ij}^{\text{теор}}}{k_j \Delta\sigma_{ij}^{\text{эксп}}} \right)^2 + \left(\frac{k_j - 1}{k_j \delta_j} \right)^2 \right\}, \tag{16}$$

где $\Delta\sigma_{ij}^{\text{эксп}}$ — статистические погрешности. Так как выражение (16) — квадратичная функция от $1/k_j$, его минимизация по величинам k_j легко делается в аналитическом виде. Результат имеет вид

$$\chi^2(\alpha_p, \beta_p) = \min_k \chi^2(k;\ \alpha_p, \beta_p) = \sum_{j=1}^{N_{\text{эксп}}} \left\{ X_j^{ee} - \frac{(X_j^{te})^2 \delta_j^2}{1 + X_j^{tt} \delta_j^2} \right\}, \tag{17}$$

где

$$X_j^{ee} = \sum_{i=1}^{n_j} \left(\frac{\sigma_{ij}^{\text{эксп}} - \sigma_{ij}^{\text{теор}}}{\Delta\sigma_{ij}^{\text{эксп}}} \right)^2,$$

$$X_j^{te} = \sum_{i=1}^{n_j} \frac{\sigma_{ij}^{\text{эксп}} - \sigma_{ij}^{\text{теор}}}{\Delta\sigma_{ij}^{\text{эксп}}} \frac{\sigma_{ij}^{\text{теор}}}{\Delta\sigma_{ij}^{\text{эксп}}}, \quad X_j^{tt} = \sum_{i=1}^{n_j} \left(\frac{\sigma_{ij}^{\text{теор}}}{\Delta\sigma_{ij}^{\text{эксп}}} \right)^2. \tag{18}$$

В уравнении (17) член X_j^{ee} учитывает статистические погрешности j-го эксперимента. Он является обычным для методики фитирования по критерию χ^2. Второй (отрицательный) член возникает благодаря оптимизации χ^2 по нормировочным параметрам k_j и описывает влияние систематической погрешности j-го эксперимента. Минимум (17) достигается при перемасштабировании экспериментальных сечений факторами

$$k_j = \left(1 + \frac{X_j^{te} \delta_j^2}{1 + X_j^{tt} \delta_j^2} \right)^{-1} \tag{19}$$

(зависящими от поляризуемостей). Возникающая функция (17) зависит только от двух параметров, что делает ее особенно удобной для фитирования в случае большого количества экспериментов.

Использование χ^2 вида (17) (или (16)) ведет к двум важным последствиям. Во-первых, поляризуемости α_p и β_p фактически определяются из исправленных значений экспериментальных сечений $k_j \sigma_{ij}^{\text{эксп}}$, что приводит к смещению (обычно в пределах полных погрешностей) значений поляризуемостей, определяемых из исходных (неисправленных) сечений $\sigma_{ij}^{\text{эксп}}$. Во-вторых, ошибки в поляризуемостях оказываются больше, чем при использовании только первого члена в (17), так как теперь они включают как статистические, так и систематические неопределенности экспериментальных сечений.

Отметим, что данные работы [4] с немечеными фотонами входят в χ^2 с учетом корреляций статистических погрешностей сечений $\sigma_i^{\text{эксп}}$, относящихся к разным энергиям ω_i. В соответствии с [4] вместо самих сечений σ_i (и экспериментальных, и теоретических) мы включаем в (17) их линейные комбинации $\sigma'_i = \sum_{i'} V_{ii'}\sigma_{i'}$, имеющие некоррелированные погрешности. Экспериментальные значения величин σ'_i и их погрешностей $\Delta\sigma'_i$, а также матрица $V_{ii'}$, диагонализирущая матрицу погрешностей сечений $\sigma_i^{\text{эксп}}$, приведены в [4].

В дальнейшем фитирование данных с помощью функции (17) проводилось в нескольких вариантах выбора теоретической модели для сечений $\sigma_{ij}^{\text{теор}}$ и отбора экспериментальных данных. При использовании низкоэнергетического приближения, описанного в разд. 3, теоретические сечения являются элементарной функцией энергии ω, угла θ и поляризуемостей α_p, β_p. При использовании дисперсионной теории сечения определяются сложным численным алгоритмом, так что для целей фитирования использовалась предварительная табуляция и последующая интерполяция теоретических сечений по четырем переменным.

Совместимость экспериментальных данных с теорией проверялась по величине оптимального значения χ^2 и вероятности P иметь такое или большее χ^2 при числе степеней свободы $N_f = n - 2$, где n — число экспериментальных точек с сечениями рассеяния. Вероятность P не должна быть слишком мала. Обычно считается допустимым, если $P > 10\,\%$, что соответствует вероятности в пределах 1,64 стандартных отклонений; нередко используются и более мягкие критерии: $P > 5\,\%$ (1,96 стандартных отклонений) и даже $P > 1\,\%$ (2,58 стандартных отклонений).

Часть фитов в разд. 5 выполнена при наложенной связи $\alpha_p + \beta_p = 14{,}0 \pm 0{,}5$ в соответствии с ПС (11). Мы рассматриваем эту связь как дополнительное «измерение» и включаем его в уравнение (17):

$$\chi^2(\alpha_p, \beta_p) \to \chi^2(\alpha_p, \beta_p) + \left(\frac{\alpha_p + \beta_p - 14,0}{0,5}\right)^2. \tag{20}$$

Здесь число степеней свободы равно $N_f = n - 1$. Такой фит приходится делать, например, в тех случаях, когда используются дифференциальные сечения γp-рассеяния при единственном угле θ.

5. ОПРЕДЕЛЕНИЕ ПОЛЯРИЗУЕМОСТЕЙ ПРОТОНА

Мы определяли поляризуемости из экспериментальных данных, делая: 1) раздельные фиты отдельно взятых экспериментов, 2) раздельные фиты по группам ранних и поздних экспериментов и 3) объединенный (глобальный)

фит по всем экспериментам. Во всех случаях, кроме описанных ниже в п. 5.4, фитирующее сечение находилось с помощью дисперсионной теории, описанной в п. 3.2.

С одной стороны, такая процедура позволяет судить о том, какие экспериментальные данные наиболее информативны с точки зрения определения поляризуемостей и правомерно ли отбрасывать старые данные в нынешней экспериментальной ситуации. С другой стороны, эта процедура позволяет сказать, совместимы ли различные группы данных друг с другом и можно ли объединять их в один глобальный фит. Ниже приводятся полученные результаты.

5.1. Поляризуемости протона, определенные по отдельным экспериментам. Поляризуемости протона α_p и β_p, определенные для каждого из экспериментов [1–4, 23, 24, 49–52], приведены в табл. 3. Так как в работах [2, 51] дифференциальное сечение измерялось при единственном угле, оба параметра α_p и β_p можно определить из них лишь при привлечении правила сумм (11).

Двухпараметрические фиты с независимыми поляризуемостями протона хорошо описывают каждый из экспериментов, рассматриваемый в отдельности, о чем свидетельствует достаточно высокий уровень достоверности P. Более того, в пределах 1–2 получаемых погрешностей большинство результатов, данных в различных строках таблицы, согласуются друг с другом и со средневзвешенными по верхней части таблицы величинами $\alpha_p \simeq 11,3$, $\beta_p \simeq 1,8$, определяемыми без привлечения ПС (11). Несколько выпадают лишь значения магнитной поляризуемости, получаемые при фитировании сечений из работ [24,49] (соответственно на 2,3 и 2,6 стандартных отклонения).

Если не обращать внимания на погрешности, то можно заметить, что дифференциальные сечения трех работ [24, 49, 50] приводят к отрицательным значениям магнитной поляризуемости протона. До сих пор по «ранним экспериментам» [49, 50] поляризуемости вообще не определялись (во всяком случае, не публиковались), и было принято считать, что только одна работа [24] указывает на отрицательное значение β_p. Однако при учете погрешностей все β_p совместимы с нулевым значением.

Другим любопытным обстоятельством является то, что значения поляризуемостей, выводимые из последнего эксперимента [4], предопределяются набором точек, полученных с немечеными фотонами. Подмножество точек, полученных с мечеными фотонами, обладает низкой точностью и, если опять забыть о погрешностях, дает рекордно большое положительное значение для β_p и для суммы $\alpha_p + \beta_p$ — см. последнюю строку табл. 3. Таким образом, измерения с мечеными фотонами, которые обладают рядом неоспоримых методических преимуществ, пока не могут сравниться по достигнутым результатам для поляризуемостей с измерениями на обычном тормозном пучке.

Для работ 90-х годов имеется близкое соответствие между результатами, приведенными в табл. 3, и оригинальными результатами самих авторов (также

Таблица 3. Поляризуемости протона в единицах 10^{-4} фм^3, найденные по данным отдельных экспериментов с помощью дисперсионной теории

Эксперимент (ссылка)	n	α_p	β_p	$\alpha_p+\beta_p$	χ^2/N_f	P, %
Oxl58 [49]	4	$17,0\pm8,1$	$-6,7\pm3,7$	$10,2\pm9,2$	4,2/2	12
Hym59 [50]	12	$13,9\pm5,6$	$-4,7\pm7,2$	$9,2\pm6,1$	0,6/10	100
Gol60 [23]	5	$10,1\pm7,8$	$9,0\pm5,0$	$19,1\pm10,2$	2,3/3	52
Fri67 [52]	16	$14,2\pm4,0$	$5,6\pm4,2$	$19,8\pm4,3$	2,4/14	100
Bar74 [24]	7	$11,4\pm1,4$	$-4,7\pm2,5$	$6,7\pm3,3$	8,0/5	15
Fed91 [1]	16	$13,7\pm3,7$	$2,1\pm3,1$	$15,9\pm4,4$	17,3/14	24
Hal93 [3]	12	$9,1\pm1,7$	$3,7\pm1,5$	$12,7\pm2,0$	5,9/10	82
Mac95 [4]	18	$12,2\pm1,7$	$3,3\pm1,8$	$15,5\pm3,1$	7,4/16	97
Ber61 [51]	2	$11,4\pm2,9$	$2,6\pm2,9$	—	0,7/1	41
Zie92 [2]	2	$10,0\pm1,4$	$4,0\pm1,4$	—	0,1/1	73
Mac95 (tagged)	8	$18,3\pm5,7$	$13,2\pm7,2$	$31,5\pm12,3$	2,2/6	90

Примечание. n — число точек в работе в области энергий до 150 МэВ. Погрешности включают статистические и систематические неопределенности. P – уровень достоверности при найденном χ^2. Сумма $\alpha_p+\beta_p$ не фиксирована в первой части таблицы. В следующей части таблицы фит сечений из работ [2,51], измеренных при единственном угле, делался при дополнительном условии (12). Последняя строка представляет результаты фита подмножества эксперимента [4] с мечеными фотонами.

найденными для случая нефиксированной суммы $\alpha_p+\beta_p$), которые также использовали дисперсионную теорию (в ее более ранней форме [36]) для определения поляризуемостей. Исключением является только работа [1] – из-за того, что первоначально измеренные там сечения были позже скорректированы (см. разд. 2); наш результат очень близок к результату обработки исправленных данных [1], приведенному в [4]. Расхождение с оригинальными результатами [3] главным образом связано с тем, что мы используем только малую часть их данных, относящуюся к допороговым энергиям ниже 150 МэВ, тогда как в [3] в фит включались данные при энергиях вплоть до 293 МэВ, где модельная зависимость становится предметом особых забот.

Как уже подчеркивалось в разд. 2, погрешности сечений при $\omega > 100$ МэВ из работы [4] обладают сильной корреляцией, которая означает наличие дополнительных связей между сечениями и тем самым их более высокую точность по сравнению с той, которая наивно следует из табл. 2. Прямолинейное использование в (17) вместо правильных линейных комбинаций сечений σ_i', упомянутых в разд. 4, самих величин из табл. 2 привело бы к увеличению α_p на $+2$, а β_p на $+3$, подняло бы сумму $\alpha_p+\beta_p$ до 21 и увеличило бы все погрешности примерно вдвое. Таким образом, учет корреляций представляет важный элемент при интерпретации сечений, полученных в [4]. Следует за-

метить, что ни в одной другой из рассматриваемых здесь экспериментальных работ учет корреляций сечений не производился. Можно думать, что сильные корреляции в [4] явились результатом разбиения энергетического интервала на слишком маленькие участки, которые были меньше реального энергетического разрешения установки. Последнее не указано явно в публикации [4].

Учитывая разброс и погрешности в поляризуемостях, приведенных в табл. 3, мы приходим к выводу о допустимости объединения данных для глобальных фитов ранних, поздних или всех работ.

5.2. Поляризуемости, полученные по всем ранним и всем поздним экспериментам. По применяемой экспериментальной методике работы [1–4, 23, 24, 49–52] четко распадаются на ранние (50–70-е годы) и поздние (90-е годы). В публикациях последних лет результаты ранних экспериментов нередко игнорируются со ссылкой на их якобы низкую систематическую точность. Чтобы количественно проверить разумность такого пренебрежения, мы провели раздельные фиты ранних [23, 24, 49–52] и поздних [1–4] экспериментов. Результаты сведены в табл. 4. Из них можно заключить, что ранние и поздние работы дают приблизительно одинаковые полные погрешности в поляризуемостях, особенно для α_p. Немного лучшая точность поздних работ достигается в основном за счет присутствия большего числа точек в области энергий выше 100 МэВ, где чувствительность к поляризуемостям выше (но выше и модельные неопределенности). Следовательно, нет достаточных оснований игнорировать ранние работы. Обе группы (ранних и поздних) экспериментов демонстрируют хорошее согласие с двухпараметрическим теоретическим сечением и показывают удовлетворительное согласие между индивидуальными работами в каждой из групп. Ранние и поздние эксперименты в целом приводят к согласующимся результатам для поляризуемостей протона, и их объединение в глобальном фите не только допустимо, но и целесообразно для уменьшения полной ошибки.

5.3. Поляризуемости, полученные при объединении всех экспериментов. Результаты глобальных фитов всех имеющихся данных при энергиях фотона до 150 МэВ как со свободным значением $\alpha_p + \beta_p$ (фит (*а*)), так и при ограничении (12) (фит (*б*)) приведены в табл. 4. В фите (*а*) найденная сумма поляризуемостей удивительно хорошо согласуется с предсказанием ПС (11). Следствием такого согласия является то, что поляризуемости, найденные в фите (*б*), почти не отличаются от поляризуемостей, найденных в фите (*а*).

Стоит отметить, что при достигнутом уровне точности измерений погрешности в поляризуемостях, полученных в фите (*б*), в значительной степени определяется не погрешностями в экспериментальных дифференциальных сечениях УРФ на протоне, а погрешностью в теоретическом значении (12). Поэтому может показаться, что наши результаты (фит (*а*)) не улучшают значения поляризуемостей, найденные в «глобальном» фите трех работ 90-х годов [4] и вошедшие в компиляцию «Particle Data Group» [69] (см. табл. 4).

В действительности «глобальный» фит в [4] был сделан при использовании теоретического ограничения $(\alpha_p + \beta_p)^{\text{теор}} = 14{,}2 \pm 0{,}5$, и погрешности в полученных средних значениях $\alpha_p^{\text{эксп}}$ и $\beta_p^{\text{эксп}}$ определяются в основном погрешностью $\pm 0{,}5$, а это может создать завышенное впечатление об уровне погрешностей в самих экспериментах. Роль ранних данных ясно видна из нашего глобального фита (*б*), погрешности в котором меньше тех, что получены в [4] (см. также рис. 1).

Таблица 4. Поляризуемости протона в единицах 10^{-4} фм^3, найденные по ранним (50–70-е гг.), новым (90-е гг.) и всем экспериментам с использованием дисперсионной теории

Эксперимент	n	α_p	β_p	$\alpha_p + \beta_p$	$\alpha_p - \beta_p$	χ^2/N_f
		(*а*) $\alpha_p + \beta_p$ не фиксировано				
50–70-е гг.	46	$12{,}8 \pm 1{,}1$	$-0{,}3 \pm 1{,}6$	$12{,}5 \pm 2{,}2$	$13{,}0 \pm 1{,}7$	33,1/44
90-е гг.	48	$10{,}8 \pm 1{,}0$	$3{,}2 \pm 1{,}0$	$14{,}0 \pm 1{,}6$	$7{,}7 \pm 1{,}2$	33,7/46
Все экспер.*)	94	$11{,}7 \pm 0{,}8$	$2{,}3 \pm 0{,}9$	$14{,}0 \pm 1{,}3$	$9{,}5 \pm 1{,}0$	73,1/92
		(*б*) $(\alpha_p + \beta_p)^{\text{теор}} = 14{,}0 \pm 0{,}5$				
50–70-е гг.	46	$13{,}3 \pm 0{,}8$	$0{,}6 \pm 0{,}9$	–	$12{,}7 \pm 1{,}6$	33,6/45
90-е гг.	48	$10{,}8 \pm 0{,}7$	$3{,}2 \pm 0{,}7$	–	$7{,}7 \pm 1{,}2$	33,7/47
Все экспер.	94	$11{,}7 \pm 0{,}5$	$2{,}3 \pm 0{,}6$	–	$9{,}5 \pm 1{,}0$	73,1/93
		(*в*) $(\alpha_p + \beta_p)^{\text{теор}} = 14{,}2 \pm 0{,}5$				
PDG98	36	$12{,}1 \pm 0{,}8$	$2{,}1 \pm 0{,}8$	–	$10{,}0 \pm 1{,}5$	

*Эти значения могут быть рекомендованы для использования PDG. Указанные погрешности включают статистические и систематические неопределенности. n — число экспериментальных точек. Отдельно показан фит (*б*) с фиксированной суммой $\alpha_p + \beta_p$, ур-е (11), а также фит (*в*) — «глобальное среднее» по работам [1, 2, 4], полученное в [4] при условии $\alpha_p + \beta_p = 14{,}2 \pm 0{,}5$ и включенное в последнее издание «Particle Data Group» [69].

Удовлетворительная величина χ^2/N_f свидетельствует в целом о совместности массива экспериментальных данных с теоретическим дифференциальным сечением. Однако интерес представляют и индивидуальные вклады χ_j^2 в суммарную величину χ^2 от сечений из отдельных экспериментов, которые позволяют количественно судить о совместности результатов разных экспериментов друг с другом. Как и следовало ожидать, наибольший вклад в χ^2/N_f дают сечения из работ [24, 49] (в [24] — фактически только точки при $\theta = 150^\circ$), которые при независимых фитах приводят к отрицательным β_p. Вероятности чисто статистического происхождения наблюдаемых χ_j^2 составляют для [49] и [24] ($\theta = 150^\circ$), соответственно, 4 и 1 %, что может считаться допустимым при мягком критерии браковки. Вклады остальных работ в χ^2/N_f заметно меньше, и аналогичные вероятности составляют 33 % и более.

Нормировочные множители k_j (уравнение (19)), корректирующие экспериментальные сечения, для большинства работ близки к единице и находятся в пределах соответствующих систематических неопределенностей. Наибольшая коррекция сечений происходит для работ [49] и [24] ($\theta = 150^\circ$), для которых $k_j = 1,08$ и 1,10 соответственно. Именно такая большая коррекция отвечает указанному выше уровню согласия этих экспериментов с глобальным фитом на уровне 4 и 1 %.

Таблица 5. Модельная зависимость при извлечении поляризуемостей протона с помощью дисперсионной теории

Изменение	$\delta\alpha_p$	$\delta\beta_p$	$\delta(\alpha_p+\beta_p)$	$\delta(\alpha_p-\beta_p)$
SAID → HDT	−0,44 (−0,19)	−0,08 (+0,03)	−0,51 (−0,16)	−0,36 (−0,22)
$M_{1+} \to +2\%$	+0,18 (+0,07)	−0,11 (−0,04)	+0,06 (+0,03)	+0,29 (+0,11)
Отсутствие двойного фоторождения	+0,00 (+0,00)	−0,09 (−0,02)	−0,09 (−0,02)	+0,09 (+0,02)
$M_1 = 500$ МэВ → 700 МэВ	−0,35 (−0,20)	+0,53 (+0,24)	+0,19 (+0,04)	−0,88 (−0,44)
$\lvert g_{\pi NN}F_{\pi\gamma\gamma}\rvert \to +4\%$	−0,14 (−0,09)	+0,10 (+0,07)	−0,04 (−0,02)	−0,24 (−0,16)
$\gamma_\pi^{(\mathrm{non}-\pi^0)} = 5,5 \to 7,3$	+0,40 (+0,18)	−0,45 (−0,15)	−0,05 (+0,03)	+0,84 (+0,32)
Оцениваемая модельная неопределенность	0,72 (0,34)	0,72 (0,29)	0,56 (0,17)	1,33 (0,62)

Примечание. Показаны изменения поляризуемостей (в ед. 10^{-4} фм^3) при использовании разных амплитуд фоторождения пионов вблизи порога (SAID и HDT), при увеличении резонансной амплитуды фоторождения пионов M_{1+}, при неучете двойного фоторождения в дисперсионных интегралах, при изменении параметров M_1, $g_{\pi NN}F_{\pi\gamma\gamma}$ и $\gamma_\pi^{(\mathrm{non}-\pi^0)}$ (см. п. 3.2). Приведенная в конце таблицы полная модельная непределенность получена квадратичным сложением указанных выше изменений. Отдельно даны непределенности при фитировании всех экспериментальных точек и (в скобках) – при фитировании только точек ниже 100 МэВ.

5.4. Модельная зависимость и модельно-независимые определения.

Важной характеристикой извлекаемых значений $\alpha_p^{\text{эксп}}$ и $\beta_p^{\text{эксп}}$ являются теоретические (модельные) неопределенности, возникающие при расчете дисперсионного дифференциального сечения. В табл. 5 приведены изменения поляризуемостей при варьировании компонент дисперсионной теории, обсуждавшихся в п. 3.2. Их квадратичное сложение дает оценку модельной

неопределенности. Наибольший вклад в нее дают факторы, связанные с t-зависимостью амплитуды A_1 («масса» σ-мезона M_1), с фоном амплитуды Лоу (параметр a_2 или $\gamma_\pi^{(\mathrm{non}-\pi^0)}$), а также с амплитудами фоторождения пионов в области энергий ниже Δ-резонанса.

При фитировании всех данных до 150 МэВ общая модельная неопределенность в α_p и β_p составляет $\pm 0{,}7$ и оказывается лишь немногим меньше, чем чисто экспериментальные погрешности, вызванные погрешностями измерений дифференциального сечения УРФ. Модельная неопределенность снижается более чем в два раза в случае, когда фитирование ограничивается областью энергий 100 МэВ. Однако при таких энергиях падает и чувствительность дифференциального сечения к поляризуемостям, так что экспериментальные статистические и систематические погрешности в поляризуемостях увеличиваются почти вдвое (см. табл. 6).

Таблица 6. Модельно-независимые фиты поляризуемостей (в ед. 10^{-4} фм^3) с использованием LEX и ELEX с неопределенной функцией $A(\theta)$). В последнем случае фитируются данные при одном угле и фиксированной сумме поляризуемостей. Для сравнения показаны результаты фита тех же точек с дисперсионной теорией (без учета модельных неопределенностей)

Тип фита	n	α_p	β_p	$\alpha_p+\beta_p$	$\alpha_p-\beta_p$
$\omega < 100$ МэВ					
LEX	53	$11{,}8 \pm 1{,}1$	$1{,}1 \pm 1{,}4$	$12{,}8 \pm 2{,}0$	$10{,}7 \pm 1{,}6$
DR		$11{,}9 \pm 1{,}3$	$1{,}0 \pm 1{,}6$	$12{,}9 \pm 2{,}2$	$10{,}9 \pm 1{,}9$
$\omega < 150$ МэВ	$(\alpha_p+\beta_p) = 14{,}0 \pm 0{,}5$				
ELEX($\theta = 90^\circ$)	28	$11{,}3 \pm 2{,}2$	$2{,}7 \pm 2{,}2$	—	$8{,}5 \pm 4{,}4$
DR($\theta = 90^\circ$)		$11{,}7 \pm 1{,}0$	$2{,}3 \pm 1{,}1$	—	$9{,}4 \pm 2{,}0$
ELEX($\theta = 135^\circ$)	28	$12{,}0 \pm 1{,}8$	$2{,}0 \pm 1{,}8$	—	$10{,}0 \pm 3{,}5$
DR($\theta = 135^\circ$)		$11{,}1 \pm 0{,}7$	$2{,}9 \pm 0{,}7$	—	$8{,}2 \pm 1{,}3$
ELEX($\theta = 150^\circ$)	6	$14{,}4 \pm 2{,}7$	$-0{,}4 \pm 2{,}7$	—	$14{,}7 \pm 5{,}4$
DR($\theta = 150^\circ$)		$14{,}6 \pm 1{,}1$	$-0{,}6 \pm 1{,}1$	—	$15{,}2 \pm 2{,}1$

Независимый контроль фитов, использующих дисперсионную теорию, может быть сделан с помощью модельно-независимых разложений LEX и ELEX, описанных в п. 3.1. Разложение LEX неприменимо при энергиях, приближающихся к пионному порогу, поэтому в фите с помощью LEX мы ограничиваемся точками с $\omega < 100$ МэВ. При таких энергиях фит с LEX и фит с дисперсионной теорией (DR) дает почти идентичный результат (табл. 6). Если бы мы включили в фит LEX все точки до энергии 150 МэВ, результаты получились бы отличными от фита DR. В частности, электрическая поляри-

зуемость получилась бы равной $9{,}4 \pm 0{,}5$ вместо значения $11{,}7 \pm 0{,}8$, получаемого с помощью дисперсионной теории. Такое отличие иллюстрирует степень важности учета высших поправок в низкоэнергетическом разложении (1)*.

В фите с помощью ELEX, в котором главные поправки следующего порядка по энергии включены в члены Δ_1 и Δ_2, результаты фитирования точек вплоть до энергии 150 МэВ получаются довольно близкими к значениям, найденным с помощью дисперсионной теории. Однако наличие дополнительных фитируемых параметров (неизвестной функции $A(\theta)$) приводит к снижению точности определения поляризуемостей. Обе эти черты иллюстрируют результаты, помещенные в табл. 6, где показаны значения поляризуемостей, найденные из двухпараметрических фитов величин α_p и $A(\theta)$ при фиксированном угле θ и при наложенном ограничении на сумму поляризуемостей (12). Углы 90°, 135° и 150° выбраны потому, что при этих углах имеются данные как при очень низких энергиях, так и при энергиях выше 100 МэВ, что необходимо для анализа энергетической зависимости дифференциального сечения.

Среднее по результатам при трех углах дает значение $\alpha_p = 12{,}3 \pm 1{,}2$ (ELEX), которое можно сравнить с величиной $12{,}0 \pm 0{,}6$ (DR), полученной фитированием тех же 62 точек с помощью дисперсионой теории и того же ограничения (12). Естественно, что погрешности в однопараметрическом фите (DR) меньше, чем в фите ELEX с 4 параметрами (α_p, $A(90^\circ)$, $A(135^\circ)$ и $A(150^\circ)$). Однако согласие получаемых средних значений подтверждает полученную выше оценку, что теоретические неопределенности в поляризуемостях, найденных с помощью дисперсионной теории, не превышают $\pm 0{,}7$.

6. ЗАКЛЮЧЕНИЕ

Проведенный анализ всех имеющихся экспериментальных данных по дифференциальному сечению УРФ при энергиях до 150 МэВ привел к наиболее полному и точному на сегодняшний день определению экспериментальных значений электрической и магнитной поляризуемостей протона. Раздельный анализ ранних и поздних экспериментов, сделанный с учетом исправлений, внесенных самими авторами оригинальных работ, показал, что их результаты совместны как по сечениям, так и по получаемым поляризуемостям. Ранние и поздние работы дают примерно одинаковые конечные погрешности для поляризуемостей, и их объединение приводит к заметному снижению результирующих погрешностей. Наиболее достоверные значения

*Некоторое увеличение погрешностей в фите типа DR происходит из-за того, что в рамках дисперсионной теории зависимость дифференциального сечения от поляризуемостей протона носит не линейный, а квадратичный характер, что уменьшает чувствительность дифференциального сечения к поляризуемостям протона.

поляризуемостей протона равны

$$\alpha_p^{\text{эксп}} = 11{,}7 \pm 0{,}8 \text{ (стат.+сист.)} \pm 0{,}7 \text{ (теор.)}, \tag{21}$$

$$\beta_p^{\text{эксп}} = 2{,}3 \pm 0{,}9 \text{ (стат.+сист.)} \pm 0{,}7 \text{ (теор.)}. \tag{22}$$

В отличие от «глобальных» значений поляризуемостей из [4], вошедших в компиляцию PDG [69], экспериментальные значения (21) определены без использования теоретической величины $(\alpha_p + \beta_p)^{\text{теор}}$, предсказываемой ПС (11). Следующая из (21) и (22) сумма поляризуемостей

$$\alpha_p^{\text{эксп}} + \beta_p^{\text{эксп}} = 14{,}0 \pm 1{,}3 \text{ (стат.+сист.)} \pm 0{,}6 \text{ (теор.)} \tag{23}$$

хорошо согласуется с теоретическим значением (12) и указывает в пределах погрешностей на нулевую аддитивную константу в правиле сумм (см. сноску на с.231). Однако отметим, что экспериментальные и теоретические погрешности в (21), (22) и (23) все еще не малы. Это прежде всего относится к значениям $\beta_p^{\text{эксп}}$ и $\alpha_p^{\text{эксп}} + \beta_p^{\text{эксп}}$.

Планирование новых экспериментальных исследований УРФ на протоне в допороговой области должно исходить из уже достигнутого уровня точности измерений. Чтобы существенно уменьшить экспериментальные погрешности в значениях $\alpha_p^{\text{эксп}}$ и $\beta_p^{\text{эксп}}$, необходимо повысить статистическую и систематическую точность измерений дифференциального сечения до 1–2 %. Уменьшение теоретической (модельной) погрешности в значениях $\alpha_p^{\text{эксп}}$ и $\beta_p^{\text{эксп}}$ может быть достигнуто, если такие измерения проводить в интервале $\omega \lesssim 100$ МэВ, где в качестве фитирующего сечения можно использовать LEX или ELEX. Для снижения погрешности в значении $\beta_p^{\text{эксп}}$ важно провести точные измерения угловой зависимости дифференциального сечения при разных энергиях. Проекты таких измерений существуют [87, 88]. Измерения асимметрии сечения рассеяния с линейно поляризованными фотонами также были бы полезны, но, по-видимому, они пока почти не реальны.

Интересно сравнить поляризуемости протона (21) с предсказаниями некоторых теоретических моделей (см. табл. 7). Значение электрической поляризуемости $\alpha_p^{\text{НКМ}} = 3{,}1$, получаемое в рамках нерелятивистской кварковой модели [31, 42], более чем в три раза отличается от соответствующего экспериментального результата. Величина $\alpha_p^{\text{НКМ}}$ слабо зависит от формы потенциала qq-взаимодействия при условии, что его параметры подобраны так, чтобы удовлетворительно воспроизводить спектр низших возбуждений протона. Указанное расхождение вызвано существенными недостатками НКМ, в частности, игнорированием мезонного облака на периферии нуклона. Уже давно было показано, что вклад пионного облака в α_p составляет величину $\sim 10{-}20$ [41, 89, 90], где численное значение зависит от параметра обрезания на малых расстояниях. Зарядовый радиус протона в НКМ ($\langle r_E^2 \rangle_p^{\text{НКМ}} = 0,29$ фм^2) также получается маленьким по сравнению с экспериментальным значением

$\langle r_E^2 \rangle_p^{\text{эксп}} = 0{,}78 \pm 0{,}03$ фм^2 [91], что также можно объяснить неучетом мезонного облака.

Таблица 7. Теоретические значения поляризуемостей протона (в ед. 10^{-4} фм^3), вычисленные в рамках нерелятивистской кварковой модели (НКМ), киральной теории возмущений (КТВ) и дисперсионных правил сумм (ПС)

Теория, ссылка	α_p	β_p	$\alpha_p + \beta_p$	$\alpha_p - \beta_p$
НКМ [31, 42]	3,1			
КТВ [92]	10,5±2,0	3,5±3,6	14,0±4,1	7,0±4,1
[47]	20,8	14,7	35,2	6,1
ПС [31, 72]	9,0±2,6	5,2∓2,6	14,2±0,5	3,8±4,7
[93]				3,2±2,6

В настоящее время для учета мезонной периферии адронов часто применяется киральная теория возмущений (КТВ) [47, 92]. В одном из вариантов такой теории с феноменологическим добавлением Δ-резонансного вклада были получены значения поляризуемостей протона $\alpha_p^{\text{КТВ}} \simeq 10{,}5$ и $\beta_p^{\text{КТВ}} \simeq 3{,}5$ [92] (см. в табл. 7), которые, на первый взгляд, хорошо согласуются с экспериментом. Однако работа [92] предсказывает слишком большое отличие суммы поляризуемостей протона от суммы поляризуемостей нейтрона, а именно величина $\Delta S = (\alpha_p + \beta_p) - (\alpha_n + \beta_n)$ получается в [92] равной $\Delta S = 14{,}0 - 21{,}2 = -7{,}2$, тогда как строгое ПС (11) дает $\Delta S = 14{,}0 - 15{,}2 = -1{,}2 \pm 0{,}3$ (см. в [16, 31]). Указанное расхождение может быть связано с непоследовательным учетом резонансных и некоторых других вкладов в КТВ. В работе [47], где сделана попытка более последовательно учесть Δ-изобару, полученные предсказания для поляризуемостей оказались далеки от экспериментальных значений (см. табл. 7).

До сих пор наиболее надежным методом расчета поляризуемостей протона остаются дисперсионные ПС. Одним из таких ПС является соотношение (11), определяющее величину $\alpha_p + \beta_p$. Более сложные соотношения существуют и для разности поляризуемостей $\alpha_p - \beta_p$ (см. обзор [31]). При вычислении разности приходится использовать результаты мультипольных анализов фоторождения пионов на протоне и опираться на плохо известные пока величины, характеризующие t-канальные обмены в УРФ. Поэтому неопределенности в получаемых предсказаниях пока не малы (см. табл. 7). Ситуация может измениться в ближайшем будущем в связи с прогрессом экспериментальных исследований УРФ при высоких энергиях.

В заключение отметим, что без учета экспериментальных значений поляризуемостей нуклонов (наряду с другими низкоэнергетическими характери-

стиками) нельзя сформулировать адекватное модельное описание их структуры на средних и больших расстояниях.

Настоящая работа поддержана грантами ИНТАС — РФФИ 97-576 и РФФИ 96-02-17590. Один из авторов (А.Л.) благодарит A.M.Nathan за предоставленные экспериментальные данные и полезные обсуждения рассмотренной проблемы.

СПИСОК ЛИТЕРАТУРЫ

1. **Federspiel F.J. et al.** — Phys. Rev. Lett., 1991, v.67, p.1511.
2. **Zieger A. et al.** — Phys. Lett., 1992, v.B278, p.34.
3. **Hallin E.L. et al.** — Phys. Rev., 1993, v.C48, p.1497.
4. **Mac Gibbon B.E. et al.** — Phys. Rev., 1995, v.C52, p.2097.
5. **Molinari C. et al.** — Phys. Lett., 1996, v.B371, p.181.
6. **Peise J. et al.** — Phys. Lett., 1996, v.B384, p.37.
7. **Blanpeid G. et al.** — Phys. Rev. Lett., 1996, v.76, p.1023; ibid., 1997, v.79, p.4337.
8. **Tonnison J. et al.** — Phys. Rev. Lett., 1998, v.80, p.4382.
9. **Александров Ю.А.** — Фундаментальные свойства нейтрона. М.: Атомиздат, 1995.
10. **Schmiedmayer J. et al.** — Phys. Rev. Lett., 1991, v.66, p.1015.
11. **Koester L. et al.** — Phys. Rev., 1995, v.C51, p.3363.
12. **Еник Т.Л. и др.** — ЯФ, 1997, т.60, с.648.
13. **Rose K.W. et al.** — Nucl. Phys., 1990, v.A514, p.621.
14. **Kolb N.R. et al.** — nucl-ex/0003002.
15. **Hornidge D.L. et al.** — Phys. Rev. Lett., 2000, v.84, p.2334.
16. **Levchuk M.I., L'vov A.I.** — Nucl. Phys., 2000, v.A674 (in press, nucl-th/9909066).
17. **Antipov Yu.M. et al.** — Phys. Lett., 1983, v.B121, p.445.
18. **Айбергенов Т.А. и др.** — Краткие сообщения по физике, 1984, выпуск 5, с.31; Cz. J. Phys., 1986, v.B36, p.938.
19. **Kaloshin A.E., Serebryakov V.V.** — Phys. Lett., 1992, v.B278, p.198; Z. Phys., 1994, v.C64, p.689.
20. **Kaloshin A.E., Persikov V.M., Serebryakov V.V.** — Phys. Atom. Nucl., 1994, v.57, p.2207.
21. **Babusci D. et al.** — Phys. Lett., 1992, v.B277, p.158; ibid., 1993, v.B314, p.112.
22. **Donoghue J.F., Holstein B.R.** — Phys. Rev., 1993, v.D48, p.137.
23. **Гольданский В.И. и др.** — Nucl. Phys., 1960, v.18, p.473; ЖЭТФ, 1960, т.38, с.1695.
24. **Баранов П.С. и др.** — Phys. Lett., 1974, v.B52, p.122; ЯФ, 1975, т.21, с.689.
25. **Powell J.L.** — Phys. Rev., 1949, v.75, p.32.
26. **Klein A.** — Phys. Rev., 1955, v.99, p.998.
27. **Baldin A.M.** — Nucl. Phys., 1960, v.18, p.318.

28. **Петрунькин В.А.** — а) ЖЭТФ, 1961, т.40, с.1148; б) Nucl. Phys., 1964, v.55, p.197; в) Труды ФИАН, 1968, т.41, с.165.

29. **Barashenkov V.S., Kaiser H.J., Ogreba A.A.** — Phys. Lett., 1962, v.2, p.33.

30. **Damashek M., Gilman F.J.** — Phys. Rev., 1970, v.D1, p.1319.

31. **Петрунькин В.А.** — ЭЧАЯ, 1981, т.12, с.692.

32. **Babusci D., Giordane G., Matone G.** — Phys. Rev., 1998, v.C57, p.291.

33. **Лапидус Л.И.** — ЖЭТФ, 1962, т.43, с.1358.

34. **Arndt R.A., Strakovsky I.I., Workman R.L.** — Phys. Rev., 1996, v.C53, p.430; ibid., 1997, v.C56, p.577 (программа SAID, описанная там).

35. **Hanstein O., Drechsel D., Tiator L.** — Nucl. Phys., 1998, v.A632, p.561.

36. **Львов А.И.** — ЯФ, 1981, т.34, с.1075.

37. **Петрунькин В.А., Львов А.И.** — В сб.: Труды 8-го Межд. семинара по электромагнитным взаимодействиям ядер при низких и средних энергиях. М.: ИЯИ, 1991.

38. **L'vov A.I., Petrun'kin V.A., Schumacher M.** — Phys. Rev., 1997, v.C55, p.359.

39. **Guiasu I., Pomponiu C., Radescu E.E.** — Ann. Phys. (N.Y.), 1978, v.114, p.296.

40. **Ахмедов Д.М., Фильков Л.В.** — ЯФ, 1981, т.33, с.1083.

41. **Weiner R. , Weise W.** — Phys. Lett., 1985, v.B159, p.85.

42. **Schoberl F., Leeb H.** — Phys. Lett., 1986, v.B166, p.355.

43. **Bernard V. et al.** — Phys. Lett., 1993, v.B319, p.269.

44. **Broniowski W., Cohen T.D.** — Phys. Rev., 1993, v.D47, p.299.

45. **Anisovich V.V. et al.** — Quark Model and High Energy Collisions. Singapore: World Scientific, 1985.

46. **Nikolov E.N., Broniowski W., Goeke K.** — Nucl. Phys., 1994, v.A579, p.398.

47. **Hemmert T.R., Holstein B.R., Kambor J.** — Phys. Rev., 1997, v.D55, p.5598.

48. **Говорков Б.Б. и др.** — ДАН, 1956, т.111, с.988.

49. **Oxley C., Telegdi V.** — Phys. Rev., 1955, v.100, p.435; Nuovo Cim. Suppl., 1957, v.2, p.953; **Oxley C.** — Phys. Rev., 1958, v.106, p.733.

50. **Hyman L. et al.** — Phys. Rev. Lett., 1959, v.3, p.93.

51. **Bernardini G. et al.** — Nuovo Cim., 1961, v.18, p.1203.

52. **Pugh G. et al.** — Phys. Rev., 1957, v.105, p.982; ibid., 1955, v.100, p.1245; MIT Summer Study, 1967, p.555;
Frish D. — priv. comm.

53. **Баранов П.С., Фильков Л.В.** — ЭЧАЯ, 1976, т.7, с.108.

54. **Nathan A.M.** — priv. comm.

55. **Thirring W.** — Philos. Mag., 1950, v.41, p.1193.

56. **Low F.** — Phys. Rev., 1954, v.96, p.1428.

57. **Gell-Mann M., Goldberger L.** — Phys. Rev., 1954, v.96, p.1433.

58. **Шехтер В.М.** — ЯФ, 1968, т.7, с.1272.

59. **Choudhury S.R., Freedman D.Z.** — Phys. Rev., 1968, v.168, p.1739.

60. **L'vov A.I.** — Preprint FIAN #344, Moscow, 1987.

61. **Максименко Н.В., Шульга С.П.** — ЯФ, 1990, т.52, с.524.
62. **Ragusa S.** — Phys. Rev., 1975, v.D11, p.1536; ibid., 1996, v.D53, p.63.
63. **Gerasimov S.B., Soloviev L.D.** — Nucl. Phys., 1965, v.74, p.589.
64. **Пронько Г.П.** — ЯФ, 1975, т.22, с.141.
65. **Guiasu I., Radescu E.E.** — Phys. Rev., 1978, v.D18, p.651.
66. **Баранов П.С., Фильков Л.В., Штарков Л.Н.** — Письма в ЖЭТФ, 1974, т.20, с.762.
67. **Терентьев М.В.** — ЯФ, 1972, т.16, с.1044.
68. **Arndt R.A., Workman R.L., Pavan M.M.** — Phys. Rev., 1994, v.C49, p.2729.
69. **Particle Data Group (Caso C. et al.)** — Eur. J. Phys., 1998, v.C3, p.1.
70. **Ритус В.И.** — ЖЭТФ, 1957, т.33, с.1264; там же, т.32, с.1536.
71. **Prange R.E.** — Phys. Rev., 1958, v.110, p.240.
72. **Львов А.И., Петрунькин В.А., Старцев С.А.** — ЯФ, 1979, т.29, с.1265.
73. **Logunov A.A., Isaev P.S.** — Nuovo Cim., 1958, v.10, p.917.
74. **Oehme R., Taylor J.G.** — Phys. Rev., 1959, v.113, p.371.
75. **Brodsky S.J., Close F.E., Gunion J.F.** — Phys. Rev., 1972, v.D5, p.1384.
76. **Close F.E., Gunion J.F.** — Phys. Rev., 1971, v.D4, p.742.
77. **Fox G.C., Freedman D.Z.** — Phys. Rev., 1969, v.182, p.1628.
78. **Breakstone A.M. et al.** — Phys. Rev. Lett., 1981, v.47, p.1778.
79. **Bauer T.H., Spital R.D., Yennie D.R.** — Rev. Mod. Phys., 1978, v.50, p.201.
80. **Ballam J. et al.** — Phys. Rev., 1972, v.D5, p.545.
81. **Bourrely C., Leader E., Wray D.** — Nuovo Cim., 1977, v.A35, p.559.
82. **Babusci D. et al.** — Phys. Rev., 1998, v.C58, p.1013.
83. **Drechsel D., Krein G., Hanstein O.** — Phys. Lett., 1998, v.B420, p.248.
84. **Hünger A. et al.** — Nucl. Phys., 1997, v.A620, p.385.
85. **L'vov A.I., Nathan A.M.** — Phys. Rev., 1999, v.C59, p.1064.
86. **Баранов П.С. и др.** — ЯФ, 1967, т.5, с.1221;
Говорков Б.Б., Денисов С.П., Минарик Е.И. — Труды ФИАН, 1971, т.54.
87. **Balin D.V. et al.** — Preprint 2104, Petersburg Nuclear Physics Institute, 1996.
88. **L'vov A.I. et al.** — Preprint 91-24, Institute of Nuclear Physics, Novosibirsk, 1991.
89. **Barashenkov V.S., Barbashov B.M.** — Nucl. Phys., 1958, v.9, p.426.
90. **Kanazawa A.** — Nucl. Phys., 1961, v.24, p.524.
91. **Rosenfelder R.** — Phys. Lett., 2000, v.B479, p.381;
Melnikov K., van Ritbergen T. — Phys. Rev. Lett., 2000, v.84, p.1673.
92. **Bernard V., Kaiser N., Meissner U.-G.** — Int. J. Mod. Phys., 1995, v.E4, p.193.
93. **Holstein B.R., Nathan A.M.** — Phys. Rev., 1994, v.D49, p.6101.

«ФИЗИКА ЭЛЕМЕНТАРНЫХ ЧАСТИЦ И АТОМНОГО ЯДРА»
2001, ТОМ 32, ВЫП. 3

УДК 539.173

ПОИСКИ МАГНИТНОГО МОМЕНТА НЕЙТРИНО

А.В.Дербин

Петербургский институт ядерной физики РАН, Гатчина, Россия

Результаты экспериментов по измерению сечения упругого рассеяния реакторных нейтрино на электроне анализируются с целью поиска вклада в сечение от магнитного момента нейтрино. Сравниваются возможности поиска магнитного момента на ускорителях и реакторе. Найден верхний предел на возможный магнитный момент нейтрино $\mu_\nu \leq 1{,}5 \cdot 10^{-10}\ \mu_B$ (90 % у. д.). Обсуждаются возможности увеличения чувствительности реакторных экспериментов до уровня $10^{-11}\ \mu_B$.

The results of measurements reactor neutrino-electron elastic scattering cross-section are processed to search for additional part connected with magnetic moment of the neutrino. The possibilities of the accelerator and reactor experiments in search for magnetic moment are compared. It is shown that the upper limit on the neutrino magnetic moment is $\mu_\nu \leq 1.5 \cdot 10^{-10}\ \mu_B$ (90 % c.l.). The possibilities to increase the sensitivity of reactor's experiments up to $10^{-11}\ \mu_B$ are discussed.

1. ВВЕДЕНИЕ

Магнитный момент нейтрино (μ_ν) в стандартной теории пропорционален массе нейтрино (m_ν), за счет которой происходит изменение спиральности нейтрино, необходимое для оператора магнитного момента нейтрино (рис. 1, *а*). Величина μ_ν равна [1]:

$$\mu_\nu = (3m_e G_F/4\pi\sqrt{2}) m_\nu \mu_B \approx 3{,}2 \cdot 10^{-19}\ (m_\nu/1\ \text{эВ})\ \mu_B,$$

где m_e — масса электрона, G_F — константа Ферми.

Современное ограничение на массу электронного антинейтрино составляет 2,5 эВ [2]. Значит, ожидаемая величина для магнитного момента нейтрино — не более чем $\sim 10^{-18}\ \mu_B$, где $\mu_B = e/2m_e$ — электронный магнетон Бора, e — заряд электрона. Такое значение на восемь порядков меньше чувствительности современных лабораторных экспериментов. Наиболее чувствительным к магнитному моменту оказывается процесс упругого рассеяния нейтрино на электроне. Измеренные значения сечения этого процесса позволяют ввести ограничения на возможный магнитный момент электронных антинейтрино $\mu_\nu \leq (1{,}5 \div 4{,}0) \cdot 10^{-10}\ \mu_B$ [3], для электронных нейтрино $\mu_\nu \leq 10{,}8 \cdot 10^{-10}\ \mu_B$ [4] и для мюонных нейтрино $\mu_\nu \leq (7{,}4 - 9{,}5) \cdot 10^{-10}\ \mu_B$ [5].

Астрофизические ограничения, использующие в основном тот факт, что рассеяние нейтрино с большим магнитным моментом на заряженных частицах приводит к эффективному образованию правых нейтрино, не участвующих в слабом взаимодействии и, таким образом, меняющих динамику звезд, находятся в районе 10^{-10}–10^{-11} μ_B [6]. Наблюдение нейтрино от взрыва сверхновой SN1987A позволило получить более сильные пределы $\sim 10^{-12}$–10^{-14} μ_B [7]. Однако предложенные сценарии резонансных переходов $\nu_l \to \nu_r$, а также возможность существования недиагональных магнитных моментов [8] позволяют согласовать даже значение $\mu_\nu \approx 10^{-11}$ μ_B с данными по сверхновой SN1987A.

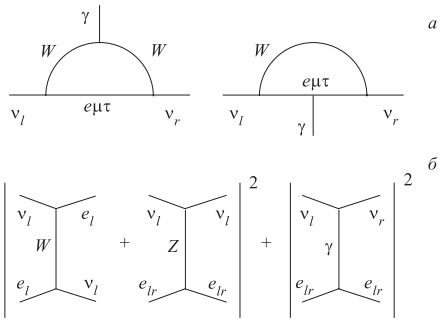

Рис. 1. *а*) Диаграммы, показывающие возникновение магнитного момента у нейтрино. *б*) Рассеяние нейтрино на электроне за счет слабого и электромагнитного взаимодействия

В теоретических моделях с правыми бозонами или расширенным сектором скалярных частиц магнитный момент может быть пропорционален массе промежуточного лептона и, как показано в работах [9], достигать значений $\sim 10^{-11}\mu_B$. Сложность этих моделей, связанная с возникновением большой массы у нейтрино, возможно, преодолевается в моделях с $SU(2)_\nu$-симметрией между ν_l и ν_r [10] или $SU(2)_H$-симметрией между электронным и мюонным семействами [11].

2. НЕДОСТАТОК СОЛНЕЧНЫХ НЕЙТРИНО И МАГНИТНЫЙ МОМЕНТ НЕЙТРИНО

Интерес к огромному (для стандартной теории) магнитному моменту нейтрино ($\sim 10^{-11}\mu_B$) связывается с проблемой недостатка солнечных нейтрино. В настоящее время имеются данные по регистрации солнечных нейтрино для пяти детекторов. Это Cl–Ar- и два Ga–Ge-радиохимических детектора, регистрирующих нейтрино по реакции обратного K-захвата, а также два детектора, регистрирующих рассеяние нейтрино на электроне по черенковскому излучению электронов отдачи. В табл. 1 приведены отношения экспериментально измеренной скорости счета нейтрино к теоретически ожидаемой в стандартной солнечной модели [12]. Первая погрешность — экспериментальная, вторая связана с неопределенностью теоретических расчетов.

Одно из возможных объяснений дефицита солнечных нейтрино состоит в том, что нейтрино имеет достаточно большой магнитный момент, взаимодей-

Таблица 1. Результаты измерений потока солнечных нейтрино в сравнении с теоретическими предсказаниями

Эксперимент	Эксперимент/теория
Cl–Ar, Homestake [13]	$0{,}28 \pm 0{,}02 \pm 0{,}04$
Ga–Ge, SAGE [14]	$0{,}53 \pm 0{,}10 \pm 0{,}03$
Ga–Ge, GALLEX [15]	$0{,}51 \pm 0{,}05 \pm 0{,}03$
Kamiokande [16]	$0{,}42 \pm 0{,}06 \pm 0{,}07$
Superkamiokande [17]	$0{,}37 \pm 0{,}02 \pm 0{,}07$

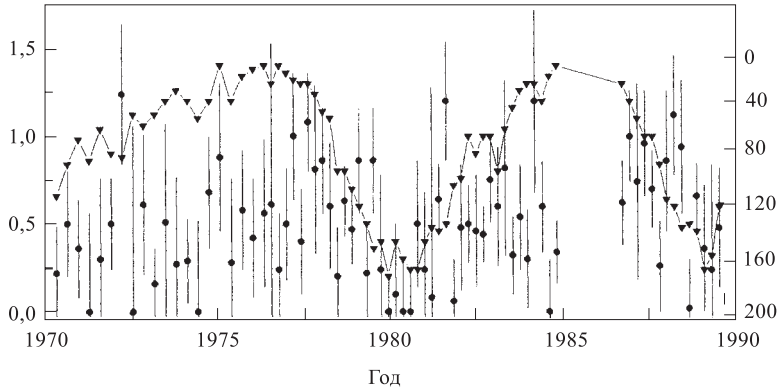

Рис. 2. Результаты Cl–Ar-эксперимента [13]. Точками показано среднее число атомов ^{37}Ar, образующихся в детекторе в сутки (левая шкала). Непрерывная кривая показывает среднемесячное число пятен на Солнце (правая шкала)

ствие которого с магнитным полем Солнца приводит к перевороту спиральности нейтрино, а правые нейтрино не участвуют в реакции заряженных токов. Эта идея получила сильную поддержку после того, как в ряде работ [18], примерно через 10 лет после начала работы Cl–Ar-детектора, появились указания на возможность существования антикорреляции между потоком нейтрино, регистрируемым в Cl–Ar-эксперименте, и числом солнечных пятен. Солнечные пятна есть результат пересечения поверхности Солнца магнитными силовыми линиями, и число солнечных пятен отражает напряженность магнитных полей вблизи поверхности Солнца. На рис. 2 показан полный 22-летний цикл солнечной активности в сравнении с результатами, полученными на Cl–Ar-детекторе [19]. Непрерывная кривая показывает среднемесячное число солнечных пятен, а точками представлено среднее число образующихся в сутки атомов ^{37}Ar [20].

В 1986 г. в работах [21] было высказано предположение, что если данная корреляция действительно существует, она могла бы быть обусловлена взаимодействием магнитного момента нейтрино с магнитным полем внутри конвективной зоны Солнца. Конвективная зона занимает ближайшую к поверхности область, примерно одну четверть радиуса. Когда Солнце активно, в конвективной зоне возникает тороидальное магнитное поле с напряженностью $H = 1 \div 10$ кГс. Пересекая магнитное поле, направленное перпендикулярно движению, спин нейтрино прецессирует, и левые нейтрино переходят в правые. Число левых нейтрино, вылетающих из Солнца, может быть оценено по простой формуле: $H \propto \cos^2(\mu_\nu HL)$, где L — глубина конвективной зоны ($L \approx 2 \cdot 10^{10}$ см). Таким образом, авторы [21] показали, что значение магнитного момента, необходимое для того, чтобы ожидаемые одиннадцатилетние (и полугодовые [21]) вариации потока солнечных нейтрино могли наблюдаться на упомянутых детекторах солнечных нейтрино, дожно быть в диапазоне $10^{-10} \div 10^{-12}\mu_B$.

В работе [22] утверждается, что антикорреляция потока нейтрино оказывается более значимой с величиной магнитного потока у поверхности Солнца, чем с числом солнечных пятен и, что интересно, она оказывается более значимой для магнитного потока вблизи центра видимого диска Солнца. В эксперименте Дэвиса регистрируются, в основном, нейтрино, возникающие в β^+-распаде ^{8}B и при K-захвате в ^{7}Be. Реакции образования этих нейтрино идут в самом центре Солнца, в области, размер которой примерно в пять раз меньше области pp-реакций. Следовательно, нейтрино, возникающие при распаде B и Be, приходящие на Землю, пересекают поверхность Солнца вблизи центра видимого диска.

Из-за большой неопределенности в погрешностях Cl–Ar-эксперимента количественная оценка коэффициента корреляции представляет сложности. Стандартный коэффициент корреляции, вычислявшийся в работах [18], соответствовал уровню значимости $\sim 1\,\%$. В вышеупомянутой работе [22] вычислялся ранговый коэффициент корреляции (коэффициент Спирмана [23]), и уровень значимости для определенного усреднения данных по сериям достигал значения 10^{-7}. Такой высокий уровень достоверности, скорее всего, связан с конкретным выбором метода усреднения данных, поскольку коэффициент Спирмана чувствителен к методу усреднения.

В других детекторах солнечных нейтрино (SAGE, GALLEX и (Super)Kamiokande) не наблюдаются сколько-нибудь значимые корреляции между регистрируемым потоком нейтрино и магнитной активностью Солнца. На рис. 3 показаны результаты коллаборации GALLEX [15]. Максимум солнечной активности был в 1991–1992 гг., минимум — в 1994–1995 гг., но нет сколько-нибудь заметных изменений в скорости счета за эти периоды. Такая же ситуация с результатами эксперимента Kamiokande (рис. 4).

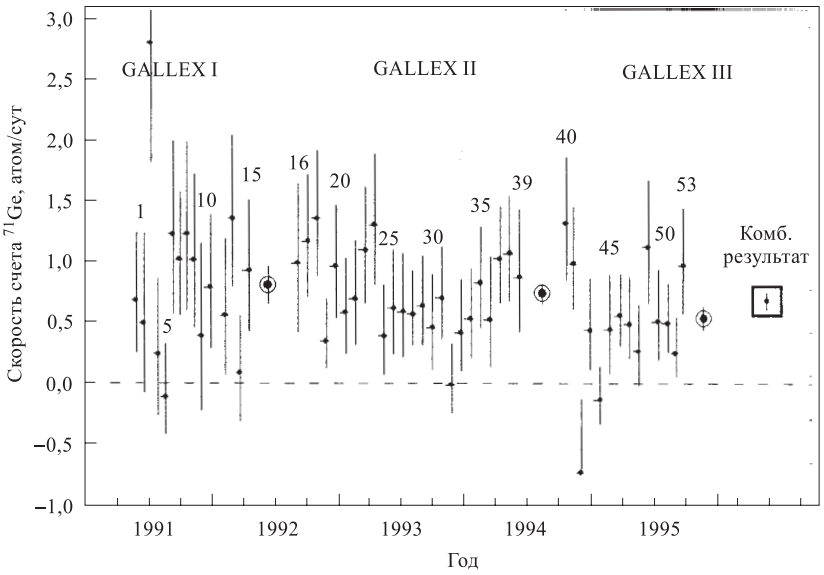

Рис. 3. Результаты эксперимента на Ga–Ge-детекторе коллаборации GALLEX [15]. Максимум солнечной активности наблюдался в 1991–1992 гг., минимум — в 1994–1995 гг.

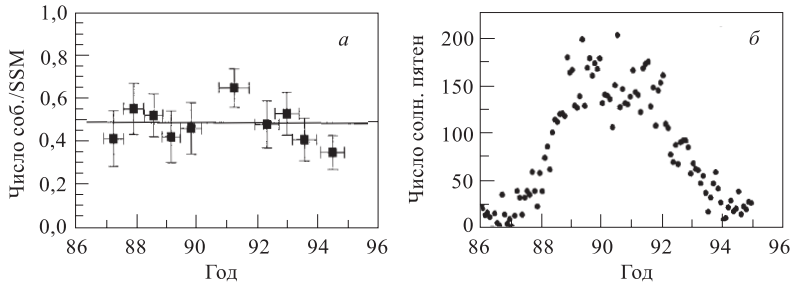

Рис. 4. *а*) Результаты эксперимента Kamiokande [16]. Отношение числа зарегистрированных событий (ν, e)-рассеяния к ожидаемому в стандартной солнечной модели. *б*) Количество солнечных пятен

Если данная корреляция действительно существует, причина расхождения может состоять в том, что все детекторы регистрируют нейтрино от различных частей энергетического спектра Солнца. Порог Cl-детектора равен 814 кэВ, Ga–Ge-детектора — 233 кэВ, порог регистрации Kamiokande 6,5–7 МэВ. При учете резонансных осцилляций нейтрино в веществе [24] вероятность перехода левого нейтрино в правое будет зависеть от энергии нейтрино, и сравнение результатов с разных детекторов усложняется [25].

3. РАССЕЯНИЕ НЕЙТРИНО НА ЭЛЕКТРОНЕ

Магнитный момент нейтрино имеет давнюю историю, восходящую к гипотезе Паули и первым вычислениям сечения рассеяния нейтрино на электроне [26]. Долгое время отрицательные результаты экспериментов по поиску взаимодействия нейтрино с электроном, чувствительность которых была далека от значения 10^{-44} см^2, интерпретировались как верхнее ограничение на возможный магнитный момент нейтрино [27]. Взаимодействие нейтрино, обладающего ненулевым магнитным моментом, с электромагнитным полем $F^{\alpha\beta}$ описывается лагранжианом

$$L = \frac{1}{2}\mu_\nu \left(\frac{e}{2m_e}\right) \bar{\nu}\sigma_{\alpha\beta}\nu F^{\alpha\beta}, \tag{1}$$

где μ_ν — магнитный момент нейтрино в единицах электронного магнетона Бора, $\sigma_{\alpha\beta}$ — матрица Паули. Такое нейтрино будет взаимодействовать с любой заряженной частицей, в том числе и с электроном.

В стандартной теории рассеяние нейтрино, имеющего магнитный момент, определяется как слабым взаимодействием, так и однофотонным обменом, причем спиральность начального и конечного состояний нейтрино в первом случае одинакова, а во втором различна. Поэтому амплитуды слабого и магнитного рассеяния не интерферируют, и полное сечение есть просто сумма сечений; при этом вклад от магнитного момента, ожидаемого в стандартной теории, пренебрежимо мал (рис. 1, *б*).

Дифференциальное сечение слабого рассеяния электронного антинейтрино на электроне в стандартной теории имеет вид [28]:

$$\frac{d\sigma}{dE} = \frac{2G_F^2 m_e}{\pi}\left(g_r^2 + g_l^2\left(1 - \frac{E_e}{E_\nu}\right)^2 - g_l g_r \frac{m_e E_e}{2E_\nu^2}\right), \tag{2}$$

где m_e — масса электрона, g_r и g_l зависят лишь от угла Вайнберга ($g_r = \sin^2\theta_W$, $g_l = 1/2 + \sin^2\theta_W$), E_ν и E_e — энергия налетающего нейтрино и энергия электрона отдачи.

Сечение рассеяния нейтрино, связанное с магнитным моментом, пропорционально μ_ν^2 [26]:

$$\frac{d\sigma}{dE_e} = \pi r_0^2 \mu_\nu^2 \left(\frac{1}{E_e} - \frac{1}{E_\nu}\right), \tag{3}$$

где $r_0 = 2{,}818 \cdot 10^{-13}$ см — классический радиус электрона, μ_ν — магнитный момент нейтрино в электронных магнетонах Бора. Зависимость сечений магнитного и слабого рассеяния от энергии E_e существенно различны; при

$E_e \ll E_\nu$ их отношение пропорционально $1/E_e$, т.е. понижение порога регистрации электронов улучшает чувствительность эксперимента к магнитному моменту, если фон при этом возрастает слабее, чем $1/E_e \ln E_e$.

Интегрируя по энергии электрона, находим, что полное сечение рассеяния, связанного с магнитным моментом, равно

$$\sigma(E_e \geqslant T) = \pi r_0^2 \mu_\nu^2 \left(\ln \left(\frac{E_{e\,\max}}{T} \right) + \frac{T}{E_{e\,\max}} - 1 \right). \tag{4}$$

В этой формуле T — порог регистрации электронов отдачи, а $E_{e\ \max} = E_\nu(2E_\nu/(2E_\nu + m_e))$ есть максимально возможная энергия электрона отдачи, которая очень близка к энергии нейтрино, если $E_\nu \gg m_e$.

Интегральное сечение (ν, e)-рассеяния в стандартной теории, как следует из (2), пропорционально E_ν. Это означает, что для того, чтобы увеличить отношение сигнал/фон (если фон связан только со слабым рассеянием), необходимо использовать нейтринные источники с малой энергией нейтрино. Например, сечение (ν_μ, e)-рассеяния, измеренное коллаборацией CHARM [29] на ускорителе SPS (CERN), составило ~ 25000 в единицах 10^{-45} см^2 (табл. 2). В то же время ожидаемое сечение для магнитного момента, равного $10^{-10}\mu_B$, составляет только 4 в тех же единицах. Это означает, что необходимо измерить сечение (ν_μ, e)-рассеяния с точностью лучше, чем 4/25000 (т.е. $\sim 10^{-4}$), чтобы почувствовать вклад от магнитного момента, равного $10^{-10}\mu_B$. Даже эксперимент в Лос-Аламосе [4], где средняя энергия нейтрино, образующихся в результате распада остановившихся π-мезонов и мюонов, составляет 33 МэВ, уступает почти на два порядка по чувствительности к вкладу в сечение от магнитного момента реакторному эксперименту.

Таблица 2. Сравнение чувствительности к магнитному моменту нейтрино для экспериментов с различными источниками нейтрино

Источник нейтрино	Средняя энергия $\langle E_\nu \rangle$	Порог регистрации $\langle T \rangle$	$\sigma_{\rm weak}$ в ед. 10^{-45} см^2	σ_μ в ед. 10^{-45} см^2 $\mu_\nu = 10^{-10}\mu_B$
SPS (CERN)	25 ГэВ	2 ГэВ	25 000	4,0
LAMPF (Лос-Аламос)	30 МэВ	15 МэВ	100	0,5
Реактор	2 МэВ	0,5 МэВ	2	1,0

Главная проблема экспериментов на реакторе состоит в том, что фон, связанный с естественной или искусственной радиоактивностью, в несколько (иногда десятки) раз превышает фон от слабого рассеяния. Отметим, что в этом случае использование нейтрино с большей энергией увеличивает соотношение эффект/фон.

4. РЕЗУЛЬТАТЫ ЭКСПЕРИМЕНТОВ ПО ИЗМЕРЕНИЮ СЕЧЕНИЯ РАССЕЯНИЯ РЕАКТОРНЫХ НЕЙТРИНО НА ЭЛЕКТРОНЕ И ОГРАНИЧЕНИЕ НА МАГНИТНЫЙ МОМЕНТ НЕЙТРИНО

К настоящему времени опубликованы результаты по измерению сечения рассеяния реакторных нейтрино на электроне, полученные на трех различных детекторах.

Первые положительные результаты измерения сечения рассеяния нейтрино на электроне были представлены в 1976 г., ровно через 20 лет после прямого обнаружения нейтрино в реакции обратного β-распада. Детектор был создан в университете Калифорнии [30], и измерения проводились на реакторе «Savana River». Центральный детектор — пластический сцинтиллятор, непосредственно регистрирующий (ν, e)-рассеяние, имел массу 15,9 кг и был окружен NaI-детектором с массой 300 кг, пассивной защитой из свинца и жидким сцинтиллятором (2000 л). Большой NaI-детектор использовался для подавления фона от реакции обратного β-распада на протоне ($\nu p \to n e^+$), поскольку центральный детектор содержал водород. Этот фон коррелирует с работой реактора, и скорость счета от этой реакции в 30 раз превышала скорость счета от (ν, e)-рассеяния в диапазоне регистрации электронов отдачи $1{,}5 \div 4{,}5$ МэВ.

Второй детектор — это кремниевый мультидетектор с общей массой 75 кг, созданный в Петербургском институте ядерной физики. Измерения сечения (ν, e)-рассеяния проводились на реакторе Ровенской атомной станции [31, 32]. Детектор представлял собой сборку из 600 отдельных детекторов диаметром 30 и длиной 125 мм. Энергетическое разрешение отдельного детектора, измеренное по линии 122 кэВ от ^{57}Co, составляло ~ 5 кэВ, из-за дополнительной емкости, связанной с выводом сигнала, увеличивалось до ~ 15 кэВ. Мультидетектор вместе с первым слоем пассивной защиты с массой 300 кг находился внутри вакуумной камеры для подавления активности радона. Пассивная защита для подавления внешней γ- и нейтронной активности состояла из слоя ртути, меди и графита.

Третий детектор был создан в Курчатовском институте, и эксперимент проводился на реакторе в Красноярске [33, 34]. Детектор с массой 103 кг представлял собой сборку из 7 идентичных сцинтилляционных детекторов на основе гексафторбензола (C_6F_6), просматриваемых с обоих концов фотоумножителями. Порог регистрации электронов отдачи был равен 3,15 МэВ и обусловлен высоким уровнем фона естественной и искусственной радиоактивности. Существенное преимущество этого детектора состоит в его подземном расположении ($\approx$ 700 м в.э.), что позволяет снизить поток мюонов на три порядка по сравнению с поверхностью Земли.

Сложность экспериментов по изучению рассеяния реакторных нейтрино на электроне состоит в том, что сечение реакции мало ($\sim 10^{-44}$ см^2), един-

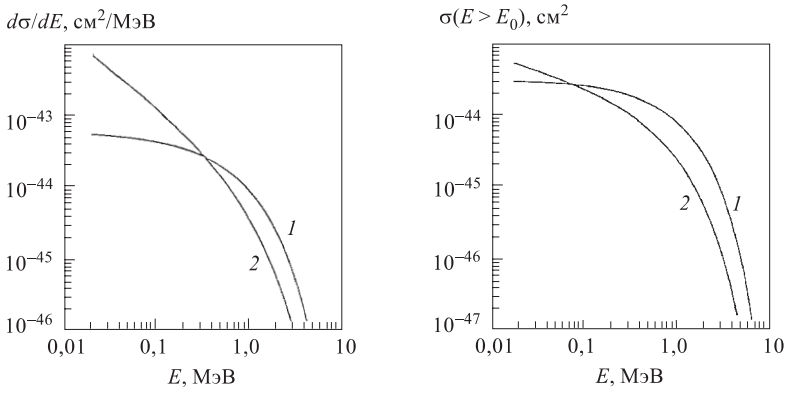

Рис. 5. Ожидаемый спектр электронов отдачи (дифференциальное сечение), возникающих при рассеянии реакторных нейтрино: *1* — стандартная теория ($\sin^2\theta_W = 0{,}23$); *2* — рассеяние за счет магнитного момента ($\mu_\nu = 10^{-10}\mu_B$)

Рис. 6. Интегральное сечение для интервала $E \div 9$ МэВ: *1* — слабое ($\sin^2\theta_W = 0{,}23$) и *2* — магнитное рассеяние ($\mu_\nu = 10^{-10}\mu_B$)

ственной регистрируемой частицей является электрон отдачи, а фон детектора, связанный с искусственной или естественной радиоактивностью, возрастает при уменьшении энергии. Поэтому приемлемое отношение эффект/фон удается получить лишь для широкого и, как правило, одного диапазона энергий электрона отдачи. Чтобы сравнить теоретические предсказания с результатами эксперимента и таким образом найти возможный вклад в экспериментально измеренное сечение от возможного магнитного момента нейтрино, необходимо сечения (2) и (3) усреднить как по спектру нейтрино, так и по интервалу энергий (E_1, E_2), в котором происходит регистрация электрона отдачи:

$$\sigma(E_1, E_2) = \int_{E_2}^{E_1} \int_{E_{\min}}^{\infty} \frac{d\sigma}{dE} N(E_\nu) dE_\nu dE_e. \tag{5}$$

Чтобы вычислить данное выражение нужно знать спектр антинейтрино от реактора. Это отдельная проблема реакторных экспериментов, выходящая за рамки данного обзора. Спектр нейтрино с энергией в интервале $2 \div 6$ МэВ известен с хорошей точностью ($\sim 4\,\%$) [35], поскольку 2 МэВ — это порог реакции обратного β-распада на протоне. При энергиях ниже 2 МэВ спектры вычислялись в работах [36], и величина погрешности в данном интервале составляет $5 \div 15\,\%$.

Ожидаемые спектры электронов отдачи или дифференциальные сечения рассеяния, усредненные по спектру реакторных нейтрино, показаны на рис. 5. Видно, что они сравниваются при энергии 320 кэВ для магнитного момента, равного $10^{-10}\mu_B$, и $\sin^2\theta_{\rm W} = 0{,}23$. Интегральные сечения для интервала от E до 9 МэВ приведены на рис. 6, и они оказываются равными лишь при энергии электронов отдачи, равной 70 кэВ.

К настоящему времени имеются экспериментальные данные по измерению сечения рассеяния нейтрино на электроне для шести различных интервалов электронов отдачи ($E_1 - E_2$), полученные на трех вышеупомянутых детекторах. Эти результаты можно представить в единицах сечения слабого рассеяния, вычисленного для установленного спектра нейтрино (табл. 3).

Таблица 3. Экспериментальные результаты измерения сечения рассеяния реакторных нейтрино на электроне и ограничения на магнитный момент

Интервал $E_1 - E_2$, МэВ	Отношение $\sigma_{\rm exp}/\sigma_{\rm weak}$	Ограничение на μ_ν в ед. $10^{-10}\,\mu_B$	Ссылка
1,0–3,0	1,36 ± 0,39	$\leq$ 1,8	[30]
3,0–4,5	2,07 ± 0,54	$\leq$ 3,4	[30]
1,0–4,0	1,15 ± 1,71	$\leq$ 2,4	[31]
3,15–5,2	1,21 ± 0,57	$\leq$ 2,4	[33]
0,6–2,0	1,23 ± 0,60	$\leq$ 1,4	[32]
3,15–5,2	0,92 ± 0,49	$\leq$ 1,9	[34]

Хотя в пределах одной погрешности пять из шести результатов согласуются со стандартной теорией, пять из них отклоняются в сторону больших сечений. Если для установления верхнего предела на возможный магнитный момент взять величину $(\sigma_{\rm exp} - \sigma_{\rm weak}) + \Delta\sigma_{\rm exp}$ (или $\Delta\sigma_{\rm exp}$, если $\sigma_{\rm exp} \leq \sigma_{\rm weak}$), то получим значения от 1,4 до 3,4 в единицах $10^{-10}\mu_B$. Предполагая, что увеличение измеренных сечений связано с магнитным моментом, и вычисляя величину χ^2 для различных значений μ_ν, получаем, что с 40 %-ной вероятностью возможно значение $\mu_\nu = 0$ (функция правдоподобия $P(\chi^2 > \chi^2_{\mu=0}) = 0{,}4$). С вероятностью 90 % $\mu_\nu \leq 1{,}9 \cdot 10^{-10}\mu_B$ ($P(\chi^2 > \chi^2_{\mu=1{,}9}) = 0{,}1$). Минимальное же значение $\chi^2_d = 0{,}7$ соответствует магнитному моменту, равному $1{,}15 \cdot 10^{-10}\mu_B$. Таким образом, гипотеза о том, что магнитный момент равен нулю, не может быть отвергнута на основе χ^2-критерия.

Для получения предела на μ_ν естественно использовать метод максимального правдоподобия. Для этого следует найти функцию правдоподобия $P(\mu)$, т.е. вычислить вероятность получения данных экспериментальных результатов для различных значений магнитного момента, в предположении, что

все результаты имеют нормальное распределение. Интегрируя эту функцию от нуля до значения μ_ν, для которого полученная площадь составляет 90 % ($\int P(\mu)d\mu = 0{,}9$), получаем, что $\mu_\nu \leq 1{,}5 \cdot 10^{-10}\,\mu_B$ для 90 %-ного уровня достоверности.

Имеющиеся экспериментальные результаты приведены также на рис. 7, показывающем зависимость отношения полного сечения магнитного рассеяния к слабому сечению от энергии. Используя погрешности нейтринных спектров, можно вычислить (задавшись определенным $\sin^2\theta_W$) связанную с ними погрешность в полном сечении, которая и будет определять возможное предельное ограничение на магнитный момент, даже если экспериментальная погрешность будет меньше, чем погрешность, связанная с неопределенностью спектра. Это верно до тех пор, пока не удастся с хорошей точностью измерить спектр электронов отдачи, чтобы можно было использовать различную энергетическую зависимость для слабого и магнитного рассеяния. Для этого необходимо, чтобы отношение вычисленных сечений, например, для двух интервалов, не зависело от спектра нейтрино. Понятно, что ширина этих интервалов должна быть существенно меньше, чем средняя ширина нейтринного спектра (~ 2 МэВ), а располагаться они должны как можно ближе к нулевой энергии. Пока это не решенная экспериментальная задача.

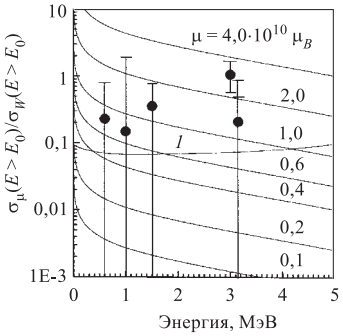

Рис. 7. Отношение полных сечений магнитного и слабого рассеяний в интервале энергий $E \div 9$ МэВ для различных значений магнитного момента (в ед. $10^{-10}\mu_B$). Кривая *1* показывает неопределенность, связанную с неточным знанием спектра нейтрино. Приведены также экспериментальные результаты (с погрешностями) в предположении, что отклонение $\sigma_{\rm exp}$ от $\sigma_{\rm weak}$ связано с магнитным моментом нейтрино

Зависимость погрешности, связанной с неопределенностью нейтринного спектра, в полном сечении для слабого взаимодействия от энергии показана на рис. 7 (кривая *1*). Неопределенность, связанная с неточным знанием $\sin^2\theta_W$, существенно ниже. Видно, что для нижнего порога $0{,}1 \div 1{,}0$ МэВ неопределенность в нейтринном спектре будет ограничивать возможный предел на магнитный момент величиной $(3{-}5)\cdot 10^{-11}\mu_B$.

5. ПЕРСПЕКТИВЫ

Каковы перспективы достигнуть точности $10^{-11}\mu_B$ в реакторных экспериментах? Единственная возможность связана с уменьшением порога регистрации электронов отдачи. Так, согласно рис. 7, для того, чтобы достиг-

нуть такой чувствительности, при пороге регистрации 1 МэВ необходимо измерить слабое сечение с точностью 0,3 %, при 100 кэВ — 0,9 % и при 20 кэВ — 1,8 %. Порог в 20 кэВ вполне реален для полупроводниковых детекторов, имеющих разрешение $\sim$ 2 кэВ. Основная проблема, конечно, связана с фоном.

На рис. 8 показаны результаты четырех экспериментов, в которых достигнуты рекордные уровни фона в низкоэнергетической области. В этих экспериментах производился поиск частиц — кандидатов на «темную материю». Если эти тяжелые частицы с массой более 1 ГэВ действительно существуют, они могут рассеиваться на ядрах, и ожидаемая энергия отдачи как раз лежит в килоэлектронвольтной области энергий. Приведенные спектры были измерены двумя HPGe-детекторами [37,38], одним Si(Li)-детектором [39] и NaI-детектором [40]. Детектор в эксперименте Гейдельберг—Москва был изготовлен из германия, обогащенного до 86 % изотопом ^{76}Ge [37]. Фон этого детектора равен 0,1 кэВ$^{-1}\cdot$кг$^{-1}$ в сутки, что почти на порядок ниже фона детектора из природного германия [38]. Фон кремниевого детектора равен 10 кэВ$^{-1}\cdot$кг$^{-1}$ в сутки.

Совершенствование пассивной и активной защит привело к тому, что в настоящее время фон детекторов связан не только с естественной (U, Th, ^{40}K) или искусственной (^{137}Cs, ^{60}Co,...) радиоактивностью, но и с активацией детекторов на поверхности Земли или радиоактивностью собственных изотопов. Так, для германиевого детектора активация изотопа ^{70}Ge быстрыми нейтронами по реакциям $(n, 3n)$ и $(n, \alpha 2n)$ приводит к скорости счета 5–10 распад/(кг·сут). Интересно отметить, что для Ge-детектора (особенно для обогащенного изотопом ^{76}Ge) не так давно открытый двухнейтринный 2β-распад может быть источником фона при поиске магнитного момента нейтрино.

Проблемы кремниевого детектора могут быть связаны с радиоактивным изотопом ^{32}Si, который образуется в атмосфере из ^{40}Ar и затем выпадает на поверхность Земли, поэтому уровень фона, связанный с данным изотопом, зависит от того, с какой глубины был взят кремний для изготовления детекторов. Концентрация ^{32}Si на поверхности Земли составляет $\sim 10^{-18}$ атом/атом, что соответствует активности 250 отсчет/(кг·сутки). Изотоп ^{32}Si ($T_{1/2} =$ 170 лет) испытывает два последовательных β-распада, которые практически не сопровождаются γ-квантами, что не позволяет подавить этот фон за счет секционирования детектора.

Исходя из обсуждавшегося выше, можно вычислить ожидаемые уровни фона для Ge- и Si-детекторов для различных интервалов энергий и сравнить эти значения с ожидаемым эффектом от слабого и магнитного рассеяния. Результаты измерений в течение одного месяца для детектора с массой 75 кг в нейтринном потоке $2 \cdot 10^{13}$ см$^{-1}\cdot$с$^{-1}$ показаны в табл. 4. Для Ge-детектора использовался уровень фона, достигнутый в эксперименте

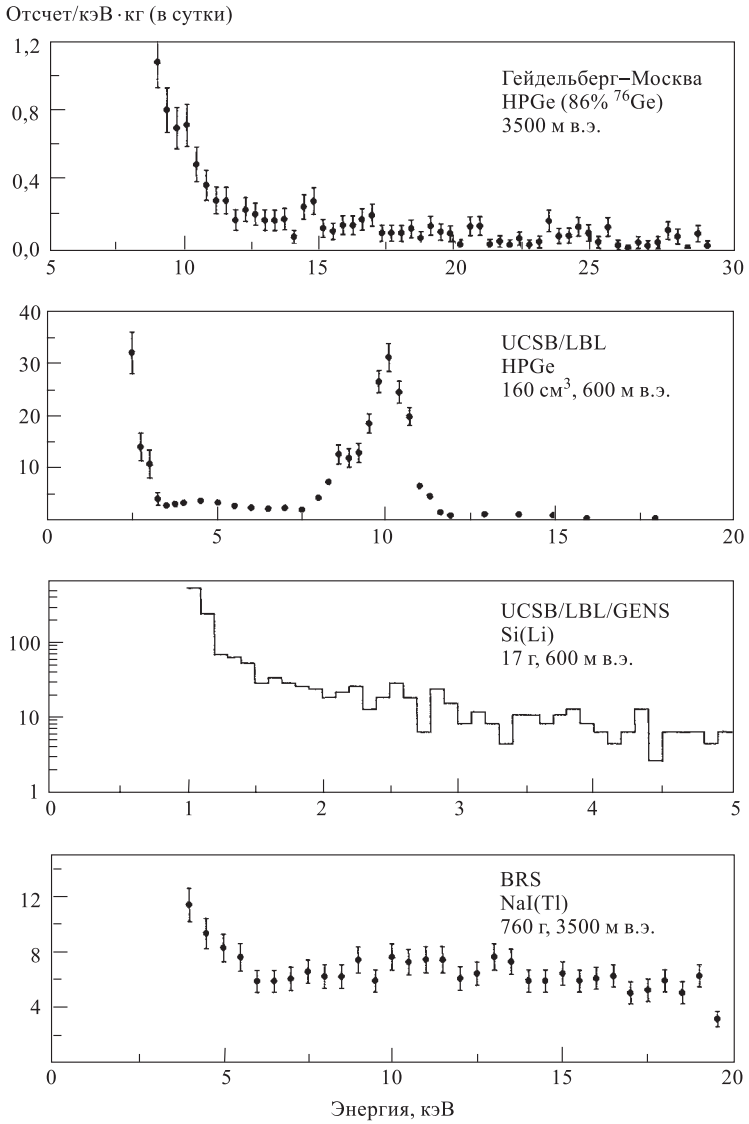

Рис. 8. Фоновые спектры в низкоэнергетической области, измеренные германиевыми и кремниевым полупроводниковыми детекторами и сцинтилляционным детектором

Гейдельберг—Москва. Фон Si-детектора вычислялся в предположении, что он связан лишь с распадами ^{32}Si с интенсивностью 100 кг$^{-1} \cdot$ сут$^{-1}$. Выбор длины энергетических интервалов определялся максимальным соотношением эффект$/\sqrt{\text{фон}}$ для фона, связанного со слабым рассеянием.

Таблица 4. Ожидаемое число отсчетов в детекторе, содержащем $2{,}25 \cdot 10^{28}$ электронов (≈ 75 кг), в потоке $2 \cdot 10^{13}$ см$^{-1}$·с$^{-1}$ за 30 дней измерений

$E_1 - E_2$, кэВ	$\mu_\nu = 10^{-11}\,\mu_B$	$\sin^2\,\theta_W = 0{,}23$	Ge	Si
2–8	35,4	69,5	2700	14900
8–30	35,0	247	4950	55500
30–120	34,5	811	20300	158000
120–500	25,6	2000	21400	125000
500–2000	9,3	2090	21100	180000
2000–8000	0,62	355		

Таблица 5. Предел обнаружения магнитного момента нейтрино (в единицах $10^{-11}\mu_B$) для различных источников фона

$E_1 - E_2$, кэВ	Слабое рассеяние	Ge	Si
2–8	0,41	1,3	2,1
8–30	0,56	1,6	2,8
30–120	0,76	2,3	3,7
120–500	1,1	2,7	4,1
500–2000	1,9	4,5	7,3
2000–8000	4,6		

Используя ожидаемые уровни фона, можно вычислить чувствительность (предел обнаружения) к магнитному моменту нейтрино для типичной кампании измерений на реакторе: один месяц до остановки реактора, один месяц во время остановки и еще месяц, когда реактор работает. Полученные результаты приведены в табл. 5.

Уменьшение порога регистрации электронов увеличивает чувствительность к магнитному моменту для всех рассмотренных источников фона. Например, если фон связан только со слабым рассеянием нейтрино, предел обнаружения для детектора с порогом 2 МэВ лишь в три раза меньше, чем современный предел на магнитный момент нейтрино. С другой стороны, переход в килоэлектронвольтную область энергии позволит иметь чувствительность к магнитному моменту реакторных нейтрино лучше, чем $10^{-11}\mu_B$, если фон будет связан лишь со слабым рассеянием. Для этого необходимо в реакторном эксперименте, практически на поверхности Земли (исключение составляет реактор в Красноярске [34]), получить уровень фона на порядок меньше, чем достигнутый в подземных экспериментах. Для поднятия чувствительности можно увеличивать массу детектора и время измерений, но поскольку сече-

ние (3) пропорционально μ_ν^2, чувствительность к магнитному моменту будет возрастать лишь как корень четвертой степени из этих величин.

Несмотря на указанные сложности, существует целый ряд проектов по измерению сечения рассеяния реакторных нейтрино или нейтрино от искусственных источников, на электроне и ядрах, с целью повышения чувствительности к магнитному моменту.

Коллаборация MUNU [41] готовит эксперимент на реакторе Буже с TPC-камерой объемом 1 м^3 с CF_4 при давлении до 5 бар. Основная проблема связана с высоким порогом регистрации электронов ($\sim 0{,}5$ МэВ). Использовать жидкоксеноновый или жидкоаргоновый детектор в экспериментах с реакторными нейтрино предлагалось в работах [42,43].

В ИТЭФ (Москва) ведутся работы над установкой, в которой сборка германиевых детекторов массой 2 кг находится внутри активной защиты из кристаллов NaI [44].

Чтобы снять проблему нейтринного спектра и получить возможность проведения экспериментов в подземных лабораториях, в ряде работ предлагается использовать искусственные источники нейтрино. Создать такие источники Б.Понтекорво предлагал еще в 1960 г. [45]. Успешное применение ^{51}Cr в экспериментах с Ga–Ge-детекторами солнечных нейтрино стимулировало новые предложения для поиска магнитного момента нейтрино с использованием источников нейтрино — ^{147}Pm [46], ^{90}Sr [47] и ^{3}H [48].

В ОИЯИ для регистрации электронов отдачи предлагается использовать низкотемпературный полупроводниковый детектор с одновременной регистрацией ионизации и тепловыделения вместе с источником нейтрино от K-захвата в ^{55}Fe [49]. В работе [50] криогенные калориметрические детекторы предлагается использовать для регистрации рассеяния нейтрино как на электроне, так и на ядрах.

В РНЦ «Курчатовский институт» предложено использовать β-распадчики ^{90}Sr–^{90}Y совместно с детектором BOREXINO для одновременного прецизионного измерения реакций обратного β-распада и (ν, e)-рассеяния [51].

6. ЗАКЛЮЧЕНИЕ

Магнитный момент нейтрино в стандартной теории мал и не может быть обнаружен на современных экспериментальных установках. Если дефицит солнечных нейтрино связан с взаимодействием магнитного момента нейтрино с магнитным полем конвективной зоны Солнца, то должны наблюдаться 11-летние вариации регистрируемого потока нейтрино, если при этом значение μ_ν не менее $10^{-11}\mu_B$. Эта величина близка к чувствительности современных лабораторных экспериментов. Такие вариации не наблюдаются в Ga–Ge-детекторах и Kamiokande.

Наиболее чувствительным к магнитному моменту оказывается процесс упругого рассеяния нейтрино на электроне. Данные по реакторным экспериментам позволяют получить ограничение на магнитный момент нейтрино $\mu_\nu \leq 1{,}5 \cdot 10^{-10}\mu_B$ (90 % у.д.). Дальнейшее увеличение чувствительности, в первую очередь, может быть связано с работой в килоэлектронвольтной области энергий электронов отдачи.

Работа выполнена при поддержке Российского фонда фундаментальных исследований (проект 97-02-16848).

СПИСОК ЛИТЕРАТУРЫ

1. **Lee B.W., Shrock R.E.** — Phys. Rev., 1977, v.D16, p.1444;
   Fujikawa K., Shrock R. — Phys. Rev. Lett., 1980, v.45, p.963.
2. **Lobashev V.M. et al.** — Nucl. Phys. B, Proc. Supll., 1999, v.77, p.327.
3. **Reines F., Curr H., Sobel H.** — Phys. Rev. Lett., 1976, v.37, p.315;
   Kyuldiev A.V. — Nucl. Phys., 1984, v.B234, p.387;
   Vogel P., Engel J. — Phys. Rev., 1989, v.D39, p.3378;
   Дербин А.В. — ЯФ, 1994, т.57, с.236.
4. **Krakaner D.A. et al.** — Phys. Lett., 1990, v.B252, p.177.
5. **Abe R. et al.** — Phys. Rev. Lett., 1987, v.58, p.636.
6. **Sutherland P. et al.** — Phys. Rev., 1976, v.D13, p.2700;
   Blinnikov S.I. et al. — Sov. Sci. Rev. Asrophys. Space Phys., 1987, v.6, p.185;
   Fokujita M., Yasaki S. — Preprint RIFP-709, 1987.
7. **Nussinov S., Rephael Y.** — Phys. Rev. Lett., 1987, v.36, p.2278;
   Barbieri R., Mohapatra R.M. — Phys. Rev. Lett., 1988, v.61, p.27;
   Lattimer J.M., Cooperstein J. — Phys. Rev. Lett., 1988, v.61, p.23.
8. **Волошин М.Б.** — Письма в ЖЭТФ, 1988, т.47, с.421;
   Стефанов М.А. — ЯФ, 1989, т.49, с.564;
   Окунь Л.Б. — ЯФ, 1988, т.48, с.967.
9. **Fukujita M., Yanagita T.** — Phys. Rev. Lett., 1987, v.58, p.187;
   Pulido J., Ralston J. — Preprint Fermilab. Pub-87, 132-t, 1987;
   Babu K.S., Mathur V.S. — Phys. Lett., 1987, v.B196, p.218.
10. **Волошин М.Б.** — ЯФ, 1988, т.48, с.804;
    Liu J. — Phys. Rev., 1987, v.D35, p.34;
    Choudhury D., Saarkar U. — Phys. Lett., 1990, v.B235, p.113.
11. **Babu K.S., Mohapatra R.M.** — Phys. Rev. Lett., 1990, v.64, p.1705;
    Ecker G. et al. — Phys. Lett., 1989, v.B232, p.217;
    Stefanov M.A., Vysotsky M.I. — Preprint ICTP IC190/67;
    Стефанов М.А., Высоцкий М.И. — ЯФ, 1991, т.53, с.1623;
    Leure M., Marcus N. — Phys. Lett., 1990, v.B235, p.113.
12. **Bahcall J.N., Pinsonneault M.H.** — Rev. Mod. Phys., 1992, v.64, p.885.
13. **Lende K. et al.** — Nucl. Phys. B, Proc. Supll., 1999, v.77, p.13.
14. **Gavrin V.N. et al.** — Nucl. Phys. B, Proc. Supll., 1999, v.77, p.20.
15. **Kirsten T.A. et al.** — Nucl. Phys. B, Proc. Supll., 1999, v.77, p.26.

16. **Suzuka Y. et al.** — Neutrino-96, World Scien. Publ., 1996, p.73.

17. **Suzuka Y. et al.** — Nucl. Phys. B, Proc. Supll., 1999, v.77, p.35.

18. **Sakurai K.** — Nature, 1979, v.279, p.146;
Базилевская Г.А., Стожков Ю.И., Чарахчьян Т.Н. — Письма в ЖЭТФ, 1982, т.35, с.273;
Гаврин В.Н, Копысов Ю.С., Макеев Н.Т. — Письма в ЖЭТФ, 1982, т.35, с.491.

19. **Davis R.** — Prog. Part. Nucl. Phys., 1994, v.32, p.13.

20. **Bahcall J.N., Press W.H.** — Astrophys. J., 1991, v.370, p.730;
Pal P.B. — Int. J. Mod. Phys., 1992, v.7, p.5387.

21. **Волошин М.Б., Высоцкий М.И.** — ЯФ, 1986, т.44, с.845;
Окунь Л.Б. — ЯФ, 1986, т.44, с.847;
Волошин М.Б., Высоцкий М.И., Окунь Л.Б. — ЯФ, 1986, т.44, с.677; ЖЭТФ, 1986, т.91, с.754.

22. **Oakley D.S. et al.** — Astrophys. J., 1994, v.437, p.L63.

23. **Корн Г., Корн Т.** — Справочник по математике для научных работников и инженеров. М.: Наука, 1977, с.642.

24. **Михеев С.П., Смирнов А.Ю.** — ЯФ, 1985, т.42, с.1441; ЖЭТФ, 1986, т.91, с.1986;
Wolfenstein J. — Phys. Rev., 1978, v.D17, p.2369.

25. **Akhmedov E.** — Phys. Lett., 1991, v.B257, p.163;
Babu K.S. et al. — Phys. Rev., 1991, v.D44, p.2265;
Pal B.P. — Int. J. Mod. Phys., 1992, v.7, p.5387.

26. **Carlson F., Openheimer J.R.** — Phys. Rev., 1932, v.41, p.763;
Bardin D.Ju., Bilenky S.M., Pontecorvo B.M. — Phys. Lett., 1970, v.B32, p.108;
Домогацкий Г.В., Надежин Д.К. — ЯФ, 1970, т.12, с.1232.

27. **Cowan C.L., Reines F., Harrison F.B.** — Phys. Rev., 1954, v.96, p.1294; Phys. Rev. Lett., 1970, v.24, p.1448; Phys. Rev. Lett., 1972, v.28, p.1406;
Толоконников С.В., Фаянс С.А. — Изв. АН СССР, 1973, т.37, с.2667.

28. **Окунь Л.Б.** — Лептоны и кварки. М.: Наука, 1981, с.302.

29. **CHARM II Collab., Vilain P. et al.** — Phys. Lett., 1992, v.B281, p.159.

30. **Reines F., Curr H., Sobel H.** — Phys. Rev. Lett., 1976, v.37, p.315.

31. **Попеко Л.А., Дербин А.В.** — Препринт ЛИЯФ, 1980, №585;
Дербин А.В., Петров Ю.В., Попеко Л.А. — Атомная энергия, 1981, т.50, с.400;
Бахланов С.В., Дербин А.В., Муратова В.Н., Попеко Л.А. и др. — Препринт ЛИЯФ, 1983, №864;
Дербин А.В., Попеко Л.А., Черный А.В., Шишкина Г.А. — Письма в ЖЭТФ, 1986, т.43, с.206.

32. **Дербин А.В., Черный А.В., Попеко Л.А. Муратова В.Н. и др.** — Письма в ЖЭТФ, 1993, т.57, с.755.

33. **Gurevich I.I., Khakimov S.Kh., Kozlov Yu.V. et al.** — In: Proc. LEWI-90, p.172. Dubna, 1991.

34. **Видякин Г.С., Выродов И.Р., Гуревич И.И. и др.** — Письма в ЖЭТФ, 1992, т.55, с.212.

35. **Кетов С.Н., Копейкин В.И., Микаэлян Л.А., Толоконников С.В.** — Письма в ЖЭТФ, 1988, т.47, с.177;
Schreckenbach K. et al. — Phys. Lett., 1985, v.B160, p.325;
Hahn A.A., Schreckenbach K. et al. — Phys. Lett., 1989, v.B218, p.365.

36. **Рубцов П.М. и др.** — ЯФ, 1987, т.46, с.1028;
Алексанкин В.Г., Родичков С.В., Рубцов П.М. и др. — Бета- и антинейтринное излучение ядер. М.: Энергоатомиздат, 1989;
Vogel P., Eugel J. — Phys. Rev., 1989, v.D39, p.3378;
Бакаляров А.М., Копейкин В.И., Микаэлян Л.А. — Препринт ИАЭ-5973/2, 1996; ЯФ, 1996, т.59, с.1225;
Копейкин В.И., Микаэлян Л.А., Синев В.В. — ЯФ, 1997, т.60, с.230.

37. **Heidelberg–Moscow Collaboration. Beck M. et al.** — Phys. Lett., 1994, v.B336, p.141.

38. **Caldwell D.O. et al.** — Phys. Rev. Lett., 1988, v.61, p.510.

39. **Caldwell D.O. et al.** — Phys. Rev. Lett., 1990, v.65, p.1305.

40. **Bacci C. et al.** — Phys. Lett., 1992, v.B293, p.460.

41. **Broggini C. et al.** — Nucl. Instr. Meth., 1992, v.A311, p.319;
Amsler R. et al. — Nucl. Instr. Meth., 1997, v.396, p.115.

42. **Baldo-Geolin M., Puglierin G., Barmin V.** — Preprint ITEP No.32-92, 1992.

43. **Cline D.B., Hong W.** — Int. J. Mod. Phys., 1992, v.7, p.4167.

44. **Beda A.G., Demidova E.V., Starostin A.S., Voloshin M.B.** — Peprint TPI-MINN -97/15-T, UMN-TH-1544-97, 1997; ЯФ, 1998, т.61, с.72.

45. **Понтекорво Б.М.** — Препринт ОИЯИ Д577, Дубна, 1960, с.39.

46. **Корноухов В.Н.** — ЯФ, 1997, т.60, с.639; ЯФ, 1998, т.61, с.1352.

47. **Bergelson B.R., Davydov A.V., Isaev Yu.N., Kornoukhov V.N.** — ЯФ, 1998, т.61, с.1347.

48. **Trofimov V.N., Neganov B.S., Yukhimchuk A.A.** — ЯФ, 1998, т.61, с.1373.

49. **Голубчиков А.В., Займидорога О.А., Смирнов О.Ю., Сотников А.П.** — ЯФ, 1996, т.59, с.1989.

50. **Инжечик Л.В., Гапонов Ю.В., Козлов Ю.В. и др.** — ЯФ, 1997, т.60, с.1993.

51. **Микаэлян Л.А., Синев В.В., Фаянс С.А.** — Письма в ЖЭТФ, 1998, т.67, с.435.

РЕФЕРАТЫ СТАТЕЙ, ПОМЕЩЕННЫХ В ВЫПУСКЕ

УДК 539.12.01

КЭД-эффекты высших порядков в ГНР. *Акушевич И., Кураев Э., Шайхатденов Б.* Физика элементарных частиц и атомного ядра, 2001, том 32, вып. 3, с. 491.

В обзоре рассмотрены эффекты высших поправок к сечению глубоконеупругого рассеяния для упругого и неупругого по протону каналов. Дифференциальные сечения вычислены с удержанием лидирующих $\sim(\alpha L/\pi)$, $(\alpha L/\pi)^2$ и нелидирующих $\sim(\alpha/\pi)$, $(\alpha/\pi)^2 L$ вкладов (здесь L есть так называемый *большой* логарифм). Также приводится явное выражение для комптоновского тензора с тяжелым фотоном, учитывающего излучение реальных и виртуальных фотонов электроном в случае продольной поляризации последнего. Детально представлен случай тормозного излучения для упругого рассеяния на протоне. Кроме того, дается анализ постановки эксперимента с детектированием только жесткого фотона как для процесса глубоконеупругого рассеяния, так и для тормозного излучения при аннигиляции электрон-позитронной пары в адроны.

Ил. 2. Библиогр.: 73.

УДК 530.12; 531.18; 531.12; 531.51; 539.12.01

Репараметризационно-инвариантная динамика релятивистских систем. *Барбашов Б.М., Первушин В.Н., Павловски М.* Физика элементарных частиц и атомного ядра, 2001, том 32, вып. 3, с. 546.

Обзор посвящен репараметризационно-инвариантному описанию динамики релятивистских систем (релятивистская частица, струна, вселенная в общей теории относительности). Такое описание достигается переходом на поверхность связей в фазовом пространстве.

Вычисление функции действия на поверхности связей (путем их решения) ведет к эквивалентным системам без связей, совместимым с простейшими вариационными принципами и с физически ясными и математически строгими определениями инвариантных измеряемых величин как в классической, так и в квантовой теориях, в частности, динамического эволюционного параметра в мировом пространстве переменных, плотности измеряемой энергии и частицеподобных (голоморфных) переменных в общей теории относительности.

Геометрический интервал времени, измеряемый часами наблюдателя, на поверхности связей становится сложным функционалом от динамических переменных. Поэтому описание эволюции переменных мирового пространства относительно геометрического интервала времени (измеряемого часами сопутствующего наблюдателя) может быть сделано с помощью специального канонического преобразования (введенного впервые Леви-Чивитой в теории дифференциальных уравнений).

Преобразование Леви-Чивита превращает энергетическую связь в канонический импульс новой переменной, совпадающей на уравнениях движения с геометрическим временем; остальные переменные мирового пространства имеют смысл начальных данных.

Исследуя репараметризационно-инвариантную динамику систем со связями на поверхности их связей, мы получаем новое представление для каузальных функций Грина в виде континуального интеграла в мировом пространстве для всех рассматриваемых релятивистских систем, и находим новые решения таких проблем, как размер-

ность пространства-времени в квантовой теории релятивистской струны, начальные космологические данные, направление стрелы времени, описание Большого Взрыва в гамильтоновской формулировке общей теории относительности в ее классической и квантовой версиях.

Табл. 1. Ил. 11. Библиогр.: 45.

УДК 514.763.4

К алгебраической классификации многообразий Калаби–Яо. Изучение пространств *K*3. *Ансельмо Ф., Эллис Дж., Нанопулос Д.В., Волков Г.* Физика элементарных частиц и атомного ядра, 2001, том 32, вып. 3, с. 605.

На основе формулировки Батырева многообразий Калаби–Яо (КЯ) как торических множеств во взвешенных комплексных проективных пространствах, ассоциированных с рефлексивными полиэдрами, предлагается индуктивный алгебраический подход к систематическому построению и классификации обобщенных многообразий КЯ для различных комплексных размерностей. Показано, как допустимые весовые векторы в низших размерностях могут быть расширены для высших размерностей. При этом отмечены роль проектирования и пересечения в их дуальном описании и естественное появление алгебраических структур Картана–Ли. Пятьдесят допустимых расширенных четырехмерных векторов могут быть скомбинированы в пары (тройки), формирующие 22 (4) цепочки, содержащие 90 (91) *K*3-пространств, из которых 94 являются особыми, а одно *K*3-пространство находится с использованием дуальности. В случае КЯ3-пространств пары (тройки) из 10270 допустимых расширенных векторов дают 4242 (259) цепочек с *K*3 (эллиптическими)-расслоениями, содержащими 730 дополнительных *K*3-полиэдров. Более полное изучение КЯ3-пространств будет проведено в последующей работе.

Табл. 30. Ил. 16. Библиогр.: 37.

УДК 539.12

Экспериментальный статус электрической и магнитной поляризуемостей протона. *Баранов П.С., Львов А.И., Петрунькин В.А., Штарков Л.Н.* Физика элементарных частиц и атомного ядра, 2001, том 32, вып. 3, с. 699.

В обзоре обсуждаются ранние и поздние экспериментальные данные по дифференциальному сечению γp-рассеяния при энергиях падающего фотона в лабораторной системе $\omega < 150$ МэВ, полученные в разных ускорительных центрах, и соответствующие безмодельные и модельные теоретические сечения, которые используются при фитировании данных и определении экспериментальных значений электрической (α_p) и магнитной (β_p) поляризуемостей протона. Впервые выполнен анализ всех имеющихся данных на совместимость и определены мировые средние значения поляризуемостей протона: $\alpha_p^{\text{эксп}} = 11{,}7 \pm 0{,}8\,(\text{полн.эксп.}) \pm 0{,}7\,(\text{теор.})$ и $\beta_p^{\text{эксп}} = 2{,}3 \pm 0{,}9\,(\text{полн.эксп.}) \pm 0{,}7\,(\text{теор.})$ (в ед. 10^{-4} фм^3). Обсуждаются также погрешности, привносимые в значения $\alpha_p^{\text{эксп}}$ и $\beta_p^{\text{эксп}}$ разными неопределенностями в использованном модельном дисперсионном сечении, и указывается интервал энергий ω, где такие погрешности минимальны.

Табл. 7. Ил. 1. Библиогр.: 93.

УДК 539.173

Поиски магнитного момента нейтрино. *Дербин А.В.* Физика элементарных частиц и атомного ядра, 2001, том 32, вып. 3, с. 734.

Результаты экспериментов по измерению сечения упругого рассеяния реакторных нейтрино на электроне анализируются с целью поиска вклада в сечение от магнитного момента нейтрино. Сравниваются возможности поиска магнитного момента на ускорителях и реакторе. Найден верхний предел на возможный магнитный момент нейтрино $\mu_\nu \leq 1{,}5 \cdot 10^{-10}\ \mu_B$ (90 % у.д.). Обсуждаются возможности увеличения чувствительности реакторных экспериментов до уровня $10^{-11}\ \mu_B$.

Табл. 5. Ил. 8. Библиогр.: 51.

«ФИЗИКА ЭЛЕМЕНТАРНЫХ ЧАСТИЦ И АТОМНОГО ЯДРА»
2001, ТОМ 32, ВЫП.3

СОДЕРЖАНИЕ

CONTENTS

Редакторы **Е.К.Аксенова, Э.В.Ивашкевич.**
Корректор **Т.Е.Попеко.**

Сдано в набор 17.12.2000. Подписано в печать 05.03.2001. Формат 60 90/16.
Бумага офсетная № 1. Печать офсетная. Усл. печ. л. 16,5. Уч.-изд. л. 20,15.
Тираж 400. Заказ 52541. Цена 15 р.

141980 Дубна Московской области
ОИЯИ, Издательский отдел, E-mail address: publish@pds.jinr.dubna.su

---

ISSN 0367—2026. Физика элементарных частиц и атомного ядра
2001. Том 32. Вып.3. 487—756.

ФИЗИКА ЭЛЕМЕНТАРНЫХ ЧАСТИЦ И АТОМНОГО ЯДРА
2001. Т. 32. ВЫП. 3

УДК 539.12.01

QED EFFECTS OF HIGHER ORDERS IN DIS

*I. Akushevich**

North Carolina Cent. Univ., Durham, NC 27707 and TJNAF, Newport News, VA 23606, USA

E. Kuraev, B. Shaikhatdenov

Joint Institute for Nuclear Research, Dubna

*On leave from the National Centre of Particle and High Energy Physics, 220040 Minsk, Belarus.

ФИЗИКА ЭЛЕМЕНТАРНЫХ ЧАСТИЦ И АТОМНОГО ЯДРА
2001. Т. 32. ВЫП. 3

УДК 530.12; 531.18; 531.12; 531.51; 539.12.01

TIME-REPARAMETRIZATION-INVARIANT DYNAMICS OF RELATIVISTIC SYSTEMS

B.M.Barbashov, V.N.Pervushin

Joint Institute for Nuclear Research, Dubna

M.Pawlowski

Soltan Institute for Nuclear Studies, Warsaw, Poland

ФИЗИКА ЭЛЕМЕНТАРНЫХ ЧАСТИЦ И АТОМНОГО ЯДРА
2001. Т. 32. ВЫП. 3

УДК 514.763.4

TOWARDS AN ALGEBRAIC CLASSIFICATION OF CALABI–YAU MANIFOLDS
Study of $K3$ Spaces

F. Anselmo

INFN–Bologna, Bologna, Italy

J. Ellis

Theory Division, CERN, CH-1211 Geneva, Switzerland

D.V. Nanopoulos

Dept. of Physics, Texas A & M University, College Station, TX 77843-4242, USA,
HARC, The Mitchell Campus, Woodlands, TX 77381, USA,
and Academy of Athens, 28 Panepistimiou Avenue, Athens 10679, Greece

G. Volkov

Theory Division, CERN, CH-1211 Geneva, Switzerland
and Theory Division, Institute for High-Energy Physics,
Protvino, Russia

ФИЗИКА ЭЛЕМЕНТАРНЫХ ЧАСТИЦ И АТОМНОГО ЯДРА
2001. Т. 32. ВЫП. 3

УДК 539.12

ЭКСПЕРИМЕНТАЛЬНЫЙ СТАТУС ЭЛЕКТРИЧЕСКОЙ И МАГНИТНОЙ ПОЛЯРИЗУЕМОСТЕЙ ПРОТОНА

П.С.Баранов, А.И.Львов, В.А.Петрунькин, Л.Н.Штарков

Физический институт им. П.Н.Лебедева РАН, Москва

ФИЗИКА ЭЛЕМЕНТАРНЫХ ЧАСТИЦ И АТОМНОГО ЯДРА
2001. Т. 32. ВЫП. 3

УДК 539.173

ПОИСКИ МАГНИТНОГО МОМЕНТА НЕЙТРИНО

А.В.Дербин

Петербургский институт ядерной физики РАН, Гатчина, Россия